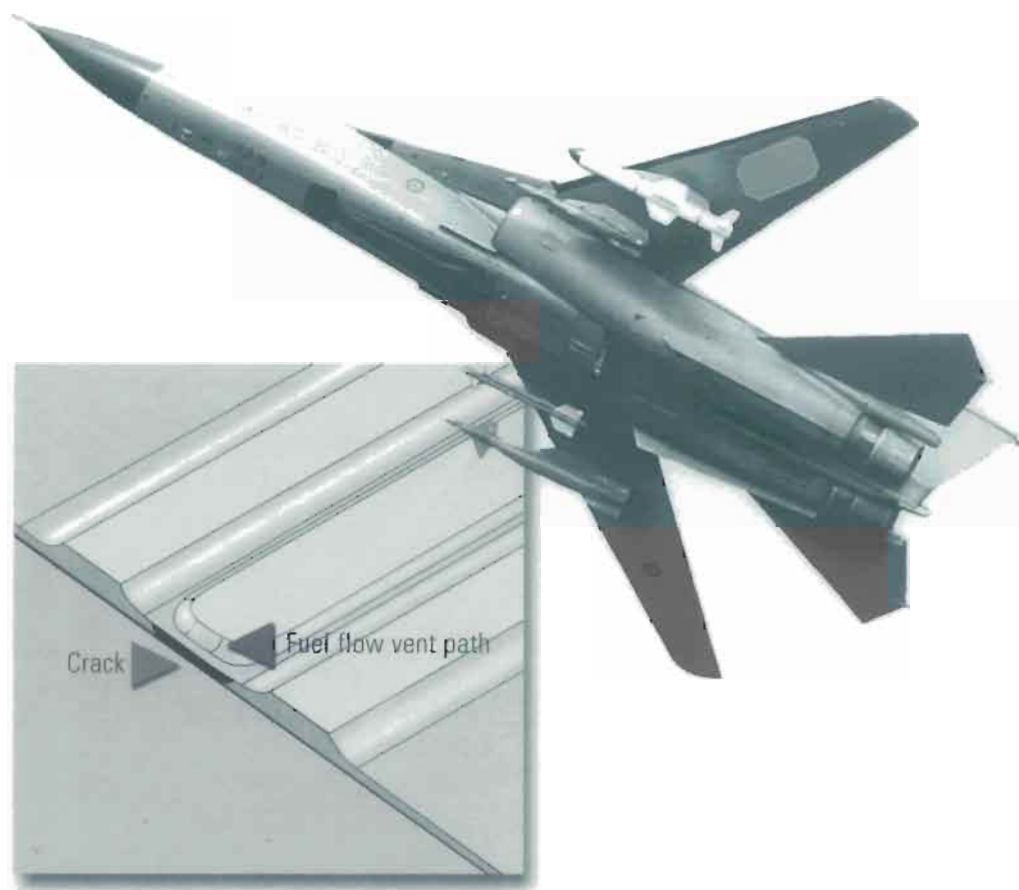


Advances in the Bonded Composite Repair of Metallic Aircraft Structure

VOLUME 2



Edited by

Alan Baker

Francis Rose

Rhys Jones

ELSEVIER

ADVANCES IN THE BONDED COMPOSITE REPAIR OF METALLIC AIRCRAFT STRUCTURE

Volume 2

Elsevier Science Internet Homepage - <http://www.elsevier.com>

Consult the Elsevier homepage for full catalogue information on all books, journals and electronic products and services.

Elsevier Titles of Related Interest

VALERY V. VASILEV & EVGENY V. MOROZOV

Mechanics and Analysis of Composite Materials

ISBN: 0 08 042702 2

JANG-KYO KIM & YIU WING MAI

Engineered Interfaces in Fiber Reinforced Composites

ISBN: 0 08 042695 6

J.G. WILLIAMS & A. PAVAN

Fracture of Polymers, Composites and Adhesives

ISBN: 0 08 043710 9

D.R. MOORE, A. PAVAN & J.G. WILLIAMS

Fracture Mechanics Testing Methods for Polymers Adhesives and Composites

ISBN: 0 08 043689 7

Related Journals:

Composite Structures - www.elsevier.com/locate/compstruct

Composites Part A: Applied Science and Manufacturing - www.elsevier.com/locate/compositesa

Composites Part B: Engineering - www.elsevier.com/locate/compositesb

Composites Science and Technology - www.elsevier.com/locate/compscitech

Major Reference Work:

Comprehensive Composite Materials - www.elsevier.com/locate/isbn/0080429939

To contact the Publisher

Elsevier Science welcomes enquiries concerning publishing proposals: books, journal special issues, conference proceedings, etc. All formats and media can be considered. Should you have a publishing proposal you wish to discuss, please contact, without obligation, the publisher responsible for Elsevier's Composites and Ceramics programme:

Emma Hurst

Assistant Publishing Editor

Elsevier Science Ltd

The Boulevard, Langford Lane

Kidlington, Oxford

OX5 1GB, UK

Phone: + 44 1865 843629

Fax: + 44 1865 843931

E.mail: e.hurst@elsevier.com

General enquiries, including placing orders, should be directed to Elsevier's Regional Sales Offices – please access the Elsevier homepage for full contact details (homepage details at the top of this page).

Book Butler logo to search for more Elsevier books, visit the Books Butler at <http://www.elsevier.com/homepage/booksbutler/>

ADVANCES IN THE BONDED COMPOSITE REPAIR OF METALLIC AIRCRAFT STRUCTURE

Volume 2

Editors

A.A. Baker

*Defence Science and Technology Organisation,
Air Vehicles Division,
Victoria, Australia*

L.R.F. Rose

*Department of Defence,
Defence Science and Technology Organisation,
Air Vehicles Division,
Victoria, Australia*

R. Jones

*Mechanical Engineering Department,
Monash University, Victoria, Australia*



2002

ELSEVIER

Amsterdam – Boston – London – New York – Oxford – Paris
San Diego – San Francisco – Singapore – Sydney – Tokyo

ELSEVIER SCIENCE Ltd
The Boulevard, Langford Lane
Kidlington, Oxford OX5 1GB, UK

© 2002 Elsevier Science Ltd. All rights reserved.

This work is protected under copyright by Elsevier Science, and the following terms and conditions apply to its use:

Photocopying

Single photocopies of single chapters may be made for personal use as allowed by national copyright laws. Permission of the Publisher and payment of a fee is required for all other photocopying, including multiple or systematic copying, copying for advertising or promotional purposes, resale, and all forms of document delivery. Special rates are available for educational institutions that wish to make photocopies for non-profit educational classroom use.

Permissions may be sought directly from Elsevier Science via their home page (<http://www.elsevier.com>), by selecting 'Customer support' and the 'Permissions'. Alternatively you can send an e-mail to: permissions@elsevier.co.uk, or fax to: (+44) 1865 853333.

In the USA, users may clear permissions and make payments through the Copyright Clearance Center, Inc., 222 Rosewood Drive, Danvers, MA 01923, U.S.A.; phone (+1) 978 750 8400, fax: (+1) 978 750 4744, and in the UK through the Copyright Licensing Agency Rapid Clearance Service (CLARCS), 90 Tottenham Court Road, London W1P 0LP; phone (+44) 207 631 5555; fax: (+44) 207 631 5500. Other countries may have a local reprographic rights agency for payments.

Derivative Works

Tables of contents may be reproduced for internal circulation, but permission of Elsevier Science is required for external resale or distribution of such material.

Permission of the Publisher is required for all other derivative works, including compilations and translations.

Electronic Storage or Usage

Permission of the Publisher is required to store or use electronically any material contained in this work, including any chapter or part of a chapter.

Except as outlined above, no part of this work may be reproduced, stored in a retrieval system or transmitted in any form or by any means, electronic, mechanical, photocopying, recording or otherwise, without written permission of the Publisher.

Address permission requests to: Elsevier Science Global Rights Department, at the mail, fax and email addresses note above.

Notice

No responsibility is assumed by the Publisher for any injury and/or damage to persons or property as a matter of products liability, negligence or otherwise, or from any use or operation of any methods, products, instructions or ideas contained in the material herein. Because of rapid advances in the medical sciences, in particular, independent verification of diagnosis and drug dosages should be made.

First Edition 2002

Library of Congress Cataloging in Publication Data

A catalog of record from the Library of Congress has been applied for.

British Library Cataloguing in Publication Data

A catalogue record from the British Library has been applied for.

ISBN: 0-08-042699-9

Ⓢ The paper used for this publication meets the requirements of ANSI/NISO Z39.48-1992 (Permanence of Paper).
Printed in The Netherlands.

BIOGRAPHIES

Dr. Alan Baker

Dr. Alan Baker is Research Leader Aerospace Composite Structures, in Airframes and Engines Division, Defence Science and Technology (DSTO), Aeronautical and Maritime Research Laboratory and Technical Adviser to the Cooperative Research Centre—Advanced Composite Structures, Melbourne Australia. He is a Fellow of the Australian Academy of Technological Sciences and Engineering and an Adjunct Professor in Department of Aerospace Engineering, Royal Melbourne Institute of Technology. Dr. Baker is a member of the International Editorial Boards of the Journals Composites Part A Applied Science and Manufacturing, Applied Composites and International Journal of Adhesion and Adhesives.

He is recognised for pioneering research work on metal-matrix fibre composites while at the Rolls Royce Advanced Research Laboratory. More recently, he is recognised for pioneering work on bonded composite repair of metallic aircraft components for which he has received several awards, including the 1990 Ministers Award for Achievement in Defence Science.

Dr. Francis Rose

Dr. Francis Rose is the Research Leader for Fracture Mechanics in Airframes and Engines Division, Defence Science and Technology (DSTO), Aeronautical and Maritime Research Laboratory. He has made important research contributions in fracture mechanics, non-destructive evaluation and applied mathematics. In particular, his comprehensive design study of bonded repairs and related crack-bridging models, and his contributions to the theory of transformation toughening in partially stabilised zirconia, have received international acclaim. His analysis of laser-generated ultrasound has become a standard reference in the emerging field of laser ultrasonics, and he has made seminal contributions to the theory of eddy-current detection of cracks, and early detection of multiple cracking.

He is the Regional Editor for the *International Journal of Fracture* and a member of the editorial board of *Mechanics of Materials*. He was made a Fellow of the Institute of Mathematics and its Applications, UK, in 1987, and a Fellow of the Institution of Engineers, Australia, in 1994. He is currently President of the Australian Fracture Group, and has been involved in organising several local and international conferences in the areas of fracture mechanics and engineering mathematics. He currently serves on the Engineering Selection Panel of the Australian Research Council and of several other committees and advisory bodies.

Professor Rhys Jones

Professor Rhys Jones joined Monash University in early 1993 and is currently Professor of Mechanical Engineering, and Head of the Defence Science and Technology Organisation Centre of Expertise on Structural Mechanics. Professor Jones' is best known for his in the fields of finite element analysis, composite repairs and structural integrity assessment. Professor Jones is the Founding Professor of both the BHP-Monash Railway Technology Institute and the BHP-Monash Maintenance Technology Institute. He is heavily involved with both Australian and overseas industry. In this context he ran the mechanical aspects of the Australian Governments Royal Commission into the failure at the ESSO plant in Victoria, and the Tubemakers-BHP investigation into the failure of the McArthur River gas pipe line in the Northern Territory.

He is the recipient of numerous awards including the 1982 (Australian) Engineering Excellence Award, for composite repairs to Mirage III, the Institution of Engineers Australia George Julius Medal, for contributions to failure analysis, a TTCP Award, for contributions to Australian, US, UK, Canada and NZ Defence Science in the field of composite structures, and a Rolls-Royce-Qantas Special Commendation, for his work on F-111 aircraft. Since 1999 Professor Jones has been Co-Chair of the International Conference (Series) on Composite Structures.

Acknowledgement

The editors are very pleased to acknowledge their appreciation of the great assistance provided by Drs Stephen Galea and Chun Wang of the Defence Science and Technology Organisation, Aeronautical and Maritime Research Laboratory, who made important contributions, in the collation and editing of this book.

FOREWORD

The introduction of the technology for bonded composite repairs of metallic airframe structures could not have come at a more opportune time. Today, many countries are facing the challenge of aging aircraft in their inventories. These airframes are degrading due to damage from fatigue cracking and corrosion. Repair with dependable techniques to restore their structural integrity is mandatory. The concept of using bonded composite materials as a means to maintain aging metallic aircraft was instituted in Australia approximately thirty years ago. Since that time it has been successfully applied in many situations requiring repair. These applications have not been limited to Australia. Canada, the United Kingdom, and the United States have also benefited from the use of this technology. The application for the solution of the problem of cracking in the fuel drain holes in wing of the C-141 is credited with maintaining the viability of this fleet.

The concept for composite repair of metallic aircraft is simple. The bonded repair reduces stresses in the cracked region and keeps the crack from opening and therefore from growing. This is easy to demonstrate in a laboratory environment. It is another thing to do this in the operational environment where many factors exist that could adversely affect the repair reliability. The researchers at the Aeronautical and Maritime Research Laboratory in Australia realized there were many obstacles to overcome to achieve the desired reliability of the process. They also realized that failures of the repair on operational aircraft would mean loss of confidence and consequently enthusiasm for the process. They proceeded slowly. Their deliberate approach paid off in that they developed a process that could be transitioned to aircraft use by engineers and technicians. The essential ingredient for application of this technology is discipline. When the applicator of this process maintains the discipline required for the process and stays within the bounds of appropriate applications, then the repair will be successful.

This book, edited by Drs A.A. Baker, L.R.F. Rose and R. Jones, includes the essential aspects of the technology for composite repairs. The editors have chosen some of the most knowledgeable researchers in the field of bonded repairs to discuss the issues with the many aspects of this technology. Included are discussions on materials and processes, design of repairs, certification, and application considerations. These discussions are sufficiently in-depth to acquaint the reader with an adequate understanding of the essential ingredients of the procedure. The application case histories are especially useful in showing the breadth of the possible uses of the technology.

It is easy to be excited about the future of composite repairs to metallic airframes. It has all the ingredients for success. Today's applications have shown that it is reliable, there is typically a significant return on the investment, and it can be transitioned to potential users. Additional research will open up possible new applications.

This book is intended to provide the reader with a good understanding of the basic elements of this important technology. It fulfills that purpose.

John W. Lincoln
Technical Adviser for Aircraft Structural Integrity
United States Air Force

DEDICATION

The Editors would like to dedicate these volumes to Dr J.W Lincoln who passed away a few months after he wrote this foreword. Jack's outstanding contributions to the many fields related to the structural airworthiness of aircraft are legend and need not be repeated here. He was very supportive of the work on bonded repair technology, as indicated in the foreword, and, indeed, was the Chairman of an international group addressing certification issues. This report is referenced in Chapter 1.

It is rare to find in science and engineering, such a giant in the field who was so modest, approachable and friendly. Jack was regarded both as a supportive father figure and the expert to be convinced on all airworthiness issues, particularly as related to the USAF.

DEFAULT NOMENCLATURE

Boron/epoxy	<i>b/ep</i>	graphite/epoxy	<i>gr/ep</i>
Shear modulus (also used for strain energy release rate)	<i>G</i>	Young's modulus	<i>E</i>
Characteristic crack length	λ	Poissons ratio	ν
Stress intensity	<i>K</i>	Crack length	<i>a</i>
Cycles	<i>N</i>	Disbond length	<i>b</i>
Paris Coefficient	<i>A</i>	Paris Exponent	<i>n</i>
Shear stress	τ	Stress	σ
Shear strain	γ	Strain	<i>e</i>
Thickness	<i>t</i>	Displacement	<i>u or δ</i>
Length	<i>L</i>	Thickness	<i>t</i>
Width	<i>W</i>	Applied load	<i>P</i>
Elastic shear strain exponent	β	Force per unit width	<i>F</i>
Inclusion factor	ϕ	Stiffness ratio	<i>S</i>
Stress Ratio	<i>R</i>	Thermal expansion coefficient	<i>a</i>
Angle	θ	Temperature range	ΔT

SUBSCRIPTS/SUPERSCRIPTS

Panel	<i>P</i>	Plastic condition	<i>p</i>
Elastic condition	<i>e</i>	Maximum value	<i>max</i>
Ultimate value	<i>u</i>	Minimum value	<i>min</i>
Adhesive	<i>A</i>	Outer adherend	<i>o</i>
Temperature	<i>T</i>	Inner adherend	<i>i</i>
Value at infinity	∞	Allowable value	<i>*</i>
Critical value	<i>c</i>		
Reinforcement	<i>R</i>		

CONTENTS

Biographies	v
Foreword	vii
Dedication	ix
Volume 1	
Chapter 1. Introduction and Overview	1
A.A. Baker	
1.1. Aim of book	1
1.2. Classification of aircraft structures for inspection and repair	2
1.2.1. Design and certification of airframe structures	2
1.2.2. Problems with ageing metallic airframe components	3
1.3. Repair requirements	5
1.3.1. Repair levels	6
1.4. Repair procedures	6
1.5. The case for adhesively bonded repairs	7
1.6. Composite versus metallic patches	9
1.7. Scope of applications	10
1.8. Some experimental comparisons of bonding versus bolting	11
1.9. R&D requirements	14
1.10. Conclusion	17
References	17
Chapter 2. Materials Selection and Engineering	19
R. Chester	
2.1. Introduction	19
2.1.1. Factors affecting adhesion	20
2.2. Materials for patches and reinforcements	21
2.2.1. Metallic materials	21
2.2.2. Non-metallic materials	24
2.2.3. Patch material selection	26
2.3. Adhesive systems	28
2.3.1. Adhesive types	28
2.3.2. Adhesive properties	29
2.3.3. Adhesive selection	30
2.4. Primers and coupling agents	32
2.5. Adhesive and composite test procedures	34
2.6. Materials engineering considerations	35
2.6.1. Residual stresses	35
2.6.2. Cure pressure and voids	36
2.6.3. Spew fillet	38
2.6.4. Composites offer the possibility of embedded strain sensors to form "SMART" repairs	39
References	39

Chapter 3. Surface Treatment and Repair Bonding	41
D. Arnott, A. Rider and J. Mazza	
3.1. Introduction	41
3.1.1. Surface energy and wetting	41
3.1.2. Bondline pressurisation and adhesive cure	42
3.1.3. Adhesive bond performance	43
3.1.4. Standards and environments for adhesive bonding	44
3.2. Mechanical tests	45
3.2.1. Loading and failure modes	45
3.2.2. Qualification of bonding procedures and performance	46
3.3. Standard tests	47
3.3.1. Wedge durability test	47
3.3.2. Fracture mechanics and the cleavage specimen	48
3.4. Fundamentals of durable bonding	48
3.4.1. Surface roughness and bond durability	49
3.4.2. Surface hydration and bond durability	50
3.4.3. Surface contamination and bond durability	51
3.4.4. Bond durability model	53
3.5. Requirements of surface preparation	56
3.5.1. Degreasing	57
3.5.2. Abrasion, grit-blasting or etching	58
3.5.3. Creation of a high energy surface oxide	60
3.5.4. Coupling agent	61
3.5.5. Adhesive primer	63
3.5.6. Drying	63
3.6. Adhesive application	64
3.6.1. Factors controlling bondline thickness	65
3.6.2. Void formation and minimisation	65
3.7. Surface treatment quality control	66
3.7.1. Waterbreak Test	66
3.7.2. Surface work function methods	67
3.7.3. Fourier transform infrared spectroscopy	67
3.7.4. Optical reflectivity	68
3.7.5. Process control coupons (traveller or witness specimens)	68
3.7.6. Practitioner education, skill and standards	68
3.8. Surface preparations for aluminium adherends	69
3.8.1. Factory processes	69
3.8.2. On-aircraft acid anodisation and acid etch processes	72
3.9. Surface preparations for titanium adherends	74
3.9.1. Factory processes	74
3.9.2. On-aircraft processes	76
3.10. Surface preparations for steel adherends	77
3.10.1. Factory processes	77
3.10.2. On-aircraft processes	78
3.11. Surface preparations for thermosetting-matrix composites	78
3.11.1. Precured patches	80
3.12. Recent surface preparation research	80
3.12.1. Sol-Gel technology for adhesive bonding	80
3.12.2. Hot solution treatment for adhesive bonding	81
References	82

Chapter 4. Adhesives Characterisation and Data Base	87
P. Chalkley and A.A. Baker	
4.1. Introduction	87
4.2. Common ASTM and MIL tests	88
4.2.1. Stress-strain allowables	89
4.3. Fatigue loading	94
4.4. Fracture-mechanics allowables	94
4.4.1. Static loading	95
4.4.2. Mode I	95
4.4.3. Mode II and mixed mode	96
4.4.4. Fatigue loading	96
4.5. FM73 database	98
4.5.1. In situ shear stress-strain allowables	98
4.5.2. Yield criterion	99
4.5.3. The glass transition temperature	99
4.5.4. Fickian diffusion coefficients for moisture absorption	100
4.5.5. Mode I fracture toughness	100
References	101
 Chapter 5. Fatigue Testing of Generic Bonded Joints	 103
P.D. Chalkley, C.H. Wang and A.A. Baker	
5.1. Introduction	103
5.1.1. Damage-tolerance regions in a bonded repair	103
5.1.2. The generic design and certification process	104
5.2. The DOFS	104
5.2.1. Stress state in the DOFS	106
5.2.2. Experimental method	108
5.2.3. Experimental results	109
5.3. The skin doubler specimen	114
5.3.1. Stress state in the skin doubler specimen	115
5.3.2. Experimental method and results	120
5.3.3. Fracture mechanics approach	123
5.4. Discussion	124
References	125
 Chapter 6. Evaluating Environmental Effects on Bonded Repair Systems	 127
Using Fracture Mechanics	
L.M. Butkus, R.V. Valentin and W.S. Johnson	
6.1. Introduction	127
6.2. Materials and specimens	128
6.2.1. Bonded material system and fabrication	128
6.3. Experimental procedures	129
6.3.1. Pre-test environmental conditioning	129
6.3.2. Testing procedures	129
6.4. Analysis	131
6.5. Results and discussion	132
6.5.1. Fracture toughness	131
6.5.2. Fatigue behavior	134
6.6. Summary and conclusions	135
References	135

Chapter 7. Analytical Methods for Designing Composite Repairs	137
L.R.F. Rose and C.H. Wang	
7.1. Introduction	137
7.2. Formulation and notation	139
7.3. Load transfer of bonded reinforcement	141
7.4. Symmetric repairs	144
7.4.1. Stage I: Inclusion analogy	144
7.4.2. Stage II: Stress intensity factor	147
7.4.3. Plastic adhesive	149
7.4.4. Finite crack size	150
7.4.5. Finite element validation	154
7.5. Shear mode	155
7.6. One-sided repairs	157
7.6.1. Geometrically linear analysis	157
7.6.2. Crack bridging model	162
7.6.3. Geometrically non-linear analysis	163
7.7. Residual thermal stress due to adhesive curing	167
7.7.1. Temperature distribution	168
7.7.2. Residual stress due localised heating	170
7.7.3. Residual stresses after cooling from cure	171
7.7.4. Thermal stress due to uniform temperature change	173
7.7.5. Validation	173
References	174
 Chapter 8. Recent Expansions in the Capabilities of Rose's Closed-form Analyses for Bonded Crack-patching	 177
L.J. Hart-Smith	
8.1. Introduction	177
8.1.1. Rose's use of the inclusion model to establish stress fields	178
8.1.2. Rose's solution for stress-intensity factor K at the crack tips	180
8.2. Universal efficiency charts for isotropic patches	183
8.3. Equivalence between octagonal and elliptical patch shapes	184
8.4. Effects of patch tapering on the adhesive stresses	186
8.5. Universal charts for the effects of corrosion	189
8.6. Design of patches to compensate for corrosion damage	191
8.7. Analysis of patches over cracks in stiffened panels	192
8.8. Designing to avoid crack initiation	194
8.9. Universal efficiency charts for orthotropic patches	196
8.10. Effects of residual thermal stresses on bonded repairs	197
8.11. Effects of adhesive non-linearity and disbonds on crack-tip stress-intensity factors	200
8.11. Out-of-plane bending effects with one-sided patches	202
8.12. Remaining challenges involving closed-form analyses	204
8.13. Concluding remarks	204
References	205
 Chapter 9. Numerical Analysis and Design	 207
R. Jones	
9.1. Analysis and design	207
9.2. The 2D finite element formulation	208
9.2.1. Element stiffness matrix	210

9.2.2.	Repair of cracks in aircraft wing skin	212
9.3.	Initial design guidelines	215
9.4.	Comparison with experimental results for non rib stiffened panels	227
9.5.	Repair of thick sections	229
9.5.1.	Experimental results	231
9.6.	Repair of cracked holes in primary structures	233
9.7.	Repair of cracked lugs	236
9.7.1.	Numerical analysis	238
9.7.2.	Experimental test	240
9.7.3.	Discussion	241
9.8.	Repairs to interacting surface flaws	242
9.9.	Material nonlinearities	243
9.9.1.	Governing differential equations for bonded joints/repairs	245
9.10.	Effect of variable adhesive thickness	251
9.10.1.	The effect of variable adhesive thickness and material non-linearity	256
9.11.	Repairs to cracked holes under bi-axial loading	258
9.12.	Findings relevant to thick section repair	262
9.12.1.	Comparison of commercial finite element programs for the 3D analysis of repairs	264
	References	266
Chapter 10.	Shape Optimisation for Bonded Repairs	269
	M. Heller and R. Kaye	
10.1.	Introduction	269
10.1.1.	Context for finite element based shape optimisation	270
10.1.2.	Finite element modelling considerations	271
10.1.3.	Outline of chapter	271
10.2.	Analytical formulation for improved stepping in patch taper region	272
10.2.1.	General configuration for symmetric stepped patches	272
10.2.2.	Analysis for single step case	273
10.2.3.	Analysis for patch with multiple steps	274
10.2.4.	Estimate for optimal first step length	275
10.2.5.	Minimum bound for peak shear strain due to patch length	276
10.2.6.	Minimum bound for peak shear strain due to stiffness of first step	277
10.2.7.	Numerical examples	277
10.2.8.	Discussion	280
10.3.	FE analysis for adhesive stress and plate stress concentration	281
10.3.1.	Configuration and finite element analysis method	281
10.3.2.	Results for no-fillet case	283
10.3.3.	Results for fillet case	283
10.3.4.	Discussion of results	283
10.4.	Gradientless FE method for optimal through-thickness shaping	285
10.4.1.	Optimal adherend taper profile at the end of a bonded joint	286
10.5.	Sensitivity FE method for optimal joint through-thickness shaping	288
10.5.1.	Initial geometry, materials and loading arrangement	289
10.5.2.	Optimisation method	289
10.5.3.	Analysis for symmetric crack repair with aluminium patch	292
10.5.4.	Analysis for non-symmetric crack repair with boron/epoxy patch	294
10.6.	Optimal through-thickness shaping for F/A-18 bulkhead reinforcement	297
10.6.1.	Initial geometry, materials and loading arrangement	297
10.6.2.	Parameters for reinforcement optimisation analyses	298
10.6.3.	Stress results for optimal reinforcement designs	300

10.6.4.	Discussion	300
10.7.	Optimisation for F/A-18 aileron hinge reinforcement	300
10.7.1.	Initial geometry, materials and loading arrangement	303
10.7.2.	Shape optimisation before reinforcement	303
10.7.3.	Iterative reinforcement design	305
10.7.4.	Discussion	308
10.8.	In-plane shaping effects	308
10.8.1.	Geometry, loading and modelling considerations	308
10.8.2.	Determination of K_I from FEA output	309
10.8.3.	Uniaxial loading and patches with aspect ratios of 2:1	310
10.8.4.	Uniaxial loading and other patch aspect ratios	310
10.8.5.	Analogy with hole-in-a-plate problem.	311
10.8.6.	Stress reduction at the centre of the patch for uniaxially loaded plate	312
10.8.7.	Summary of results and discussion	312
10.9.	Conclusions	313
	References	314
Chapter 11.	Thermal Stress Analysis	317
	R.J. Callinan	
11.1.	Introduction	317
11.2.	Analytical expression for initial stresses in a circular plate due to heating	318
11.2.1.	Comparison of F.E. and analytic results	324
11.2.2.	Orthotropic solution	328
11.2.3.	Thermal stresses in a one-dimensional strip	330
11.2.4.	Peel stresses	332
11.2.5.	Coefficients of thermal expansion of a laminate	333
11.3.	Finite element thermal stress analysis	335
11.3.1.	Two-dimensional strip joints	337
11.3.2.	Three-dimensional strip joints	339
11.4.	Application of analysis to large repairs of aircraft wings	341
11.4.1.	F.E. analysis	343
11.4.2.	Edge restraint factor	346
11.5.	Conclusions	349
	References	350
11.6.	Acknowledgment	350
	Appendix	351
Chapter 12.	Fatigue Crack Growth Analysis of Repaired Structures	353
	C.H. Wang	
12.1.	Introduction	353
12.2.	Crack-closure analysis of repaired cracks	354
12.2.1.	Small-scale yielding	354
12.2.2.	Large-scale yielding solution for a stationary crack	357
12.2.3.	Plasticity induced crack closure under large-scale yielding solutions	361
12.3.	Overload effect and validation using finite element method	361
12.4.	Thermal residual stresses and comparison with experimental results	365
12.4.1.	Thermal residual stresses	365
12.4.2.	Experimental results under spectrum loading	367
12.5.	Conclusions	372
	References	373

Chapter 13. Boron/epoxy Patching Efficiency Studies	375
A.A. Baker	
13.1. Introduction	375
13.2. Stress intensity analysis of patched cracks	376
13.2.1. Model for estimating stress intensity	376
13.2.2. Use of model to estimate crack growth	378
13.2.3. Extension of the model for growth of disbond damage	379
13.3. Experimental approach	379
13.4. Fatigue studies	381
13.4.1. Disbond damage in the patch system	381
13.4.2. Influence of stress range	383
13.4.3. Influence of patch thickness	384
13.4.4. Influence of R ratio	384
13.4.5. Influence of temperature	386
13.4.6. Influence of panel thickness variation	387
13.4.7. Residual strength of patched panels	389
13.5. An approach to b/ep patch design	392
13.5.1. Cyclic loading	392
13.5.2. Spectrum loading	394
13.5.3. Check on residual strength	396
References	396
Chapter 14. Glare Patching Efficiency Studies	399
R. Fredell and C. Guijt	
14.1. Introduction	399
14.1.1. Overview and background of fibre metal laminates	399
14.2. Parametric studies of various patch materials	400
14.3. Experimental results	408
14.4. Discussion	410
14.5. Summary and conclusions	412
References	413
Chapter 15. Graphite/epoxy Patching Efficiency Studies	415
P. Poole	
15.1. Introduction	415
15.2. Repair of thin skin components	416
15.3. Repair of thick sections	418
15.4. Graphite/epoxy versus boron/epoxy	424
15.5. Effect of bondline defects	427
15.6. Effect of impact damage	433
15.7. Effect of service temperature	435
15.8. Effect of exposure to hot-wet environments	436
15.9. Repair of battle damage	438
15.10. Future work	440
15.11. Acknowledgements	440
References	441
Chapter 16. Repair of Multi-site Damage	443
R. Jones and L. Molent	
16.1. Introduction	443
16.2. Specimen and loading	444

16.2.1.	Boeing lap joints	444
16.2.2.	Airbus lap joints	449
16.3.	Repairs	450
16.3.1.	Repair philosophy	451
16.3.2.	Repair details	452
16.4.	Stress analyses	453
16.4.1.	Thermo-elastic analysis	453
16.4.2.	Finite element analyses	456
16.5.	Specimen fatigue test results	459
16.5.1.	Unreinforced baseline fuselage lap joint specimens	459
16.5.2.	Reinforced baseline fuselage lap joint specimens	464
16.5.3.	Environmental evaluation of repairs	464
16.5.4.	Hot/wet	465
16.5.5.	NaCl aqueous	466
16.6.	Damage tolerant evaluation of specimens	468
16.6.1.	Adhesive disbonds	468
16.6.2.	Impact damage	469
16.6.3.	Tension testing	472
16.7.	Full scale repair demonstrators	474
16.7.1.	Airbus A330/A340 fatigue test article	474
16.7.2.	Boeing 727, 747 and 767 in-flight demonstrators	477
16.7.3.	Doubler inspections	479
16.7.4.	Demonstrator summary	480
16.8.	Conclusions	480
	References	482
Chapter 17.	Damage Tolerance Assessment of Bonded Composite Doubler Repairs for Commercial Aircraft Applications	485
	D. Roach	
17.1.	Introduction	485
17.1.1.	Damage tolerance and fracture control plan	486
17.1.2.	Damage tolerance establishes fracture control plan	488
17.2.	Composite doubler damage tolerance tests	491
17.3.	Conformity inspection and FAA oversight	492
17.4.	Test results	500
17.4.1.	Fatigue tests	500
17.4.2.	Strain field measurements	506
17.5.	Conclusions	514
	References	515
Chapter 18.	Validation of Stress Intensity Estimations in Patched Panels	517
	B. Aktepe and A.A. Baker	
18.1.	Introduction	517
18.2.	The K -gauge	518
18.2.1.	K -gauge equations	518
18.3.	Theory of K_I measurement using strain gauges	519
18.3.1.	Westergaard equations	519
18.3.2.	Rose's inclusion model for stress intensity	521
18.3.3.	Wang's crack-bridging model	521
18.4.	Experimental procedure	522
18.5.	Strain surveys	524
18.5.1.	Unpatched specimen	524

18.5.2. Patched specimen	525
18.6. Crack length	526
18.7. Time-dependent behaviour	527
18.8. Conclusions	529
18.9. Nomenclature	529
References	530

Volume 2

Chapter 19. Bonded Repair of Acoustic Fatigue Cracking 531

R.J. Callinan and S.C. Galea

19.1. Introduction	531
19.2. Cracking history	533
19.2.1. Inlet nacelle	533
19.2.2. Aft fuselage cracking	536
19.3. Sound pressure levels	536
19.3.1. Inlet nacelle	536
19.3.2. Aft fuselage	536
19.3.3. Power spectral density	537
19.4. Random response analysis	537
19.5. Stress intensity factors	538
19.6. FEA of cracked nacelle inlet	539
19.6.1. Crack growth study	540
19.6.2. Summary of repair failure investigation	546
19.7. Highly damped repairs for cracked panels	546
19.7.1. Design of highly damped patch	547
19.7.2. Damping of highly damped patch	547
19.7.3. Analysis of repaired cracked plate	551
19.7.4. Results and discussion	551
19.8. Aft fuselage finite element model	557
19.8.1. Modes and frequencies	558
19.8.2. Acoustic fatigue crack growth data	559
19.8.3. Residual thermal stresses	560
19.8.4. Damping data	561
19.8.5. Adhesive data	561
19.9. Thermal environment for F/A-18	562
19.10. Analytical results	563
19.11. Experimental work	566
19.12. Conclusions for aft fuselage repair	568
References	568

Chapter 20. Smart Patch Systems 571

S.C. Galea

20.1. Introduction	571
20.2. Smart patch approach	573
20.3. Damage detection studies	578
20.3.1. Load transfer (strain) technique	578
20.3.2. Residual strain technique	588
20.3.3. Electro-mechanical impedance, transfer function and stress wave technique	593
20.3.4. Adhesive bond degradation sensors – active sensing technique	597
20.4. Laboratory smart patch conceptional demonstrators	599

20.5.	In-flight demonstrator	604
20.5.1.	Finite element analysis – damage sensing technique	604
20.5.2.	Health monitoring systems	607
20.6.	Conclusions	611
	References	612
Chapter 21.	Adhesively Bonded Repairs: Meeting the Safety Requirements Implied within Existing Aviation Industry Certification Regulations D. Bond	615
21.1.	Introduction	615
21.2.	Certification of an adhesively bonded repair	617
21.2.1.	The need to certify a repair	617
21.2.2.	Adhesively bonded repairs	617
21.2.3.	Regulatory deficiencies	618
21.3.	Repair design information	619
21.3.1.	Existing requirements	619
21.3.2.	Additional guidance	621
21.4.	Analysis and development testing	621
21.4.1.	Design allowables	621
21.4.2.	Static analysis	626
21.4.3.	Fatigue and damage tolerance analysis	630
21.4.4.	Development testing	635
21.5.	Full scale testing	637
21.5.1.	Existing requirements	637
21.6.	In-service management and inspection	637
21.6.1.	Existing requirements	637
21.6.2.	Additional guidance	637
21.7.	Future approaches to bonded repair certification	638
21.8.	Conclusions	638
	References	639
Chapter 22.	Certification Issues for Critical Repairs A.A. Baker	643
22.1.	Current limitations of crack patching	643
22.2.	Justifying credit for patching efficiency – fatigue concerns	644
22.2.1.	Influence of fatigue on patching efficiency	645
22.2.2.	Obtaining patch system fatigue allowables	646
22.2.3.	Validation of patching analysis	648
22.3.	Justifying credit for patching efficiency – environmental durability concerns	648
22.3.1.	Assurance of patch system environmental durability	650
22.3.2.	Australian experience on service durability	653
22.4.	Justifying credit for patching efficiency – the Smart Patch approach	654
22.5.	Discussion	655
22.6.	Conclusions	656
	References	656
Chapter 23.	Nondestructive Evaluation and Quality Control for Bonded Composite Repair of Metallic Aircraft Structures D.P. Roach and C.M. Scala	659
23.1.	Introduction	659
23.1.1.	NDI needs and damage tolerance	660

23.1.2.	NDI assessments	663
23.2.	Inspection for delaminations, disbonds and adhesion failure	664
23.2.1.	Pulse-echo ultrasonics	665
23.2.2.	Through-transmission ultrasonics	679
23.2.3.	Guided waves	680
23.2.4.	Resonance test inspection method	683
23.2.5.	Thermography	685
23.2.6.	Other techniques	689
23.3.	Inspections for cracks in parent material beneath composite doublers	694
23.3.1.	Eddy-current inspections	694
23.3.2.	X-radiographic inspections	701
23.3.3.	Challenges in crack monitoring	703
23.4.	Quality control issues in service	714
23.4.1.	Quality assurance	714
23.4.2.	Use of realistic calibration standards	715
23.5.	Conclusions	719
23.6.	Acknowledgements	723
	References	724
Chapter 24.	Practical Application Technology for Adhesive Bonded Repairs	727
	M. Davis	
24.1.	Introduction	727
24.1.1.	Management of repair technology	730
24.2.	Repair application technology	730
24.2.1.	Materials selection	731
24.2.2.	Surface preparation	732
24.2.3.	Heating procedures for on-aircraft repairs	742
24.2.4.	Repair pressurisation	748
24.3.	Occupational health and safety (OHS)	750
24.3.1.	Solvents	751
24.3.2.	Grit	752
24.3.3.	Fibres	752
24.3.4.	Risks to aircraft	752
24.4.	Quality management	752
24.5.	Facilities	754
24.6.	Training and certification	755
24.7.	Deficient repair concepts	755
24.8.	Conclusion	757
	References	757
Chapter 25.	Rapid Application Technology: Aircraft Battle Damage Repairs	761
	R. Bartholomeusz, P. Pearce and R. Vodicka	
25.1.	Introduction	761
25.2.	Aircraft battle damage repair	762
25.2.1.	Battle damage	762
25.2.2.	ABDR criteria	763
25.2.3.	Types of ABDR	764
25.3.	Comparison of metallic mechanically fastened repairs to bonded composite repairs for ABDR	765
25.3.1.	Adaptation of bonded composite repairs for battle damage	766
25.3.2.	The composite laminating resin and adhesive	766
25.3.3.	Fibre	767

25.3.4.	Simplified design methods for ABDR	767
25.3.5.	Surface treatment	768
25.3.6.	Forming the bonded composite patch	768
25.3.7.	Mechanically fastened, metallic repair	769
25.3.8.	Fatigue and static testing of specimens	769
25.3.9.	Comparison of test results	769
25.4.	Development of a bonded composite ABDR system	771
25.4.1.	Resin development	772
25.4.2.	Repair durability, strength and surface treatment	773
25.4.3.	Mechanical properties	774
25.5.	Application of the DSTO/ABDR system	776
25.5.1.	Resin measurement, mixing and dispensing	776
25.5.2.	Pre-bonding surface treatment procedures	777
25.5.3.	Repair consolidation and application	777
25.5.4.	Heating procedures	777
25.5.5.	Vacuum moulding tool	778
25.6.	Conclusions	779
	References	779
Chapter 26.	Standardized Training and Certification for Bonded Repair Specialists	783
	Marty A. Smith	
26.1.	Introduction	783
26.1.1.	Benefits of improved training and process control – an example	783
26.2.	The task at hand – a uniform approach	784
26.2.1.	Advantages of standardization	784
26.2.2.	Building a database of reliable repairs – “We’re all in this together”	785
26.3.	Current approaches to training and certification	785
26.4.	Formalized trade structure	786
26.4.1.	The purpose of a trade structure	786
26.4.2.	A four-tiered trade structure – the ARTI model	786
26.5.	The ARTI model for training of bonded repair specialists	787
26.6.	Certification of bonded repair specialists	791
26.6.1.	The Boeing wedge test (BWT) – an accepted standard	791
26.6.2.	Administration of certification tests	793
26.7.	Conclusion	795
	References	795
Chapter 27.	Case History: F-111 Lower Wing Skin Repair Substantiation	797
	K.F. Walker and L.R.F. Rose	
27.1.	Introduction	797
27.2.	Crack location and residual strength	798
27.3.	Repair substantiation requirements	800
27.3.1.	Design load cases	800
27.3.2.	Fatigue loading	801
27.4.	Validation strategy	801
27.5.	Design validation (finite element analysis)	802
27.5.1.	Uncracked, unpatched wing model	802
27.6.	Cracked, patched model including thermal effects	803
27.7.	Repair substantiation (representative specimen testing)	805
27.7.1.	Representative bonded joints	805

27.7.2. Panel specimens	807
27.8. Box specimens	809
27.9. Repair history	809
27.10. Conclusion	811
References	811
 Chapter 28. Case History: Composite Doubler Installation on an L-1011 Commercial Aircraft	 813
D. Roach	
28.1. Introduction	813
28.2. Fuselage door surround structure tests	814
28.2.1. Full-scale structural testing philosophy	814
28.2.2. L-1011 fuselage structure	815
28.2.3. Repair of fuselage test article with a composite doubler	815
28.2.4. Biaxial test facility description	817
28.3. Fuselage door surround structure test results	819
28.3.1. Structural tests before composite doubler installation	819
28.3.2. Structural tests after composite doubler installation	820
28.3.4. Validation of finite element model analytical results	825
28.3.5. Nondestructive inspection	826
28.4. Component level tests: door corner specimen	826
28.4.1. Door corner test overview	826
28.4.2. Subsize door corner test results	828
28.5. L-1011 composite doubler installation	832
28.5.1. Composite doubler repair of L-1011 aircraft passenger door	832
28.5.2. Non-destructive inspection of door surround structure and composite doubler	836
28.5.3. Inspection intervals for L-1011 aircraft	839
28.5.4. Quality assurance measures	839
28.6. FAA and industry approvals	840
28.7. Conclusions	841
References	842
 Chapter 29. Case History: F-111 Wing Pivot Fitting Reinforcement	 845
R. Chester	
29.1. Introduction	845
29.2. Reinforcement design	846
29.3. Selection and evaluation of materials	849
29.4. Selection and evaluation of the reinforcement	850
29.4.1. Mechanical test evaluation	851
29.4.2. Cure characterisation and formability studies	851
29.4.3. Selection and evaluation of candidate adhesives	852
29.4.4. Selection and evaluation of surface treatment procedures	853
29.4.5. Modifications to doubler system	853
29.4.6. Residual stress minimisation	853
29.5. Doubler application technology	854
29.5.1. Temperature	854
29.5.2. Pressure	854
29.6. Doubler fitment	855
29.7. Fitment to fleet aircraft	856
29.8. Conclusions	857
References	858

Chapter 30. Case History: Bonded Composite Reinforcement of the F/A-18 Y470.5 Centre Fuselage Bulkhead	859
R.A. Bartholomeusz and A. Searl	
30.1. Introduction	859
30.1.1. Background	860
30.2. FE analysis of bulkhead and reinforcement	860
30.2.1. Results of the bulkhead FE analysis	862
30.2.2. Measurement of adhesive through-thickness stresses	862
30.3. FE design of representative specimen (curved beam specimen)	864
30.4. Experimental test program	864
30.4.1. Static testing of curved beam specimen	864
30.4.2. Durability testing of the curved beam specimen	865
30.4.3. Residual strength after fatigue	866
30.5. Trial installation of reinforcement to full-scale fatigue test article	866
30.6. Discussion	867
30.6.1. Pre ECP reinforcement	867
30.6.2. Post ECP reinforcement	868
30.7. Conclusions	869
30.8. Acknowledgments	869
References	869
Chapter 31. C-5A Fuselage Crown Cracking	871
C. Guijt and S. Verhoeven	
31.1. Introduction	871
31.2. Damage tolerance analysis	872
31.3. Repair options	874
31.4. Design of the bonded repair	875
31.5. FEM model of the patched crack	879
31.6. Conclusions	883
References	884
Chapter 32. Case History: F-16 Fuel Vent-hole Repairs	885
C. Guijt and J. Mazza	
32.1. Introduction	885
32.2. Damage tolerance analysis	885
32.3. Repair options	887
32.3.1. Mechanically fastened aluminum patch	888
32.4. Design of the bonded repair	889
32.4.1. Operating temperatures	890
32.4.2. Maximum operating temperature	890
32.4.3. Cumulative temperatures	891
32.5. Testing	892
32.5.1. Fatigue analysis of the aluminum doubler	892
32.6. Bonded repairs	892
32.6.1. Repair installation procedures	894
32.7. Conclusions	895
References	895
Chapter 33. Reinforcement of the F/A-18 Inboard Aileron Hinge	897
R. Chester	
33.1. Introduction	897

33.2.	Load cases	898
33.3.	Design and stress analysis	899
33.4.	Static testing and repair validation	903
33.5.	Certification and implementation to aircraft	905
33.6.	Conclusions	906
	References	906
Chapter 34.	UK Applications	907
	P. Poole	
34.1.	Introduction	907
34.2.	Design studies	908
34.3.	Repairs to RAF aircraft	909
	34.3.1. Secondary structure repairs	909
	34.3.2. Primary structure repairs	911
	34.3.3. Birdstrike protection	912
34.4.	Repairs to EH101 development airframe full scale fatigue test specimen	913
34.5.	Acknowledgements	918
	References	918
Chapter 35.	Case History: Repair Applications On DC-10/MD-11 Aircraft	919
	D. Roach	
35.1.	Introduction	919
35.2.	Repair development and validation tasks to support on-aircraft installation	921
	35.2.1. Repair design	921
35.3.	Repair analysis	921
35.4.	Repair design validation	926
35.5.	Nondestructive inspection	933
35.6.	Current status of DC-10/MD-11 commercial aircraft repairs	934
Chapter 36.	Case History: CF-116 Upper Wing Skin Fatigue Enhancement Boron Doubler	937
	D. Raizenne	
36.1.	Introduction	937
36.2.	Background	937
	36.2.1. Compression induced fatigue cracking	939
36.3.	Repair considerations	940
36.4.	Bonded composite doublers	941
36.5.	Doubler design and analysis	941
36.6.	Doubler manufacturing and installation procedures	946
	36.6.1. Doubler qualification testing	947
36.7.	Doubler fractographic analysis	949
36.8.	Fleet experience	951
36.9.	Discussion	954
36.10.	Conclusions	954
36.11.	Composite repair lessons learned	955
36.12.	Acknowledgements	956
	References	956
	Appendix A	957
	Material properties	957

Chapter 37. In-service Durability of Bonded Composite Repairs – Commercial Demonstrator Programs	959
R.A. Bartholomeusz and R.C. Geddes	
37.1. Introduction	959
37.2. Demonstrator doublers	960
37.2.1. QANTAS demonstrator program	960
37.2.2. Ansett keel beam reinforcement	962
37.3. In-service environment and repair location	962
37.3.1. Temperature	962
37.3.2. Foreign object damage.	963
37.3.3. Airflow and erosion	964
37.3.4. Aircraft fuels, hydraulics and lubricants	964
37.3.5. Miscellaneous	964
37.4. Bond durability and surface treatment	964
37.5. Case study results	965
37.5.1. QANTAS program	965
37.5.2. Ansett keel beam demonstrator reinforcement	968
37.6. Discussion and lessons learnt	970
37.6.1. Erosion protection by the use of shields	971
37.6.2. Repair location and design	971
37.6.3. Applicability of demonstrator programs	971
37.7. Conclusions	972
References	972
 Chapter 38. Case History: Bonded Composite Repair of A CH-47 Cargo Hook Beam	 973
B.J. Harkless, A.P. Kerr and M.A. Shupick	
38.1. Introduction	973
38.2. Defect description	973
38.3. Justification of approach	974
38.3.1. Loads analysis	975
38.3.2. Design loads	975
38.3.3. Static strength analysis	975
38.3.4. Fatigue analysis	977
38.3.5. Proof testing	977
38.4. Patch system and environmental protection	978
38.5. Repair procedure	978
38.6. Continuing airworthiness/inspection	979
References	979
 Chapter 39. Case History: Application of Bonded Repair Technology to Large Areas	 983
B. Harkless and A. Kerr	
39.1. Background	983
39.2. Examples of applicability to large areas	984
39.2.1. Full length rotor blade doublers	984
39.2.2. Large scale wing reinforcement	984
39.2.3. Large scale fuselage reinforcement	894
39.3. Current state of the technology	985
39.3.1. Critical features of the bonding process	985
39.3.2. Grit blast/silane process steps	986

39.4.	Process areas requiring adaptation	987
39.4.1.	Solvent scrubbing step	987
39.4.2.	Grit blast step	988
39.4.3.	Heating methods	988
39.5.	Large area repairs in a production environment	989
39.6.	Conclusions	994
	References	995
Chapter 40.	Case History: Composite Patch Reinforcement of T-38 Lower Wing Skin	997
	M.M. Ratwani, J. Helbling, B. Heimerdinger and N.M. Ratwani	
40.1.	Introduction	997
40.2.	Validation testing	999
40.2.1.	Test specimen description	999
40.2.2.	Composite reinforcement fabrication and bonding	1000
40.2.3.	Strain gage installation	1000
40.2.4.	Test spectrum and equipment	1001
40.3.	Test results	1001
40.3.1.	Strain gage results	1001
40.3.2.	Crack growth results	1003
40.4.	Comparison between test results and analytical predictions	1005
40.5.	Application of composite reinforcement to a full scale wing test	1007
40.6.	Conclusions	1007
	References	1008
Chapter 41.	Case History: Advanced Composite Repairs of USAF C-141 and C-130 Aircraft	1009
	W.H. Schweinberg and J.W. Fiebig	
41.1.	Background	1009
41.2.	Repair design	1012
41.3.	Installation development	1016
41.4.	Industrialization and repair	1014
41.5.	Success and failures	1017
41.6.	Other applications	1020
41.7.	Cost savings	1024
41.8.	Additional research	1025
41.9.	Lessons learned	1029
41.10.	Summary	1032
	References	1032
Chapter 42.	Case History: Bonded Composite Reinforcement of Ship Structures	1035
	I. Grabovac	
42.1.	Introduction	1035
42.2.	Materials development and characterisation	1038
42.3.	Installation of composite reinforcement	1042
42.4.	Reinforcement efficiency assessment	1044
42.5.	Service performance	1046
42.6.	Technology improvement	1047
42.7.	The current status – year 2000	1048
42.8.	Conclusion	1048

42.9.	Acknowledgement	1049
	References	1049
	Index	1051

Chapter 19

BONDED REPAIR OF ACOUSTIC FATIGUE CRACKING

R.J. CALLINAN and S.C. GALEA

Defence Science and Technology Organisation, Air Vehicles Division, Fishermans Bend, Victoria, 3207, Australia

19.1. Introduction

Acoustic fatigue is due to a very high intensity excitation as a result of pressure waves caused by either engine or aerodynamic effects. Acoustically-induced cracking has occurred on the external surface of the lower nacelle and aft fuselage skins on the F/A-18, as illustrated in Figure 19.1. In the former region, overall sound pressure levels greater than 170 dB have been measured in flight [1]. These high sound pressure levels appear to be a result of an aerodynamic disturbance at the inlet lip [1]. Typical cracks occur along a line of rivets or run parallel to the rivet line and may turn into the centre of the panel, as shown in Figure 19.1. Cracking generally occurs along the longer side of the panel where the bending stresses due to out-of-plane vibrations are a maximum. Up to a third of the F/A-18's in the RAAF fleet are affected by these cracks.

The standard repair for such cracking is to remove and replace the panel. The standard long term fix is to incorporate additional stiffeners on the inside to stiffen the panel. This has two effects; firstly to reduce the panels response, i.e. lower stress for a given load and secondly it increases the resonant frequencies of the panel to frequencies well outside the recorded excitation frequencies.

In order to reduce the cost of repairing such cracked structures a bonded composite repair would be preferred. The benefits of such a repair are reflected in the time required to carry out the repair. For example, the inlet nacelle repair typically requires a repair time of 60 h for the mechanical repair and approximately 15–25 h for the bonded repair. In the case of the repair to the aft fuselage the time for the mechanical repair is 15–30 h spread over three or four days. This repair also requires engine removal and installation which takes a three man team approximately 8 h followed by engine ground runs.

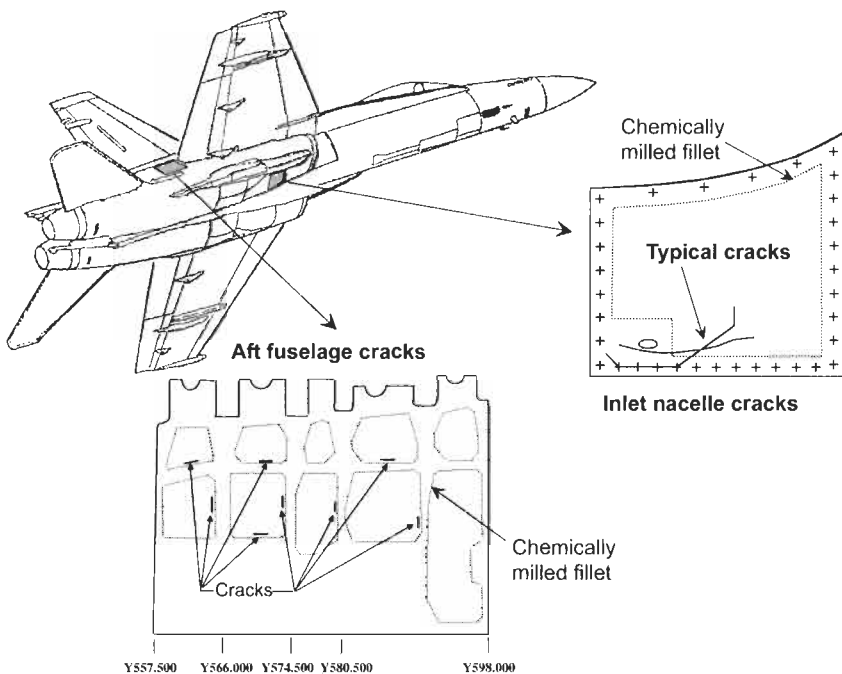


Fig. 19.1. Location of the cracking in the lower nacelle inlet and the aft fuselage skins. (Chemically milled fillets are indicated by dotted line.).

A bonded repair was designed for the inlet nacelle area, based on a standard repair design procedure, and implemented on an existing cracked aircraft. While in the past boron fibre/epoxy resin patches have been extremely successful, in repairing cracked metallic secondary and primary structures [2], (see also Chapters 13 and 16) in this case significant crack growth occurred after the application of the repair. This unsuccessful application of a bonded repair to a cracked metallic structure was due to the fact that the standard design procedure [3] is based on in-plane low cycle (quasi-static) loading condition (See Chapter 7). However for the acoustic environment a new design approach for bonded repairs is required, i.e. a design procedure based on dynamic out-of-plane high-cycle loading. Work carried out by [4,5] showed that the addition of damping to a bonded repair can result in significant reductions of crack growth. These authors showed that a low-damping patch covering the entire panel resulted in a reduction of the mode I stress intensity, K_I , from $18 \text{ MPa m}^{1/2}$, for a cracked unrepaired panel, to $6 \text{ MPa m}^{1/2}$. Although this is not a high value in comparison with the fracture toughness value, K_{IC} , in an environment of high-cycle fatigue it leads to a high crack growth rate. They found that by further increasing the damping of the repaired structure, from a loss factor of 0.032 to 0.128, reduced the stress intensity to $4 \text{ MPa m}^{1/2}$. Work carried out by [6,7] also indicates that the addition of damping can significantly reduce the crack growth rate.

This chapter firstly investigates the failure of the low damped boron/epoxy repair. Secondly the report details the design of a highly-damped bonded repair, incorporating constrained layered damping (CLD), using finite element analysis (FEA) of the structure subject to simulated acoustic loading conditions. CLD material incorporates a layer of visco-elastic material (VEM) with a constraining layer attached to the top of the VEM. The study involves the estimation of the root mean square (rms) stress intensity factor (K) in the cracked and cracked/repared cases. Various patch design parameters, such as reinforcing patch dimensions, thicknesses of the (viscoelastic) damping material and thickness of the constraining layer are considered in order to maximise the effectiveness of the patch and thus lower the stress intensity. Finally it is theoretically verified that the highly-damped patch can significantly reduce crack growth and therefore yield acceptable crack lengths for a 6000 h lifetime condition.

19.2. Cracking history

19.2.1. Inlet nacelle

As a result of the failure of the boron/epoxy repair to prevent crack growth, the particular panel was removed from the aircraft for replacement and assessment, [8], of the fracture surface. The inside surface of a section of the cracked panel is shown in Figure 19.2, and the missing section was that used for the examination. It was found that the crack had started on the inside of the thicker section, and developed as a semi-elliptical surface crack, as indicated in Figure 19.3, until it became deep enough to penetrate the thickness of the panel. The crack proceeded as a through crack, with crack fronts being inclined as shown in Figures 19.4 and 19.5 corresponding to a final crack length of 135 mm. The central region of the crack just before the boron/epoxy repair was applied is shown in Figure 19.6 and indicates rubbing of the crack faces due to transverse movement. This would

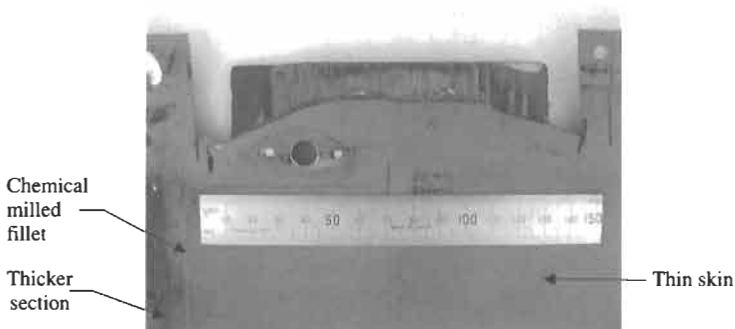


Fig. 19.2. Interior view of cracked panel with boron/epoxy repair [8].

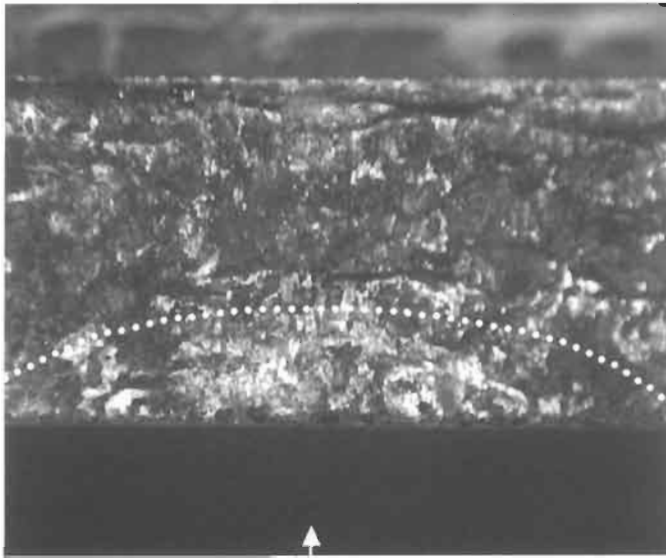


Fig. 19.3. The origin of the crack in the panel (arrowed). The remains of the semi-elliptical surface crack can be seen just below the dotted line. This crack was located on the inside surface of the thicker section of panel. Note the smooth rubbed character of the surface, indicating large relative motions between the two halves of the crack [8].

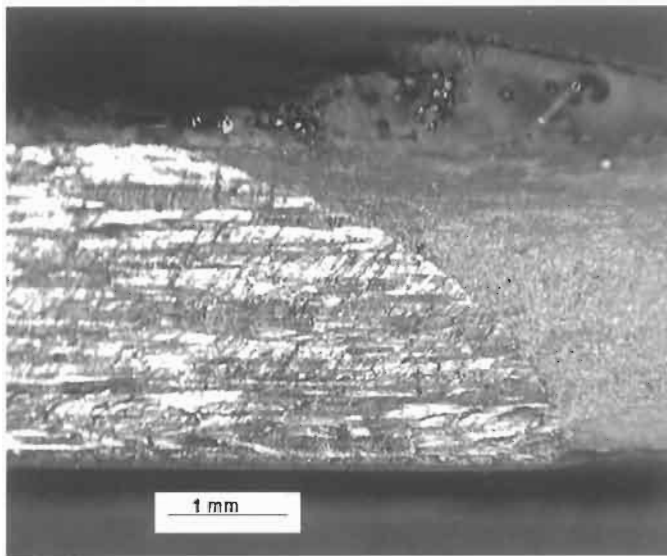


Fig. 19.4. View of the tip of the crack in the thick end of the panel. The fatigue crack surface is the bright faceted region to the left and the deliberately broken surface is the mottled grey area to the right. Note the shape of the crack, much longer along the inside surface of the panel, indicating that a degree of bending was involved in the development of the crack. Also note that the fatigue crack surface is bright and highly detailed, and does not appear to have been rubbing [8].

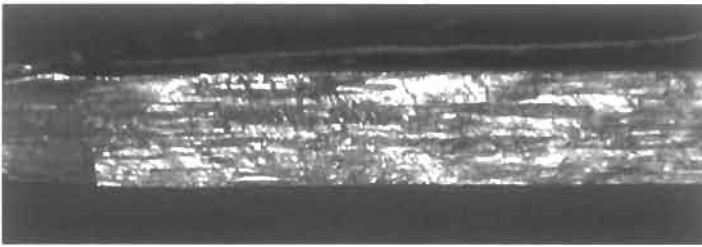


Fig. 19.5. View of the tip of the crack in the thinner part of the panel. The same comments as above for Fig. 19.4 apply here [8].

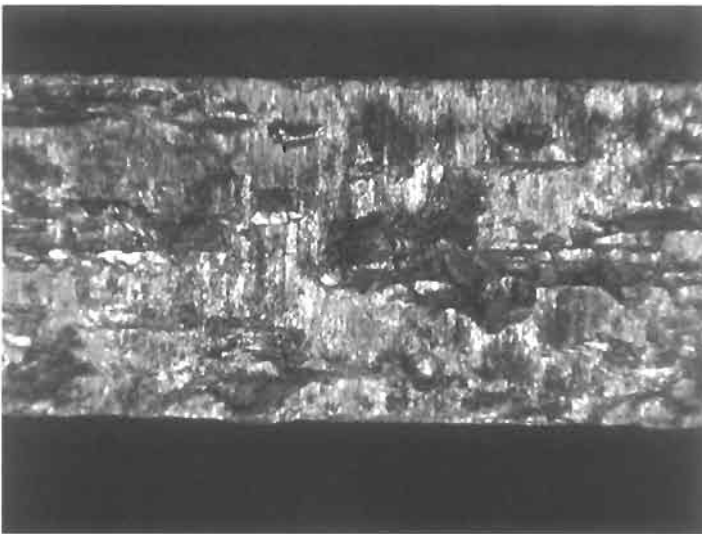


Fig. 19.6. View of the central area of the crack, showing the presence of pronounced rubbing [8].

correspond to a mode III crack tip driving force. However after the patch was applied a change in crack growth mode occurred. This is seen in Figures 19.4 and 19.5 where the crack is bright and highly detailed in comparison to that shown in Figure 19.6. After the repair the shape of the crack front indicates that bending was involved. This is consistent with a neutral axis offset caused by the bending of both the boron/epoxy and panel in which the maximum stress occurred in the inner surface of the panel.

Both the length of the crack tip after the repair and flight hours are known for the right hand crack tip shown in Figure 19.2, and is 2 mm/flight hour. While the crack growth rate before the repair is unknown it is thought to be considerably less than that after the repair. There is a possibility that before the repair, the rubbing of the crack faces provided some friction damping to the panel, this in turn led to a lower crack growth rate.

19.2.2. Aft fuselage cracking

The chemically milled steps for panels in the aft fuselage are shown dotted in Figure 19.1. Cracks occur in the chemically milled step region, and are generally parallel to the longest side and midway along the side. The aft fuselage section shown in Figure 19.1 contains a composite of all known cracking locations which occur between fuselage stations Y557.500 and Y598.000. The conventional repair involves removal of the crack and use of a metallic doubler attached by mechanical fasteners. To carry out this type of repair the engine needs to be removed.

19.3. Sound pressure levels

19.3.1. Inlet nacelle

One third octave sound pressure measurements have been made in flight [1], using microphones located at the nacelle inlet area, and are plotted in Figure 19.7. The spectrum level, relative to the overall sound pressure level (OASPL), is derived from this data and is also shown in Figure 19.7. In this case the higher than expected sound pressure levels (SPL) were caused by an aerodynamic disturbance at the inlet lip. At present no data exists for the calculation of SPL's in the aft fuselage.

This spectrum is now used as the excitation pressure on the inlet nacelle F.E. model.

19.3.2. Aft fuselage

Since the cracking on the inlet nacelle preceded that in the aft fuselage then it is conservative to assume the same PSD, as shown in Figure 19.7. This is greater than the design value of the OASPL of 160 dB for the airframe [1]. Premature acoustic fatigue cracking in the aft fuselage suggests that an additional aerodynamic

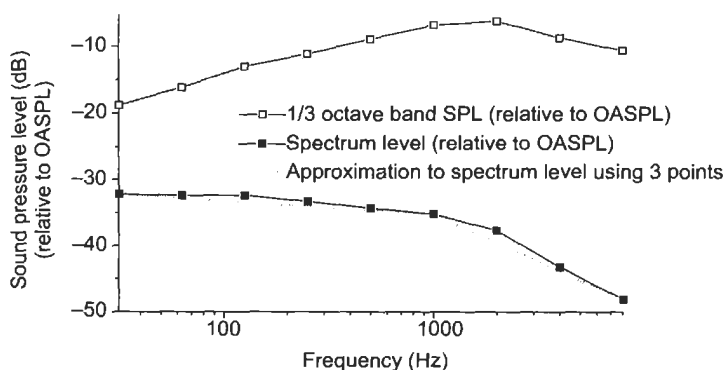


Fig. 19.7. Spectrum and one-third octave band levels of sound pressure over the external nacelle inlet, (where OASPL = 172.2 dB), [1].

Table 19.1
Power spectral density for inlet nacelle.

Frequency (Hz)	Three points for curve (dB)	Pressure spectrum level (dB)	$S_I(f)$ (MPa) ² /Hz
31.5	-32.2	140	4.0×10^{-8}
1000.0	-35.2	137	2.005×10^{-8}
8000.0	-48.1	124.1	1.028×10^{-9}

disturbance is responsible for the higher than expected SPL. The possibility exists that the flap may be responsible for this. In the case of the B52, [9], it was found that cracking in the aft fuselage skin was a result of the aerodynamic disturbance caused by the deflected flap position during take-off. However aerodynamic disturbances can also be caused by high angle of attack manoeuvres resulting in separation of airflow over the flap.

19.3.3. Power spectral density

The relationship between the spectrum SPL and the r.m.s. fluctuating pressure (p) is given in [10] as:

$$P_{\text{rms}} = 10^{(\text{SPL}/20 - 4.69897)}, \quad (19.1)$$

and the power spectral density (PSD) of acoustic pressure, i.e. PSD of the excitation, at any given frequency is given by:

$$\text{PSD} = p_{\text{rms}}^2 = 10^{(\text{SPL}/10 - 9.3979)} \quad (19.2)$$

The spectrum curve in Figure 19.7 has been approximated with the three points listed in Table 19.1.

19.4. Random response analysis

The random response analysis capability of the NASTRAN program has been used to solve this problem [11]. This involves a solution in the frequency domain after the transfer function, $H(\omega)$, is generated. Together with the PSD of the excitation, $S_I(\omega)$, the PSD of the response, $S_J(\omega)$, is determined:

$$S_J(\omega) = |H(\omega)|^2 S_I(\omega) \quad (19.3)$$

This analysis allows the statistical properties of the system to be evaluated. Random vibrations considered here involve all frequencies at any one instant in time. After calculating the PSD, the root mean square (r.m.s.) of the response can

be determined by computing the square root of the PSD area:

$$j_{\text{rms}} = \sqrt{\frac{1}{2\pi} \int_0^{\infty} S_j(\omega) d\omega} \quad (19.4)$$

A similar application of finite element techniques to undertake a PSD analysis to acoustic fatigue problems has been reviewed by [10]. The response of interest are the displacements near the crack tip from which stress intensity factors are computed. For the adhesive the quantities of concern are shear and peel stresses. These quantities are considered in Sections 19.5 and 19.9 respectively.

19.5. Stress intensity factors

In the F.E. model the depth of the plate is modelled using 20 noded brick elements, which allows the model to account for the bending behaviour of the skin. The skin thickness is approximately 1 mm, hence the condition of plane stress is assumed. The computation of the stress intensity factor may be determined directly from the crack tip element used around the crack tip or from displacements using a crack opening displacement (COD) formula. The rms crack tip stress intensity factors for mode I, II and III are derived from the standard asymptotic relations:

$$K_{\text{I rms}} = \frac{Eu_{\text{rms}}}{4} \sqrt{\frac{2\pi}{l}}, \quad (19.5)$$

$$K_{\text{II rms}} = \frac{Ev_{\text{rms}}}{4} \sqrt{\frac{2\pi}{l}}, \quad (19.6)$$

$$K_{\text{III rms}} = Gw_{\text{rms}} \sqrt{\frac{2\pi}{l}}, \quad (19.7)$$

where

E = Young's modulus,

G = Shear modulus

u_{rms} = mode I crack opening rms displacement (i.e. displacement out-of-plane of the crack)

v_{rms} = mode II crack opening rms displacement (i.e. displacement in-plane, parallel to the plane of the crack)

w_{rms} = mode III crack opening rms displacement (i.e. displacement in-plane, transverse to the plane of the crack)

l = length of the crack tip element

19.6. FEA of cracked nacelle inlet

In order to study the cracking mechanisms of the cracked and repaired/cracked nacelle skin cases, a simplified model has been developed in which the skin is considered to be a flat rectangle. However, to take account of all shear deformation the structure has been idealised as a fully 3D structure using 20 noded brick elements. The geometry of the structure is shown in Figure 19.8. The mesh size of the skin structure is 75×60 elements, while the patch and skin is 40×40 elements. As shown, the uni-directional patch only extends partially across the panel. It also covers an adjacent panel as shown in the dotted outline. Sufficient elements have been used to define the minimum crack length considered. Material properties for the skin, adhesive and boron are shown in Table 19.2. The Young's modulus of the composite in the 0° fibre direction is E_1 , and E_2 in the transverse direction. The main reason that 20 noded bricks were used in the skin is that calculations for K can be made corresponding to a bending field. Also, the behaviour of the adhesive has been modelled as a 3D element, to allow for shear deformation. A loss factor of 0.016 has been used [1].

The boundary conditions for this model are considered to be fully clamped except for the crack region which is not restrained. The patch above the crack also remains fully constrained. Clearly crack closure will occur at an increasing distance away from the crack tip, however the complexity in introducing such constraints has not been included in this preliminary study. The crack is initially 50 mm long with it's centre located within the patch. A number of crack lengths have been

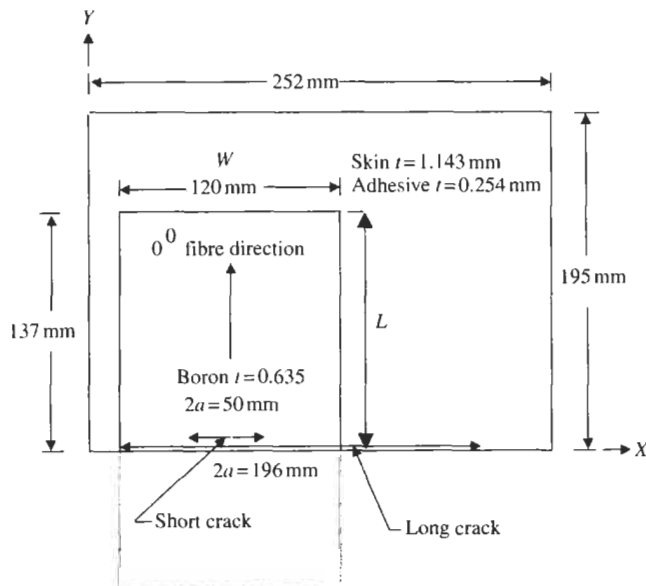


Fig. 19.8. Dimensions of simplified F/A-18 nacelle inlet panel, with crack and patch.

Table 19.2
Material properties used in the FEA.

Material	Young's modulus (MPa)	Ratio of Young's modulus (E_1/E_2)	Poisson's ratio (ν_{12})	Shear modulus (MPa)	Density ($\times 10^{-9}\text{Mg/mm}^3$)
Aluminium	71000.0	1.0	0.33	26691.0	2.77
Adhesive	2273.0	1.0	0.35	842.0	1.2
Boron	207000.0	10.89	0.21	4800.0	2.0
VEM (20 °C)	5700.0	1.0	0.30	2192.0	1.75

considered to simulate the crack growth. The crack is assumed to grow symmetrically until the left hand crack tip extends to the edge of the patch. At this point no more crack growth occurs due to the proximity of the panel boundary. The only growth that occurs is at the right hand crack tip. In this study the maximum crack length considered is 196 mm.

19.6.1. Crack growth study

Figure 19.9 illustrates the variation of natural frequencies with increasing crack length for the cracked un-repaired panel and also the cracked repaired panel for the first 3 resonant modes. In the case of the cracked un-repaired structure, increasing the crack length significantly reduces the resonant frequencies of the panel. Also as expected, repaired panels have little variation in natural frequencies with crack length. Furthermore, the repaired panels have substantially higher natural frequencies for all modes than the un-repaired panels. The results indicate that the boron repair has a definite influence on the panel stiffness.

Mode shapes have been computed for various crack lengths for the un-repaired and for the repaired panel and are presented in [4]. Results presented here are for

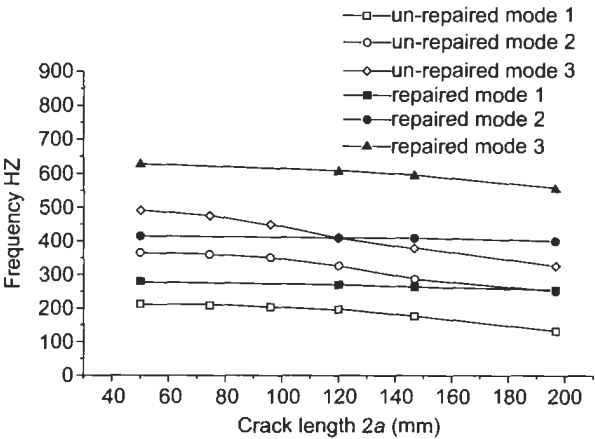


Fig. 19.9. Frequency versus crack length for un-repaired and repaired cases.

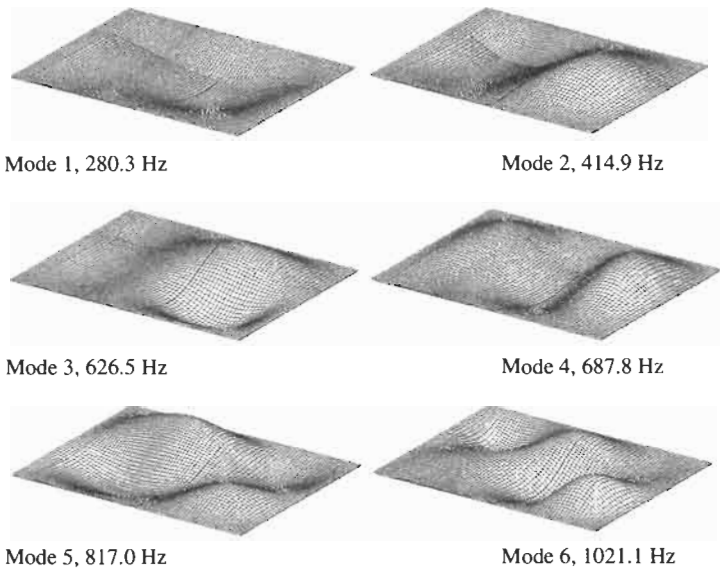


Fig. 19.10. Mode shapes for the repaired panel containing a short crack ($2a = 50$ mm).

short and long cracks for the un-repaired and repaired panel. The first six mode shapes for a repaired panel containing a short, 50 mm crack, are shown in Figure 19.10. Clearly the mode shapes in Figure 19.10 indicate that the crack tip behaviour is dominated by the mode I stress intensity factor K_I . Figure 19.11 shows

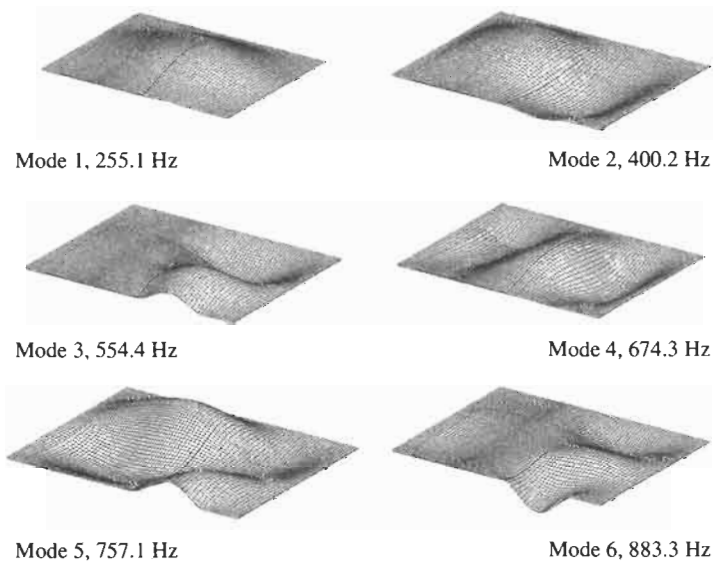


Fig. 19.11. Mode shapes for the repaired panel containing a long crack ($2a = 196$ mm).

the mode shapes of a repaired panel where the long, 196 mm, crack now extends outside the patch (see Figure 19.8). These mode shapes indicate that the unsupported crack tip behaviour will now have significant contributions from mode III stress intensity factor, K_{III} .

The modal analysis indicates that all the mode I, II and III stress intensity factors will be significant. The rms mode I stress intensity factor $(K_I)_{rms}$ for the cracked un-repaired panel is shown in Figure 19.12. As expected, the general response is an increase of $(K_I)_{rms}$ with crack length. The left hand crack tip is always closer to the clamped edge of the panel than the right hand crack tip, and since the bending stresses are a maximum midway along the boundary, the right hand tip gives the highest value of $(K_I)_{rms}$. The values of $(K_I)_{rms}$ in relation to the fracture toughness, are significant and explain crack growth. For crack growth, threshold values of $(K_I)_{rms}$ are shown in Figure 19.26.

In the repaired panel the neutral axis is offset and as a result $(K_I)_{rms}$ is evaluated at both inner and outer surfaces of the skin; the repair being applied to the outer surface. Being a one sided repair the repair is more effective on the outer surface which is more closely restrained [12]. These bending effects are clearly shown in Figure 19.13. The right hand crack results in the highest values for $(K_I)_{rms}$ located on the inner surface. These values of $(K_I)_{rms}$ are significantly high before the crack grows out from under the patch and explain continued crack growth. For a normal "static" repair in which the only significant events are manoeuvre and gust loads, the repair would be successful. However, in the acoustic excitation environment, the resonant frequency of the actual nacelle panel is of the order of 300–400 Hz thus causing the repair to be ineffective.

The rms mode II stress intensity factor, $(K_{II})_{rms}$ for the cracked un-repaired panel is shown in Figure 19.14. Little through thickness variation of $(K_{II})_{rms}$ has been found, hence only one value is presented for each crack tip. Numerical values are similar to $(K_I)_{rms}$ and the existence of $(K_{II})_{rms}$ explains the tendency of long cracks to turn into the centre of the panel. For the case of the repaired panel shown in

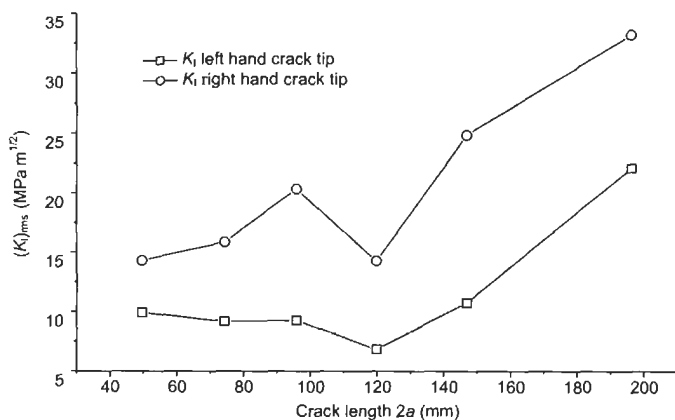


Fig. 19.12. Stress intensity factor $(K_I)_{rms}$ in un-repaired panel for left and right hand crack tips.

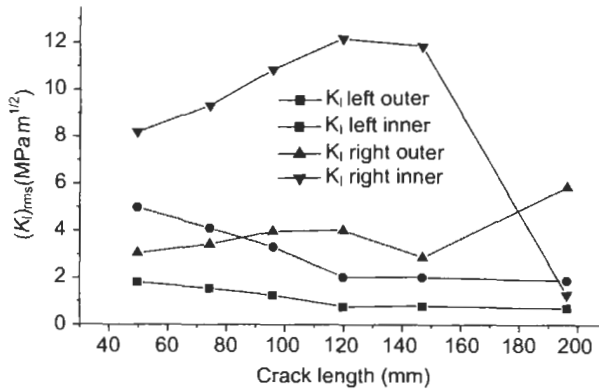


Fig. 19.13. Stress intensity factor $(K_I)_{rms}$ in repaired panel. (Note the change in scale compared to Fig. 19.12.)

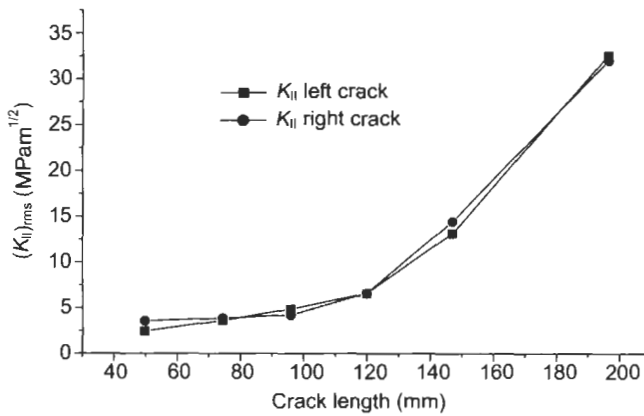


Fig. 19.14. Stress intensity factor $(K_{II})_{rms}$ for un-repaired panel.

Figure 19.15, $(K_{II})_{rms}$ has been substantially reduced. Note that when the right hand crack tip grows out from under the repair, the value for $(K_{II})_{rms}$ for the right hand outer crack tip exceeds the value for the right hand inner crack tip. This is due to the transverse bending of the higher order vibration modes that can only occur when the crack-length exceeds the width of the patch illustrated in Figure 19.11. Also it would be expected that the right hand inner and outer values would converge approaching the right hand boundary. The transverse bending is also shown by the values of $(K_{III})_{rms}$ in this region, Figure 19.17.

The rms of the mode III stress intensity factor $(K_{III})_{rms}$ for the cracked un-repaired panel is shown in Figure 19.16. The values of $(K_{III})_{rms}$ increase significantly with crack length for both left and right hand crack tips, and the

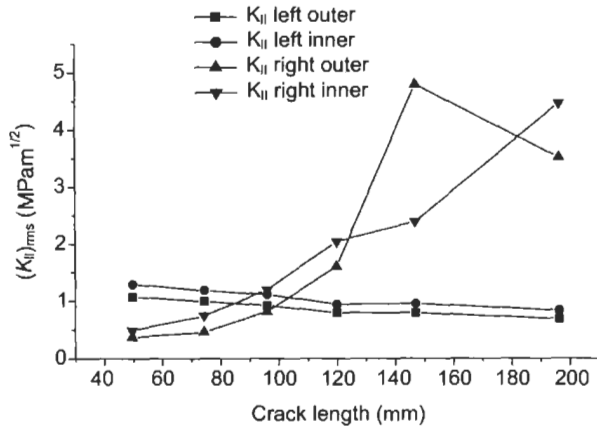


Fig. 19.15. Stress intensity factor $(K_{II})_{rms}$ for repaired panel.

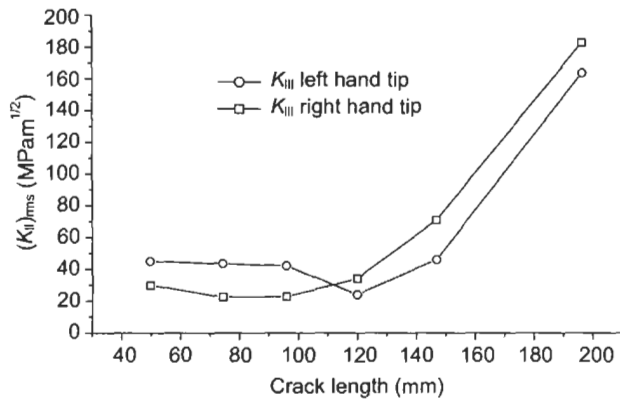


Fig. 19.16. Stress intensity factor $(K_{III})_{rms}$ for un-repaired panel.

numerical value of $(K_{III})_{rms}$ is greater than $(K_I)_{rms}$. Clearly $(K_{III})_{rms}$ will contribute significantly to crack growth. In the case of the repaired panel, shown in Figure 19.17, the values of $(K_{III})_{rms}$ for a crack tip under the patch are low, but not zero. However, once the crack grows outside the patch (i.e. for crack lengths > 120 mm) $(K_{III})_{rms}$ increases significantly.

The PSD of the displacement response, u , behind the right hand crack-tip is shown in Figure 19.18. Equation (19.3) implies that the u displacement behind the crack-tip is proportional to $(K_I)_{rms}$. Similarly the displacement response for w is proportional to $(K_{III})_{rms}$. Therefore the PSD shown in Figure 19.18 indicates the relative response of K with increasing frequency. Although not shown the PSD has been computed for the two different crack lengths for both un-repaired and repaired cases.

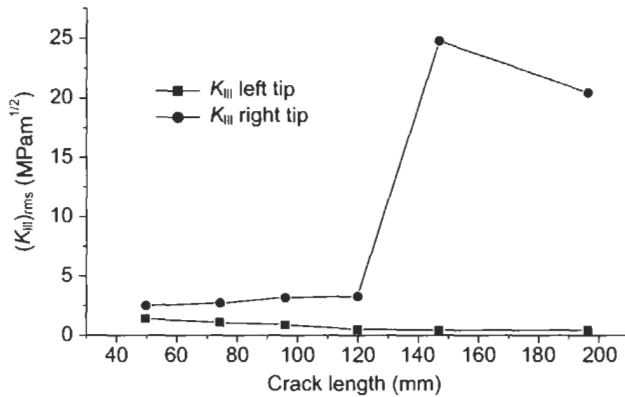


Fig. 19.17. Stress intensity factor $(K_{III})_{rms}$ for repaired panel. (Note change in scale compared to Fig. 19.16).

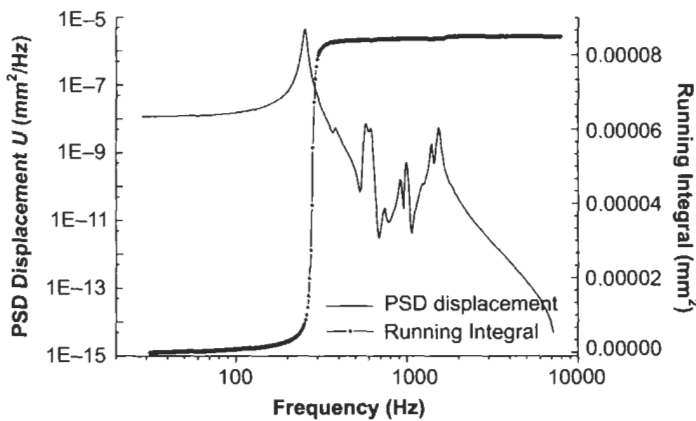


Fig. 19.18. PSD of displacement u ($\propto (K_I)_{rms}$) and running integral of the PSD for repaired panel of crack length $2a = 50$ mm.

Figure 19.18 shows the PSD for the case of a repaired panel with $2a = 50$ mm. In this case each peak will correspond to the resonant frequencies illustrated in Figure 19.10. For example the fundamental resonant mode occurs at a frequency of 280 Hz in Figure 19.10 which corresponds to the maximum response in Figure 19.18. Absence of peaks at certain resonances, e.g. Mode 2 at 414.5 Hz, indicates that the crack tip is located at or near the nodal line of the corresponding mode shape. A running integral of the PSD response will indicate the relative contribution of each of the modes to the overall K_{rms} and is also shown in Figure 19.18. This shows that 98% of the overall $(K_I)_{rms}$ is due to the first mode.

In all other cases, with one exception, mode 1 makes the major contribution to the overall $(K_I)_{rms}$ or $(K_{III})_{rms}$ response. The exception is shown in Figure 19.19 for

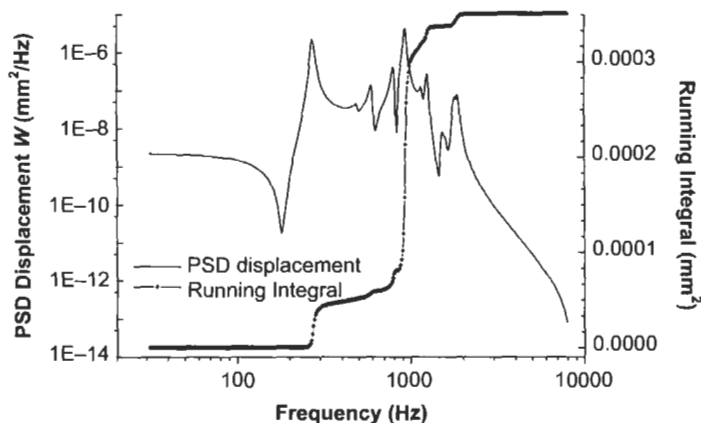


Fig. 19.19. PSD of displacement $w(\alpha(K_{III})_{rms})$ and running integral of the PSD for repaired panel of crack length $2a = 196$ mm.

a repaired panel with a crack length of 196 mm and shows that mode 6 makes the major contribution to the overall $(K_{III})_{rms}$ response.

19.6.2. Summary of repair failure investigation

The fractographic analysis has revealed that the cracks in the panel initiated at a single site on the inside surface of the thicker section. Also that before the panel was repaired the mode III stress intensity provided the crack tip driving force. However after the repair is applied, transverse displacement at the crack was eliminated, and resulted in a mode I stress intensity factor at the skin surface providing a majority of the crack tip driving force. Interestingly, the crack growth after the repair was significantly higher than before the repair. It is possible that the rubbing of the crack faces provided friction damping to the system, which did not occur under mode I. The analysis carried out has simulated and characterised the growth of the crack in both the cracked unrepaired and cracked repaired panel. It was found that a relatively high stress intensity factor still existed on the inner surface of the right hand crack tip after the repair was applied. This value was $12 \text{ MPa m}^{1/2}$ compared to a value of $35 \text{ MPa m}^{1/2}$ for the unrepaired panel. For an aircraft component subjected to manoeuvre and gust loads this reduction in stress intensity factor would have been adequate, however crack growth corresponding to a fundamental frequency of 300 Hz will be significant.

19.7. Highly damped repairs for cracked panels

The work carried out in this section is based on [5,15]. It is evident from the previous section that a change in direction is necessary to design an effective long

term solution for bonded composite repair systems subject to acoustic loading conditions.

19.7.1. Design of highly damped patch

The cracking surveys undertaken by [6] indicates that typical crack lengths, before repair, are 100 mm long and occur in a skin thickness of approximately 1 mm. The repair must restore the stiffness of the structure, with an equivalent amount of composite material, and also reduce the dynamic stress levels.

Since the repairs are on the external surface there is a requirement to preserve aerodynamic smoothness. Therefore patch development is undertaken with the restriction that the patch must be tapered and the thickness must not exceed approximately 3 mm (1/8"). This was considered, [6], to be an adequate thickness since such an intrusion would not be significant with respect to the boundary layer on the aft 80% of any surface. Also the possible crack growth for a 6000 h lifetime must be considered.

19.7.2. Damping of highly damped patch

One of the most effective mechanisms to substantially reduce the dynamic stress level in the repaired structure is to increase the damping performance of the repair and, therefore, of the repaired structure. Callinan, *et al.* [4,5], Rogers, *et al.* [6] and Liguour [7] reported on the use of a highly-damped composite patch (or "Durability Patch"), i.e. composite repairs that incorporate VEM, to prevent the further growth of costly "nuisance" cracks. This is a passive damping technique aimed at reducing high-cycle fatigue. Rogers, *et al.* [6] noted that the general application of passive damping techniques which involve using VEM were rarely used for high-cycle fatigue environments because the necessary design information such as operating temperatures, resonant frequencies, and strain levels were difficult to obtain. They further reported that aircraft structures are often susceptible to resonant high-cycle fatigue due to the low intrinsic damping of the material since rms stress levels are highly dependant on modal damping. Thus in order to increase damping the authors considered the use of constrained layer damping (CLD), incorporated in the patch, which increases the structural damping of the repaired structure and will assist in stopping or substantially reducing acoustically-induced crack growth in the panel. CLD consists of a layer of VEM attached to the structure with a constraining layer attached to the top of the VEM.

There are numerous case studies, noted by [13], of the use of damping in the aeronautical scene to alleviate problems associated with resonant vibrations. In this section the modal loss factor of a reinforced panel is calculated for various bonded doubler reinforcement geometries, add-on damping treatment geometries and constraining layer effective stiffnesses. This damping study is undertaken on a panel similar to that shown in Figure 19.8 except that no crack is present and the reinforcement now has its centreline (i.e. the centre of the W dimension) aligned with the centreline of the long dimension of the panel.

Initially an investigation into the effect of reinforcement geometry on modal loss factor is undertaken. In this case a 250 mm long by 166 mm wide by 1.2 mm thick aluminium panel, fixed on all four sides, is modelled. The entire aluminium panel is treated with CLD. Typical “off-the-shelf” CLD treatments are 0.5 to 2 mm thick with a 0.125 mm thick constraining layer of aluminium. Material properties for the damping (VEM) material, aluminium and boron/epoxy are given in Table 19.2. The material loss factor for the viscoelastic material is taken as 1.0 and the constraining layer is an aluminium sheet 0.125 mm thick. The panel is reinforced with a unidirectional boron/epoxy laminate with fibres aligned in the y -direction, see Figure 19.8. The thickness of this reinforcement is determined such that the stiffness of the reinforcement and the aluminium plate are matched, i.e. using Eq. (19.8)

$$E_{al}t_{al} = E_r t_r \tag{19.8}$$

These studies were conducted with a reinforcement of constant length (L) of 75 mm and varying widths (W) of 50 mm, 100 mm and 125 mm. The effects of these different size reinforcements on the structural loss factor of the panel are determined and are given in Table 19.3. It must be pointed out at this stage that the damping properties of the boron/epoxy laminate and aluminium are not included in the analysis, i.e. these values are assumed to be zero. Therefore, the actual structural damping is expected to be higher than that predicted in this study, hence, the results from this study are conservative. The modal loss factor is calculated from the finite element analysis by assuming that, given the material damping, the modal loss factor [14] can be calculated by:

$$\eta_s = \sum_{i=1,n} \frac{\eta_i e_i}{e} \tag{19.9}$$

where η_s is the structural loss factor and η_i is the material loss factor of the i th

Table 19.3
Loss factor of aluminium panel (with no crack) reinforced with unidirectional boron/epoxy with a 1 mm thick damping treatment and 0.125 mm thick aluminium applied to whole panel.

Mode	Damped natural frequency (Hz)	Loss factor	Specimen description
1	290	0.139	Patch dimensions are 75 mm (L) \times 50 mm (W)
2	460	0.113	
3	769	0.081	
1	288	0.135	Patch dimensions are 75 mm (L) \times 100 mm (W)
2	441	0.118	
3	723	0.093	
1	289	0.132	Patch dimensions are 75 mm (L) \times 125 mm (W)
2	442	0.116	
3	732	0.085	

element. The modal energy, e , is calculated with Eq. (19.10);

$$e = \int \delta^T [K] \delta dV, \quad (19.10)$$

where δ is the eigenvector and the stiffness matrix is denoted by $[K]$. Equation (19.9) is implemented as a post-processing option in the finite element analysis package and was first validated prior to its use.

The results in Table 19.3 show that the size of the unidirectional boron/epoxy reinforcement has a small effect on the structural damping. However, [15] observed that when the reinforcement was made from aluminium changing the size of the reinforcement caused a large change in the modal loss factor. For example, when the size of the boron/epoxy reinforcement is increased from 75 mm by 50 mm to 75 mm by 125 mm, there is only a 5% reduction in the modal loss factor for mode 1 compared to an 11% reduction for the aluminium reinforcement.

Table 19.4 shows the results for modal loss factors when only the boron/epoxy patch is treated with constrained layer damping. This table shows that the structural damping derived with this scheme of damping treatment is not very effective. These results therefore confirm that damping treatment should be applied to the entire panel for more effective damping of the structure.

The study is extended to investigate the effect of varying the VEM thickness and constraining layer properties on the overall loss factor. In this analysis only one patch size is considered, viz. 77 mm long by 125 mm wide, and the VEM thickness, t_{VEM} , is varied from 0.5 mm to 2.0 mm. The constraining layer is now boron/epoxy and two laminates are modelled, viz. a two ply [0/90] laminate and a four ply [0/90]_{sym} laminate.

The predicted results given in Table 19.5, show a significant increase in modal loss factor as the VEM thickness is increased. For mode 1 an increase of 32% and 90% is observed when the VEM thickness is increased from 0.5 mm to 1.0 mm and

Table 19.4

Loss factor of aluminium panel (with no crack) reinforced with unidirectional boron/epoxy with a 1 mm thick damping treatment and 0.125 mm thick aluminium constraining layer applied to the reinforcement only.

Mode	Damped natural frequency (Hz)	Loss factor	Specimen description
1	324	0.03	Patch dimensions are 75 mm (L) \times 50 mm (W)
2	543	0.011	
3	852	0.022	
1	316	0.049	Patch dimensions are 75 mm (L) \times 100 mm (W)
2	501	0.03	
3	833	0.036	
1	315	0.053	Patch dimensions are 75 mm (L) \times 125 mm (W)
2	492	0.036	
3	830	0.036	

Table 19.5

Loss factor of aluminium panel (with no crack) reinforced with a unidirectional boron/epoxy patch of dimensions 77 mm (L) \times 125 mm (W) with the constrained layer damping treatment applied to whole panel.

Mode	Damped natural frequency (Hz)	Loss factor	Specimen description
1	258	0.122	
2	449	0.106	$t_{\text{vem}} = 0.5$ mm
3	641	0.078	[0/90] boron/epoxy constraining layer
1	240	0.161	
2	411	0.132	$t_{\text{vem}} = 1.0$ mm
3	597	0.091	[0/90] boron/epoxy constraining layer
1	217	0.232	
2	368	0.178	$t_{\text{vem}} = 2.0$ mm
3	528	0.126	[0/90] boron/epoxy constraining layer
1	245	0.216	
2	423	0.163	$t_{\text{vem}} = 1$ mm
3	585	0.122	[0/90] _{sym}] boron/epoxy constraining layer
1	222	0.274	
2	378	0.203	$t_{\text{vem}} = 2$ mm
3	528	0.1	[0/90] _{sym}] boron/epoxy constraining layer

0.5 mm to 2.0 mm, respectively. With the increase in thickness of the VEM there is also a corresponding drop in damped natural frequency which is mainly due to the increase in mass. Also increasing the effective stiffness of the constraining layer substantially improved the modal loss factor of the panel. For the 1.0 mm thick VEM case the loss factor, for the first resonant mode, increased by 34% when the effective stiffness of constraining layer is increased by substituting the [0/90] laminate with a [0/90]_{sym}] laminate. The increase in loss factor is less pronounced for the 2.0 mm thick VEM case where an increase in 18% was observed when the constraining layer thickness is increased from two to four plies.

Overall this theoretical study has shown that the modal loss factor of the reinforced panel can be significantly improved by incorporating constrained layered damping. Further improvements can be achieved by increasing (i) the thickness of the VEM and (ii) the effective stiffness of the constraining layer. The values of modal loss factor of panels incorporating highly-damped patches, tabulated in Table 19.5, are used in the next section as inputs for the FE models of repaired cracked panels.

It has been established that, Section 19.6.1, the stress intensity in the cracked (un-repaired) plate is as shown in Figure 19.12. Here the right hand crack tip refers to the crack tip located midway along the plate shown in Figure 19.8. The higher stress intensity for the right hand crack tip is due to the larger dynamic bending stresses that occur midway along the panel. For a crack length of 80 mm $K_I = 15 \text{ MPa m}^{1/2}$. Although this is not a high value in comparison with the fracture toughness value, K_{IC} , in an environment of high-cycle fatigue it leads to a high crack growth rate.

19.7.3. Analysis of repaired cracked plate

Firstly, the panel is idealised as a three dimensional flat plate using 20 noded brick elements. Sufficient elements are used to define the crack length considered. Also, the behaviour of the adhesive and viscoelastic damping materials is modelled as a 3D element, to allow for shear deformation. The boron/epoxy patch and boron/epoxy constraining layer are sufficiently thin such that 2D shell elements are an adequate representation.

The geometry of the structure is shown in Figure 19.8. The mesh size of the skin and viscoelastic structure is 75×60 elements. As shown, the unidirectional boron/epoxy reinforcing patch only extends partially across the panel. It also covers an adjacent panel as shown in the dotted outline. The boron/epoxy repair has length, L , and width, W . In this section the length is fixed at 77 mm, however three widths are considered, viz. 80 mm, 99 mm and 126 mm. The entire panel is covered with the CLD material. Material properties for the skin, adhesive, VEM and boron are shown in Table 19.3.

The boundary conditions for this model are considered to be fully clamped except for the crack region which is not restrained. For this study the crack length was 80 mm. The patch above the crack also remains fully constrained. Clearly crack closure will occur at an increasing distance away from the crack tip, however the complexity in introducing such constraints is not included in this preliminary study.

19.7.4. Results and discussion

19.7.4.1. Modal shapes and frequencies

As previously mentioned, one of the main concerns regarding a particular repair is the change of frequency of the plate to the excitation frequencies. The first three frequencies of the original uncracked un-repaired plate are shown in Table 19.6. For a highly-damped patch consisting of a 1.0 mm thick damping layer with a [0/90] boron/epoxy constraining layer the variation of resonant frequencies with increasing patch width (W) is shown in Table 19.7. The reinforcing patch length (L) is 77 mm. In all cases the addition of the highly-damped patch configuration resulted in a reduction of frequency. The resonant frequency increases by 5%, 10% and 13% for vibration modes 1, 2 and 3, respectively, when the patch width increased from 80 to 126 mm. Typical modes of vibration predicted by the F.E.A. are shown in Figure 19.20. The resonant frequencies for a 2.0 mm thick damping

Table 19.6
Frequencies for original
uncracked un-repaired plate.

Mode	Resonant frequency (Hz)
1	218
2	374
3	506

Table 19.7
Resonant frequencies for various patch widths (W) and thicknesses of damping material with [0/90] boron/epoxy constraining layer (t_{VEM}).

	Case 1.0/80*	Case 1.0/126*	Case 2.0/80*	Case 2.0/126*
Mode	Resonant frequency (Hz)			
1	208	216	193	200
2	335	341	308	319
3	442	461	403	417

* refers to values of t_{VEM}/W in mm.

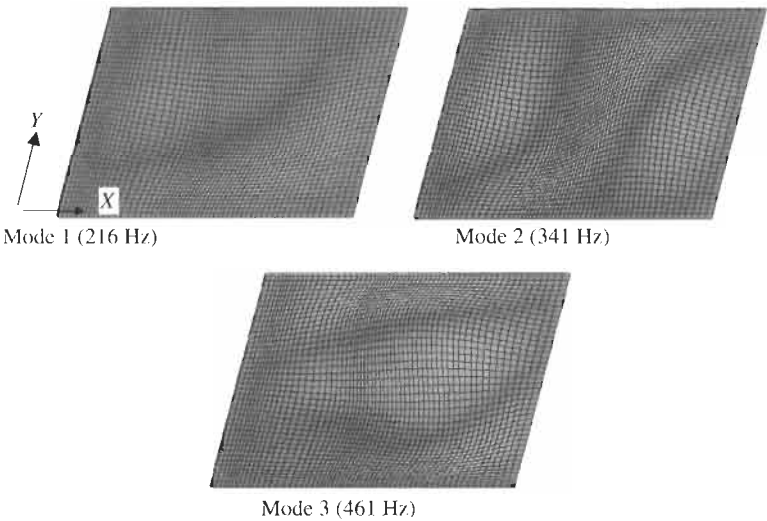


Fig. 19.20. Mode shapes for cracked panel with highly damped repair ($w = 126$ mm, $t_{\text{vem}} = 1.0$ mm and [0/90] boron/epoxy constraining layer).

layer with a [0/90] boron/epoxy constraining layer for various patch widths (W) are shown in Table 19.7.

19.7.4.2. PSD of the displacement

Since the area under the displacement PSD curve is the mean square displacement response, then a running integral of the displacement PSD illustrates the contribution of each vibration mode to the overall displacement response, as shown in Figure 19.21. Since the stress intensity is proportional to the crack opening displacement, then a running integral of the displacement response will indicate the contribution of each vibration mode to the overall stress intensity. Figure 19.21 shows the PSD displacement response at the right hand (inner side) crack for the case of a 1.0 mm thick damping layer with [0/90] boron/epoxy

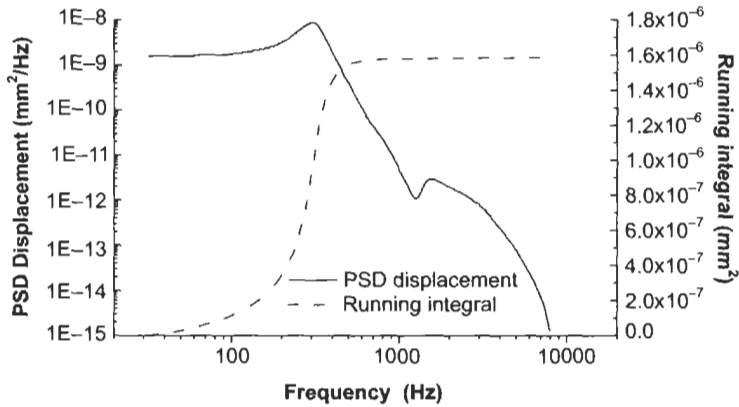


Fig. 19.21. PSD of displacement $u(x) (K_I)_{rms}$ and running integral of the PSD for a cracked panel with a 1.0 mm thick damping layer with [0/90] boron/epoxy constraining layer and an 80 mm wide by 77 mm long boron/epoxy reinforcement.

constraining layer and a 80 mm wide by 77 mm long boron/epoxy patch. This figure shows that vibration mode 1 contributes up to 99% of the overall stress intensity $(K_I)_{rms}$. Similar results were found for all the other highly damped repair configurations investigated.

19.7.4.3. Stress intensity factor

Stress intensity factors are computed at the inside and outer surfaces of the skin. Since the repair results in a neutral axis shift the maximum values exist at the inner surface. The most critical crack tip position is the tip located midway down the longest side of the panel, as shown in Figure 19.8. The maximum values have been plotted in Figures 19.22–19.25. Various highly-damped patch configurations, involving 0.5, 1.0 and 2.0 mm thick damping VEM, are considered. In all cases the highly-damped patch has a boron/epoxy reinforcement/repair with dimensions 77 mm long and varying widths of 80 mm, 99 mm and 126 mm. Overall the highly damped repairs show a significant reduction in $(K_I)_{rms}$ compared to the low damped repair case. Introducing damping reduces the mode I stress intensity by about a factor of 10. Over the range of damping thickness considered the configuration that give the lowest values of $(K_I)_{rms}$ is for the 77 mm long by 126 mm wide reinforcement/repair with the 1.0 mm thick VEM and [0/90] constraining layer case. Also, the 0.5 mm thick VEM with [0/90] constraining layer case gave similar stress intensities as shown in Figure 19.23.

Although no crack growth data corresponding to $(K_{II})_{rms}$ or $(K_{III})_{rms}$ stress intensities are available, the numerical values of $(K_{II})_{rms}$ are lower than those for $(K_I)_{rms}$, as shown in Figure 19.24. Also, the numerical values for $(K_{III})_{rms}$, as shown in Figure 19.25, are numerically comparable to $(K_I)_{rms}$. All of the damped repairs are equally effective in reducing $(K_{II})_{rms}$, and show a considerable reduction in comparison to the low damped design. Also the results for $(K_{III})_{rms}$ show that all

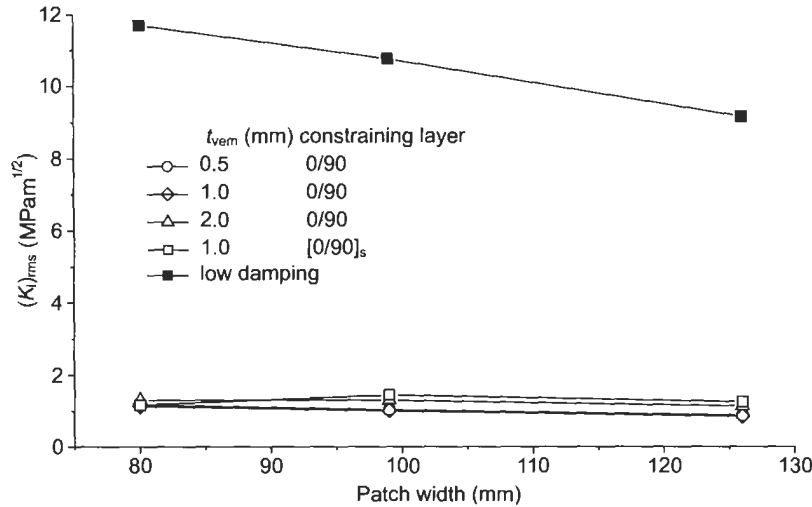


Fig. 19.22. Stress intensity factor, $(K_I)_{rms}$, for various highly-damped and low damped patch configurations.

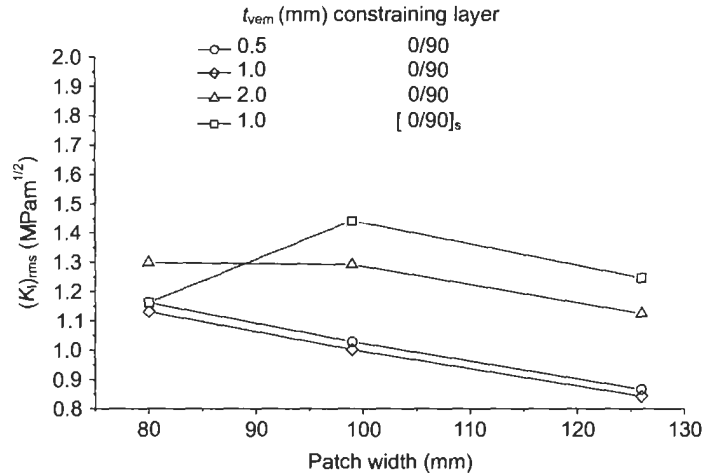


Fig. 19.23. Stress intensity factor, $(K_I)_{rms}$, for various highly-damped patch configurations.

the configurations, except the 0.5 mm, [0/90] configuration, gave equally low values of $(K_{III})_{rms}$. Overall, comparisons with the low damped patch, i.e. a repair with no CLD included, have shown the highly-damped patch to be very effective. The best overall results appear to be for the 1.0 mm [0/90] configuration.

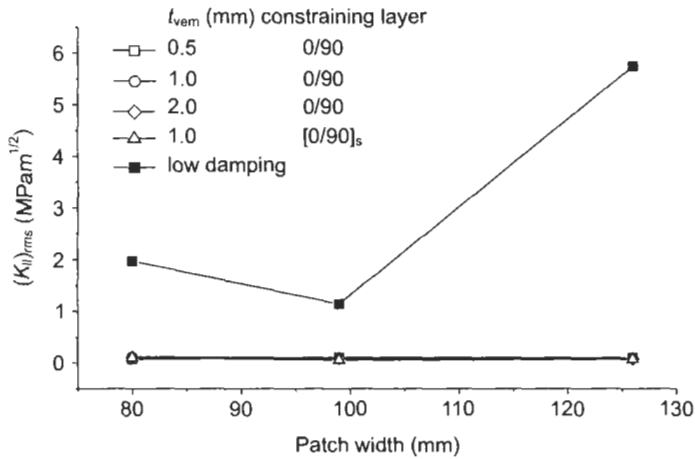


Fig. 19.24. Stress intensity factor, $(K_{II})_{rms}$, for various highly-damped and low damped patch configurations.

19.7.4.4. Crack growth predictions

The crack growth data shown in Figure 19.26 is for 7075-T6 aluminium alloy corresponding to long crack growth data for panels tested subject to uniaxial loading [16]. As a result of the neutral axis offset the curve of $R=0$ most closely represents the crack growth curve for the bending fatigue case. While these data are for low frequency loading conditions, evidence exists that high frequency testing results in slightly lower crack growth rates [17,18]. In our case high frequency

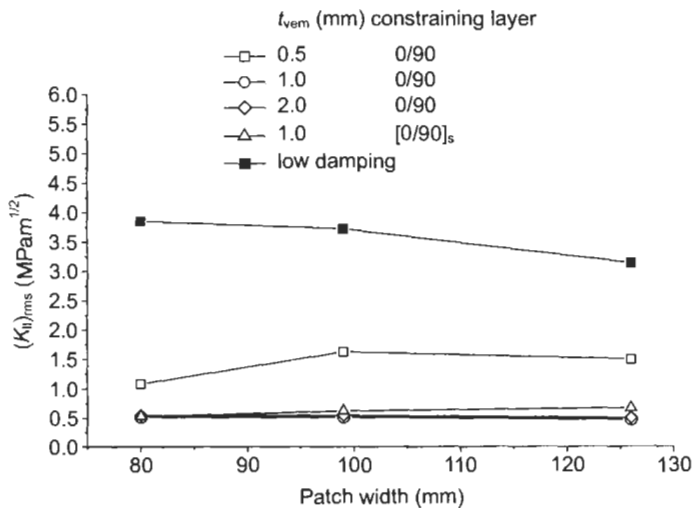


Fig. 19.25. Stress intensity factor, $(K_{III})_{rms}$, for various highly-damped and low damped patch configurations.

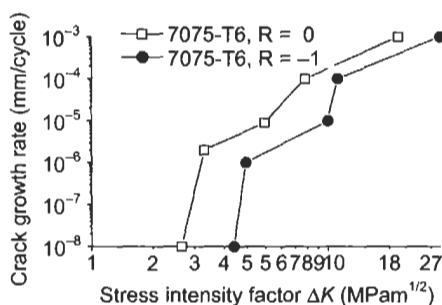


Fig. 19.26. Crack growth rate for 7075-T6 with increasing K_I , [16].

bending is involved, therefore taking crack growth rates from Figure 19.26 will lead to conservative estimates of crack length. The curve in Figure 19.26 has been extrapolated to determine the approximate crack growth rate for cases less than 10^{-8} mm/cycle. Using these data insignificant crack growth has been calculated, after the 6000 h, for all the highly-damped patch configurations considered. Crack growth data for 4% Cu-Al alloy subjected to high frequency bending, given in [16], also indicates negligible crack growth for all the highly-damped patch configurations considered. Although no crack growth data corresponding to K_{II} or K_{III} stress intensities are available the K_{III} results shown in Figure 19.25 indicate possible crack growth for the 0.5 mm [0/90] configuration. Note that the above results are highly dependent on the material loss factors used in the modelling. This loss factor is also dependent on the operating temperature. Therefore in order to design an effective highly damped repair knowledge of the temperature condition when the high SPL are generated is required.

19.7.4.5. Summary

A methodology is proposed to enable the design highly-damped patches for cracked structures subject to intense acoustic loading. The highly-damped patch incorporates a boron/epoxy reinforcement/repair, to restore structural strength, as well as a constrained layered damping layer in order to enhance damping and thus reduce dynamic stresses. The proposed highly-damped patches reduce the response at resonance of the patched panel compared to the un-repaired uncracked panel. A study investigating the effects of various reinforcement dimensions, VEM thicknesses and constraining layer configurations on the modal loss factor of the plate has also been undertaken. It was found that for the various reinforcements studied, no significant variation in loss factor was observed. However significant increases in loss factor are observed with increasing VEM thickness and constraining layer effective stiffness. The inclusion of damping in the repair enables the stress intensity factor to be substantially reduced. Predictions of K_I indicate that no crack growth is expected for all the highly-damped patched configurations considered. However this result is based on the assumption of a modal loss factor of the viscoelastic material of 1.0. The modal loss factor does

however vary with both temperature and frequency and it is not possible to achieve 1.0 over a wide temperature range. These issues will be considered in the next section.

19.8. Aft fuselage finite element model

In order to study the cracking mechanisms of the cracked and repaired/cracked aft skin cases, a simplified model has been developed in which the skin is considered to be a flat rectangle. Most of the skin panels in which cracking occurs have a chemical milled step in which the panel is reduced in thickness to 0.91 mm. While the width and height dimensions of each panel vary, the F.E. model has representative dimensions as shown in Figure 19.27. The mesh is shown in Figure 19.28. Since the crack lies near the boundary, the repair will continue across the adjacent panel as outlined in Figure 19.27. In order to more accurately represent the bending of the panel, two layers of 20 noded brick elements have been used through the thickness. A local boron/epoxy repair [O₃] has been applied to make up for material lost as a result of the crack, but does not cover the entire

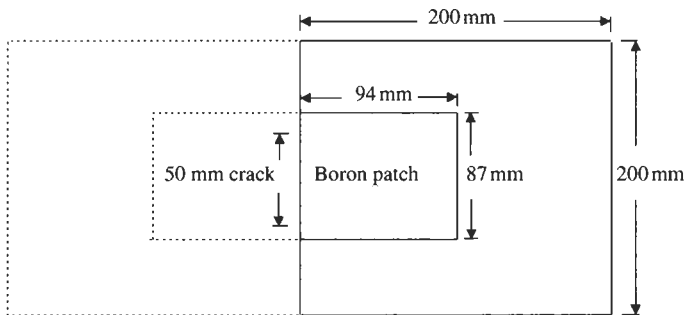


Fig. 19.27. Dimensions of repair, plan view.

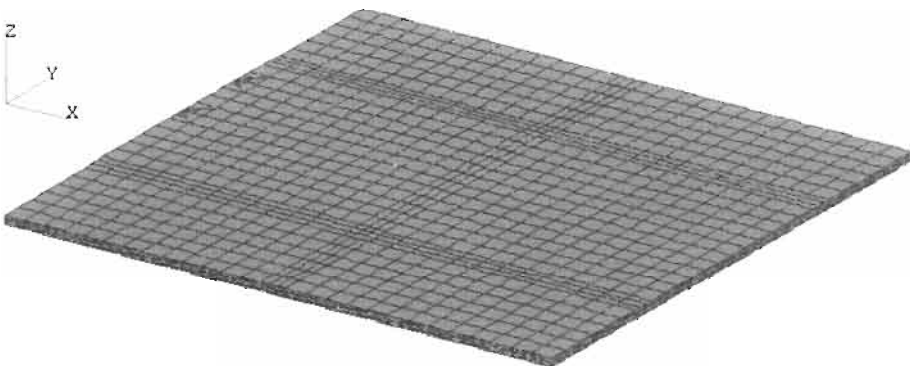


Fig. 19.28. Finite element model of multi-layer highly damped repair, containing a 50 mm long crack.

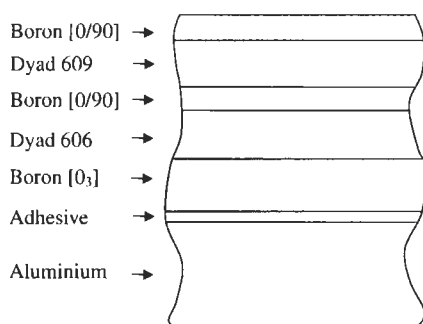


Fig. 19.29. Components of the highly damped repair.

panel. The highly damped section of the repair covers the entire panel including the local boron patch. This section consists of two viscoelastic layers with two boron/epoxy [0/90] constraining layers as shown in Figure 19.29. The viscoelastic layers and adhesive have been modelled using 3D elements as are the constraining layers. The total structure consists of 7000 elements and 29000 nodes.

19.8.1. Modes and frequencies

A modal analysis has been carried out using NASTRAN program, [11], to determine the mode shapes and frequencies. The first four mode shapes are shown in Figure 19.30. The PSD of the response is plotted in Figure 19.31. From this curve it is clear that mode 1 provides the greatest contribution to the response at a frequency of 203 Hz. The mean square contribution of the other modes is more than one order of magnitude smaller than that for mode 1.

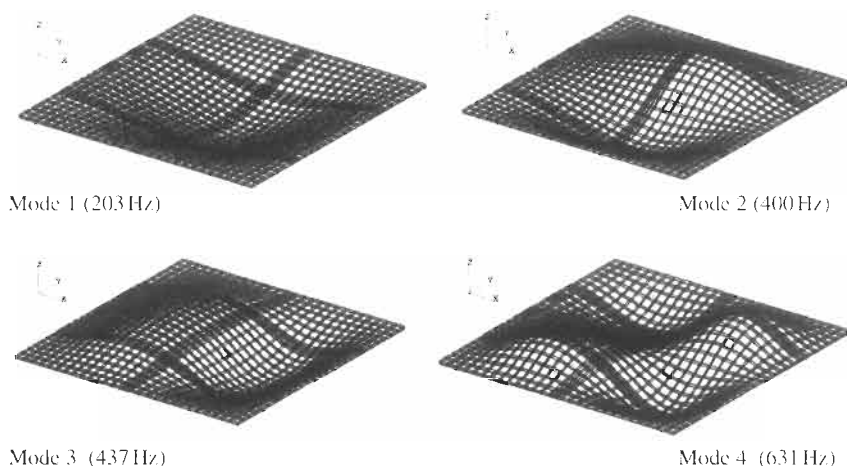


Fig. 19.30. Modes and frequencies for aft fuselage repaired skin.

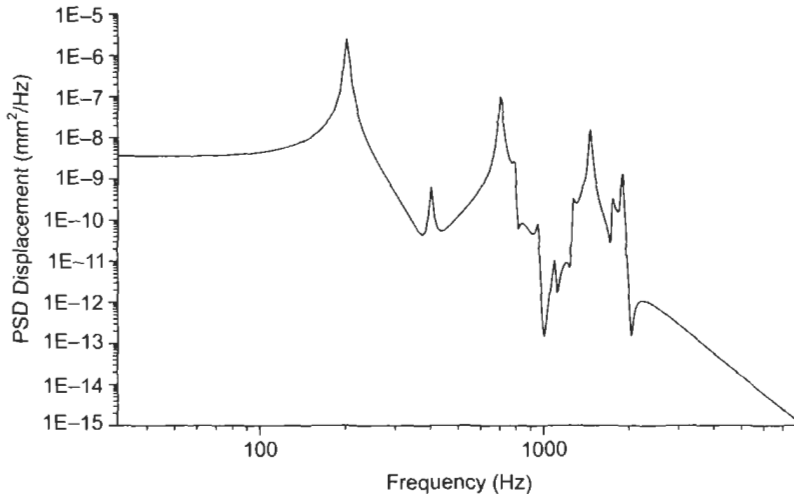


Fig. 19.31. PSD of the response (i.e. mean square of the displacement near the crack tip).

19.8.2. Acoustic fatigue crack growth data

In this study, it has been necessary to show that standard crack growth laws can be applied to structures subject to high frequency out-of-plane bending excitation. While acoustic fatigue data is very limited a comparison has been made with L73 data (U.K. spec.) and a standard crack growth law. The L73 (clad) alloys, [18], shown in Figure 19.32, is equivalent to 2014-T6. The crack growth law for 2014-T6 is given by [19] as:

$$\frac{da}{dn} = \frac{C_f(\Delta K)^m}{(1-R)K_f - \Delta K} \text{ (mm/cycle) ,} \quad (19.11)$$

where $C_f = 1.0 \times 10^{-5}$, $m = 2.87$, $K_f = 59.9$, $R = \sigma_{\min}/\sigma_{\max}$ and here ΔK is assumed to be equal to ΔK_{rms} .

The crack growth law is usually determined from testing at a frequency of typically 4–10 Hz. Also Eq. (19.11) is only valid for a range of 6–50 MPa m^{1/2}. A comparison between the crack growth law prediction and the 2014-T6 data is shown in Figure 19.33. The experimental data corresponds to a sinusoidal data at 175 Hz and shows surprisingly good agreement. The random data has not been used since the slopes of the curves show significant disagreement, with similar strain levels.

To determine results for 7075-T6 consider Eq. (19.11) with the following coefficients:

$$C_f = 1.37 \times 10^{-5}, \quad m = 3.02, \quad K_f = 63.9$$

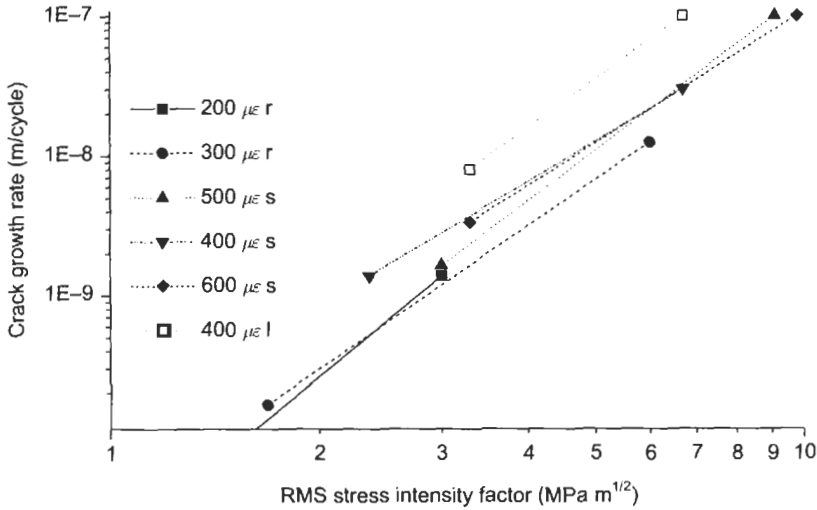


Fig. 19.32. Acoustic fatigue crack growth data for clad 2014-T6, ($\mu\epsilon$ denotes micro-strain, r denotes random, s denotes sinusoidal and l denotes low reversal rate, [18]).

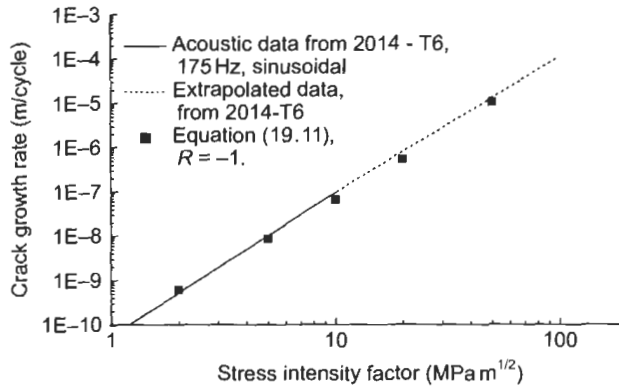


Fig. 19.33. Crack growth data and crack growth law, [18].

19.8.3. Residual thermal stresses

Thermal stresses arise due to the different coefficients of thermal expansion of the materials involved and may be significant at the extremes of the operating temperatures. Furthermore it is known that the residual thermal stresses due to the bonding process may be significant. Typically the bonding process results in curing at a temperature of approximately 80–120 °C. In the case of a boron/epoxy repair to an aluminium plate there is a large difference in the coefficients of thermal expansion. As a result the residual stress intensity for a repair involving boron/

epoxy is comparable to the stress intensity for the out-of-plane vibration. At high operating temperatures this effect is alleviated. However the shear modulus of the adhesive bonding the boron/epoxy to the plate softens and increases the stress intensity factor.

19.8.4. Damping data

Two commercially available structural damping materials have been evaluated such as Soundcoat and Isodamp. From this testing the Soundcoat Dyad 606 and 609 [20], have been chosen as being the most suitable materials that are available for this application. The manufactures data for Dyad 606 and 609 are shown in Figures 19.34 and 19.35. A combined plot for Dyad 606 and 609 is shown in Figure 19.36 for a frequency of 200 Hz and gives a guide for the expected performance using a combination of 606 and 609.

19.8.5. Adhesive data

Stress strain data is available for FM300, [21], and is shown in Figure 19.35 as a function of temperature. The service temperature for this adhesive ranges from -55°C to 150°C . Only two data points exist for each temperature case, as a result values for shear modulus have been extrapolated. Using dry data the shear modulus is given by: $G = 1281 - 7.419T$ (MPa), where T is the temperature in $^{\circ}\text{C}$.

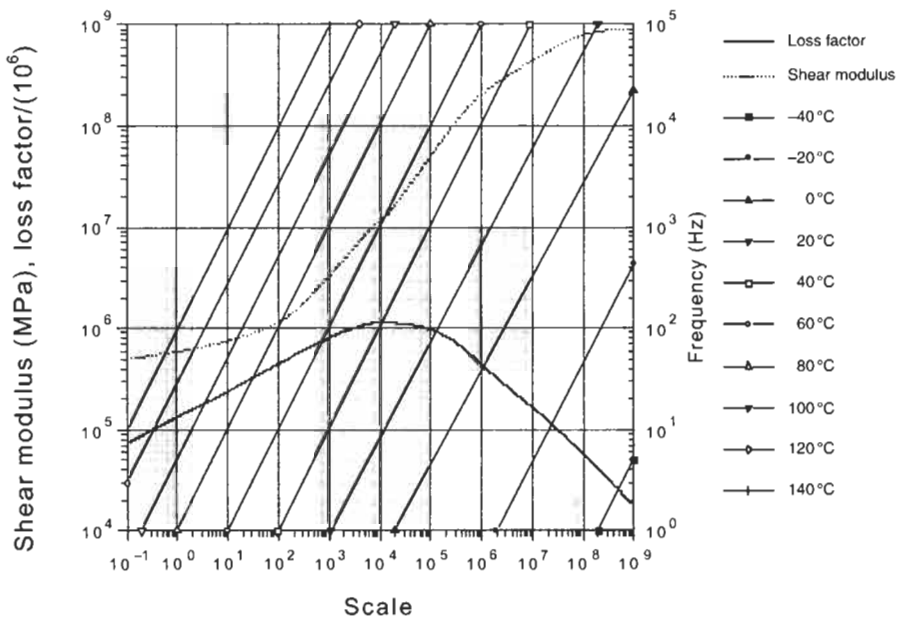


Fig. 19.34. Dyad 606 material data. (To obtain loss factor divide shear modulus scale by 10^6).

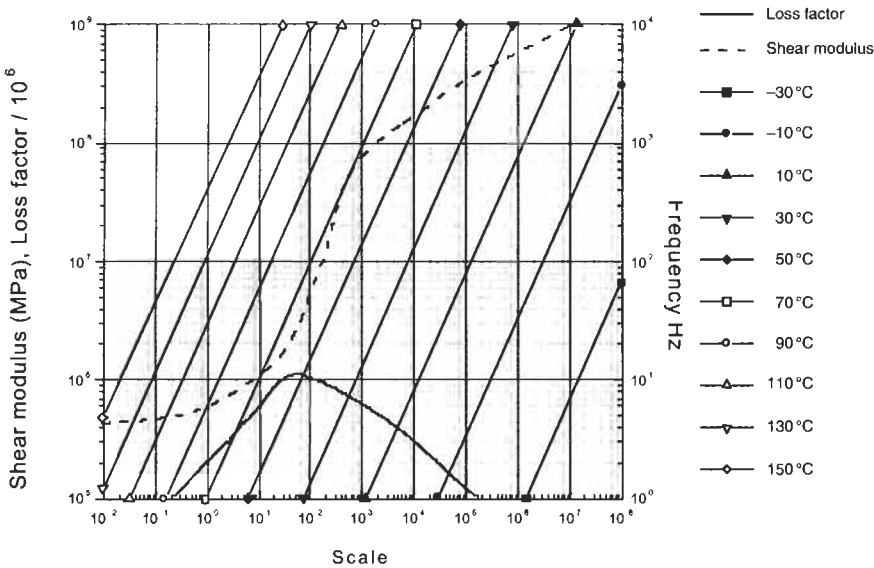


Fig. 19.35. Dyad 609 material data. (To obtain loss factor divide shear modulus scale by 10⁶.)

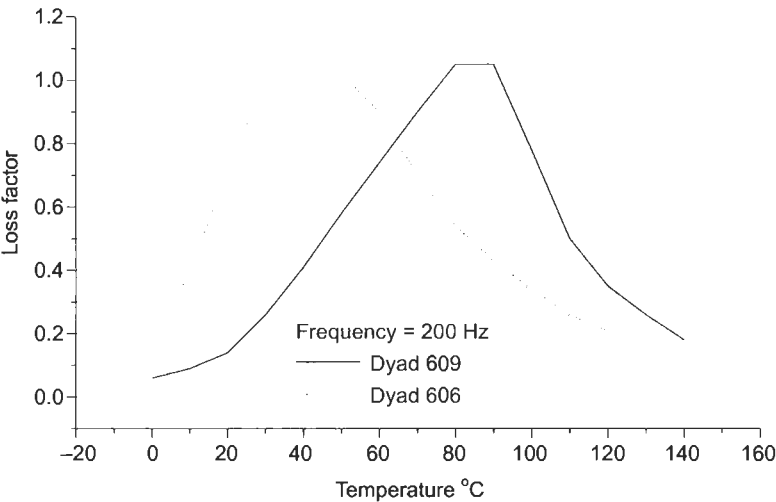


Fig. 19.36. Comparison of Dyad 606 and 609 over the entire temperature range.

19.9. Thermal environment for F/A-18

Results of a thermal profile of the F/A-18 have been obtained from [22]. These flight tests were performed to establish the thermal profile at the edges of the flight envelope in order to provide design information for bonded repairs. The operating

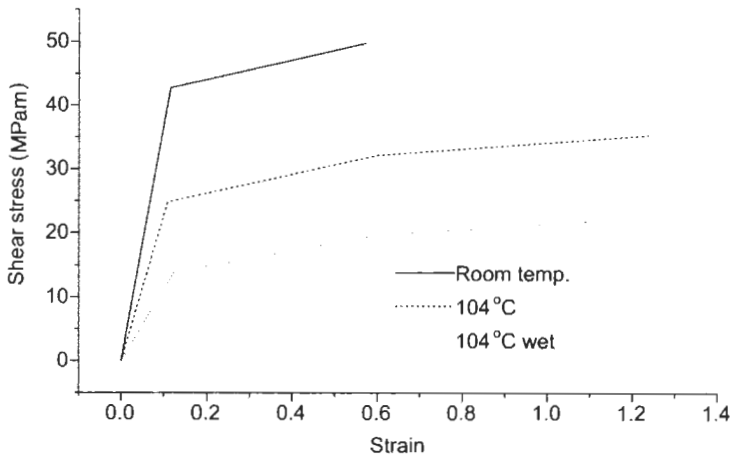


Fig. 19.37. Stress strain diagram for FM300 for the temperature range shown.

Table 19.8

Thermal conditions for F/A-18 aft fuselage.

Condition	Altitude	Mach no.	Temperature °C
ISA	SL	1.1	78
ISA	FL350	2.0	103
Coldest day	FL500	0.74	- 63
Hottest day	SL	1.1	114
Hottest day	FL350	2.0	141

extremes are shown in Table 19.8 for the aft fuselage in the area in which cracking has occurred. The most relevant conditions are those at high dynamic pressures which can lead to maximum temperatures of the order of 141 °C. This would be the extreme limit for the highly damped repair. Temperatures for the coldest condition correspond to minimum power and would not be expected to contribute to acoustic fatigue damage. It is unlikely that even temperatures of 0 °C would contribute since this would be at low engine power. Hence without additional data, the highly damped repair will be expected to perform over a temperature of 0–141 °C. Since temperatures close to the hottest day of the year only occur several times each year, the ISA condition is more likely with a temperature range of 78–103 °C.

19.10. Analytical results

In Figure 19.38 a plot is shown for the ratio of stress intensity factor for the cracked unpatched plate to the stress intensity of the repaired plate. This includes the thermal residual stress contribution and softening effect of the adhesive. A

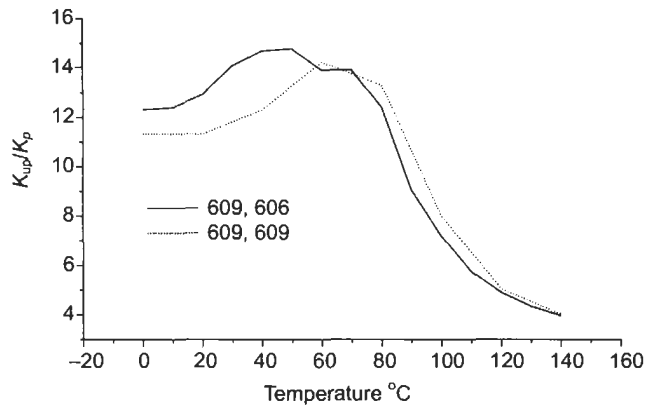


Fig. 19.38. Plot of K_{up}/K_p versus temperature for configurations using 609 and 606.

significant reduction of K_{up} is shown over the complete temperature range. Results using two layers of 609 are also shown in Figure 19.38. These results show a slight improvement at the higher temperature range but reduced performance at temperatures below 60 °C.

Figure 19.39 shows the crack growth rate for 7075-T6, over the temperature of interest. Equation (19.11) is used to obtain the crack growth rates, with relevant coefficients, including both thermal residual stresses estimated from a closed form solution and adhesive softening. The crack growth rate is relatively low for temperatures of 80 °C, beyond this the crack growth increases significantly. In

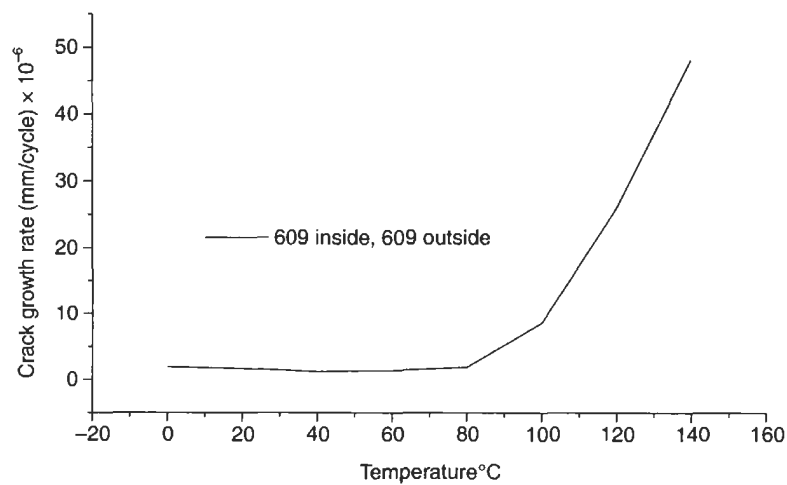


Fig. 19.39. Crack growth rate for highly damped repair.

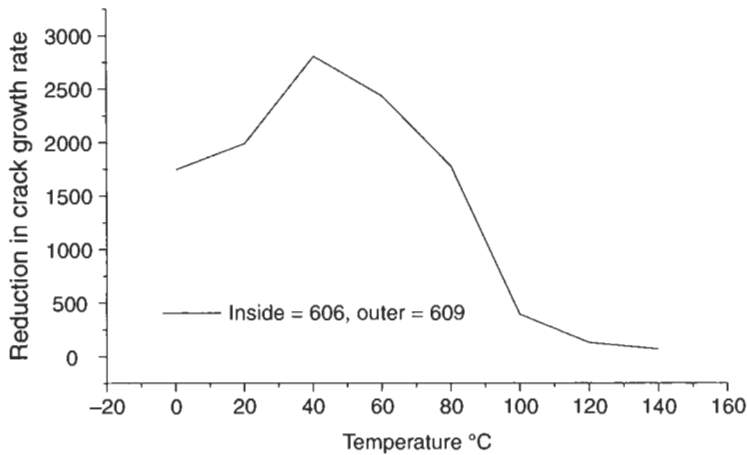


Fig. 19.40. Reduction in crack growth rate for highly damped repair compared to cracked un-repaired plate.

comparison Figure 19.40 shows that the crack growth rate for the cracked un-repaired panel to the repaired panel is approximately 2700 times greater for temperatures up to 40°C. Even at 140°C the crack growth rate of the cracked un-repaired panel is 70 times the crack growth rate of the repaired panel.

The adhesive shear and peel stresses bonding the boron repair to the aluminium are shown in Figure 19.41 corresponding to room temperature. In comparison with Figure 19.37, it is evident that for room temperature at this particular SPL the stresses are relatively low and no yielding will occur under peel or shear.

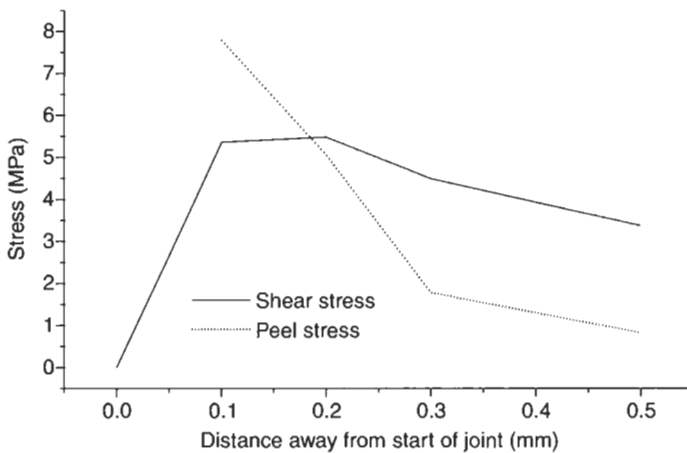


Fig. 19.41. Adhesive stresses bonding boron to aluminium at room temperature.

19.11. Experimental work

Limited experimental work has been carried out in [23–25] in support of the analytical work. While differences exist between the aft fuselage geometry and specimens, similar experimental trends are expected. This work covers testing butterfly specimens which involve the flexing or bending motion shown in Figure 19.42, provided by a shaker, in order to simulate the acoustic excitation. The specimen is excited at the first resonant frequency and the geometry of the specimen is shown in Figure 19.43. These specimens consist of bare aluminium specimens with boron/epoxy patches and Dyad 609 and 606 VEM layers with $[0,90]_s$ constraining layers. The highly damped repair was applied using RT curing adhesive Hysol EA9320. All panels were pre-cracked with a crack length of 25 mm. The damping materials are the same as those used in the aft fuselage F.E. model. In each case the maximum force applied to the specimen by the shaker was 90 N. This forcing level achieved a nominal rms strain of about $1000 \mu\epsilon$ ahead of the crack. Comparative results are shown in Figure 19.44. In the case of bare aluminium specimens approximately 100000 cycles were obtained before the resonant frequency dropped by 15%. A 15% drop in resonant frequency was used as a criteria to indicate extensive crack growth. For boron/epoxy repairs approximately 1000000 cycles were obtained before the resonant frequency of the specimen dropped by 15%. In the case of the highly damped repair the first test with a shaker force of 90 N gave no reduction in frequency at 10000000 cycles, as shown by the dotted line. A second run was made with the shaker force increased to 180 N. The results for this run are shown in Figure 19.44. At approximately 10000000 cycles a 15% reduction of resonant frequency has occurred. The highly damped repair tested is slightly different to that analysed above in Section 19.8.0 in that the constraining layers of $[0/90]_s$ are used in the experimental test rather than the $[0/90]$ plies in the aft fuselage F.E. model. However the experimental results indicate that highly damped repairs are very effective in reducing the crack growth rate.

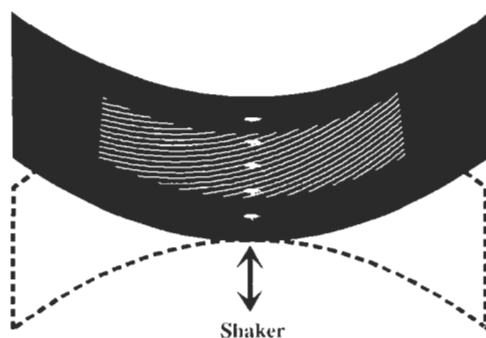


Fig. 19.42. Flexing motion for butterfly specimen provided by an electrodynamic shaker.

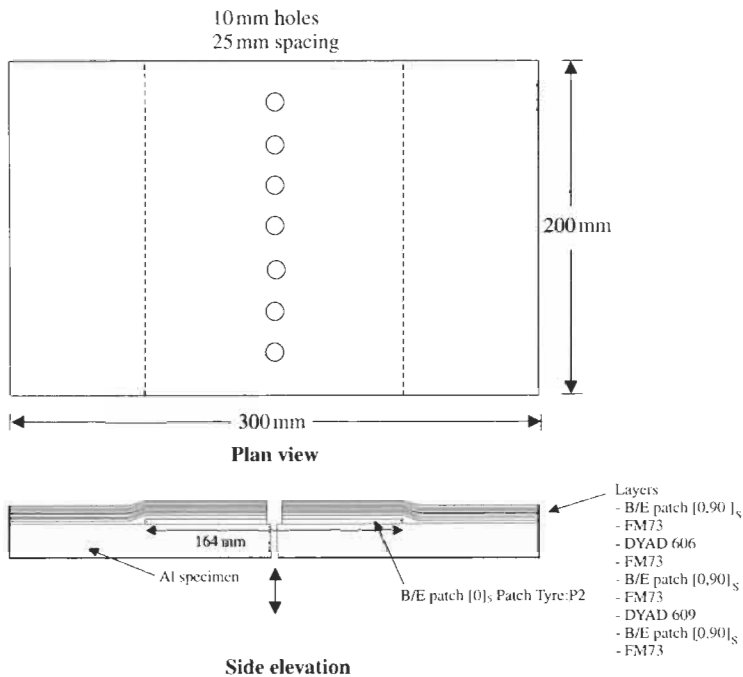


Fig. 19.43. Highly damped repair specimen configuration, from [24].

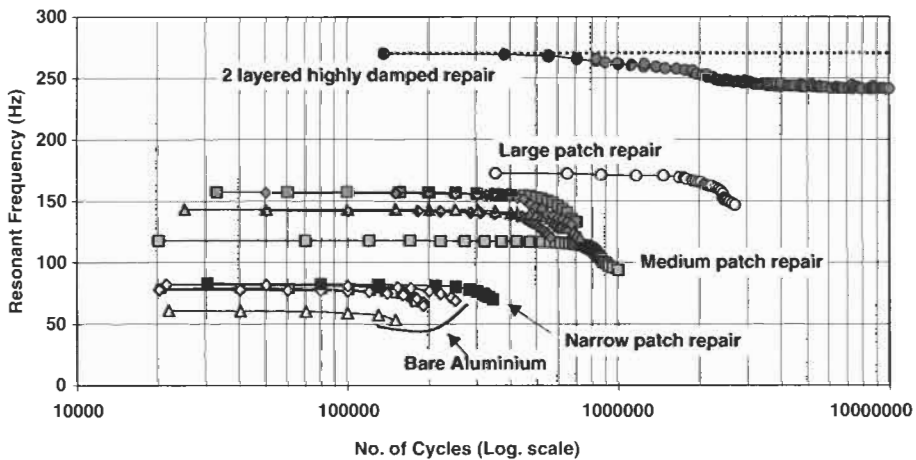


Fig. 19.44. Comparative test lives for various specimens, from [24]. (Narrow, medium and large patch repair refers to reinforcing patch lengths of 56 mm, 164 mm and 210 mm respectively).

19.12. Conclusions for aft fuselage repair

While sufficient data is not available to precisely define the acoustic/thermo environment, operating temperatures for extremes of the design envelope have been identified. Using two different damping materials, Soundcoat Dyad 606 and 609, enable the repair to be effective over a wide temperature range. Results show that the highly damped repair is effective in reducing the stress intensity factor in intense acoustic excitation conditions. Crack growth laws which have to be validated for limited acoustic fatigue are used to predict crack growth rates for cracks for the un-repaired and repaired cases. The FEA results indicated that, compared to unpatched cracked panels, the application of the proposed highly damped repairs would reduce the crack growth rates by a factor of 2700, at temperatures around 40 °C, and 70 for temperatures around 140 °C. The damping materials, boron and FM300 adhesive will survive temperatures up to 140 °C.

References

1. A/B/C/D Aircraft Lower Nacelle Skin Acoustic and Strain Measurements and Sonic Fatigue Analysis. MDC 94B0044. March, 1994.
2. Baker, A. (1994). Bonded Composite Repair of Metallic Aircraft Components. *AGARD-CP-550 Composite Repair of Military Aircraft Structures*, Paper 1.
3. Composite Materials and Adhesive Bonded Repairs. RAAF Standard Engineering C5033, Draft – January 1994.
4. Callinan, R.J., Galea, S.C. and Sanderson, S. (1997). Finite element analysis of bonded repairs to edge cracks in panels subjected to acoustic excitation. *Composite Structures*, **38**(1–4), pp. 649–660.
5. Callinan, R.J., Chiu, W.K. and Galea, S.C. (1998). Optimisation of a composite bonded repair to cracked panels subjected to acoustic excitation. *Proc. of the 21st Congress of the Aeronautical Sciences (ICAS 98)* Melbourne, Australia, 1–18 September. (Paper A98–31631 ICAS Paper 98–5.3.2).
6. Rogers, L., Maly, J., Searle, I.R., *et al.* (1997(b)). Durability patch: Repair and Life Extension of High-cycle Fatigue Damage on Secondary Structure of Ageing Aircraft, 1st Joint DoD/FAA/NASA Conference on Aging Aircraft, Ogden, Ut, 8–10 July.
7. Liguour, S., Perez, R. and Walters, K. (1997). Damped Composite Bonded Repairs for Acoustic Fatigue, AIAA Paper 97–1689 (A97–26775) 3rd AIAA/CGAS Aeronautics Conference, Atlanta, GA, May 12–14, pp. 774–783.
8. Goldsmith, N. (1998). Fatigue and Fracture Detection and Assessment Investigation Report. Examination of Cracked Panel from an FA-18 Fuselage. DSTO DDP-0316, August.
9. Hauge, E., Johson, P.S., Smith, D.L., *et al.* (1999). Durability Patch and Damage Dosimeter: A Portable Battery Powered Data Acquisition Computer and Durability Patch Design Process. The Third Joint FAA/DoD/NASA Conference on Aging Aircraft. Sept 20–23. Albuquerque, New Mexico.
10. Climent, H. and Casalengua, J. (1994). Application of a PSD Technique to Acoustic Fatigue Stress Calculations in Complex Structures. AGARD Symposium on Impact of Acoustic Loads on Aircraft Structures, Lillehammer, Norway, May.
11. Blakely MSC/NASTRAN, Basic Dynamics Analysis, User's Guide. The MacNeal-Schwendler Corporation, December 1993.
12. Wang, C.H. and Rose, L.R.F. (1999). A crack bridging model for bonded plates subjected to tension and bending. *Int. J. of Solids and Structures*, **36**, pp. 1985–2014.
13. Soovere, J. and Drake, M.L. (1985). Aerospace Structures Technology Damping Design Guide – Volume II: Design Guide, AFWAL-TR-84–3089.

14. Johnson, C.D. and Kienholz, D.A. (1982). Finite element prediction of damping in structures with constrained viscoelastic layers. *AIAA Journal*, **20**(9), September.
15. Chiu, W.K., Galea, S.C. and Callinan, R.J. (1998). Damping of Repaired Structures subject to acoustic fatigue: a numerical study. *Polymers and Polymer Composites*, **6**(3), pp. 133–142.
16. Newman, J.C. and Edwards, P.R. Short-Crack Growth Behaviour in Various Aircraft Materials. AGARD-12-767.
17. Hartman, A., Jacobs, F.A., Nederven, A., *et al.* (1967). Frequency Effect on 1 mm 7075-T6 Clad Sheet. NLR TR M 2182, May.
18. Byrne, K.P. (1972). Strains Affecting the Growth Rate of Edge Cracks in Acoustically Excited Panels. ISVR Tech. Rep. 59, November.
19. Schwarmann, L. (1988). Material Data of High-Strength Aluminium Alloys for Durability Evaluation of Structures. Aluminium-Verlag, Dusseldorf.
20. Anon. Soundcoat data sheets for Dyad 606 and 609.
21. Anon. FM300 Film adhesive. Manufactures data. Cytec Fiberite Inc. S. Barlow
22. Determination of F/A-18 Thermal Profile. Formal Report Task 00176. AR-009-066. July 1985.
23. Bohret, D. (2000). Acoustic fatigue testing of bare aluminium panels with boron/epoxy patch repairs. Aerostructures document ER-FA18-54-APM100, 19 June.
24. Bohret, D. (2000). Acoustic fatigue testing of bare aluminium panels with highly damped repairs. Aerostructures report ER-FA18-54-APM101, 29 June.
25. Bohret, D. (2000). Acoustic fatigue testing. Aerostructures report ER-FA18-54-APM086, 19 June.

Chapter 20

SMART PATCH SYSTEMS

S.C. GALEA

Defence Science and Technology Organisation, Air Vehicles Division, 506 Lorimer Street, Fishermans Bend, Victoria, 3207, Australia

20.1. Introduction

The application of bonded composite patches or doublers to repair or reinforce defective metallic structures is becoming recognised as a very effective and versatile repair procedure for many types of problems [1]. Various applications of this technology are discussed in Chapters 1 and 22, and include the repair of cracking, localised reinforcement after removal of corrosion damage and for reduction of fatigue strain. The bonded repair to the cracked metallic structure – crack patching – allows the restoration of strength and stiffness of the structure, as well as slowing crack growth by reducing stress intensity. The application of bonded composite patches to fix defective secondary structures has become routine in recent years. However, as stated in Chapters 21 and 22, the application of bonded composite repairs (CBR) to cracked primary structure is generally acceptable only on the basis that a margin on design limit-load (DLL) capability is retained if the repair fails (total absence) [2].

This is essentially the application of a fail-safe approach, viz.:

- When a cracked single-load-path component maintains sufficient residual strength to withstand DLL times a safety factor (often 1.2). In this case regular inspection is required, to ensure that the critical crack length for failure at this stress is not exceeded, based on the predicted growth rate for the *unpatched crack*.
- When a redundant (multiple) load path component can withstand DLL times the safety factor if the cracked path has failed. This is a standard procedure now for such structures so should not pose any particular problems. In this case inspection is required to ensure that the alternate load path is not cracked to the extent that it would not withstand the elevated stress.

The conservative approach in the single load path case eliminates the possibility of repairing a crack already above critical size or a small crack with high growth rate. However, as discussed in Chapter 27, a repair to a crack greater than critical size was undertaken in Australia to the lower wing skin of an F111 aircraft, following an extensive certification program [2,3]. To certify the repair a substantial analysis and testing program, to ascertain (1) residual strengths, (2) damage tolerance and (3) durability, was required.

In single load-path cases the inspection requirement based on growth of the unpatched crack may be acceptable where the initial crack size is small (or non-existent, for example in the case of a preventative doubler rather than a patch). However, there will be many repairs, for example those with cracks approaching critical size, where this inspection requirement will not be cost-effective. The repair can then be undertaken only by accounting for the restoration of residual strength and reduction of the rate of crack growth provided by the reinforcement. That is when the cracked/patched structure can be managed as on a slow crack growth or damage tolerant basis. Essentially, as discussed in Chapter 22, there is a need to prove that the cracked/patched structure meets damage tolerance requirements – this includes slow crack growth, even if the original structure was designed on a safe-life basis.

Assuming that the static requirements are satisfied, then full credit for the patch in slowing crack growth could be justified by:

1. *Safe life approach in safe-life zone*: Based on demonstrating that strains are below threshold in the safe life zone

PLUS

2. *Damage tolerance approach in damage tolerance zone*: Based on predictable slow disbond growth.

OR

3. *Continuous safety by inspection approach*: Based on self-assessment of the patch system integrity using the “smart patch” approach [2,4].

Figure 20.1 illustrates the safe-life and damage tolerant zones at the ends and in the middle, respectively, of a generic patch.

The aim of the “smart patch” approach is for continuous monitoring of patch performance to ensure that load transfer is maintained. That is, the basic form of this concept will incorporate in-situ sensors to monitor in-service the structural condition (health or well-being) of the patch system and the status of the remaining damage in the parent structure. The need to follow the correct patch design and process procedures is unchanged. The smart approach simply allows a relaxation of the probability of failure requirements, particularly in relation to environmental degradation. However, it must be stated from the outset that the viability of any smart approach now depends on establishing its reliability or probability of detection – which is similar to the problem of probability of detection in non-destructive inspection (NDI). Certainly self-checking and significant redundancy would have to be included in the system to provide the required level of confidence.

“Smart patch” approaches are technically feasible but will be economically viable only for repairs to very significant and costly primary structure. For

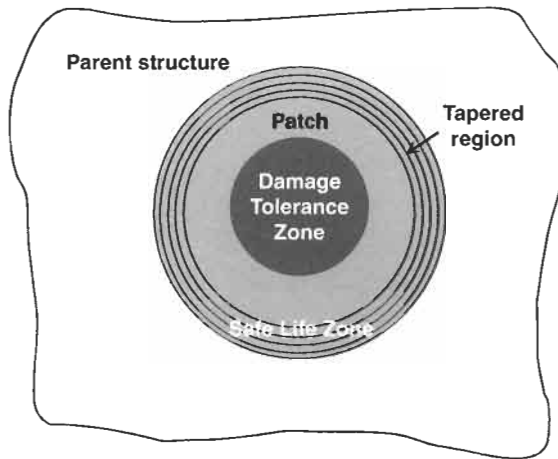


Fig. 20.1. Schematic of a generic external bonded repair showing safe-life zone (no disbonding allowed in this zone) and damage tolerant zone (stable disbonding growth allowed in this zone) [2].

certification and management of critical repairs for very high cost components, this approach may be an acceptable solution from the airworthiness perspective by allowing some relaxation of the certification requirements. This technology should also allow operators to move away from current costly time-based maintenance procedures toward real-time health condition monitoring of the bonded repair and the repaired structure – thus allowing a more cost effective methodology for managing critical structures. These systems would allow timely decisions on preventative and scheduled maintenance before failure of the repair or repaired structure.

This chapter focuses on various issues associated with the development and implementation of the smart patch concept. Section 20.2 outlines a background to the smart patch approach. Section 20.3 gives an overview of a number of *in situ* damage detection studies, undertaken by DSTO, applied to CBR systems. A laboratory concept demonstration of the smart patch system, using two types of skin doubler specimens, is described in Section 20.4. Section 20.5 describes the development of a system for an in-flight demonstration of the smart patch on an F/A-18 aileron hinge. The smart patch systems developed to-date, comprises of fully self-contained remotely-interrogated miniaturised sensor signal conditioning and data acquisition electronic hardware, attached in close proximity to sensors on a repair, for storing recent in-flight readings of patch health.

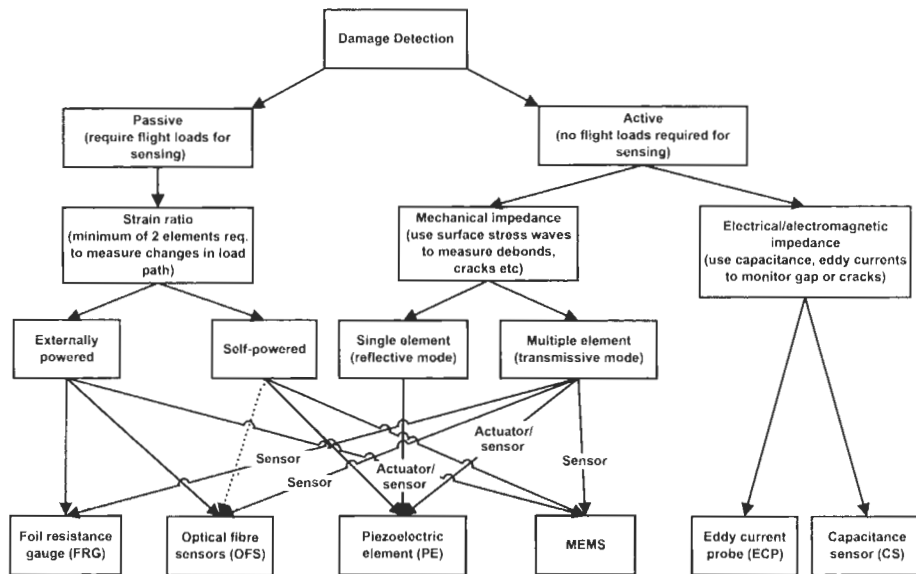
20.2. Smart patch approach

The generic patch system, shown in Figure 20.1, consists of (1) a safe life region where disbands in the adhesive grow rapidly, leading to repair failure, and (2) a

damage tolerant region of the patch system over the damaged parent region where limited disbond growth is acceptable since growth is generally stable [2]. Therefore the specific objectives of the smart patch or in-situ patch-health monitoring system, are to detect disbond growth in the safe life zone of the patch (which is unacceptable) and monitor damage growth in the parent material (below the damage tolerance zone), i.e. delaminations for composites or cracks for metals. Current research, at the DSTO and the DSTO-Centre of Expertise for Structural Mechanics [5,6], is focused on the development and assessment of new sensing techniques and sensors, which may be incorporated in bonded repair systems, to detect and monitor (1) disbonds in the adhesive layer, (2) delaminations in the patch system, (3) quality of the bond [7] and (4) crack growth rates in the underlying metallic substrate [8].

The detection technique chosen for the smart patch system will depend on a number of factors including, area of detection, numbers of transducers available, on-line/off-line capability, power requirements and, system complexity, reliability, robustness, sensitivity and accuracy. Some techniques are more amenable to wide field interrogation, such as acousto-ultrasonic or stress-wave based techniques, whereas some techniques need to be located in the region of interest, such as in-situ eddy current and strain based techniques. Some of the “passive sensory” smart structure techniques [5,6] would require real-time interrogation during flight (on-line) whereas the “active sensory” techniques can be activated on demand (off-line) at the operator’s convenience. In order for in-situ health monitoring to be accepted and implemented an approach that achieves acceptable redundancy, reliability and probability of detection, would be required. Therefore it is envisaged that systems including a variety of sensors and damage sensing techniques would assist in facilitating both airworthiness and operator acceptance. The sensing techniques currently being considered for health monitoring of composite patch systems are (1) strain sensing (load transfer monitoring) using electrical-resistance foil strain gauges [8,9,10], piezoelectric film sensors [10,11,12] and optical fibres [13–17] (ideally embedded, for robustness, in the composite patch or more simply bonded to its surface), (2) residual strain monitoring using electrical-resistance foil strain gauges [6,8] and optical fibre sensors, (3) the electro-mechanical impedance, transfer function and stress wave techniques using low profile piezotransducer elements [6,18–20] and (4) embedded bond degradation sensors using MEMS-based sensors [7]. These techniques are discussed in more detail in Section 20.3. The other major issue is the power supply, which is closely interrelated with the choice of sensor (and actuator) and damage detection technique used. Figure 20.2 illustrates possible power sources associated with some more promising combinations of sensors/actuators and damage detection techniques being investigated.

The most direct approach, currently adopted by DSTO, to assess the “health” of the patch system is to measure the level of load transfer in the safe-life zone. This is achieved by monitoring the ratio of strains at the ends of the tapered region to those away from the patch. Any decrease in this ratio is an indication of disbonding of the patch in this critical region. In this approach there is no requirement for measurement of the actual loading; disbonding is indicated by the reduction in



Source	Device	Storage	Transducer					
			FRG	OFS	PE	ECP	CS	MEMS
aircraft power			Y	Y	Y	Y	Y	Y
manufacture time		primary cell	Y	Y	Y	Y	Y	Y
strain energy	PZT	capacitor/secondary cell	N	N	Y	Y	Y	Y
interrogator	RF	capacitor/secondary cell	N	(Y)	Y	Y	Y	Y
solar	PV	capacitor/secondary cell	Y	(Y)	Y	Y	Y	Y

Fig. 20.2. Flow diagram showing some promising damage detection techniques, with possible corresponding transducers and power sources (MEMS – Micro-electro-mechanical systems).

relative strain. Ideally, the sensors are automatically monitored by an on-board miniaturised system, which would provide a warning (e.g. via a wireless link) should the indication of disbonding become significant, as shown schematically in Figure 20.3. This could be combined with the damage-tolerance approach in the cracked region or alternatively the “smart” capability could also include monitoring of crack and disbond growth.

An important early potential application was in the large (120 + ply) boron/epoxy (b/ep) doubler reinforcement for the wing pivot fitting (WPF) of Australian F-111 aircraft (Figure 20.4). Fatigue cracks can initiate in the upper-skin of the F-111 wing pivot fitting (WPF) stiffener runout region shown in Figure 20.4(a). A strain reduction of over 30% is required in this region to avoid plastic yielding during cold proof load testing (CPLT), [21] and also to increase the in-service

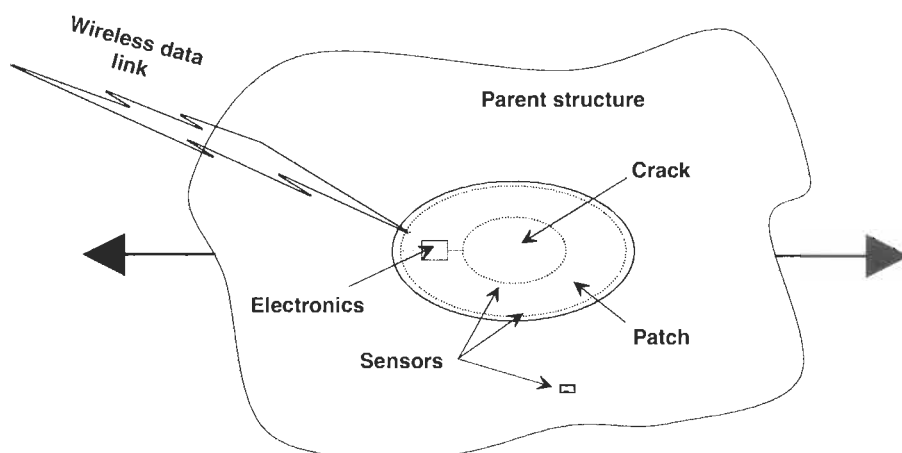
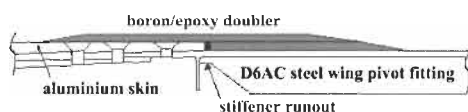
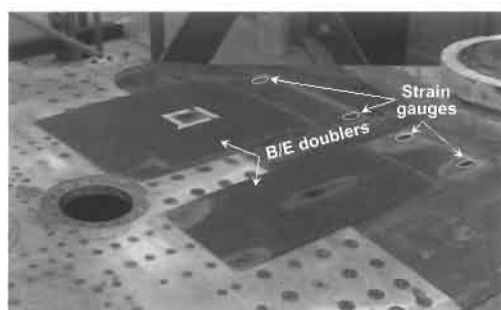
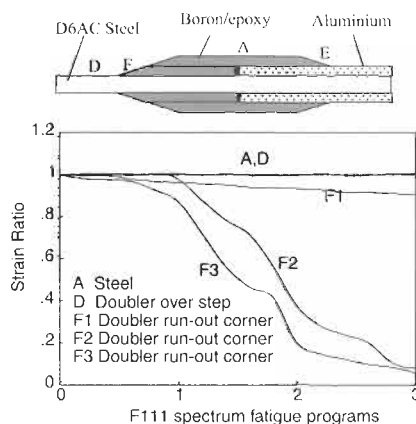


Fig. 20.3. Schematic of the smart patch concept.



(a)



(b)

Fig. 20.4. (a) (top) Photograph of b/ep doublers on an F-111 with the location of resistance-foil strain gauges for doubler health monitoring and (bottom) schematic showing location of critical area and the 120 ply thick doubler [9]. (b) Plot of strain ratio reduction due to disbond growth as a result of fatigue cycling (bottom) and representative bonded joint specimen showing strain gauge positions (top). The F gauge results plotted are on the corners of the doubler [9].

inspection interval. The required strain reduction is particularly challenging because of the thick steel structure and high loading and was achieved by designing and implementing b/ep doublers, as depicted in Figure 20.4(a) (see Chapter 29) [9,22]. The approach taken to monitor patch health was to apply resistance-foil strain gauges (see Figure 20.4(b)) on the ends of the tapered section of the b/ep doubler and on the surface of the steel WPF away from the doubler and monitor the ratio (doubler strains) / (strain in the steel fitting) during service life. Any decrease in this ratio is an indication of disbonding of the doubler. Figure 20.4(b) shows results obtained from tests on F-111 representative bonded joint specimens (representing a section through the doubler) subjected to CPLT loads and the F-111 loading spectrum. Disbonding is indicated by the reduction in relative strain, where disbands initiated and grew mainly from the corners of the doubler and growth was very much less in the centre. In the aircraft doubler system the sides are tapered normal to the doubler axis, so stress concentrations in these corners will be much less severe; however, the results amply demonstrate the effectiveness of the monitoring approach proposed. This early attempt at in-service monitoring of the doubler gauges, although highly effective for aircraft undergoing the CPLT, proved too cumbersome for in-flight use (but should be possible with the current “smart patch” approach). A similar approach is being used to monitor the structural integrity of a large (5 m × 1 m) 6 mm thick doubler used to reduce cracking around welds in the aluminium deck of an Royal Australian Navy Frigate as described in Chapter 42 [23].

The objective is to develop an autonomous remotely-accessed patch health monitoring (smart patch) system. To facilitate rapid acceptance of these systems by the operators and certification authorities, the systems need to be fully autonomous with wireless access. The wireless feature will assist in allowing this smart patch concept to gain acceptance in practice, since wiring associated with the sensors, actuators and instrumentation will be difficult, if not impossible, to implement on real aircraft structures without OEM approval. This approach will allow smart patch systems to be incorporated in “difficult-to-access” locations. The long-term goal is to achieve maintenance free devices by incorporating a wireless and *self-powering* capability within the systems. These low maintenance wireless systems will enable minimum interruption to relatively rigid and well-established logistic and maintenance procedures associated with ageing aircraft. This approach will allow easier acceptance by the operator and logistic support staff and incur minimum additional through-life-support costs. As stated above these systems are initially aimed at high value applications; this is because initial systems may be expensive to manufacture and install. In the future, the miniaturisation of such systems should lead to reductions in the costs of manufacture and installation enabling application of this technology to a wide range of secondary bonded structural applications.

20.3. Damage detection studies

20.3.1. Load transfer (strain) technique

Piezoelectric films. Figure 20.4(b) shows the results using conventional resistance-foil strain gauges on an F-111 representative bonded joint (skin doubler) specimen. Similar experimental results were achieved on other skin doubler specimens, shown in Figure 20.5, using both resistance-foil strain gauges and piezoelectric film sensors. These specimens reflect the important structural features around region E of the representative bonded joint specimen shown in Figure 20.4(b). In this case both resistance-foil strain gauges and 28 μm thick piezoelectric polyvinylidene fluoride (PVDF) film sensors were used to detect and monitor damage growth in the tapered region of the bonded doubler.

Sensors were located on the taper of the b/ep doubler and on the surface of the aluminium inner adherend, away from the doubler, (sensors A and C, respectively, in Figure 20.5(a)) in order to monitor the ratio (doubler strains) / (strain in the far-field). Any decrease in this ratio is an indication of disbonding of the doubler. A notable advantage of this approach is that there is no requirement to measure the actual loading. In these studies the piezofilm sensor was used in a manner similar to that for the resistance-foil strain gauge: by monitoring (loss of) load transfer over the tapered region of the patch. However, in the piezofilm case, the sensing area was generally much larger compared to the resistance-foil strain gauge, thus this sensor monitors damage progress over a larger area. In this case a 10 mm by 10 mm sensor was used on the first two steps of the doubler (sensor A in Figure 20.5(a)) [12]. The specimen used in this study was a skin-doubler (SD) Type I specimen consisting of a 3.13 mm thick aluminium inner adherend with tapered 29 ply unidirectional b/ep doublers bonded to each side to retain symmetry as shown in Figure 20.5(a). The doublers are bonded to the aluminium substrate using FM73 epoxy structural adhesive. The boron doublers were tapered at a step-up rate of two plies every 4 mm, with the first step consisting of a single ply. The uniaxial loading was applied at a frequency of about 4 Hz.

Another approach using PVDF sensors was to place the sensor over the edge of the patch, as indicated by sensor B in Figure 20.5(a) [6]. This approach uses the fact that as the disbond between the patch and the aluminium adherend initiates and grows there is an increase in relative movement between the edge of the patch and the adherend. Therefore a piezofilm sensor placed across this region detects disbonding by monitoring an increase in strain. In this study a 7 mm by 4 mm sensor was placed over the patch edge, at a location indicated by sensor B in Figure 20.5(a). However, in this case, the specimen used was a skin-doubler (SD) Type II specimen consisting of a 6.4 mm thick aluminium inner adherend with tapered 11 ply unidirectional b/ep doublers bonded to each side to retain symmetry as shown in Figure 20.5(b). As for the previous specimen, the doublers were bonded using FM73 epoxy structural adhesive. This specimen had a similar ply drop off rate as the Type I specimen. The uniaxial loading was applied at a frequency of about 3 Hz. A more detailed description of the specimen and experimental set-up is given in Chapter 5.

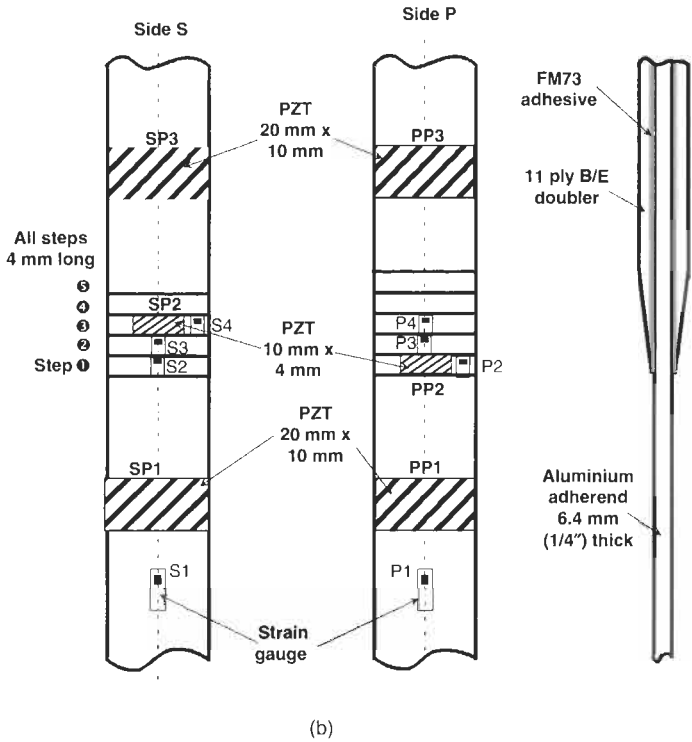
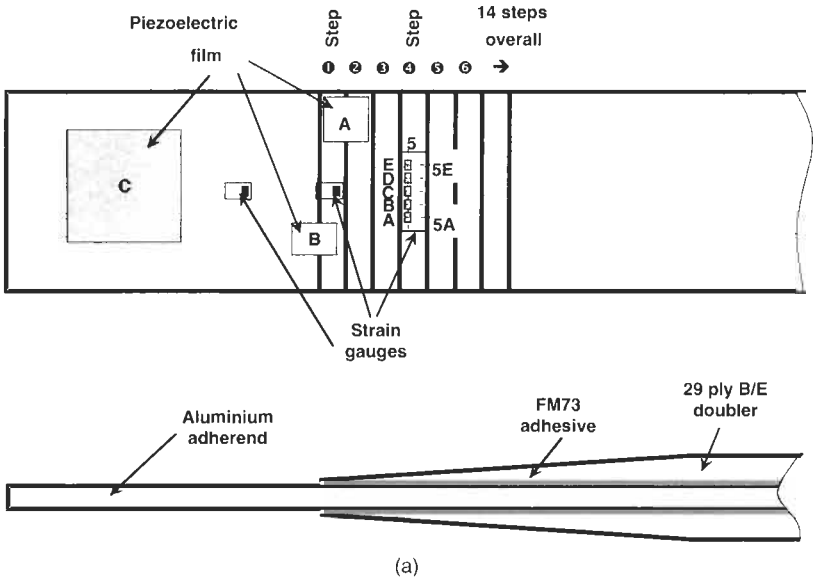


Fig. 20.5. Schematic of skin-doubler (SD) specimens with transducer locations for (a) Type I specimen and (b) Type II specimen.

Figure 20.6(a) and (b) shows the piezofilm response with increasing loading cycles. In Figure 20.6(a) disbond growth under the sensor was indicated by a significant reduction in piezoelectric film voltage ratio (sensor A / sensor C), which correlates well with the resistance-foil strain ratio results. Figure 20.6(b) shows the results for the piezofilm sensor when positioned over the patch edge, and indicates a significant increase in sensor output (approx 60% increase in signal compared to the non-damaged case) due to the presence of damage. The magnitude of the increase in sensor signal will depend on the relative proportion of the sensor area over the patch edge compared to the total sensor area. As indicated in this figure, this technique detects disbond initiation, and reaches a maximum sensor output well before the resistance-foil strain gauge detects any sign of damage – as would be expected.

The piezoelectric film sensors have the advantage of not requiring power to function and may be manufactured to suit any size, geometry and substrate curvature. Note also that, better sensitivity would be achieved using piezofilm sensors manufactured to cover smaller areas of critical regions. These sensors were also tested under hot/wet conditions where it was found that their environmental durability was very good although they were sensitive to damage from rough handling – thus handling, sealing and assembly (wiring) need to be considered carefully if implementing such sensors in practical applications [12].

Bragg grating optical fibre sensors

An optical fibre-based intrinsic distributed sensing technique, viz. fibre bragg grating (FBG), was used here to monitor damage in composite bonded patch systems. A FBG sensor consists of a periodic modulation of the core refractive index of an optical fibre. Such a sensor is fabricated by forming defect sites in the glass matrix through exposure to intense UV light [24]. The effect of this periodic refractive index variation on propagating light is to reflect a narrow band of wavelengths back down the fibre, as is illustrated in Figure 20.7. The peak wavelength of this reflected light is the Bragg wavelength of the grating (λ_B) and is given by

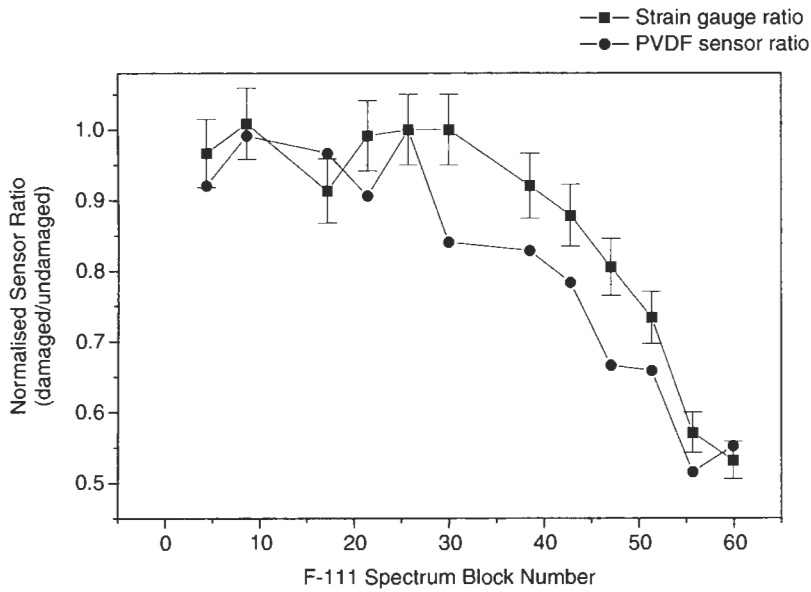
Eq. (20.1):

$$\lambda_B = 2n\Lambda , \quad (20.1)$$

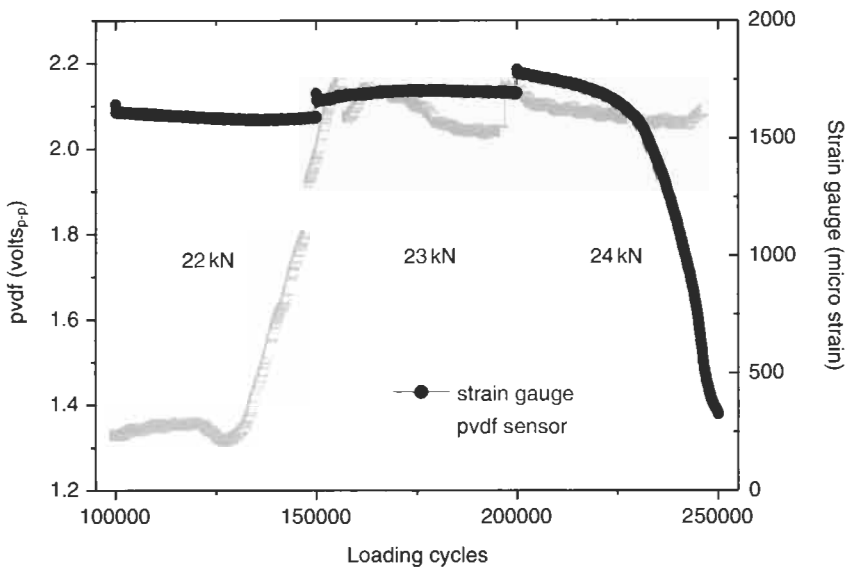
where n is the effective core refractive index of the fibre and Λ is the period of the grating.

Temperature and strain both influence the Bragg wavelength as they affect the physical properties of the fibre, resulting in changes to the refractive index and the period of the grating. The wavelength shift $\Delta\lambda_{BS}$, for an applied longitudinal strain $\Delta\epsilon$ is given by:

$$\Delta\lambda_{BS} = \lambda_B(1 - p_x)\Delta\epsilon , \quad (20.2)$$



(a)



(b)

Fig. 20.6. Results for piezoelectric film sensors and resistance-foil strain gauges on skin doubler Type I specimen: (a) Sensor ratio A/C and (b) Sensor B (see Fig. 20.5(a)).

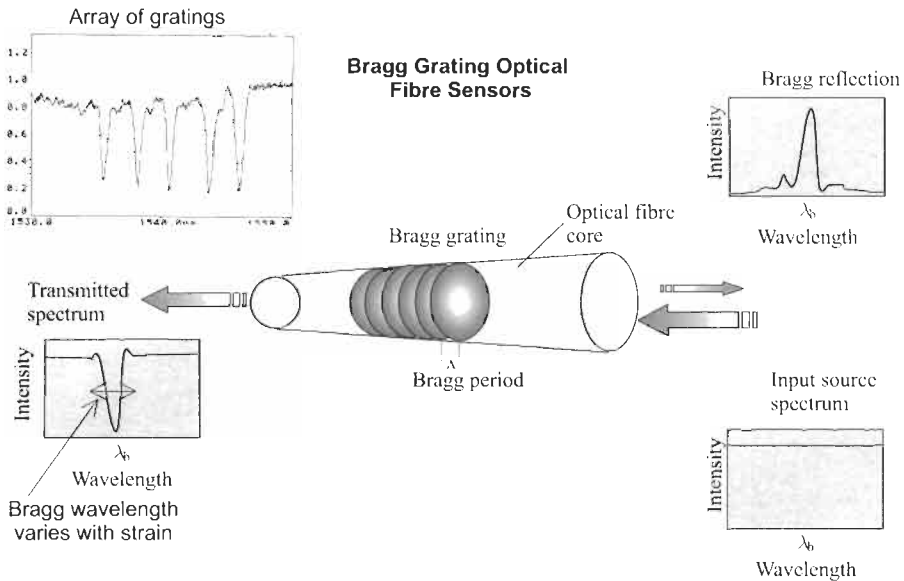


Fig. 20.7. Schematic of a fibre Bragg grating.

where p_x is the photo elastic coefficient of the fibre and is given by:

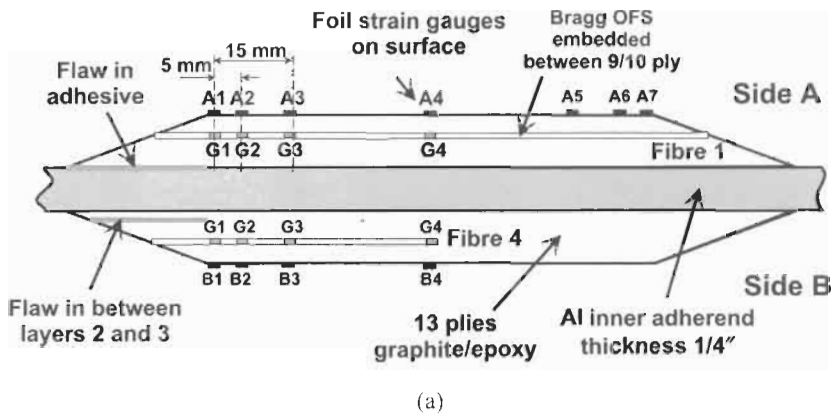
$$p_x = \frac{n^2}{2[p_{12} - \nu(p_{11} - p_{12})]} \quad (20.3)$$

where p_{11} and p_{12} are the components of the fibre optic strain tensor and ν is Poisson's ratio. Similarly for a temperature change of ΔT , the corresponding wavelength shift is given by:

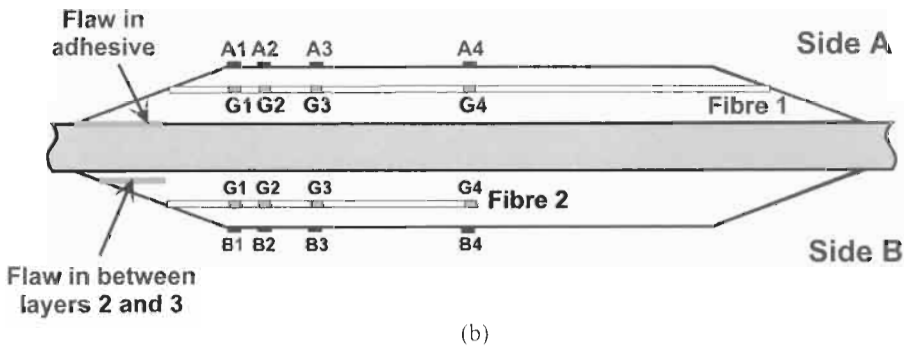
$$\Delta\lambda_{BT} = \lambda_B(1 + \xi)\Delta T \quad (20.4)$$

where ξ is the fibre thermo-optic coefficient. For silica fibre, the wavelength sensitivities of a FBG with λ_B of $1.55\mu\text{m}$ have been measured as $1.15\mu\text{m}/\mu\epsilon$ and $13\mu\text{m}/^\circ\text{C}$ [25].

A theoretical and experimental study on the use of embedded FBG sensors in measuring strains and structural-health of bonded composite repairs was reported on in [6,15]. The specimens and sensor positions, considered in these studies, are shown in Figure 20.8. The specimen consisted of a 6.35 mm thick aluminium inner adherend with two 140 mm long 13 ply graphite/epoxy (gr/ep) doublers with the tapered ends consisting of a ply drop-off of 3 mm/step. A 0.2 mm thick layer of Hysol EA 9320, room temperature curing, adhesive was used to bond the reinforcements onto the aluminium. There are two artificial damage regions within the specimen, one is in the adhesive/aluminium interface within the tapered region of the reinforcement (on side A), which is referred to as a disbond, and the other is between plies two and three of the patch within the tapered region (on side B),



(a)



(b)

Fig. 20.8. Schematic showing specimen details and position of sensors for specimen (a) TTCP 1 and (b) TTCP 2.

which is referred to as a delamination (see Figure 20.8). Specimen TTCP one and two had disbonds and delaminations along the full length and half-length of the taper (about 41 mm and 18 mm long), respectively. Figure 20.8 also shows the locations of FBGs, between the 9th and 10th plies, and surface mounted conventional strain gauges. The grating lengths (i.e. the sensing lengths) were typically 3–4 mm long and the surface mounted resistance-foil gauges were 2 mm long. The experimental program consisted of strain surveys conducted under static-loading. These strain measurements were then compared to finite element predictions. Finally, a fatigue study was undertaken to evaluate the performance of these sensors in monitoring damage growth.

Figure 20.9(a) and (b) shows a comparison between the measurements taken from fibres four and one, respectively, and corresponding surface strain gauges with increasing applied load for specimen TTCP 1. All gratings of fibre four showed positive linear responses, increasing in magnitude from grating G1 to grating G4. Good agreement was observed between sensors B4 and G4. Note that, each corresponding pair of sensors, at positions 1, 2 and 3, (i.e. B1/G1, B2/G2 and

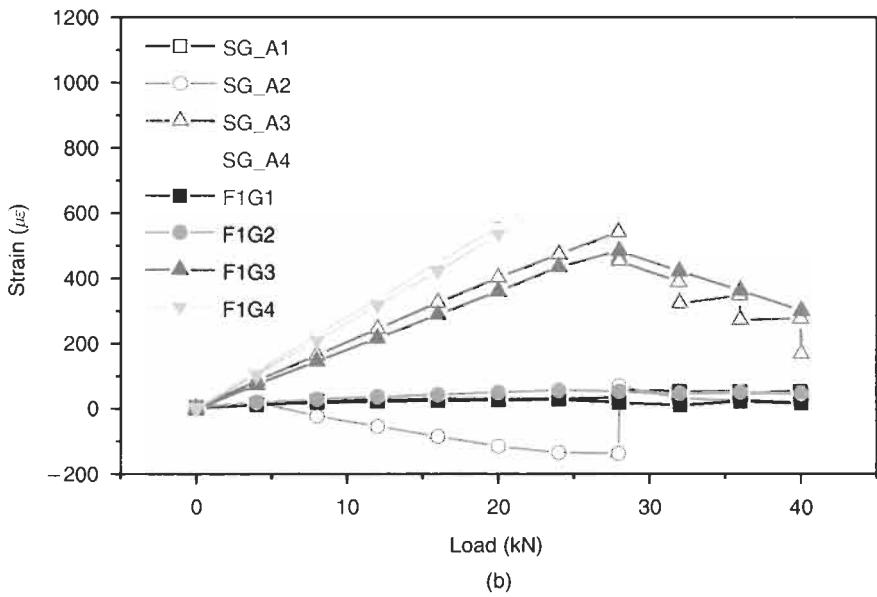
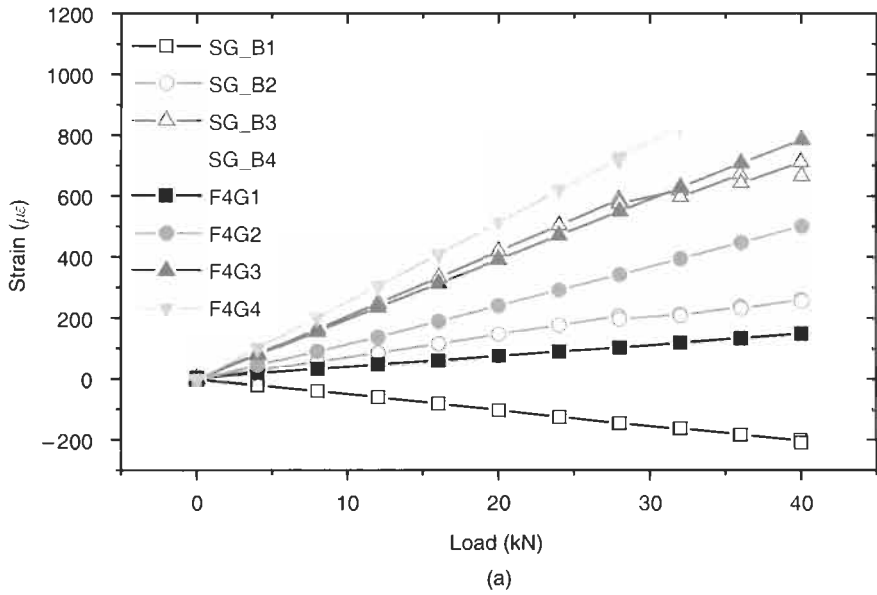


Fig. 20.9. Response of FBG from (a) fibre 4 and (b) fibre 1, with corresponding surface gauge measurements, with increasing loads for specimen TTCP 1.

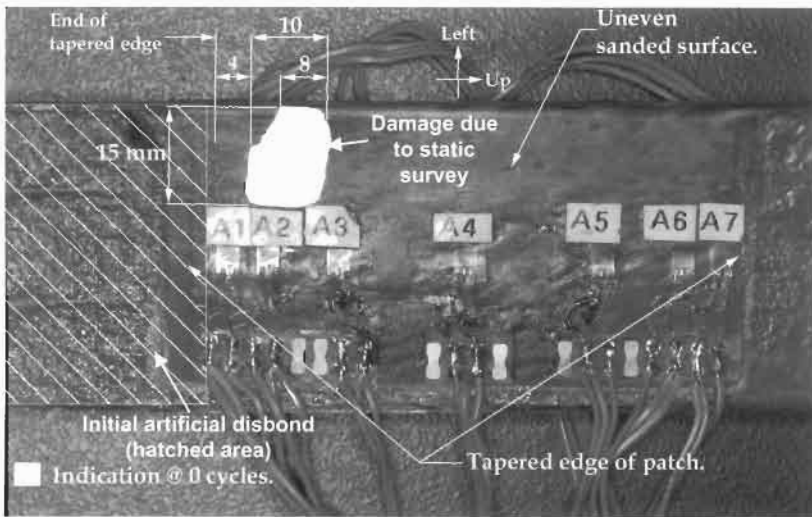


Fig. 20.10. Damage indicated by the ultrasonic A-scan of specimen TTCP 1 after the static strain survey.

B3/G3, respectively) showed a higher response for the Bragg grating than for the surface strain gauge – this was due to the shear lag effect. Although not shown here, similar trends were observed for gratings G1, G2 and G3 of fibre two compared to gauges A7, A6 and A5 respectively for specimen TTCP 1 at the non-damaged end [15]. For fibre one (see Figure 20.9(b)), gratings G1 and G2 showed little response, consistent with the response at surface gauge A1, since no load has yet been picked up by the patch due to the presence of the artificial disbond. Grating G3 showed a significant reduction in response at 28 kN, consistent with the response of gauges A2 and A3. This drop in signal (and hence-forth a null response) when the load exceeded 28 kN is indicative of the formation of a disbond, in the adhesive layer, located outside the initial artificial disbond under sensors A2/G2 and A3/G3. These observations were confirmed by an NDI examination consisting of manual ultrasonic A-scans in this region, as shown in Figure 20.10.

The fatigue study also showed that embedded FBGs could easily monitor damage in the adhesive layer of a bonded composite patch specimen. Figure 20.11 shows the strain response of gratings in fibre two, on side B of specimen TTCP 2. This figure illustrates the excellent sensitivity of embedded FBGs in monitoring damage growth. These results confirm the ability of strain measurements within the reinforcement (as a measure of load transfer) to reflect damage growth in high load transfer regions of composite bonded repairs.

Measured surface and embedded sensor strains were also compared with predicted strains. In this case specimen TTCP 1, shown in Figure 20.8(a), was modelled by an elastic stress analysis using the linear static analysis code of MSC.NASTRAN. Figure 20.12 shows the predicted and measured longitudinal strains on side A for a static load of 24 kN (before the disbond propagated) for the

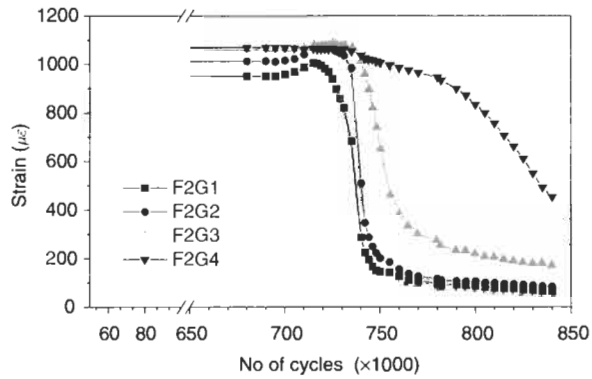


Fig. 20.11. Strain response of Bragg gratings of fibre 2 (at 40 kN), on Side B of specimen TTCP 2, with increasing number of applied loading cycles.

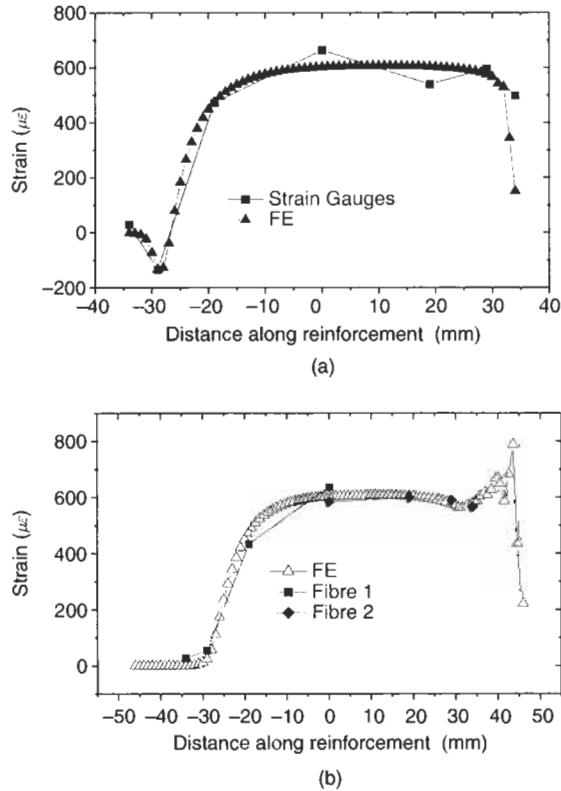


Fig. 20.12. Comparison of measured and predicted FEA strains, from (a) surface mounted strain gauges and (b) Bragg grating optical sensors embedded between the 9th and 10th plies, for a load case of 24 kN and for an initial disbond length of 41 mm on side A of specimen TTCP 1.

first strain survey. The maximum predicted value of strain on sides A and B compares reasonably well with the measured values from both the surface gauges and the Bragg gratings. Figure 20.12 shows the excellent correlation between the measured and predicted longitudinal strains at both the surface and 9th/10th ply interface. In general, the measurements from the surface electrical-resistance foil strain gauges and the embedded FBG sensors correlated well with the finite element analysis. In conclusion, these results indicate that the embedded FBG measure, with reasonable accuracy, the longitudinal strain in a composite patch.

One cautionary note, however, is that the measurement of strain from the Bragg grating spectral response can be complicated when the grating is located in regions of high strain gradients. These high strain gradients can substantially distort the Bragg reflected spectral shape, thus leading to strain conditioning problems with certain demodulation techniques. However, such distortion to the spectra can be minimised by the use of short gratings, and where possible apodising the grating to suppress sidelobe structure. This distortion can be clearly seen in Figure 20.13, which shows the response for an array of gratings in a fibre surface mounted on a bonded composite repair (i.e. a repair to a cracked aluminium skin as shown in Figure 20.15(a)). The fibre is placed perpendicular to the direction of crack growth and the sensor with the spectrum with the lowest Bragg wavelength (i.e. peak on the left in Figure 20.13(a) and (b)) is located over the crack (see sensor 7 in Figure 20.15(c)). The broadening of the response and the appearance of sub-peaks reflects a chirping of the grating caused by high strain gradients (due to severe local secondary bending) induced by the crack. In this case what was originally a fairly standard Bragg reflection spectra (Figure 20.13(a)) has become a complex spectra containing multiple peaks (Figure 20.13(b)). Such complex spectra are poorly handled by standard Bragg grating interrogation instruments, which typically rely on simple peak detection algorithms (viz. zero crossing of the reflected Bragg wavelength spectra). However, this feature could be exploited to enable optic fibre technology to monitor delamination under the patch [5,16].

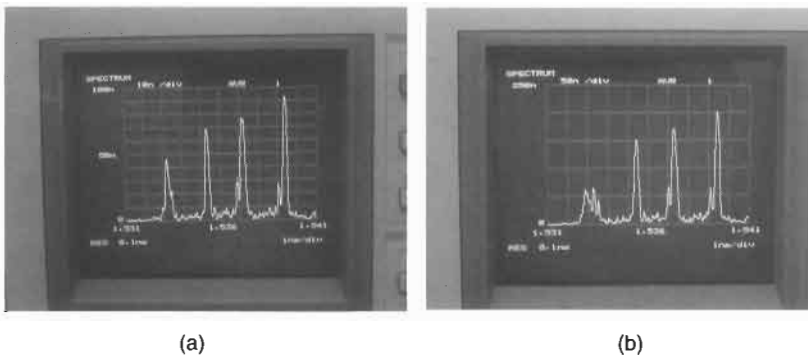


Fig. 20.13. Optical spectra from an array of Bragg gratings (a) before and (b) after the crack passed under the sensor.

20.3.2. Residual strain technique

This section discusses the use of residual strains within the patch system as an in-situ health monitoring technique. This passive technique relies on the fact that when a composite repair is applied to a metallic substrate the difference in the coefficient of thermal expansion (CTE) between the composite and the metal results in significant residual thermal stresses in the patch system at room temperature (see Chapter 11). Disbonding or damage in the patching system should lead to a redistribution of the residual strains. Therefore monitoring the residual strains in the component gives an indication of the presence of damage. The magnitude of the change in residual strains depends on the type, severity and location of damage, the curing temperature, the relative stiffness between the patch and the substrate, and the differences between the CTE of the patch and the substrate.

To illustrate this technique strain measurements were undertaken during the fatigue studies on skin-doubler specimens Types I and II, see Figure 20.5(a) and (b) [6]. The doublers are bonded to the aluminium substrate using FM73 epoxy structural adhesive at a cure temperature of 80 °C, respectively. Figure 20.14(a) and (b) show the residual strain (strain at zero load) response, with increasing number of loading cycles, measured using resistance-foil strain gauges, 5A and 5E, on the 4th step of Type I specimen (Figure 20.14(a)), and, P3, on the 2nd step of Type II specimen (Figure 20.14(b)). Both figures show an increase in residual strain due to the disbonding process, reaching a constant level of about 300 and 400 $\mu\epsilon$, respectively. The higher value of residual strain for the sensor on the 2nd step compared to sensors on the 4th step is due to the high stiffness of the aluminium substrate compared to the patch at these locations. Consequently, higher residual strains, and hence better sensitivity, to disbonds is expected for regions on the outer, thinner, portion of the patch. The strain levels measured in these studies can be easily detected using either optical fibre sensors or resistance-foil strain gauges. Therefore, it appears that these studies illustrate the feasibility of residual strain measurements as an alternative method of monitoring patch health.

Residual strains were also successfully used to detect and monitor fatigue cracks in the metallic substructure of patched-cracked specimens. The experimental program was conducted on similar cracked-patched specimens to that used for the b/ep patching efficiency studies discussed in Chapter 13. The cracked-patched specimens consist of two 3.14 mm thick 2024 T3 skins with 10 mm long starting cracks. These specimens were repaired with unidirectional boron/epoxy 7 ply (0.9 mm) thick semicircular patches. A layer of FM 73 film adhesive was co-cured onto the boron/epoxy bonding surface. The patches were then bonded onto the aluminum cracked skin with adhesive FM 73 at 120 °C, following surface treatment of the metal using the silane process and of the boron/epoxy patches by blasting with alumina grit on the co-cured adhesive layer [1]. The aluminium skins were tested in a back-to-back honeycomb sandwich arrangement by bonding each skin onto aluminium honeycomb as shown in Figure 20.15(a). More details on this specimen can be found in Chapter 13.

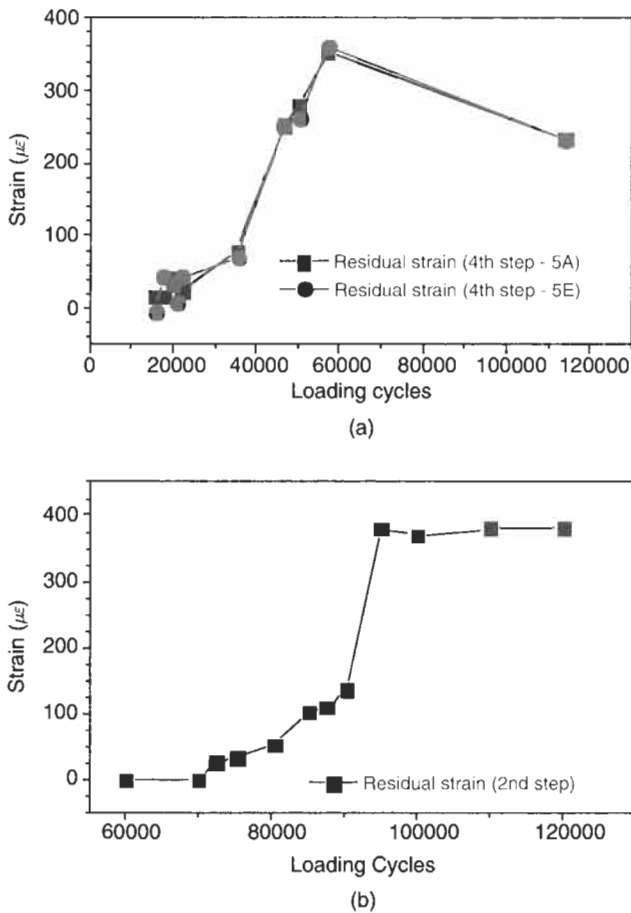
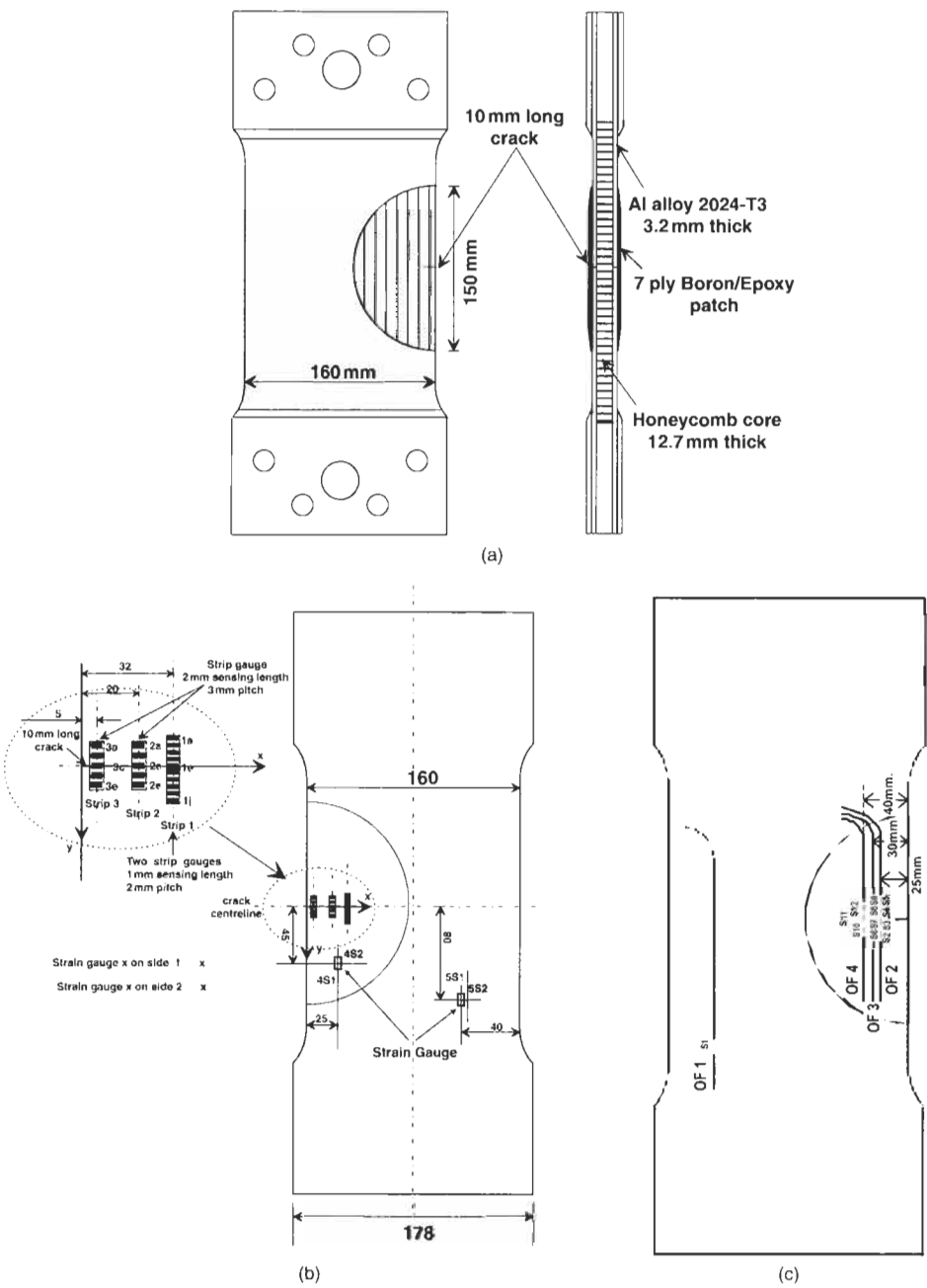


Fig. 20.14. Variation of residual strains in the tapered region of a patch with increasing number of loading cycles for sensors: (a) 5A and 5E on the 4th step of skin-doubler specimen Type I and (b) P3 on the 2nd step of skin-doubler specimen Type II.

In order to study the surface strain behaviour of the patch as the crack grows, strain gauges and optical fibres were attached as shown in Figure 20.15(b) and (c), respectively. One specimen had resistance-foil strip gauges attached at three x stations along the crack centreline (see Figure 20.15(b)). The strain gauge strips 1, 2 and 3 were located at 32 mm ($x = 32$), 20 mm and 5 mm from the specimen edge, respectively. The centreline of each strip of gauges was aligned perpendicular to the crack centreline. The second specimen had an array of FBG sensors on four optical fibres OF1 – OF4 attached as shown in Figure 20.15(c). OF1 contained a single far-field sensor, S1, and was bonded to the aluminium skin using a cyno-acrylate adhesive. The remaining three optical fibres, containing sensors S2–S12, were bonded to the top surface of the repair also using a cyno-acrylate adhesive. Sensors



S2–S5, S6–S9 and S10–S12 were located in OF2, 3 and 4, respectively. These fibres were aligned perpendicular to the crack centreline and located 25, 30 and 40 mm from the specimen edge, respectively. The fibres were completely buried beneath a thick layer of room temperature curing adhesive so as to protect the optical fibres and to also provide a smooth surface for eddy current measurement of the crack length.

The strains measured at zero load (residual strains) are shown in Figure 20.16(a), for resistance-foil strain strip gauge 1 at $x = 32$ mm (sensors 1d and 1i) and in Figure 20.16(b) for OF3 at $x = 30$ mm (sensors S6–S9). These figures show the significant variation in residual strains as the crack progresses past the sensors. Note that the strains presented here are not the absolute residual strains, since they do not contain the baseline component of residual (thermal) strains due to bonding

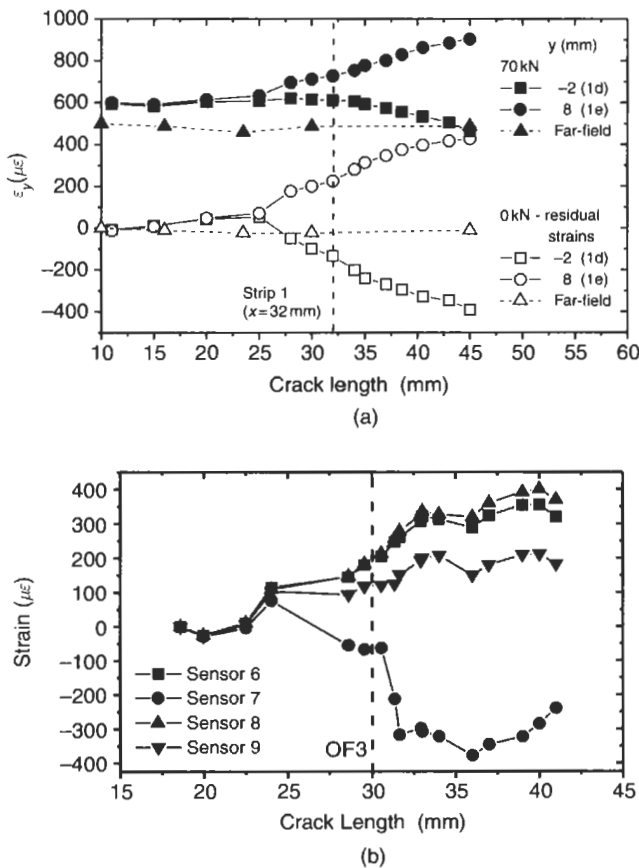


Fig. 20.16. Variation of (relative) residual strain, with increasing crack length, measured by (a) resistance-foil strip strain gauges 1d and 1i at $x = 32$ mm (see 0 kN load case) and (b) FBG sensors six to nine on OF three at $x = 30$ mm.

of the patch onto the aluminium skin, but reflect the relative change in residual strain in the patch as the crack propagates. As previously mentioned, this change is believed to be caused by the redistribution of residual thermal strains as the crack propagates under the patch – hence these effects are limited to the immediate vicinity of the crack. A similar redistribution of residual thermal strains is observed in composite laminates in response to an impact event. The change in residual strain appears to mimic the surface strain distribution observed under load, for the same damage state condition. This can be observed in Figure 20.17 where the spatial distributions of residual strains and strains measured at a 70 kN load, Figure 20.17(a) and (b) respectively, produce similar distributions. That is, the sensors over the crack show negative strains while those above and below the crack show positive strains.

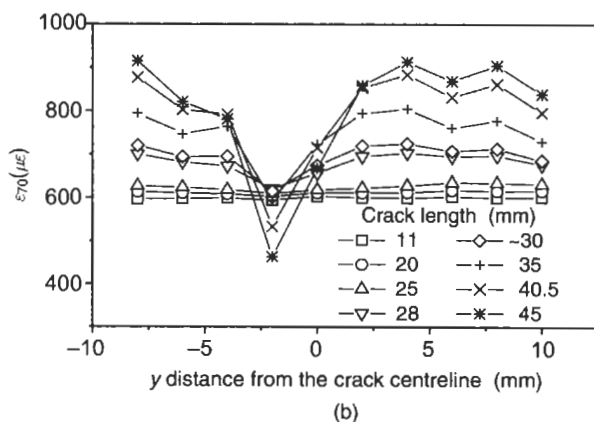
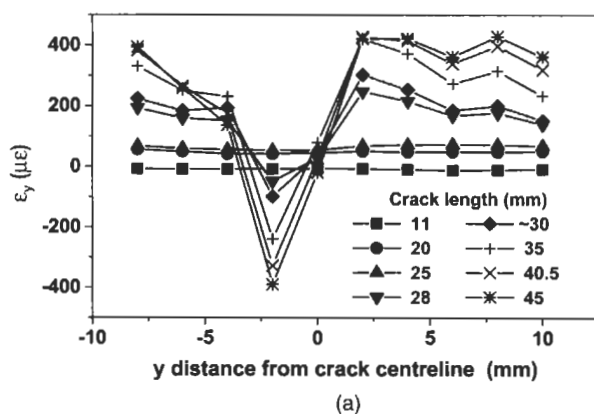


Fig. 20.17. Variation of (relative) strain distributions normal to the crack at $x = 32$ mm (for resistance-foil strip strain gauge 1), with increasing crack length: (a) residual strain distributions (i.e. 0 kN load case) and (b) strains at 70 kN (strains at 0 kN have been set to zero).

The results for both types of sensor arrays show that the residual strain over the crack (minimum strain response) drops by $-400\mu\epsilon$ and the strains above and below the crack (maximum strain response) increase by $400\mu\epsilon$ as the crack passes under the sensor array. Changes in residual strains, due to the presence of the crack, appear to occur when the crack tip is about 5–7 mm from the sensor – this is consistent with the strains measured under load. Figure 20.16 shows that, for this particular repair system, the residual strains are sensitive to changes in crack length. The degree of sensitivity will be determined by issues such as adhesive cure temperature, adhesive type, substructure stiffness, the geometry of the repair, *etc.* These results do indicate that the measurement of residual strains may be an alternate method for detecting and monitoring crack growth in the cracked substructure.

20.3.3. *Electro-mechanical impedance, transfer function and stress wave technique*

Low profile piezotransducer elements for sensing and actuation offer an encouraging alternative in-situ structural health monitoring technique for composite repair systems. Recent work has underscored the practical versatility of these materials with elements applied to in-situ health monitoring in the following configurations, as: surface mounted devices [26], embedded devices [27] and combinations of embedded and surface mounted devices [28]. The primary practical advantage in using piezoelectric materials like polymer film and piezoceramic wafers over strain gauges is that they do not require an external power source and they generate signals far stronger than those of traditional amplified strain gauges. These elements offer at least three modes of interrogation: electro-mechanical impedance, transfer function and stress wave propagation modes.

Electro-mechanical impedance method

The impedance-based method utilises a single piezotransducer element and exploits variations in the element electrical impedance, which arises from changes in the structural stiffness of the underlying host due to damage growth. The mechanical impedance is defined as the ratio of the applied force to the resulting velocity. In this case, the excitation of a surface mounted piezoceramic element, by applying a varying voltage (force) across the element, induces a vibrational response in the host that serves to modulate the current flowing (velocity) through the piezoelement. Consequently, the measured electrical impedance of the piezoelement (voltage/current) conveys information relating to the structural characteristics of the host, including any structural change arising from the formation and/or growth of damage. A damage parameter, D_I , was used to quantify the overall electrical impedance and is the basis for monitoring structural change (i.e. damage growth) in the skin-doubler specimen. The parameter D_I was defined as

$$D_I = \int Z(f)df, \quad (20.5)$$

where f is the frequency, Z is the impedance and the integration limits are 0 to 3.5 kHz. The upper limit is chosen to exclude the first structural resonance. The D_I -parameter was normalised with respect to the value obtained prior to the application of cyclic loading. In essence D_I is the mean square response of the impedance over the frequency range of interest.

Figure 20.5(b) shows a schematic drawing of the skin-doubler Type II specimen, considered in this experimental study, as well as the transducer locations. In this case the piezoceramic material was PZT (Lead Zirconate Titanate) wafers. A constant-amplitude sinusoidal load, with a fixed frequency of 5 Hz, was applied to the specimen. The maximum cyclic load started at 15 kN (minimum load was 0.1 kN) and was increased in 1 kN steps every 50000 cycles until damage was observed, after which the loading level was kept constant. During the experiments the disbond growth was monitored on Side P using element PP2 on step one and resistance-foil strain gauge P3 on step two (see Figure 20.5(b)). The electrical impedance of PP2 was measured at discrete frequencies in the range 400 Hz – 5 kHz, using an impedance analyser with a constant rms excitation voltage of 2 V.

The variation in D_I measurements, with increasing loading cycles, for transducer PP2 are shown in Figure 20.18 [6,20]. This figure suggests that disbond growth commenced at about 200000–205000 cycles, relatively soon after increasing the load amplitude to 20 kN after exposure to some 200000 loading cycles at lesser amplitudes. A systematic drop in the D_I -parameter was observed until about 210000–215000 cycles, whereafter the response remains relatively constant indicating, presumably, that the disbond had progressed past the PZT element where further disbond growth would have no effect on the element impedance. Note the overall drop in D_I is nominally about 4% relative to the initial value. Sensor P3 showed a reduction in strain after 205000 cycles reaching a minimum value at about 215000 cycles, indicating that the disbond does exist and had

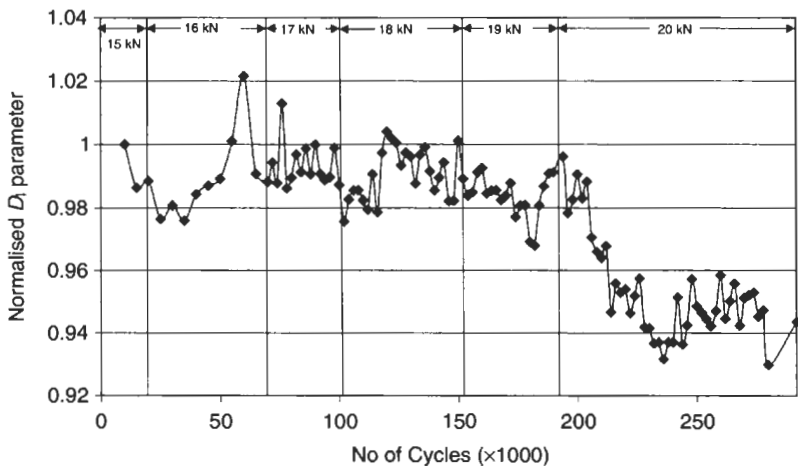


Fig. 20.18. Variation of D_I (of piezotransducer PP2) with increasing number of loading cycles.

nominally progressed passed the first step after about 215000 cycles. Sensor PP2 detects growth of a disbond (under step one) before it is detected by sensor P3 (on step two) – as would be expected. Even though the measured response is broadly consistent with the behaviour measured for similar bonded repair scenarios [19], the reduction in D_I is not as significant as previous studies. Currently a detailed numerical investigation of this specimen configuration is being undertaken to understand the behaviour of the transducer with varying position and amounts of damage.

Transfer function method

The transfer function method presented here is based on the system transfer function between a pair of piezotransducers on a bonded repair system. One element acts as a sensor the other as an actuator and the structural damage is assessed on the basis of changes in the transfer function between the transducer pair. The transfer function method is particularly attractive because the actuating piezoceramic element, which is quite brittle, can now be located in a low stress region, whilst the sensor, which can be a more fatigue-resistant piezoelectric film, can be placed in the high stress region. The damage parameter, D_{TF} in this case is calculated from the transfer function ($T.F.$) and is defined as

$$D_{TF} = \int T.F.(f)df, \quad (20.6)$$

where the integration limits are the same as the D_I case. Note that the D_{TF} parameter presented here has been normalised with the D_{TF} value for the no-damage case. The transfer function method was carried out for three different combinations using elements PP1, PP2 and PP3 on the skin-doubler Type II specimen shown in Figure 20.5(b). The transfer functions between the piezoelement pairs were measured using broadband random excitation with a frequency bandwidth of 250 Hz to 20 kHz with an rms excitation amplitude of 2 V.

Figure 20.19 shows the D_{TF} , with actuator PP3 and sensor PP2 [6,20]. As damage initiated at around 200000 cycles the value of D_{TF} decreases by about 30% after about 210000 cycles, indicating that damage had progressed past step one. This result was consistent with the impedance and strain gauge measurements described above. Similar results were observed for the piezotransducer pair PP1 (actuator) and PP2 (sensor), however after about 230000 cycles the D_{TF} parameter was observed to increase. The results using element pairs PP3 (actuator) and PP1 (sensor) showed no significant changes in D_{TF} with damage growth after about 210000 cycles. Further experimental and theoretical studies are underway with the view of establishing optimal transducer spatial distributions whilst maintaining adequate damage detection sensitivity.

Stress wave (acousto-ultrasonic) technique

The excitation of elastic stress waves is relatively straightforward given the broadband frequency response characteristic of piezoceramic materials. One of the

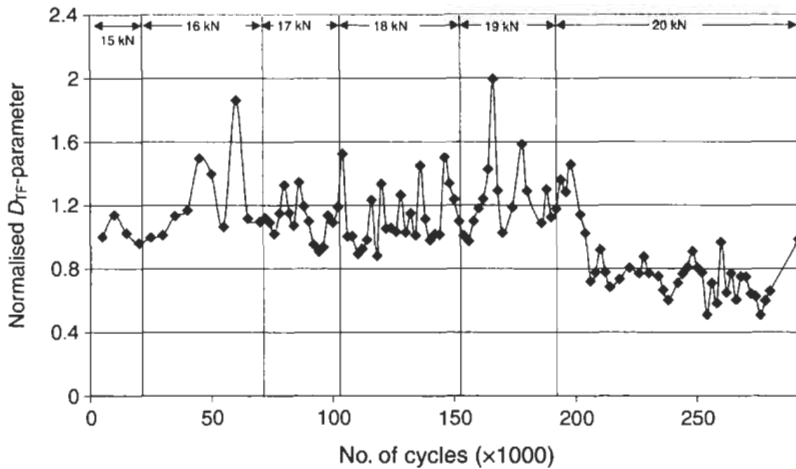


Fig. 20.19. Variation of D_{TF} (of actuator PP3 and sensor PP2) with increasing number of loading cycles.

inherent advantages of the stress-wave arrangement over the impedance, transfer function and the strain-based load transfer approaches, discussed above, is that it does not require *a priori* knowledge of the likely location of damage initiation and should therefore allow for a lower sensor density where large structures are considered. The broader sensitivity range also provides a better basis for the quantitative assessment of disbond growth.

Referring to the experimental arrangement shown in Figure 20.5(b), the approach here is to excite elastic stress waves in the host by applying a short voltage pulse to a piezoelement, SP1, surface mounted to the metal substrate some distance from the patch. Part of the elastic energy is transmitted through the bond-line into the patch and received at the two piezosensor locations (SP2, located on step three of the patch, and SP3, located on the far-field region of the patch). The expectation is that continuous monitoring of the elastic energy at this sensor location should provide a robust basis for the assessment of disbond growth from the patch edge, which was readily confirmed by experimentation.

Damage in composite bonded repairs was assessed by monitoring the sensor power (P) within a prescribed time window give by,

$$P = \int_{t_1}^{t_2} v(t)^2 dt, \quad (20.7)$$

where $v(t)$ is the measured sensor voltage, t_1 and t_2 are the lower and upper bounds of the time window, respectively. The lower bound was determined to allow the inclusion of the fast-wave mode of interest (but allowed the omission of spurious signals due to high RF effects) and the upper bound was set by the need to exclude boundary reflections.

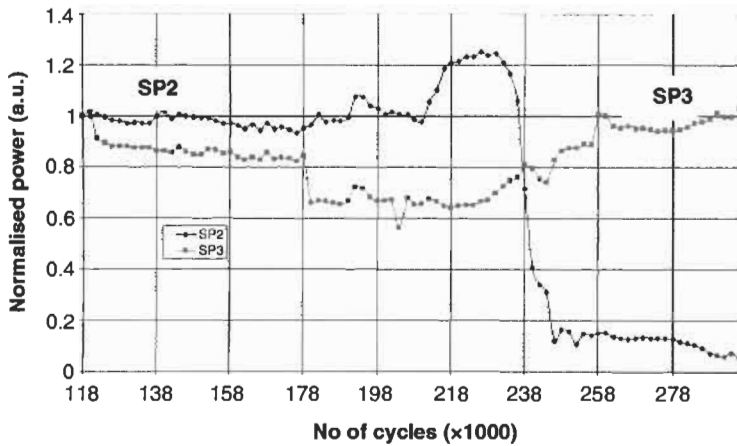


Fig. 20.20. Signal power versus number of cycles for piezosensor SP2 and SP3.

Computations of the power of the received signal were made at frequent intervals in the course of fatigue testing. The signal power at both sensor stations is plotted as a function of the number of loading cycles in Figure 20.20 [6,20]. Several interesting observations can be made here. Firstly, the response at sensor SP2 reflects a higher level of sensitivity to disbond growth than that recorded at sensor SP3. This is an intuitive result since the former element is located directly above the region where disbond growth occurred. It should be noted here that the results presented show good correlation with the strain results observed by strain gauge S3. Another interesting aspect is the markedly superior noise-effective sensitivity relative to that of the impedance and transfer function measurements (see Figures 20.18 and 20.19). In the case of SP2 for example, disbond growth through the sensor footprint results in a systematic drop in signal of some 90%, compared to 4% and 30% for the impedance and transfer function measurements, respectively. One potentially concerning aspect of these measurements is the apparent complexity of the relationship between disbond growth and the evolution of signal power. In the case of SP3 for example this is demonstrated by the 20% increase in power immediately preceding the more substantial long-term decline in signal. Such complexities are attributable to wave propagation physics and will include diffraction and mode conversion. Work is presently underway to try to understand such behaviour with a view to exploiting it for the quantitative assessment of disbond growth.

20.3.4. Adhesive bond degradation sensors – active sensing technique

Another more direct approach of monitoring bond-line degradation and failure is by the use of the adhesive bond degradation (ABD) sensor developed by DSTO and Analatom [7] and consists of a number of small, independent, wireless sensors that can be mounted within the adhesive bond-line. The basic concept is shown

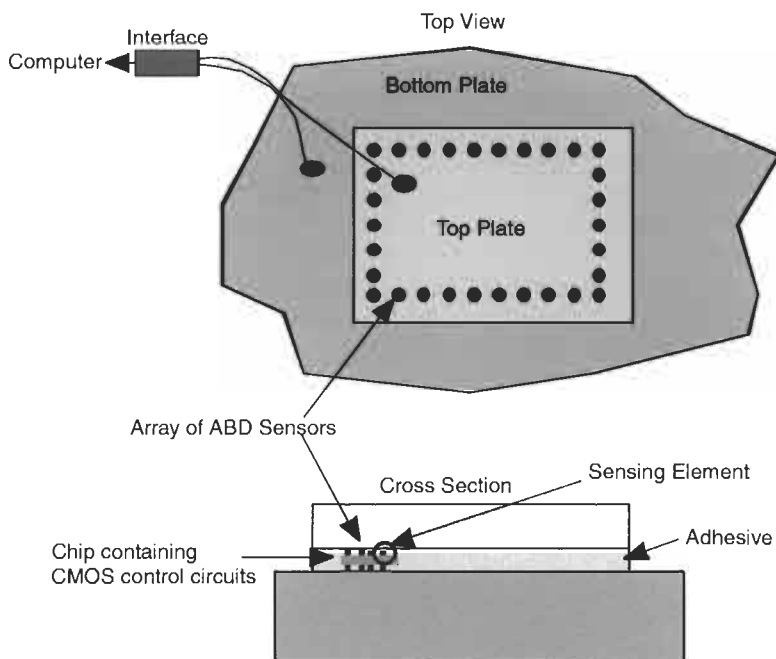


Fig. 20.21. Schematic of a bonded repair with an upper metal plate over a lower metal plate and an array of ABD sensors in the adhesive bond-line. In the metal/metal implementation the sensors have metal studs, which contact the metal plates to make these plates the power and communications “wires” [7].

schematically in Figure 20.21. A number of the ABD sensors would be included in any bonded repair or component to monitor the condition of the whole bond.

An adhesive bondline can be as thin as $80\text{ }\mu\text{m}$. Consequently, these sensors must be less than this minimal thickness and contain circuitry for sensing and communication. CMOS circuitry has been developed, to produce sensors less than $80\text{ }\mu\text{m}$ thick. Other studies have shown that void densities of up to 17% have little impact on the strength of a bonded joint [29]. Therefore, the projected size of these devices (1 mm^2) and wireless or minimal 2-wire interface will have no impact on the strength of the bonded joint that they are included in. The projected area fraction taken up by the ABD sensors is less than 0.5%. In the case of metal bonded to metal, as indicated in Figure 20.21, the sensor chips have metal studs that contact both metal plates. All power and communication requirements are met through these connections so a truly wireless sensor can be implemented. This concept could be extended to composite-to-composite or metal or honeycomb by either using RF or a 2-wire interface for power and communication.

In the study documented here the focus is on a metal-to-metal repair bonded using a thermoset epoxy film adhesive. The sensors are sensitive to the condition of the metal/epoxy interface that is the principle locus of failure due to environmental

degradation. The ABD MEMS sensor contains sensing elements which measure the conductivity between the sensor and the opposing metal plate, and CMOS circuitry required for the sensor to be semi-autonomous. The sensing elements consist of metal studs mounted on both the top and bottom surfaces of a silicon chip. Some of the sensing elements are in contact with the metal plates whilst others are not giving the sensor two modes of operation. The sensor detects gross disbonding or poor bonding by loss of electrical continuity for the elements initially touching the metal plate. This loss of continuity from a particular sensor indicates the loss of bonding at this point between the upper and lower plates. Sensing elements that are not initially connected to both the top or bottom plates act as chemical ion detectors. These elements detect the build up of metal ions between the stud and the metal plate due to chemical activity associated with water penetrating the bond causing degradation of the metal/epoxy interface which causes the loss of bonding. The ABD device also contains CMOS circuitry for control of the environmental sensitive probes and for communication. Details of the CMOS circuitry and fabrication processes are given in reference [7].

To demonstrate the technique sensing elements were laid up in a Boeing Wedge test (ASTM D3762–79, re-approved 1988) configuration using the Australian Silane treatment, as described in Chapter 3, placed in 50 °C water and loaded at a constant slow rate which ensures that the environmental degradation of the metal/epoxy interface is faster than the crack opening rate. The experimental set-up is illustrated in Figure 20.22. The voltage required to pass $\pm 100 \mu\text{A}$ between the sensing element and the Al plate was measured every 4 h after the specimen was immersed in water. The results in Figure 20.22(b) initially show an open circuit, region 1, until the conductivity increases indicating the presence of ions at the interface, region 2. The conductivity decreases again, region 3, until the sensor once again shows the presence of ions (region 4) indicative of bond degradation due to water ingress up the metal/epoxy interface. At the end of the period in region 4 the conductivity starts to decrease. This decrease is thought to be due in part to attack of the sensing element itself. Complete degradation is observed in region 5. More detailed studies are being performed to relate the nature and position in time along the graph with the mechanical condition of the bonded joint.

20.4. Laboratory smart patch conceptional demonstrators

The laboratory demonstrator of the “smart” approach was based on a strain measurement technique, with resistance-foil strain gauges and piezoelectric film sensors bonded to the ends of the taper region and on the surface of the component away from the critical end region of the patch for the skin doubler specimens shown in Figure 20.23. The concept, as discussed in Section 20.3.1, was to monitor the ratio (critical patch strains)/(far-field strain in the component) during service life and any decrease in this “patch health” ratio would be an indication of disbonding of the patch in this critical end region. In this approach there was no requirement to measure the actual loading, disbonding is indicated by the reduction in relative

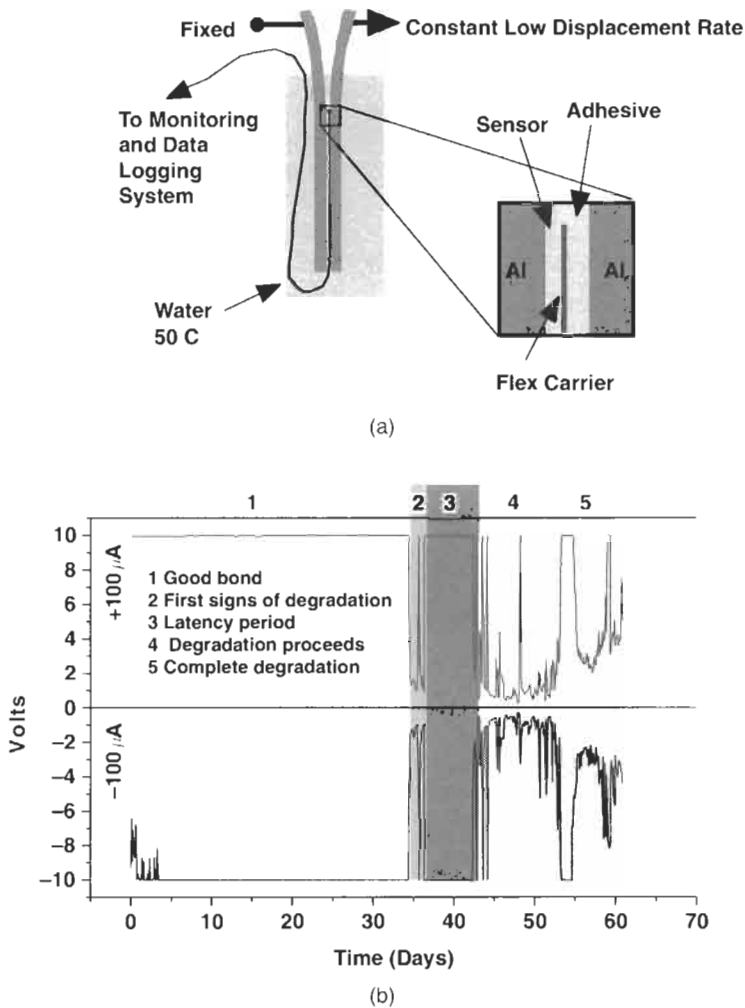


Fig. 20.22. (a) Lay up for accelerated ageing test of the ABD sensor (b) Bond degradation sensor signal variation with exposure to 50 °C water. The two data sets are the voltages required to pass $\pm 100 \mu A$ current through the sensing element. The $\pm 10 V$ reading reflects the maximum voltage available and indicates a high impedance (undegraded) state. The noise at the start of the $-100 \mu A$ trace is thought to be due to the fact that the sensing element is very close to the Al [7].

strain. The above ratio is forthwith referred to as the patch-state-of-health value (PSH). Another damage parameter mentioned below is the patch damage quotient (PDQ) given as a percentage defined by $100 \times (\text{far-field strain} - \text{critical patch strain}) / \text{far-field strain}$.

The laboratory demonstrator was based on electrical devices that monitored single sensor pairs (i.e. a two channel device). The device continually monitors the

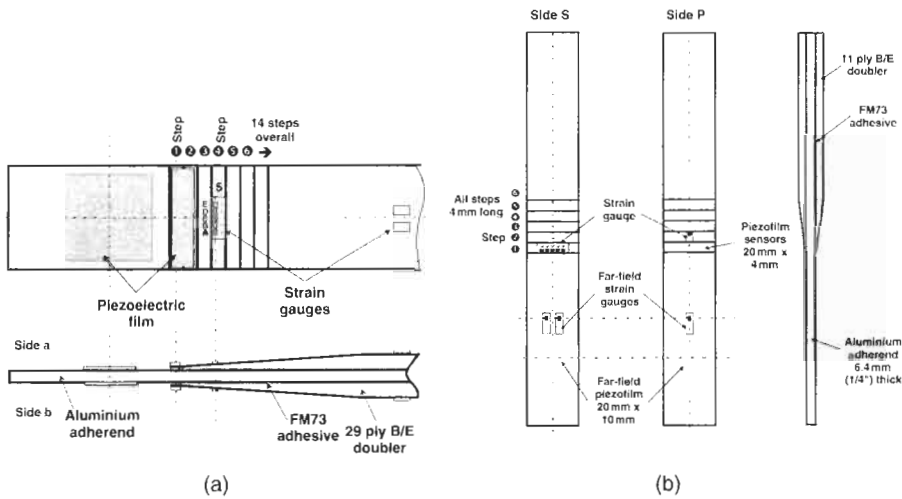


Fig. 20.23. Schematic of specimens showing resistance-foil strain gauge and piezoelectric film sensor locations for smart patch laboratory demonstration studies: (a) Skin doubler Type I specimen and (b) Skin doubler Type II specimen.

strain sensor pair and processes and stores the “patch health” information and then transmits this data to an external computer by an IR link when required – as shown in the flow diagram of Figure 20.24. The prototype device, shown in Figure 20.24 was not optimised for size and weight; however, it easily fits in the palm of an average hand and has a mass of about 25 grams and is powered by a single 3 Volt battery. In these experiments, infrared (IR) (rather than radio frequency, RF) waves were used for data transmission, since IR emissions are unlikely to interfere with any of the aircraft electrical functions. A potential problem with infrared

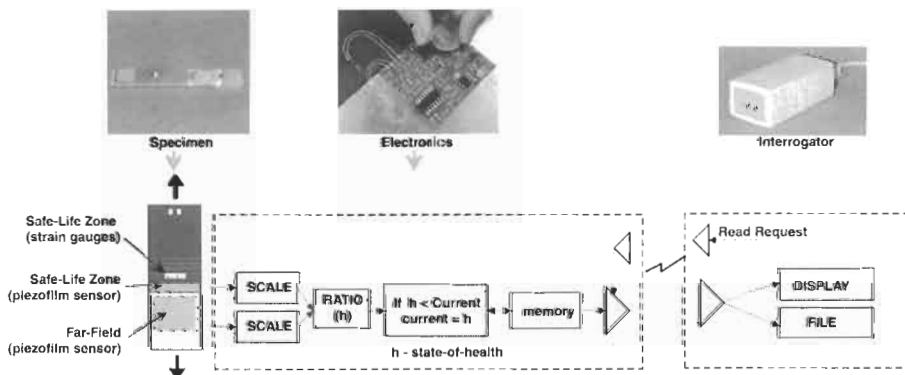


Fig. 20.24. Photographs and flow chart of the laboratory demonstrator experimental set-up.

transmission is that it requires direct line of sight which may be difficult to achieve where a repair is located deep within the airframe structure. However, in these cases, a possible workaround may be to "pipe" the IR signal through optical fibres.

Two triggering approaches were initially considered. The first involves a device which is normally in a dormant state, (a so-called sleep-mode), and is activated by some external trigger event. The external trigger could be supplied by an appropriate transducer, possibly a piezoelectric element. This option was not used in the conceptual prototype because of the complexity added by the external triggering system and its consequent impact on overall system reliability. The second approach, and the one employed in the prototype, involves sampling the device on a periodic basis. In order to meet the limited power requirements variable sampling rates were employed. That is the sampling rate was varied as a function of the (activity) strain level of the parent strain gauge, where the maximum sample rate was about 3 samples/sec during times of high (activity) strain and the minimum sample rate was about 10 samples/hour during periods of low (activity) strain. It was envisaged that this technique would still achieve about 3–5 years of life for the device, based on the use of conventional resistance-foil strain gauges.

The skin doubler Type I and Type II specimens were used in these studies and are shown in Figure 20.23. The Type I specimen, Figure 20.23(a), had resistance-foil strain gauges located in the far-field (on the patch) and on the 4th step of the boron doubler, and 28 μm thick piezoelectric PVDF film sensors located in the far-field (on the aluminium) and on the first two steps of the doubler [4]. In the Type II specimen, Figure 20.23(b), the side of interest, side P, had a piezoelectric film sensor on the 1st step of the doubler and in the far-field, and resistance-foil strain gauges on the 2nd step of the doubler and in the far-field [10]. The smart patch devices were connected to the piezoelectric film sensors on side A of the Type I specimen and the piezofilm sensors on Side P of the Type II specimen. The device was programmed to calculate PSH and PDQ for specimens Type I and II, respectively. The resistance-foil strain gauges were monitored using conventional PC-based data acquisition systems. Specimens were subject to the same loading conditions as that described in Section 20.3.1, and patch health data from the smart patch devices were interrogated at frequent intervals in the course of the fatigue testing.

Figure 20.25(a) and (b) show data from the prototype devices, which monitored the ratio of step 1 + 2 strains/far-field strains (PSH) and (far-field – 1st step) strains/far-field strains (PDQ), respectively. It is seen that the device successfully monitors the damage growth at the tapered end of the doubler. For the Type I specimen there is a clear reduction in PSH after about 54000 cycles. The response of the strain gauges on step 4, which exhibits a noticeable change at about 72000 cycles, confirms the presence of damage in that specimen. The smart patch system used on the Type II specimen also successfully detects damage in the doubler. Once again, damage is confirmed by independent resistance-foil strain gauge measurements. However in this case the PDQ has exceeded the 100% value expected when damage has passed the 1st step. It is believed that this occurred because of the strain induced by the adhesive "spew fillet" at the edge of the patch restraining the natural extension of the patch caused by relaxation of thermal strains due to disbond

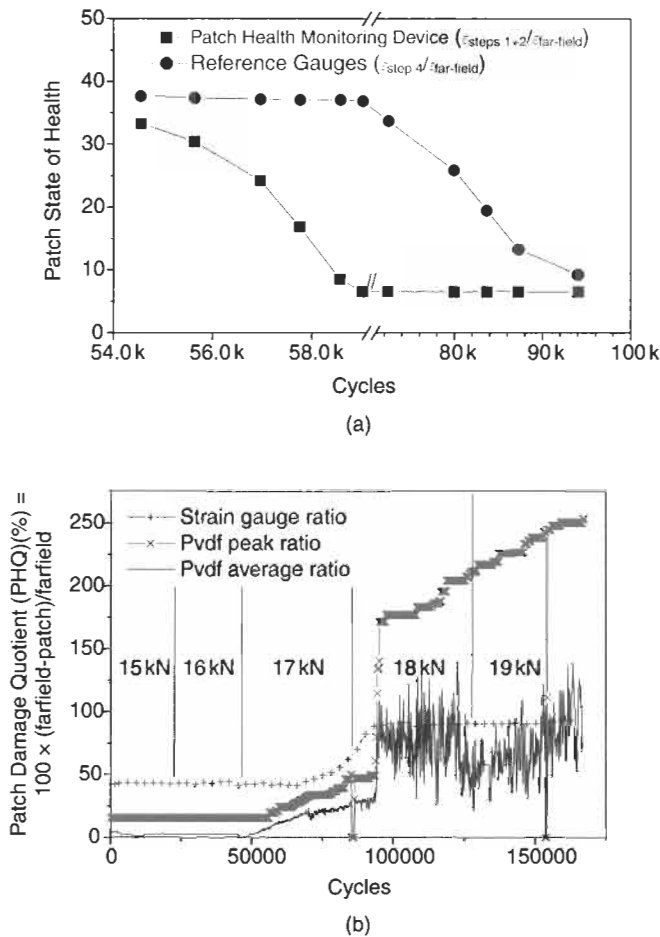


Fig. 20.25. (a) Plot of variation of patch state of health (ratio of critical region strain/far-field strain) with increasing number of applied loading cycles for specimen Type I shown in Fig. 20.23(a) [4]. (b) Variation in patch damage quotients, as measured by the PVDF smart patch device, and strain gauge ratio with increasing number of cycles for side P on specimen Type II (Fig. 20.23(b)).

growth. This phenomenon complicates the calculation of the PSH or PDQ based on the strain ratio technique [10], suggesting that a more robust method of determining the patch health may be required in flight. For example, instead of simply calculating a single patch health value it may also be necessary to look for linearity between far-field and patch strains at various load levels. Overall, the experimental programs to date have shown that the laboratory demonstration of the “Smart Patch” concept, employing piezoelectric film and conventional strain sensors, are able to detect disbonding of a composite patch.

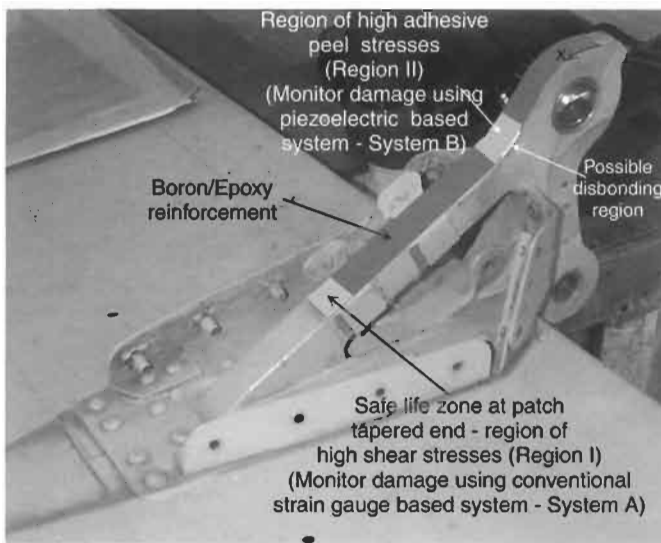
20.5. In-flight demonstrator

The viability of these smart system approaches depends on whether requisited levels of reliability, robustness and sensitivity can be demonstrated under the aircraft temperature and environmental operating conditions. In this context, flight trials of the technology are essential. Currently DSTO are planning flight trials to monitor the performance of a b/ep doubler system recently developed to extend the life of F/A-18 aileron hinge [30]. F/A-18 inboard aileron hinges, as shown in Figure 20.26(a), suffer from a fatigue cracking problem in the hinge aft strut, for which the only current solution is replacement of the component. DSTO has designed reinforcements for hinges that have not yet developed cracks as well as a method for restoring cracked hinges to an airworthy condition, as described in Chapter 33 [31]. A combined analytical and experimental program has shown that the proposed structural rework and reinforcement restores static strength to the hinge. These reinforcements reduce the stresses in the hinge by more than 25%, and have been tested up to 150% of Design Limit Load. The flight trial consists of applying a composite bonded reinforcement to an F/A-18 aileron hinge and then implementing and demonstrating two in-situ health monitoring systems. The sections below describe some of the preliminary activities undertaken during the development of the system. Two main issues will be discussed, viz., (1) the damage detection technique and (2) the electronic approach.

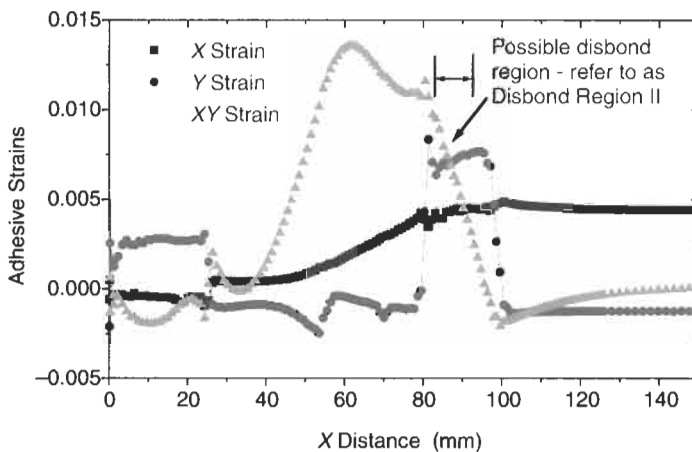
20.5.1. Finite element analysis – damage sensing technique

In situ techniques for detecting and monitoring damage in the bondline of the aileron hinge reinforcement need to be established and calibrated. Therefore a finite element study was undertaken to evaluate various in-situ damage detection techniques. Previous conventional bonded reinforcements/repairs had two likely disbond sites, namely in the damage tolerant region, which is over the damaged substructure, and in the safe-life zone (in the tapered region of the patch) – see Figure 20.1. The aileron hinge bonded reinforcement is considerably different to conventional bonded patches in that the concave shape of the hinge introduces high peel stresses in the bonded patch system. The reinforcement outlined in Chapter 33 is for a reinforcement applied to an optimally blended hinge. However in the demonstrator case the reinforcement will be applied to an unaltered hinge.

A finite element analysis of the hinge with a b/ep reinforcement was undertaken to determine the most likely regions of damage and to assess various damage detection techniques [30]. Figure 20.26(b) shows the peel, shear and longitudinal stresses in the adhesive of the reinforcement. These results indicate that two critical regions exist, viz., the tapered region at the end of the repair on the hinge strut (Region I in Figure 20.26(a)) and the region of high adhesive shear/peel stresses in the mid-section of the reinforcement (Region II in Figure 20.26(a)). Figure 20.26(b) does not show the high adhesive shear stresses at the end of the patch (Region I) since this region was not modelled here. Also note that the repair termination on the top of the lug (at $x=0$) is not under load and therefore the adhesive shear



(a)



(b)

Fig. 20.26. Smart patch reinforcement flight trial on F/A-18 aileron hinge: (a) regions of high adhesive peel and shear stresses are indicated on the hinge reinforcement and (b) predicted adhesive stresses in the reinforcement with no blending and no disbonds present (Note disbond to be modelled in region II is indicated here).

stresses are low in this region. Therefore, only the location of high shear/peel stresses (Region II) and high adhesive shear stress region at the end of the patch (Region I) will be considered in this case. A study was then undertaken to observe the effects of disbond damage on the surface stresses of the reinforcement. The two

damage cases considered were disbonds in the (1) high adhesive peel stress region of the reinforcement (Damage case II) and (2) tapered region of the reinforcement (Damage case I). The damage was simulated by introducing a 10 mm long disbond in the adhesive layer. Two load cases were considered in the FE analysis, viz., load case WO39 a tensile design ultimate load condition and WO42 a compressive design ultimate load condition. The results shown here are for the former case only. Plots of surface strains are given in Figure 20.27(a) for the various disbond

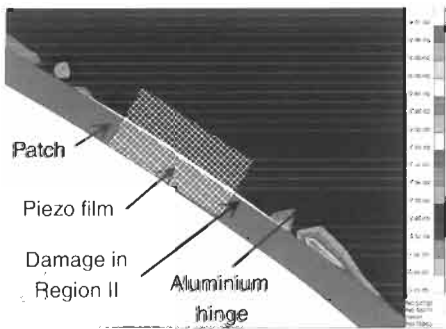
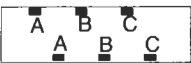
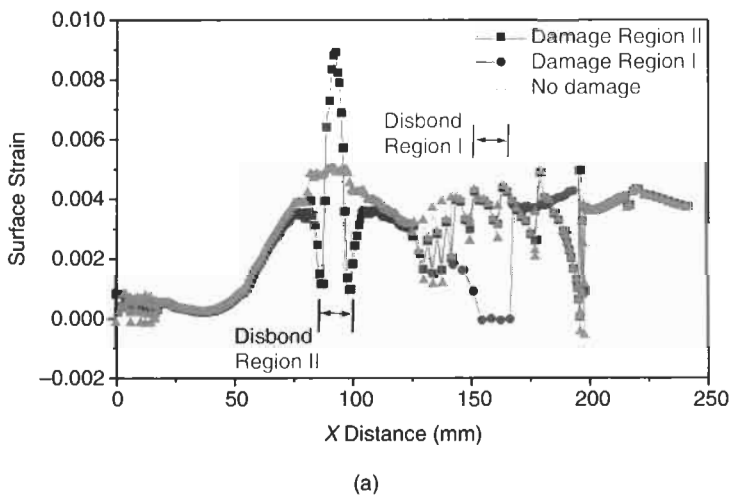


Fig. 20.27. Smart patch reinforcement flight trial on F/A-18 aileron hinge: (a) longitudinal surface strain profile on a b/ep doubler, applied to an aileron hinge, due to 10 mm disbond in the various regions indicated and (b) damage detection schemes for damage in Region II (top) sensor array and (bottom) piezoelectric film placed over the disbond (i.e. the piezoelectric film basically measures the amount of disbond opening).

conditions. The results and recommendations from this study are summarised below:

- i Region I – damage at the tapered end: For disbonding in the tapered region the patch surface strains above the disbond drop to zero under all load conditions considered. Therefore it appears that measuring the simple ratio of strain over the taper to strain in the far-field (aluminium) will give an adequate indication of damage in this region.
- ii Region II – damage at the adhesive high peel stress region: Significant increases in surface strains compared to the no damage case are predicted, for both load cases, indicating that damage detection is possible using surface strain sensors. Figure 20.27(a) shows a distinctive sharp peak in the surface strains (peak occurs over a 5–6 mm length for the 10 mm long disbond). However, the sharpness of the peak means that it may be difficult to detect if the sensor is not carefully positioned with respect to the damage. Also, the presence of a strain trough means that the averaging effect due to finite length of the strain sensors may mask the peak. Thus sensors will only detect the damage if the sensing length is small, compared to the peak-trough distance, and if the sensors are positioned over the damage or when the damage reaches a substantial size. Also, it is quite likely that the damage will initiate on one side without growing through the width to the other side. Therefore, in order to achieve a reasonable chance of detecting damage an array of sensors, on both sides of the reinforcement, is required. In order to reduce the number of sensors required then one approach may be to have a staggered array as shown in Figure 20.27(b). However this would require several dual channel devices or one multi-channel device to cover a reasonable area of about 20–30 mm long. Another approach is to make use of the disbond opening under load, which appears to be substantial, and use a piezoelectric film bonded on the edge of the aileron (over the repair, adhesive layer and some of the aluminium), as shown in Figure 20.27(b), to detect disbond opening. FEA and experimental studies are evaluating the performance of the sensor for different sensor positions and sizes. In summary two regions are to be monitoring during the flight demonstrator, viz. Region II: the region of high peel stresses located at the region of high curvature, and Region I: at the end of the doubler, and are indicated in Figure 20.26(a).

20.5.2. *Health monitoring systems*

Normally it is desirable to detect damage over a reasonable area. This could potentially be achieved by having one large sensor or several elements connected to act effectively as a large sensor. However, the disadvantage with this configuration is that an averaging effect is produced, reducing the sensitivity of the system. One alternative is to have individual channels for each of a number of individual (or small groups) sensors. This appears attractive but if the centralised electronics fail the whole device may be inoperative. Another alternative is to have individual autonomous pairs of far field and area of interest sensors. This alternative has the potential to provide a degree of robustness against single sensor or electronics

failure, and provides a system which is easily scalable for different geometry patches. It also provides information on the extent of damage – that is the system can track the damage (even in the event of an element failing). Therefore, as for the laboratory concept demonstrator, the flight demonstrator system is based on devices that monitor single pairs of strain sensors. As there was only one window of opportunity to get access to a service aircraft it was decided to use two independently developed sets of electronic devices, using (where possible) different components. It was anticipated that this would maximize the chances of having a successful demonstration, within the confines of the current budget and time frame. Both units combine strain-sensing elements with sophisticated electronics that track the health of a bonded composite patch. The two units are [30]:

1. System A. Smart patch system demonstrator – conventional strain gauge based version (SPSD-CG) which is a low technological risk device utilising a Li-based battery and conventional electrical-resistance foil strain gauges to measure patch strains.
2. System B. Smart patch system demonstrator – piezoelectric film based version (SPSD-P) which is a medium-high technological risk device utilising piezoelectric film (PVDF) for both self-powering and strain ratio measurement.

Some of the main broad specifications of these systems are that they need to be small low-powered devices capable of operating in a nominally autonomous manner. The device should be robust enough to survive in the harsh operational environments likely to be encountered, with the main concern being that the device should be able to tolerate a temperature range of -40°C to about 80°C . (Note that, operator data [30] suggests that the F/A-18 hinge operates in temperatures in the range -40°C to 60°C .) The current smart patch system arrangement is shown in Figure 20.28. The systems consist of surface mounted solid-state electrical

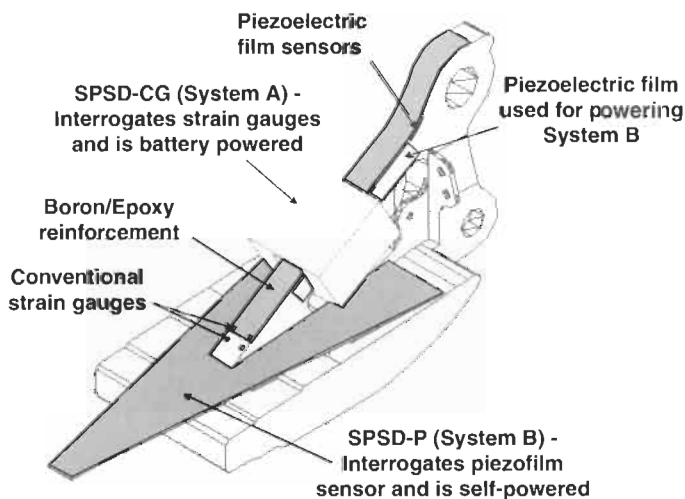


Fig. 20.28. Sketch of the aileron hinge with proposed smart patch demonstrator arrangement.

components on standard printed circuit boards, however future work will look at developing MEMS-type devices for flight.

System A

The device in system A lies dormant until it is activated by a vibration sensing switch. Once the device is activated both the temperature and battery voltage are continually monitored, but the device interrogates the strain gauges only when (1) the system temperature is in the range of 0 °C to 25 °C, (2) the voltage is within prescribed limits and (3) a measurement has not been recorded in the past hour. This procedure is used to increase battery life, minimize strain gauge errors and to prevent the device from operating outside the specifications of the electronics. Two hundred pairs of simultaneous far-field and patch strain samples are taken over a 5 s period – these samples are called a “measurement”. If the far-field strain for a specific sample pair is less than the minimum threshold strain (currently set at 100 $\mu\epsilon$) then the data pair is discarded, otherwise the data pair are added to running totals for patch and far-field, respectively. Assuming at the end of the measurement a sufficient number of good samples have been taken (e.g. 10% or 20 good samples out of 200) then a patch health value (as a percentage) is calculated by using the simple ratio $100 \times \text{patch}_{\text{total}} / \text{farfield}_{\text{total}}$. Data stored in the device not only includes the patch health value, but also other parameters such as time stamps, temperature and a limited amount of strain time-history data. This additional data will allow a level of confidence in the operation of the device. In this demonstrator some degree redundancy is achieved by incorporating two SPSD-CG systems monitoring two pairs of strain gauges. The devices are encapsulated in epoxy and enclosed in aluminium cartridges as shown in Figure 20.28. The device is interrogated using an IR wireless link.

System B

An effort is currently underway to develop a system with self-powering capability since a completely autonomous system, i.e. systems with an indefinite life, is considered highly desirable – even though this activity involves substantial technical risk. The system under development will be powered from its environment (local changes in strain) in order to achieve readings during flight. During interrogation, for data uploading, power for the device will be attained from a magnetic field produced by the interrogation unit (when plane is on the ground). The initial demonstration involves the development of a relatively simple system, using sheets of PVDF to convert strain energy from the structure to electrical energy. Geometric and other constraints have limited the amount of power available using this technique to the fractions of a milliWatt range. As it is difficult to get a reasonable amount of signal processing done on this kind of power budget, the harvested power was stored in a capacitor. Once sufficient energy was available for a complete reading cycle, and the structure was experiencing significant strain, then a reading was taken. The initial design uses a large footprint, the area of which is illustrated in Figure 20.28, however the design is such that it should be a relatively straightforward process to reduce the unit to very small proportions using

standard CMOS technology. Figure 20.28 shows the size and mounting arrangement of the SPSD-P system, and the location of the transducers on the aileron hinge. The sensors used with this part of the system are also made from PVDF sheet. The three main factors influencing this choice being, no excitation power required, modest signal conditioning requirements and high fatigue life. These virtues however come at a cost, in this case, in the form of poor low frequency response. As there is a high probability of a substantial amount of the strain being in the low frequency region it is important to ensure the frequency roll-off characteristics are fairly accurately matched. This in itself can be tedious, but as high impedances are involved the greater challenge is ensuring that they remain matched in an adverse environment. To assist with this problem buffer amplifiers with low input leakage were incorporated, but the need for thorough protection against moisture ingress remains a critical issue.

To minimize system power requirements the patch health measurement was obtained using an analogue technique, the signal from the “reference” transducer was fed through a divider chain and compared to the signal from the active transducer via a chain of 10 comparators (10% resolution). In a very elementary case the only value needed would be the last ratio measured. However this was considered not to be sufficiently robust, since a single noise “spike” could cause a misleading reading and, if a sequence of readings showed no change, there would be no indication that the system was still functioning properly. This led to the conclusion that some other confidence building indicators were required. A timestamp was considered but thought to be a little challenging using the technologies readily available, therefore a reading counter was chosen as a compromise. Unfortunately the only place to maintain the count is in the nonvolatile memory, thus necessitating a “measurement cycle” to consist of (1) reading the memory (2) taking the measurement, and (3) writing the updated information back into memory. This of course considerably increases the energy requirement, but was considered necessary for a practical system. In an attempt to reduce the effects of spurious spikes a simple slew rate filter algorithm was employed. This was thought to be appropriate as the damage is expected to grow relatively slowly with respect to the reading rate, and even if it suddenly failed this would be indicated after only 10 reading cycles at most. During a reading cycle the system is synchronized to an internal 5 MHz clock, the speed being basically chosen to minimize the energy required. Initially the logic to control the device was intended to be implemented in a commercially available off-the-shelf low power programmable logic device. However no acceptable device was available, hence the current system uses standard SSI/MSI CMOS devices. A temperature dependant lockout was fitted to the supply circuit to prevent any operations being attempted if the operating temperature was outside specified temperature limits of the “industrial grade” off-the-shelf electronics used in this device.

The prototype design is capable of reading two ratios, with respect to a common reference (to 10% of full scale), and maintains a count of the cumulative number of readings (that wraps back to zero at approx. 16.7 million counts). Initial indications are this prototype will consume about 210 nJ of energy to perform the digitization

and division functions, 60 nJ to perform the storage and retrieval functions and 10 nJ for clocking. On the supply side, the PVDF material is capable of providing a strain dependent energy density of $0.37 \text{ nJ/m}^2/\mu\epsilon$. Initial experiments have indicated that for a bank of PVDF sensors with an effective area of about 204 cm^2 (in the location indicated in Figure 20.28) peak applied strain levels of about $300 \mu\epsilon$ at frequencies greater than 3 Hz should provide enough energy for the device to operate. Limited flight strain data have indicated that this strain loading scenario should be easily achieved at the aileron aft hinge strut. In this system the patch health data is up-loaded by the operator using a magnetic transceiver.

20.6. Conclusions

The “smart patch” approach, which is based on self-monitoring, would considerably alleviate the certification concerns for implementing bonded composite repairs to primary aircraft structures. This approach relies on the ability to automatically detect disbonding in the patch, i.e. the “smart patch” approach is basically a continuous safety-by-inspection approach for the bonded repair. However, this approach brings its own problem of reliability assurance. Currently the approach appears technically feasible but, in the short term, only economically viable for repairs to very significant and costly primary structure.

An overview of various *in situ* patch health monitoring techniques and sensor types was undertaken. This overview mainly detailed experimental studies using conventional resistance-foil strain gauges, optical fibre sensors, low profile piezotransducer elements and MEMS-based sensors. All techniques appear to be successful in detecting disbonding in the bonded patch. The latter technique has the added benefit of also indicating bond degradation, thus giving the operator some indication of the state of the bond and therefore some warning of impending bond failure.

Studies on laboratory coupon specimens at DSTO, outlined in this chapter, have shown that the concept of the “smart” approach using autonomous patch health monitoring systems appears to be viable. These systems establish, store and allow the operator (at their convenience) to up-load patch health values (i.e. ratios of patch strain at a critical location to far-field strain). This ratio gives an indication of the level of load transfer into the patch. Any decrease in this ratio is an indication of disbonding of the patch in this critical region. In this approach there is no requirement for measurement of the actual loading: disbonding is indicated by the reduction in relative strain.

The main aspects of the development of two different *in-situ* autonomous remotely interrogated patch health monitoring systems, which will be used on a flight demonstrator on an operational F/A-18, were also outlined in this chapter. The two systems being developed consists of a piezoelectric (PVDF) film-based and a conventional electrical-resistance foil strain gauge-based sensing system. The latter system uses a primary cell (Lithium-based battery) as the power source, which should enable an operating life of 1–2 years. The patch health data is

up-loaded by the operator using an IR link. The piezoelectric film-based sensing system is self-powered and has been designed to operate using the electrical power generated by an array of piezoelectric films, which convert structural dynamic strain to electrical energy. These transducers power the electronics which interrogate the piezoelectric film sensors, and process and store the patch health data on non-volatile memory. In this system the patch health data is up-loaded by the operator using a magnetic transceiver.

References

1. Baker, A.A. (1994). Bonded composite repair of metallic aircraft components, AGARD-CP-550 Composite Repair of Military Aircraft Structures, Paper 1.
2. Baker, A.A. (1997). On the certification of bonded composite repairs to primary aircraft structures. *Proc. of 11th Int. Conf. on Comp. Mat. (ICCM-11)*, Gold Coast, Australia.
3. Baker, A.A., Rose, L.R.F., Walker, K.F., *et al.* (1996). Repair substantiation for a bonded composite repair to a F-111 lower wing skin. *Proc. of the Air Force 4th Aging Aircraft Conf.*, Colorado, July.
4. Baker, A.A., Galea, S.C. and Powlesland, I.G. (1998). A smart patch approach for bonded composite repairs to primary airframe structures. *Proc. of the 2nd Joint FAA/DOD/NASA Conf. on Aging Aircraft*, Williamsburg VA.
5. Galea, S.C. and Baker, A.A. (2000). Smart structures approaches for health monitoring of aircraft structures. *Proc. of the SPIE 2000 Symposium on Smart Mat. and MEMS: Smart Structures and Devices Conf.*, Melbourne, Australia, 13–15 December, Paper 4235–39.
6. Galea, S.C., Rajic, N., Moss, S.D., *et al.* (2001). *In situ* health monitoring of composite bonded repairs. *Proc. of the 3rd Int. Workshop on Structural Health Monitoring*, Stanford University, 12–14 September.
7. Wilson, A.R., Hopcroft, M. and Sbiaa, Z. (2000). MEMS adhesive bond degradation sensor. *Proc. of the SPIE's 2000 Symposium on Smart Mat. and MEMS, Smart Electronics and MEMS Conf.*, 13–15 December, Paper 4236–32.
8. Galea, S.C. (1997). Monitoring damage in bonded composite repairs of cracked metallic components using surface strain measurements. *Proc. of 11th Int. Conf. on Comp. Mat. (ICCM-11)*, Gold Coast, Australia.
9. Baker, A.A., Chester, R.J., Davis, M.J., *et al.* (1993). The development of a Boron/Epoxy doubler system for the F111 wing pivot fitting – materials engineering aspects. *Composites*, **24**, pp. 511–521.
10. Moss, S.D., Galea, S.C., Powlesland, I.G., *et al.* (2000). *In situ* health monitoring of a bonded composite patch using the strain ratio technique. *Proc. of the SPIE's 2000 Symposium on Smart Mat. and MEMS, Smart Structures and Devices Conf.*, Melbourne, Australia, 13–15 December, Paper 4235–41.
11. Rees, D., Chiu, W.K. and Jones, R. (1992). A numerical study of crack monitoring in patched structures using a piezoelectric sensor. *Smart Mat. and Structures* **1**, pp. 202–205.
12. Vodicka, R. and Galea, S.C.P. (1998). Use of PVDF strain sensors for health monitoring of bonded composite repairs. DSTO Technical Report 0684, June.
13. Chang, C.-C. and Sirkis, J. (1996). Multiplexed optical fibre sensors for air frame repair patch monitoring. *Experimental Mechanics*, **36**, pp. 353–359.
14. McKenzie, I., Jones, R., Chiu, W.K., *et al.* (1997). The monitoring of crack growth beneath bonded repairs using a bragg grating array. *Proc. of the Far East and Pacific Rim Symposium on Smart Mat., Structures, and MEMS*, Adelaide, Australia, 10–13 December, Vol. 3242, pp. 272–283.
15. Whitehead, S., Galea, S.C. and McKenzie, I. (2000). *In situ* health monitoring of bonded composite repairs using embedded optical fibre sensors. *Proc. of the Int. Conf. on Comp. Eng. ICES'2K*.

16. Kowalik, M., McKenzie, I. and Galea, S.C. (2000). Detection of disbonds in secondary bonded structures using embedded Bragg grating optical fibre sensors. *Proc. of the SPIE's 2000 Symposium on Smart Mat. and MEMS, Smart Structures and Devices Conf.* Melbourne, Australia, 13–15 December, Paper 4235–44.
17. Ikegami, R. (1999). Structural health monitoring: assessment of aircraft customer needs structural health monitoring. *Proc. of the 2nd Int. Workshop on Structural Health Monitoring*, Stanford University, Stanford CA USA, September 8–10.
18. Chiu, W.K., Galea, S.C., Koss, L.L., *et al.* (2000). Damage detection in bonded repairs using piezoceramics. *Smart Mat. and Structures*, **9**, pp. 1–10.
19. Koh, Y.L., Rajic, N., Chiu, W.K., *et al.* (1999). Smart structure for composite repair. *Composite Structures*, **47**(1), pp. 745–752.
20. Koh, Y.L., Chiu, W.K., Rajic, N., *et al.* (2002). The application of piezoceramic elements to the detection of disbond growth in a bonded composite repair patch. *Proc. of Australian Congress on Applied Mechanics (ACAM 2002)*, Sydney, Australia, February.
21. Cox, A.F. (1988). Fatigue cracking in the upper plate of wing pivot fittings in F111 aircraft. *Defence Science and Technology Organisation, Aeronautical Research Laboratory*, Report ARL-MAT-R-121.
22. Molent, L., Callinan, R.J. and Jones, R. (1989). Design of an all boron/epoxy doubler reinforcement for the F-111C wing pivot fitting: structural aspects. *Composite Structures*, **11**, pp. 57–83.
23. Grabovac, I., Bartholomeusz, R.A. and Baker, A.A. (1993). Composite reinforcement of a ship superstructure - project overview. *Composites*, **24**, pp. 501–509.
24. Hill, K.O., Fujii, F., Johnson, D.C., *et al.* (1978). Photosensitivity on optical fibre waveguides: application to reflection filter fabrication. *Appl. Phys. Lett.*, **32**, pp. 647–649.
25. Rao, Y.J., Ribeiro, A.B.L., Jackson, D.A., *et al.* (1995). Combined spatial- and time-division-multiplexing scheme for fibre grating sensors with drift-compensated phase-sensitive detection. *Opt. Lett.*, **20**, pp. 2149–2151.
26. Penn, L.S., Jump, J.R., Greenfield M.J., *et al.* (1999). Use of the free vibration spectrum to detect delamination in thick composites. *Journal of Comp. Mat.*, **33**, pp. 54–72.
27. Chaudry, Z., Lalande, F., Ganino, A., *et al.* (1995). Monitoring the integrity of composite patch structural repair via piezoelectric actuators/sensors. *AIAA/ASME/ASCE/AHS/ASC 36th SDM Conf.* New Orleans LA, **4**, pp. 2243–2248.
28. Islam, A.S. and Craig, K.C. (1994). Damage detection in composite structures using piezoelectric materials. *Smart Mat. and Structures*, **3**, pp. 318–326.
29. Pearce, P.J., Arnott, D.A., Camilleri, A., *et al.* (1998). Cause and effect of void formation during vacuum bag curing of epoxy film adhesives. *J. Adhesion Sci. Technol.*, **12**(6), pp. 567–584.
30. Galea, S.C., Powlesland, I.G., Moss, S.D. *et al.* (2001). Development of structural health monitoring systems for composite bonded repairs on aircraft structures. *Proc. of the SPIE 8th Annual Int. Symposium on Smart Structures and Mat.: Smart Structures and Integrated Systems Conf.*, Newport Beach, CA, USA, 4–8 March 2001. Paper 4327–33.
31. Chester, R. (1999). Life extension of F/A-18 inboard aileron hinges by shape optimisation and composite reinforcement. DSTO-TR-0699, January.

Chapter 21

ADHESIVELY BONDED REPAIRS: MEETING THE SAFETY REQUIREMENTS IMPLIED WITHIN EXISTING AVIATION INDUSTRY CERTIFICATION REGULATIONS

D. BOND

Department of Mechanical, Aerospace and Manufacturing Engineering, UMIST, Manchester, UK

21.1. Introduction

The process of aircraft structural certification has evolved over many years. However, the objective remains the same; to ensure that the structure is airworthy (i.e. safe to operate) based on accepted standards. The evolution is the result of an ever-improving understanding of the threats to structural integrity and its incorporation into the accepted standards. *Ergo*, certification of modern aircraft structures is essentially a process of identifying possible failure modes, assessing their probability of occurrence and developing guidelines to ensure that this probability is reduced to an acceptable level. Guidance on the certification of aircraft is provided in a variety of regulatory authority documentation such as the United States (US) Federal Aviation Authority (FAA) Regulations (FARs), European Joint Aviation Authority (JAA) Regulations (JARs), United Kingdom (UK) Ministry of Defence (MoD) Defence Standards (e.g. DEF STAN 00-970 [1]) or US Department of Defence (DoD) Military Guide Specifications (e.g. MIL-A-8860 [2] and MIL-A-83444 [3]).

Early aircraft designers and certification authorities were primarily interested in failures caused by static overloading of the aircraft. Since then, increases in engineering knowledge and/or in-service failures have led authorities to add additional requirements for *inter alia*, metallic fatigue, corrosion, multi-site damage and, for composite structures, the effects of environmental exposure and impact damage. Mature, proven requirements exist and are used for certification of conventional metallic, mechanically fastened aircraft structures as a result of the vast amount of experience with this form of assembly. The introduction of composite materials into modern aircraft structures forced a review of these certification procedures which resulted in few alterations to the regulations

developed for metallic structures, but required the publication of interpretative and advisory material to ensure that the unique behavioural aspects of composite materials were addressed [4–6].

The use of bonded repairs should create much less of an impact than the introduction of composite materials but nonetheless, requires a similar review of the standards. To repair an aircraft implies that the resultant configuration will still meet the original certification basis (i.e. the standards to which the production aircraft have been shown to comply). The review must address the significant differences between traditional mechanically fastened repairs and those adhesively bonded including (see Figure 21.1):

- The adhesive being the sole mechanism for load transfer in the repair whereas, in a mechanically fastened joint, multiple fasteners provide multiple load paths.
- The high dependency of bonded repairs on production processes where any inadequacies can result in unexpected and unobservable degradation of repair performance.
- The inability to reliably predict and/or non-destructively inspect bonded repair for their long-term durability post-installation.

The intention of this chapter is to examine the applicability of existing requirements to certify bonded repairs and to identify any deficiencies, omissions or ambiguities. Additional guidance to that included in the existing standards is provided throughout to assist in the development of repairs that not only conform to the existing structural certification regulations but also to the safety levels implied within them.

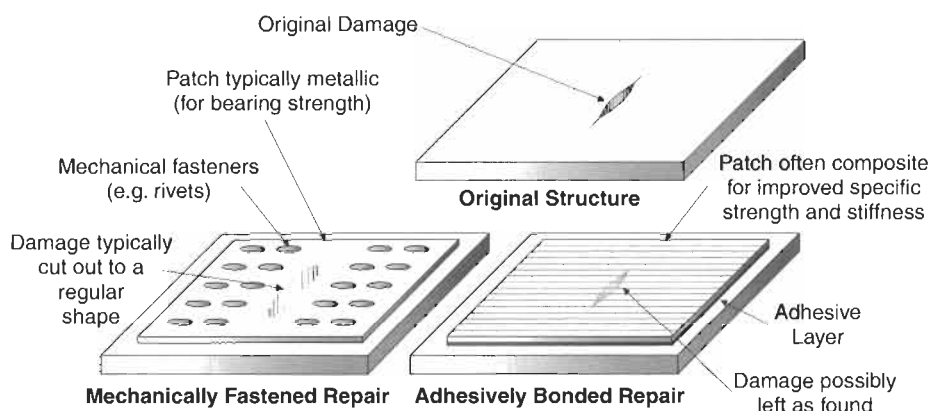


Fig. 21.1. Comparison between traditional and adhesively bonded repairs.

21.2. Certification of an adhesively bonded repair

21.2.1. The need to certify a repair

Most engineers involved in the repair of aircraft structures would be unfamiliar with the need to consider certification issues. Typically a repair will be applied in accordance with the manufacturer supplied structural repair manual (SRM) or Airworthiness Authority directives. What is not recognised is that each of these repairs has had to be shown by the relevant design authority to return the aircraft to its original certification basis. This is to ensure that a repaired aircraft is no less airworthy than a new aircraft.

Adhesively bonded repair technology has only “come-of-age” over the last ten to fifteen years and as a consequence is not often included as an option in SRMs or the practices included are obsolete at best and ineffective at worst. Hence, to utilise the latest advances in this technology which offer reduced repair downtime, more effective repair designs and the possibility of repairing structures unable to be repaired by traditional methods, certification issues must be clearly and concisely stated for field level repair designers so they can understand exactly what design and testing requirements must be met for certification purposes.

21.2.2. Adhesively bonded repairs

To certificate a bonded repair there must be a clear understanding of what the repair is expected to do and the potential failure mechanisms associated with its design and use. To this must be added criteria defining the required level of confidence that the repair will not fail under any of these mechanisms. Once this understanding and these criteria are established, certification of the repair is essentially a process of considering, conducting and accepting methods which can be used to demonstrate compliance of the repair to these criteria.

By definition, a repair “... restores the structure to its original type certification status, or to the certification status that has been modified by the use of approved Supplementary Inspection Documents (SIDS) ...” [7] or Aircraft Structural Integrity Programs (ASIP) [8]. As the repair is expected to restore an original certification basis, the procedures required to certificate it must require the repaired structure to meet the same set of acceptability criteria as was used to gain the original type status for the aircraft. However, the method by which compliance is shown may vary from that used for the original structure.

The potential failure modes that can occur in a structure repaired by a bonded patch are shown in Figure 21.2. With the benefit of hindsight we now know that some of the adhesive bonding procedures used in the past on production aircraft were inadequate and did/will not provide long term durability against adhesive to adherend interfacial failure (Figure 21.2 mode (c)). Yet these techniques must have passed the required tests to gain regulatory authority approval. The problem has most likely arisen from utilising regulations written to cover traditional mechanically fastened procedures but which are inadequate to ensure the required

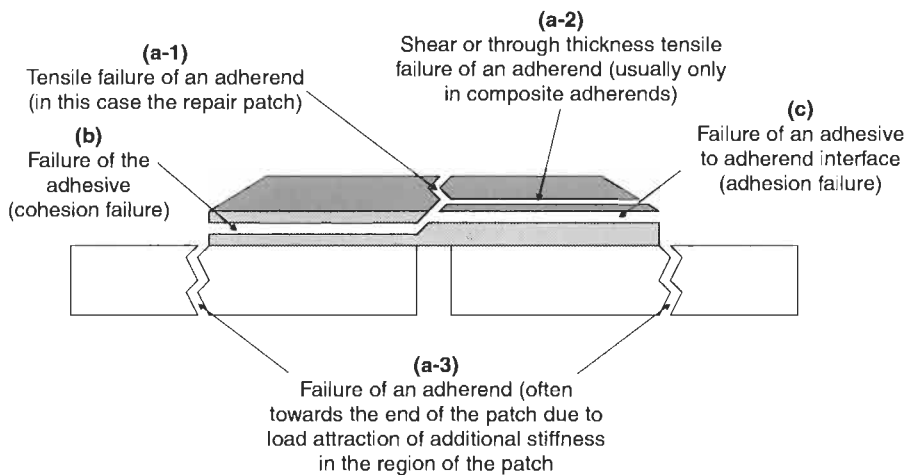


Fig. 21.2. Failure modes in an adhesively bonded repair.

level of performance in a bonded repair. Interfacial failure is highly dependent upon the repair application process, which is the main difference between certification of this type of repair and more traditional approaches. Failure mechanisms in the other three modes are reasonably well understood and predicted using standard analysis techniques provided the other differences between bonded and mechanically fastened repairs are considered, including:

- The structural properties of polymeric materials (e.g. resins and adhesives) often vary significantly more with their operating environments than do those of metallics.
- The adhesive is not entirely in its elastic state and bond strength is dominated by the contribution of plastically deformed adhesive.
- Through-thickness stresses developed as a result of load path eccentricity must be carried by the adherends as well as the adhesive¹ (as opposed to mechanically fastened repairs where such stresses are carried predominantly by the fasteners).

21.2.3. Regulatory deficiencies

As mentioned above, the problem with current certification requirements is that, in principle, they allow the use of bonded repairs that pass inadequate proof-of-compliance tests, but later fail in service. Most such failures are associated with material and process deficiencies including poor material selection, ineffective

¹ Failure of composite adherends due to this factor does raise some analytical problems as current techniques struggle to adequately address this failure mode near the surfaces bonded to the adhesive. However, failure in the matrix is the preferred mode for composite adherends as this indicates that the critical design condition is not associated with the adhesive/adherend interface and is a property of the adherend material and repair.

surface preparation process or poor work practices [9]. These problems represent not only the absence of appropriate guidance on specific adhesive bonding issues in the existing regulations but also a lack of understanding of the technology.

Regulatory authorities are moving away from providing specific methods of how a certain level of airworthiness is to be achieved, preferring to state the requirement and provide guidance on how the requirement has been complied with in the past. This approach allows more flexibility and ingenuity in any certification program and is ideal for the certification of traditional forms of structure, which the industry has extensive experience with. However, as the industry has significantly less experience with bonded repair technology it would not be inappropriate for certification requirements on bonded structures to be more stringent and specific until experience is gained. For example, most regulatory bodies require the design of the aircraft structure (including repairs) to "... protect the safety of flight structures from potentially deleterious effects of material, manufacturing and processing defects through proper material selection and control, control of stress levels, use of fracture resistant design concepts, manufacturing and process controls and the use of careful inspection procedures" [3]. However, such requirements are often misinterpreted to mean that the repair must exhibit an acceptable fatigue life. While this is not incorrect, what is not recognised is that bond durability is not demonstrated by fatigue testing alone. Even fatigue tests conducted under extreme environmental conditions do not fully address the interfacial durability phenomena in bonded repairs that are dependent on time as much if not more than on load cycles.

This chapter utilises the United States Air Force (USAF) structural integrity program breakdown from MIL-HDBK-1530 [10] to describe currently documented and relevant certification requirements related to bonded repairs, utilising extracts from both military and civil regulations as examples. The issues associated with structural certification and the management of structural integrity are almost identical and the handbook provides a logical breakdown of the relevant aspects of design, construction and on-going fleet management.

21.3. Repair design information

21.3.1. Existing requirements

Typically the design service life of a repair will be set to ensure it exceeds the remaining service life of the aircraft or some period of time or flying hours to allow the structure to operate until a more significant repair can be introduced. If using traditional repair techniques, varying qualities of repair application process may be used depending on the required life of the repair (choice of fastener, surface treatment *etc.*). However, with the current knowledge of bonding technology a bonding process cannot be varied depending upon its required service life (i.e. a shorter service life does not mean a less rigorous process can be specified) as the effect of process parameters on the durability of the interface has yet to be fully characterised.

There are varying requirements for determining the design usage spectra depending on the certifying authority. The USAF for example, require the development of two spectra; the first being the usage of an aircraft in a fleet above which severity only 10% of the fleet would be expected to operate (i.e. the 90th percentile severity) which is then used for durability analysis and testing and the second being the median fleet usage (i.e. the 50th percentile severity usage) which is used for damage tolerance analysis [2]. In contrast, the UK MoD only require the establishment of the mean fleet usage spectrum for both analyses but utilise different safety factors to those used by the USAF to achieve a similar probabilistic level of safety in the structure [11]. For a bonded repair, the spectra used for analysis and/or testing should be consistent with that used for the original structure.

The service environment of the repair must be determined considering issues such as temperature and moisture profiles and the various fluids the assembly may encounter (e.g. fuel, sealant, hydraulic fluid) [6]. In this way the certification of a bonded repair against environmental degradation is similar to the certification of a composite structure. The FAA and JAA rely upon an Advisory Circular (FAA – AC & JAA – ACJ) to address the specific needs of composite structures not adequately covered in the actual regulations. “The extent of testing and/or analysis and the degree of environmental accountability required will differ for each structure depending upon the expected service usage, the materials selected, the design margins, the failure criteria, the database and experience with similar structures, and on other factors affecting a particular structure” [4,5]. Specifically, for design purposes, “... environmental design criteria should be developed that identify the most critical environment exposures including humidity and temperature, to which the material in the application under evaluation may be exposed ...” [4,5].

For civil aircraft, critical design conditions for temperature/load interaction are frequently associated with solar heating on the ground in combination with the high loads generated on take-off. These temperatures are a function of aircraft livery, wind conditions and local humidity (i.e. wind chill factor). Maximum aircraft design temperatures of greater than 80 °C are possible on civil aircraft under worst-case conditions. UK Military requirements [12] provide detailed temperature limits for design purposes based on the analysis of air temperature measured regularly at various locations throughout the world. For example, the maximum air temperature at sea level in which an aircraft must be able to operate is taken as 45 °C (although it is noted that this is not the highest ever recorded but simply a realistic upper design level). The minimum air temperature at sea level from the data recorded indicates that a level of –40 °C should be specified.

Tests on metallic wings in Australian dry tropic conditions have shown that upper temperatures may reach 87 °C, 5 to 10 times per annum and can possibly exceed 100 °C on rare occasions. To account for this solar radiation heating, UK military requirements specify that the aeroplane and its equipment must be able to operate when they have acquired a temperature of 70 °C. “In addition, to allow for the absorption of heat due to solar radiation, the aeroplane and its equipment when

subjected to a temperature of 90 °C should not be damaged and should be capable of immediate operation without adjustment when the temperature drops to 70 °C” [12].

To account for environmental moisture effects, composite components are typically designed using parameters equivalent to those of the material when it has been conditioned to saturation in an 85% RH environment [6]. This condition can be read directly to mean that the adhesive must also be designed to perform in a similar condition. Realistically though, the adhesive is unlikely to reach saturation as it usually only has its edges exposed to these atmosphere. However, these edges will approach saturation and this is where the majority of the adhesive load capacity is developed hence the requirement is reasonable and conservative. This has limited effect on lower temperature design cases and usually only becomes critical at elevated temperatures. As with the design usage spectra, the environment used for analysis and/or testing should be consistent with that used for the original structure.

21.3.2. Additional guidance

Of particular concern to bonded repairs are the extreme hot/wet and cold/dry conditions as in the former the adhesive is at its most compliant (i.e. low stiffness), while in the latter condition the adhesive is at its most brittle. Both these conditions must be considered in the design process even if they do not correlate with the condition at which the repair must carry its maximum load/stress as they represent extremes for the load capacity of the adhesive.

21.4. Analysis and development testing

21.4.1. Design allowables

21.4.1.1. Materials

Existing requirements

The design and analysis of the original aircraft structure would have required that materials and processes with well-established performance allowables be used. The same is therefore necessary for the materials and processes used in the repair of the structure. Typically, aircraft certification authorities require the material allowables such as strength and stiffness to be determined using stringent statistical approaches often involving numerous coupon tests (e.g. MIL-HDBK-5 [13]). Civil regulations for material allowables provide an excellent summary of the general requirements for development of such data requiring that, “... the suitability and durability of materials used for parts, the failure of which could adversely affect safety, must:

- be established on the basis of experience or test,
- conform to approved specifications that ensure their having the strength and other properties assumed in the design data, and
- take into account the effects of environmental conditions, such as temperature and humidity expected in service” [14].

Additional guidance

Bonded repairs should not be designed on the basis of adhesive material properties derived from short overlap strength tests as such tests do not accurately determine the adhesive system parameters necessary to calculate the adhesive load capacity. Existing standards [15,16] usually specify that single lap shear specimens are acceptable without distinguishing between tests such as (ASTM D 1002 [22]) and thick adherend tests (such as ASTM D 3983 [17]) [15]. Adhesive load capacity is estimated from adhesive shear stress-strain data and lap shear specimens typically fail due to out of plane bending in the adherends developing significant peel stresses in the adhesive. Lap-shear strength data is only valid for joints expected to exhibit such adherend deformation [18]. Adhesive load capacity should be derived from thick adherend tests as they eliminate significant adherend bending.

21.4.1.2. Processes

Existing requirements

Process allowables are particularly critical in adhesive bonding where the surface preparation and type of bonding process utilised can have significant effects on bond performance. A typical example of the regulations detailing processing allowables can be found in the FARs, "... The methods of fabrication used must produce a consistently sound structure. If the process requires close control to reach this objective, the process must be performed under an approved process specification, ... and ... each new aircraft fabrication method must be substantiated by a test program ..." [19].

A bonding process involves a number of steps including; adherend surface preparation, repair lay-up and temperature and pressure application for bond cure. A sound bonded repair is dependant upon the successful formation of durable chemical and attractive polar bonds between the adhesive and the adherend surface [20]. Poor execution of any of the aforementioned steps can be critical to the performance of the repair with surface preparation being the step most difficult to perform effectively. For example, during surface preparation the requirement to have a clean bonding surface with adequate surface energy to facilitate adhesive wetting is obvious and usually obtained. However, the need (particularly with metallic adherends) for an enhanced level of surface chemical activity is often not appreciated but is required to increase the resistance of the bond to hydration and improve its service life. Currently the ability of a bonding process to produce hydration resistant bonds may only be fully determined from service experience or similar long term testing.

For example, many older aircraft components were made using an FPL etch and sealed chromate-anodising process. Royal Australian Air Force (RAAF) experience with this process is that many bonded components suffer interfacial failure in service and now only allow this process to be used with painting.² Clearly, while the

² FPL combined with unsealed chromate anodising does however, produce a good surface for adhesive bonding.

process ensures that the adherend surfaces have been adequately cleaned, the required resistance of the bond to hydration has not been achieved. The experience with some SRM recommended repair processes is similar. The “scuff sand and solvent clean” surface preparation method used for bonded repairs in the early days of F-111 service also fails to provide a hydration resistant bond. These and many other processes often provide an uncontaminated wettable surface, but fail to develop the enhanced surface chemical activity required for environmental durability and, although they demonstrated adequate short-term strength, frequently disbond in service. If the ability to resist hydration had been interrogated as part of a certification program for these repair processes, none of them would have been approved for use.

The requirement to investigate the environmental durability of bonded repairs is analogous to the need for fatigue testing of mechanically fastened structures. The difficulty is in how a bond can be demonstrated to possess acceptable durability. The approach typically adopted is to evaluate the process by which the bond was formed. Many commonly used surface preparation processes have relied solely upon static strength [21] through use of lap-shear tests (such as ASTM D1002 [22]) to indicate the durability of the adhesive bond produced. Other test programs [23] have used uniaxial fatigue loading however, such tests do not interrogate the resistance of the bond to hydration. Tests such as the load-endurance test (ASTM D 2919 [24]) rely on the application of a static load that places the bond in shear whilst exposed in a hostile environment. While this approach appears representative of the in-service conditions experienced by the bond, it does not produce consistent results and service experience has shown that some preparation methods validated using this test do not produce durable bonds [25].

Should an acceptable process be identified through appropriate testing then, as required by [19] for a fabrication method requiring close control, quality management procedures must be used to provide confidence that the repair bond has been correctly installed so as to result in adequate strength and durability. Current civil regulations provide little guidance on this issue although the RAAF adhesive bonding handbook [26] does provide detailed requirements for an appropriate quality management process. The handbook includes the need to develop detailed process specifications, a requirement to ensure competent trade-persons perform the work and describes the type of process documentation that should be used to increase the likelihood for success with the process.

Additional guidance

The presence of moisture absorbed into or adsorbed onto either the adhesive or the adherends will compromise the integrity of any repair formed between the two [27,28]. Care should be taken to prevent excessive exposure to moisture for the adhesive and the repair process should include mandatory drying of all adherends. Analysis tools do exist to calculate optimum drying times [27,28] although they are complex and require a significant amount of specialised material data. A general approach that has proven to work well for the RAAF is to require a minimum of

1 h at 110 °C for monolithic metallic and composite adherends and 2 h at the same temperature for honeycomb core.

The environment where bonding is to be performed is important when dealing with polymeric materials since it can affect the final properties of the joint. The conditions for in-situ repairs need extra scrutiny since an ideal environment is more difficult to obtain or control than in a production environment. Cure cycle temperatures, pressure and the humidity in the area where uncured adhesives or composites are exposed are all critical parameters. Data from the Defence Science and Technology Organisation (DSTO) in Australia showed that exposure of one type of film adhesive to 85% RH and 29 °C (85 °F) for one hour resulted in excessive micro-voiding when cured under vacuum and the shear and peel strength decreased by approximately 50% [42]. An acceptable bonding environment for adhesives in common use today is shown in Figure 21.3. This envelope controls; (a) the humidity level to reduce moisture absorption into both the adhesive and composite (if used) and (b) the temperature to ensure that an acceptable level of tack is maintained in both products during the bonding process.

As previously mentioned, surface preparation is the single most important factor influencing the ultimate success or failure of a bonded joint. Obtaining initial bond strength is not difficult, however moisture degradation of the interface between the adherend and the adhesive is the critical mechanism to consider in any testing. This is especially true for adhesive to metal bonding. The degradation process is primarily time dependant (although elevated loading and thermal cycling have also been reported to contribute to the rate of the process [27]). Use of a “knock-down” factor to account for inadequate surface preparation is inappropriate, as the “knock-down” for poor surface preparation would have to approach 100% over time. The capability of bonded interfaces between adhesives and metal components to withstand the effects of environmental exposure should be demonstrated separately and in addition to static strength or fatigue related load tests.

The (Boeing) wedge test is currently acknowledged as the most reliable, low-cost method for discriminating (qualitatively) between various surface preparation processes. In the test, the adhesive and interface are placed under tension (the worst loading case for adhesives) at or near the ultimate strength of the adhesive. Any

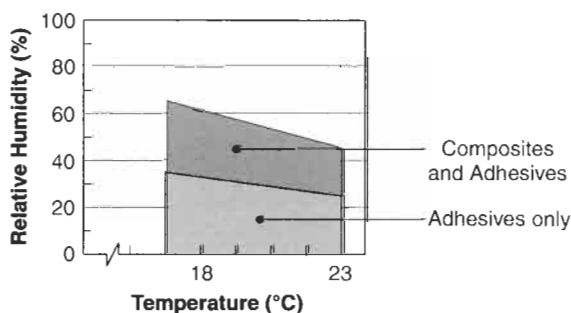


Fig. 21.3. RAAF engineering standard [26] bonding environment.

weakness in the interface results in the propagation of a crack through the interface indicating that it is unable to support the full adhesive capability. An acceptable procedure for the wedge test is contained in ASTM D 3762 [29], but the stated acceptance criteria are not sufficient for the aerospace industry. The following are considered more appropriate [25,26,42]:

- Tests should to be performed at 50 °C, 95% humidity, non-condensing.
- Initial crack lengths are to be measured one hour after insertion of the wedge while exposed in a laboratory environment. The crack length measured must not exceed 1.2 times the crack length obtained from specimens prepared using the same adhesive to bond aluminum (2024) adherends prepared using phosphoric acid anodising to BAC 5555.
- In all cases, the initial crack length must not exceed 50.8 mm (2 in.).
- The average crack growth must not exceed 5.08 mm (0.2 in.) after 24 h nor exceed 6.35 mm (0.25 in.) after 48 h exposure.
- The surface generated during exposure must not exhibit greater than 10% adhesion (interfacial) failure.

Experience has shown that adhesive bonds produced using processes that comply with these criteria demonstrate acceptable in-service durability. As a broad guide, processes that comply include phosphoric acid anodising (PAA) and the grit-blast and silane method [30].

Most quality control programs currently employed for adhesive bonding processes rely upon companion coupon tests and post-bond NDI [31] even though such practices do little to either increase the likelihood of success or provide any real evidence of an acceptable repair installation. The companion coupons are typically lap-shear samples that, as previously mentioned, do not adequately test bond durability. Preferred tests such as the wedge test often take too long to be of value in production and even when schedules allow this test to be conducted, the acceptance values currently prescribed by ASTM D3762 [29] are so low that the companion coupons only occasionally fail. Even if appropriate acceptance values are used, the performance of a companion coupon does not guarantee that the bond formed on the aircraft component will be acceptable. Similarly, there is no NDI method currently available that will assure bond integrity. Ultrasonic and X-ray methods may detect the presence of voids, disbonds and other defects that may be significant, but the absence of these is insufficient as a measure of bond quality. The main concerns are that no method evaluates the degree of cure of the adhesive and the resistance of the adhesive-adherend interface to hydration.

For these reasons, quality management practices rather than quality assurance testing should be used to achieve adhesive bond integrity. Quality management requires the task to be performed by competent technicians following approved process specifications that have been validated as being capable of providing durable bonds. Each facet of this statement is important; the technicians should be appropriately trained and assessed as competent in performing the process unsupervised (i.e. self-signing) and the process specification must follow exactly the process that has been validated. While most production shops do follow process

specifications, there are numerous examples where local process variations have been introduced without validation and, in many cases, “industry standards” have been applied in the development of the process specification, rather than appropriate testing [32].

The process specification should detail the adhesive cure cycle since this greatly influences the mechanical properties of the bonded joint. Many adhesives have multiple cure cycles so the specification should identify those that are acceptable. The temperature at the bondline during cure should be monitored and recorded through the use of multiple, separately controlled, heat sources [33] as this provides additional evidence of the adherence to the specification and ensures that heat up rates and dwell temperatures were in accordance with the validated process. The temperature should also be monitored in areas likely to exceed the bondline temperature to ensure that these locations are not overheated.

The method by which pressure is applied to the bond should also be addressed by the specification following the method by which the application process was validated. Although pressure is not required for the chemical cure of the adhesive, the mating of the adherends, wetting of the adherends by the adhesive, the cure pressure and the method of its application all affect the bondline thickness and porosity. Vacuum bag techniques are commonly used for in-situ repairs and when using adhesives prone to porosity, the bagging procedure requires strict adherence to the validated process to avoid excessive voiding.

21.4.2. Static analysis

21.4.2.1. Existing requirements

The structure of an aircraft, whether it be original or repaired, bonded or not, must have static margins of safety³ (MoS) that are zero or greater at the design ultimate load cases. Existing regulatory static strength requirements are relatively uncomplicated and differ only slightly between the various design standards. Typical military regulations require that, “... for all design considerations, strength shall be provided so that the material yield allowable stresses will not be exceeded at limit loads, and material ultimate allowable stresses will not be exceeded at ultimate loads ...” [2]. While this requirement is appropriate for traditional mechanically fastened repairs using materials almost entirely within their elastic range, bonded repairs utilise the plastic performance of the adhesive so some interpretation of the requirements is necessary. Similar civil regulations provide less proscriptive requirements, “The structure must be able to support limit load conditions without detrimental permanent deformation ... and at any load up to limit loads, the deformation may not interfere with safe operation ... The structure must be able to support ultimate loads without failure for at least 3 seconds ...” [34].

³ MoS = (Actual performance/Design requirement) – 1.

Design limit loads (DLL) are defined to be the maximum loads the aircraft is expected to experience in service while Design ultimate loads (DUL) are derived by applying suitable safety factors to the DLL conditions. A value of 1.5 is typically accepted as the base safety factor for DUL, but other factors may be required in specific circumstances to take into account additional variability or uncertainty associated with the design. Guidelines for developing the safety factors are included in the design standards and some consideration to appropriate factors for bonded repairs is appropriate when seeking certification. Typically the safety factors required for composite materials would be applicable for a bonded repair (see [4,5]).

21.4.2.2. Additional guidance.

The critical DUL case for a location determines the minimum notched material strength required and hence the minimum allowable thickness (t_{\min}). Should the component be designed thicker than this (t_{actual}), the structure may be able to withstand a greater load than DUL i.e. the Structural ultimate load (SUL). The capability of the repaired structure to withstand any of these loads is required to be demonstrated by an appropriate combination of analysis and test.

In the absence of pre-existing test data the minimum extent (i.e. number and type of specimens⁴ of the test program should be based on the predicted adhesive load capacity of the repair although additional testing may be required if the critical failure is found to be other than cohesion failure in the adhesive. Any static testing should ideally be done at representative service conditions. However, it may be acceptable to perform the testing in an ambient atmosphere provided the effects of the environment on the materials are treated in the same manner as accepted by the original certification basis for the aircraft. The adhesive load capacity at a given location (with a given thickness t_{actual}) can be compared to the original structural design loads and found to be (see also Figure 21.4):

- **Condition 1:** Greater than the material ultimate load (MUL) of one of the adherends,
- **Condition 2:** Greater than the SUL,
- **Condition 3:** Greater than the DUL,⁵
- **Condition 4:** Greater than the DLL,⁵ or
- **Condition 5:** Less than the DLL.

Should the adhesive load capacity fall in condition 4 or 5 the repair will not achieve the requisite certification standard of the original aircraft. However, repairs that fall into condition 4 may be used to provide fatigue life enhancement modifications but only where the existing structure is capable of sustaining the

⁴ As a general guide; coupons are specimens used to derive basic design parameters for bulk materials (e.g. dog-bones or thick adherend test specimens), elements derive design parameters for generic structure (e.g. double or single overlap specimens), detail specimens expand the element parameters to a specific design geometry and subcomponents investigate the combining of specific design details.

⁵ Calculated for the repaired structure considering any additional factors introduced by the repair.

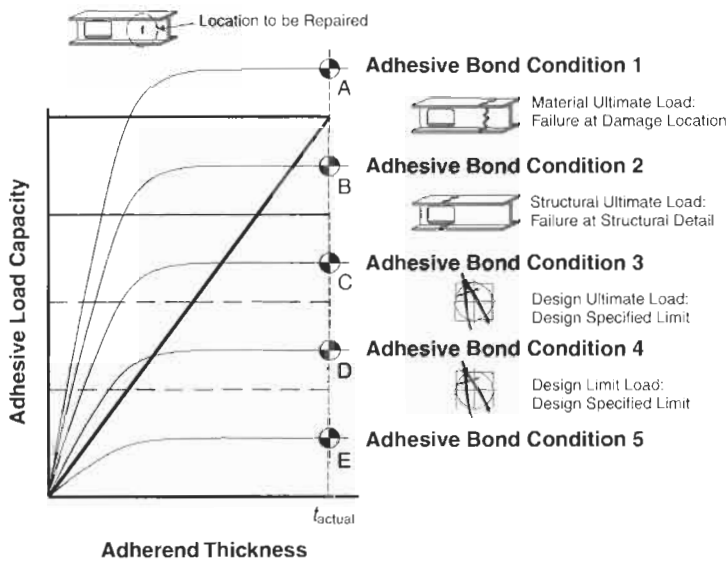


Fig. 21.4. Design conditions for an adhesively bonded repair.

required residual strength⁶ in the absence of the repair. Condition 5 is unacceptable for any structure other than for repairing aircraft operating under flight restrictions (e.g. emergency ferry flights). The flight restrictions are required to reduce the expected in-service loads of the structure to a level where the repair's adhesive load capacity would be sufficient to move the joint into a higher design condition. The certification requirements/guidance for that condition then become applicable to the repair.

As a general rule, the minimum level of test specimen and aim of the test program recommended for providing proof of compliance for bonded repairs is shown in Table 21.1. The recommendations included in the table assume that the repair designer is confident that the identified loading used for the design is accurate and uses modelling techniques validated through previous testing to provide consistent, conservative results. Should static testing using the recom-

⁶ A structure must be demonstrated to maintain a level of residual strength "... in the presence of the defect (damage)" and must be "... able to withstand loads (considered as static ultimate loads) developed by ... limit symmetrical manoeuvre conditions, ... limit rolling conditions, ... limit yaw manoeuvring conditions..." [34]. This ensures that "... the structure has been evaluated to ensure that should serious fatigue, corrosion, or accidental damage occur within the operational life of the airplane, the remaining structure can withstand reasonable loads without failure or excessive structural deformation until damage is detected" [7]. "Static ultimate loads" in this context means that the magnitude of the limit load conditions is not factored to become ultimate loads, but that the structure under these limit load values must meet the ultimate failure criteria. Typically the residual strength requirements vary between 1.0 and 1.2 DLL.

Table 21.1
Recommended aims and specimens for certification testing of bonded repairs.

Condition	Aim of test program	Recommended minimum level of test specimen
1	<ul style="list-style-type: none"> • Static testing should demonstrate that for a generic joint configuration, the load capacity of the adhesive exceeds the adherend material ultimate load. • Fatigue testing should demonstrate that disbonds in the safe life region of the patch do not grow under the expected usage spectra. • Some additional testing or analysis may be required to account for creep and load rates effects. 	REPRESENTATIVE ELEMENT
2	<ul style="list-style-type: none"> • Static testing should demonstrate that for the particular repair configuration, the load capacity of the adhesive exceeds the SUL (which itself could be determined by test or analysis) • Fatigue testing should demonstrate that disbonds in the safe life region of the patch do not grow under the expected usage spectra. • Some additional testing or analysis may be required to account for creep and load rates effects. 	REPRESENTATIVE DETAIL SPECIMEN
3	<ul style="list-style-type: none"> • As the adhesive is the critical element in the new structure certification of the adhesive bond should require a full development testing program (i.e. up to full-scale sub-component level) to demonstrate that the adhesive load capacity is greater than DUL. • Fatigue testing should demonstrate that disbonds in the safe life region of the patch do not grow under the expected usage spectra. • Some additional testing or analysis may be required to account for creep and load rates effects. 	FULL-SCALE SUB-COMPONENT
4	<ul style="list-style-type: none"> • As fatigue enhancement repairs are not necessarily designed to carry DUL, there is only a need to perform static testing to validate that the adhesive load capacity exceeds DLL and as such prevent the repair/modification from failing on an aircraft operating within its design envelope. • Fatigue testing should demonstrate that disbonds in the safe life region of the patch do not grow under the expected usage spectra. • Consideration of the effect of patch departure when in flight is especially important should a load in excess of DLL be encountered. • Note: detailed testing and analysis of the damaged structure would have to be performed in accordance with existing standards to confirm its ability to meet the residual strength requirements 	REPRESENTATIVE ELEMENT
5	<ul style="list-style-type: none"> • Testing applicable to the revised design condition (based on appropriate operational restrictions) should be conducted • For limited operations (such as single ferry flights) and where sufficient experience with the desing and application of bonded repairs exists, there may be cause to further reduce the level of testing required for repairs in this condition. Note that this must be at the discretion of the relevant Airworthiness Authority. 	AS APPLICABLE

mended specimen types demonstrate failure in other than a cohesive mode⁷ in the adhesive or as expected in the adherends, peel stresses resulting from load path eccentricity in the region of the adhesive bond need to be investigated.

Localised bending moments will exist at the end of the repair, resulting in through-thickness stresses in the adhesive and adherends. If these stresses exceed the peel or through-thickness strength of the repair materials, failure will occur. Because peel failures may occur in poorly designed repairs at loads well below those that could cause shear failure, the associated stresses must be considered in repair designs and all efforts made to minimise them. Analysis and testing at the specimen level recommended in Table 21.1 should also consider the factors that affect the peel strength of the final repair configuration. This requires that specimens should reflect as close as possible the geometry of the location to be repaired within the level of specimen complexity suggested (e.g. element adherend thicknesses should match those of the damaged area and proposed repair patch overlap and tapers should match those proposed for the actual repair design). If the peel stresses in a specific repair configuration are not well understood then the minimum level of specimen tested should be increased to provide such understanding (e.g. element to details for Condition 1).

Note that reliable design data for peel strengths of adhesives is difficult to obtain. Typical peel tests such as climbing drum peel (ASTM D 1781 [35]) or T-peel (ASTM D 1876 [36]) do not provide acceptable design data. Designs may often use a rule-of-thumb approach where peel stresses are kept below known acceptance limits for ductile and brittle adhesives [37]. In a similar manner, reliable data for laminate through-thickness strength is also hard to obtain. Because such failures are resin-dominated, the transverse tensile strength of uni-directional laminae or the resin tensile strength are acceptable alternatives.

21.4.3. Fatigue and damage tolerance analysis

21.4.3.1. Existing requirements

General

Both military and civil regulations covering the fatigue and damage tolerance⁸ of an aircraft structure require similar performance:

- “Strength shall be provided so that the fatigue life of the structure will equal or exceed the specified life, including specified scatter factors” [2].
- “The structural design of the aircraft will be such that repeated loads shall not cause failure or permanent deformation of any part of the airplane, interfere with

⁷ Note that full cohesive failure in the adhesive is likely only with metallic adherends and even then some mixed mode failure is likely. Provided that cohesive failure is the dominant mechanism then peel stresses are unlikely to have had significant effect on the demonstrated load capacity.

⁸ In this sense damage tolerance refers to the ability of a structure to tolerate the presence of a defect or damage and for example, can refer to cracks in metallic structures, delaminations in composite materials or disbonds in bondlines.

its mechanical operation, or effect its aerodynamic characteristics ... for the planned service life of the airplane..." [38].

- "An evaluation of the strength, detail design, and fabrication must show that the catastrophic failure, of the structure, due to fatigue, corrosion, or accidental damage, will be avoided throughout the life of the airplane" [39].

Interpretation of these concepts and means of showing compliance is more complex than is the case for static strength. A complexity is that aircraft have been accepted using different philosophies *viz.* Safe-Life, Fail-Safe and Safety-by-Inspection.

Safe-life

In a Safe-Life aircraft fatigue and damage tolerance is managed by demonstrating a specified service life during which the aircraft will be free of critical defects. The fatigue life is typically determined by full scale test scaled by appropriate safety factors e.g. "... the usage spectra will not cause structural defects (cracks, deformations, loss of modulus, delaminations, disbonds, *etc.*) within four lifetimes if proven by analysis, and 2 lifetimes if proven by full scale tests," [38] or "... the cornerstone of safe-life substantiation is a full scale test of a complete airframe to a factor of 5 times the service life." [40]. Damage tolerance is usually assessed on a probabilistic basis for safe-life aircraft and only limited testing on the most extreme cases is conducted (e.g. birdstrike).

This approach is quite reliable for metallic and traditionally fastened structures due to the degradation of such parts only being slightly affected by the environment and the factors used having been developed on similar structure [41]. An equivalent approach for bonded repairs would have to account, not only for the variation in performance of the constituent materials (i.e. adherends and adhesives), but also for the variability in the adhesive bond introduced by having repairs installed in non-standard environments, with slight alterations to each application process and as conducted by a variety of technicians.

Fail-safe

The Fail-Safe methodology of structural certification ensures ongoing structural integrity by requiring the design provide an alternate load path should a structural component fail. The use of the Fail-Safe methodology is critical for components that are difficult or costly to inspect as such structures can be left until failures can be identified by inexpensive techniques. Repair of a Fail-Safe structure by adhesive bonding is the ideal opportunity to utilise the full benefits of such a repair as even should the repair unexpectedly fail, the certification basis of the overall aircraft would not be compromised and the required level of safety maintained. Care must be taken however, to ensure that the application of a bonded repair does not mask the detection of failure of a Fail-Safe structure e.g. if a bonded repair was used to patch a crack in a Fail-Safe structure and for some reason failed to prevent the crack growth, the eventual complete failure of the repaired structure must be as easy to detect as it would have been in the original structure.

Safety-by-inspection

The “Safety-by-Inspection” approach (also known as “Slow-Crack-Growth” when used to consider fatigue crack growth in metallic structures [3,42]) is used when the structure has no alternate load path and relies upon regular inspections to maintain the safety of the structure. The initial “safe” operating period of the structure (the threshold) is equivalent to the minimum time over which the worst expected initial flaw in the fleet population would be expected to grow to a critical size or in which accidental damage leading to a defect of critical size is expected (critical size being that at which the structure would not be able to demonstrate an acceptable residual strength). The threshold value, “... can be established using either ... (1) fatigue analysis and test with appropriate scatter factors, or (2) slow crack growth analysis based on appropriate initial manufacturing damage ...” [43] and requires the assumed initial flaw to be “... of the maximum probable size that could exist as a result of manufacturing or service induced damage ...” [43]. For adhesive bonds, “slow crack growth analysis” is analogous to an assessment of disbond growth. The time to the first inspection is this threshold value divided by a safety factor, typically 2 [2,38] or greater [11]. After an inspection, if no damage is found, the flaw in the structure is assumed to be equivalent to the largest flaw that the inspection technique used could not reliably find. Should a flaw be found, it may either be left or repaired depending on its effect on structural integrity. A revised inspection period is then calculated for the new structural configuration.

The Safety-by-Inspection methodology lends itself to the application of bonded repairs especially when used to provide service life extension through their ability to reduce crack growth rates in metallic structures or to reduce delamination growth rates in composite structures. However, the lack of confidence in patch durability and the current interpretation of regulatory guidelines (such as quoted from [43] in the preceding paragraph) have led authorities to require the structural integrity of the repaired structure to be assessed in the absence of the repair i.e. the full degradation of the adhesive bond is considered as a possible initial or induced flaw. Such a practice within the USAF requires the damaged structure to be capable of withstanding at least DLL in the absence of the repair while amendment proposals for the UK MoD design standard [44] requires a capability to withstand 1.2 DLL (the UK MoD definition of Residual Strength). Bonded repairs using these practices are nothing more than fatigue life enhancements having ignored the structural contribution of the repair. Indeed the USAF and UK approaches require inspection intervals to be calculated ignoring the stress reduction/damage growth rate reduction produced by the repair. This is essentially due to the inability to guarantee the integrity of the bond by post-repair NDI.

One organisation, which has taken the step to consider the contribution of a bonded repair, is the RAAF in its management of fatigue cracking in the lower wing skin of a F-111 aircraft [45–47]. Initial investigations suggested that the cracking was close to critical length for the aircraft operating in its normal flight envelope. The repair design, based on a combination of the Hart-Smith [48] design principles and the Rose model [49] was validated by finite element analysis (FEA) and a detailed experimental program. Fatigue testing performed on representative

sub-components [50] confirmed the modelling predictions that the crack growth under the patch would be retarded significantly and remain slow and stable for a period several times the anticipated remaining life of the aircraft. After incorporation of the repair, the wing saw a further 665 operating hours prior to being retired for use as a fatigue test article. NDI assessment using several inspection methods was unable to detect any crack growth from when the patch was applied. This approach was adopted due to RAAF experience demonstrating that a combination of highly trained technicians and quality management procedures provide high confidence in the integrity of the applied repair.

Damage tolerance

The airworthiness standard covering the substantiation of composite rotorcraft structure has recently been revised [51] and provides the only available regulatory guidance on how to deal with damage tolerance certification for bonded joints. Specifically "... unless the ultimate strength of each critical bonded joint can be reliably substantiated in production by NDI techniques ... then limit load capability must be guaranteed by either of the following or a combination thereof: (A) The maximum disbond of each critical bonded joint ... is established by test, analysis or both. Disbonds greater than these values are typically prevented by design features. (B) Each critical bonded joint on each production article should be proof tested to the critical limit load." While these requirements are quite demanding for a production component they may be impossible to conform to on bonded repairs and a more general approach is necessary.

21.4.3.2. Additional guidance

Fatigue

Currently no information has been publicly released to quantify the appropriate scatter factors to account for the variability associated with adhesive bonding. In view of this, Safe-Life qualification of a bonded repair through extended fatigue testing as required for aircraft structures would be difficult to accept for certification purposes without significant additional testing to determine the appropriate factors. This approach has however been used for production bonded structures where the approving airworthiness authority has been confident that the bond has been applied under closely controlled circumstances that could be guaranteed to directly relate to the coupon, element, or sub-component tests that were included in the substantiation data.⁹

Experience has shown that adhesive bonds are very fatigue resistant [48] provided that adhesive peel strains are kept low and shear strains in the adhesive are kept predominantly in the elastic range. Existing RAAF bonded repair design methodology [26] utilises a pseudo Safe-Life approach and has had success in

⁹This approach was adopted for production bonding processes used on F/A-18 and Eurofighter due to the increased confidence by the relevant Airworthiness Authorities in manufacturers being able to control production process variables to produce a consistent bond.

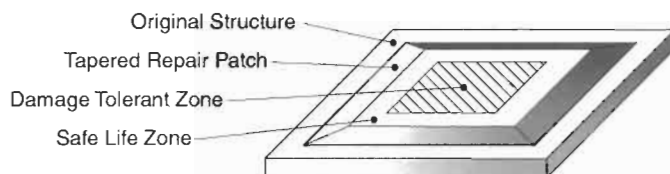


Fig. 21.5. Safe-life and damage tolerance zones in an externally bonded repair.

preventing fatigue failures from occurring in bonded repairs using ductile adhesives by ensuring that the adhesive shear strain is less than twice its elastic limit ($2\gamma_e$) when the repair is subjected to 60% of DLL. For brittle adhesives the strain allowable recommended is the elastic limit (γ_e). Recent reviews of this philosophy have suggested increasing the corresponding load level from 60% to 80%. This recommendation is supported by Baker [52] who demonstrated that loading producing only limited plastic deformation in the adhesive of a representative bonded joint is able to be tolerated over a significant number of cycles. However, it should be noted that in later studies on similar joints, representing generic repairs with boron/epoxy patches, it was found that fatigue failure occurred in the matrix resin of the boron/epoxy, rather than in the adhesive. As reported in Chapter 5 this failure mode is thought to be dependant, at least for disbonding over the crack in the parent structure, on the shear-strain range experienced by the adhesive.

As a certification approach, such a methodology, being based on allowable strains or other similar criteria, requires extensive knowledge and experience of the specified repair adhesives and the stresses developed in the particular bond geometry. The necessity for this background information makes use of such an approach difficult for “new” employers of bonded repair technology.

Baker [53] provides a novel concept for bonded repair design for conditions where fatigue failures may be of concern suggesting that the patch be considered in two zones (as shown in Figure 21.5):

- **Safe-life zone** at the tapered ends of the patch where damaging strains in the adhesive system are shear and peel.
- **Damage tolerant zone** in the middle where damaging strains are predominantly shear.

To prevent rapid loss of the patch due to fatigue disbonding, adhesive strains in the safe-life zone at the patch ends should not exceed the level that would produce disbonding in the service life of the repair. Even slow initial disbond growth in this region is unacceptable since once the disbond grows outwards and reaches the inner edge of the taper region, strains dramatically increase and growth becomes rapid. Thus the patch system in this region must be designed on a Safe-Life basis. This should be achieved by limiting strains in the critical regions through design (e.g. appropriate end tapering, increased adhesive thickness *etc.*) and use of appropriate strain allowables (possibly taken from the RAAF experience above). With considered patch design for thin adherends (approx. <3mm) quite low strain levels can be achieved so as not be a concern in most repairs. In the damage

tolerance zone, limited disbond growth in the patch system is acceptable as such growth is typically stable and, if not large, has only a minimal effect on the repair efficiency. This approach is already recognised as being possible by some certification authorities [6]. Testing to demonstrate the compliance of a repair to these requirements should be conducted at a specimen level equivalent to that recommended for the corresponding static strength design conditions (see Table 21.1).

In repairs to thick cracked structures (approx. >3 mm) with high load requirements, the bond line around the defect is highly stressed and damage growth can be expected and tolerated. In such a condition the minimum level of testing recommended is a sub-component program to demonstrate the stability of such disbond growth up to the critical defect size. A certification approach similar to “slow-crack-growth” for metallic structures may then be used to certify the structure based on the knowledge of expected disbond growth rates for the given usage spectra.

Damage tolerance

The damage tolerance evaluation of a repaired structure is intended to ensure that should serious fatigue, corrosion, accidental damage or other form of defect occur within the design service life of the repaired structure, the remaining structure will withstand reasonable loads without failure, or excessive structural deformation until the damage is detected. When considering failure scenarios and residual strength, the behaviour of the global aircraft structure in the presence of the repair should be considered and not just the macro details of the repair elements.

Initial flaws should be assumed to exist as a result of material, manufacturing and assembly of both the original structure and the bonded repair as required by existing regulations. Initial flaws in the immediate area of the repair should be those associated with the detectable limits of the post-repair NDI procedure. The damage tolerance evaluation should cover the simultaneous occurrence of the most adverse combination of flaws in both the original and repair elements of the structure as well as the existence of a defect in the bondline. Note that this defect is assumed to be limited to voids or disbonds (detectable by NDI) due to the use of acceptable bonding processes and a quality management system resulting in a repair resistant to environmental degradation. Where a bonded repair is located directly over a defect without that defect first being removed, this defect should be considered as integral to the new structure and its behaviour under the repeated load environment evaluated in combination with the most critical initial defect(s) assumed to exist in the repair element and bondline.

21.4.4. Development testing

21.4.4.1. Existing requirements

The current process for testing bonded structures closely resembles that used for the certification of composite structures i.e. a building block process that

progressively interrogates the design typically including coupon, element, detail, sub-component and component testing to prove the design meets strength, fatigue, damage tolerance and durability requirements. Ideally the effects of the environment should be considered in such testing. However, this results in expensive testing programs and is often substituted for by the use of suitable “knock-down” factors applied to material allowables (developed from the less expensive environmental testing of elements and coupons) and/or testing at elevated load levels.

The test program typically utilises the coupons and elements to develop basic material and generic design allowables and the more complex specimens to evaluate the effect that mapping the generic structure onto specific details and components has on the allowables and/or analysis techniques. This is aimed at providing the certifying authority with the required level of confidence that the design calculations and expected performance of the structure will be realised in the production items. Development testing for bonded repairs should not be significantly different to that used for the original structure on the aircraft certification program. However, unlike for the original structural clearance (that proceeds onto full-scale testing), it represents the highest (realistic) level of testing that can be used to provide the necessary proof of repair performance. The format of the element/detail/sub-component test matrix will vary between individual repairs (see the recommendations of Table 21.1) and Airworthiness Authorities. A possible approach to save time and cost in such a test program may be to utilise representative joints (detail to component level) to simultaneously generate material (coupon), detail and scaling effect allowables [54].

21.4.4.2. Additional guidance

Static testing to provide proof of compliance to regulations typically uses a 1.5 load enhancement factor to prove that the structure is capable of meeting the DUL requirements. This factor does not however, account for the variability in material or assembly performance but only for that in loading. In the design process the variability in material/assembly performance is accounted for by the use of “B” basis allowables. However, testing to a design envelope factored by 1.5 does not provide clearance against the material/assembly variability as it only provides evidence of compliance for the requirement to account for loading variability (i.e. the 1.5 factor used in the design process to determine DUL). Testing to DUL for metallic and mechanically fastened structures has traditionally been acceptable as the variability in these types of structure is sufficiently low (typically less than 0.05) that any correction factor is insignificant. When the variability in material and/or assembly performance exceeds this level (not uncommon with bonded joints), special consideration should be given to the effect of the variability on the necessary load enhancement factor for proof of compliance testing. In such cases, the material and assembly variability should be accounted for in testing by increasing the ultimate load capability that has to be demonstrated.

21.5. Full scale testing

21.5.1. Existing requirements

Full scale testing of an original aircraft design demonstrates the performance of the complete structure under representative loading (and ideally environment) conditions. Such testing of an original design acts as the final proof of concept stage and is required by existing Airworthiness Authority regulations [11]. A similar final proof of concept stage is not expressly required for bonded or mechanical repairs in any existing regulations. Clearly this level of testing is impractical for non-standard repairs (SRM recommended standard repairs should be developed and proven during the certification testing of the full aircraft article) or newly developed repair techniques/processes such as adhesive bonding. Hence the reliance of repair certification programs upon a thorough development test program although, “If the modification significantly alters loads in other parts of the airplane ... or if the modification is significantly different in structural [performance] ... additional full-scale fatigue test evidence would be necessary ...” [43].

21.6. In-service management and inspection

21.6.1. Existing requirements

The force management issues associated with bonded repairs are essentially the same as those for any other repair or modification made to an aircraft structure. The manufacturer or organisation developing the repair is required to update all analyses to reflect the results of any development testing [10]. Additionally, a tracking program for ensuring the operational loading environment of the repair is consistent with that used for the analysis and test program should be implemented. The tracking of a bonded repair might require special provisions not needed for more traditional repairs, such as disbonding inspections or sub-patch crack growth NDI.

21.6.2. Additional guidance

NDI plays an important role in the adhesive bonding process and its in-service use even if it presently cannot detect bond environmental degradation. Current NDI techniques can identify, within certain limits, porosity and disbonds in adhesive bondlines and must be able to detect as a minimum, the maximum allowable defect size calculated in the design process and accounted for in the repair damage tolerance assessment. NDI can provide some information about bond integrity though, and this can become an important part of in-service monitoring of repairs (e.g. of crack status under bonded patches). Using the inspection intervals determined from the assumption that the repair is effective in reducing crack growth in damaged structure, NDI can give assurances that the structure is performing as expected; the corollary to which is that the bond is

maintaining an acceptable level of integrity. Given a baseline standard, NDI techniques can also be used to monitor bondline or patch integrity with respect to disbonds and delaminations that enables the possible fatigue failure modes of a repair to be regularly inspected for.

The use of a “smart patch” (a patch able to automatically signal its own structural health) may be able to fill the technology gap currently existing due to the lack of an inspection capability for bond integrity. The use of strain gauges or other means to detect the loss of load carrying capacity in such patches is the source of much promising research [53,54].

21.7. Future approaches to bonded repair certification

The current approaches adopted by the majority of the aviation industry for the use and certification of bonded repairs, whilst conservative, tend to be overly restrictive in not considering the contribution of the repair to structural integrity. Provided adequate requirements and/or guidance are added to existing regulations the beneficial effects of such a repair could be included with no degradation in the safety implications for aircraft operations. The utilisation of the contribution of a bonded repair should be conditional upon appropriate regulatory overview being in place to ensure that a mature quality system is used to provide consistency in the employed bonding processes. Future advances in NDI and “Smart Patch” technology [54] may provide additional or alternative methods to this “quality management” approach of assuring bond integrity.

Prediction of structural performance is an important factor because even limited static, durability and damage tolerance tests are very expensive. To avoid Airworthiness Authorities requiring such testing they must have reasonable confidence that the analysis and design development testing will accurately predict full-scale behaviour. At present, the key to satisfying Airworthiness Authorities is sound analytical procedures that have been verified by test and experience. This is the hallmark of currently used metallic materials. For these materials, critical strength failure modes in tension, compression, shear and bearing are predictable. Further, the availability of crack growth laws for metals permits the damage tolerance capability to be established. For bonded and composite structures, the analytical procedures are still emerging. Difficulties persist in the prediction of inter-laminar stresses and the growth of delaminations resulting from impact damage. As these procedures mature and become accepted and validated by experience, the confidence in and cost-effectiveness of bonded repairs are likely to result in their increased usage.

21.8. Conclusions

Adhesive bonded repair is an emerging technology that has potential gains for aircraft operators. This chapter has dealt with issues of certification and proposed

that existing criteria in the current aircraft design standards are applicable for the certification of bonded repairs.

Additional guidance material has been presented to aid in the interpretation of these standards and to ensure that the unique characteristics of bonded repairs are adequately considered during a certification process. The most important of these characteristics is the demonstration of long-term durability, as this is not currently addressed by the static and fatigue strength testing methods in current use. Additional testing in the form of wedge tests should be included in certification programs to address this behaviour. The difficulty in proving the reliability and durability of a bonded repair is also identified and suggestions for a quality management system proposed to provide satisfactory proof of compliance to design standard requirements.

References

1. UK MoD, DEFSTAN 00-970, Design and Airworthiness Requirements for Service Aircraft, Issue 2, 1 Dec. (1999).
2. US DoD, MIL-A-8860, General specification for airplane strength and rigidity, 20 May (1987).
3. US DoD, MIL-A-83444, Airplane damage tolerance requirements (superseded by Mil-A-87221), 27 March (1987).
4. FAA, Composite Aircraft Structure, AC 20-107A, 25 Apr. (1984).
5. JAA, Composite Aircraft Structure (Acceptable means of compliance), ACJ 25.603, (1986).
6. UK MoD, DEFSTAN 00-970, Design and Airworthiness Requirements for Service Aircraft, Part 1 Section 3 Leaflet 40, Fatigue: Fibre-Reinforced Components, Issue 2, 1 Dec. (1999).
7. FAA, Instructions for continued airworthiness of structural repairs on transport airplanes, AC25.1529-1, 1 Aug. (1991).
8. Kerr, A. (1999). Certification of Bonded Repairs, *Proc. of the (1999) USAF ASIP Conference*, December.
9. Davis, M.J. (1997). Deficiencies in regulations for certification and continuing airworthiness of bonded structures. *Int. Aerospace Congress*, Sydney, 25-27 February.
10. US DoD, MIL-HDBK-1530, General guidelines for aircraft structural integrity program, 31 Aug. (1996).
11. UK MoD, DEFSTAN 00-970, Design and Airworthiness Requirements for Service Aircraft, Part 1 Section 3.2, Fatigue, Issue 2, 1 Dec. (1999).
12. DEFSTAN 00-970 Issue 2, Part 1, Section 7, Leaflet 2, Dec. (1999).
13. US DoD, MIL-HDBK-5, Metallic materials and elements for aerospace vehicle structures, 1 Dec. (1998).
14. FAA, FAR 25-603, Materials, 30 Oct. (1978).
15. UK MoD, DEFSTAN 00-970, Design and Airworthiness Requirements for Service Aircraft, Part 1 Section 4 Leaflet 17, Processes and Working of Materials: Adhesive Bonding of Structural Parts - Recommended Design Practice, Issue 2, 1 Dec. (1999).
16. US DoD, MIL-A-25463B, Adhesive, film form, metallic structural sandwich construction (superseded by SAE-AMS-A25463), 30 Sep. (1999).
17. ASTM D3983-98, Standard Test Method for Measuring Strength and Shear Modulus of Nonrigid Adhesives by the Thick-Adherend Tensile-Lap Specimen, (1998).
18. Hart-Smith, L.J. (1993) The bonded lap-shear coupon - useful for quality assurance but dangerously misleading for design data. *Proc. of the 38th Int. SAMPE Symp. and Exhibition*, Anaheim. 10-13 May.
19. FAA, FAR 25-605, Fabrication, 30 Oct. (1978).

20. Kinloch, A.J. (1987). *Adhesion and Adhesives – Science and Technology*, Chapman and Hall, London.
21. Bonk, R.B., Osterndorf, J.F., Ambrosio, A.M., *et al.* (1996). Evaluation of adhesives for adhering carbon/epoxy composites to various metallic substrates. *Proc. of the 41st International SAMPE Symposium and Exhibition*, pp. 1472–1485, Anaheim, 24–28 March.
22. ASTM D1002-99, Standard Test Method for Apparent Shear Strength of Single-Lap-Joint Adhesively Bonded Metal Specimens by Tension Loading (Metal-to-Metal), (1999).
23. Boeing, Report D658-10401-1 Evaluation of Bonded Boron Epoxy Doublers for Reinforcement of Commercial Aircraft Metallic Structures, Contract 6-1171-10A3397R4, 27 Mar. (1996).
24. ASTM D2919-95, Standard Test Method for Determining Durability of Adhesive Joints Stressed in Shear by Tension Loading, (1995).
25. Davis, M.J. and Bond, D.A. (1996). Towards a certification methodology for adhesively bonded structures and repairs. *The symposium of the International Committee on Aircraft Fatigue 99*, Seattle, 12–16 July.
26. RAAF, Standard Engineering for Composite Materials and Adhesive Bonded Repairs, No. C5033, Issue 1, Sep. (1995).
27. Bond, D. (1996). Ph.D. Thesis, University of Surrey.
28. Bond, D., Swan, G., Bader, M. and Smith, P. (1998). The effect of matrix moisture content on the repair of carbon fibre reinforced epoxy. *Proceedings of the 21st ICAS Congress*, 13–18 September.
29. ASTM D3762-98, Standard Test Method for Adhesive-Bonded Surface Durability of Aluminum (Wedge Test), (1998).
30. Baker, A.A. and Chester, R.J. (1998). Minimum surface treatments for adhesively bonded repairs. *Int. J. Adhes Adhes*, **12**, pp. 73–78.
31. UK MoD, DEFSTAN 00-970, Design and Airworthiness Requirements for Service Aircraft, Part 1 Section 4 Leaflet 16, Processes and Working of Materials: Adhesive Bonding of Structural Parts – Processes and Control, Issue 2, 1 Dec. (1999).
32. Middleton, D.H. (ed.), (1990). *Composite Materials in Aircraft Structures*, Longman Scientific & Technical, London, p. 114.
33. Davis, M.J. and Bond, D.A. (1999). Principles and practices of adhesive bonded structural joints and repairs. *Int. J. Adh.* **19** (2–3), pp. 91–105.
34. FAR 25.305, Strength and Deformation, 9 Feb. (1996).
35. ASTM D1781-98, Standard Test Method for Climbing Drum Peel for Adhesives, (1998).
36. ASTM D1876-95, Standard Test Method for Peel Resistance of Adhesives (T-Peel Test), (1995).
37. Hart-Smith, L.J. (1972). Design and Analysis of Adhesive Bonded Joints, USAF Conference on Fibrous Composites in Flight Vehicle Design, Dayton OH, 26–28 September.
38. US DoD, MIL-A-8866C, Airplane strength and rigidity reliability requirements, repeated loads, fatigue and damage tolerance, 3 Oct. (1994).
39. FAR 25.571, Damage-tolerance and fatigue evaluation of structure, 28 Apr. (1998).
40. UK MoD, DEFSTAN 00-970, Design and Airworthiness Requirements for Service Aircraft, Part 1 Section 3 Leaflet 35, Fatigue: Safe-Life Substantiation, Issue 2, 1 Dec. (1999).
41. Payne, A.O. (1961). Full-scale fatigue testing of aircraft structures, *Proceedings of the Symposium held in Amsterdam, 5–11 June 1959, Determination of the fatigue resistance of aircraft wings by full-scale testing*, Pergamon Press, New York.
42. TTCP Subgroup H Action Group 13, Draft report on the Certification of Bonded Repairs, June (2000).
43. FAA, AC 25-571-1C, Damage Tolerance and Fatigue Evaluation of Structure, 29 Apr. (1998).
44. Poole, P. and Bond, D.A. (1999). Draft chapter 803 and leaflet 803, UK MoD, DEF STAN 00-970, Issue 1, January.
45. Callinan, R.J., Sanderson, S. and Keeley, D. (1997). Finite Element Analysis of an F-111 Lower Wing Skin Repair, DSTO TN 0067, January.
46. Davis, M.J., Kearns, K. and Wilkin, M. (1995). Bonded Repair to Cracking in Primary Structure: A Case Study, PICAST2-AAC6, Melbourne, 20–23 March.

47. Rose, L.R.F., Callinan, R.J., Baker, A.A. *et al.* (1995). Design Validation of a Bonded Composite Repair for the F-111 Lower Wing Skin, PICAST2-AAC6, Melbourne, pp. 20–23.
48. Hart-Smith, L.J. (1995). An Engineer's Viewpoint on Design and Analysis of Aircraft structural Joints, Mc Donnell Douglas Paper MDC 91K 0067, also published in *Proc. Institution of Mechanical Engineers, Part G, Journal of Aerospace Engineering*, **209**, pp. 226–238.
49. Rose, L.R.F. (1987). Crack reinforcement by distributed springs. *J. Mech. Phys. Solids*, **V35**, pp. 383–405.
50. Boykett, R. and Walker, K. (1996). F-111C Lower Wing Skin Bonded Doubler Repair Substantiation Testing, DSTO TR-0480, dated November.
51. FAA, AC 29 MG 8, Airworthiness Standards Transport Category Rotorcraft – Miscellaneous Guidance: Substantiation of Composite Rotorcraft Structure, 30 Sep. (1999).
52. Baker, A.A. (1988). Crack Patching: Experimental Studies, Practical Applications, Chapter 6 in *Bonded Repair of Aircraft Structures*, (A.A. Baker and R. Jones eds.), Martin Nijhoff, pp. 107–173.
53. Baker, A.A. (1999). Issues in the certification of bonded composite patch repairs for cracked metallic aircraft structures. *Proceedings of the 20th Symposium of the International Committee on Aeronautical Fatigue (ICAF)*, Seattle, USA, July.
54. Baker, A.A. (1997). On the certification of bonded composite repairs to primary aircraft structure. *The International Conference on Composite Materials* – 11, Gold Coast, 14–18 July.

Chapter 22

CERTIFICATION ISSUES FOR CRITICAL REPAIRS

A.A. BAKER

Defence Science and Technology Organisation, Air Vehicles Division, Fishermans Bend, Victoria 3207, Australia

22.1. Current limitations of crack patching

The economic benefits of patching are fully realised only when full credit is given to the patch for the restoration of residual strength and reduction in fatigue crack-growth rate. However, as discussed in Chapter 21 application of bonded composite repairs to cracked *primary structure* is acceptable only on the basis that a margin on design limit-load (DLL) capability is retained in the loss (total absence) of the patch [1].

This is a fail-safe approach, which can be applied:

- When a cracked single-load-path component maintains sufficient residual strength to withstand DLL times a safety factor (often 1.2). In this case inspection is required to ensure that the critical crack length for failure at this stress is not exceeded, based on the predicted growth rate for the *unpatched crack*.
- When a redundant (multiple) load path component can withstand DLL times the safety factor if the cracked path has failed. This is a standard procedure now for such structures so should not pose any particular problems. In this case inspection is required to ensure that the alternate load paths are not cracked to the extent that they could not withstand the elevated stress caused by the failure. The single load path and redundant load path structural designs are respectively typical of fighter and large transport aircraft.

The inspection requirement based on growth of the unpatched crack in the single load-path case may be acceptable (for example if it coincides with the current inspection interval) where the initial crack size is small (or non-existent, for example in the case of a preventative doubler rather than a patch). However, while the fail-safe approach is highly desirable, there will be some repairs, for example

those with the crack approaching critical size or with small cracks having a predicted high (unpatched) growth rate, where this inspection requirement will not be cost-effective. The repair is then only economically feasible if full credit can be given to the reinforcement in restoring residual strength and reducing the rate of crack growth. This requirement is of course essential if the crack already exceeds critical size.

This chapter considers approaches by which full credit can be given to the patch system in these situations.

If credit for the patch is accepted, management of the repaired region is on a slow crack-growth approach to damage tolerance in which inspection intervals are set on the basis of predictable crack-growth characteristics. The aim being for at least two inspection intervals before the crack grows to critical size. In the case of a bonded repair the crack growth is that of the patched crack so the prediction must take account of significant changes in patching efficiency during the patch life.

Patching efficiency is defined here as (a) the recovery in residual strength following patching and (b) the reduction in crack-growth rate of the fatigue crack provided by the patch. The patching efficiency [2] depends largely on the reduction of stress intensity following patching and possibly on the level of mean stress resulting from thermal mismatch between the patch and parent structure.

There are essentially two alternative ways of justifying full credit being given to the patch system. These are by showing:

- (a) that the risk of significant loss in patching efficiency is acceptably low, *or*
- (b) that significant loss can be detected before it becomes a safety issue.

Fatigue strength of the patch system is considered not to be an issue where the static strength of the repair joint (crack spanned by the patch) is designed to exceed greatly the ultimate strength of the parent material [3,4]. However, fatigue is a concern with highly loaded primary structure where this margin cannot be achieved.

In all repairs, thin or thick skin, environmental durability of the patch system is a major concern.

Thus two approaches are discussed here: The first which addresses (a) is based on a demonstrated ability to predict the patch system's fatigue behaviour and to assure its environmental durability.

The second, which addresses (b), is based on the "Smart Patch" concept in which the patch system monitors its own health. The smart patch concept is described in Chapter 20.

22.2. Justifying credit for patching efficiency – fatigue concerns

This section addresses the situation where reduction in patching efficiency due to fatigue damage is the main concern. This includes consideration of degradation in fatigue properties of the patch system due to environmental agents such as temperature, moisture, fuel, hydraulic oil etc.

Essentially the airworthiness requirement is to prove by test or analysis that the patch can restore the residual strength of the cracked structure to the required level (generally $> 1.2 \times \text{DLL}$) for the remaining service life. Thus it is important to show that unacceptable loss in patch efficiency cannot result from the service cyclic loading (or from mechanical damage) and that the fatigue crack in the parent structure will grow at an acceptable rate which can be predicted for the purpose of setting inspection intervals.

It may be feasible to modify (e.g. stop drill or reshape) the crack to increase residual strength to the required level. However, it is in accord with damage tolerance philosophy to assume the presence of a crack at the limits of detectability in the modified crack.

22.2.1. Influence of fatigue on patching efficiency

Patching efficiency could fall due to fatigue failure through the fibres (an unlikely event because of the relative fatigue immunity of these composites when loaded in the fibre direction, fibre dominated mode) or to disbonding caused by fatigue crack growth through one or more of the following matrix/interface dominated modes:

- The adhesive
- The adhesive (or primer) to metal interface
- The adhesive composite interface
- The surface matrix resin of the composite
- The near-surface plies of the composite.

To discuss the influence of fatigue disbonding of the patch system the patch can be considered as made up of two zones [5], Figure 22.1(a):

- **Safe-life zone** at the tapered ends of the patch where damaging strains in the adhesive system are shear and peel.

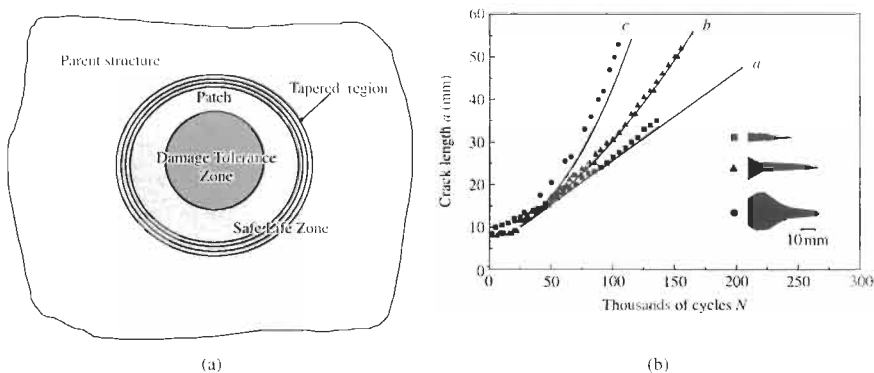


Fig. 22.1. (a) Schematic of an external bonded patch showing safe-life zone (no cracking allowed in patch system) and damage tolerance zone (slow crack growth allowed in patch system). (b) Plot of crack growth versus cycles for three panels tested at 138 MPa, showing inset disbond size over crack. Taken from reference [1].

- **Damage-tolerant zone** in the middle where damaging strains are often mainly shear.

To prevent potential loss of the patch due to fatigue disbonding, strains in the safe-life zone at the patch ends should not exceed the fatigue damage initiation threshold for a significant number of cycles. Even slow initial disbond growth in this region is a concern since once the disbond reaches the inner end of the taper region, strains may increase significantly (depending on the thickness of the patch) and growth may become rapid. Thus the patch system in this region must be designed on a safe-life basis. This is achieved [6] by limiting strains in the critical regions by design (e.g. appropriate end tapering, increased adhesive thickness etc.) and use of appropriate strain allowables. With optimum patch design (see Chapter 10) the strain levels in the tapered region can be designed to be quite low [7] so should not be a concern in most repairs.

The forgoing considerations apply mainly to thick highly loaded structure. In thin-skin structure disbonding in the tapered region can be tolerated [8] as the load transfer stresses are acceptably low, even in the absence of the taper.

In the damage-tolerance region, Figure 22.1(a), limited disbond growth in the patch system is quite acceptable. Damage growth in this region is generally stable, and, if not large, has only a fairly small effect on reinforcing efficiency, Figure 22.1(b); see also Chapter 13. Since the patch-metal bond line is highly stressed in this region significant damage growth can be expected, particularly in repairs to primary structure involving thick skins and high loads.

Thus, assuming the initial residual strength requirements are satisfied, full credit for the patch in slowing crack growth could be justified by demonstration that: (a) strains are below threshold for fatigue damage initiation in the *safe-life zone* and (b) disbond growth is slow and predictable in the *damage-tolerant zone*, as described in the next section.

22.2.2. Obtaining patch system fatigue allowables

To minimise certification costs suitably designed bonded joints [1] can be tested to provide a generic data base on patch system fatigue allowables. The proposed tests are outlined in Table 22.1 and discussed. The joints, shown inset in Table 22.1, have been used as the generic joints [9] to assess disbond initiation and growth rate in b/ep patch repairs to aluminium alloy specimen. These tests are detailed fully in Chapter 5, but are also mentioned again here as they are central to this discussion.

To characterise the allowable strains in the double-overlap joint, representing the crack region, an approach evaluated is to use the theoretical or the measured strain range in the adhesive $\Delta\gamma$ as the damage severity criteria. This is plotted against disbond growth rate db/dN , as shown in Figure 22.2, where b is the disbond width and N the number of cycles. The dotted line is arbitrarily defined as the initiation threshold in this case.

The patch-termination specimen shown in Table 22.1 is the more applicable generic joint specimen for characterising the threshold for damage growth in the safe-life zone, since this is representative of the geometry of this region and also

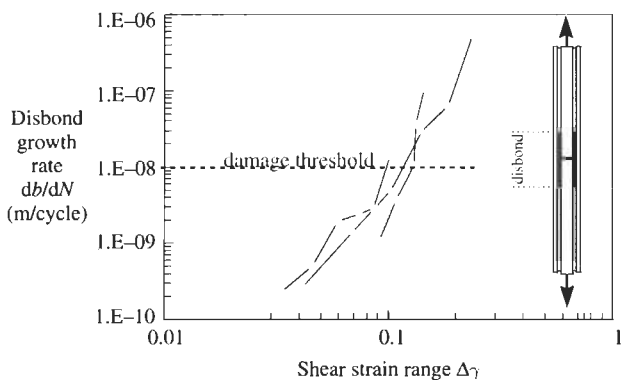




Fig. 22.2. Plot of disbond growth rate in the adhesive versus shear strain range obtained from tests on a double-overlap joint, shown inset. The adhesive is FM73, around 0.3 mm thick, the inner adherend is 2024 T6 aluminium, around 3 mm thick, and the outer adherends are b/ep, around 1 mm thick.

Table 22.1
Generic joint test program to obtain repair system allowables.

Requirement	Approach
<p>To find joint static and fatigue strain allowables and confirm validity of failure criteria based on coupon test data.</p> <p><i>The failure criteria must hold for similar geometrical configurations, e.g. adherend thickness and stiffness and adhesive thickness.</i></p>	<ul style="list-style-type: none">● Undertake static strength tests to:<ul style="list-style-type: none">– check strength against predictions based on coupon data● Undertake fatigue tests to:<ul style="list-style-type: none">– obtain B-basis threshold for fatigue disbond growth– rate of disbond growth at constant amplitude and spectrum loading
 <p>Generic double-overlap joint (represents cracked region)</p>	<ul style="list-style-type: none">● Find knockdown factors for:<ul style="list-style-type: none">– hot/wet conditions– non-optimum manufacture– typical damage– other aircraft fluids e.g. fuel
 <p>Generic reinforcement termination joint</p>	<ul style="list-style-type: none">– more representative loading conditions

represents the combination of peel and shear stresses that develop at the ends of the patch. The total energy release rate G_T may prove to be a suitable parameter to use as a damage severity criterion, the threshold level which could be used as a materials allowable for patch design.

Since the patch system is expected to be insensitive to low loads and load sequences, the allowables can probably be based directly on elevated stress constant-amplitude loading rather than using the constant-amplitude data to predict life under spectrum loading. A conservative approach could be to eliminate cycles at low loads from the spectrum (shown in prior testing) not to be damaging, then elevate all other loads to DLL and base the allowable life on the number of cycles to damage initiation or acceptable damage growth.

A major issue is the relation of the generic joint to the actual loading situation in a particular repair. Providing the generic test is similar to the practical situation, limited testing using representative joints, more representative of the actual repair, could be undertaken to find the knock-down factor for the difference.

22.2.3. *Validation of patching analysis*

The aim is to validate patch design approaches based on generic repair configurations. The approach is based on tests on a range of generic structural detail specimens, as indicated in Table 22.2. Again limited testing may be required on representative structural detail specimens to validate actual repair design, if this differs significantly from the generic structural detail [1].

The validation testing is described more fully in Chapter 13. Two of the figures from that chapter are repeated here.

Figure 22.3(a) depicts a structural detail specimen tested under constant-amplitude loading and Figure 22.3(b) plots $\log da/dN$ versus $\log \Delta K$ predicted using Rose's patching model [10]; where a is the crack length and K the stress intensity. These and other results help to validate use of this model as a practical approach for predicting K in simple cracking geometries. The growth of disbonds in the damage-tolerant zone can be incorporated in the model based on data from the generic joint tests [Chapter 5].

As discussed in Chapter 18, in addition to the fatigue studies, for direct comparison with model predictions the stress intensity K was measured using K gauges bonded at the tip of a patched crack. As shown in Figure 22.4 agreement between measured and predicted K is quite good up to a temperature of around 70°C.

22.3. Justifying credit for patching efficiency – environmental durability concerns

The key need with the use of adhesive bonded repairs (as with structural adhesive bonding generally) is to assure adequate environmental durability of the adhesive bond. Environmental durability in bonded repairs impacts directly on the structural integrity of the repair. Unlike the fatigue case, it is not feasible to define

Table 22.2

Validation of design approaches based on generic structural detail program.

Requirement	Approach
Validate (F-E/analytical) design procedures and assess repair damage tolerance	Undertake tests to assess: <ul style="list-style-type: none">• Static strength under various environments• Fatigue strength, threshold for damage initiation in patch system• Threshold for growth and rate of growth of residual damage, e.g. cracks in metals• Influence of spectrum loading and environment Assess damage tolerance: <ul style="list-style-type: none">• Residual strength before and after fatigue damage to patch system and residual damage• Influence of impact damage to patch and deliberate disbonds in patch system
Generic external patch	

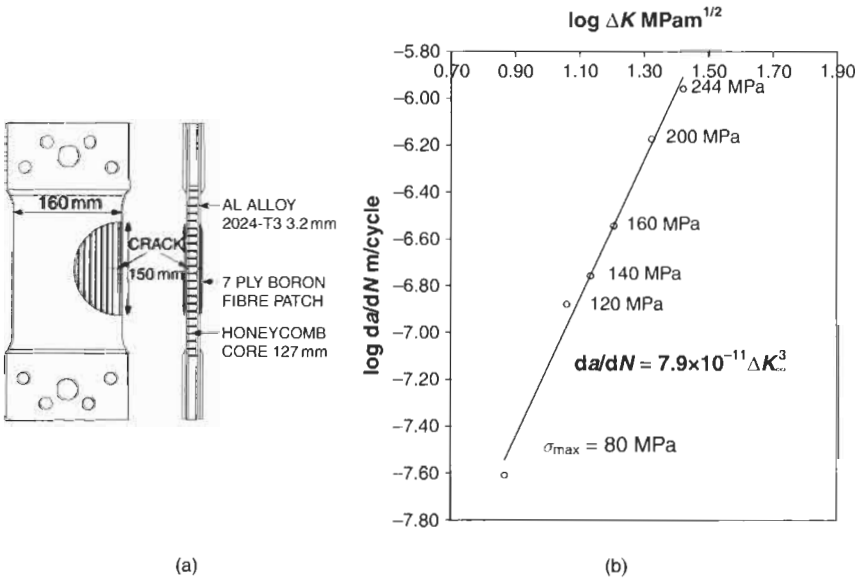
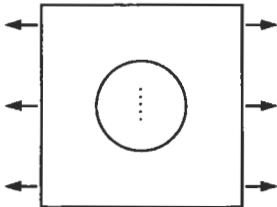


Fig. 22.3. (a) Generic structural detail test specimen for patched cracks in metallic structures used to validate the patching model and obtain crack-growth parameters and (b) plot of experimental $\log da/dN$ versus $\log \Delta K$, predicted from Rose's [10] analytical patching model.

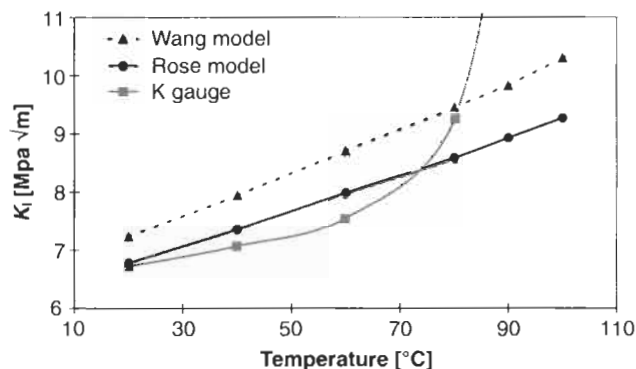


Fig. 22.4. Comparison of experimental and theoretical results for K_I for $a = 30$ mm, patched specimen. The models used for the theoretical predictions are Rose's model and a related model developed more recently by Rose and Wang. See Chapter 18.

either a strain threshold for environmental disbonding or a disbond growth rate. With inadequate environmental durability the threshold for disbonding can fall to zero so the disbond growth rate can be catastrophic. Thus it is not possible to set a safe inspection interval for this type of degradation.

It is important to note that while environmental durability is generally a significant problem with metals it is not with polymer-matrix composites such as b/ep or gr/ep. This is because of the moisture sensitivity of the metal interface if pre-bonding surface preparation is inadequate. Hydration of an unstable surface metal oxide results in a weak, easily disrupted interface.

Unfortunately current and foreseeable NDI techniques can detect only disbonds, voids etc. Bonds with potentially poor environmental durability cannot be detected as long as intimate thermal and mechanical contact at the bond interface is maintained. Developing an NDI capability to detect weak bonds is a very long-term prospect and may well prove infeasible. However, pre-bond NDI, which is the development of techniques to check that the surfaces are correctly treated prior to bonding is feasible, as discussed later.

22.3.1. Assurance of patch system environmental durability

The requirement is to provide assurance at an acceptable level of probability that patch bond failure will not occur in the service environment during the required lifetime of the repaired component – or alternatively that the risk of bond failure is acceptable for the required service life.

This assurance revolves about quality control of the pre-bonding process because:

- This is the most critical process in the repair and is often applied under difficult conditions.

- The danger of incorrect application or surface contamination, for example by organic species from fuel etc. in the repair environment is significant.

Thus a simple to apply (non-hazardous) surface-treatment, such as the silane process [11], increases application reliability, even though other more complex repair surface treatments, for example those based on phosphoric-acid anodising, may provide bonds with marginally superior environmental durability. Chapter 3 discusses bonding surface treatment issues.

To develop data on which an assessment of potential bond durability can be made a suitable test is required. Such a test is needed to (a) assess the process evaluation, (b) assess that it has been correctly applied and (c) qualify technicians.

It is proposed that the Boeing Wedge Test (BWT), depicted in Figure 22.5, fulfils this requirement for the following reasons:

- The BWT has been a US industry standard for adhesively bonded airframe components for many years and is an ASTM test.
- The BWT is a simple low-cost test which requires a minimum of equipment.
- Australian experience based on assurance of bond durability through BWT testing has been very positive, as described in the next section. Assurance is now based on RAAF Engineering Standard C5033 Composite Materials and Adhesive Bonded Repairs [4].

However, there are questions concerning if the severity of the BWT is appropriate and how to quantify it in terms of a failure probability. Neither of these questions can satisfactorily be answered at present.

Efforts are being made to establish if the required statistical data is available in the literature. There may be also a suitable statistical database held by the major aircraft manufacturers, but this is likely to be of a proprietary nature. At present the only information on which a decision can be based is the extensive service experience of the Royal Australian Air Force, discussed in Section 3.2.

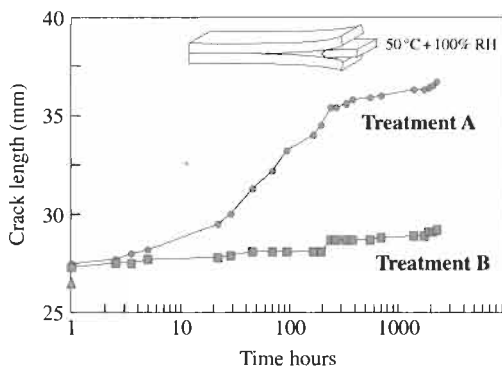


Fig. 22.5. Boeing wedge test to assess bond durability. The metallic adherends are made the aluminium alloy under investigation, generally about 3 mm thick bonded with the appropriate adhesive. The wedge is driven in under standard conditions.

Australia uses a severe version of the standard BWT. For example, an acceptable test result is generally less than 19 mm growth of the disbond in 1 h; while the requirement is less than 5 mm growth in 24 h or 7 mm in 48 h.

More severe tests can be performed. These include the double-cantilever beam test, the constant-compliance cantilever-beam test [12] and the slow strain-rate test [13]. The advantage of these is that they are quantitative in that a Mode I-fracture energy can be measured and correlated with exposure conditions and time. This is generally not possible with the BWT as with tougher adhesives some plastic bending of the metal adherend arms occurs when the wedge is driven in.

The disadvantages of the alternative tests are that they are much more costly to make and test compared with the BWT and they (probably) cannot be correlated with service behaviour, since a suitable database related to these tests is unavailable. The ability to quantify a durability parameter, e.g. Mode I strain energy-release rate G_I , is of limited practical value since it is not a useable design parameter. Thus these tests are more suitable for research purposes, for example in the evaluation of new surface treatments.

Another issue is the value of a BWT made during the repair process, rather than simply to qualify technicians and processes. Separate test specimens made up in parallel and, as far as possible, under the conditions of the repair cannot capture all the variables associated with the repair process; for example, in the exact parent material, in the type and degree of contamination and in the cure cycle. Nevertheless, it is reasonable to assume that a good BWT result from these specimens will provide considerable extra confidence in the repair procedure.

Other than the BWT for quality control of surface treatment there is also the possibility of pre-bond NDI, including simple wetting measurements. However, more sophisticated measurements for assessing, for example, contamination, degree of surface blasting [14], and production of the correct surface condition are also feasible and can be adapted for field use. These include surface potential measurement and infrared surface analysis.

22.3.2. Australian experience on service durability

Table 22.3 provides details on Australian bonded composite repair applications. Many repairs have survived over 20 years service, without evidence of environmental or fatigue durability problems.

However, a few environmental durability failures were found in the Mirage III wing repairs. In these repairs the surface treatment was based on the phosphoric-acid gel-anodising process (PAA). The failures were attributed to (a) the extreme porosity, which developed in the bond line of some of these repairs caused by moisture absorption under the tropical conditions in which these repairs were applied and (b) the absence of corrosion-inhibiting primer. Use of staged adhesive and more careful drying of the surfaces prior to bonding would have reduced the moisture problems.

Fatigue durability of the patch system has been a problem in only one case: the F-111 wing-pivot-fitting boron/epoxy doublers which were primarily designed to

Table 22.3

Australian bonded patch repairs to military aircraft, experience on environmental durability.

Aircraft	Problem	Surface treatment (patch system)	Remarks on bond durability
C130	Stress corrosion cracked stiffeners in wing, aluminium alloy 7075.	GB initially GB + S later (b/ep + FM73)	Over 20 years of service. No bond durability problems where bonding carried out as specified
Mirage III	Fatigue cracking in lower wing skin, aluminium alloy AU4SG.	PANTA (b/ep + FM73)	180 wings repaired or reinforced. Eight bond durability problems over around 8 years. Failures were associated with adhesive voiding caused by extreme humidity in the tropical repair station.
F-111-C	Secondary bending in wing pivot fittings leading to a fatigue problem. Steel D6ac fastened to aluminium alloy wing skin.	GB + S (b/ep + FM73)	No bond durability failures to steel or aluminium surface over 10 years.
F-111-C	Stress corrosion cracking in weapon bay longeron flange, aluminium alloy 7075T6.	GB + S (gr/ep cloth + ep)	Over 10 aircraft repaired. No bond durability problems over around 8 years.
F-111-C	Stress corrosion cracking in longeron adjacent to refuel receptacle, 7049-T6.	GB + S (B/ep + EA 9321)	Over 10 aircraft repaired. No bond durability problems in 8 years.
F-111-C	Metal-to-metal and sandwich structure repairs. RAAF adopted GB + S and changed to FM 300 adhesive in 1992.	GB + S FM300 FM 73, EA 9321	No bond durability failures in over 7 years.
F-111-C	Pork-chop panel (lower fuselage). Panels rebuilt after repeated in-service failures.	GB + S FM 300	Repeat rebuild rate reduced from 95% to zero. No bond durability failures in 7 years.
C-141 (USAF)	Fatigue cracking in wing riser weep holes, 7075T6.	GB + S + P (b/ep + FM73)	No bond durability problems around 5 years
P-3C	Full depth corrosion damage in horizontal tail, aluminium alloy 7075 T6.	GB + S (al alloy + FM73)	No bond durability problems over around 10 years
Boeing 747	Simulated repairs to several regions including fuselage lap-joint, wing leading edge, trailing edge flap and engine thrust reverser cowl.	GB + S + P (b/ep + FM73 or acrylic)	Demonstrator repairs: 37 000 flying hours, 7020 landings over a 9-year period with no significant bond durability problems
Sea King Helicopter	Fatigue crack in frame	GB + S + P (b/ep + FM73)	Operated in an offshore ship-borne environment for 4 years with no problems
F-111-C	Fatigue cracking in lower wing skin at fuel flow hole under forward auxiliary spar.	GB + S B/ep	No bond durability problems in over 2.5 years service.

Notes: GB = alumina grit blasting; S = Silane; P = Primer; PANTA = Phosphoric acid non-tank anodising
 b/ep = boron/epoxy; gr/ep = graphite/epoxy; AF 126, FM73, FM300 epoxy-nitrile film adhesives. ep = epoxy-paste adhesive; acrylic = toughened acrylic adhesive Flexon 241 EA 9321 epoxy paste adhesive.

reduce strains in the fitting during a cold (-40°C) proof load test – this they did successfully. A secondary aim for the doublers was to reduce fatigue strains in the fitting in service to increase the inspection interval (by a factor of around 3); however, fatigue failures are being experienced. Failure occurs mainly in the surface resin of the boron/epoxy. While the cause of this failure is not fully understood, it is

thought to result from use of an excessive taper angle at the ends of the doubler, resulting in adhesive strains above the fatigue threshold. There is also some evidence, as yet unconfirmed, that peroxide components in some fuels can soften the adhesive [15].

22.4. Justifying credit for patching efficiency – the Smart Patch approach

An alternative to certification procedures based on testing is the “Smart Patch” approach [1,16] Figure 22.6 – see also Chapter 20. The aim here is to develop a capability for continuous autonomous (self) monitoring of patch performance to ensure that the patch is performing in service as required. Although the need to follow the correct patch design and process procedures is unchanged, the “smart” approach should allow considerable relaxation in the certification requirements. However, failure of the patch system will still be a costly and therefore a highly undesirable event.

The most direct approach to assess the “health” of the patch system is to measure the level of load transfer in the safe-life zone, Figure 22.1. This approach was successfully demonstrated on test specimen during the development of the b/ep doubler for the F-111 wing-pivot fitting [17], using resistance strain gauges bonded at the ends of the tapered region, but was premature for in-flight application. The monitoring could also include automatic assessment of cracking in the parent structure and disbond growth in the patch system in the damage-tolerance zone. The use of bonded or embedded piezoelectric elements for *in situ* monitoring appears to be highly promising.

The viability of this smart approach revolves largely on how to prove its reliability under the aircraft temperature and environmental operating conditions. This is the reason why flight trials will be so important.

An alternative “smart” approach, being developed by Wilson [18], is based on the use of special chemical sensors embedded in the adhesive layer. These sensors detect chemical species produced at the metal surface during the process of bond

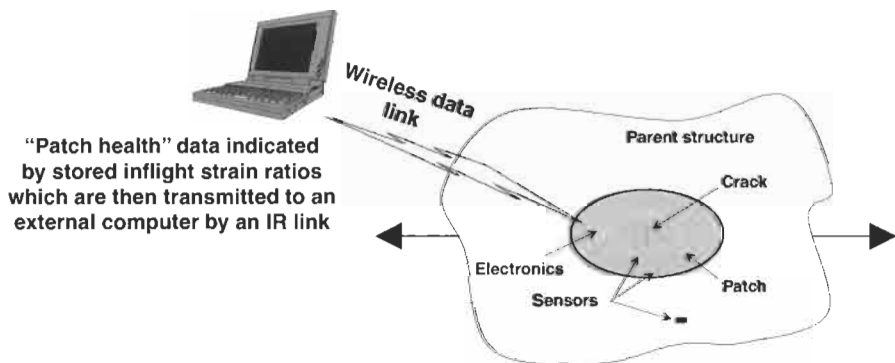


Fig. 22.6. Schematic diagram of the smart patch concept.

degradation. This approach, complementary to the strain approach previously discussed, should provide warning of impending bond deterioration.

22.5. Discussion

A decision chart for management by slow-crack growth is provided in Figure 22.7, based on the previous discussion. This shows that certification requirements can be made much less stringent by the “smart-patch” approach, as imminent loss or degradation of patch reinforcing ability will be immediately detected. However, where certification is based on this approach the key requirement becomes proving the smart system reliability in the aircraft operating environment. Generally, the

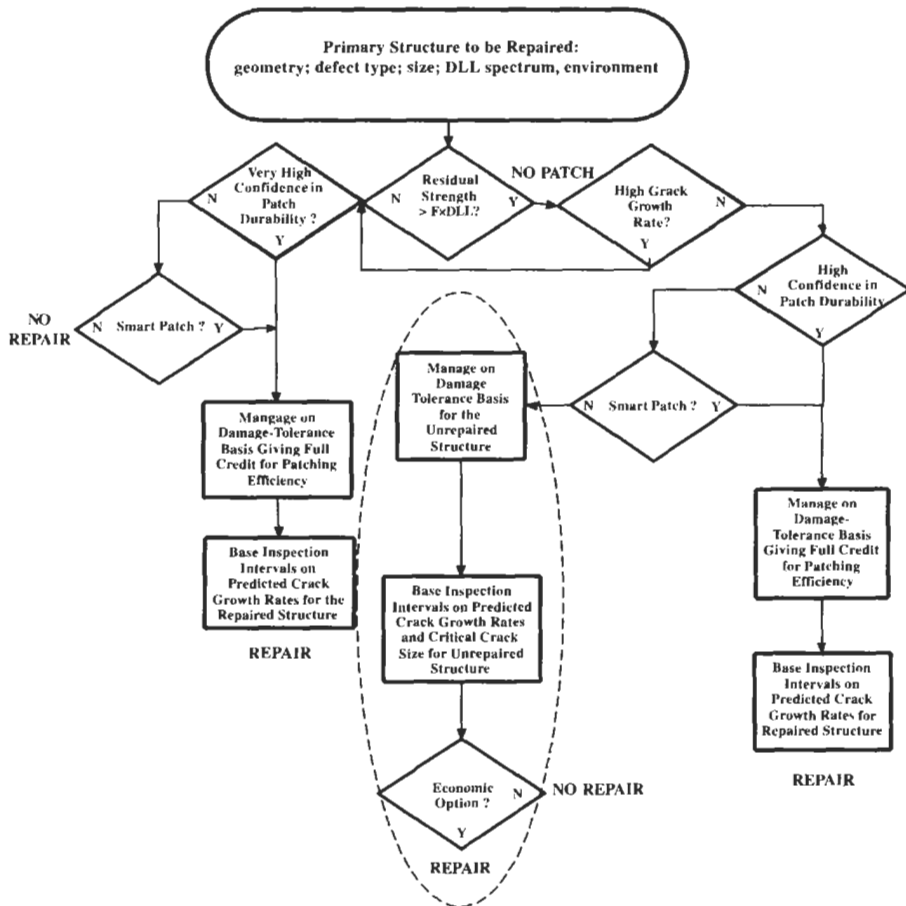


Fig. 22.7. Decision chart for certification of bonded patch repairs to cracked structure. The actions inside the dotted ellipse represent the conservative fail-safe approach.

smart patch approach appears technically feasible but will be economically viable mainly for repairs to costly primary structure.

Where the smart-patch approach is not used, the key issue is how to provide assurance that the probability of unacceptable loss in patching efficiency is acceptably low. If bond environmental durability is shown not to be a concern then management can be based on patch system fatigue allowables, giving full credit for the patch in slowing crack growth and recovering residual strength. However, bond degradation is generally the major concern so the main issue here is of providing confidence that environmental degradation of the patch system will not occur. If this is not possible in the absence of the smart patch approach the repair must be based on a fail-safe approach, giving no credit to the patch.

To provide assurance of bond durability a validated accelerated test of bond quality is required. It is proposed that the BWT or some derivative of it is a suitable test. The BWT can be used to qualify surface treatment processes and technicians, as in the C-141 repair program [19] and can be used for in-line quality control purposes. The question of what BWT result is and what is not acceptable is the current challenge. Sufficient information on service experience may exist in the literature on bonded aircraft components and in the Australian experience on bonded repairs to help provide the answer.

22.6. Conclusions

The certification requirements to permit management of bonded composite repairs by allowing full credit for the presence of the patch in slowing crack growth and recovering residual strength have been addressed.

The major structural integrity issue is to assure that disbonding of the patch due to environmental degradation will not occur during the required service life.

Methods based on a combined safe-life/damage-tolerance approach can be applied to the patch system where bond environment durability is not a concern, based on patch system fatigue allowable and knockdown factors.

It is proposed that the BWT should be adopted as the principal accelerated test for quality control for bonding surface treatment. The main challenge is to correlate the BWT with a probability of failure, possibly based on service experience.

Use of the smart-patch approach, based on self-monitoring would considerably alleviate the certification requirements, since loss of patching efficiency would be detected automatically. However, this approach brings its own problem of reliability assurance.

References

1. Baker, A.A. (1997). On the certification of bonded composite repairs to primary aircraft structures. *Proc. of 11th Int. Conf. on Comp. Mat. (ICCM-11)*, Gold Coast Australia, Volume 1, pp. 1-24.

2. Baker, A.A. (1996). Fatigue studies related to certification of composite crack patching for primary metallic structure. *Proc. FAA/NASA Symp. Cont. Airworthiness Aircraft Structures*, Atlanta USA pp. 313–330.
3. Davis, M. (1994). The development of an engineering standard for composite repairs. *AGARD-CP-550 Comp. Rep. Mil. Aircr. Strucs.*, Paper 24.
4. Royal Australian Air Force Engineering Standard for Composite Materials and Adhesive Bonded Repairs, No C5033 Issue 1. Department of Defence, Australia.
5. Baker, A.A. (1997). On the certification of bonded composite repairs to primary aircraft structures. *Proc. 11th Int. Conf. Comp. Mat. (ICCM-11)*, Gold Coast Australia.
6. Hart-Smith, L.J. (1991). An engineers viewpoint on design and analysis of aircraft structural joints. Douglas Paper MDC 91K0067. *Proc. Int. Conf. on Aircraft Damage Assessment Repair*. Australian Institute of Engineers, Melbourne, Australia, August.
7. Tran-Cong, T. and Heller, M. (1997). Reduction in Adhesive shear strains at the ends of bonded reinforcements. DSTO, AMRL Research Report, DSTO-RR-0115.
8. Naboulsi, S. Mall, S. and Denny, J.J. (1997). Analysis of fatigue crack growth in imperfectly bonded composite patch repair of cracked aluminium panels. *Proc. of Int. Conf. on Aeronautical Fatigue (ICAF97)*.
9. Chalkly, P. and Baker, A.A. (1999). Development of a generic repair joint for certification of bonded composite repairs. *Int. J. of Adhesion*, **19**, pp. 121–132.
10. Rose, L.R.F. (1988). Theoretical analysis of crack patching. Chapter 6 in *Bonded Repair of Aircraft Structures* (A.A. Baker and R. Jones eds.) Martinus Nijhoff, pp. 107–173.
11. Baker, A.A. and Chester, R.J. (1992). Minimum surface treatments for adhesively bonded repairs. *Int. J. of Adhesives and Adhesion*, **12**, pp. 73–78.
12. Kinloch, A.J. (1987). Chapter 7 Fracture mechanics of adhesive joints. *Adhesion and Adhesives: Science and Tech.*, Chapman Hall.
13. Kindermann, M.R., Wilson, A.R. and Arnott, D.R. (1997). A multiple constant displacement-rate tensile testing machine. *Measurement Science Technology*, **8**, Arnott, pp. 390–397.
14. Olsson-Jacques, C.L., Arnott, D.R., Lambrianidis, L.T., *et al.* (1997). Toward quality monitoring of adherend surfaces prior to adhesive bonding in aircraft repairs. *The Proc. Int. Aerospace Cong. 1997 7th Australian Aeronautical Conference*, Institution of Engineers Australia, 24–27 February Sydney, Australia, pp. 511–520.
15. Chalkly, P.C. and Gedds, R. Fatigue testing of F111 wing pivot fitting repair representative joints to be published.
16. Baker, A.A., Galea, S.C. and Powlesland, I.G. (1998). A smart patch approach for bonded composite repairs to primary airframe structures. *Proc. Sec. Jt. FAA/DOD/NASA Conf. on Aging Aircraft*, Williamsburg, VA.
17. Baker, A.A., Chester, R.J., Davis, M.J., Retchford, J.A. and Roberts, J.D. (1993). The development of a boron/epoxy doubler system for the F111 wing pivot fitting – materials engineering aspects. *Composites* **24**, pp. 511–521.
18. Baker, A. and Meadows, L. (1998). Air force research area critical issues paper: smart materials and structures for military airframes. Defence Science and Technology Report *DSTO-GD-0176*, May.
19. Schweinberg, W., Jenson, R. and Fiebeg, J. (1995). Advanced composite repairs of the C141 wing structure. *Int. Conf. of Comp. Mat. ICCM 10*.

Chapter 23

NON-DESTRUCTIVE EVALUATION AND QUALITY CONTROL FOR BONDED COMPOSITE REPAIR OF METALLIC AIRCRAFT STRUCTURES

D.P. ROACH

Sandia National Laboratories – USA

C.M. SCALA

*Defence Science and Technology Organisation, Maritime Platforms Division,
Fishermans Bend, Victoria 3207, Australia*

23.1. Introduction

This Chapter describes the utilization of conventional and advanced nondestructive inspection (NDI) techniques to detect flaws in bonded composite doublers and metallic aircraft substrates. The Chapter focuses mainly on the extensive nondestructive evaluation (NDE) capability which has been developed by research at both the DSTO in Australia and the U.S. FAA/AANC in developing crack reinforcement/repair technology for military and civil aircraft.

While composite doublers have long been used by DSTO on military aircraft, their application in commercial aviation in particular has been suppressed by uncertainties surrounding their application, subsequent inspection, and long-term endurance. Before the use of composite doublers could be accepted for widespread use in the civil aviation industry, the FAA/AANC program was necessary to ensure that methods were available to quickly, easily, and reliably assess the integrity of a doubler.

The main goals in developing NDI techniques for composite doubler installations are: (1) proper accuracy and reliability in detection and sizing of flaws or degradation, (2) increased speed and decreased cost of inspection, (3) improved scanning techniques, (4) improved flaw imagery (signal processing), and (5) upgrading existing techniques and procedures as new technology becomes available. New technology need not be a completely different approach and/or a new device used to perform an inspection. It could merely be an advanced probe or signal readout equipment which is integrated into an existing technique.

Baker, A.A., Rose, L.R.F. and Jones, R. (eds.).

Advances in the Bonded Composite Repairs of Metallic Aircraft Structure

Crown Copyright © 2002 Published by Elsevier Science Ltd. All rights reserved.

Nondestructive inspection is affected by the geometry and material properties of the doubler installation. For example, the thickness of the doubler creates lift-off effects during eddy-current inspections and signal attenuation during ultrasonic examinations. Furthermore, lightning protection ply (when used) creates an undesirable side effect by disrupting the eddy-current signals. Laminate taper, which will occur at the extremities of doublers and may also occur over changing thicknesses within the parent structure, creates a need for careful, and possibly multiple, equipment set-ups and inspections.

A major inspection requirement for doublers is the identification of disbonds between the composite laminate and metallic substrate, and delaminations between adjacent composite laminate plies. Detection of voids, or porosity, is also critical since these defects can reduce the strength of the doubler. The absence of disbonds, delaminations, and porosity in an installation quality assurance check indicates that the doubler is able to perform its duty [1–5]. However, due to the relative newness of the technology and lack of performance data under actual flight conditions, the current approach is to continue inspections of the substrate material. Thus, in the case of doubler reinforcements, inspection for new cracks in the substrate beneath the composite doubler is necessary. For doubler repairs, accurate monitoring of existing cracks is essential.

NDI requirements (sensitivity and inspection intervals) are driven by damage tolerance analyses (DTA). However, the stack of metallic substrate (isotropic), composite lamina (anisotropic), and adhesive layers makes the analysis quite complex and hinders the calculation of an exact DTA. It is difficult to determine the effects of flaw size and the point at which a flaw size/location becomes critical. This is especially true of disbond, delamination, and porosity flaws. NDI is often asked to compensate for this analysis uncertainty and consequently the thresholds for flaw detection can become quite conservative. Also, an increased emphasis is placed on quantifying the probability that a flaw of a particular size and location will be detected by a piece of NDT equipment.

23.1.1. NDI needs and damage tolerance

Detailed discussions on DTAs for composite doubler installations are presented in references [3,6–9]. An overview of damage tolerance for bonded composite doublers is given below in order to present NDE needs in light of damage tolerance issues.

Damage tolerance is the ability of an aircraft structure to sustain damage, without catastrophic failure, until such time that the component can be repaired or replaced. The U.S. Federal Aviation Requirements (FAR 25) specify that the residual strength of the component shall not fall below, σ_L , the component stress at limit load, P_L . The limit load is anticipated to occur once in the life of an aircraft. This establishes the minimum permissible residual strength $\sigma_P = \sigma_L$. To varying degrees, the strength of composite doubler repairs is affected by crack, disbond, and delamination flaws. The residual strength as a function of flaw size can be calculated using fracture mechanics concepts. Figure 23.1 shows a sample residual

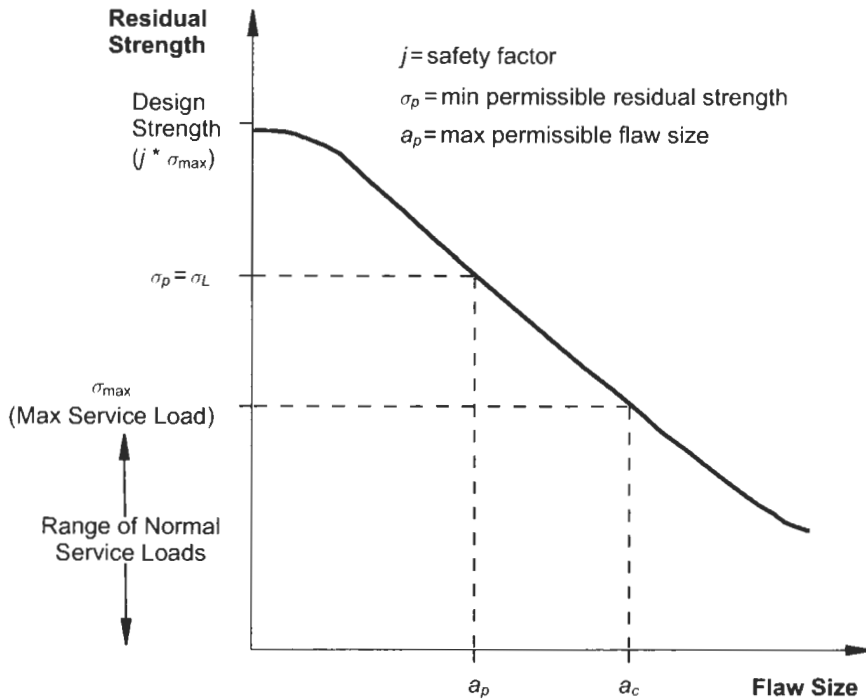


Fig. 23.1. Residual strength curve.

strength curve. The residual strength curve is used to relate the minimum permissible residual strength, σ_p , to a maximum permissible flaw size, a_p .

A fracture control plan is needed to safely address any possible flaws which may develop in a structure. Nondestructive inspection is the tool used to implement the fracture control plan. Once the maximum permissible flaw size is determined, the additional information needed to properly apply NDI is the flaw growth versus time or number of cycles. Figure 23.2 contains a flaw growth curve. The first item of note is the total time, or cycles, required to reach a_p . A second parameter of note is a_d which is the minimum detectable flaw size. A flaw smaller than a_d would likely be undetected and thus, inspections performed in the time frame prior to n_d would be of little value. The time, or number of cycles, associated with the bounding parameters a_d and a_p is set forth by the flaw growth curve and establishes $H(\text{inspection})$. Safety is maintained by providing at least two inspections during $H(\text{inspection})$ to ensure flaw detection between a_d and a_p .

An important NDI feature highlighted by Figure 23.2 is the large effect that NDI sensitivity has on the required inspection interval. Two sample flaw detection levels a_{d1} and a_{d2} are shown along with their corresponding intervals n_{d1} and n_{d2} . Because of the gradual slope of the flaw growth curve in this region, it can be seen that the inspection interval $H_1(\text{inspection})$ can be much larger than $H_2(\text{inspection})$ if NDI

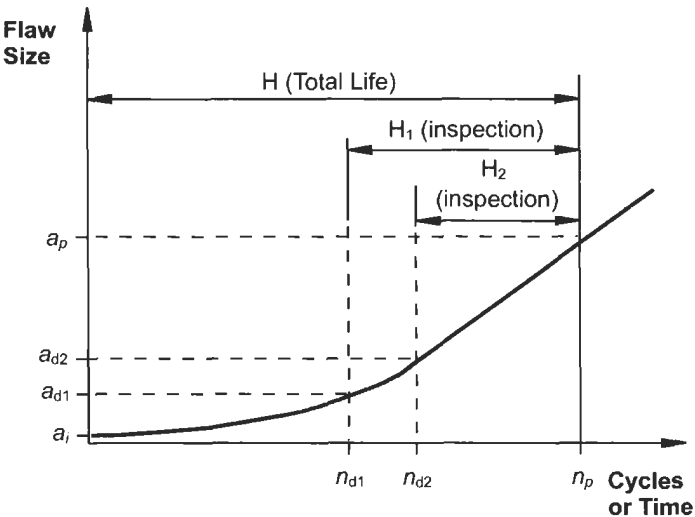


Fig. 23.2. Crack growth curve showing time available for fracture control.

can produce just a slightly better flaw detection capability. Since the detectable flaw size provides the basis for the inspection interval, it is essential that quantitative measures of flaw detection are performed for each NDI technique applied to the structure of interest. This quantitative measure is represented by probability-of-detection (POD) curves such as those shown in Figure 23.3. Regardless of the flaw size, the POD never quite reaches 1 (100% possibility of detection). Inspection sensitivity requirements normally ask for a 90% POD with a 95% confidence limit

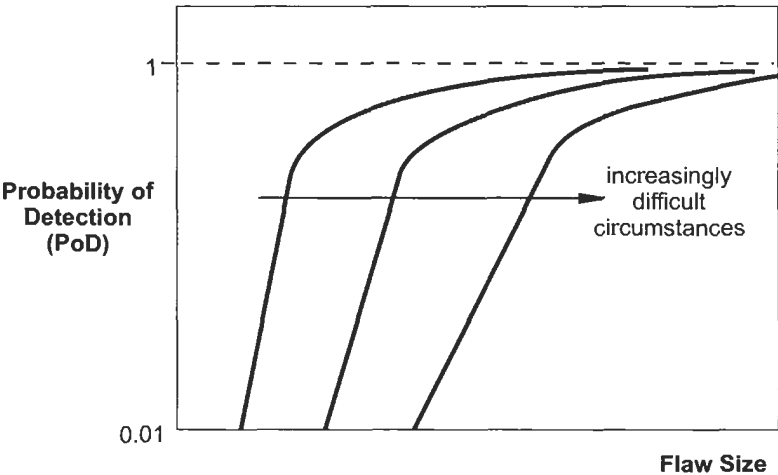


Fig. 23.3. Effect of circumstances on probability-of-detection.

at a_p . For any given inspection task, the POD is affected by many factors such as: (1) the skill and experience of the inspector, (2) accessibility to the structure, (3) exposure of the inspection surface, and (4) confounding attributes such as underlying structure or the presence of rivets. Thus, the effects of circumstances on POD must be accounted for in any NDI study. Figure 23.3 shows how increasingly difficult circumstances can degrade the POD of an NDI technique.

In any surveillance of aircraft structure there are three main aspects to the inspection requirements: (1) the DTA which determines the flaw onset and growth data (especially critical flaw size information), (2) the sensitivity, accuracy, and repeatability of NDI techniques which, in concert with the DTA, establishes the minimum inspection intervals, and (3) the impediments which the NDI techniques must contend with while achieving the required level of sensitivity. NDI studies strive to detect flaws "as small as possible". However, in order to avoid unnecessary maintenance, and possibly harmful structural modifications, the NDI techniques should be directed at flaw levels as determined by DTA.

23.1.2. NDI assessments

Test specimen design and utilization are key considerations in producing relevant NDI assessments. The specimens should possess statistically relevant flaw densities and profiles. In order to provide realistic, comprehensive, and yet controlled flaw scenarios it is best (if at all feasible) to include a mix of test specimens from all four of the following categories:

Type	Specimen category description
1	Reference Standards: used to set up equipment at maintenance depots; provide immediate feedback through knowledge of flaw locations/types.
2	Engineered Test Specimens: representative flaws in realistic structures; well characterized flaws used for blind NDI performance studies.
3	Full-Scale Aircraft Sections: sections cut from aircraft which provide exact structure and natural flaws.
4	Complete Aircraft Test Beds: allows deployment issues to be addressed using actual structure and geometry.

This approach avoids a complete dependence on any one type of structure. The sections cut from aircraft provide the most realistic specimens. However, since the flaw profiles cannot be determined until post-experiment disassembly, the engineered specimens provide a necessary element of experimental control.

Quantitative assessments require that a statistically representative number of flaw sites and detection opportunities exist in the test specimens. Flaw sizes should not be so large that they are always found or so small that they are always missed; the flaw sizes should cover the expected range of increasing reliability. The human vigilance factor can only be assessed if there are sufficient unflawed inspection sites in the test specimens. A specimen design goal is to make the number of unflawed sites large enough to permit some estimate of false call rate.

Both the FAA/AANC and DSTO research and development programs have employed the full range of specimen types, including Types 3 and 4. For the FAA/AANC program, a hangar facility was established at the Albuquerque International Airport for housing an assortment of transport and commuter aircraft. Full-scale aircraft structures included a complete 737 aircraft, two fuselage barrel sections from a DC-9 aircraft, two L-1011 fuselage sections, and three C-141 wing planks. An L-1011 fuselage section had a door corner composite doubler installed and was tested extensively at the facility. A composite doubler was also installed on a door corner of an in-service Delta Airlines L-1011 aircraft in order to demonstrate composite repair technology in-service. Since the early 1970s, the DSTO programs have continued to pioneer composite repair technology for in-service RAAF aircraft. Over this time, composite doublers have been developed for the repair of stress-corrosion cracks in Hercules wing planks and F111 console-trusses and fatigue cracks in Mirage lower wing skins, Macchi landing wheels, F111 upper wing pivot fittings, F111 lower wing skins and F/A-18 aileron hinges.

Based on the extensive experience of both the FAA/AANC and DSTO, the following sections of this chapter address the sensitivity, accuracy, and repeatability of NDI techniques, NDI impediments, and the measurement of probability of flaw detection. The inspection for delaminations, disbonds and adhesion integrity employing pulse-echo and through-transmission ultrasonics, guided waves, resonance testing, thermography, acoustic emission, and holographic thermography is presented in Section 23.2. In Section 23.3, eddy-current sensitivity and POD issues relating to inspection for cracks beneath composite doublers are presented. X-radiographic crack inspection and challenges in crack monitoring are also presented in this section. Quality assurance and calibration standards are discussed in Section 23.4. Concluding remarks are presented in Section 23.5.

23.2. Inspection for delaminations, disbonds and adhesion failure

The two main potential causes of structural failure in composite doubler installations are cracks in the metallic substrate and adhesive disbonds/delaminations. When disbonds or delaminations occur, they may lead to joint failures. By their nature, they occur at an interface and are, therefore, always hidden. A combination of fatigue loads and environmental weathering effects can combine to initiate these types of flaws. Periodic inspections of the composite doubler for disbonds and delaminations (from fabrication, installation, fatigue, or impact damage) are essential to assuring the successful operation of the doubler over time. The interactions at the bond interface are extremely complex, with the result that the strength of the bond is difficult to predict or measure. Even a partial disbond may compromise the integrity of the structural assembly. Therefore, it is necessary to detect all areas of disbonding or delamination, as directed by DTA, before joint failures can occur.

The overall goals of a composite doubler inspection effort should be to: (1) utilize suitable NDI techniques to detect interply delaminations and metallic substrate

interface disbonds, and (2) generate an inspection procedure for use by NDT technicians in aircraft maintenance depots. This includes the development of appropriate equipment calibration standards.

23.2.1. Pulse-echo ultrasonics

Ultrasonic (UT) inspection is a nondestructive method in which beams of high frequency sound waves are introduced into materials for the detection of surface and subsurface flaws in the material. The sound waves, normally at frequencies between 0.1 MHz to 25 MHz, travel through the material with some attendant loss of energy (attenuation) and are reflected at interfaces. The reflected beam is displayed and then analyzed to define the presence and location of flaws.

The principal advantages of UT inspection as compared to other NDI techniques are:

- good penetrating power for detection of deep flaws.
- high sensitivity permitting the detection of extremely small flaws.
- accuracy in determining size and position of flaws.
- only one surface needs to be accessible.
- nonhazardous operations with no effect on personnel and equipment nearby.
- portability.
- output can be digitally processed.

The disadvantages are:

- operation requires careful attention by experienced personnel.
- extensive technical knowledge is required for the development of inspection procedures.
- couplants are needed to provide effective transfer of ultrasonic wave energy into parts being inspected.
- suitable reference standards are needed both for calibrating equipment and for characterizing flaws.

23.2.1.1. A-scan vs C-scan mode

In conventional pulse-echo ultrasonics (PE UT), A-scan signals represent the response of sound waves, in amplitude and time, as they travel through the material. As the waves interact with defects or flaw interfaces within the solid and portions of the pulse's energy are reflected back to the transducer, the flaws are detected, amplified and displayed on a visual display screen. The interaction of the ultrasonic waves with defects and the resulting time vs amplitude signal produced on the screen depends on the wave mode, its frequency and the material properties of the structure. Flaw size can be estimated by comparing the amplitude of a discontinuity signal with that of a signal from a discontinuity of known size and shape. Flaw location (depth) is determined from the position of the flaw echo along a calibrated time base. The latter is useful for distinguishing between disbonds and delaminations.

Figure 23.4 shows a Quantum device being used to perform a PE UT bondline inspection of a composite doubler bonded to an L-1011 fuselage structure. Figure 23.5 contains two A-scan signals produced by the hand-held transducer inspection



Fig. 23.4. Pulse-echo ultrasonic inspection of door corner composite doubler using a Quantum A-scan device.

(gel couplant) of another doubler specimen which contained intentional, engineered flaws at discrete locations. Changes in the A-scan signal (i.e. lack of reflected signal from aluminum back wall), caused by the presence of the disbond, are clearly visible. The primary items of note in Figure 23.5 are: (1) the unique signature of the amplitude vs time waveform which allows the user to ascertain the transmission of the ultrasonic pulse through various layers of the test article and which indicates a good bond, and (2) the absence of signature waveforms indicating a disbond.

In the case of disbond and delamination inspections, it is sometimes difficult to clearly identify flaws using the A-scan signals alone. Small porosity pockets commonly found in composites, coupled with signal fluctuations caused by material nonuniformities can create signal interpretation difficulties. These inspection impediments are primarily troublesome in thicker composite laminates which exceed 20 plies. Significant improvements in disbond and delamination detection can be achieved by taking the A-scan signals and transforming them into a single 2D C-scan image of the part being inspected. C-scan technology uses information from single point A-scan waveforms to produce an area mapping of the inspection surface. By employing a number of electronic gates it is possible to simultaneously collect data from various interfaces/depths within the doubler and substrate.

23.2.1.2. Use of scanning technology

In recent years, fieldable, portable, NDI scanner systems have made great inroads into aircraft maintenance practices. The scanners are used to generate

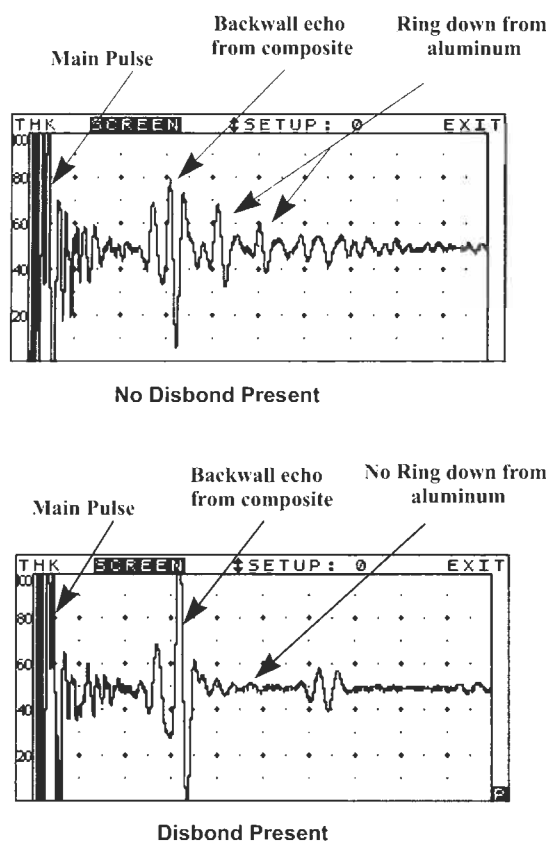


Fig. 23.5. A-scan waveform from bonded and disbonded portions of a composite doubler test specimen.

C-scan images of eddy-current, ultrasonic, or bond-tester inspection data. Scanner designs include manual scanners, semiautomated scanners, and fully automated scanners. Reference [10] contains information on the usability and performance of commercially available scanner systems as they apply to aircraft NDI. Several of these scanner systems are discussed here as they pertain to composite doubler inspections. When addressing scanner system capabilities and limitations, key performance factors include: design, portability, deployment, articulation and access to enclosed areas, speed of coverage, accuracy, usability (human factors), and computer hardware/software.

A basic C-scan system (SAIC/Ultra Image Inc.) that has been used to inspect bonded composite doublers is shown in Figure 23.6. The scanning unit containing the transducer is moved over the surface of the test piece using a search pattern of closely spaced parallel lines. A mechanical linkage connects the scanning unit to X-axis and Y-axis position indicators which feed position data to the computer. The echo signal is recorded, versus its X-Y position on the test piece, and a color

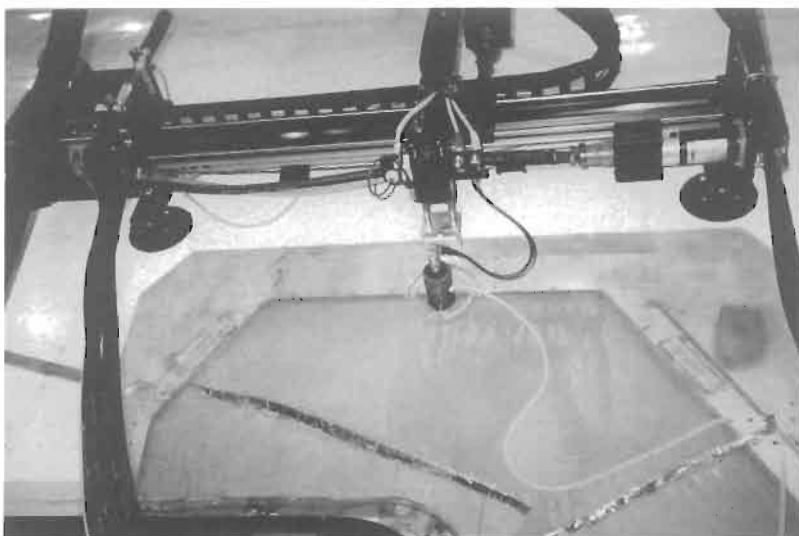


Fig. 23.6. Ultrasonic scanner system inspecting a tapered region of the L-1011 door corner doubler.

coded image is produced from the relative characteristics of the sum total of signals received. The entire ultrasonic C-scan device is attached to the structure using suction cups connected to a vacuum pump. The unit is tethered to a remotely located computer for control and data acquisition. Pneumatic pressure is used to maintain a constant transducer force against the part being scanned.

Normal UT coupling is achieved through the use of a gel or other liquid medium which can: (1) conform to the time varying gap between the UT transducer and the test surface, and (2) transmit acoustic energy with minimum attenuation. In most UT inspections, this couplant is initially applied to the surface and then periodically replenished as the couplant is pushed away by the scanning motion. When proper coupling is lost, a corresponding loss of UT signal (signal “drop out”) is observed. Once a scanner has been set in motion, a preset area is inspected and any signal drop-out areas must be revisited. In order to avoid this potentially time consuming process, an optimized and continuous source of UT coupling is highly desirable.

Scanner systems can be enhanced through the use of, for example, “dripless bubbler” [11] or “weeper” systems to optimize ultrasonic coupling. A weeper system integrated with the Ultra Image scanner is shown in Figure 23.7. The weeper forms the transducer arm of the scanning unit and consists of a UT emitter/receiver transducer in a water column. The weeper body is a cylinder with a plastic membrane at the base. Within the weeper body, a column of water is contained between the membrane and the transducer. The membrane is pierced several times to produce a suitable water flow between the membrane and the inspection surface. Water is continuously pumped into the weeper body in order to maintain the water column and the water couplant “pool” between the weeper body and the inspection surface. This water column and associated water pool beneath the membrane

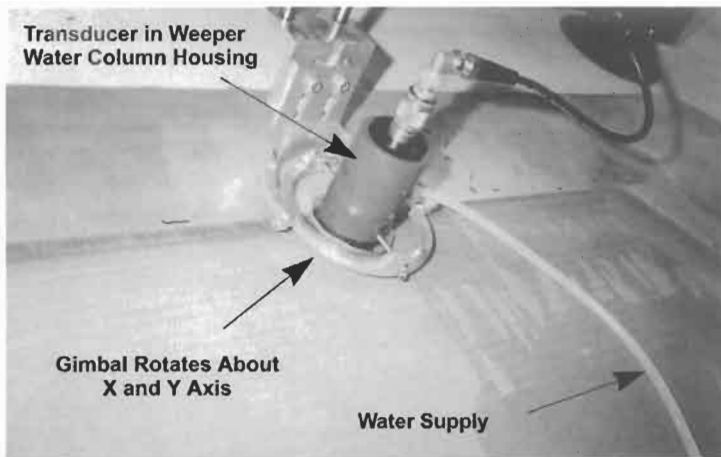


Fig. 23.7. Close-up view of ultrasonic transducer and weeper system for optimized coupling.

provides very uniform and consistent coupling for the ultrasonic waves moving into and out of the test article. This eliminates data irregularities, provides more energy at the inspection point, and produces better output signals (less dispersion). The end results are: (1) improved signal-to-noise (amplitude), (2) better time-of-flight data, and (3) greater flaw detection resolution.

23.2.1.3. Use of customized, focused transducers with pulse-echo ultrasonics

The detection of disbonds at the aluminum bondline interface is often quite challenging. When using 0.5" (12.7 mm) diameter focus transducers, the echo amplitude change observed at the disbond may be only slightly different than that due to unflawed portions of the composite bondline. A noticeable improvement in the bondline echo response at a disbond was obtained at the FAA/AANC by using a 1" (25 mm) diameter, 2" (51 mm) focus transducer. The echo response was further enhanced by placing a 0.38" (9.7 mm) diameter cork stop in the center of the transducer [12].

The diagram in Figure 23.8 shows ray traces, drawn from the 1" (25 mm) diameter transducer, which focus on the aluminum bondline interface of a 72-ply boron-epoxy repair patch. The large refracted angles for the outer rays of the ultrasonic beam are due to the elastic anisotropy of the composite that changes significantly from the thickness direction to the transverse direction of the composite. The refracted angles in the composite shown in Figure 23.8 were calculated using L-wave velocity values that were measured in a small 72-ply boron-epoxy laminate coupon.

From Figure 23.8 it is seen that by placing a stop comprising a 0.38" (9.7 mm) diameter, 0.25" (6.4 mm) thick, cork button in the center of the transducer, the zero degree ray together with all low angle rays are blocked so that only the faster velocity rays are transmitted in the sample at large refracted angles. The faster

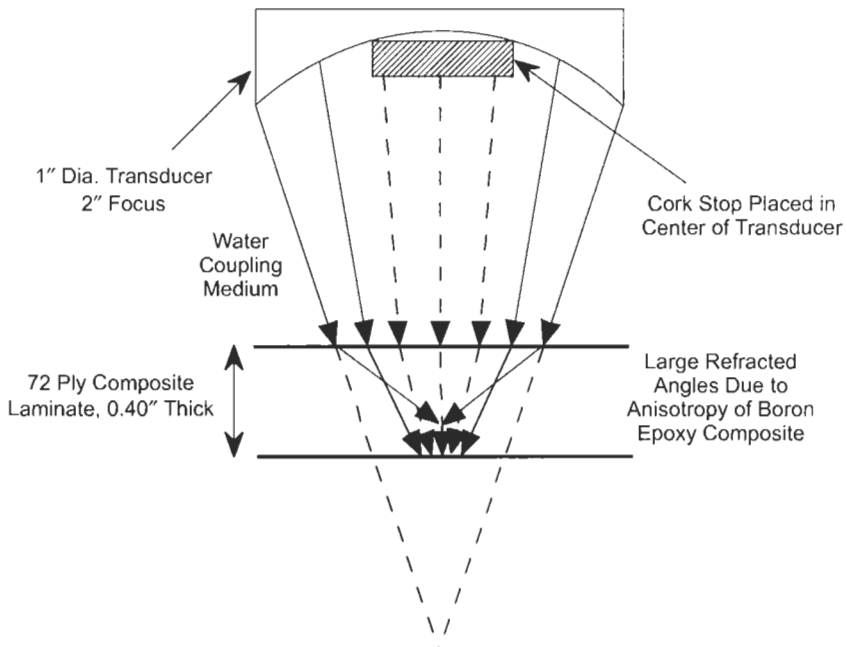


Fig. 23.8. Ray traces for a 1.0" (25 mm) diameter, 2" (51 mm) focus transducer and a 72-ply boron-epoxy sample.

velocity rays interact with the bondline interface in a way to enhance the difference of the echo response between bonded and non-bonded conditions of the interface.

23.2.1.4. Results from pulse-echo ultrasonic inspections

Using an ultrasonic scanner system and a weeper coupling device, a series of NDI validation tests were performed at the FAA/AANC. The tests used a complete array of aircraft and bench top, engineered composite doubler specimens. Design variables which were varied in the test specimens included: footprint of doubler, number of boron-epoxy plies, taper ratio around the perimeter of the doubler, doubler lay-up (quasi-isotropic vs uniaxial), use of protective fibreglass cover plies, and cure cycle (temperature and pressure variations within allowable limits). The specimens contained different skin thicknesses and substructure elements beneath the doublers while the doublers themselves ranged in thickness from 4 plies to 72 plies, i.e. approximately 0.027" to 0.410" (0.69 mm to 10.4 mm) thick.

Evaluation of technique on L-1011 test specimens with engineered flaws

A series of C-scan images of various bonded composite doubler installations were obtained to evaluate the PE UT inspection technique and also to establish optimum gate settings for an actual L-1011 inspection (Figure 23.6). C-scan images (based on amplitude) for 8-ply and 72-ply bonded composite doublers with engineered flaws are shown in Figures 23.9 and 23.10, respectively. Test specimen

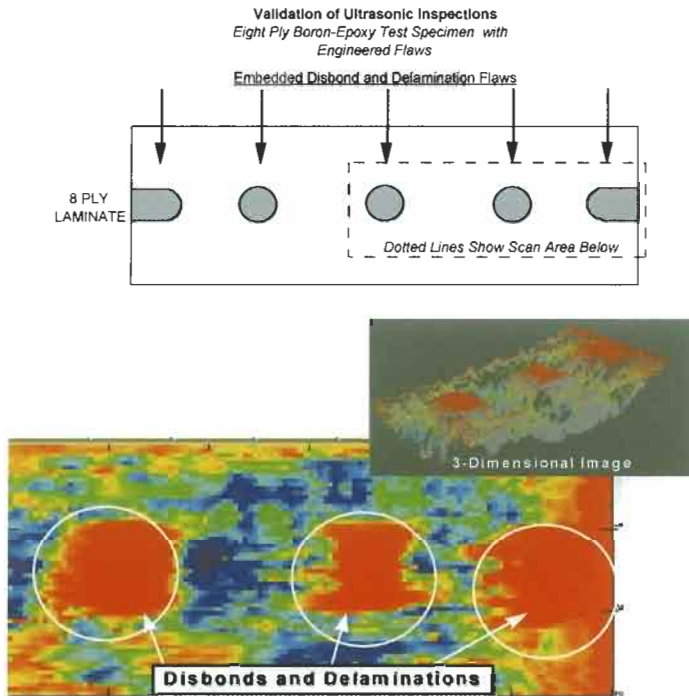


Fig. 23.9. Pulse-echo ultrasonic C-scan of 8-ply bonded composite doubler specimen with engineered flaws.

schematics are included with each NDI image to provide doubler lay-up information and profiles on the embedded flaws. Three-dimensional contour plots are also shown to demonstrate another means of displaying the data and interpreting the results. Disbond and delamination flaws are revealed by continuous and distinct signal loss areas which, depending on the color palette chosen, are either relatively bright or dark compared to the surrounding colors. It was found that: (1) the flaws were clearly visible when viewed side-by-side with adjacent, unflawed material, (2) flaws as small as 0.25" (6.4 mm) in diameter could be mapped even through 0.41" (10.4 mm) thick laminate, (3) inspections could be performed through impediments such as fibreglass cover plies or lightning protection mesh, and (4) the thickness and substructure configuration of the parent aluminum structure did not affect the inspections, although gate adjustments were necessary. In these images, the color scales were adjusted to produce the greatest variation between flawed and unflawed material. In addition,

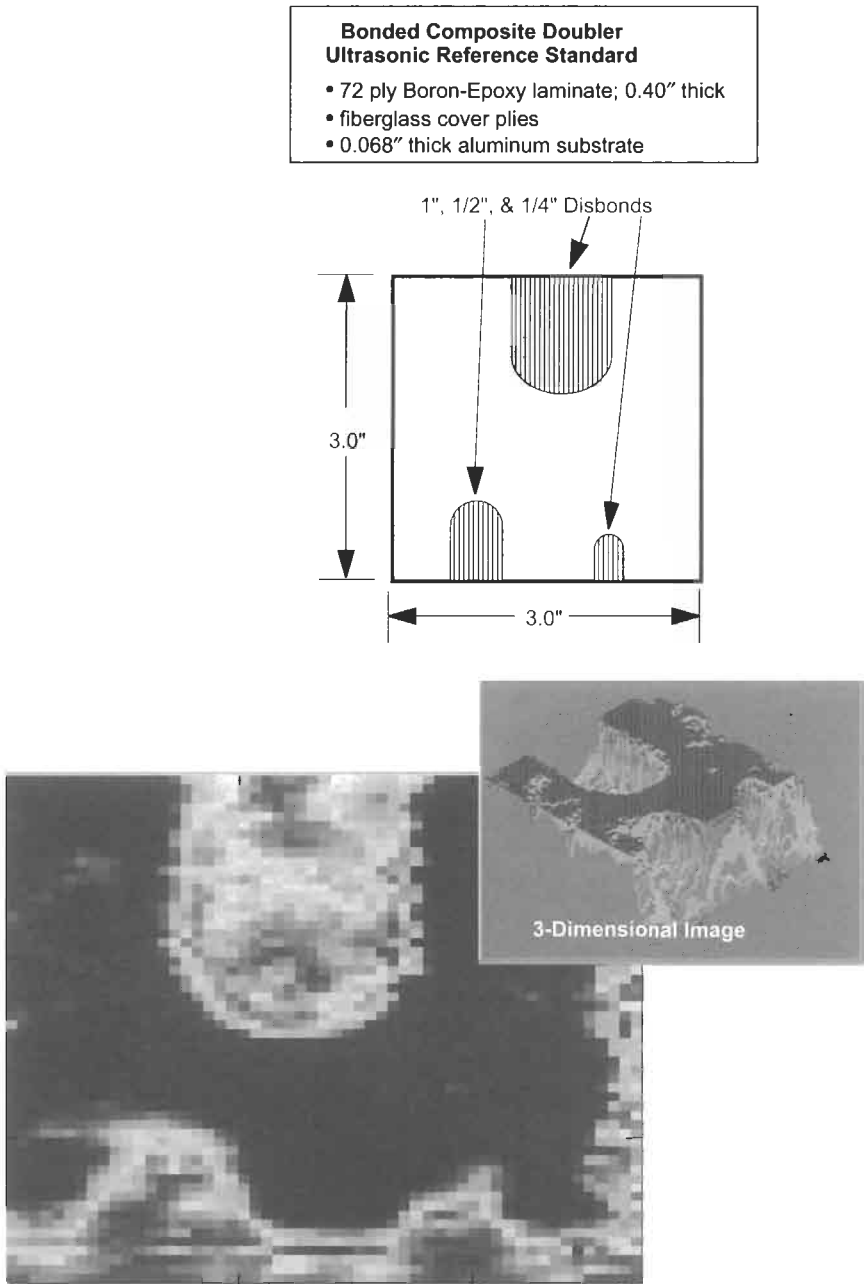


Fig. 23.10. Pulse-echo ultrasonic C-scan of 72-ply bonded composite doubler specimen with engineered flaws.

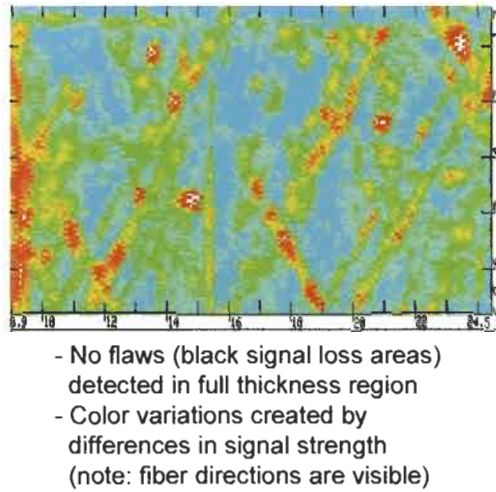


Fig. 23.11. Pulse-echo ultrasonic C-scan of composite doubler on L-1011 fuselage specimen (constant thickness area above the door cut-out).

time-of-flight information was also displayed in image format to help locate the depth of the damage.

Evaluation of technique on L-1011 door surround structure doublers

Delta Air Lines and Textron installed a Lockheed-designed composite doubler on a door surround structure fuselage section (Figure 23.4) cut from a retired L-1011 aircraft. A UT inspection procedure was developed by the AANC and approved for use on L-1011 aircraft by Lockheed-Martin [13]. This procedure was applied to the doubler on the door surround structure test article. Figure 23.11 contains a sample C-scan image from an ultrasonic inspection of this composite doubler. Although no flaws were found in the L-1011 demonstration installation, it can be seen that a complete map of the composite doubler, which highlights any irregularities, can be obtained. Nonuniformities in the composite laminate and singular features, such as the boron fibres, create color variations in the C-Scan. This demonstrates the sensitivity of the technique.

Evaluation of technique on AANC 737 test bed (composite doubler with engineered flaws)

The Ultra Image scanner system was deployed on the 737 Transport Aircraft Testbed at the AANC hangar to inspect a 6-ply thick octagon shaped doubler. Figure 23.12 shows a schematic of the doubler depicting the size and location of the implanted flaws while Figure 23.13 shows a C-scan image produced by the scanner system. (A similar result was obtained with another scanning system which employed a dripless bubbler transducer arrangement [14].) In the gray-scale image, the flaws are shown as the brighter colored areas within the dark baseline. It can be

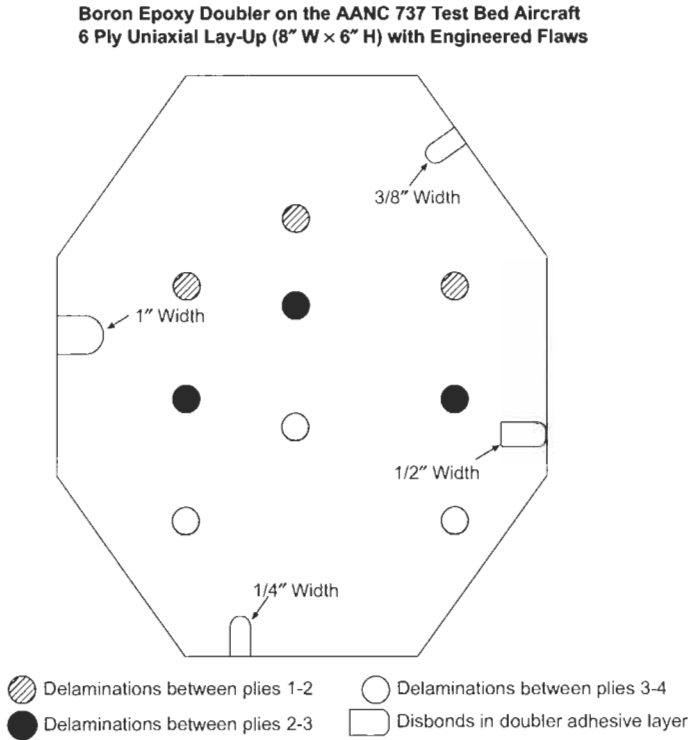


Fig. 23.12. Schematic of 737 testbed doubler showing engineered flaws.

seen that this inspection was able to detect flaws at a wide range of depths in a single image. Also, flaw imaging is most difficult at the edge of the doubler where the thickness is only one or two plies. This is because there is very little difference in UT transmission time between the front of a one ply doubler surface and the front of the aluminum surface beneath it. This makes it difficult, but still possible, to delineate differences which occur in this time frame.

23.2.1.5. *Evaluation of PE ultrasonic techniques on large carbon-epoxy composite reinforcement to aluminum substrate*

The present assessment of NDE for the composite repair technology is directed specifically towards aircraft applications but a recent DSTO feasibility study of the application of repair technology to a ship structure also provided relevant information on inspection for disbonds and delaminations for the case of large reinforcements. In this maritime trial of the composite repair technology, two large (5 × 1 m²) carbon-fibre reinforcements were applied to the deck of a Royal Australian Navy FFG-7 frigate. The NDE investigation included both ship monitoring and laboratory studies using test panels which simulated typical ship superstructure and potential defects associated with FFG-7 deck composite

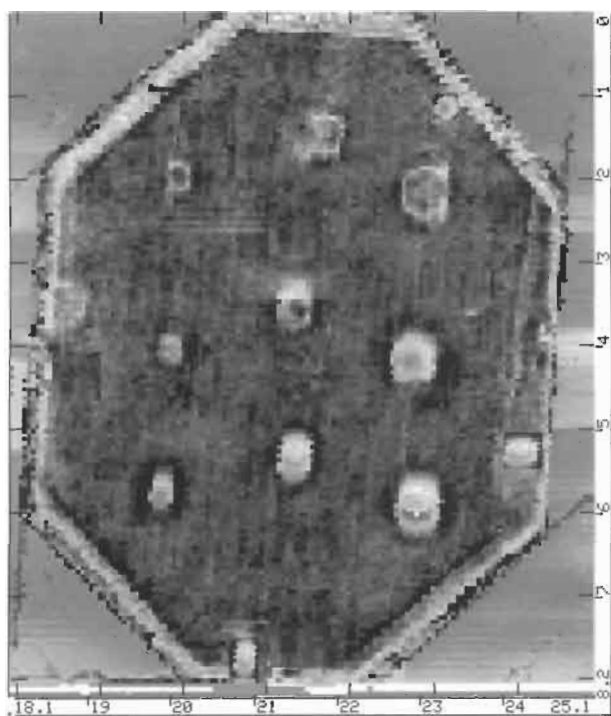


Fig. 23.13. Grey-scale C-scan image of 737 doubler produced by the scanner system.

reinforcement. Ultrasonic techniques were examined for bond and delamination detection using simulated specimens [15].

The specimens were designed to match as closely as possible the actual reinforcement applied to the upper deck of HMAS *Sydney*. The specimens were constructed using 10 mm thick marine-grade aluminum alloy similar to the Al 5456 deck alloy. The composite reinforcement was built up using a thin woven fibreglass layer bonded to the metal followed by 25 plies of unidirectional carbon fibres in a modified vinyl-ester matrix and then overlaid with several layers of woven glass material. The lower fibreglass layer was required to provide electrical isolation between the carbon fibres and the metal deck plate, and the upper woven fibreglass overlay was applied to provide a degree of wear protection and to minimize water ingress at the edges of the reinforcement. The carbon fibre layup had a maximum thickness of 25 plies, tapering to zero thickness at the edges. The total thickness of the reinforcement was approximately 7 mm.

The minimum disbond or delamination size required to be detected on FFG-7 frigates was estimated to be approximately 25 mm in diameter so that the test specimens were manufactured to contain defects both above and below this target diameter. In all, four specimens were prepared for the disbond/delamination study:

- Specimen I was manufactured as a control specimen and did not contain any simulated defects.
- Specimen II (Figure 23.14) was made to study severe composite reinforcement disbonding. Drilled holes in the decking at the reinforcement/deck interface were used to represent the case where the disbonded surfaces are well separated, resulting in an air gap. The holes ranged in diameter from 10 mm to 20 mm and were located at a range of positions under the reinforcement.
- Specimen III was also constructed to study composite reinforcement disbonding but, rather than using holes (as in Specimen II), more subtle disbonds were simulated by placing teflon inserts at the reinforcement/deck interface. The proposed inserts in this specimen varied from circular disbonds of diameter from 10 mm to 30 mm to rectangular shapes from 25 mm by 25 mm to 25 mm by 150 mm.
- Specimen IV (Figure 23.15) was made to study composite delaminations which were simulated using teflon inserts at a wide-range of locations within the composite reinforcement bonded to the deck; the proposed location of the inserts were at three different depths within the reinforcement (at the top carbon ply, ply 12 and ply 25).

C-scan ultrasonics was trialed for detection of disbonds and delaminations in the simulated FFG-7 reinforcement specimens. The ultrasonic testing system used was a Krautkramer Branson USIP20 which was linked to an ANDSCAN position scanning system to enable 2D presentation of C-scan ultrasonic data. The C-scan data were acquired using a single longitudinal ultrasonic probe operating at normal incidence with water as couplant. Use of a range of different ultrasonic probes operating from 0.2 MHz to 10 MHz was investigated. Finally, a probe operating at 0.5 MHz was selected for acquisition of the C-scan data presented later in this section. This probe was well-suited to the present study because its diameter was 30 mm which was therefore comparable to the critical defect size to be detected; moreover, the relatively large active area of this probe facilitated scanning of the large test specimens. However, the entire face of the transducer had to be maintained in good contact with the surface for best results, invalidating acquisition of data within 15 mm of any edge of the reinforcement and causing difficulties on the contour-line where the composite-reinforcement depth profile changed abruptly from uniform thickness to a stepped wedge.

Application of the ultrasonic probe to the control Specimen I containing no defects resulted in the detection of a series of ultrasonic pulses. These were identifiable as multiple reflections and mode conversions within the probe itself, at the probe/reinforcement interface, at the composite/deck interface and at the back face (interior side) of the deck. The longitudinal pulse reflected from the back face of the deck was particularly strong. Hence, a variable time gate was set to acquire the amplitude of this reflection in all subsequent C-scan studies of Specimens II, III and IV, as reinforcement disbonding or delamination would be expected to significantly reduce the amplitude of this reflection. The amplitude of this reflection did not vary significantly in a C-scan of Specimen I indicating that, as planned, this control specimen did not contain any significant defects.

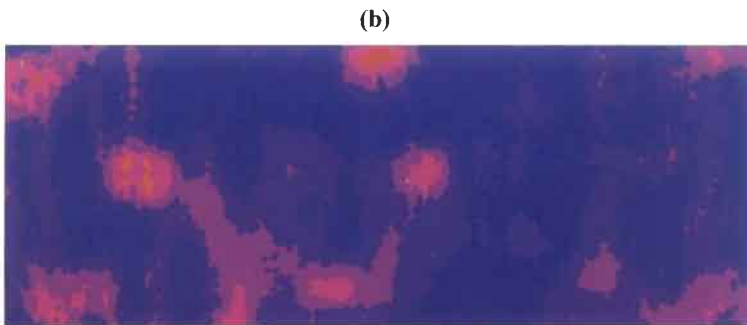
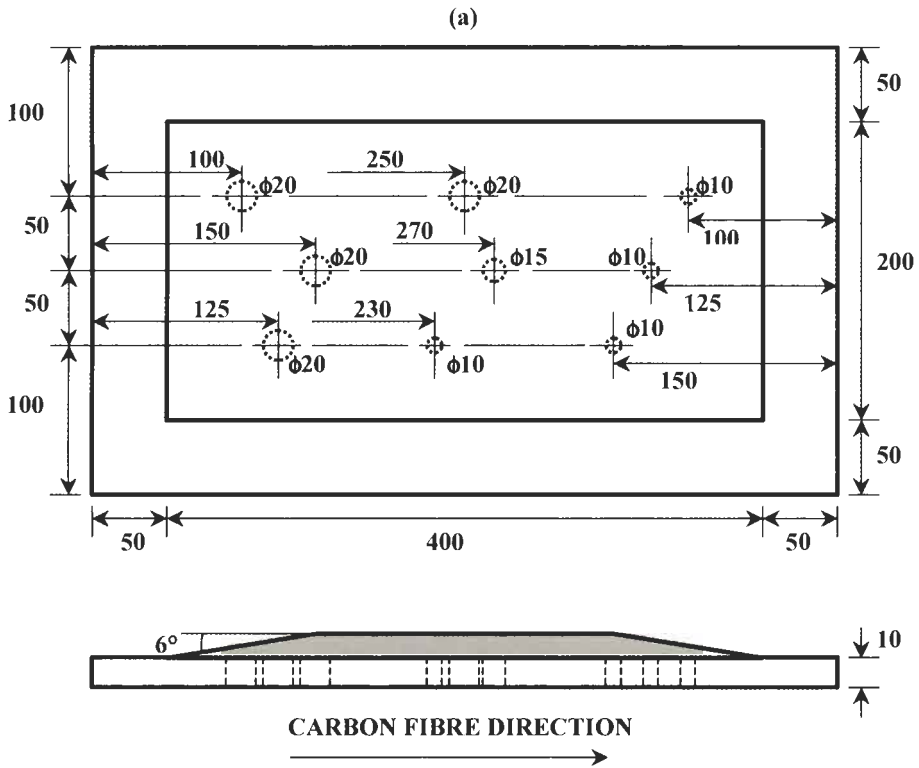


Fig. 23.14. Simulated specimen II: (a) severe disbands between composite reinforcement and frigate deck simulated using through-thickness holes in the 10 mm thick substrate; (b) corresponding C-scan result for the scanned region. (The color scale in order of decreasing ultrasonic sensor amplitude is blue to orange.) [15]

Figure 23.14 shows the *C*-scan results from Specimen II containing holes in the decking material at the reinforcement/deck interface to simulate air-gap disbonds. Comparison of (a) and (b) in Figure 23.14 shows that all holes were detected with the exception of a 10 mm diameter hole whose location coincided with the change in reinforcement profile from uniform thickness to a wedge, making probe coupling difficult. The ultrasonics results also indicate that some disbonding was present in the specimen, particularly near the edges of the reinforcement and in some cases associated with the presence of the holes.

For Specimen III containing teflon inserts at the reinforcement/deck interface to simulate disbonds, all inserts were detected, regardless of their size or location. As in the case of Specimen II, the ultrasonics results indicated that some disbonding was also present in Specimen III, particularly near the edges of the reinforcement where large teflon inserts were located.

Figure 23.15 shows the *C*-scan results from Specimen IV which contained teflon inserts at wide-ranging locations within the composite reinforcement to simulate delaminations within the reinforcement. Comparison of (a) and (b) in Figure 23.15 shows that all delaminations were detected regardless of their location, with the exception of a 10 mm diameter insert located close to the composite/deck interface. As in the cases of Specimens II and III, the *C*-scan results for Specimen IV also indicate that some disbonding was present in the specimen, particularly near the edges of the reinforcement where large teflon inserts were located and between the inserts.

The results on the large carbon-epoxy composite simulated specimen demonstrate the value of combining *C*-scan data with variable time gating – this allowed monitoring of disbonds/delaminations in the tapered ends of reinforcement where their occurrence is often most critical.

The above results demonstrate that ultrasonics is applicable to detecting delaminations and disbonds not only in boron-epoxy composite repairs but also in large carbon-composite. Whereas the minimum disbond or delamination size required to be detected on FFG-7 frigates was estimated to be approximately 25 mm in diameter, much smaller defects were detectable by *C*-scan ultrasonics in the present work. Under the ultrasonic experimental conditions used here, all disbonds and delaminations larger than 15 mm in diameter were detectable and in most cases defects as small as 10 mm in diameter were observable. If necessary, smaller defects could be resolved by appropriate choice of a higher frequency transducer. However, use of the large transducer in the present work facilitated rapid scanning of the large reinforcement necessary for the FFG-7 upper deck.

23.2.2. Through-transmission ultrasonics

Through-transmission ultrasonics (TTU) passes a beam of sound energy through a component under test and, rather than interpreting the returned wave as PE UT does, it uses the signals which are transmitted through the test piece. Two transducers must be accurately aligned with each other on opposite sides of the

component under test. Disbonds, delaminations, or porosity in the test piece will prevent all or part of the transmitted sound from reaching the receiver transducer.

To perform an inspection using TTU, both sides of the test piece must be accessible. A water medium is used to provide the UT coupling. Inspections are performed with the test piece immersed in a water tank or positioned between water jets (UT squirter set-up).

Since this technique requires the sending-receiving transducer pair to be located in front and back of the structure being inspected, accessibility and deployment issues severely restrict the field application of TTU techniques. The motion of the transducer pair must be linked and water coupling to the structure, through complete immersion of the part or through focused water jets, is necessary. This further complicates field deployment and affects the size of the structure that can be inspected. As a result, TTU was not deemed to be a viable inspection technique for composite doubler installations on aircraft. However, TTU is a very accurate NDI technique and can be used to establish a basis of comparison for other, more fieldable techniques. It was used in FAA projects to evaluate basic UT phenomena and aid in the deployment of the PE UT scanner system.

23.2.3. Guided waves

23.2.3.1. Lamb waves for disbond detection

Lamb waves (alternatively known as plate waves), generated in plate-like structures by piezoelectric transducers or laser pulses, are proving to be useful for the evaluation of composite repairs. In addition to the detection of disbonds and delaminations, this ultrasonic technique offers improved large area or global detection of those defects together with the potential for assessing the quality of the adhesive bond. The multi-mode property of Lamb waves potentially offers enhanced sensitivity to the different defects through the judicious use of the different modes.

Research to date has been directed primarily at bond/disbond monitoring. In recent studies, Rose *et al.* [16,17] used test specimens with simulated disbonds inserted between both boron-epoxy and carbon fibre layers and aluminum substrates. They employed both pitch-catch and pulse-echo piezoelectric transducer arrangements on lap-joint and overlay test specimens. Optimal sensitivity of a pitch-catch arrangement for the boron/aluminum lap-joint test specimen was based on the theoretical matching of phase velocities in both materials. However, due to the complexity of modelling a three layer structure, final optimization of sensitivity by this resonance matching criterion was achieved experimentally by fine tuning of the angle of the receiver transducer. Previous work [18] had indicated that, for layers of different materials, if the same angles were used by the sender and receiver transducers less than optimum reception would result. Pulse-echo scanning with the S_0 mode (aluminum) was then performed on the lap-joint specimen. The reflected signal amplitude was low for a good bond (due to the leakage of energy between plates) while a strong reflection occurred for a disbond. Pitch-catch scanning with the S_0 mode was also performed, with the receiver transducer on the overlap region

of the joint and at the appropriately tuned angle. The received signal amplitude was high for a good bond and low for a disbond. The same inspection modes were employed for pitch-catch scanning of the carbon fibre patch test specimen and found to give good detection of the disbonds.

23.2.3.2. *Leaky interface waves for adhesion integrity*

A major constraint on the more extensive use of composite repair technology is that there is no readily applicable NDI technique to distinguish a good bond from a weak bond between overlay and substrate or the long-term durability of the bond to degradation.

One possible approach to this problem is the use of leaky interface waves which, when they exist, propagate along the boundary between two materials, decaying into the slowest available bulk wave. This approach is of interest because of the anticipated link between changes in interfacial stiffness and leaky interface wave propagation. Theoretical work was carried out at DSTO [19–22] to determine whether such waves would exist for boron-epoxy overlays applied to typical metallic aircraft substrates (aluminum, steel, and titanium). For these overlay/metal combinations, the theory showed that the characteristics of such waves were highly dependent not only on substrate properties but also on the elastic constants of the overlay. Hence, a methodology was developed and applied for one-sided measurement of elastic constants in the overlay, as would be necessary in practice. Using experimental results both for the boron-epoxy overlay elastic constants and other requisite material parameters, theoretical modelling was then carried out which predicted that leaky interface waves could exist travelling perpendicular to the fibre direction for boron-epoxy composite combined with typical aircraft substrates. Experiments were conducted on test specimens to firstly confirm the existence of these waves and secondly to investigate their use for distinguishing between good and suspect bonds. One set of test specimens comprised 10 mm thick 2024-T351 aluminum substrates with dimensions $98 \times 300 \text{ mm}^2$. Boron-epoxy overlays of approximately 3 mm thickness with dimensions $49 \times 200 \text{ mm}^2$ were well-bonded to the substrates using standard procedures for boron-epoxy reinforcement of aircraft. For another set of aluminum/boron-epoxy specimens, the substrate surface was moderately contaminated with a 1% aqueous solution of hydraulic oil (which is a typical contaminant in aircraft maintenance facilities). A Nd:YAG laser line-source incident on the substrate beyond the overlay was used to generate a Rayleigh wave, most of which was converted to an interface wave when it reached the overlaid region (Figure 23.16). This was demonstrated by piezoelectric detection of both the leaked quasi-shear waves reaching the top of the overlay, and of the diminished Rayleigh wave that was transmitted to the substrate beyond the overlay. Significant differences were observed in the attenuation of the quasi-shear waves for specimens which were prepared with either good or poor adhesive bonds (Figure 23.16). It is interesting to note that no differences were detected with conventional C-scan ultrasonic inspection.

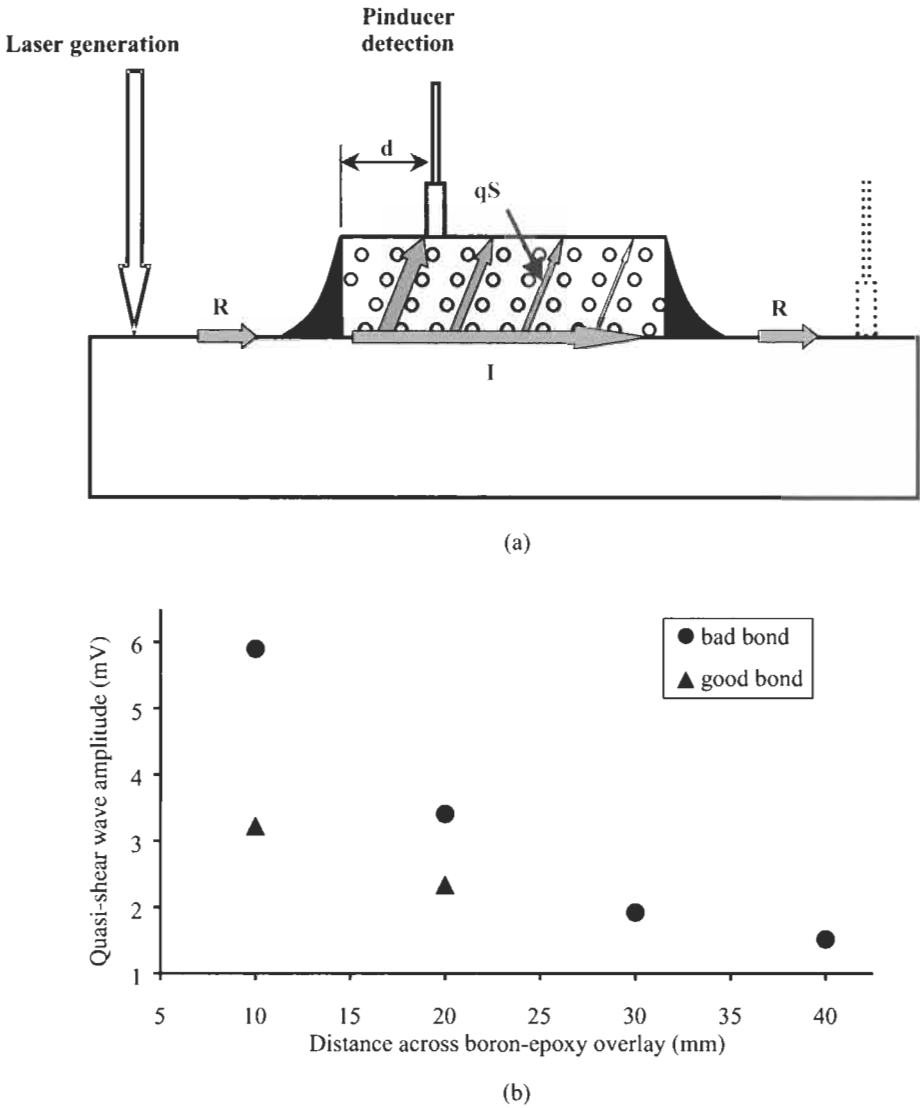


Fig. 23.16. (a) Experimental arrangement for the generation and detection of leaky interface (I) waves between an overlay and metallic substrate. The I-waves are generated when Rayleigh (R) waves reach the overlay. This was demonstrated by piezoelectric detection of both the leaked quasi-shear waves propagated to the top of the overlay and of the diminished R-waves propagated to the substrate beyond the overlay. (b) Quasi-shear wave peak amplitude as a function of distance, d , across the overlay for aluminum/boron-epoxy specimens. The results show the effect of the different interface properties for good and contaminated bonds. [22]

Following on from the DSTO work, QANTAS [23] trialed a variant of the above leaky interface wave technique on test specimens comprising aluminum substrates and composite overlays with simulated disbonds (teflon inserts and pull-out tabs). Waves were generated in the substrate using a 1 MHz transducer and detected on top of the overlay using a 2.5 MHz roller transducer. Disbonds in boron-epoxy and graphite-epoxy overlays were detectable with careful manual scanning. When trialed on boron-epoxy overlays on a Boeing 747 aircraft, the success of the technique was limited due to a number of additional issues including poor transducer coupling, more complex signals, proximity to rivets, and, for overlays on honeycomb structures, higher attenuation of flexural waves. Other more conventional techniques were also trialed, including pulse-echo ultrasonics and resonance testing. Overall, the results indicated that, for simple bond/disbond testing, application of the more conventional techniques is a better option. Notwithstanding these results, for assessment of adhesion integrity the more complex leaky interface wave or other emerging technologies will need to be further developed and implemented. One such technology would be electronic speckle interferometry which has recently shown some promise [24].

23.2.4. Resonance test inspection method

In high frequency bond testing (HFBT), often referred to as resonance testing, a transducer with a hard wear-surface is acoustically coupled to the item under inspection using a liquid couplant. Inspection frequencies normally range from 25 kHz to 500 kHz and are dependent on the thickness and type of material to be inspected. HFBT utilizes special narrow-bandwidth transducers, which, when coupled to the item under test, produce a continuous or standing UT wave in the material. The test material, in turn, has a damping effect on the transducer, increasing its bandwidth as well as changing its resonance frequency and signal amplitude. Anomalies, such as disbonds or delaminations in composite doublers, result in changes in the standing wave pattern of the material. Changes in the acoustic impedance create changes in the electrical impedance which are monitored by the Bondmaster instrument and displayed in the form of an amplitude/phase plot. In the general sense, the phase information is related to the depth of the disbond in the doubler or a thickness variation caused by the slope in the taper. Signal amplitude is predominately affected by the relative size or severity of the disbonds in the composite doubler. Sensitivity, the angle of the dot movement (rotation), and operating frequency can be adjusted on the instrument to maximize the differences between flawed and unflawed inspection sites. Figure 23.17 shows some sample output from the Bondmaster device and how the screen plots are used to detect the presence of a flaw.

High frequency ultrasonic resonant bond inspection was evaluated at the FAA/AANC on an array of composite doubler test specimens. A Staveley Sonic Bondmaster instrument was used to perform the inspections. A narrow banded 0.5" (12.7 mm) diameter transducer was driven at its resonant frequency of 330 kHz and placed on the composite doubler with the use of gel couplant [25]. The boron-

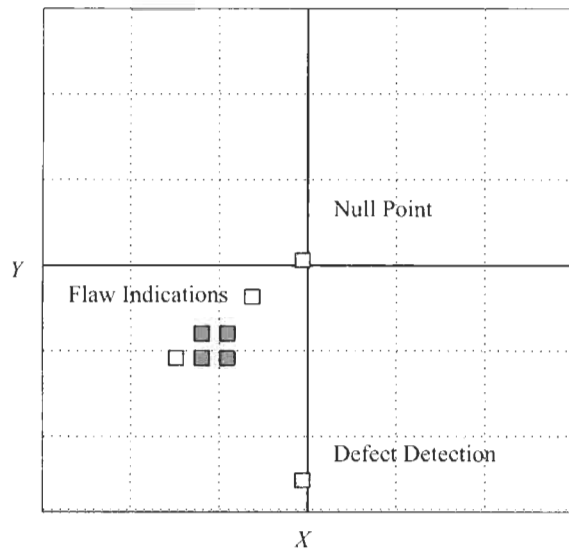


Fig. 23.17. Representative bondtester output for disbond and delamination inspections on 13-ply fatigue coupons.

epoxy had a damping effect on the transducer. The primary results were increased bandwidth, shift in resonant frequency, and change in signal amplitude. The transducer was nulled on an unflawed composite area on a calibration standard. The transducer was then moved to the composite doubler being inspected. Changes in the acoustic impedance of the transducer as it moves over a flawed area were detected. The flaw changed the standing wave pattern in the material. These changes were subsequently detected as differences in the acoustic impedance at the surface of the material caused by loss of material damping.

As with other contact UT methods, the inspection surface must be relatively smooth to allow adequate acoustic coupling. This fact, combined with the need for a liquid couplant, can sometimes limit the application of HFBT and make large area inspections somewhat tedious. On painted surfaces, poor paint adhesion can increase the overall acoustic impedance of the structure and may cause erroneous indications. When inspecting relatively thick, multi-ply composite doublers, detection of delaminations in the bottom few plies can be difficult. This is due to the relatively small change in total material impedance seen by the probe. The use of well characterized calibration standards is essential to properly set-up the resonant HFBT device [26]. However, even with the use of calibration standards it was found that material nonuniformities, inherent in composites and more prevalent in thicker laminates, can create difficulties in the application of the HFBT resonance testing. The results from this evaluation showed that it was difficult to obtain consistent signals from doublers in excess of approximately 0.115"

(2.92 mm) thick (approximately 20 plies). In regions above this thickness, changes in the signal amplitude and phase occurred even during inspections of unflawed portions of the doubler. The signals at a single point continuously fluctuated from “unflawed” to “flawed” indications, thus, it was difficult to clearly interpret the readings. Additional experimentation may be able to alleviate these difficulties and expand the useable range of HFBT inspections.

23.2.5. Thermography

Thermography is a nondestructive inspection method that uses thermal gradients to analyze physical characteristics of a structure, such as internal defects. This is done by converting a thermal gradient into a visible image using a thermally sensitive detector such as an infrared (IR) camera or thermally-sensitive film materials.

The temperature distribution on an aircraft skin or component can be measured optically by the radiation that it produces at infrared wavelengths. Many defects affect the thermal properties of materials. Examples are corrosion, disbonds, cracks, impact damage, panel thinning, and fluid ingress into composite or honeycomb materials. By the judicious application of external heat sources, these common aircraft defects can be detected by an appropriate infrared survey. Several organizations have demonstrated infrared structural inspection techniques on aircraft in field tests at maintenance facilities [27–31]. The U.S. Air Force is currently integrating thermography into the inspection of composite structures on its C-130, C-141, and F-15 aircraft. The applications include both composite honeycomb and bonded composite doubler structures. In the commercial aircraft arena, validation efforts are underway to certify thermography for select tear strap disbond and skin corrosion detection applications. In the AANC composite doubler study, a turn-key thermography inspection system developed at Wayne State University – the thermal wave imager (TWI) – was used to assess the merits of thermography to detect disbonds and delaminations in composite doublers [14]. The discussion and results which follow pertain to the TWI system.

Thermal wave imaging is accomplished using high-power flash lamps, an IR video camera, and image processing hardware and software, all of which are controlled by a personal computer. The flash lamps put out a short, high-power pulse of radiation, which raises the surface temperature of the aircraft approximately ten degrees when it is absorbed by the surface. The temperature pulse propagates into the material as a thermal wave and gets reflected by any defects which may be present in the material. The resulting temperature distribution is then recorded by the IR camera and displayed on the computer monitor. In practice, the computer actually obtains several images at progressively later times after each flash. This method is particularly useful for imaging and determining the depths of disbonds and delaminations in boron-epoxy repair doublers on aircraft structures.

TWI inspections were performed on composite doubler installations containing engineered flaws. Figure 23.18 shows a schematic of a composite doubler with

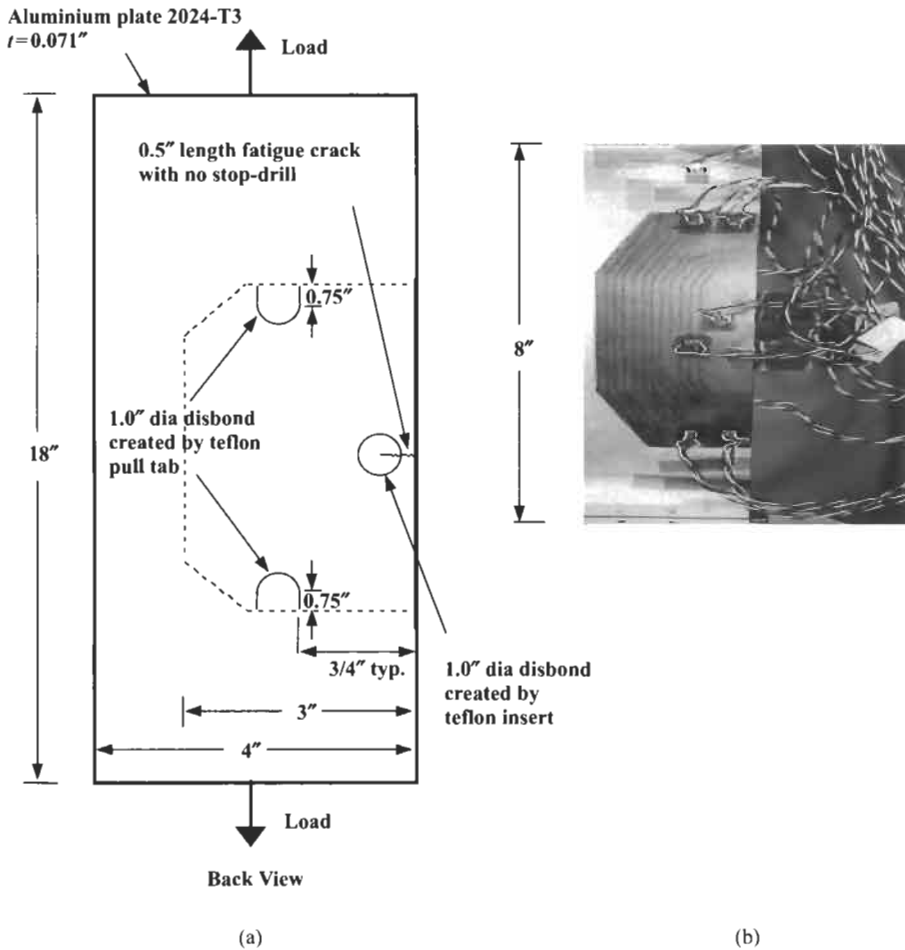


Fig. 23.18. 13-ply boron-epoxy composite doubler coupon: (a) schematic showing embedded flaws comprising a fatigue crack with a 1.0" (25 mm) diameter co-located disbond centered over the crack tip and 1.0" (25 mm) diameter disbonds in the load transfer region (edges of bondline); (b) photograph of the coupon during fatigue test.

disbond and crack flaws installed on an aluminum fatigue coupon while a sequence of images produced at different times during TWI inspection of this test specimen are shown in Figure 23.19. The early time images following the flash clearly resolve the ply drop-off at the edges of the 13-ply composite doubler. Beginning at around 0.68 s, intentionally placed disbonds between the doubler and the aluminum at the left and right edges (where the doubler is thinnest) begin to appear. As time progresses, these disbonds begin to show in thicker and thicker layers of the doubler. Between 4 and 8 s it is possible to see the circular disbond which was implanted over the crack tip and a "tail" extending downward along the induced

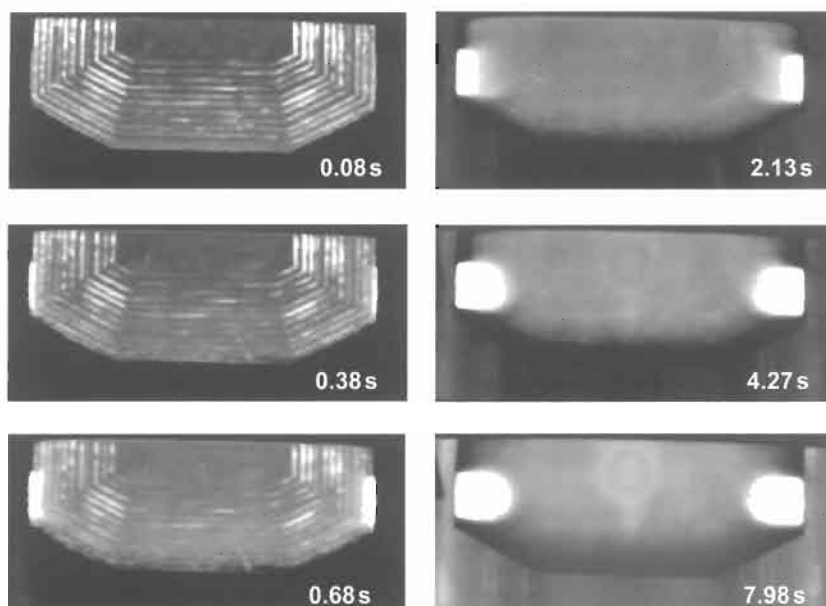


Fig. 23.19. Sequence of thermal wave images for a composite doubler coupon with embedded flaws.

fatigue crack. The circular disbond was located 13 plies deep in the doubler installation. The disbond tail was also located between the 13-ply doubler and the aluminum skin and was associated with a cohesive fracture of the adhesive layer immediately adjacent to the crack growth.

TWI was also applied to a boron-epoxy doubler which was installed on a DC-9 fuselage section in the AANC hangar. Figure 23.20 shows a schematic of the 10-ply doubler installation which identifies the size, shape, and location of the embedded flaws. The resultant sequence of images produced by a TWI inspection are shown in Figure 23.21. The features seen at early times are defects closest to the outside surface of the doubler (note appearance of flaws #1 and #2 in the first few frames). The disbonds, located at the base of the 10-ply doubler, and the deeper delaminations appear in the later frames corresponding to their delayed effect on the thermal field. All six embedded flaws were identified in the TWI images and flaws smaller than 0.5" (12.7 mm) in diameter could be detected. Another item of note is that the flaws around the perimeter of the doubler, at its thinnest region, are clearly imaged and do not induce the imaging difficulties observed in the UT C-scan results.

During the course of this composite doubler development effort, thermography was applied to over a dozen different doubler installations. The two examples above highlight the viability of thermography for inspecting bonded composite doublers. More comprehensive and structured tests were performed to better determine the sensitivity and resolution of thermography in detecting composite doubler disbonds, delaminations, and porosity. The Airworthiness Assurance

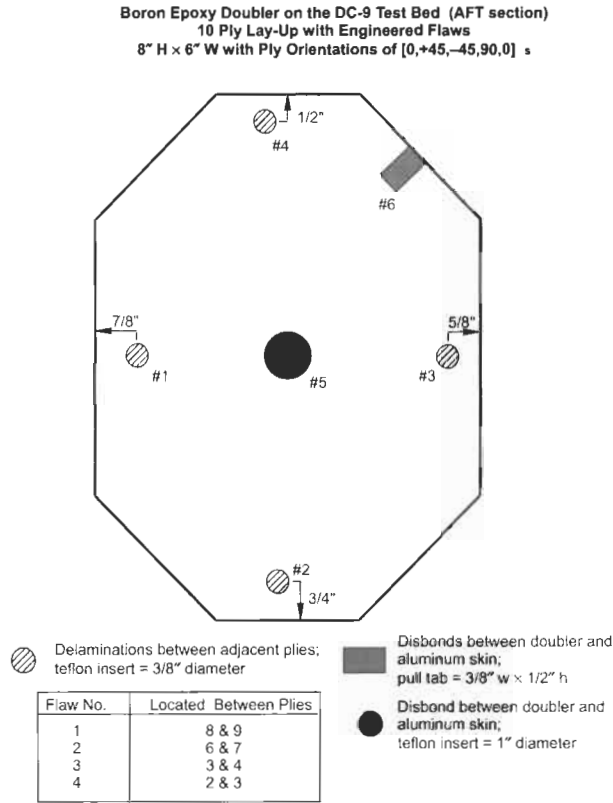


Fig. 23.20. Composite doubler installation on DC-9 testbed.

Center at Sandia National Labs conducted tests of this nature to apply thermography inspections to aircraft maintained by Warner Robins Air Force Base [32]. The tests ascertained the effects of a host of inspection impediments (e.g. underlying structure, doubler protective coatings) on the overall probability of flaw detection. It was demonstrated that flaws smaller than 0.5" (12.7 mm) in diameter could be reliably detected using thermography and their depth could be accurately determined.

- Summarizing, the advantages of thermography are as follows:
- thermography can be performed without physical contact with the surface.
 - single images can include relatively large areas, 1–2 ft² (0.09–0.4 m²), allowing for rapid inspections of large surface areas.
 - 2D image of the inspected surface helps the operator visualize the location and extent of any defect.
 - electronic recording of the image data allows for more thorough data analysis while other maintenance activities are being performed in the inspection area.
 - coats of paint are not an obstacle, however, their presence must be taken into consideration.

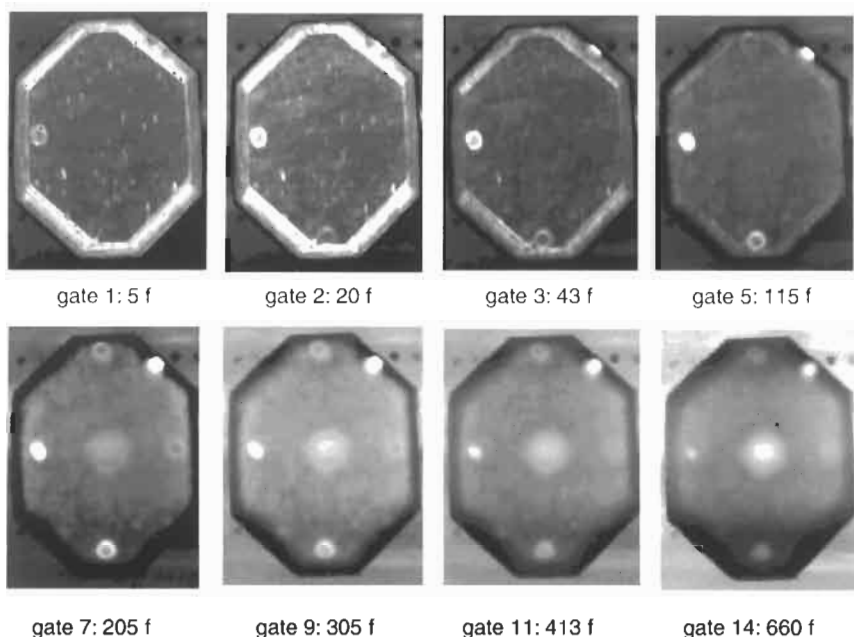


Fig. 23.21. Sequence of thermal wave images from DC-9 composite doubler inspection. (Frame time, $f = 1/60$ of a second.)

- nonmetallic materials can be inspected more easily than metals because of a difference in thermal properties.

The disadvantages are that:

- it is often necessary to apply a high-emissivity coating during inspections to obtain an acceptable image; steps have been taken to minimize the labor time associated with this task.
- damage to layers deep within a structure is more difficult to detect than damage in surface layers because the larger mass of material tends to dissipate the applied heat energy; preliminary experiments have shown that TWI can inspect doublers up to 40 or 50 plies, i.e. 0.25" to 0.30" (6.4 mm to 7.6 mm) thick.
- image interpretation requires an understanding of the physics of thermography and may require a high level of operator expertise; sophisticated data analysis and presentation software has minimized this dependency on in-depth expertise in thermography physics.

23.2.6. Other techniques

23.2.6.1. Acoustic emission

DSTO has pioneered the use of acoustic emission (AE) in several aircraft-related applications [33–35], including disbond detection for boron-epoxy reinforcements. The disbond application on which AE was trialed [36] was one of the most

challenging boron-epoxy reinforcement applications, viz. reinforcement of the complex wing pivot fitting (WPF) region in the F-111 aircraft. Fatigue cracking in the upper WPF of F-111 aircraft had led to the catastrophic failure of several wings during cold-proof testing. Conventional repair methods were impractical due to fitment problems. Therefore, an all boron-epoxy bonded external doubler repair was proposed in 1988 to extend the life of the WPF (Figure 23.22).

Validation of the doubler repair was made at DSTO in two stages by (i) proof-testing of an F-111 wing, and (ii) fatigue and cold-proof testing of a laboratory specimen designed to simulate the complex repaired F-111 section comprising

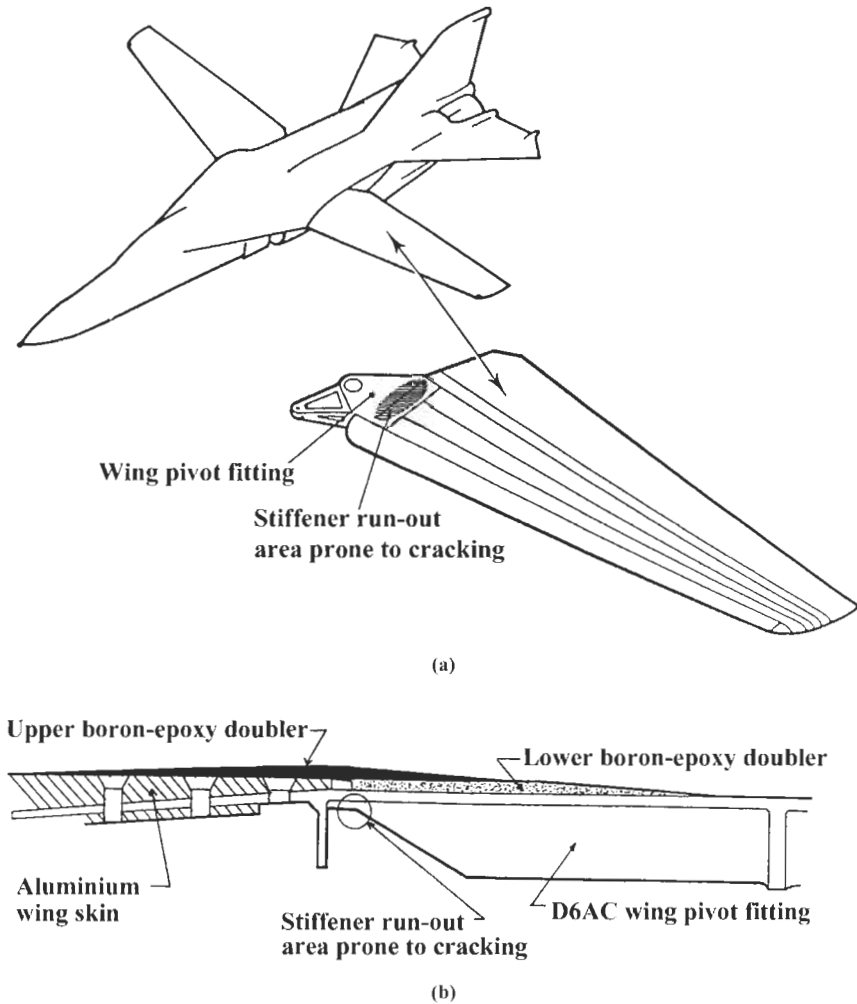


Fig. 23.22. (a) F-111C aircraft wing pivot fitting (WPF); (b) cross-section of the WPF and wing skin showing boron-epoxy doublers deployed over the region prone to cracking. [36]

WPF, wing-skin, bolts and doublers. AE was used to monitor possible disbonding of the boron doubler during both stage (i) and stage (ii) testing, because of the difficulties in applying more conventional techniques.

During stage (i) AE monitoring, AE sensors were attached to the WPF at each of the four corners of the largest of two doublers installed on the WPF. AE data acquisition was performed using a multi-channel Dunegan DART system interfaced to a computer for data processing. AE signals were accepted or rejected on the basis of their times of arrival at the four sensors. No AE signals could be attributed to disbonding of the large doubler, a result which was consistent with the fact that the repaired wing satisfactorily passed the stage (i) proof testing.

At the time of stage (ii) AE monitoring, the DART was required for other AE testing. Therefore, an AET-5000 locator was selected for AE signal processing. The locator allowed linear location of AE from two sensors which were attached at both ends of the long simulated WPF specimen (Figure 23.23). Acceptance/rejection criteria for AE from disbonding were specified in terms of arrival times of signals at the two sensors. Stage (ii) AE monitoring of possible disbonding in the simulated WPF specimen was carried out during two series of fatigue cycling and cold-proof testing. No AE events were detected during either series of fatigue cycling. A comparison of the AE results from the two cold-proof tests indicated that more AE events were detected in the second test, which suggested that damage had occurred in the latter test. The damage predicted by AE was confirmed by visual inspection of the specimen after the second cold-proof test – considerable disbonding in a tapered section of the reinforcement was apparent. Given the promising results obtained, AE is considered to be a promising technique for disbond detection for future applications.

23.2.6.2. Holographic interferometry

In the typical laser-based holographic interferometry system for NDI, a double exposure of an object corresponding to two different stressed states of the object produces a hologram of the object with fringes superimposed on the hologram. The fringe pattern corresponds to out-of-plane differential displacements (contour map) of the surface, revealing localized distortions in the vicinity of surface and sub-surface structural defects (if present). Such systems have a displacement resolution of about $0.3\text{ }\mu\text{m}$ and inherently have a wide field of view enabling rapid inspection of large areas. Vacuum loading is a typical method for applying stress.

Holographic interferometry for detecting bonding defects has existed for some 20 years but a significant problem experienced in the past with this NDI technique was that it usually required a vibration isolation table for the object under test. This operational constraint was obviated in a portable holographic interferometry system (PHITS) developed and demonstrated by the Australian Defence Force Academy (ADFA). Some work performed at ADFA [37] with the PHITS was directed at its potential application for the NDI of composite repairs. For a boron overlay on an aluminum substrate, it could be clearly seen that interfacial disbands, simulated by teflon inserts, were detected. The assessment of adhesion integrity

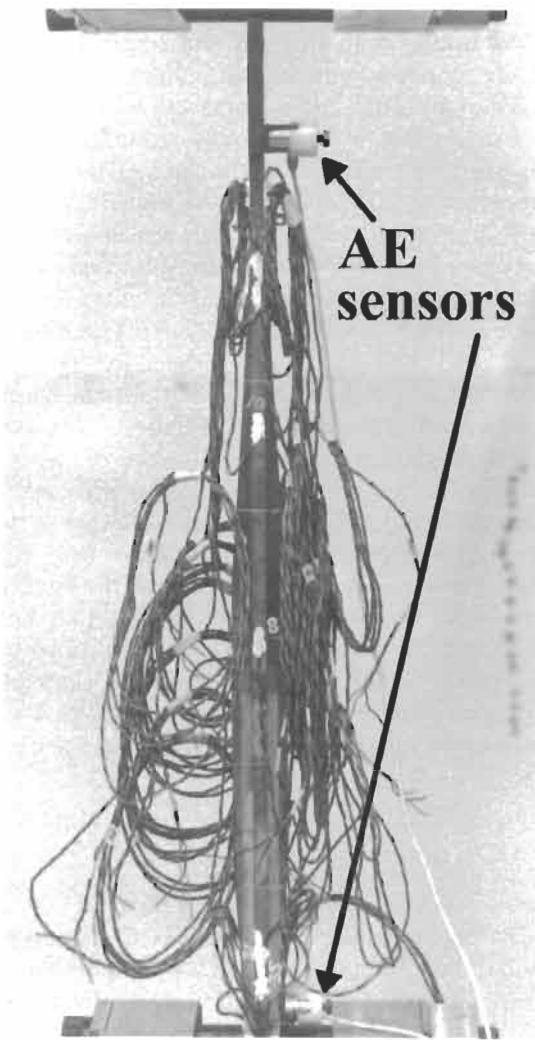


Fig. 23.23. Simulated WPF specimen. [36]

employing the PHITS was also investigated but the results for a weakened bondline, simulated by oil contaminated adherend surfaces, were inconclusive.

23.2.6.3. *Thermography-stress analysis/defect detection*

The design and development of composite repairs usually requires the testing of specimens which are as representative as possible of the local geometry, the degree of local constraint, and the operational stresses. Thermal emission techniques are sometimes employed as an alternative or complementary approach to strain gauge techniques during testing of specimens but also have a role in the detection of sub-

surface defects. The techniques depend on the reversible conversion between mechanical and thermal energies when a body is subjected to cyclical tensile or compressive stresses. For adiabatic conditions, the relationship between the reversible temperature change and the corresponding change in the sum of the principal stress is linear and independent of loading frequency. Thermographic systems have been used and developed at DSTO for problems and studies associated with boron-epoxy reinforced specimens representative of wing skin repairs of corrosion and crack damaged sites on military aircraft.

A study [38] employing a SPATE (stress pattern analysis by thermal emission) system was undertaken for a number of specimen types. The SPATE system was a single detector system which detected the infrared radiation emitted from a specimen surface as a result of the minute temperature changes during cyclically stressing of the specimens. For specimens with boron-epoxy overlays over surface cracks, SPATE image data and numerical modelling data indicated the possibility of using thermal emission techniques to monitor crack growth or delamination beneath the overlays. The study also considered corrosion occurring on wing skins, particularly on or adjacent to skin splices. Of interest were corrosion repairs where the corroded region is cut out and replaced by a metal plug with a composite overlay bonded over the plug and the surrounding region. Bonded plug simulated repair coupons (Figure 23.24) were fabricated from aluminum substrates and boron-epoxy overlays. During fatigue testing of these coupons, SPATE images were employed not only for stress analysis but also for indicating delamination and its growth after defined increments in the load spectrum. A SPATE image indicating minor delamination near one end of the overlay as well as a delamination region in from the end is shown in Figure 23.24.

A new thermographic stress analysis system known as FAST (focal-plane array for synchronous thermography) was developed at DSTO [39]. The FAST system employed a staring array thermal imager instead of a single detector enabling it to operate many times faster than the SPATE system. Its potential for NDI applications was of interest for structures containing sub-surface features which can affect the FAST images via two phenomena, viz. (i) the effect of hidden features on the surface stresses and (ii) the effect of through-thickness diffusion as a result of high stress induced temperature gradients [39]. The FAST system has been

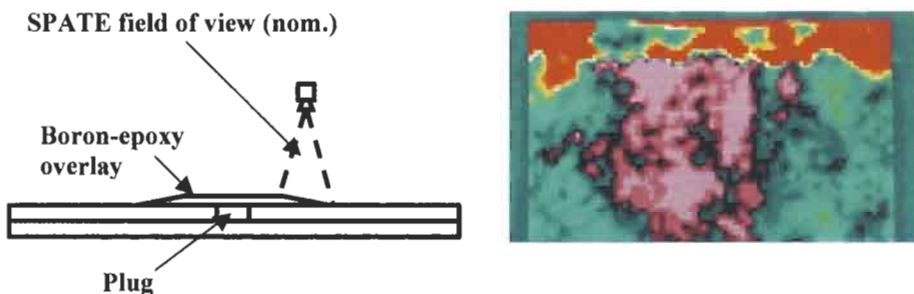


Fig. 23.24. Bonded plug simulated repair coupon and SPATE image. [38]

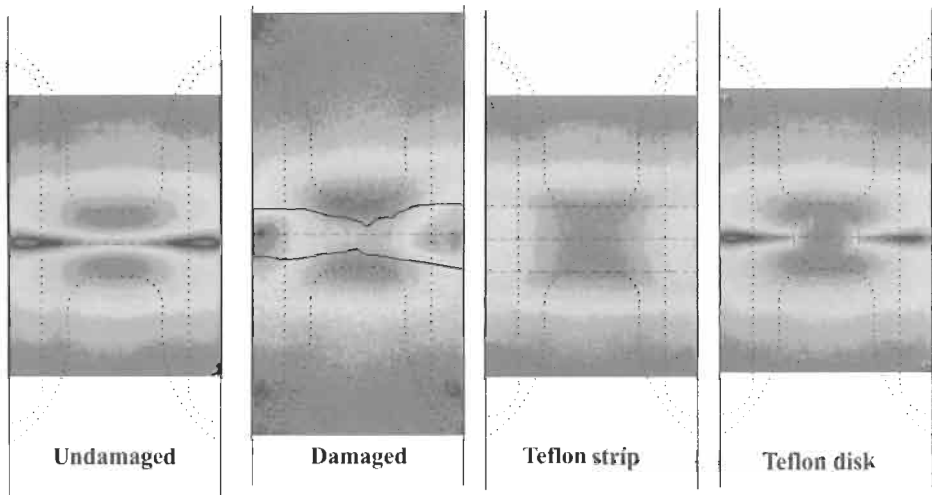


Fig. 23.25. FAST images of F-111 lower wing skin coupon specimens. [40]

employed in a number of composite repair studies, e.g. F-111 lower wing skin tests (Section 23.3.3.1). For the wing-skin coupon specimens of those tests, the FAST images [40] shown in Figure 23.25 were collected for an undamaged specimen, a fatigued damaged specimen, and specimens with simulated disbonds (teflon inserts). Superimposed on the images (as broken lines) is the hidden detail showing through-the-thickness variations of the aluminum inner adherend (refer Figures 23.33 and 23.34). The damage profile indicated by ultrasonic NDI is superimposed on the image for the fatigued specimen. The shape and location of the teflon inserts are superimposed on the simulated disbond specimen images. The central regions of the images for the undamaged and damaged specimens show two highly stressed regions. The inclusion of the simulated disbonds caused these regions to coalesce with the effect increasing as the disbond area increases.

As indicated by the examples presented above, thermoelastic techniques such as SPATE and FAST currently can only provide qualitative indications of defects. Further development would be required to enable the techniques to be used for quantitative NDI.

23.3. Inspections for cracks in parent material beneath composite doublers

23.3.1. Eddy-current inspections

Eddy-current (EC) inspection uses the principles of electromagnetic induction to identify or differentiate structural conditions in conductive metals [41,42]. The presence of a crack is indicated by changes in the flow of eddy currents in the metal. EC signals are physically monitored using impedance-plane plots which show the

reactive and resistive components of a coil as functions of frequency, conductivity, or permeability. When using EC to detect cracks in an aluminum skin, there are inspection impediments produced by the composite laminate.

External surface inspections which may key off visible attributes such as rivet head locations (normal origin of fatigue cracks) must now be performed blind since the doubler covers the aluminum surface. Mylar maps of the doubler area, which include rivet and substructure element locations, can alleviate this difficulty and minimize false calls. Although the doubler does not interrupt an eddy-current signal it does create a lift-off effect which reduces the signal strength. Lower frequency probes can be used to produce a greater depth of EC penetration. However, this is accompanied by a loss in sensitivity versus higher frequency probes. Thus, the thicker the doubler, the greater reduction in crack detection sensitivity.

The depth of penetration of eddy currents is inversely proportional to the product of magnetic permeability, electrical conductivity, and frequency of the inducing currents. Therefore, eddy-current tests are most sensitive to discontinuities on the surface next to the coil, which makes them very effective for detecting fatigue cracks in the near surface. High frequency eddy current (HFEC) is generally considered to be in the range 100 kHz and above and is used to detect near-surface flaws. Low frequency eddy current (LFEC) is in the 100 Hz to 10 kHz range and is used to penetrate deeper to detect flaws in underlying structure. The detectable flaw size usually becomes larger as the frequency is lowered. Eddy currents deeper in the material are weaker and lag in phase compared to the currents near the surface. By measuring the phase, it is possible to determine whether the defect is near the surface or at an inner wall.

Because eddy currents are created using an electromagnetic induction technique, the inspection method does not require direct electrical contact with the part being inspected. The composite doubler, between the EC transducer and the aluminum being inspected, does, however, create a lift-off effect which changes the EC signal. This lift-off effect can mask important aspects of flaw detection and must be counteracted by careful equipment set-up, use of suitable calibration standards, and experience in EC signal interpretation. Eddy currents are not uniformly distributed throughout the skin; rather, they are densest at the surface immediately beneath the coil (transducer) and become progressively less dense with increasing distance below the surface. Thus, the inspection sensitivity through composite doublers is decreased by the lift-off effects and the associated need to inspect below the surface of the EC transducer. The depth of EC penetration can be increased by decreasing the inspection frequency. As noted above, these lower frequency inspections are accompanied by a loss in sensitivity. Therefore, EC inspection through composite doublers becomes a balance between signal resolution and the frequency required to inspect beneath a particular laminate.

23.3.1.1. Sensitivity assessment

Structured EC testing was performed at the FAA/AANC in an attempt to quantify EC performance through composite doublers. Both sliding and surface

(pencil) probes were evaluated. The sliding probe, with its lower frequency and larger footprint, is normally preferred for these type of inspections, particularly where large areas need to be scanned, the doubler is thick and/or the cracks are 2nd layer ones. When the doubler is thin enough and the approximate crack location is known, the pencil probe with its higher frequency can provide an improved inspection sensitivity. When inspecting the coupon specimen shown in Figure 23.18, a 30 kHz pencil probe was able to reliably detect the crack tip – which was changing during the course of the fatigue testing – through a 13-ply doubler. Eddy-current and microscopic inspections on the back side of the specimen (non-doubler side) confirmed the accuracy of the EC inspections through the doubler.

Figure 23.26 shows representative EC signals from cracked structure located beneath boron-epoxy doublers. Two variations are shown to demonstrate the ability of EC to detect both first (surface) and interlayer (substructure) cracks in aircraft structure. Initial testing conducted by the AANC on composite doubler specimens with cracks in the parent aluminum skin established the following general limits of crack detectability through composite doublers:

- i a 0.060" (1.5 mm) long first layer (surface) crack can be detected in the aluminum through a 0.310" (7.87 mm) thick doubler;
- ii a 0.15" (3.8 mm) length surface crack can be detected through a 0.5" (12.7 mm) thick laminate; and
- iii a 0.15" (3.8 mm) long subsurface (2nd layer) crack can be detected through a 0.310" (7.87 mm) thick doubler and a 0.040" (1.0 mm) thick surface plate.

In the case of the L-1011 application, the addition of the copper mesh lightning protection created difficulties in carrying out the standard EC inspections for

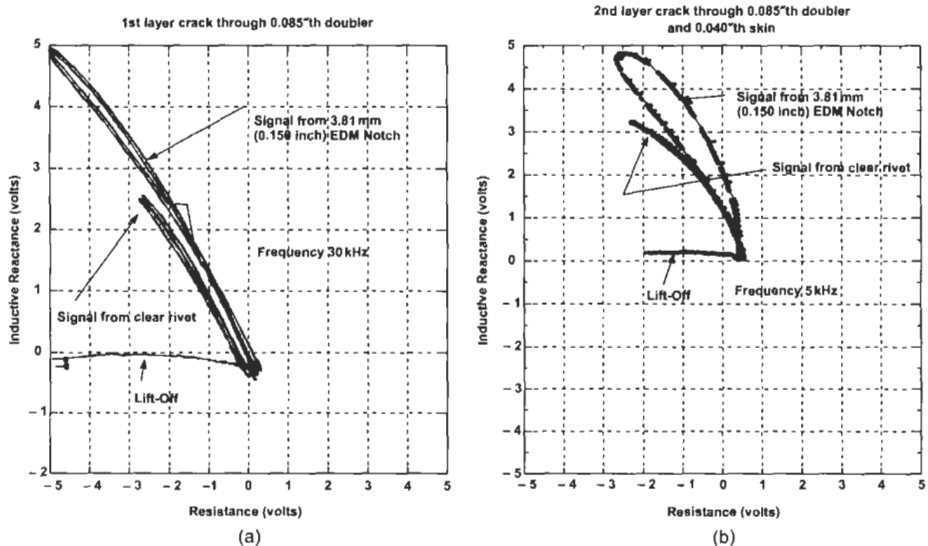


Fig. 23.26. EC signal for (a) 1st layer crack through 0.085" (2.2 mm) thick doubler and (b) interlayer crack through 0.085" (2.2 mm) thick doubler and 0.040" (1.0 mm) thick skin.

cracks using a pencil or sliding probe. Since the copper mesh is a conducting material, it disrupts the flow of eddy currents at the surface of the laminate. This, in turn, causes the balance point on the impedance plane display to vary with probe orientation. The use of ultra-low frequencies (500 Hz) to inspect the part helped the EC inspection to look “past” the copper mesh and into the area of interest. However, the signal resolution was significantly diminished and key location pointers such as fasteners were no longer evident. This study determined that the combined detrimental effect of probe lift-off (doubler thickness) and copper mesh lightning protection was not a problem until the doubler reached approximately 15 plies thick, i.e. 0.10" (2.5 mm). Beyond this thickness, the signal-to-noise ratio was below acceptable levels. The unstable signal movement alone was greater than the expected signal variation due to the presence of a crack. If copper mesh is not present in an installation, the results presented above indicate that acceptable crack detection can be obtained through doublers in excess of 40 plies thick.

23.3.1.2. Probability of crack detection

The limits of crack detection listed above were not arrived at in a blind manner. That is, the operator knew the locations of the cracks and made a judgment call as to whether the variation in EC signal was sufficient to justify a flaw call. True flaw detection performance must be measured through blind experiments where the inspector must make flaw calls from an assortment of cracked and uncracked rivet sites. The specimen set must be statistically relevant and provide: (1) opportunities for flaw calls over the full range of applicable crack lengths, and (2) sufficient unflawed sites to assess the Probability of False Alarm. In order to make a valid measurement of the flaw detection capabilities of EC inspections through composite doublers a structured POD study was performed.

The POD study utilized a series of surface crack and subsurface crack aircraft panels. These panels, which mimic a Boeing lap splice joint, contained an assortment of fatigue cracks with specific lengths which were carefully engineered in the upper or lower skins [43]. To determine the limits of crack detectability through composite doublers of various thicknesses, a composite laminate step wedge was superimposed over the lap splice crack panels as shown in Figure 23.27. In these specimens, the cracks were located in the upper rivet row of the outer skin (i.e. surface cracks).

Surface crack POD

A suite of 18 lap splice panels was inspected through four laminate thicknesses (Table 23.1). Figure 23.28 shows the resulting POD curves which were generated from the inspections on surface crack panels using a sliding probe. It can be seen that all cracks of 0.17" (4.3 mm) length and greater were found regardless of the thickness of the composite doubler. Also, the family of curves follow the general trend presented earlier in this chapter where the POD performance diminishes with increasingly difficult circumstances (Figure 23.3). Thus, as the doubler becomes thicker the POD drops off slightly. These results are quite good in light of the damage tolerance requirement to find fatigue cracks beneath doublers before they

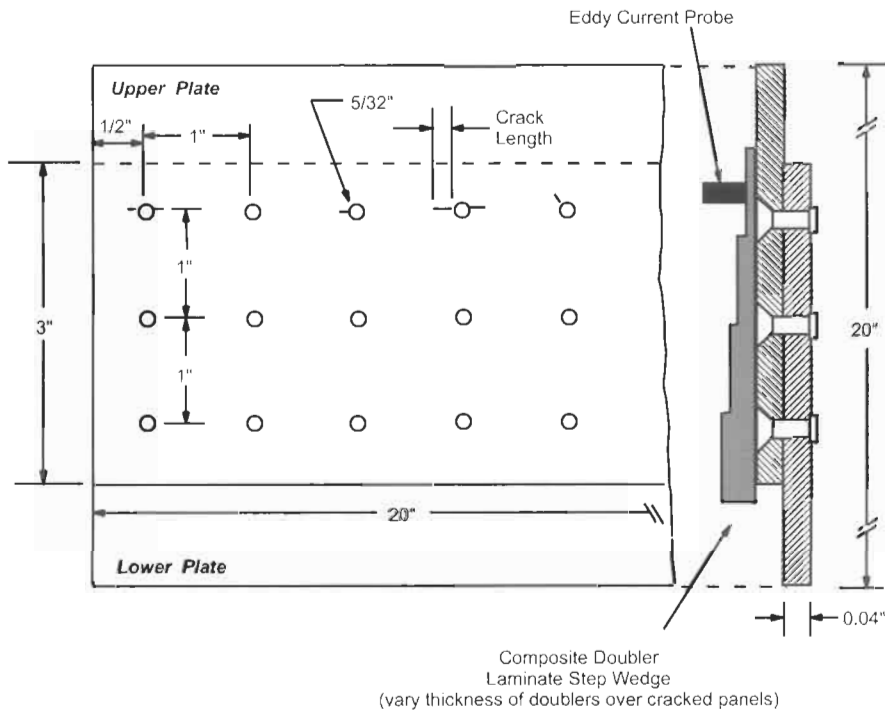


Fig. 23.27. Test set-up for detection of surface cracks through composite doublers.

reach 1" (25 mm) in length. The EC detection capabilities corresponding to the standard 95% POD goal are summarized in Table 23.1.

The surface crack probability-of-detection experiment used the 18 aircraft panels with a total of 360 rivet inspection sites (upper row of lap splice outer skin only). Since 81 of these inspection sites were cracked, there were 279 opportunities for false calls. Two false calls were made on the panels which were inspected without a composite doubler (0.7%) while no false calls were recorded during any of the inspections through the various composite doublers. Overall, it can be said that the

Table 23.1
Eddy-current surface crack detection performance through bonded composite doublers.

Composite doubler thickness	Number of plies	Surface crack length at 95% POD threshold
No doubler	0	0.053" (1.3 mm)
0.031" (0.79 mm)	5	0.059" (1.5 mm)
0.085" (2.2 mm)	15	0.091" (2.3 mm)
0.143" (3.63 mm)	25	0.103" (2.61 mm)
0.199" (5.05 mm)	35	0.121" (3.07 mm)

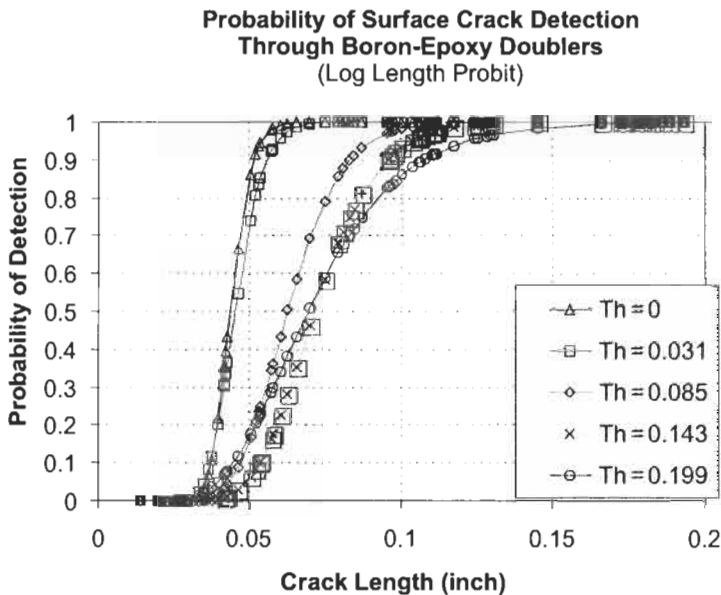


Fig. 23.28. Probability-of-detection curves for eddy current surface crack inspections through different thicknesses of composite doublers.

false call rate for inspections through composite doublers in the 5- to 35-ply regime is less than 1%. It should be noted that the above results pertain to a single ASNT level II inspector's findings. While the quantitative results are certainly valid, additional inspections, performed by other aircraft certified inspectors, are needed to draw final POD conclusions.

Interlayer (third layer) crack POD

A second POD study was performed to assess eddy-current crack detection of subsurface cracks through composite doublers. The subsurface crack test panels were also lap splice joints with two different skin thickness sets: (1) top plate, bonded doubler, and bottom plate were all 0.40" (10.2 mm) thick, and (2) top plate, bonded doubler, and bottom plate were all 0.36" (9.1 mm) thick. Figure 23.29 shows the lap splice configuration where the cracks are in the lower row of the inner skin (third layer). The major difference between these specimens and the surface crack panels shown in Figure 23.27 is the presence of the bonded aluminum doubler between the upper and lower skins. Thus, this experiment challenged eddy-current inspections to detect third layer cracks through either 0.80" (20.3 mm) thick material comprising two 0.40" (10.2 mm) thick layers or 0.72" (18.3 mm) thick material comprising two 0.36" (9.1 mm) thick layers.

A suite of 17 lap splice panels was inspected without a doubler in place and then again after placing the 0.031" (0.79 mm) thick (5 plies) doubler over the cracked panels. Figure 23.30 shows the resulting POD curves which were generated from

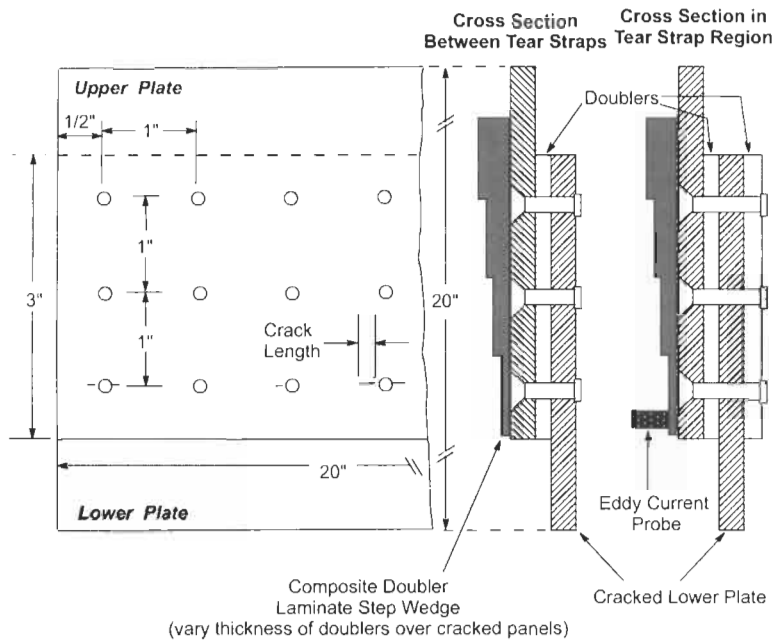


Fig. 23.29. Test set-up for detection of subsurface cracks through composite doublers.

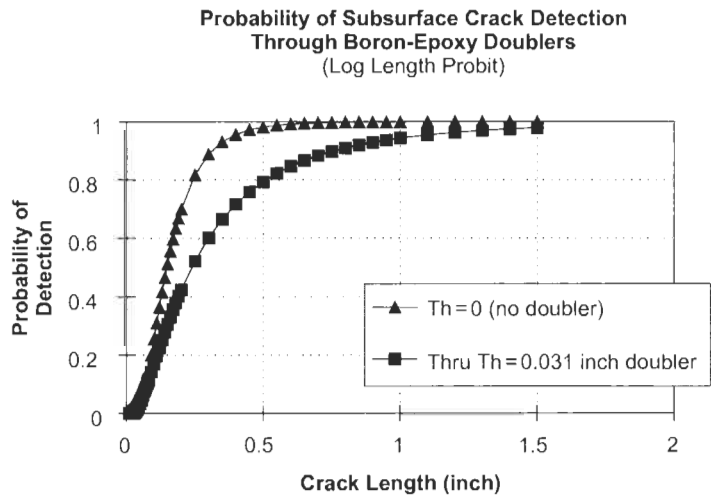


Fig. 23.30. Probability-of-detection curves for eddy current subsurface crack inspections through different thicknesses of composite doublers.

the inspections on the interlayer crack panels, again using a sliding probe. The interlayer crack detection is shifted to the right relative to the surface crack POD curves because of the added depth of penetration required for the eddy current (and the associated loss in resolution). However, the curves do infer that cracks of 1" (25 mm) and greater can be detected in subsurface structures beneath composite doublers. It should be noted that the curves were generated by producing a fit through the data. There were insufficient crack detections to fully populate the curve and thus portions of the curves are extrapolations using accepted POD curve fitting algorithms. Therefore, a table of 95% POD values, which would be primarily extrapolation numbers, is not presented for the interlayer POD study.

The interlayer crack POD experiment used the 17 aircraft panels with a total of 340 rivet inspection sites (lower row of lap splice inner skin only). Since 98 of these inspection sites were cracked, there were 242 opportunities for false calls. One false call was made on the panels which were inspected without a composite doubler (0.4%) and one false call was recorded during the inspections through the 0.031" (0.79 mm) thick composite doubler. The number of cracks detected in this experiment could have been higher but the penalty may have been a higher number of false calls. Once again, while the quantitative results are certainly valid, additional inspections, performed by other aircraft certified inspectors, are needed to draw final POD conclusions. Additional tests would also help highlight the relationship between an inspector's experience and qualification and false calls with probability of crack detection.

23.3.2. *X-radiographic inspections*

Radiographic inspection is a nondestructive method of inspecting materials for surface and subsurface discontinuities [41]. The method utilizes very short wavelength radiation in the form of either X-rays or gamma rays. The waves penetrate the material and are absorbed depending on the thickness or density of the material being examined. By recording the differences in absorption of the transmitted waves, variations in the material can be detected. Figure 23.31 shows an application of X-radiography in a hangar environment.

In the particular case of the L-1011 composite doubler, evaluating X-radiographic results through composite doublers was important as an X-radiographic inspection requirement was already called out to detect cracks in the door corner region [44]. If acceptable results could be obtained through the door corner doubler, then it would not be necessary to modify any existing procedures or introduce any new inspection techniques. Delta Air Lines would merely perform the same X-radiographic inspection as before the doubler was installed and acceptable flaw detection would be achieved. The following section describes the effort to: (1) assure that composite doublers do not adversely affect X-radiographic inspections, and (2) identify proper exposure time and power settings to optimize the sensitivity of the X-radiographic technique when inspecting through thick doublers [45].

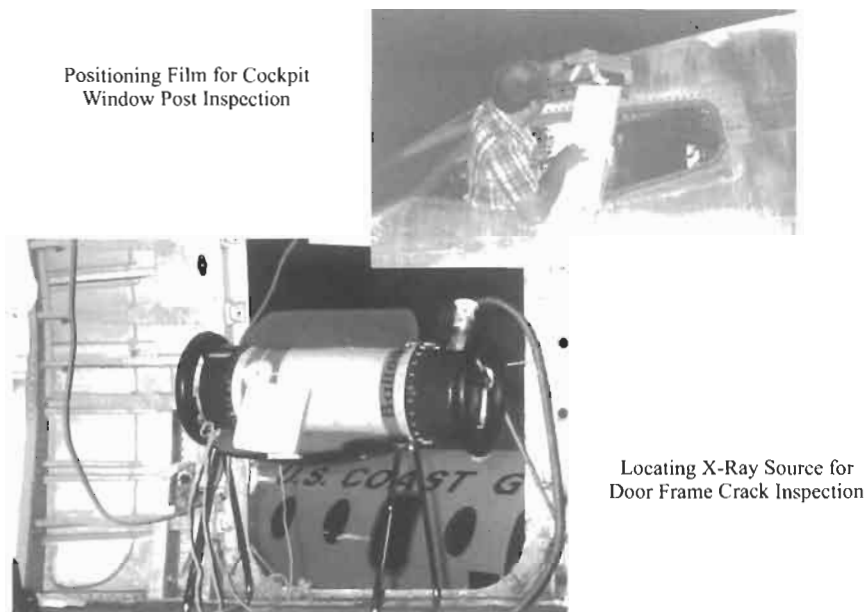


Fig. 23.31. Aircraft fuselage inspection for cracks using X-radiography.

Resolution and sensitivity – image production through composite doublers

Several specimens with 1st and/or 2nd layer EDM notches or fatigue cracks ranging from 0.05" (1.3 mm) to 1.0" (25 mm) in length as well as the L-1011 fuselage test article were inspected through a 72-ply composite doubler. To form a basis of comparison, X-radiographs were also taken without the doubler placed over the cracked specimens. Details of the doubler are as follows: 72 ply, multi-axial lay-up with a fibreglass top coat (as per the Lockheed L-1011 doubler design drawing). A single screen lightning protection ply was placed on top of the doubler to assess any degradation in the X-radiograph caused by this copper mesh.

X-radiography was found to be a very effective inspection method to interrogate the interior of the parent material covered by a composite doubler. This technique provides the advantage of a permanent film record. To increase the contrast on the film, the X-radiographic inspection was performed at low kilovoltage (80 kV).

The specified damage detection threshold for cracks under the doubler is 1.0" (25 mm) (for L-1011 application). Test results showed the ability to detect cracks less than 1" (25 mm) in length. The EDM notches, length range of 0.25" to 1.0" (6.4 mm to 25 mm), were readily apparent in the X-radiographs. Further, fatigue cracks of the order of 0.38" (9.7 mm) in length were found under 0.41" (10.4 mm) thick (72 ply) boron-epoxy doublers. A sample X-radiograph of a crack imaged through a 72-ply composite doubler is shown in Figure 23.32. (Note that significant resolution is lost in translating the X-radiograph to a black and white graphic.) Comparisons with X-radiographs taken without composite doublers revealed that while the doubler may darken the X-radiograph image slightly it does not impede

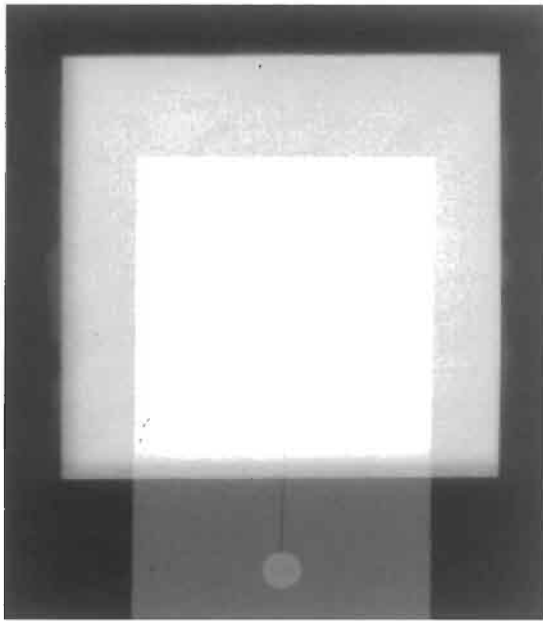


Fig. 23.32. Sample X-radiograph of a cracked aluminum structure beneath a 72-ply composite doubler.

the X-radiographic inspection. Power and exposure times were adjusted in order to restore the desired contrast and maintain the specified film density of between 2 and 3. The initial set-up, employing 80 kV, 12 mA, 6'' (150 mm) source-to-film-distance, 30 s exposure time, and medium speed film, produced a film density of 0.98. Increasing the exposure time to 90 s produced a film density of 2.64. Image quality indicators (IQI), inserted into the field of view, verified the resolution and sensitivity of the radiographic technique. IQI lines with widths of 0.010'' (0.25 mm) and dots with diameters of 0.10'' (2.5 mm) were clearly imaged on the X-radiograph. These results showed that X-radiographic inspections are as effective as before a doubler is installed.

The X-radiographic tests performed in this study determined that there are no additional impediments brought on by the presence of composite doublers. X-radiographic inspections were able to achieve high levels of resolution when inspecting through thick composite doublers and the films were very comparable with films acquired on similar structures without doublers. All difficulties associated with X-radiographic inspections – shadowing from substructure elements, accessibility, and safety issues – are the same as in structures without composite doublers.

23.3.3. Challenges in crack monitoring

The above has shown how the sensitivity and reliability of EC and X-ray crack inspections are affected by impediments generated by composite doublers installed

on typical aircraft panel structures with through-thickness cracks. Composite doublers installed over partial back-face cracks and cracks in complex-shaped components present even greater impediments. The novel solutions developed by DSTO to several of these problems are given below.

23.3.3.1. Through-and Partial-thickness cracking of F-111 lower wing skin

Experimental testing was undertaken at DSTO to verify a bonded boron-epoxy repair to a 48 mm long through-thickness fatigue crack in a fuel-flow passage area of the lower wing skin of an F-111C aircraft of the Royal Australian Air Force (RAAF) as shown in Figure 23.33. The crack had reduced the residual strength of the wing to below the Design Limit Load. This was the first time that a bonded composite repair had been applied to a critical defect in a primary aircraft structure and represented the most critical application of bonded repair technology yet undertaken anywhere in the world.

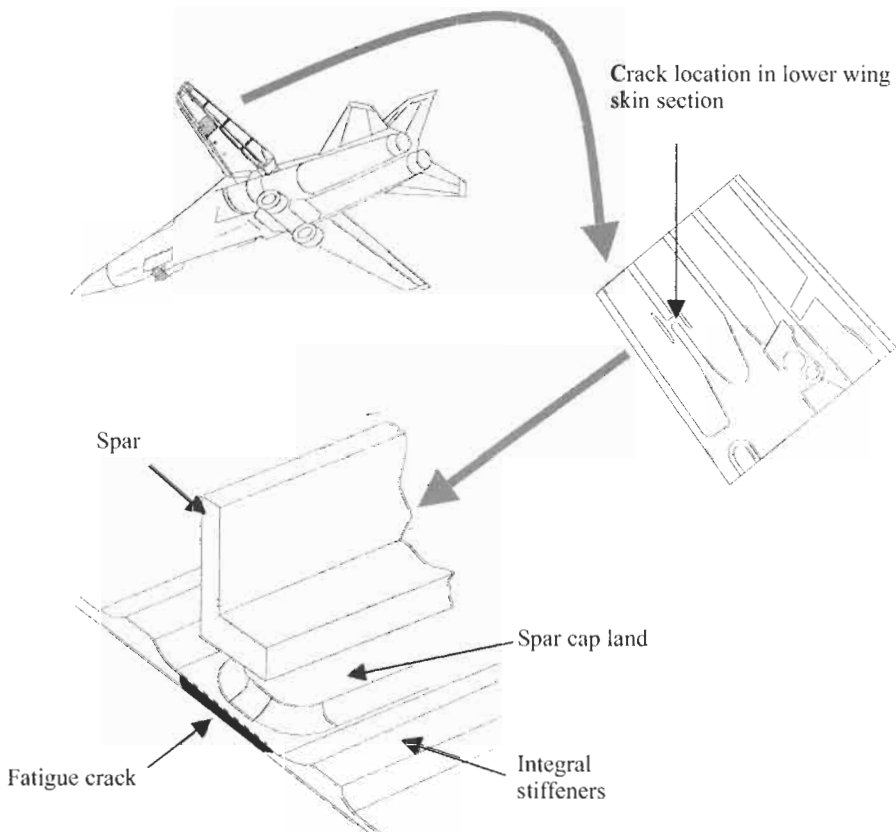


Fig. 23.33. Fuel flow passage area of F-111 lower wing skin.

NDE for through-thickness cracking

NDE was used in the substantiation of the repair which required both static and fatigue testing of a range of representative specimens [38,46]. Tests were performed on simple coupon and panel specimens, and more complex, quasi full-scale, box specimens. All but a few of the test specimens had a through-thickness crack defect introduced mechanically in the area corresponding to where cracking initiated in the aircraft wing. Boron-epoxy reinforcements were applied to the coupon specimens, to most of the panel specimens, and to both of the box specimens.

RAAF eddy-current techniques were used to measure the through-thickness crack lengths to within 1 mm through the reinforcements on both the panel and box specimens and were used to monitor crack growth behavior during fatigue testing. Ultrasonic C-scan inspection was performed on the boron-epoxy reinforcements after specimen fabrication to confirm reinforcement and bond integrity. Ultrasonic C-scan inspection was also employed to verify the location and size of simulated disbonds (teflon inserts) in a number of the coupon specimens. Ultrasonic A- and C-scan inspection of fatigue loaded panel and box specimens indicated disbonding along the cracks for widths up to ~6 mm (Figure 23.34) and, for the box specimens, also some disbonding at the ends of the reinforcements. Teardown inspections were performed but were inconclusive as to the extent of disbonding.

NDE for partial-thickness back-face cracking

The need for monitoring of back-face cracking arose as an extension of the successful application of the boron-epoxy repair technology to the repair of primary structure in the case of the F-111 lower wing skin. The main focus of the F-111 lower wing skin problem was to repair a through-thickness crack (as described above). However, there was also interest in developing a capability for (i)

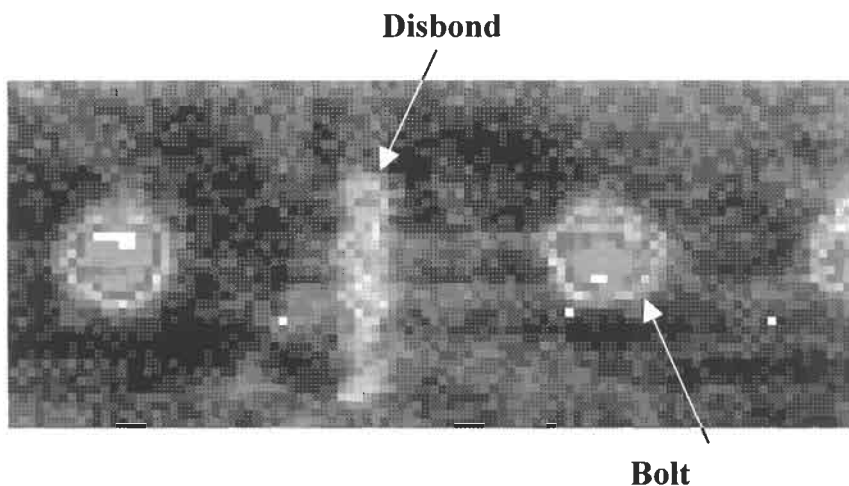


Fig. 23.34. Ultrasonic C-scan of central region of a box specimen showing disbonding around crack. [47]

reinforcement of uncracked wings and (ii) repair of future back-face cracks in other F-111 wings. Clearly it would be useful to repair such cracks at an early stage in cracking rather than when the cracks became through-thickness. Hence there was a requirement for NDE development to assess minimum detectability limits for partial-thickness back-face cracking for the F-111 lower wing configuration.

As illustrated above, eddy-current techniques are routinely used for the accurate monitoring of the length of through-thickness cracks under boron-epoxy repairs. They are also usually applicable for monitoring of partial-thickness front-face cracks emanating from the reinforced/repair surface. However, monitoring of partial-thickness back-face cracks under boron-epoxy repairs required new technique development.

Both eddy-current and ultrasonic techniques were investigated using specimens (3.2 mm thick plates) to simulate the F-111 forward auxiliary wing-spar station 281.28. A series of rectangular partial-thickness slots were inserted in the back-face of the plates to allow verification of minimum defect detectability limits for this lower wing skin problem. For each slot studied, the length-to-depth aspect ratio was selected to simulate the expected cracking profile in the wing skin. The length/depths used were 20.4 mm by 2 mm, 5 mm by 1.2 mm, 2.5 mm by 0.6 mm, and 1.8 mm by 0.4 mm, respectively. The smallest slot in this series was well below the detection limits required in the RAAF F-111 procedure for an unreinforced lower wing spar. Two different sets of specimens were prepared, one set having a multi-directional boron reinforcement lay-up and configuration identical to that used in the F-111 wing repair and the second set differing only in the use of a unidirectional boron as reinforcement. A multi-directional boron-reinforced specimen which simulated the actual geometry of the reinforced 281.28 station lower wing skin was also prepared and tested to assess geometric limitations of techniques for the actual wing-skin.

The ultrasonic techniques trialed were based on variants of the 45° shear-wave ultrasonic procedure developed by the RAAF for the unreinforced F-111 lower-wing skin problem. The techniques used either a single or multiple skip (i.e. three or five skip) approach with the ultrasonic probe applied on the reinforcement. In practice, only the single-skip approach could be applied to the present wing-skin problem but the multiple-skip technique was also investigated to gain a better understanding on the detection of back-face cracks under boron reinforcements. The ultrasonics pulser/receiver used was a Krautkramer USIP20. Two probes were trialed: (i) an Aerotech ABFP-SM 45° 5 MHz shear-wave probe with a square active element 4.7 mm × 4.7 mm, and (ii) a Krautkramer SMSWS 45° 5 MHz shear-wave probe with a circular active element of 3.18 mm diameter. Each probe was used with an ANDSCAN manual scanner to allow accurate defect mapping. The eddy-current technique trialed used a 4 kHz probe in combination with a MIZ40 eddy-current flaw detector and the ANDSCAN system.

For both the multi- and uni-directional boron reinforcement types, all four slots were detected using the multiple-skip shear-wave ultrasonic procedure on the plates. For the unidirectional reinforcement, all four defect types were also detectable using the single-skip approach. For the multi-directional boron

reinforcement, the single-skip ultrasonic technique easily detected the largest slot in the plate specimen but was only just able to resolve the second largest slot, due to the problems of additional wave reflections in the reinforcement.

Independent of reinforcement type, the eddy-current technique was easily able to detect the largest slot but, as in the case of ultrasonics, was only just able to resolve the second largest slot. Thus, in terms of techniques currently applicable to the present F-111 spar station 281.28 wing-skin geometry with a multi-directional reinforcement type, the detectability limits of the eddy-current and single-skip ultrasonic techniques are comparable.

For both the ultrasonic and eddy-current techniques, the application of 2D imaging proved most valuable for defect mapping and would be worth implementing in practice for accurate assessment of crack growth.

In summary, the present study demonstrated the feasibility of detecting partial-thickness back-face cracking and established minimum detectability limits. However, it is noteworthy that such limits are critically dependent on the lay-up of the boron-epoxy reinforcement applied.

23.3.3.2. Crack monitoring under reinforcements to complex-shaped components

While eddy-current testing is used routinely to detect and monitor cracks under repairs, the fact that increasingly complex-shaped components are being considered as candidates for repairs is providing challenges in terms of NDE monitoring. This is particularly the case for repairs to curved surfaces such as recently trialed repairs/reinforcements to several F/A-18 components, including (i) repair/reinforcement of cracked F/A-18 aileron hinges and (ii) reinforcement to the F/A-18 bulkhead crotch region [48,49].

NDE through the reinforcement to crotch region of F/A-18 Y470.5 bulkhead

The crotch region of the Y470.5 bulkhead (made from aluminum alloy 7050 T7451) was identified as a potential site for fatigue cracks early in the life of the F/A-18 aircraft (Figure 23.35). The RAAF requested DSTO to investigate the use of a bonded composite reinforcement that could be applied to this region to extend the life of the bulkhead. This also necessitated NDE research associated with the bulkhead reinforcement. The NDE research was carried out in conjunction with the full-scale testing of an F/A-18 aircraft using test article FT-55 in Canada.

The development of NDE techniques to detect cracks through the boron-epoxy doubler repair to an F/A-18 Y470.5 bulkhead was undertaken using simulated specimens containing EDM slots. The slots were 2 mm long \times 1 mm deep and were inserted in the critical root radius, radius run-out region and flat section on the simulated repair specimen. An initial eddy-current investigation using standard probes showed that a defect could be detected beneath the 1 mm thick repair on a flat region of the specimen but could not be detected beneath the repair in the more critical root radius and radius run-out regions. Further investigations were carried out using a range of relatively large diameter unshielded ferrite-cored probes, similar to those used in the past to inspect the reinforcement on Macchi aircraft wheels. These tests, performed using a commercial unshielded probe and also two

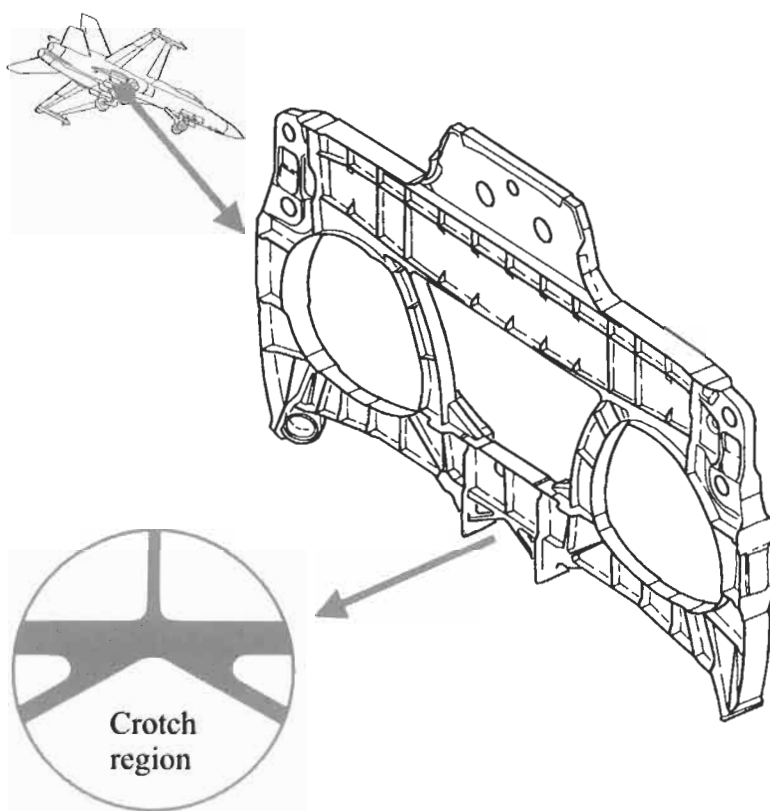


Fig. 23.35. Crotch region of Y470.5 bulkhead of F/A-18 aircraft.

unshielded probes fabricated at DSTO, were also unsuccessful due to the difficulty in identifying the defect signal in the presence of large probe lift-off variations. Recently, a prototype sliding probe was fabricated at DSTO and trialed for this work but also proved unsuccessful.

Ultrasonic techniques are not routinely applied to the detection of cracks in metallic components underneath composite reinforcements because (i) eddy currents are usually readily applied to this problem (as shown earlier in this chapter), and (ii) understanding the generation and detection of waves on the surface of the reinforcement, the propagation of these waves in a three layer system (composite/adhesive/metal), and the interaction/scattering of waves by the crack is a complex process. However, given the problems in applying eddy currents to the F/A-18 Y470.5 bulkhead crotch reinforcement, ultrasonic techniques were trialed.

In a preliminary investigation, various routine ultrasonic techniques proved capable of detecting a defect beneath the B-Ep repair on a flat region of the specimen but did not detect defects beneath the repair in the more critical root

radius and radius run-out regions. A range of more complex ultrasonic procedures were trialed in these curved regions, including single transducer techniques and variants of pitch-catch techniques. The optimum ultrasonic procedure involved the use of two 5 MHz probes which were each mounted in wedges to enable the generation and detection of shear waves in aluminum at 45 degrees. The wedge of the transducer used for generation was machined so that it was no longer flat but curved on its leading edge to conform to surfaces in the F/A-18 radius run-out and root radius regions.

The transducers were scanned in tandem with the first transducer used as generator and the second as detector. The transducers were applied as close together as their geometry allowed (Figure 23.36). The transducers were used in conjunction with a Krautkramer USIP20 pulser/receiver. When the transducer used for generation was applied in the proximity of the crack, a strong signal was reflected back to the detector, following leakage of energy back along the metal/adhesive/composite system.

For an isolated bulkhead, it would clearly be easier to apply ultrasonic procedures from the non-reinforced side of the crotch repair section. However, if this were not possible, the present section shows that an alternative technique exists for inspection from the reinforcement side. The technique would clearly need to be validated on other bulkhead specimens or on related problems where inspection under repairs to curved surfaces was required, such as in the F/A-18 aileron hinge problem below.

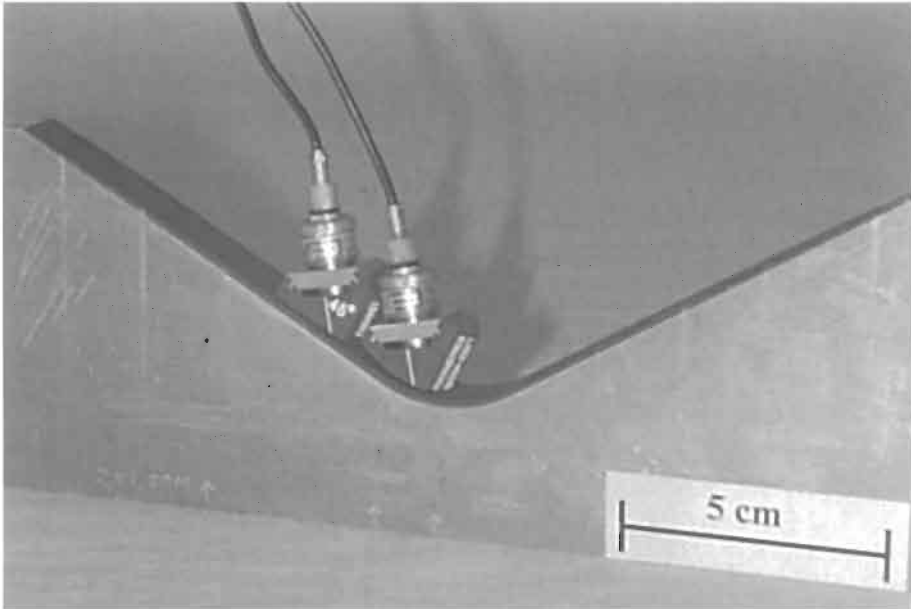


Fig. 23.36. Generator and detector transducer configuration applied to the crotch region of a simulated specimen.

*NDE through the reinforcement to F/A-18 aileron hinges**Ultrasonic procedure*

US Navy and more recently RAAF experienced fatigue cracking in the aft strut fillet of inboard aileron hinges (Figure 23.37). Options considered were either replacement of the hinges or composite reinforcement of uncracked hinges or hinges from which the fatigue cracks have been removed [48]. NDE research formed an integral part of the program to develop a composite reinforcement for the hinges.

The ultrasonic procedure which was successfully applied to the F/A-18 bulkhead problem above was also trialed for detection of cracks under the repair to F/A-18 aileron hinges. However, the scope of the problem was quite complex as modifications to the curvature of the hinge were under review as part of the hinge refurbishment program. As such, the curvature of the wedge used with the ultrasonic probe used for generation was left at that machined for the crotch repair case rather than being optimized for the aileron curvature. Time constraints also meant that no special arrangements could be put in place for transducer scanning on aileron hinges (see below for possible improvements to scanning). The hand-held arrangement used made it difficult to maintain a constant generator-detector separation, variation in which was expected to result in some variations in the time of arrival of signals at the detector.

The manual procedure was applied to three hinge specimens:

- i Specimen no. 1, which contained a crack assessed prior to reinforcement to be at least 2 mm deep.

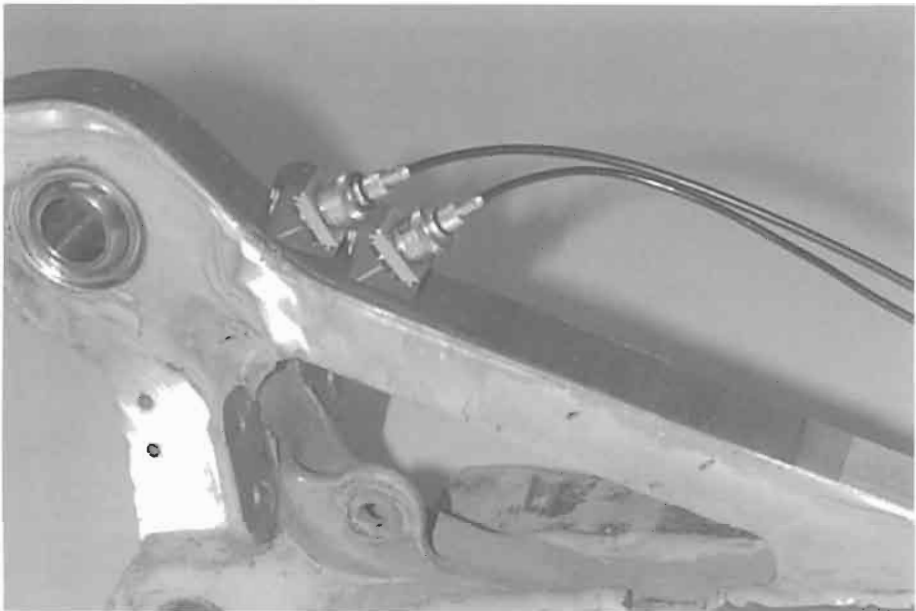


Fig. 23.37. Generator and detector transducer configuration applied to an aileron hinge.

- ii Specimen no. 9, which contained a crack assessed prior to reinforcement to be to be 4 to 4.5 mm long.
- iii Specimen no. 7, which contained three EDM slots. The slots were all 1.5 mm long and 0.5 mm deep and were designated A, B, and C in order of increasing distance from the bearing location. Hence, the slot locations were such that slot A was in a region of greater curvature than slot B followed by slot C [48].

A strong ultrasonic signal from the crack was evident for each of the cracked hinge specimens (denoted 1 and 9) as illustrated in Figure 23.38 for Specimen no. 9. In addition, each of the slots in Specimen no. 7 were also detected (Figure 23.38), indicating that differences in curvature did not affect the effectiveness of the ultrasonic technique. However, small variations in time for which crack/slot signals were observed in the three Specimens was attributed to the impossibility of maintaining a constant generator-detector separation with the curvature on different parts of the specimen (see notes above and suggestions for modifications to procedures given below). There were also significant differences in adhesive thickness in the three specimens tested which caused differences in wave propagation times.

A number of checks were made to ensure that in all the specimens studied, the signals attributed to cracks/slots were indeed due to these defects. In particular:

- i results were checked by scanning the tandem generator-detector combination in two opposite directions, either towards or away from the bearing. In these cases, the signals from the cracks/slots were expected to occur at approximately the same time for each case (as indeed they were) whereas signals from other reflectors due to specimen boundaries would be expected to be different.
- ii where cracks/slots were at the edge of the specimen, the intensity of the signals attributed to cracking decreased as the tandem pair was moved sideways across

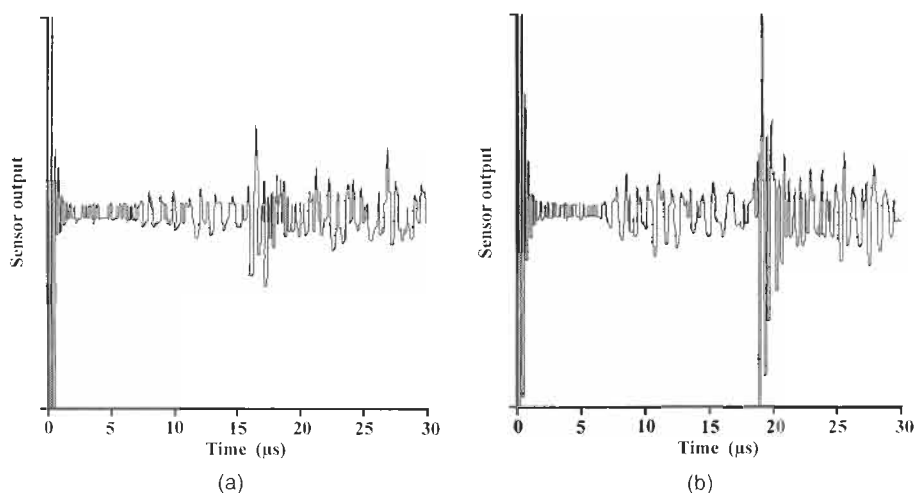


Fig. 23.38. (a) A-scan waveform for Specimen no. 9 with strong signal evident from the crack around 17 μ s; (b) A-scan waveform for Specimen no. 7 with strong signal evident from slot B around 19 μ s.

the specimen. Similarly, for cracks/slots which were known to be in the center of the specimen, the intensity decreased on either side of the center-line.

In summary, the ultrasonic procedure described in the section proved highly successful in detecting cracks/slots in the F/A-18 aileron hinge. For the future, it would clearly be easier to apply ultrasonic procedures from the back face of the strut (for which technique development was also carried out [48]). However, if this were not possible, the present section shows that a viable technique exists for inspection from the reinforcement side.

Eddy-current procedures

In the past, eddy-current inspection has been very successfully applied by DSTO for both detection and monitoring cracks under bonded composite reinforcements, with applications ranging from the repair of Macchi landing wheels to the bonded reinforcement of the F-111 lower wing skins. In fact, one of the criteria for selecting boron-fibre composites for repair and reinforcement applications is that the low electrical conductivity of the material makes it essentially "transparent" to eddy-current inspection. However, despite this previous success, experimental tests at DSTO using eddy-current inspection techniques with a wide variety of probes have so far failed to detect fatigue cracking under the aileron-hinge bonded composite reinforcement [48].

There are three reasons, when combined, which explain why conventional eddy-current techniques have so far failed in this case, while they had succeeded in the past:

- i *The aileron hinge cracks are not through-thickness cracks:* The signals arising from the typically 3–4 mm long surface breaking cracks in the aileron are small compared with the signals arising from the through-thickness cracks encountered in many of the previous reinforcement applications.
- ii *The reinforcement is relatively thick:* The geometrical attenuation of the eddy-current signal increases exponentially as the separation between the probe and the metal surface increases. The aileron reinforcement is significantly thicker (nominally 1.5–2.0 mm thick) than, for example, the 0.5 mm thick reinforcements used for the Macchi wheels where the cracking was also not through-thickness. The nature of the curved surface at the cracking location is also likely to result in thicker adhesive bondlines than would be the case for a flat doubler, and any such increase will further attenuate the signal.
- iii *The cracking occurs in a curved region of the surface:* The curvature of the surface, together with variations in the bondline thickness, produces variations in probe lift-off and probe-tilt resulting in unwanted background signals which cannot be wholly eliminated by phase plane analysis.

The combined effect of the relatively small defect signal and reinforcement thickness is illustrated in Figure 23.39 where the eddy-current signal due to the 3 mm fatigue crack in an un-reinforced aileron hinge (Specimen no. 3) is plotted as a function of probe lift-off from the metal surface, or equivalently, as a function of the thickness of the reinforcement. (As the reinforcement is a poor electrical conductor, varying the probe lift-off from the metal surface is equivalent to varying

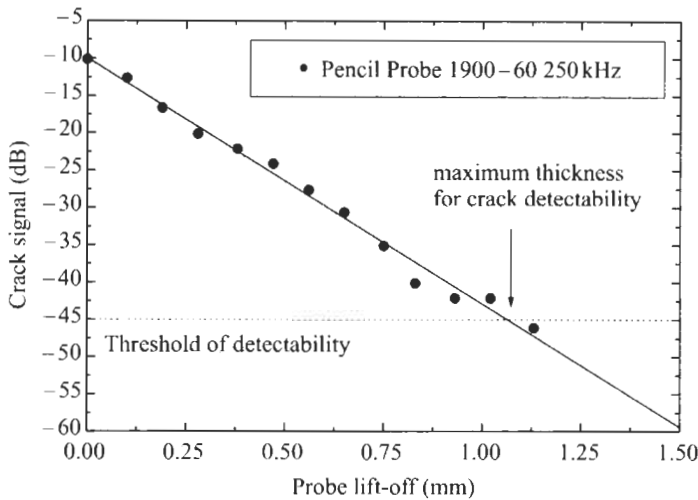


Fig. 23.39. Eddy current signal due to 3 mm long fatigue crack in an aileron hinge (Specimen no. 3) as a function of probe lift-off from the metal surface. [49]

the thickness of the reinforcement with the probe on the upper surface of the composite.) The probe was a shielded 90° pencil probe (Zetec 1900-60) and the crack signal is defined as the maximum excursion in the impedance plane perpendicular to the lift-off locus. The plot shows that this particular crack would be detectable if the thickness of the reinforcement was less than or approximately equal to 1.0 mm.

The effect of reinforcement thickness on crack detectability was investigated in more detail using a model system consisting of a 2024-T3 Al alloy plate containing a 5 mm long \times 1.2 mm deep EDM slot. Four probes were used: three were conventional ferrite-cored probes with varying diameter, and one was a DSTO eddy-current “sliding probe”. The sliding probe was a driver-pickup type probe where the driver and pickup coils are arranged side-by-side. The DSTO prototype sliding probe consisted of two 4 mm ferrite-cored probes with a center-center spacing of 7.5 mm. As shown in Figure 23.40, the signal due to the crack decreases rapidly with probe lift-off for the three conventional probes, the rate of decay increasing with decreasing probe radius. In contrast, the signal detected by the sliding probe decreases only slowly with lift-off, albeit with a smaller initial signal than for the conventional probes. The relative insensitivity to lift-off, and hence reinforcement thickness, suggests that the sliding probe concept may be a potential solution to the problem of eddy-current detection of cracking under the hinge reinforcement. Work is currently in progress to design, manufacture and test the performance of a range of eddy-current sliding probes.

In summary, the ultrasonic technique developed at DSTO is capable of detecting aileron hinge cracks through the composite reinforcement and with further work this could be developed into a procedure capable of being routinely applied in the

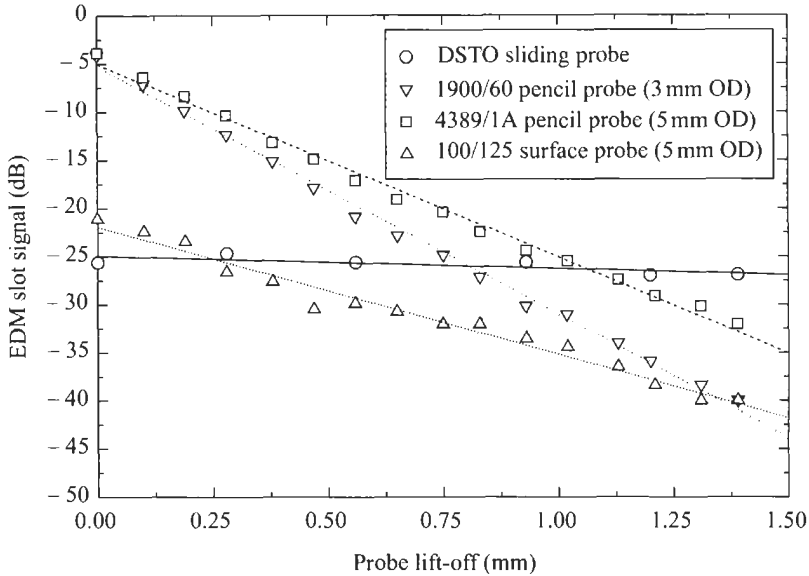


Fig. 23.40. Eddy current signal due to a 5 mm \times 1.2 mm EDM slot in 2024-T3 aluminum alloy as a function of probe lift-off for a range of eddy current probes. The signal from the sliding probe is insensitive to lift-off and hence reinforcement thickness. [49]

field. Eddy-current techniques are currently unable to detect cracking through the doubler due to the small size of the cracks, the thickness of the reinforcement, and the curvature in the region. Further eddy-current development would be valuable, given the increasing acceptance of eddy-current testing as a routinely applied crack monitoring technique in other reinforcement applications. The solution in terms of eddy-current development may even be in terms of the smart patch concept described in Chapter 20.

23.4. Quality control issues in service

23.4.1. Quality assurance

An overall approach to managing the implementation of composite doubler technology is proposed in reference [50]. Reference [50] suggests the use of an Engineering Standard to guide all design, analysis, and QA issues. A series of QA procedures were included in the FAA/AANC project's composite doubler installation process [51] to assure: (1) sufficient strength in the adhesive layer, (2) sufficient strength in the boron-epoxy laminate, (3) proper surface preparation to allow the best opportunity for complete adherence of the doubler, and (4) the

detection of any flaws in the composite doubler. DSTO has also implemented similar procedures.

The first four QA procedures for the FAA/AANC given below involve test specimens which are generated at the same time the doubler is installed. All test specimens are produced using the same temperature and pressure profile as the aircraft doubler cure. The final AANC QA procedure is nondestructive inspection which is used for the initial acceptance of a composite doubler installation and for continued surveillance over the life of the doubler.

The QA procedures were:

- i *Wedge test* – Two aluminum strips bonded to the parent structure immediately adjacent to the doubler are prized off with a phenolic wedge. The test indicates whether adhesive fracture (cohesive failure) rather than disbonding (adhesive failure) occurs, and thus whether the surface preparation is good and the full adhesive strength has been achieved.
- ii *Lap shear test* – Bonded lap joint specimens are pulled to failure to determine the ultimate strength of the adhesive layer. Six specimens tested for the L-1011 door corner doubler exceeded the minimum strength requirement of 3000 psi (20.68 MPa) [14].
- iii *Short beam shear test* – Coupons are tested for laminate shear strength. Three L-1011 boron-epoxy doubler coupons were tested. The average shear strength value, 10.7 ksi (73.8 MPa), was within the specified range [14].
- iv *Four point bend test* – Coupons are tested for ultimate tensile strength. Three L-1011 boron-epoxy doubler coupons were tested. The average tensile strength, 212 ksi (1.46 GPa), exceeded the minimum strength requirement [14].
- v *Nondestructive inspection* – The tests outlined above determine the strength properties of the installation. However, it is still necessary to detect any flaws in the installation. Initially, the status of flaws in the doubler and bondline must be ascertained to accept the installation. Thereafter, the flaw status of the doubler, bondline, and parent material must be periodically measured. Nondestructive inspection provides the last line of defense in this regard. NDI is the only means for determining if the structural integrity of the repair area changes over time.

23.4.2. Use of realistic calibration standards

A critical element in the application of any piece of NDT equipment is the use of realistic calibration standards. The standards must have representative flaws which are engineered in a reliable manner and possess the appropriate structural configuration (e.g. doubler thickness and lay-up, skin thickness). Furthermore, all flaw detection challenges, with the exception of full scale accessibility and deployment issues, should be included in the calibration standard. Once the inspection equipment is set-up using feedback from the calibration standards, aircraft inspections can proceed with the knowledge that acceptable probability-of-detection numbers can be achieved. In the case of bonded composite doublers, the calibration or reference standards must include disbonds and delaminations in the

doubler and cracks in the parent aluminum material. Disbond and delamination inspections can be accommodated with a single standard while another standard is used to support crack inspections.

23.4.2.1. Calibration standards for disbond and delamination inspections

A representative calibration standard containing artificial flaws of known size and depth should be used to ensure a repeatable inspection. The flaws must be engineered in the standards in a well-controlled manner and they must adequately represent the size, depth, and signal variation effects of actual disbond and delamination flaws. Amplifier gains and UT signal gates should be established during scans of the calibration standard. Depending on the physical size of the composite doubler and the degree of thickness variation, the inspector can determine the number of scans (unique set-ups) necessary to completely cover the doubler. Material properties and the doubler thickness will determine the frequency of the transducer needed to resolve the composite front and back surfaces and whether the doubler is scanned with a contact or water column configuration.

The initial reference standard developed by the FAA/AANC for 13-ply fatigue coupon inspections did not possess a taper in the laminate. The inspection null point was created using an unflawed 13-ply thick area. In the case of the Bondmaster (resonance mode) inspection device this moved the dot to the center of the screen. The transducer was then placed on a 13-ply area with an engineered disbond. The instrument gain and rotation were used to position the dot three divisions away from the center of the screen and on the axis. When the tapered sections of the fatigue samples were inspected – especially areas with only a few plies – low signal indications were found. The low signal levels provided a less than desirable detection reliability. To obtain better inspection results on the taper sections of the test specimens a new inspection standard was designed. Figure 23.41 shows this reference standard which can be used to support UT inspections in composite doublers up to 15 plies thick. This reference standard contains disbonds between the composite doubler and aluminum skin, delaminations between adjacent composite lamina, and nulling areas in both the full thickness and tapered/thin regions.

System set-up and use of calibration blocks

Special precautions must be taken in order to produce a good inspection in areas where the doubler thickness changes (taper regions). Thickness variations require the user to track the front surface of the doubler and set the depth gates as appropriate. By employing a series of gates in one scan, it is possible to collect data over a wide range of depths. However, in the case of extremely thick doublers (the L-1011 doubler was 72 plies thick) it may be necessary to use several different scans each containing their own unique set of gates. For example, on the L-1011 doubler, separate scans may be obtained for 30-ply, 50-ply, and 72-ply thicknesses. This process improves the resolution in the area of interest and avoids the acquisition of potentially misleading signals.

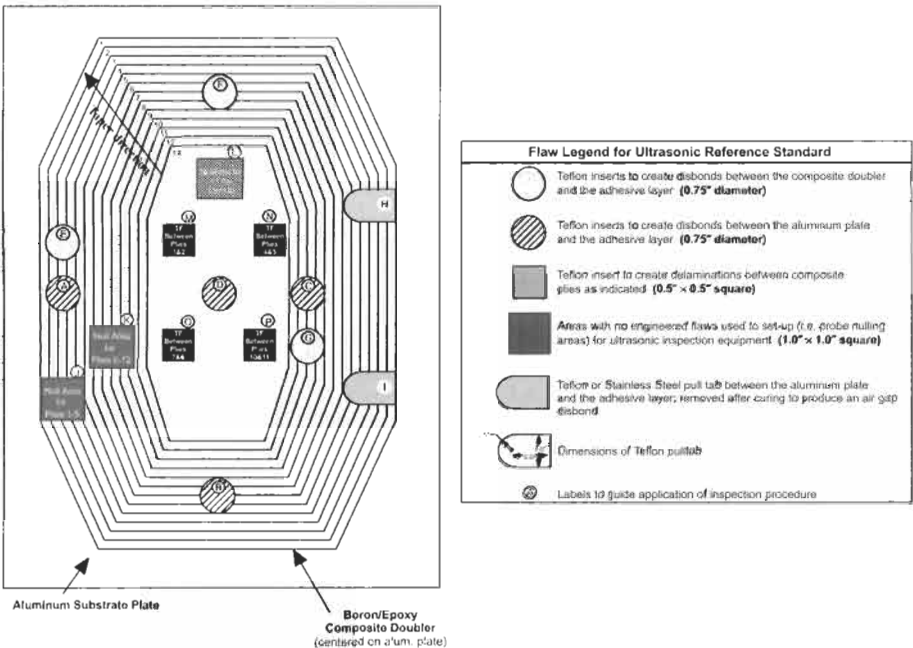


Fig. 23.41. Configuration of composite doubler reference standard to support disbond and delamination inspections.

The L-1011 investigation determined that it is helpful to employ multiple calibration sites when inspecting composite doublers with thickness variations in excess of 10–12 plies. Specifically, it was found that a new set-up null point should be established after every 10–12 ply drop off in the tapered region (or change in thickness of 10 plies). In the case of the 13-ply fatigue coupons, a second calibration site for disbands and delaminations is required. The reference standard shown in Figure 23.41 makes this provision by including disbands, delaminations, and null areas in each of the important laminate thickness regions. This eliminates sporadic low signal flaw indications and improves flaw detection reliability.

Fabrication of disbands and delaminations

There are several methods which can be used to produce controlled flaws in test specimens. The basic specimen flaws consist of disbands between the laminate and the substructure (aluminum skin) and interply delaminations between adjacent composite plies. To create a disbond at an adhesive/substrate interface or an interply delamination, a contamination site that interferes with the wetting action of the adhesive is required. The most successful techniques are: (1) inserting a teflon or stainless steel pull tab on the bondline surface or between plies, (2) cutting a hole in the adhesive and adding a teflon insert or other “pillow” insert which can

interrupt an interrogating NDT signal, and (3) coating the disbond area with a mold release (chemical agent which resists adhesion, e.g. silicone, teflon).

Using assorted nondestructive inspection techniques, the AANC evaluated the flaw realism for each of the following experimental approaches:

- i *Pull tab* – These inserts, which are removed after the adhesive curing process, produce a true “air gap” disbond or delamination in a specimen. A piece of stainless steel shim stock, 0.003” to 0.004” (0.08 mm to 0.10 mm) thick, is placed between adjacent composite plies or between the base of a laminate and the mating aluminum structure. The stainless steel shims are treated with a chemical release agent to prevent any permanent bond to the adhesive. Prior to their use, the coated pull tabs are baked at a temperature greater than the doubler cure temperature. This assures the performance of the release agent during the doubler installation.
- ii *Pillow insert* – Special inserts are placed in the laminates during the lay-up operation to produce interply delaminations. The inserts will interrupt an inspection signal and simulate an air gap between adjacent plies. Teflon, or a stacked assembly of sheet materials (“pillow”), can be used as inserts. Pillow inserts are composed of Kapton tape surrounding three layers of tissue paper. This pillow insert assembly can be fabricated with a total thickness of 0.008”–0.009” (0.20 mm–0.23 mm). This helps to minimize the amount of local deformation of the doubler in the area of the inserts. Teflon or pillow inserts can be fabricated with unusual or “random” shapes in order to model real life flaws.
- iii *Pin hole* – This flaw engineering method allows for the production of random shaped (and less controllable) disbonds between a boron-epoxy doubler and its parent aluminum structure [52]. In this process, small “pin holes” are drilled through the parent metallic material. This causes a vacuum leak path and results in adhesive being pulled away from the hole area during the cure process. The resulting disbonds have irregular shapes with small tentacles. This approach produces more realistic disbond flaws, however, the flaw shape is uncontrolled and the reliability is uncertain.

23.4.2.2. Calibration standards for crack detection in parent material

Since these inspections pertain to the original aircraft structure, it is often possible to utilize existing crack reference standards as called out in the aircraft manufacturer’s NDT manuals. Most commonly, the crack reference standards take the form of single or riveted plate assemblies with EDM notches. The notches are used to simulate cracks emanating from holes (rivet sites). In the FAA/AANC testing, conventional crack standards were used to set-up the NDT equipment. As in normal deployment of eddy-current equipment, the standards must match the structure of interest with regards to material type, material thickness, rivet type and/or hole size, crack depth (surface or subsurface), and crack length. To complete the standard for use with bonded doublers, a composite doubler laminate (cured without adherence to a parent metallic structure) is placed over the crack standard to simulate the aircraft doubler. The laminate should match the key

characteristics of the aircraft composite doubler. The most critical characteristics to match are: (1) doubler thickness/number of plies, and (2) the presence of wire mesh lightning protection plies. Fibreglass environmental protection plies are less essential except for the additional lift-off effects they produce, which may be only 0.004"–0.008" (0.10 mm–0.20 mm). Ply orientation does not appear to have a significant effect on eddy-current inspections so an exact match of the doubler lay-up is not necessary in this case. Finally, it is essential that the doubler laminate conform properly to the crack standard. This will eliminate unintentional, and unrealistic, probe lift-off which will change the resolution of the inspection.

Thus, it is possible to simply superimpose a composite laminate over existing crack reference standards as called out in the manufacturer's NDT manuals. By adjusting the laminate overlay to match the repair of interest, it is possible to use the same crack standards to support many different repair inspections. Figure 23.42 shows a sample eddy-current reference standard for use with bonded composite doublers. It has a number of similarities with the conventional eddy-current standards which are called out in the Boeing NDT Manuals. The standard in Figure 23.42 contains an array of rivet sizes with cracks of different lengths and orientations emanating from the fasteners. It includes riveted joints in case there are any effects of second layer skin on the detection of cracks in the surface skin. It also includes skin cracks which are not associated with fastener holes. This area can be used to set up equipment for inspections through composite doublers which are repairing skin dents or corrosion grind-outs.

23.5. Conclusions

The unavoidable by-product of aircraft use is that crack and corrosion flaws develop throughout the aircraft's skin and substructure elements. Economic barriers to the purchase of new aircraft have created an aging aircraft fleet and placed even greater demands on efficient and safe repair methods. The composite doubler reinforcement/repair technology provides a safe and cost-effective solution to aircraft repair challenges. The engineering advantages associated with composite doubler use should accelerate their use in civil and defence aviation repairs. Periodic field inspections of the composite is essential to assuring the successful operation of the doubler over time. Primary among inspection requirements for these doublers is the identification of disbonds, between the composite laminate and aluminum parent material, and delaminations in the composite laminate. Surveillance of cracks in the parent aluminum material beneath the doubler is also a major concern.

By combining the ultimate strength, disbond growth, and the crack mitigation results obtained in the FAA/AANC program, it was possible to truly assess the capabilities and damage tolerance of bonded boron-epoxy composite doublers. In this test series, relatively severe installation flaws were engineered into the test specimens in order to evaluate boron-epoxy doubler performance under worst case, off-design conditions. The engineered flaws were at least two times larger than

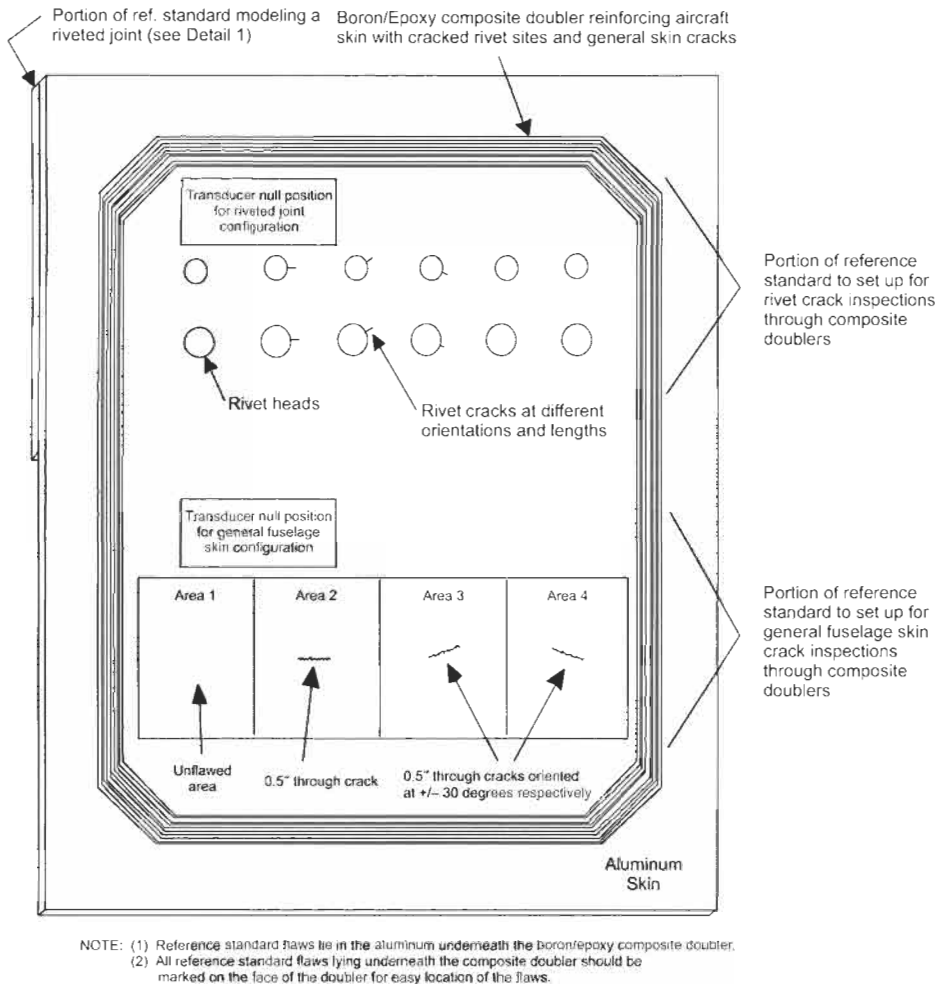


Fig. 23.42. Eddy current reference standard used to support inspections for cracks in aluminum beneath composite doublers.

those which can be detected by NDI. It was demonstrated that even in the presence of extensive damage in the original structure (cracks, material loss) and in spite of non-optimum installations (adhesive disbonds), the composite doubler allowed the structure to survive more than four design lifetimes of fatigue loading. Furthermore, the added impediments of impact – severe enough to deform the parent aluminum skin – and hot-wet exposure did not affect the doubler's performance. Since the tests were conducted using extreme combinations of flaw scenarios (sizes and collocation) and excessive fatigue load spectrums, the performance parameters were arrived at in a conservative manner. This damage tolerance assessment indicates that the current composite doubler inspection

requirements are very conservative. Even in view of these encouraging doubler performance results, the cautious NDI approach is necessary in order to accumulate data on the operation of bonded doublers in actual flight environments. A strong history of success may allow the inspection intervals on these repairs to be lengthened or eliminated.

Several ultrasonic methods have been successfully applied to the problem of disbond and delamination detection. Through-Transmission ultrasonics is a highly sensitive technique but deployment issues severely restrict its field application. The ultrasonic resonance test method works well in mapping out flaw shapes and delineating the flaw edges. Inspection results depend upon effective acoustic impedance match between the aluminum and the composite doubler. In thinner laminates, resonance testing is able to repetitively detect disbond flaws as small as 0.25" (6.4 mm) in diameter. Furthermore, the bond-tester technique is also able to map out a changing flaw profile – a cohesive failure in the adhesive caused by the crack propagating through the aluminum – during fatigue testing of the composite doubler. Material nonuniformities inherent in composite laminates produce inconsistent signals when resonance ultrasonics is applied to laminates greater than 0.115" (2.92 mm) thick (20 plies). In this region, it is difficult to interpret the equipment's readings.

Pulse-Echo ultrasonics can be easily implemented on an aircraft using hand-held inspection devices. Anomalies in A-scan signals can be used to detect laminate flaws although signal fluctuations, caused by material nonuniformities, can create interpretation difficulties. The optimum method to achieve both field deployment and ease of signal interpretation involves the use of Pulse-Echo C-scan ultrasonics. C-scan views are area maps of the inspection surface. They provide the inspector with easier-to-use and more reliable data with which to recognize flaw patterns. Specific emphasis can be placed on the UT signal, highlighted in the color-mapped C-scan, based on user specified amplitude gates, time-of-flight values and signal waveforms.

Extensive testing has shown that the 2D, color coded images produced by manual and automated ultrasonic scanners are able to reliably detect disbond and delamination flaws of the order of 0.50" (12.7 mm) in diameter. Time savings, human factors issues, and repeatability are some of the main advantages associated with C-scan ultrasonics. Key to implementing this NDI technique is the use of representative calibration standards which allow for accurate equipment settings (amplifier gains and signal gates) over the full range of laminate thickness.

During the course of the FAA/AANC composite doubler development effort, thermography was applied to multiple doubler installations. Successful results demonstrated the viability of thermography for inspecting bonded composite doublers. Flaws smaller than 0.5" (12.7 mm) in diameter could be detected using thermography and their depth could be accurately determined. Furthermore, while ultrasonics has difficulty resolving flaws in the thin (one to three ply) doubler region around the tapered perimeter, studies at both DSTO and the FAA/AANC show that thermography does not appear to have difficulty with this configuration. More comprehensive and structured tests are underway to better determine the sensitivity

and resolution of thermography in detecting composite doubler disbonds, delaminations, and porosity.

Crack detection in the parent aluminum material can be accomplished using conventional eddy-current and X-radiographic techniques. The success of the eddy-current technique is primarily determined by two installation factors: (1) lift-off effects due to the thickness of the composite doubler, and (2) signal disruption from other conductive medium such as copper mesh lightning protection.

Testing conducted by the AANC on composite doubler specimens with cracks in the parent aluminum skin established the following general limits of crack detectability through composite doublers: (1) a 0.060" (1.52 mm) long first layer (surface) crack can be detected in the aluminum through a 0.310" (7.87 mm) thick doubler, (2) a 0.15" (3.8 mm) length surface crack can be detected through a 0.5" (12.7 mm) thick laminate, and (3) a 0.15" (3.8 mm) long subsurface (2nd layer) crack can be detected through a 0.310" (7.87 mm) thick doubler and a 0.040" (1.0 mm) thick aluminum surface plate. A blind, probability of crack detection study was performed using a statistically valid set of fatigue crack panels and composite doublers of various thicknesses. It was found that even through doublers as thick as 35 plies, i.e. 0.199" (5.05 mm) thick, the probability of finding surface cracks of 0.2" (5.1 mm) in length exceeds 95%. The results were achieved with a false call rate of less than 1%. These results are quite good in light of the damage tolerance requirement to find fatigue cracks beneath doublers before they reach 1" (25 mm) in length.

The FAA/AANC completed a study to: (1) demonstrate that composite doublers do not interfere with the ability to perform X-radiographics inspections for cracks in aluminum, and (2) identify proper exposure time and power settings to optimize the sensitivity of X-radiographic technique when inspecting through extremely thick doublers (72 ply). Radiography was demonstrated to be a very effective inspection method to interrogate the interior of the parent material covered by the composite doubler. X-radiographic inspections are as effective as before the doubler was installed. The boron-epoxy material does not impede the X-radiographic inspections. Power and exposure times can be adjusted to accommodate the presence of the doubler and achieve the required film density and resolution. Again, the required damage detection threshold for cracks under the doubler is 1.0" (25 mm). X-radiographs showed the ability to detect fatigue cracks on the order of 0.38" (9.7 mm) in length beneath 0.40" (10.2 mm) thick (72 ply) boron-epoxy doublers.

Clearly, a series of conventional and advanced NDI techniques now exist for the routine application of composite doubler technology. The techniques include those developed by the FAA/AANC as outlined above and also by DSTO in wide-ranging applications, including:

- i PE ultrasonics which has been successfully applied for the detection of delaminations and disbonds in large doubler repairs;
- ii leaky interface waves which have shown some promise for good bond/weak bond discrimination and for determining the long-term durability of bonds to degradation;

- iii acoustic emission monitoring which has been applied for disbond detection during the validation of boron-epoxy doubler repairs to the complex wing pivot fitting region of F-111 aircraft;
- iv thermoelastic techniques such as SPATE and FAST for qualitative indications of defects; and
- v novel ultrasonic and eddy-current solutions for crack inspections for challenging problems such as partial back-face cracks (F-111 lower wing skin) and cracks in complex-shaped components (crotch region of F/A-18 bulkhead and aft strut fillet of F/A-18 inboard aileron hinge).

While there have been many successes in the past, DSTO, as originator of the boron-epoxy reinforcement/repair technology, continues to “push the boundaries” of the technology. This includes “pushing the boundaries” in terms of requirements for development of new NDE capabilities. Thus, DSTO is particularly interested in the further development of improved NDE for crack detection and sizing under reinforcements to curved surfaces, such as discussed in Section 23.3 of this chapter. Future applications could even include crack detection under complex 3D reinforcements which are being trialed in a joint Canadian/Australian fatigue test on the F/A-18 aircraft.

For the future, DSTO is also interested in any new developments related to the bond durability problem. Although some progress has been made in this area as outlined in Section 23.2 of this chapter, there is no readily applicable NDI technique to distinguish a good bond from a weak bond between overlay and substrate or the long-term durability of the bond to environmental degradation. This significant problem is limiting the wider application of the repair technology to primary structures. The current perspective is that techniques for NDE to determine bond durability are unlikely to be successful in the short-to-medium term, especially given difficulties in solving the simpler metal-metal bond durability problem. For this latter problem, a range of innovative techniques are being investigated world-wide, including the feasibility of using non-linear ultrasonic techniques. However, for the boron reinforcement technology, smart patches such as addressed in Chapter 20 may well be the best approach to this bond durability problem for the foreseeable future.

23.6. Acknowledgements

The authors wish to sincerely thank Mr David Hatt who contributed significantly to the preparation of this chapter. They also acknowledge the invaluable contribution of Mr Phil Walkington to the FAA/AANC NDI development described in this chapter as well as to the reporting of these activities. The authors also gratefully acknowledge the substantial scientific contributions of Drs Steve Burke, Geoffrey Hugo and Robert Ditchburn, and Ms Susan Bowles to the DSTO research outlined in this chapter.

References

1. Roach, D.P. (1995). Performance analysis of bonded composite doublers on aircraft structures. In: *Int. Symp. on Composite Repair of Aircraft Structures in concert with ICCM-10*, August.
2. Belason, E.B., Rutherford, P., Miller, M., et al. (1994). Evaluation of bonded boron/epoxy doublers for commercial aircraft aluminum structures. In: *FAA/NASA Int. Symp. on Aircraft Structural Integrity*, May.
3. Baker, A.A. (1997). Fatigue studies related to certification of composite crack patching for primary metallic aircraft structure. In: *FAA-NASA Symp. on Continued Airworthiness of Aircraft Structures*, Dept. of Transportation Report No. DOT/FAA/AR-97-2, I, July.
4. Fredell, R.S., van Barnveld, W. and Vlot, A. (1994). Analysis of composite crack patching of fuselage structures: high patch modulus isn't the whole story. In: *SAMPE Int. Symposium 39*, April.
5. Rose, L.R. (1987). Influence of disbonding on the efficiency of crack patching. *Theoretical Applied Fracture Mechanics*, 7.
6. Fredell, R.S. (1994). Damage Tolerant Repair Techniques for Pressurized Aircraft Fuselages [Ph.D. dissertation]. Delft University.
7. Rice, R., Francini, R., Rahman, S., et al. (1993). Effects of Repair on Structural Integrity. Dept. of Transportation Report No. DOT/FAA/CT-93/79, December.
8. Roach, D.P. and Graf, D. (1998). Damage Tolerance Assessment of Bonded Composite Doublers for Commercial Aircraft Applications. Sandia National Laboratories/Dept. of Energy Report No. SAND98-1016, June.
9. Jones, K.M. and Shah, S. (1996) Composite Repair – Upper Forward Corner of P-3 Door – Model L-1011 Aircraft, Strength and Damage Tolerance Analysis. Report No. LG95ER0157, Part of Documentation Package for FAA Atlanta Aircraft Certification Office Project No. SP1798AT-Q, analysis plan December, (1995), final report October.
10. Gieske, J.H. (1994). Evaluation of Scanners for C-Scan Imaging in Nondestructive Inspection of Aircraft. Dept. of Energy Sandia Report, SAND94-0945, April.
11. Barnard, D.J. and Hsu, D.K. (1996). NDI of aircraft fuselage structures using dripless bubbler ultrasonic scanner. In: *SPIE Nondestructive Evaluation Techniques for Aging Infrastructure and Manufacturing Conf.*, 2945.
12. Gieske, J.H., Roach, D.P. and Walkington, P.D. (1998). Ultrasonic inspection technique for composite doubler/aluminum skin bond integrity for aircraft. In: *SPIE Nondestructive Evaluation Techniques for Aging Infrastructure and Manufacturing Conf.*, 3258, April.
13. Walkington, P. and Roach, D. (1997). Ultrasonic Inspection Procedure for Bonded Boron-Epoxy Composite Doublers. Sandia Labs AANC Specification AANC-PEUT-Comp-5521/4-004, Sandia National Laboratories, Albuquerque, NM; also included in FAA Document SNL96ER0007 under Atlanta ACO Project SP1798AR-Q, FAA approval January.
14. Roach, D. and Walkington, P. (1998). Development and Validation of Nondestructive Inspection Techniques for Composite Doubler Repairs on Commercial Aircraft. Sandia National Laboratories/Dept. of Energy Report No. SAND98-1014, May.
15. Scala, C.M., Burke, S.K., Pearce, P.J., et al. (1997). NDE for composite reinforcement/repair of ship superstructure. *Nondestructive Testing-Australia* 35, p. 67–71.
16. Rose, J.L., Rajana, K.M. and Pelts, S. (1995). Guided waves for metal to composite adhesion bond inspection. In: *Proc. of the 18th Annual Meeting of the Adhesion Society*; February 19–22, p. 340–342.
17. Rose, J.L., Rajana, K.M. and Barshinger, J.N. (1996). Guided Waves for Composite Patch Repair of Aging Aircraft. In: (D.O. Thompson and D.E. Chimenti eds.). *Review of Progress in QNDE*, 15, p. 1291–1298.
18. Rose, J.L., Pilarski, A. and Rajana, K.M. (1995). Ultrasonic Guided Waves for Lap Splice Joint Inspection in Aging Aircraft. In: (D.O. Thompson and D.E. Chimenti eds.). *Review of Progress in QNDE*, 14, p. 1417–1424.
19. Doyle, P.A. and Scala, C.M. (1991). Ultrasonic Measurements of Elastic Constants for Composite Overlays. In: (D.O. Thompson and D.E. Chimenti eds.). *Review of Progress in QNDE*, 10B, p. 1453–1459.

20. Scala, C.M. and Doyle, P.A. (1992). Elastic Constants for Unidirectional Boron-Epoxy Composites. In: (D.O. Thompson and D.E. Chimenti eds.). *Review of Progress in QNDE*, **11**, p. 585–592.
21. Doyle, P.A. and Scala, C.M. (1993). Toward laser-ultrasonic characterization of an orthotropic-isotropic interface. *J. Acoust. Soc. Am.*, **93**(3), p. 1385–1392.
22. Scala, C.M. and Doyle, P.A. (1995). Ultrasonic leaky interface waves for composite-metal adhesive bond characterization. *J. Nondestructive Eval.*, **14**(2), p. 49–59.
23. Hockings, C. and Robertson, C. (1994). Evaluation of simple test methods for inspection of boron epoxy repair patches to aircraft outer surfaces. *Nondestructive Testing-Australia* **31**(6), p. 153–158.
24. Addison, R.C., Yang, Q.D. and Rugg, K.L. (2001). NDE of composite bonded doublers. In: *33rd Int. SAMPE Technical Conf. "Advancing Affordable Materials Technology"*, November.
25. Krautkramer, J. and Krautkramer, H. (1983). *Ultrasonic Testing of Materials*. 3rd edn. New York: Springer-Verlag; p. 174–179.
26. Moore, D., Roach, D., Swanson, M., *et al.* (1996). Nondestructive inspection of adhesive bonds in composite and metallic materials. In: *41st Int. SAMPE Symp.*, March.
27. Favro, L.D., Ahmed, T., Han, X., *et al.* (1995). Thermal Wave Imaging of Aircraft Structures. In: (D.O. Thompson and D.E. Chimenti eds.). *Review of Progress in QNDE* **14A**, p. 461–466.
28. Syed, H., Winfree, W., and Cramer, K. (1992). Processing Infrared Images of Aircraft Lap Joints. In: *Thermosense XIV, SPIE* **1682**.
29. Large Area Nondestructive Inspection Scanner. Southwest Research Institute Project 17–3205, U.S. Air Force contract #F4606–89-D-0039-SA-01, October, 1991.
30. Bishop, C. (1995). Composite structure repair evaluation using pulsed infrared imaging. In: *Nondestructive Evaluation Techniques for Aging Infrastructure and Manufacturing Conf.*, **2455**.
31. Spicer, J., Kearns, W., Aamodt, L., *et al.* (1993). Characterization of Hidden Airframe Corrosion by Time-Resolved Infrared Radiometry (TRIR). In: *Review of Progress in QNDE*, **12**.
32. Valley, M., Roach, D., Dorrell, L., *et al.* (1998). Evaluation of commercial thermography systems for quantitative composite inspection applications. In: *2nd Joint NASA/FAA/DoD Conf. On Aging Aircraft*, September.
33. Beattie, A., Dahlke, L., Gieske, J., *et al.* (1994). Emerging Nondestructive Inspection Methods for Aging Aircraft. SAND92–2732 Sandia National Laboratories, Chapter 1, p. 1.1–1.16.
34. Scala, C.M., Bowles, S.J. and Scott, I.G. (1989). The development of acoustic emission for structural integrity monitoring of aircraft. In: (W.J. McGonnagle, ed.) *Int. Advances in Nondestructive Testing*, **14**. New York: Gordon and Breach, p. 219–257.
35. Scala, C.M., McCardle, J.F. and Bowles, S.J. (1991/92). Acoustic emission monitoring of a fatigue test of an F/A-18 bulkhead. *J. Acoustic Emission*, **10**(3–4), p. 49–60.
36. Scala, C.M., Bowles, S.J., McCardle, J.F., *et al.* (1990). AE Monitoring of Military Aircraft. *Non-Destructive Testing-Australia*, **27**(1), p. 4–8.
37. Heslehurst, R.B., Baird, J.P., Williamson, H.M., *et al.* (1993). Portable Holographic Interferometry Testing System: Application to Crack Patching Quality Control. In: (T. Chandra, A.K. Dhingra, eds.). *Advanced Composites 93, Int. Conf. on Advanced Composite Materials: The Minerals, Metals, and Materials Society*, p. 687–692.
38. Molent, L., Enke, N., Wallace, G., *et al.* (1994). Thermomechanical Analysis of Bonded Repaired Skin Splice Joint Test Specimens. ARL-TR-24, Aeronautical and Maritime Research Laboratory, Australia.
39. Ryall, T.G. and Wong, A.K. (1994). The use of thermal imaging for stress analysis and failure detection. In: *Proc. IMMA Conf., Failure Analysis in Materials Engineering*. IEAust, Melbourne, Australia, March.
40. Mirabella, L., Galea, S. and Sanderson, S. (1999). Validation of a Bonded Repair to an F-111C Wing-Coupon Testing Program (Phase 1). DSTO report in preparation, Aeronautical and Maritime Research Laboratory, Australia.
41. Volume 17 Nondestructive Evaluation and Quality Control. In: *Metals Handbook* 9th edn., *ASM Int.*, 1989, p. 241–246.
42. Ansley, G., *et al.* (1992). Current Nondestructive Inspection Methods for Aging Aircraft. U.S. Dept. of Transportation, FAA Report No. DOT/FAA/CT-91/5, June.

43. Spencer, F., Borgonovi, G., Roach, D., *et al.* (1993). Reliability Assessment at Airline Inspection Facilities, Volume II: Protocol for an Eddy Current Inspection Reliability Experiment. Dept. of Transportation Report, DOT/FAA/CT-92/12-II, May.
44. L-1011 Nondestructive Testing Manual, Section 53-15-80, X-ray Inspection of Passenger, Galley, and Cargo Door Frame Corners. Lockheed California Co., Burbank, CA., Nov., 1979.
45. Roach, D.P., Moore, D. and Walkington, P. (1996). Nondestructive inspection of bonded composite doublers for aircraft. In: *Proc. of SPIE Conf. on Nondestructive Evaluation of Aging Aircraft*, December.
46. Boykett, R. and Walker, K. (1996). F-111C Lower Wing Skin Bonded Composite Repair Substantiation Testing. DSTO-TR-0480, Aeronautical and Maritime Research Laboratory, Australia.
47. Ryan, M. (1996). NDT Inspection Report No. 691/102 [unpublished], Aeronautical and Maritime Research Laboratory, Australia.
48. Virtue, P., Morton, H., Ward, D., *et al.* (1999). Life Extension of F/A-18 inboard aileron hinges by shape optimization and composite reinforcement. In: (R. Chester, ed.) DSTO-TR-0699, Aeronautical and Maritime Research Laboratory, Australia.
49. Scala, C.M. and Burke, S.K. (1999). NDE to assess the effectiveness of boron-epoxy repairs to complex-shaped aircraft components. In: *9th Int. Symp. on Nondestructive Characterization of Materials*, June-July.
50. Davis, M.J. (1995). A call for minimum standards in design and application technology for bonded structural repairs. In: *Int. Symp. on Composite Repair of Aircraft Structures in concert with ICCM-10*, August.
51. Berg, S.D. (1995). Process Specification for the Fabrication and Application of Boron/Epoxy Doublers onto Aluminum Structures. Revision No. 6, Textron Specialty Materials Specification No. 200008-001, Dec.
52. Schweinberg, W., Jansen, R. and Fiebig, J. (1995). Advanced composite repairs of the C-141 wing structure. In: *Int. Symp. on Composite Repair of Aircraft Structures in concert with ICCM-10*, August.

Chapter 24

PRACTICAL APPLICATION TECHNOLOGY FOR ADHESIVE BONDED REPAIRS

M. DAVIS

Directorate General of Technical Airworthiness, Royal Australian Air Force

24.1. Introduction

While the main focus of this book is on repair of cracks in metallic structure, adhesive bonded repairs have been used on sandwich panels for some considerable time. Many of the repair application methods for sandwich panel repairs are used for repair of cracked metallic structure. In general, service experience with adhesive bonded repairs on sandwich panels has been extremely varied, with some structural repairs providing excellent service and others failing or requiring early replacement after a comparatively short service life. A survey of bonded repairs at one Deeper Maintenance facility in the Royal Australian Air Force (RAAF) [1] has shown that 53% of significant defects on structures such as F-111 were associated with adhesive bond failures (see Figure 24.1). The survey also showed that in 1993 43% of all bond defects (21% of the total defects) were associated with failures of previous bonded repairs.

The RAAF has experience that shows the importance of process performance to effective repair technology. Concurrent with the survey detailed above, the RAAF has introduced improved process specifications based on validated procedures and upgraded training courses. In the period of seven years subsequent to the changes, *only one repair* has been found to be defective in service, and that defect constituted less than 5% of the bond area. In other words, by use of properly validated processes, improvements in training standards and implementation of quality management systems, the RAAF has been able to cut the repeat-repair rate at its largest bonding facility to nearly zero.

The overall poor performance of adhesive bonded structures has led to a perception that adhesive bonding is not a reliable method for construction or repair. This is despite the fact that bonded structures have been shown to be far

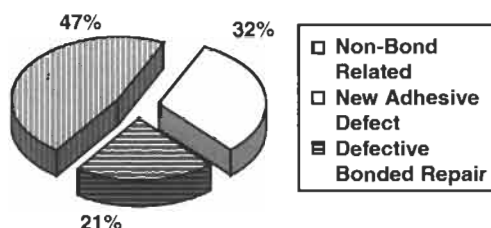


Fig. 24.1. Results of a 1992 survey of defect reports at a major RAAF Base.

more fatigue resistant than equivalent mechanically fastened structures [2]. When correctly designed, bonded joints can sustain higher load levels than equivalent mechanically fastened joints (up to unnotched material ultimate for thin materials). Bonded joints are also lighter due to the absence of the fasteners. The joint is more easily inspected for significant flaws and disbonds using NDI because of the absence of fasteners.

Deficient bonding processes have been the major factor in the inferior performance of adhesively bonded structures and repairs. Because of the perceived poor performance of repair patches, the USAF requires that structures for which adhesive bonded repairs are proposed must be able to demonstrate limit load capability *without the repair*. Thus, components, which could be made serviceable if the effectiveness of the bonded repair was considered in the design, are scrapped. Baker [3] indicated that designs which allow for the contribution of the repair can only be permitted where the designer (and regulator) has absolute confidence in the manner in which the repair was implemented. There have been a number of calls [4–7] for processes used in adhesive bonding to be part of the certification program for bonded structures and repairs.

Hart-Smith [8] has shown that for thin metallic adherends, bonded joints may be designed such that the adhesive load capacity is greater than the unnotched strength of the parent material, assuming of course that the bond does not fail due to other causes such as environmental degradation. (Environmental degradation is not a design issue. The resistance of a joint to degradation is determined by the surface preparation at the time of manufacture.) Such adhesive bonds should thus *never* fail, because the structure would have failed away from the joint before the load necessary to fail the adhesive could be achieved. Therefore it may be concluded that adhesive bonds in thin adherends (up to 3.5 mm thick for typical aircraft aluminium alloys) do not fail because of deficient design. In only a few cases are the failure caused by poor materials selection. Deficient repair bonding processes are the most common cause, and the deficiencies are more usually in the effectiveness of the processes themselves rather than in their implementation. Even though many manufacturers and repair stations may implement the approved processes very well, there are examples of poor process performance contributing to bond failures. No matter how well the process was performed, in these cases the bond was destined to fail because of the ineffectiveness of the process in producing bond durability.

The difference between a design deficiency and a processing deficiency can often be determined by examination of the failure surface produced when the bond breaks [9]. *Design deficiencies* are typically characterised by fracture of the adhesive (cohesion failure) with adhesive material present on both surfaces (see Figure 24.2). Cohesion failure is typical of the failure surfaces observed from adhesive strength tests such as lap-shear or peel tests. The adhesive would also contain minimal voids and obvious defects. *Processing deficiencies* are usually characterised by interfacial (adhesion) failure of the bond such that adhesive remains on only one of the adherend surfaces, with the matching surface being free of adhesive, or by the presence of voids or other bondline defects in the adhesive. Although interfacial failures occasionally occur due to contamination, the most usual cause of in-service adhesion failures is poor environmental durability due to the inadequacy of the surface preparation used when the bond was formed (see Figure 24.3).

Joints that fail by adhesion are generally considerably weaker than for those that fail by cohesion, but of more importance, the bond strength may degrade with time. Even if a structure that is susceptible to adhesion failure can demonstrate sufficient strength by static test, there is a high probability that the same structure will eventually fail in service as the weak bonds deteriorate. Therefore the conclusion



Fig. 24.2. Types of failure in adhesive bonds.

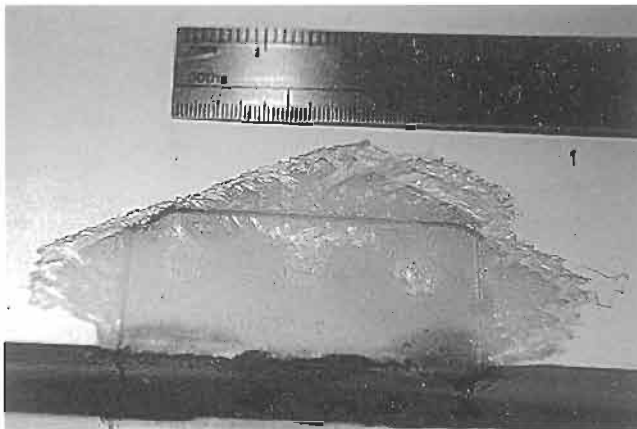


Fig. 24.3. A photograph of an interfacial failure of a bond in an aircraft elevator trim tab hinge. Note the replication of the part serial number and the smooth surface, clearly indicating an interfacial failure due to poor production processes. (Photograph courtesy Steve Emery, civil aviation safety authority, Canberra.)

may be drawn that interfacial failures are directly attributable to inadequate surface preparation processes used during manufacture. The absence of a requirement to demonstrate environmental durability for adhesive bonds is a major deficiency in the current FARs [5].

While the requirement for use of validated processes in adhesive bonded construction is important, it is essential for bonded repairs. Repairs are usually implemented under adverse environmental conditions using application methods that are significantly different from those used in production. The outcome is often a bond with a lower strength and durability than for production joints using the same materials. However, if the appropriate basic principles are followed, acceptable repair strength and durability can be achieved under repair conditions.

24.1.1. Management of repair technology

A formal management system is a fundamental requirement for the successful implementation of effective bonded repairs. The RAAF has developed RAAF Standard Engineering C5033 to provide direction in composite and adhesive bonded repair technology. This document directs the standards required for control of repair design and implementation, as well as specifying facilities, training requirements and procedures for design authorisation. Associated with this standard are two handbooks, AAP 7021.016-1 which provides methods for field level repair design, and AAP 7021.016-2 which contains process specifications for repair fabrication and application. While these publications are intended for management of simple repairs, the RAAF maintains an Aircraft Structural Integrity section, which has access to a Defence Support Network for design and validation of more complex repairs. This structure provides control over repairs through design, certification, specification and implementation. Organisations should not attempt bonded repairs unless such a structure is available and is competent in repair technology.

24.2. Repair application technology

The basic requirements of an on-aircraft surface preparation are:

- Primarily, it must produce a durable bond.
- It must be sufficiently robust and transportable that it can be performed in non-ideal conditions.
- It should not cause secondary damage to the surrounding structure.
- It must be applied by technicians who are appropriately trained and qualified.

The basic principles for adhesive bonding for repair under depot or field level maintenance are essentially the same as for production. The importance of procedural controls is not diminished just because the adhesive bond is for repair. Surface preparation and quality management procedures are usually adaptations of production processes. The successful implementation of a bonded repair requires management of a number of factors which, if incorrectly implemented, would result

in formation of an inadequate bond with a consequent reduction in performance of the repair. The factors, which strongly influence bond strength, are:

- Materials selection.
- Surface preparation.
- Repair heating for elevated temperature cure.
- Repair pressurisation.
- The manner in which repair quality is managed.

24.2.1. Materials selection

The engineering reasons for selection of repair materials is addressed in other chapters. This section deals with practical reasons for selection of repair materials. Common practice for bonded repairs on existing bonded or composite aircraft structure is to select the appropriate materials to the approved materials list. Almost invariably, the approved materials list contains the same materials used for manufacture of the component because these were the materials on which the structure was certified. However, automatic selection of the same materials is not always justified. Many composite materials and adhesives require very high pressures and temperatures to achieve adequate cure with an acceptable void content. Methods for heating and pressurisation in production are usually autoclave based and high positive pressures and relatively uniform temperatures are readily achieved. Unless the component can be removed from the aircraft, repair is usually performed using localised methods for heating and pressure. These invariably can not produce the same conditions as occur in production. Therefore, if a material has specific cure requirements that can not be achieved under field conditions, that material should not be selected for repair purposes, even if it was the material used to attain certification.

An example of this problem is the use of foaming core-splice adhesives for repair of sandwich structure. These materials contain a blowing agent that out-gasses during cure, causing the adhesive to expand to fill gaps. When cured under positive autoclave pressures, the resultant voids are small and the splice attains the required strength. However, if the same adhesive is cured for repair by using vacuum to apply pressure, the negative pressure expands the gas dramatically, resulting in extreme void content, with a substantial loss of shear strength for the splice.

A related issue is the selection of an adhesive or resin system with the same cure temperature as the original structural materials. In some cases, adhesives and resins are selected for their high temperature properties derived from their high glass transition temperature. For such cases, selection of materials with similar cure temperatures would be appropriate. However, in many cases, the selection of the cure cycle is driven by requirements to operate autoclaves using a common cure cycle because of high production costs. Selection of materials with differing cure temperatures would require separate autoclave cycles. The consequence of this production-driven materials selection is that many operators struggle to achieve the same cure temperatures to repair components even though these do not experience

service conditions that would necessitate the resulting high glass transition temperature.

The basic principle for selection of repair materials may be stated as:

Materials selected for repair must be appropriate for that repair and must be capable of being utilised using processes available where the repair is to be installed.

24.2.2. Surface preparation

Most adhesive bond failures can be attributed to poor processes during fabrication, with lack of quality surface preparation being the most common cause of bond failure. The very best joint design will not be durable if the surface preparation is inadequate.

For effective surface preparation the surface must be:

- Free of contamination,
- Sufficiently chemically active to enable formation of chemical bonds between the adhesive and the adherends, and
- Resistant to environmental deterioration in service, especially by hydration.

The first step is to remove surface contamination that would inhibit chemical reactions with the bonding surface. A clean surface is an essential condition for adhesion but it is not sufficient for bond durability. Most structural adhesives function by the formation of chemical bonds between the adherend surface atoms and the adhesive [10]. These chemical links are the load transfer mechanism between the adherends. While the surface must be clean (free of contamination) it does not necessarily follow that a clean surface is sufficiently chemically active to enable formation of chemical bonds. Further, even a clean surface that can form chemical bonds is not a sufficient condition for bond durability; the chemical bonds themselves must be resistant to chemical dissociation in service for the adhesive bond to be durable.

The possible outcomes of surface preparation conditions are shown in Table 24.1. Short-term strength is relatively easy to obtain with minimal surface preparation; however, these bonds degrade during service, leading to debonding. If a simple lap-shear test (ASTM D1002) is undertaken shortly after completion of the bonding process, acceptable lap-shear strengths can be obtained even with minimal preparation. However, longer-term bond strength depends on the resistance of the chemical bonds to degradation over time. In many cases, poorly prepared metallic surfaces form hydrated oxides which displace the chemical bonds between the adhesive and the surface. The consequence being that the adhesive bond fails along the interface some time after fabrication (adhesion failure).

Surface preparation should never be termed "cleaning" nor should the chemicals used be termed "cleaning agents" as these expressions lead to confusion between the different activities which combine to form the whole surface preparation process. In many cases, surface-modifying chemicals applied to contaminated surfaces do not dissolve the contaminants, resulting in an ineffective bond if the

Table 24.1.

The influence of surface condition on the short and long term strength of adhesive bonds.

Condition	Evidence	Short term effect	Long term effect
Contaminated surface.	Adhesion failure.	Chemical reactions are inhibited. Bonds are weak.	Weak bond which fails soon after manufacture.
Clean surface.	Short term: Mixed adhesion-cohesion failures. Long term: Adhesion failure.	Short-term bonds are strong.	Gradual degradation leads to interfacial failure. The joint strength will decay to zero.
Clean surface which is chemically active and hydration resistant.	Cohesion failure, if failure occurs at all.	Short-term bonds are strong.	Bond maintains integrity throughout its service life.

solvent degreasing step is not performed adequately. The degreasing step has sometimes been eliminated in process specifications or performed with indifference by operators, in the mistaken belief that the “cleaning agent” is the important part of the process and it will remove any contamination. Processing chemicals such as etchants require contact with the substrate, and their effectiveness is diminished if the surface is contaminated. This is especially true for coupling agents, which do not etch the surface being prepared.

The basic principles of surface preparation dictate a number of aspects, which are often violated by process specifications even from reputable manufacturers [4,11]. The requirements for adequate surface preparation dictate the sequence in which the surface preparation process should be conducted. There are three basic steps:

1. Remove surface contamination by solvent degreasing.
2. Expose a fresh chemically active surface (typically by chemical etching or surface abrasion).
3. Chemically modify the surface to produce an interface resistant to hydration.

Note: Most thermosetting polymer matrix composite adherends usually do not require the chemical modification process.

24.2.2.1 Solvent degreasing

Surface contamination should be removed as the first step in surface preparation. It must be scrupulously undertaken such that all contamination is removed. While the use of vapour-degreasing tanks is an effective method, this approach is not practical for on-aircraft repairs or repairs to large components. In these cases solvent degreasing must be performed by hand. This is usually slow, tedious work which is made more difficult by the necessity to wear personal protective equipment (PPE) including respirators, gloves, eye protection and disposable clothing for protection against the solvents used. The arduous nature of this task, together with production demands often leads to short cuts being taken by some technicians. To

overcome this, the RAAF requires a water break test to be performed after solvent degreasing to assure integrity of the procedure. Most production procedures and repair manuals which use the water break test usually apply it after the surface is fully prepared (again, the “clean” surface syndrome). The effect of surface roughness caused by abrasion and etching can under some circumstances lead to poorly prepared surfaces actually passing the test, whereas the use of the water break test immediately after solvent degreasing will force the operator to maintain a high standard.

A common mistake presented in many aircraft repair manuals [4] is to specify solvent degreasing after abrasion of the surface. Degreasing after abrasion or chemical treatment will result in a layer of partially solvent dissolved contamination remaining on the prepared surface [12] and this may inhibit adhesion.

The type of solvent is also important. Care is required to ensure that the solvent does not degrade the structure being degreased. For example many chlorinated hydrocarbon solvents can cause stress corrosion cracking [17]. Solvents with a rapid evaporation rate are best for hand degreasing, because any residual unevaporated pools of solvent will spread partially dissolved contamination as the material evaporates; the faster the solvent evaporates, the less surface is contaminated. The RAAF currently uses methyl ethyl ketone (MEK) as its primary surface degreasing solvent. Despite the common perception that MEK is a dangerous material, it has some properties that actually improve safety when compared to other solvents. MEK can be detected at 2 ppm, with clear recognition at 25 ppm. This gives the technician a clear warning of the onset of failure of the breathing protection system. Other solvents, such as trichloroethane tend to reduce nasal sensitivity after exposure.

Degreasing must be performed using a solvent rather than a detergent. Detergents function by wetting the surface better than the contamination, thus displacing it from the surface. This means that the detergent will become a contaminant unless it can be removed from the surface. Note that water solubility of a detergent is not a guarantee of removal.

Another important issue is the selection of an appropriate wipe cloth that will not contaminate the surface. Shop rags, cheesecloth and even some proprietary wipe cloths may contain contaminants. Others contain dyes which are solvent soluble. Some wipe cloths contain lanolin to reduce skin abrasion on the hands of the user. These must be avoided. The RAAF uses a high strength aircraft wipe cloth that is very resistant to tearing, but fresh white non-perfumed tissues are an acceptable alternative.

24.2.2.2 Exposing a chemically active surface

Solvent degreasing is important, because it removes contaminant materials, which inhibit the formation of the chemical bonds. However, solvent degreasing alone is never an adequate surface preparation. In a similar manner, the standard surface preparation in many aircraft repair manuals, repair procedures and texts [13,14] involving a “scuff-sand and solvent clean” whilst producing a clean, moderately chemically active surface, will not produce a surface which is resistant

to degradation in service. Even application of an adhesive primer (see for e.g. [15]) to a clean surface will not produce a durable bond unless that surface is chemically active and capable of formation of stable chemical bonds with the primer. Durability requires the formation of a surface chemistry and morphology, which will result in chemical bonds between the surface atoms and the adhesive that are resistant to hydration during later service.

For any adhesive bonding process, a fresh, chemically active surface is essential. This may be generated by etching, but may also be produced by abrasion. Production facilities usually use tank etching methods for metallic surfaces, and field level facilities usually rely on abrasion of the surface. The function of abrasion is often mistakenly believed to be to enable the adhesive to key into the surface. The error in this argument can be seen in any number of rough surfaces that have disbanded interfacially (see Figure 24.4). The real purpose is to expose a fresh, active surface.

In field facilities, abrasion is usually performed either by hand, with abrasive pads or paper, or by grit blasting. Hand abrasion is less effective than grit blasting, and tends to produce folded material on the surface as abrasion tracks roll material into adjacent scouring from previous passes. Those areas of folded material trap contaminants and moisture [16]. Removal of sanding debris is difficult, leading many specifications to require solvent cleaning after abrasion. Because bonding relies on the chemical activity of the surface and the absence of contamination, solvent cleaning after abrasion only succeeds in partially dissolving contaminants

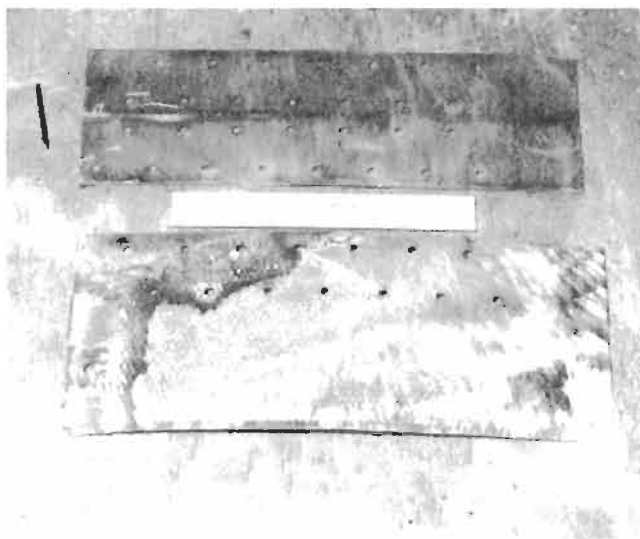


Fig. 24.4. A failed doubler splice plate repair on F-111. Note the rough abrasion of the surface performed during the original repair. The failure is interfacial, with minimal adhesive remaining on the failure surface, indicating poor surface preparation (scuff sand and solvent clean). This example demonstrates that abrasion alone is not sufficient to produce a durable bond.

and spreading them over the surface, reducing surface activity. Sanding debris is best removed using a dry wipe process until all debris is removed [17].

Light grit blasting is far more effective in production of an active surface, mainly because it is a non-contact process with a clear visible measure of effectiveness. The objective in grit blasting is to just remove the surface layer sufficient to expose a chemically active surface. Small pencil blaster systems are recommended and the large grit blasters used for removing paint and rust from large areas must be avoided. One requirement for grit blasting is that the abrasive must cut the surface, not deform surface. Thus abrasives such as glass beads, walnut husks, sand and steel shot are not suited. Aluminium oxide powder and zirconia have been found to be effective [18]. It is important that the abrasive powder is not recycled, to prevent re-contamination of exposed surfaces.

The grit should be delivered in a dry inert gas stream. Compressed air (from a compressor) is not suitable, due to oil and water contamination. Current practice in the RAAF repair applications is to use dry nitrogen gas that is readily available at maintenance stations because of its use for inflation of tyres and shock struts. Dust may be blown off the surface using nitrogen. Particles may break into fine needles, pass through fuel filters and cause fuel system malfunctions. Grit particulates must be contained within the worksite, and extracted using a vacuum system that must exhaust away from the aircraft.

Caution: Failure to contain and extract fine dust from fuel tanks has led to in-flight engine failures on RAAF and USAF aircraft.

The level of abrasion by grit blasting has an influence on the adhesive void content after cure. Excessive abrasion by either high pressures or slow pass rates can cause folding of the surface [18] on softer metals such as aluminium, leading to trapped moisture which evaporates during heat cure of the adhesive causing voiding in the adhesive layer. The grit blast should be light enough to avoid folding, but sufficiently heavy to remove the surface oxides. This can be easily controlled by abrasion until the surface sheen is removed, but not so hard that the surface of aluminium alloys turn a dull, dark grey. With limited training, most operators easily master the appropriate level of abrasion.

Common arguments advanced against grit blasting for repair application include the fact that most repair facilities do not have the equipment and it is too messy and difficult to perform in a repair environment. These logistics management and training issues are not sufficient justification for the use of inferior processes that may result in bond failure.

24.2.2.3. Exposing a chemically active surface on polymer matrix composite surfaces

For thermosetting plastic matrix composite surfaces, common practice is to use tear films (also known as peel plies), a sacrificial layer placed on the surface during the laminating process. The tear film remains in place until the adhesive is to be applied. It is then removed, supposedly taking surface contaminants with it. However, this concept is flawed for the reasons given in the following discussion.

Typically, three forms of tear films are used. The first type is a thin fibreglass layer that is difficult to remove, and may cause delamination damage in thin

laminates. There is a real danger of removing the first few layers of laminate with the tear film. The second type is usually a nylon product. Unfortunately, nylon forms quite strong bonds with epoxy resins so some form of release agent is often applied to the fibres to enable the operator to remove the tear film without causing excessive damage to the laminate. Tests [19] have shown that this release agent is transferred to the bonding surface thus reducing the effectiveness of any adhesive bond formed. Most reputable manufacturers clearly state that all coated fabrics have the potential to transfer release agent to the surface exposed by removal of the tear film. The third form of tear film uses heat setting or corona discharge treatment to glaze the surface of the fibres. This is the usual process for polyester tear films. The glazed surface is so slick that it releases from the resin when required. Unfortunately, it leaves a replicate of the glazed surface on the laminate surface again resulting in reduced bond effectiveness on that surface. While the surface remaining is clean, it is not chemically active, apart from a few locations where the weave bundles cross over each other and the resin is fractured.

The only recommended surface preparation for thermoset matrix composites is a light aluminium oxide grit blast in dry nitrogen. The abrasion should just remove the surface of the resin without exposing or fracturing bare fibres. This process may be effective on moulded and corona treated tear film surfaces, and has been shown to reduce silicone contamination when coated nylon tear films are used [19]. Dust should be blown off the prepared surface using a nitrogen gas stream. Because the epoxy surface bonds well to other epoxies, no chemical modification is required. Hand abrasion may be used, but the outcome is never as effective as grit blasting.

24.2.2.4. Chemical modification processes

The formation of a suitable surface chemistry is the most important step in the surface preparation process because the integrity of this surface directly influences the durability of the adhesive bond. Past practice (on F-111 aircraft for example) has frequently relied on the "clean surface" approach of a scuff sand and solvent clean only. This treatment results in bonds with abysmally poor durability as it does not generate a stable oxide on aluminium alloys (see Figure 24.4).

There are three basic groups of surface modification methods for aluminium alloys; etchants, anodising processes and coupling agents. Etchants remove surface oxides and generate a micro-rough surface with a large number of active bond sites, at the same time as forming oxides which are relatively resistant to hydration. Anodising in chromic or phosphoric acid solutions produces a thin oxide film, with a high degree of micro-roughness and an oxide form that is highly resistant to hydration. Phosphoric acid anodising produces the most durable adhesive bonds of the variety of anodising methods [20] and field experience has shown that the "sealed chromate" anodise method is not sufficiently durable (see Figure 24.5).

The use of coupling agents for adhesively bonded repairs was pioneered by the Aeronautical and Maritime Research Laboratories (Melbourne) in the mid 1980s [21]. One end of the long-chain polymers in the coupling agents form covalent bonds with the surface oxides and hydroxides on the aluminium while the other end links with the adhesive during cure. In this way the polymers effectively couple the

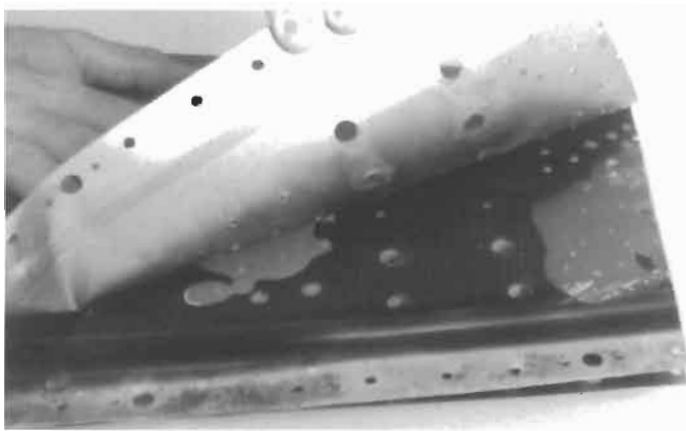


Fig. 24.5. An in-service disbond of a panel fabricated using the sealed chromate anodising process. Note also the failed injection "repairs".

adhesive and the surface. Because the coupling agent does not modify the oxides on the surface (as would occur with etching or anodising) the freshness of the exposed surface is essential to the success of the bonding process. Any delay in application of the couplant after exposure of the chemically active surface will result in the formation of thick oxides with fewer bond sites and thus, reduced durability. When properly performed, the use of coupling agents on grit blasted surfaces provides bonds with durability approaching that of phosphoric anodising [20,22]. The durability of hand abraded surfaces which have been treated with coupling agents is inferior so this method should not be used.

A major advantage of the grit blast and silane method is that it has been shown to be effective on a range of substrates including, aluminium alloys 2024 and 7075, titanium 6Al-4V, D6AC steel and stainless steel. Therefore with care this method may be used as the sole preparation method for adhesive bonding for a range of applications. For repairs to aluminium structures where steel or titanium fasteners are used, this can be a significant advantage. For such surfaces, applications involving etching or anodising necessitate application of a protective coating over every fastener to prevent corrosion, electroplating effects and hydrogen embrittlement.

The most durable bonds are formed using phosphoric acid etching (PAA) [20]. Problems with control of acid spillage in this process have been largely overcome by the phosphoric acid contained system (PACS) [23] where a double vacuum bag is used to contain the acid. However, this system has its own drawbacks. Tests [24] have shown that if the process is performed on structure at a temperature above 85°F (29°C), a severe reduction in durability results [25]. The process is susceptible to vacuum leaks, and may cause corrosion between dissimilar metals such as fasteners and skin surfaces. All fastener heads must be coated with a fast-setting epoxy barrier before anodising is undertaken. A consequence is that the bond to the

fasteners is not durable, and may lead to in-service disbonding. A further limitation with any anodising process is that the area that can be processed is limited by the power capacity of the anodising power supply. This is typically 300 mm square (one square foot). For larger areas, anodising is performed in stages and measures must be undertaken to avoid acid damage of the previously prepared surfaces. The problems which can arise are demonstrated in one example [26] of this practice, where the surface was protected with a tape which uses a silicone based adhesive in direct contact with the prepared surface, risking contamination of the bond in the area where the tape was located.

Extensive research into the use of an organo-functional silane based coupling agent for surface preparation [21,27] has been followed up by Wright Laboratories through the University of Dayton [25]. The grit-blast and silane process is now widely accepted as an ideal field level process. Durability of joints formed using the silane coupling agent is only marginally lower than those formed using PAA processes. Additionally, the silane solution is not acidic nor does it promote galvanic corrosion and has been shown to be effective on a range of metals, eliminating the need for the protective coating of fasteners. The process is quite simple and does not require complex support equipment. A major advantage is that the area that can be treated is only limited by the area that can be kept wet by the operator and the ability to correctly dry the surface after treatment.

24.2.2.5. Primers

Common practice in bonding production is to treat surfaces with a corrosion inhibiting primer immediately after preparation. The primer provides a stable protective coating that enables parts to be stored for extended periods until required. The primer also provides corrosion resistance in service. Wedge test results [28] also show that bond durability is significantly enhanced. However, care is required to obtain the correct primer thickness; primer layers less than 0.005 mm (0.0002 in.) are not effective against corrosion and layers thicker than 0.01 mm (0.0004 in.) create a weak layer through which failure occurs. Most corrosion inhibiting primers in current use present environmental and occupations health risks due to the use of chromates, although chromate-free primers have been developed and shown to be reasonably effective.

Experience in the RAAF shows that with the grit blast and silane preparation method a primer may not be required to obtain durable repairs. The silane coupling agent is effectively a primer and its use as a corrosion prevention method has been reported [29]. The RAAF does not use primers with the grit-blast and silane method because of difficulties in obtaining the required level of thickness control while performing repairs in confined spaces, especially when wearing the personal protective equipment necessary to protect the operator against the chromate products. The RAAF has not experienced any bond failure or corrosion in such bonds where the grit blast and silane process was used. In one case on D6AC steel where significant corrosion occurred adjacent to a repair, the previously prepared surface was still well bonded to the adhesive even though the corrosion extended in the steel under the repair by inter-granular corrosion.

24.2.2.6. Validation of processes

There is no post-bond non-destructive test that will verify the integrity of an adhesive bond. NDI and companion test specimens only provide information about *necessary* conditions for bond integrity. For example, ultrasonic inspection will detect significant air gaps in the bond. This is necessary for bond integrity because air gaps indicate areas of voiding that may result in a low strength bond or regions of disbonding. However, the absence of voids does not, in itself, imply a strong bond. Similarly, a lap-shear test coupon prepared at the same time as the bond can only verify the short-term strength of the bond, but does not assure bond durability. There is no test that is *sufficient* to *guarantee* the strength and durability of a bond.

To determine if an adhesive bond has bond integrity, the processes used to fabricate the bond must be properly validated **BEFORE** the bonding is undertaken, i.e. it is the processes that must be validated, not the product produced. The validation usually requires some form of mechanical testing. A lack of understanding of the principles required for adhesion has in the past, led to the use of inappropriate validation tests. Many of the tests have been based on strength tests such as ASTM D1002 Lap-Shear Strength Tests or D1876 Peel Strength Tests. While shear and peel strength are essential for bond integrity, they are not sufficient to assure durability.

Because bond degradation by hydration of the surface oxide is time dependent, the results of strength tests will depend on how long after fabrication the joints were tested. This can be easily demonstrated by performing a simple lap-shear test on aluminium specimens prepared using only a simple solvent wipe. If tested immediately after fabrication, reasonable results can be obtained and failures will occur by a mixture of adhesion and cohesion. Identical specimens allowed to stand in a humid environment will usually fail at very low loads after limited exposure and all will display adhesion failure. Hence, it may be concluded that quality control lap-shear results do not verify surface preparation because of the time-dependence of bond degradation. Such tests will identify badly contaminated bonds, but success in these tests does not provide assurance that the bond is durable.

Validation testing for the adhesive bonding processes must evaluate the time dependent resistance to hydration of the chemical bonds formed at the adhesive/adherend interface. The most appropriate test for evaluation of surface preparation are wedge tests such as the Boeing Wedge Test, ASTM D3762 (see Figure 24.6). Specimens prepared using the required bonding processes are fabricated from 150 mm (6 inch) square 3 mm (0.125 inch) aluminium alloy. After bonding together,

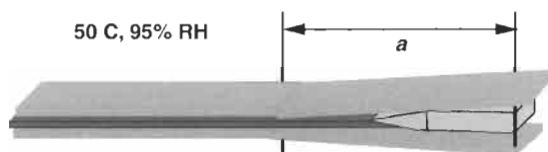


Fig. 24.6. A Boeing wedge test specimen.

the plates are cut to produce five 25 mm (1 inch) specimens. A wedge is driven between the adherends, cracking the adhesive. The specimens are then exposed to a hot, humid environment (50 °C and 95% RH) and the crack tends to grow with prolonged exposure to the combined effects of the environment and the peel stresses introduced by the wedge. The crack length is periodically measured and the results compared against acceptance values to determine the comparative durability of the surface preparation. In a poor durability bond the crack locus will move to an adhesive/adherend interface indicating a loss of adhesion between the adhesive and the adherends.

The wedge test is ideal for evaluation of bond durability because the adhesive bonds are placed under the most aggressive stress (tension at near the adhesive material ultimate) while being exposed to conditions that promote hydration of the surface oxide. However, even though this is a reliable test, a lack of understanding of the basic principles of adhesion has frequently resulted in the use of inappropriate acceptance criteria for results derived from the test. The ASTM Standard itself states that for an acceptable bond, specimens should achieve an average of 12 mm (0.5 inches) growth in one hour with a maximum from any specimen of 18 mm (0.75 inch). Experience has shown that such acceptance values are grossly inadequate with processes meeting these requirements producing bonds with poor durability in-service. The acceptance limits are too high and the exposure time is too short to allow hydration to occur. Current practice within the RAAF [6,30] and at Wright Laboratories (USAF) is to require no more than 5 mm growth (0.2 inches) in 24 h, and no more than 6.2 mm (0.25 inches) in 48 h. The surface generated during the test must also not exhibit more than 10% adhesion (interfacial) failure.

Other test methods have been developed for evaluation of the durability of adhesive bonds. The slow strain test developed by AMRL [31] is an effective method for discriminating between surface preparation methods. In this method, the wedge opening of the Boeing Wedge Test is replaced by a test rig that peels the adherends apart at a slow, constant rate while the specimens are exposed to the test environment. This system allows a constant opening force to be generated, whereas the stress applied at the crack front in the Boeing Wedge Test diminishes as the crack length increases. The strain-endurance test [29] subjects lap shear specimens to a sustained shear load whilst being exposed to a hot-humid environment. This system does have the advantage that the loading is in shear which is more representative of service loads. However, because the bonds are exposed to a shear load well below the ultimate for the adhesive, the tensile stresses acting on the bondline will be considerably lower than for the wedge type tests and this test method will not be as effective in discriminating between acceptable and poor processes.

Even minor changes in production processing must be validated before use on an aircraft to avoid the danger of poor in-service durability. An example where inadequate validation has resulted in an inadequate process may be found in the adaptation of the common optimised FPL chromic acid etch process from production to field applications. In production, large tanks of acid etchants are

used to prepare surfaces for bonding. This is not practical for on-aircraft repairs and the acid is usually gelled to form a thick paste to help prevent spills and the accidental corrosion of surrounding structure. Lap-shear test results indicate acceptable bond strength for joints formed using the gelled acid etchant, but wedge test results frequently indicate poor performance when compared to the tank process and other field processes [32]. The reason that the chromic acid etch is not as effective in gel form is that the tanks are usually maintained at a set elevated temperature of 71 °C (160 °F) and this level of temperature control is impractical for on-aircraft repairs. Thus, while the etchant materials are essentially the same for tank and gelled applications, one critical aspect of the process was omitted for the sake of practicality. Without reliable validation, the change in the process appears acceptable, but when subjected to wedge testing, the inferior performance is evident.

24.2.3. Heating procedures for on-aircraft repairs

If hot-bonding is performed for aircraft component construction, global heating systems are usually used, where the entire component is heated in an autoclave or oven giving relatively uniform temperature distributions for cure of the adhesive. Heating procedures for on-aircraft repairs can not employ global heating methods, due to the size of most airframes and components, and the need to remove the component to enable such heating methods to be used. Heat for bonded repairs is therefore usually supplied by use of localised heating methods such as heater blankets or heat lamps.

One consequence of heating for on-aircraft repairs is that the presence of substructure, co-location of materials with different conductivity and the localised nature of the heat sources usually results in non-uniform temperature distributions, which may cause overheating of the structure, undercure of the adhesive and/or residual thermal stresses. These conditions can be avoided if basic principles are considered when the heating system is configured and installed. Unfortunately, many deficient heating procedures have become standard practice even in approved aircraft repair manuals.

To effectively heat a structure for repair, that structure must be divided into separate zones on the basis of the thermal conductivity combined with the mass of material to be heated. Each zone is then to be heated by a separate heat source with a power capacity selected to match the thermal mass within the zone. For example, consider a thin aluminium skin attached to a relatively thick spar and a moderately thick longeron (see Figure 24.7). This structural configuration would necessitate separate heated zones for each structural element. The blankets over the thin skin would only provide a relatively small amount of power while the smaller blankets over the longeron and frame would be required to provide significantly more power.

The location, number and method of installation of temperature sensors will also have a direct influence on the effectiveness of a repair heating procedure. Temperature sensors perform two functions; they ensure that the structure is not overheated during heating and provide a measure of assurance of cure of the bond

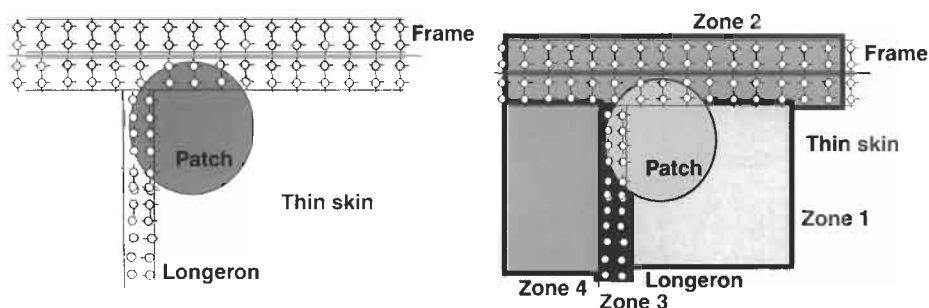


Fig. 24.7. The zoned methodology for heating a relatively complex structure.

adhesive. Both functions are equally important and a *single* temperature sensor can not perform both functions.

The location of the sensors for control must be at the point in each zone where the heated zone is expected to be hottest. Sensors for acceptance of the repair must be located around the repair such that the coldest point is measured (see Figure 24.8). A common error in setting up heating systems is to use a “standard” sensor configuration, such as three sensors located 120 degrees apart around the repair. Such a standard system will never guarantee to meet the basic principles of temperature measurement and control because there is no assurance that the hottest/coldest points will be those where the sensors are located. A further error is to control the system by the coldest point in an effort to drive the minimum temperature up to the required cure condition. Such a practice will risk overheat damage to the existing structure. There are more reliable ways of ensuring the adhesive experiences the required cure cycle, based on the time to cure the adhesive at the minimum observed temperature around the repair.

Testing at AMRL has shown that many epoxy adhesives can be cured at temperatures below the manufacturer’s recommended cure cycle, provided the time of the cure cycle is appropriately extended to suit. A typical “cure cycle envelope” is shown in Figure 24.9. By controlling the system by the hottest temperature in each

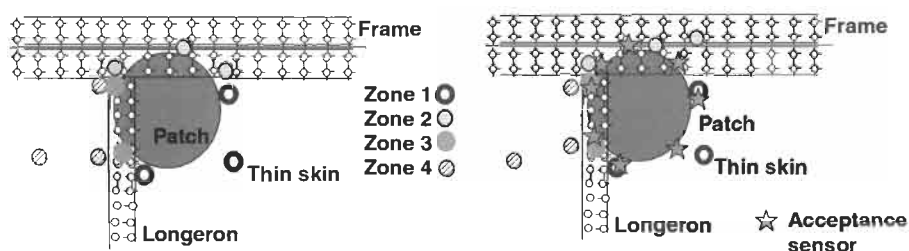


Fig. 24.8. Configuration of temperature sensors (a) for temperature control by estimation of the hottest point in each heated zone and (b) for cure assurance by location at the anticipated coldest points around the repair.

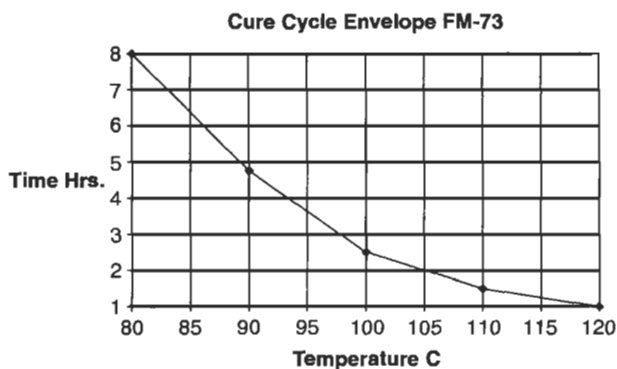


Fig. 24.9. A typical cure cycle envelope for a common film adhesive.

zone, overheating damage is avoided. The lowest temperature is then used to determine the cure cycle duration from the cure cycle envelope.

Control of processes for heating a structure requires measurement of the temperatures at these specific locations:

1. Where the hottest temperature is anticipated within each heated zone. This point will be used to provide temperature control to ensure that the structure is not overheated.
2. Where the coldest point is anticipated to occur around the repair. This point will be used to provide assurance that the repair adhesive has received a full cure cycle.

For cases where sub-structural heat sinks exist, a heat trial is strongly recommended before attempting repair installation. Sufficient temperature sensors must be used to assure measurement of these conditions. These should be installed prior to assembly of the heater system. The objectives of a temperature survey are firstly to ensure that the proposed heater system can achieve an acceptable temperature distribution, secondly to identify which thermocouples should be used for control and acceptance and thirdly to identify hot or cold areas so that corrective action can be undertaken. When the correct heater configuration is established, any thermocouples that are providing unnecessary information may be omitted from the final configuration to be used during repair installation.

Another issue in connection with heating systems that needs to be addressed is that of multi-zone heater blankets. A number of manufacturers sell these items with the claim that they provide a more uniform temperature distribution. These blankets usually consist of a number of concentric separately controlled zones (circular or rectangular) and usually have thermocouples embedded in the blanket. Some also feature a self-sealing vacuum system. In practice, these systems are unsuited to even moderately complex structure, because the distribution of the heat sources rarely match those found on practical aircraft structure (see Figure 24.10 for example).

The outcome of the heating process will depend upon where the sensors happen to be positioned on the structure. The unsuitability of these systems is

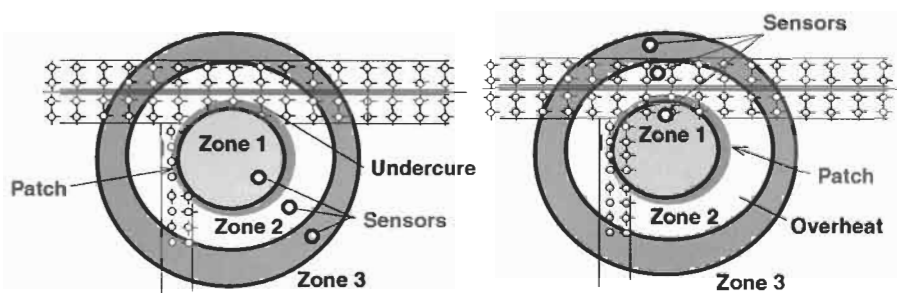


Fig. 24.10. Different outcomes for the same multi-zone heater system, depending on the location of the embedded sensors relative to the heat sinks.

demonstrated by the two conditions shown; either the adhesive in the repair over the thicker structure is undercured, or that over the thinner structure is overheated. The self-sealing vacuum system is susceptible to leaks at fasteners. A loss of vacuum will result in a defective repair and possibly, for repairs performed on lower surfaces of a component, the entire heating system may fall away from the part, creating a difficult (if not dangerous) situation for the operator. In comparison, the conventional vacuum bag system usually holds the assembly in place even with significant vacuum leaks.

The type of temperature controller (hot bonder) used to perform repairs also has a direct influence on the quality of the repair. There is a wide range of temperature control kits available on the market and unfortunately, many are not adequate for the performance of acceptable bonded repairs. The requirements for a temperature control device for adhesive bonded repair include:

- All heating processes are to be performed using a closed loop temperature control system for each heated zone. Heater systems that rely on operator manipulation to achieve correct temperature control are unsuitable.
- Cure cycles are to be temperature based, irrespective of the time of the cure cycle. Systems that undertake a cure cycle based on elapsed time without reference to the actual temperature are unsuitable.
- Control units should have the capacity for at least three controlled outputs. Single output temperature controllers have limited use in realistic structures, and encourage the use of single heat sources. Groups of single channel systems may be used simultaneously to provide control of multiple heat zones.
- Units must record maximum zone temperatures and minimum adhesive layer temperatures to provide recorded evidence that the cure cycle has been undertaken. Units that record temperatures at arbitrary locations that are neither the temperature being used for control nor the adhesive bondline temperatures are unsuitable.
- Units must have the capacity to measure at least two temperatures for each heated zone, plus at least two temperatures around the repair patch.
- Units must display all measured temperatures in digital form simultaneously in one area on the control unit. Units which display more than one temperature,

but require the operator to select the channel being displayed result in confusion for the operator, especially when a large number of thermocouples are involved. These systems are unsuitable. Units which display some temperatures in digital form and others in analog form cause operator confusion and are unsuitable.

- Units should have the capacity to operate on three-phase power, to achieve an acceptable power capability. Single-phase multi-channel controllers draw excessive electrical current and are therefore unsuitable.
- Fault occurrence must be reported in visual and audible manners and recorded in hard copy. Clear identification of the fault should be provided. Systems that use a single alarm that does not indicate the source of fault are unsuitable.
- Data should be presented in colour and differentiation made between various control states and alarm conditions. Color systems greatly enhance operator interpretation of the process state and improve safety of operation.
- The system should be capable of resuming a control cycle on command following resumption of power after a power failure, provided that power is restored within an acceptable period of time, say 15 min. Power failures longer than this may require the repair to be removed and repeated.

Care must be exercised in the selection of a hot-bonding unit. Many such devices, even from reputable manufacturers, have peculiarities that may result in deficient bonded repairs. Some deficiencies that have been observed include:

- Devices can control only one or two heat sources. Only in very rare cases will such systems be adequate for effective repair. A minimum of three controlled outputs is essential. As a general rule, the more controlled outputs the better the system can be configured to provide acceptable temperature distributions.
- Devices can only measure a limited number of temperatures. This is a severe limitation on even knowing that an unacceptable heating condition exists.
- Many controllers have a limited power capability due to the use of single phase input power. Most domestic power supplies are limited to about 2200 to 2400 Watts (20 A at 110 V or 10 A at 240 V). Connection of two or more moderate sized heater blankets to such devices usually results in activation of circuit breakers when the device is operated. For effective repair installation on even moderately complex structure, connection to three phase power is essential.
- In some devices, temperature is reported in digital form on displays, but analog form on channels recorded for quality purposes. In emergency situations, this requires the operator to interpret data while trying to assess the cause of a fault. Data should be presented in a consistent form, either all analog or all digital.
- One system which had been configured with a low-power heat source actually started to time the soak part of the cycle even though the temperature was actually 40 °C below the set point.
- The temperature recorded on many systems using a tape-printer was neither the hottest nor the coldest point. Such data is meaningless as a quality control measure. The minimum requirement is to record the hottest point under each heat source and the coldest point around the repair.
- During operation of one system with a deficient thermocouple located in the control input socket, the system was indicating very high temperatures from all

adjacent sensors. The operator (correctly) swapped the control sensor such that control would be driven by the one indicating the highest temperature. The system interpreted the removal of the control thermocouple as an open circuit, and automatically transferred control to the next thermocouple in the sequence, which unfortunately by then was the defective thermocouple that had just been swapped.

The RAAF were unable to purchase commercially available controllers that met all requirements, so they employed a contractor to develop such a system. The Novatech HBC-43 is a PC based unit capable of control of six powered outlets from data collected from sixteen temperature sensors, with a proposed extension to thirty-two. The sophisticated software enables automatic control to the hottest point in each designated zone and also has the capacity to automatically adjust the cure cycle duration on the basis of the coldest point around the repair using stored temperature profiles such as shown in Figure 24.9. Cure cycle settings, temperature sensor status and heater status can be changed from the keyboard even while the system is running.

24.2.3.1. Manufacture of thermocouples

Thermocouples rely on the different atomic structure of dissimilar materials to generate a potential difference due to electron deficiencies. The voltage output by the joint is dependent on the temperature and when properly calibrated, measurement of the voltage enables a direct measure of temperature. A range of metals and alloy pairs are used such as iron-constantan (J-type), copper-constantan (T-type) or chrome-alumel (K-type). At least another five types of thermocouples are available. Each measuring device is made to match a particular wire type, because the calibration characteristics of each wire pair are unique to that combination. Use of the incorrect wire type will result in incorrect temperatures being reported, with a consequent risk of overheat damage to the structure or undercure of the repair.

The manner in which the thermocouple junction is formed can have a significant effect on temperatures measured. Sufficient electrical contact is required to ensure adequate integrity of the joint. The most effective way to join the wire ends is by welding by either an oxy-acetylene flame or by use of a resistance-welding device. Silver solder must not be used to join the wire pairs. The junction between wire A and the solder will set up a potential difference which may not be the opposite of the potential difference between wire B and the solder. The resulting total potential difference across the joint may not be the same as that which would result in direct contact between the two metals.

While some manufacturers of hot bonders supply thermocouples with the wire ends twisted together, that joining method must be avoided. The author is aware of at least one case where adhesive flowed between the wires during a repair application. The increased resistance of the joint resulted in a lower temperature being reported, with the controller increasing power output to suit the reported temperature situation. Severe damage to the structure was only avoided by intervention by the technicians performing the repair.

24.2.3.2. Installation of thermocouples

Effective temperature measurement and control requires that the sensor must be located on the surface where the temperature is to be measured. This may at first seem obvious; if you wish to have a region reach a particular temperature, then the temperature on the surface of that structure must be measured. In practice this obvious rule is frequently overlooked, with temperature sensors often being located on a copper sheet (used to more evenly distribute heat in systems where a zonal system is not practiced) placed over the repair area. In some cases bleeder layers and release materials also act to insulate the sensor from the surface. A further example of wrong practice is to use temperature sensors embedded in the heater system itself. Such sensors only indicate the temperature of the blanket, which may be only remotely dependent on the surface temperature. In these examples, the sensors will not be recording the surface temperature on the component and therefore are not conveying data necessary to avoid overheat damage and to assure adhesive cure.

Sensors should be located on the surface being heated and held in place with heat resistant *non silicone* tape. A small piece of insulation should be placed over the sensor to isolate it from the heater blanket to avoid the system incorrectly indicating the blanket temperature (see Figure 24.11).



Fig. 24.11. Method for installation of thermocouples for measuring surface temperatures.

24.2.4. Repair pressurisation

Application of pressure during repair is required to provide consolidation of the repair and reduction of void content in the bondline. Similar requirements apply for composite patches being cured or cobonded *in situ*. In production processes positive pressure is usually applied by an autoclave. In on-aircraft repair applications, such pressurisation methods are impossible. Several methods are commonly used including:

- Vacuum bagging
- Inflated bladders
- Mechanical clamps
- Dead weights

In the vacuum bag method (see Figure 24.12) a conformable heat-resistant plastic membrane is located over the repair area and the air within the sealed region is evacuated. Atmospheric pressure acting on the outside of the plastic and on the back face of the structure will apply pressure over the repair. Vacuum bagging has the advantages of simplicity, flexibility of application, the ability to conform to

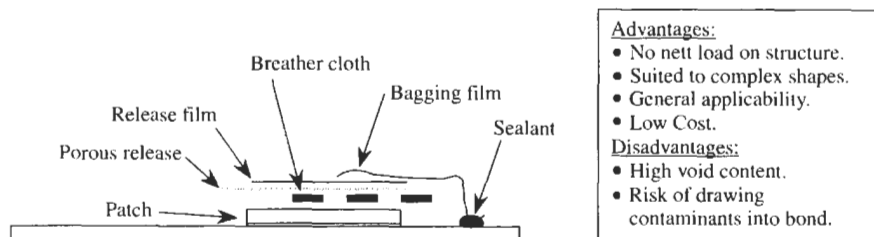


Fig. 24.12. The vacuum bag method for pressurisation of repairs.

complex shapes and the process does not cause distortion because there is no net load on the structure. A major disadvantage of the process is that the low pressure enhances the release of volatiles and where volatile gasses are trapped, the low pressure increases their volume. This causes a significantly higher void content than would occur under positive pressure. Current RAAF practice is to apply maximum vacuum to a repair during the heat-up phase so that as many volatiles are drawn out as possible. When the lowest cure temperature for the adhesive is achieved (see Figure 24.9) the vacuum is backed off to 250 mm Hg. This causes a reduction in the size of trapped volatiles.

The inflated bladder method (see Figure 24.13) of pressurisation has much of the flexibility of the vacuum bag method with the added advantage of the use of positive pressure to reduce the void content in resins and adhesives. In this pressurisation method, a flexible bladder that is in contact with the repair area is attached to a rigid plate which in turn is held in place by a clamping device to hold the assembly against the surface to be repaired. The space between the bladder and the rigid plate is pressurised using compressed air. This forces the bladder against the repair surface and provides the pressure required for repair installation. A major limitation in the inflated bladder method is that the system will produce a net load on the structure, and care is required to avoid damage by overloading the region. The system also requires some clamping method to react out the pressure loads.

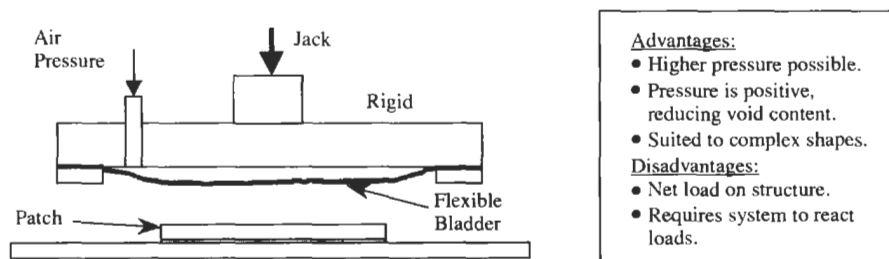


Fig. 24.13. The inflated bladder method for pressurisation of repairs.

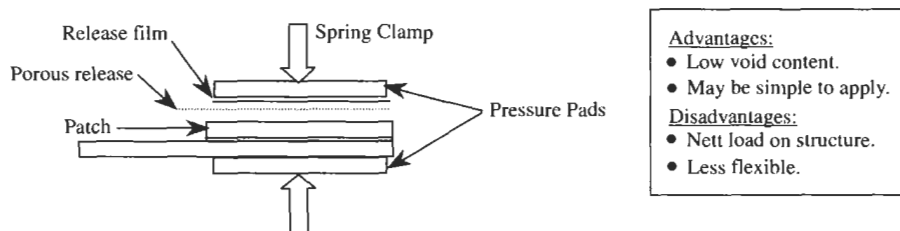


Fig. 24.14. Mechanical clamping methods for pressure application.

Mechanical clamping, (see Figure 24.14) may be an effective method for pressure application during repair. The method of clamping will depend upon the geometry of the structure surrounding the repair. If access to both the front and back faces is possible, a simple “C-clamp” may suffice. In other cases, the ability to react loads from an adjacent piece of structure (or even a hangar floor) will enable the use of hydraulic or screw jacks. This method of pressurisation is not as flexible as the vacuum bagging or inflated bladder methods, because some form of pressure distribution plate will be required. Care must be exercised to avoid local over-pressurisation of the region directly under the clamp. This can be verified by performing a flow check before applying the repair. (A piece of adhesive is sandwiched between thin Teflon film and cured in the same manner as is proposed for the repair. Examination of the cured adhesive will show regions of deficient pressurisation.) Care is also required to avoid damage to the structure from the pressure loads.

Dead weights are usually inappropriate for structural repairs, particularly where film adhesives are used. Typical film adhesives require high pressures, and even the use of vacuum bagging is a compromise. A simple calculation of the weight required to produce 110 kPa (~15 psi) over a bond area would show that the load required would be impossible to attain by the use of weights. For high temperature repairs, the thermal mass of the weights will also cause significant problems in achieving the correct cure conditions. The use of dead weights for pressure application is only appropriate where contact pressure is sufficient for the adhesive being used.

24.3. Occupational health and safety (OHS)

Occupational health and safety (OHS) is a primary concern in modern employment systems. Gone are the days where the repair manual instructed “Continue to dry solvent (insert carcinogen name here) until the odour disappears”. Safe work practices dictate that every hazardous material is identified and all staff should have for their perusal all material safety data sheets (MSDS) for any product they encounter. The MSDS details the hazards, exposure limits, personal protective equipment (PPE) and methods for hazard management.

In many cases, materials used for adhesive bonding do present hazards when not correctly used or stored. While protection of workers from hazards is a primary consideration in process selection, the engineering requirements for effective bonding practices must not be compromised by actions taken to provide protection. The classic example of conflict between engineering and OHS is the provision of protective hand creams to prevent dermatitis from contact with solvents and resin systems. Many such creams contain silicone products, lanolin or other fatty materials, all of which are release agents and therefore are totally incompatible with the requirements for adhesive bonding. Care must therefore be exercised in the provision of such materials for personnel working in bonding processes.

24.3.1. Solvents

The most common hazardous exposure for bonding technicians comes from the requirement to use significant amounts of solvents for surface preparation. Exposure risks are from respiratory or dermal contact. Appropriate mechanical exhausting and/or breathing protection can reduce respiratory exposure to well within acceptable limits. The type of solvent also is significant in management of risks. The solvent type used for hand wiping processes should have a rapid evaporation rate. Materials that evaporate slowly will permit spreading of contamination. The RAAF currently relies almost exclusively on methyl ethyl ketone (MEK), also known as Ethyl Methyl Ketone and Butanone. While many consider MEK to be a risky material because of the chance of reduced liver function, the material may be considerably safer than alternative materials [33] because of the ease of recognition of the odour. A worker can easily recognise the product and take corrective measures by replacing respirator cartridges or adjusting the fit of masks. Many other solvents tend to cause a reducing response to detection with exposure, and may risk excessive exposure before the operator recognises the risk.

Management of dermal contact is more intractable because of contact with hands during solvent wiping processes. Although most MSDS data suggests that butyl rubber gloves should be used, they are expensive and must be re-used to minimise cost. Repeated use of gloves for surface preparation represents a significant risk of cross-contamination between tasks. The RAAF currently uses surgical gloves in combination with a strict policy of changing gloves after every five minutes exposure to MEK. Tests undertaken for the RAAF [34] have shown that, even though MEK break-through occurs in a short time after immersion, the total body load by dermal contact from ten minutes complete immersion in MEK is less than 0.3% of the permitted body load due to respiratory exposure at the Time Weighted Average exposure limit. Note that disposable “inspection” gloves should not be used because the rubber is considerably thinner and provides negligible protection.

24.3.2. Grit

As discussed in *Surface Preparation*, light grit blasting with aluminium oxide is the most effective method for exposure of a fresh chemically active surface during preparation for bonding. Experience in the RAAF has shown that grit breaks down into particles about 5 microns diameter and about 30 microns long. These represent a threat to fuels systems because the particles can pass through fuel filters and have caused several cases of in-flight engine failures. Grit must be contained and extracted away from the aircraft. Also of concern, the small particle size is of concern for deep lung contamination. However, some evidence does exist, as reported in the material safety data sheet (MSDS) for aluminium oxide, which suggests that mice exposed to even finer aluminium oxide dust did not display symptoms of lung disorders usually associated with deeper lung penetration by fine fibres. The MSDS does note a reduction in liver function after exposure to the material.

24.3.3. Fibres

Repairs to composite structures usually involve machining or sanding to remove damaged material. The dust produced may present a respirable particulate hazard. However, it must be noted that the size of all common composite fibres is larger than the 5 microns usually associated with deeper lung penetration believed to cause asbestosis. Breathing protection should always be used for operations that produce respirable dust.

The major risk when handling composite materials is skin penetration by fibres or bundles of fibres. Boron fibres present a significant threat because of the large fibre diameter, high stiffness and extreme hardness. Splinters of composite fibres should not be squeezed or rubbed because the fibres may break up, making complete removal difficult. Removal can be aided by use of a low power microscope.

24.3.4. Risks to aircraft

Many operations undertaken during repair installation can present a hazardous condition with risks of damage to the aircraft being repaired (see Table 24.2).

24.4. Quality management

Common practice in many adhesive-bonding shops is to rely on post-production NDI to assess the integrity of the bond. This may be coupled with companion specimens that are tested for quality assurance. While these tests and inspections will eliminate bonds with obvious defects, they do not provide a positive assurance of bond integrity. If a bond passes a NDI it simply means that the test method used could not detect any flaws with an air gap larger than the given threshold value for

Table 24.2

Repair procedures with the risks of possible damage to the aircraft.

Process	Possible impact on Systems
Damage removal	Further impact damage by tool drop. Dust, swarf contamination of hydraulics, fuel or electrical systems.
Surface preparation	Corrosion if acidic etchants and anodising materials are used. Contamination of bearings, fuel systems and electronics by grit and dust. Solvent degradation of plastics, paints. Chemically induced hydrogen embrittlement or stress corrosion cracking.
Heating	Fire. Melting of plastics, metallurgical damage to metals, overheating hydraulic oils, sealants and paints. Sandwich panel disbonding and composite panel delamination. Damage to electrical wire and electronic equipment. Thermal distortion of panel.
Pressurisation	Distortion of structure.
Inspection	Contamination by ultrasonic coupling materials.

the NDI. A deficient surface preparation will not necessarily result in an air gap, and therefore the test is not conclusive evidence that the process has produced a durable bond. Similarly, there is no NDI method that will measure the degree of cure of an adhesive. Lap-shear and peel tests on companion coupons should detect ineffective adhesive cure and, to a limited extent, poor surface preparation but, as discussed before, strength tests do not indicate a durable bond has been formed.

Because quality assurance is not valid for adhesive bonding, quality must be derived from quality management. In other words, it is far better to correctly manage a process to produce a valid outcome than to test a poorly performed process to see if it achieved nominal acceptance criteria. Adhesive bonding is what is termed a “Special Process”, one where there is no post-event method for measurement of the success of the process. Such processes should be controlled by certification of compliance with approved and validated process specifications. While most bonding shops use a method of certification of compliance with process specifications, it is usually the validation of those processes that is deficient. Further, the process tracking method often only requires one signature at the end of a few sub-steps, those usually being steps that could be verified by quality control. Adhesive bonding is so process-sensitive that compliance must be demonstrated at even minor process steps and any material or process changes must be strictly validated. Care is required to ensure that process specifications exactly match the process that has been validated.

Certain aspects of bonding processes can have dramatic effects on bond integrity. One example is the quality of film adhesives at the time of usage. Testing is usually required to certify acceptance of new materials. Material which is out of shelf life or which has been packaged, stored or handled incorrectly can lead to defective bonds

that are difficult to detect. Film adhesives (which are usually stored and transported frozen) must be packed in heat sealed packaging and must only be opened after the entire package has reached room temperature. Packaging must be free of tears and damage which allows exposure of the adhesive to atmospheric moisture. Adsorbed moisture will boil off during elevated temperature cure, resulting in a high void content in the adhesive layer. Sealing of packaging by adhesive tapes or the use of self-sealing plastic bags is not acceptable because even a minor air leak in the packaging will result in moisture contamination of the adhesive.

24.5. Facilities

RAAF STD ENG C5033 indicates that a bonded repair facility should have three separate areas for performance of adhesive bonded repairs:

- An open work-space for damage removal, inspection, hot bonding, moisture evacuation and fabrication of metallic repair patches.
- An enclosed room with controlled environment for surface preparation.
- An enclosed room with controlled environment for composite fabrication and application of adhesives and vacuum bagging.

Film adhesives must be handled in controlled environments (see Figure 24.15) where the humidity levels are within limits because epoxy film adhesives absorb atmospheric moisture that boils off during elevated temperature cure, forming micro-voids. Exposure of FM300 adhesive to 30 °C for 1 h can result in over 60% void content in adhesive bonds, with a subsequent reduction of peel and shear strength of approximately 50% [18].

Measures must be undertaken to exclude contaminants from the enclosed rooms. Dust and other air borne particulates may be excluded by operating the air conditioning system to provide a higher pressure in the enclosed rooms. Air locks should also be used. To minimise the chance of contamination and to reduce the health risks, consumption of foods and beverages should be prohibited within the area. Access to the area should be restricted to essential personnel only.

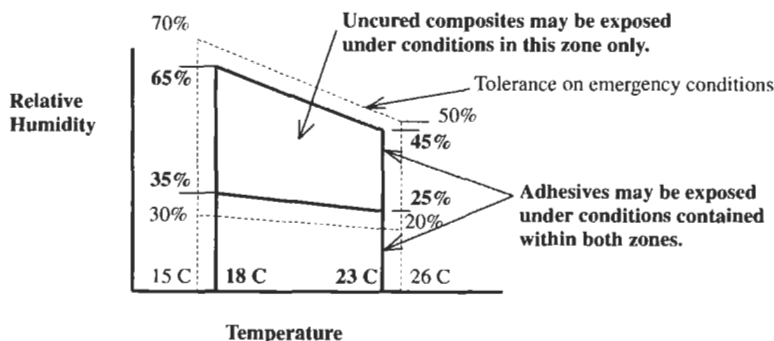


Fig. 24.15. Humidity and temperature requirements for adhesive bonding.

24.6. Training and certification

Because adhesive bonded repairs are so strongly dependent on processes, it is important that technicians who perform repairs are well trained and can regularly demonstrate competency. In this respect, a clear delineation must be made between “composites” training and training in adhesive bonding to eliminate a common error in training specifications. The ability to laminate a composite does not have any relevance to competency in surface preparation of a metallic surface for bonding. Similarly, extensive experience in performance of bad practices in a “bonding shop” is not of itself an appropriate qualification for performance of processes to produce durable bonds.

To ensure competency in adhesive bonding the RAAF has developed its own competency based training at three levels, with courses for technicians, supervisors and design engineers. A competency standard has also been developed to qualify technicians and that standard is to be assessed annually to assure continuing competence of technicians.

24.7. Deficient repair concepts

There are a number of common accepted practices in adhesive bonding that can not be justified on the basis of a reasoned consideration of the basic principles outlined above. This chapter would not be complete without addressing a few of those practices that have contributed to the poor acceptance of adhesive bonding. The simplest deficient practice in adhesive bonding is to believe that surface preparation is required for strength, and, by corollary, a lightly loaded structure does not require surface preparation because the bond will only experience very low loads. There are a number of examples of this policy that have resulted in total disbond and corrosion damage where moisture has been trapped between the disbanded surfaces.

There are also a number of commonly practiced “repair” methods which are performed on a regular basis on both civil and military aircraft, which have no chance of success, and which in most cases lead to an early onset of further damage to the component. The most common deficient repair practice is the use of injection repairs, where liquid adhesive is forced under pressure into adhesive bond defects with the intention of re-bonding regions where disbonds have occurred. This practice has been used on bonded joints as well as sandwich panels [4,11,35]. If one accepts the basic principle that a bond requires a chemically active surface on which to bond, injection repair methods are doomed to failure. Because no surface preparation is possible, the surface will not be active, and in many cases is usually contaminated with aircraft fluids or environmental moisture.

There are in reality only two positive outcomes from injection repair of adhesive bonds. Firstly, the air gap is filled to the extent that the NDI technician can no longer find the defect, and secondly, the repair technician is contented because he has complied with the repair instruction. A large number of negative outcomes

from injection repairs can be identified. Restoration of strength is not achieved so a defective component is returned to service with an unjustified airworthy rating. The injected adhesive bond in the component almost always fails again. (See the repeated injection repairs in Figure 24.5, where there were at least nine attempts to repair the panel by injection of adhesive.)

A longer term result of injection repairs is that they provide a moisture entry path, which may lead to corrosion of the component. This is particularly the case with honeycomb sandwich panels. Corrosion is caused by entrapment of moisture that diffuses slowly through epoxy adhesives. Injection repairs give the moisture the shortest possible diffusion path; through the thickness of the adherends. Unfortunately, the component is usually withdrawn from service because of corrosion, rather than correctly attributing the failure to the previous repair. The bulk of RAAF maintenance of adhesive bonded structures on F-111 can be traced directly to previous injection repairs. This author would welcome any data that demonstrates that injection for repair of adhesive bonds is a valid repair method.

In a recent survey of seven defect reports conducted at one RAAF base, not one injection repair had actually rebonded the defect to be repaired. In two cases where a repair had been attempted in a metal-to-metal bond, the injection holes had missed the disbond, and no adhesive had flowed into the gap at all. Another four injection repairs had been attempted into sandwich structure. The panel had been made using two layers of adhesive and a void existed where the lower adhesive layer had sagged away from the other layer. All of the injection holes passed through the skin and both layers of adhesive and the adhesive had been injected into the core cavity. No adhesive flowed into the void being repaired. In the final example, an injection was successful in getting adhesive to flow into a disbanded metal-to-metal joint. However, even though there had been intimate contact between the adhesive and both surfaces, the adhesive had failed to re-bond the surfaces together. In three cases, there was evidence of the initiation of corrosion.

Another ineffective form of repair commonly known as potted repairs involves removal of damaged skin and core in a sandwich panel and filling the cavity with an epoxy filler. The filled cavity is smoothed to match the contour of the panel to complete the repair. Clearly, this is not a structural repair because no patch is bonded over the area. Invariably, these repairs directly cause corrosion of surrounding core because of moisture absorption into the epoxy material. Approximately 40% of repair effort currently expended by the RAAF in support of sandwich structure on F-111 involves repair of previous injection and potted repairs. The RAAF has now prohibited injection repairs.

One other common problem experienced in aircraft repairs is the insistence by some authorities on the use of mechanical fasteners in bonded joints or repairs. The fasteners contribute little to bond strength, because the load transfer lengths for the bond are usually less than the minimum edge distances for the fasteners, and therefore almost all load is transferred by the bond before the fastener can pick up any load. Fasteners provide moisture paths for degradation of the bond, and also provide fatigue initiation sites. They also reduce the effectiveness of NDI of the bond. The use of rivets in sandwich panel repairs is a major cause of corrosion

damage, even when the fasteners are installed wet with sealant. Further, if a crack develops at a fastener in an adhesive bond, it tends not to grow along the fastener line as commonly occurs in fastened joints, but will grow into the adjacent structure due to the higher stiffness of the reinforced joint area [36].

24.8. Conclusion

This chapter has addressed a number of basic principles for adhesive bonding and repairs and given examples of the consequences of failure to observe those principles. Adhesive bonds require only minimal design to achieve substantial strengths, but require meticulous attention to detail in process selection, validation, specification and performance. Poor practices and processes can produce strong bonds that will pass testing requirements if tested immediately after bonding. However, only well prepared and performed processes can produce durable, long lasting adhesive bonds. From this, it is concluded that any test program for certification of a bonded structure must also address certification of the bonding processes used to form the structure. Certification of structures on the basis of static and fatigue tests alone (without consideration of certification of the bonding processes) will approve those that pass structural requirements but which will have a real chance of structural failure within a relatively short period of service due to lack of structural durability. These points have been included in a proposed methodology for certification of adhesive bonded structures and repairs that is based on comparisons between the potential load capacity for the adhesive and the structural load requirements for the design [37,38].

References

1. Davis, M.J. and Bond, D.A. (1999). Principles and practices of adhesive bonded structural joints and repairs. *Int. J. Adhesion*, **19**(2–3), pp. 91–105.
2. Hart-Smith, L.J. (1995). An Engineer's Viewpoint on Design and Analysis of Aircraft structural Joints. Mc Donnell Douglas Paper MDC 91K 0067, also published in *Proc. Inst. Mech. Engrs., Part G, J. of Aerospace Engineering*, **209**, pp. 226–238.
3. Baker, A.A. (1999). Certification of bonded composite patch repairs for cracked metallic primary aircraft structures. *Proc. of the 20th Symposium of the International Committee on Aeronautical Fatigue (ICAF)*, Seattle, USA, July.
4. Davis, M.J. (1995). A call for minimum standards in design and application technology for bonded structural repairs. *Proc. Symp. on Composite Repair of Aircraft Structures*, pp. 4-1, 4-15, Vancouver, August.
5. Davis, M.J. (1997). Deficiencies in regulations for certification and continuing airworthiness of bonded structure. *Int. Aerospace Congress*, Sydney 25–28 February.
6. Davis, M.J. and Bond, D.A. (1999). Towards a Certification Standard for Adhesive Bonded Structures and Repairs, The Symposium of the International Committee on Aircraft Fatigue ICAF-99, Seattle, 12–16 July.
7. Kerr, A. (1998). Certification of Bonded Repairs. The Aging Aircraft Conference, Williamsburg, VA, 30 August, 02 September.

8. Hart-Smith, L.J. (1985). The Design of Repairable Advanced Composite Structures, Douglas Paper 7550, presented to SAE Aerospace Tech. Conf. Long Beach CA., 14–17 October.
9. Davis, M.J. and Bond, D.A. (1999). The importance of failure mode identification in adhesive bonded aircraft structures and repairs. *The International Conference on Composite Materials* – 12, Paris, 05–09 July.
10. Kinlock, A.J. (1987). Adhesion and Adhesives, p 78, Chapman and Hall.
11. Davis, M.J. (1996). The role of materials and processes in defective bonded structural repairs. *Proc. 41st Int. SAMPE Symp. and Exhib.*, pp. 936–950, Anaheim, March.
12. Olsson-Jacques, C. Rider, A. and Arnott, D. (1995). The influence of pre-bond MEK exposure on bond durability. *Proc. Int. Aerospace Congress, PICAST 2-AAC 6*, pp. 599–604, Melbourne, 20–23 March.
13. Bell Helicopter Textron Product Support, Kiowa Roof Shell Repair 92RL-132 dated 23 December 1992.
14. Wegman, R.F. and Tullos, T.R. (1992). Handbook of Adhesive Bonded Structural Repairs, p. 119, pp. 136–137, p. 147, Noyes Publications.
15. NAP 7210.024-2-015 B3 (Sikorsky Seahawk Repair Manual).
16. Wilson, A., Kindermann, M. and Arnott, D. (1995). Void development in an epoxy film adhesive during vacuum bag cure. *Proc. Int. Aerospace Congress, PICAST 2-AAC 6*, pp. 625–630, Melbourne, 20–23 March.
17. Perl, D. R. (1994). Evaluation of Damage to F/A-18 Advanced Composite Honeycomb Sandwich Parts Caused by Elevated Temperature Cure Cycles, 39th Int. SAMPE Symp. and Exhibition, April.
18. Arnott, D. Pearce, P., Wilson, A., et al. (1995). The effect on mechanical properties of void formation during vacuum bag processing of epoxy film adhesives. *Proc. Int. Aerospace Congress, PICAST 2-AAC 6*, pp. 811–816, Melbourne 20–23 March.
19. Hart-Smith, L.J., Redmond, G. and DAVIS, M.J. (1996). The curse of the nylon peel ply. *41st Int SAMPE Symp. and Exhib.*, Anaheim 25–28 March.
20. Askins, B. (1993). Surface preparation using the phosphoric acid containment system (PACS). *Proc. 3rd. Int. Wkshp. on Composite Repair of Metallic Aircraft Structures*, Ottawa, 14–15 September.
21. Baker, A.A. (1988). Crack Patching: Experimental Studies, Practical Applications, Bonded Repair of Aircraft Structures, (A.A. Baker, R. Jones, eds.). Martinus Nijhoff.
22. Arnott, D.R., Wilson, A.R., Rider, A.N., et al. (1997). Research Underpinning the Adherend Surface Preparation Aspects of the RAAF Engineering Standard C5033, *Int. Aerospace Congress*, Sydney 25–28 February.
23. Boeing Document No. D650-10101-1, May (1990).
24. Askins, B. (1993). Surface preparation using the phosphoric acid containment system (PACS). *Proc. 3rd. Int. Wkshp. on Composite Repair of Metallic Aircraft Structures*, Ottawa, 14–15 September.
25. Kuhbander, R.J. and Mazza, J.J. (1993). Understanding the Australian silane surface treatment. *38th Int. Symp. and Exhib. SAMPE*, Anaheim.
26. Roach, D. (1995). Performance and analysis of bonded composite doublers on aircraft structures, *Proc. Symp. on Composite Repair of Aircraft Structures*, pp. 4-1, 4-15, Vancouver, August.
27. Arnott, D.R., Wilson, A.R., Rider, A.N., et al. (1997). Research underpinning the adherend surface preparation aspects of the RAAF engineering standard C5033. *Proc. Int. Aerospace Congress*, Sydney 24–27 February pp. 27–40.
28. Baker, A.A. (1994). Bonded composite repair of metallic aircraft components – overview of Australian activities. *AGARD Conference Proceedings 550, Composite Repair of Military Aircraft Structures*, Seville, 3–5 October.
29. Pitrone, L.R. and Brown, S.R. (1988). Environmental Durability of Adhesively Bonded Joints, Adhesively Bonded Joints; Testing, Analysis and Design, ASTM STP 981. W.S. Johnson, Ed., ASTM, Philadelphia, pp. 289–303.
30. RAAF Engineering Standard C5033, Logistics Systems Agency, Royal Australian Air Force, September. (1995).

31. Arnott, D.R. and Kindermann, M.R. (1989). A Constant Displacement Rate Test to Estimate the Durability of Adhesive Bonds Formed Between 2024 Aluminium Alloy Sheet Adherends. The Australian Aeronautical Conference 1989, Melbourne October.
32. Davis, M.J. and Bond, D.A. (1999). The Importance of Failure Mode Identification in Adhesive Bonded Structures and Repairs, *Proc. ICCM 12*, Paris 5–9 July.
33. Safe Handling of Advanced Composite Materials, (1991). 2nd Edition, Suppliers of Advanced Composite Materials Association, Arlington VA, July.
34. Evaluation of Gloves for use with Methyl Ethyl Ketone for the Aeronautical and Maritime Research Laboratory, Australian Government Analytical Laboratories, October (1994).
35. F/A-18 Structural Repair Manual SRM 250.
36. Hart-Smith, L.J. (1981). Effects of Flaws and Porosity on Strength of Adhesive-Bonded Joints, Douglas Aircraft Company Report MDC J4699, November.
37. Davis, M.J. and Bond, D.A. (1999). Towards a Certification Methodology for Adhesively Bonded Structures and Repairs, presented at ICAF 99, Seattle, 10–16 July.
38. Davis, M.J. (2000). Certification of Adhesive Bonds for Construction and Repair, Aging Aircraft Conference 2000, St. Louis MO, 15–18 May.

Chapter 25

RAPID APPLICATION TECHNOLOGY: AIRCRAFT BATTLE DAMAGE REPAIRS

R. BARTHOLOMEUSZ, P. PEARCE* and R. VODICKA

Defence Science and Technology Organisation, Air Vehicles Division, Fishermans Bend, Victoria 3207, Australia

25.1. Introduction

During times of conflict rapid repairs are required to keep aircraft operational with a useful level of mission capability, or to return them safely to a depot for major maintenance if acceptable mission capability cannot be restored. This technology, known as Aircraft Battle Damage Repair (ABDR), maximises aircraft availability so can prove to be a decisive factor in times of conflict. During peacetime the technology is also relevant as aircraft can sustain damage at remote locations where full depot facilities are unavailable. In such cases, there is a requirement to perform temporary repairs with minimum equipment so that the aircraft can be flown back to a depot.

Essentially ABDR must restore the aircraft to as near original design static strength and capability that the time, equipment and personnel constraints imposed by the operational situation allow. Battle damage repairs are undertaken at forward operational bases or under field conditions without access to full workshop facilities. At present conventional ABDR is based on the use of metallic, mechanically fastened patches. However, since such repairs require the introduction of many new fastener holes the component is made more difficult to repair permanently later and may need to be replaced. Bonded composite repairs, in contrast, do not damage the component, since fastener holes are not required and, unlike metallic repairs, composites are highly formable so can readily be applied to complex contours.

This chapter describes the development of a battle damage repair approach based on adhesive bonding combined with high-performance composite reinforcement developed at the Defence Science Technology Organisation (DSTO). Techniques for the repair of thin-skinned metallic aircraft structure with simulated battle damage were investigated. Early practical applications demonstrated the

effectiveness of such field bonded-repair schemes. Lightning damage to the fuselage of a Royal Australian Air Force (RAAF) Lockheed P3-C Orion aircraft was successfully repaired using carbon-epoxy composite patches formed and cured on the damaged fuselage skin and subsequently bonded on with an epoxy adhesive [1]. Although applied as temporary repairs, these patches survived over 20 years before being deliberately removed to check durability.

Most of the early work at DSTO was focused on the testing of commercially available composite laminating resins and adhesives. It was quickly apparent that the resin or adhesive determined the processing speed and flexibility of bonded-composite battle-damage repair. A resin system that cures quickly, at low temperatures and is capable of bonding to surfaces with only minimum surface preparation reduces application time and complexity.

This early work also showed that many commercially available resin systems were unsuitable for ABDR and thus a proprietary in-house resin system was developed by DSTO. This in-house resin system provided excellent adhesive and composite properties as well as providing a wide range of processing options. As part of the work, traditional pre-bond surface treatment procedures were modified in order to be less time consuming and simpler to implement under field conditions. Application techniques designed to save time during repair were also devised and evaluated. The final ABDR system was found to meet all criteria and demonstrated excellent performance when compared to traditional mechanically fastened metallic repairs on representative specimens.

25.2. Aircraft battle damage repair

25.2.1. Battle damage

During operational missions aircraft are prone to a range of damage, many of which do not result in catastrophic failure. This can include ground fire (Figure 25.1), missile strike, foreign object damage, shrapnel and component degradation induced by excessive “g” manoeuvres. In most cases damage can be classed into four main categories [2]:

1. Projectile damage – leading to holes, section loss, spalls, gouges, cracking, tearing of thin skins and deformation.
2. Blast and overpressure damage – that can cause structures to buckle, cripple, misalign and lead to the separation of joints and deformation.
3. Fire damage – prolonged heating can weaken materials (particularly aluminium alloys) and high temperatures can cause them to melt and burn.
4. Secondary damage – caused by serviceable structure being overloaded and damaged as the aircraft exceeds its allowable flight envelope. This may result in cracks, crippling or buckling.

During wartime, fatigue and corrosion are also of concern and ABDR may be used as a short term solution for these problems.

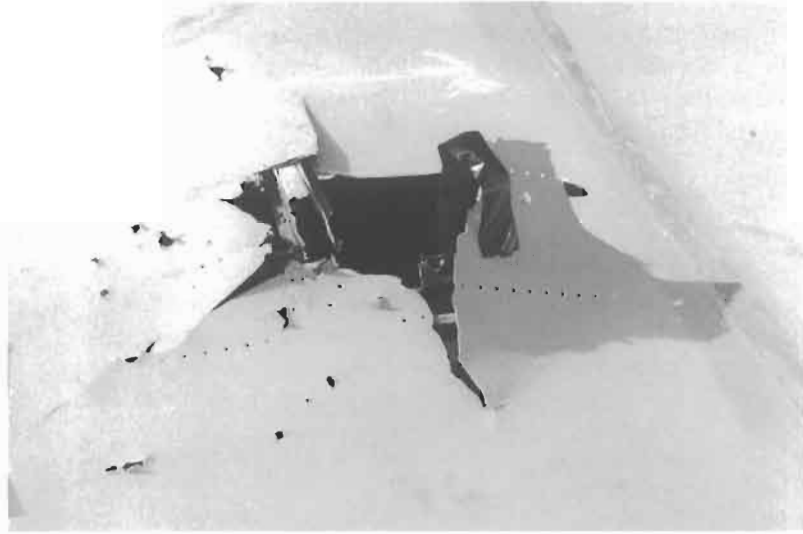


Fig. 25.1. Battle damage in a Lockheed Hercules C130 aircraft caused by penetration of a high explosive impact projectile. The total area of damage is approximately 1 m in diameter.

25.2.2. *ABDR criteria*

The primary aim of ABDR is to restore damaged aircraft to a minimum level of operational readiness in the shortest possible time with the minimum of equipment, personnel and facilities [2].

Thus, the main difference between peacetime repair methods and ABDR is the need to restore quickly the aircraft to an operational status. This usually means simplification of peacetime repair techniques and the reduction or removal of the fatigue requirement for the repair primarily achieves this. Normally a peacetime repair is required to have the same fatigue life as that of the aircraft. However, the US Airforce require ABDR to have a fatigue life of only 100 h [3] and this means that the repair process may be simplified considerably and therefore save time. Considering this, the main requirements for successful ABDR are:

1. Restoration of the ultimate load capability for an operating life of around 100 h. This means that the repair is designed for static strength and fatigue or environmental durability of the repair is relatively unimportant.
2. Rapid repair techniques are required to restore the aircraft to operational availability quickly.
3. The repair technique must be simple, as it must be possible to implement at a forward operational base or in the field with the minimum of equipment and personnel.
4. The repair must be able to be designed using very simple analytical tools, charts or a simple personal computer application.
5. Materials used in the repair must have long storage lives at room temperature.

6. All repair equipment and materials must be easily transportable to the repair site. If possible, the repairs should be packaged in kit form for ease of use.
7. ABDR is considered a temporary repair that must cause minimum further damage to the structure and be able to be removed easily so that a permanent depot-level repair can be undertaken later.

25.2.3. Types of ABDR

ABDR for airframes is currently mainly based on mechanical fasteners and metallic patches (Figure 25.2). The advantages of this approach are:

1. Only simple tools and low technical skill levels are required.
2. Repairs can be made to internal as well as external structure.
3. Materials for the repairs are easy to store and have unlimited shelf lives.

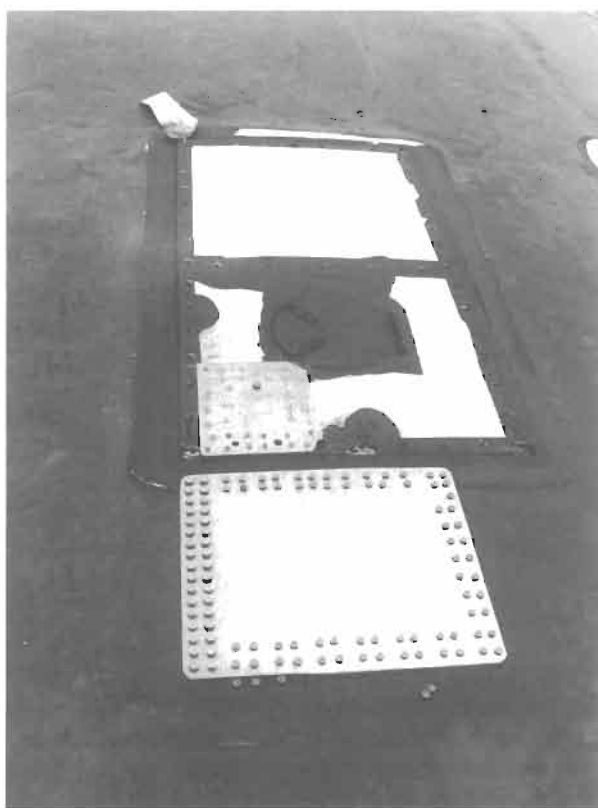


Fig. 25.2. A mechanical repair applied to damage on a Lockheed Hercules C130 wing skin caused by a high explosive impact round typical of ground fire.

The disadvantages of the approach are:

1. A large number of new fastener holes are required, which considerably enlarge the size of the damaged region.
2. Repairs to highly contoured surfaces may not be possible in the field.
3. Repair efficiency is often relatively low because of poor load transfer from the damaged structure.

The use of adhesive bonding with metallic patches overcomes some of these problems but is still limited to repair of structure with simple contours. The use of composite patches removes this limitation and additionally composites have the advantages of high strength and stiffness combined with low weight.

The major drawbacks with adhesive bonding are the need for rapid and effective surface pre-bonding treatments for the metal or composite skin (although with a suitable adhesive this could be limited to paint removal) and the need for new skills and techniques to be learnt.

25.3. Comparison of metallic mechanically fastened repairs to bonded composite repairs for ABDR

To demonstrate the effectiveness of bonded composite repairs, an experimental program was undertaken to compare the performance of traditional mechanically fastened, metallic ABDR to a bonded-composite battle damage repair as developed at DTSSO. The two techniques were compared by tests including static strength and fatigue durability. The tests were carried out on 7075-T6 aluminium alloy panels, provided by the United States Air Force (USAF) as part of a collaborative program, representative of thin-skinned metallic aircraft fuselage (see Figure 25.3).

The composite repairs were formed by wet lay-up of dry carbon fibre with resin followed by cure under a vacuum bag as described below. The metallic, mechanically fastened repairs were applied by USAF tradesmen using standard ABDR techniques [3].

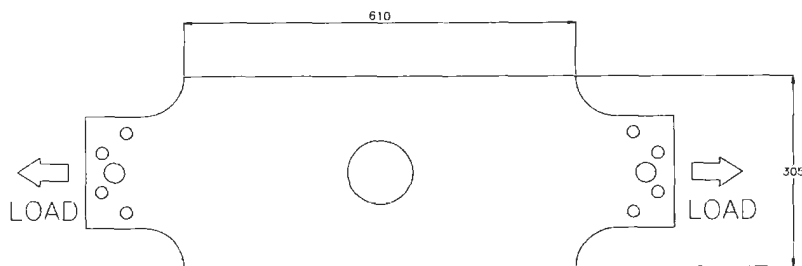


Fig. 25.3. Representative specimen used for comparative testing of ABDR. The central hole, diameter 102 millimetres, was representative of the battle damage. All dimensions in millimetres.

25.3.1. Adaptation of bonded composite repairs for battle damage

Current bonded composite repairs rely on materials and application techniques that require [5]:

1. Storage in a freezer and thus have very limited shelf life at room temperature. These include pre-preg composite tapes and elevated temperature curing film adhesives.
2. Materials that cure at high temperatures and pressures and thus often require the use of an autoclave or temperature controlled mechanical press to form the composite or the adhesive bond.
3. Rigorous pre-bonding surface-treatment techniques to ensure bond strength and durability.
4. High levels of operator skill and adherence to strict quality control for the design and application of the repair.

In order to utilise bonded composite repairs for ABDR we require:

1. Materials that have a long shelf life at room temperature, such as two-part resin systems with dry carbon, glass or boron fibres to manufacture the composite and form the bond.
2. The use of minimum pre-bonding surface-treatment procedures.
3. Resins that cure at room temperature and can form a composite using vacuum pressure or a roller to consolidate the repair.
4. Simplified methods to quickly design repairs.
5. Ideally a resin system that can be used to form the composite and the adhesive bond simultaneously. This removes a step in the repair manufacturing process and can save a considerable amount of time.

25.3.2. The composite laminating resin and adhesive

Work at DSTO is based on the use of two simplified forming and bonding techniques for composite repairs:

1. Simultaneously forming the adhesive bond and composite repair by placing dry fibre on the damaged surface, applying liquid resin and curing under vacuum pressure at ambient temperature, or
2. Pre-curing the composite repair on the surface by placing dry fibre on a sheet of release film on the damaged surface, applying liquid resin, consolidating under vacuum pressure, at ambient temperature and subsequently bonding the cured composite patch.

A third technique, not described here, is to wet laminate the composite, using a suitable resin, directly onto the damaged surface. The dry fibres are consolidated using a roller and the resin allowed to cure at ambient temperature. This simple approach would produce a rough but effective repair in a very short time using minimum equipment.

All the above techniques are based on a wet lay-up approach. This has the advantage of avoiding storage problems, as the neat resin and hardener can be

stored at ambient temperature for extended periods, and no curing reaction will occur until the components are mixed together. In addition, for ease of use the resins may be packaged into cartridge dispensing units that mix and dispense resins simultaneously.

Three resin systems were trialed for this repair program:

1. A rubber toughened vinyl-ester system, previously employed in a DSTO ship repair program [6].
2. An epoxy laminating resin.
3. An acrylic adhesive.

The vinyl-ester system had the advantage of allowing the simultaneous bonding and forming of the composite repair to the damaged area. The epoxy resin was used to form some of the composite patches and then these were bonded later with the acrylic adhesive. The acrylic adhesive requires minimum surface treatment procedures prior to bonding.

25.3.3. Fibre

Carbon fibres were chosen for the experimental work at DSTO because of their excellent mechanical properties and high drapability. Other available fibres include dry glass fibre or dry boron tape, however, they were discounted because of the relatively low mechanical performance of glass fibre composites and the difficulty of forming stiff boron fibre composites to surfaces with complex curvature. Although boron has a number of advantages it is also very costly compared with carbon.

A high modulus non-crimp uni-directional carbon fibre fabric was used in this experimental program. The cloth is made up of large tows of carbon fibre that are knitted together, rather than woven, by a polyester yarn. The fibres in this cloth are relatively straight (compared with other types of cloth) so it is termed a “non-crimp” fabric.

25.3.4. Simplified design methods for ABDR

The design of bonded joints is based on the determination of the required bond length to transfer load from the damaged structure to the repair or reinforcement. Analytical methods exist for the design of bonded joints [7,8], however, for battle field repair, simplified design methods [9] may be used which provide estimates of overlap length, taper length, repair thickness, repair width, laminate stiffness and strength with a sufficient degree of accuracy. Importantly, use of these approximations will provide conservative results for the design of bonded composite ABDR. The bonded repairs for this program were designed using the analytical techniques described in the RAAF standard for adhesive bonded repairs [8]. These methods can easily be converted into design charts or ideally be programmed into a portable computer.

25.3.5. Surface treatment

For ABDR, only simple surface-preparation techniques can be considered, as the reduction of repair application time is imperative. Ideally, a pre-bonding surface treatment (standard DSTO surface treatment) would include [8,10]:

1. Solvent degreasing and cleaning.
2. Pad abrade.
3. Grit blast with alumina grit.
4. Chemical modification of the metallic surface, such as application of an aqueous solution of epoxy-silane coupling agent.
5. Application of a corrosion inhibiting primer to improve bond strength and durability.

An experimental program was undertaken to simplify the surface treatment procedure for ABDR [4]. The results of this program indicated that for the toughened vinyl-ester resin only the last of the above steps could be omitted without affecting the strength and durability of the adhesive bond. However, for the acrylic adhesive the surface treatment could be limited to solvent degreasing and cleaning, followed by mechanical abrasion (pad abrade or grit blast). For the early laboratory experiments at AMRL it was decided to accept the increased complexity and application time to obtain good bond performance with the above resins. A more rapid application resin and surface treatment system was to be developed under a parallel program, as described later.

25.3.6. Forming the bonded composite patch

The bonded composite repairs were either simultaneously formed and bonded under a vacuum bag using the vinyl-ester resin (Figure 25.4) or pre-cured with the epoxy resin and subsequently bonded with the acrylic adhesive. The average time for application of the repairs was approximately 100 min¹ for both cases, however, both the vinyl-ester and epoxy resins used in this program cured in 24 h at room temperature, which would be considered too slow for ABDR. Increasing the cure

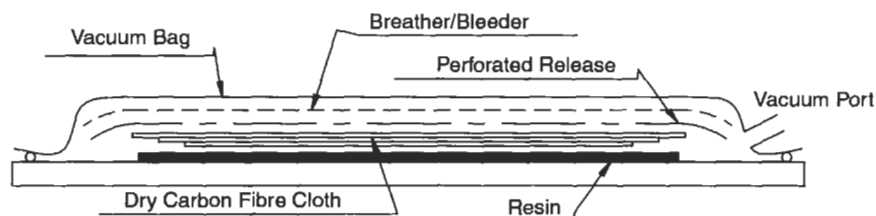


Fig. 25.4. Schematic view of bonded composite repair being formed and bonded to specimen.

¹ This assumes two people working and all materials and equipment ready at hand for the surface treatment and application procedure.

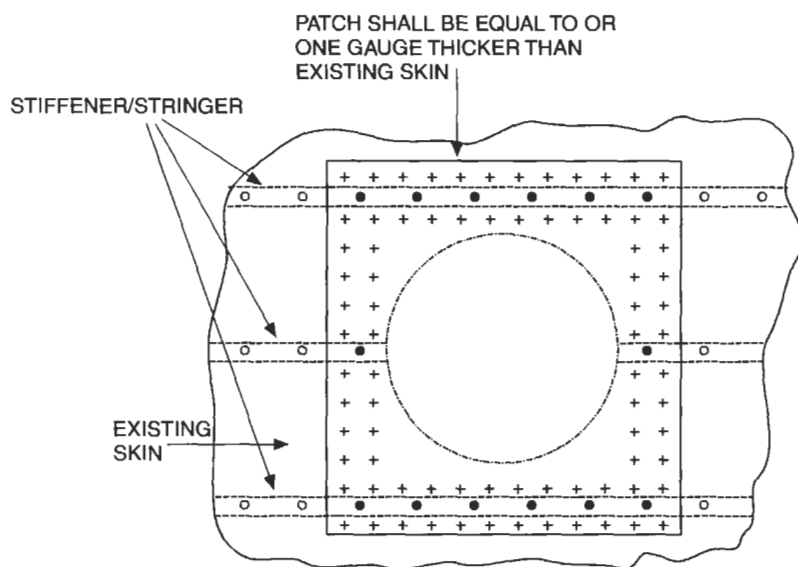


Fig. 25.5. Schematic drawing of mechanically fastened, metallic repair.

temperature of resins and adhesives decreases this cure time. For the epoxy resin it is possible to reduce the cure time to 1 h at 100 °C and at 50 °C the resin cures in 4 h.

25.3.7. Mechanically fastened, metallic repair

The mechanically fastened repairs (Figure 25.5) were 1.6 millimetre thick 7075-T6 aluminium alloy (to match skin stiffness), and the patch measured 178 by 178 millimetres in size. The patch was fastened to the test panel using blind rivets. The USAF tradesmen required only 64 min to apply each repair on average.

25.3.8. Fatigue and static testing of specimens

The specimens were fatigue tested to the equivalent of 100 flight hours based on a RAAF F-111 aircraft loading spectrum, then loaded in compression to 80% of design limit load (DLL) and finally in tension to design ultimate load (DUL) or failure. In this case, 150% of DLL was equal to DUL and DUL was equal to 503 MPa, the material ultimate strength of the 7075-T6 aluminium alloy. The results of the test program are shown in Table 25.1.

25.3.9. Comparison of test results

The mechanically fastened metallic repair required only 64 min to apply and withstood both the applied fatigue loading and the static compression test.

Table 25.1

The results of the static compression and tension tests for representative ABDR.

Specimen	Average compression test %DLL	Average tensile test %DLL	Notes
No-damage, no-repair	80	130	Premature failure at deep scratch in panel
Damaged, no-repair	Not tested	107	Panel failed through central hole.
Metallic, mechanically fastened repair	80	136	Failure at first row of rivets in patch
Vinyl-ester bonded-composite repair	80	118	Adhesive bondline failure.
Epoxy/acrylic bonded-composite repair	80	150	Repair withstood DUL.

However, during the static tensile test to DUL the repair failed through the first row of rivets at 130% DLL which is below the 150% required. Visual inspection of the failure showed that some fatigue damage was evident at the rivet holes, which probably caused the premature failure of the specimen.

The vinyl-ester resin system had the advantage of allowing simultaneous forming and bonding of the composite repair. Unfortunately, it was shown that the system was sensitive to surface treatment and application procedures increasing application time and complexity. The repair withstood the fatigue and compressive loading but prematurely failed the tensile test. Inspection of the failure surfaces showed that a combination of voiding and disbonding caused these failures.

The epoxy/acrylic system had the advantage of allowing minimum surface treatment procedures to be employed prior to bonding of the composite. The repair was applied in 100 min, however, at ambient temperature, 24 h was required to fully cure the epoxy resin and with an additional 2 h of cure time for the acrylic adhesive. However, as mentioned earlier the epoxy resin could have been cured in 4 h at 50 °C.

The epoxy/acrylic repairs were the only repairs that withstood the spectrum fatigue loading, static compression and tension tests with no failure or damage to the repair.

In summary, the metallic repairs had the advantage of being simple and quick to apply, however, were unable to withstand the DUL static tensile case. The repair based on the vinyl-ester resin also was unable to withstand the DUL static case. The only repair that was capable of surviving the DUL static case was based on the epoxy-composite patch bonded with the acrylic adhesive. Unfortunately, due to the cure characteristics of the resins used, the application of the repair was somewhat complex and time consuming. It was shown however that the bonded composite repair technique would provide better mechanical performance than a mechanically fastened, metallic repair.

25.4. Development of a bonded composite ABDR system

The requirements for bonded composite ABDR were outlined in Section 3.1. These requirements mainly deal with application speed, ease and flexibility. For bonded composite repairs this is mainly determined by the properties of the adhesive or resin used. Unfortunately, it was found in the early experimental work described above that it was difficult to meet all of these requirements with commercially available adhesives and resin systems. Work was undertaken to develop an in-house resin formulation with the processing flexibility required for ABDR. The resin system was designed to meet the following specification:

1. The resin should be mixed from off-the-shelf components, as synthesis of small batches of specific resins is very expensive and impractical.
2. The resin should perform well at temperatures ranging within the operational envelope of the aircraft.
3. The cured resin should have good shear modulus, fracture toughness and peel strength so that it can be effective in providing high interlaminar and interfacial adhesion.
4. The resin system should have a viscosity range such that over a reasonably wide temperature range it will wet out the composite fibres effectively when either using hand rollers or vacuum bag techniques.
5. The resin should have a wide processing window so that it can be cured from room temperature to 100°C and be post cured if required.
6. A two component (resin and hardener) system is preferred to simplify mixing and increase shelf life.
7. The resin system should be relatively stable, easily stored and not present a significant occupational health and safety hazard.

Early work at DSTO [6] had shown that commercially available composite laminating resins do not possess high fracture toughness or peel strength precluding their use as adhesives. However, for some thermosetting resin systems, a significant improvement in toughness, with minimal change in critical properties, can be achieved by reaction with 5 to 20% of a suitable chemically modified elastomer, usually a carboxyl-terminated butadiene-acrylonitrile (CTBN) rubber. Improvements in fracture toughness have been noted with structural epoxies [11] and vinyl esters [12], but for this study only epoxy resins were considered since the latter resins are less convenient, do not allow minimum surface treatment procedures and have a relatively short shelf life.

An in-house ABDR resin system was developed based on the blending of two off-the-shelf epoxy-laminating resins that were modified by the addition of CTBN elastomer [13]. The two resins were based on:

1. A common difunctional diglycidyl ether of bisphenol A (DGEBA).
2. A higher functionality Novolac system.

Previous work [14] has shown that DGEBA based epoxies are relatively easy to toughen with CTBN elastomer. In contrast, the higher functionality Novolac epoxies, do not respond well to elastomer toughening but have good high temperature properties. The two resins were blended to meet the requirements of

acceptable toughness coupled with elevated temperature properties for ABDR. This meant that the one resin system could be used to laminate the composite, bond it simultaneously to the damaged structure and retain good mechanical properties at elevated temperature.

25.4.1. Resin development

25.4.1.1. Resin blend optimisation

The effect of blending the two resin systems is shown in Table 25.2. Adducts containing 13, 23 and 50% of Novolac resin, all with 10% of elastomer, were produced by simultaneous mixing of all the ingredients followed by addition of a catalyst, heating and stirring. The T-Peel [15], double torsion (DT) Mode I Fracture Toughness [16] and heat deflection temperature (HDT) [17] were measured. There was a small drop in T-Peel strength as the proportion of Novolac was increased. Acceptable properties were found by using a 50% blend of both resins with 10% of elastomer, giving a HDT of 89 °C, T-Peel strength of 53 N/mm and a DT fracture toughness of 384–1567 J/m² if the elastomer is adducted with the Novolac resin. This resin was designated AMORLUX 1310.

25.4.1.2. Viscosity of AMORLUX 1310

The viscosity of the resin in part determines its practical wetting properties and is important for low-pressure composite and bond forming techniques such as wet layup under a vacuum bag. The viscosity of the resin mixture, measured [18] at 15, 20 and 40 °C, was approximately 4500, 1200 and 550 cps respectively. Within this range, fibre and bond surface wetting would not present a problem.

25.4.1.3. Cure of AMORLUX 1310

The cure schedule for the resin was determined at various temperatures. It was found that at a cure temperature of 110 °C full cure was achieved in 45 min. At other cure temperatures, mild post-cure is necessary to ensure adequate cure. Therefore, a combination of cure at moderate temperature followed by post cure between 60 and 80 °C is recommended. If no capability is available to heat the resin the system can be cured at 25 °C in 24 h.

Table 25.2
Properties of toughened epoxy resin blends.

DGEBA Resin (%)	Novolac Resin (%)	Elastomer (%)	T-Peel (N/25.4mm)	DT fracture toughness (J/m ²)	HDT (°C)
87	13	10	64.6	—	74
77	23	10	58.9	—	79
50	50	10	52.9	218–1068	89

25.4.2. Repair durability, strength and surface treatment

The surface treatment of metal adherends prior to bonding largely determines the strength and durability of an adhesive bond. As mentioned earlier, for ABDR only simple surface preparation techniques can be considered, as the reduction of repair application time is imperative. As ABDR is considered temporary, some of the long-term durability of the adhesive bond may be sacrificed in order to save time (ABDR's are temporary and are usually replaced after the conflict or during a major servicing). The durability and bond strength of AMORLUX1310 was investigated through comparing levels of pre-bonding surface treatment for aluminium alloys.

25.4.2.1. Adhesive durability and strength

Both Boeing Wedge Test (BWT) [19] and contoured cantilever beam test (CCBT) [20] specimens were manufactured with the AMORLUX 1310 resin bonded to 2024 T3 aluminium alloy. The adherends were prepared by using the different Levels of surface treatment as described in Table 25.3.

The results of fracture toughness tests are shown in Table 25.4. Level one treatment resulted in low fracture toughness. Examination of the specimens after testing showed adhesive failure. Surface treatment at Levels Two and Three showed progressive improvement in fracture toughness and the failure surfaces were now observed to be cohesive. Note that a large increase in application time was observed if the Level Three surface treatment was used.

Table 25.3

Levels of surface treatment used in test program.

Level	Surface treatment	Time for application*
One	Solvent clean, pad-abrade with solvent and solvent wipe	30 min
Two	Solvent clean, pad-abrade with solvent, solvent wipe and grit blast with alumina grit	60 min
Three	Solvent clean, pad-abrade with solvent, solvent wipe, grit blast with alumina grit, apply aqueous solution of epoxy-silane and dry	120 min

* The times shown assume that all materials and equipment required are prepared and ready for use prior to commencing surface treatment.

Table 25.4

Results of fracture toughness tests on AMORLUX 1310 resin.

Surface treatment	Fracture toughness (J/m^2)	Failure mode
Level One	540	Adhesive
Level Two	777	Mixed
Level Three	1590	Cohesive

25.4.2.2. Addition of epoxy-silane to AMORLUX

Work by Kerr and Walker [21] and Hong and Boerio [22] showed that the addition of small amounts of epoxy-silane to liquid resins improves bond durability. To reduce application time, it was decided to trial the addition of epoxy-silane to the liquid AMORLUX 1310 resin prior to mixing with the hardener.

A series of CCBT specimens were prepared with epoxy-silane concentrations in the resin varying from 0 to 5%. The hardener was then added to the resin and epoxy-silane mixture, stirred and the prepared metal surfaces bonded together (surfaces treated at Level Two). The results (Figure 25.6) showed that for concentrations of 1% of epoxy-silane in the liquid resin the fracture toughness was comparable to that for the tests with the epoxy-silane applied to the surface in aqueous solution. In addition, the failure surfaces indicated cohesive failure of the bond.

BWT specimens were also manufactured and bonded with AMORLUX 1310 with 1% epoxy-silane mixed into the resin as detailed above. The results of the BWT for all Levels of surface treatment (see Figure 25.7) show that the addition of epoxy-silane to the resin improved the environmental durability of the bond when compared to grit blasting or pad abrading alone.

25.4.3. Mechanical properties

25.4.3.1. Adhesive strength and stiffness

The Kreiger TALS test was used to determine the adhesive shear properties of AMORLUX 1310. The metal surfaces were treated by solvent cleaning, pad

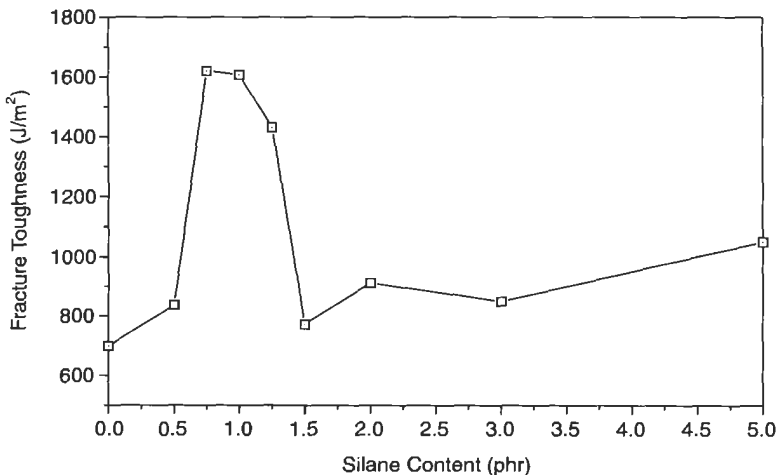


Fig. 25.6. The effect of the epoxy-silane concentration on the CCBT fracture toughness of AMORLUX 1310.

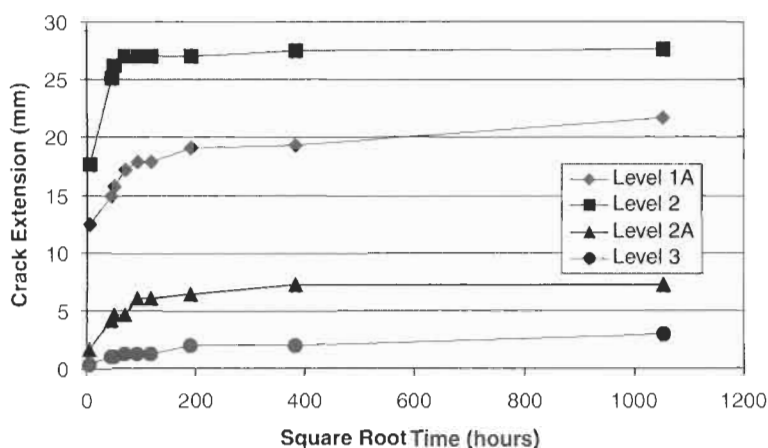


Fig. 25.7. Results of BWT's for AMORLUX 1310 resin with varying Levels of surface treatment procedures. The Level 1A and 2A treatments indicate the addition of epoxy silane to the resin mixture prior to bonding.

abrasion and grit blasting prior to bonding with the AMORLUX 1310 resin. 1% of epoxy-silane was added to the resin, which was then mixed with the hardener. The results are summarised below in Table 25.5.

Table 25.5

Summary of AMORLUX 1310 properties.

The neat resin properties are:

DT Mode I Fracture Toughness	1567 J/m ²
T-Peel Strength (Aluminium adherends)	60 N/25 mm width
Heat Deflection Temperature	89 °C
Viscosity range at application temperatures	4500 to 550 cps
Cure temperature range	Ambient to 110 °C

The adhesive properties are:

Shear Yield Stress	24 MPa
Elastic Shear Strain Limit	0.066
Plastic Shear Strain Limit	0.21
Shear Modulus	605 MPa
CCBT Fracture Toughness	1607 J/m ²
Surface Treatment (Metallic)	Solvent degrease, pad abrade, grit blast

The carbon fibre/AMORLUX 1310 composite properties are:

Mode I fracture toughness	1000 J/m ²
Fibre Volume Fraction	36% to 48%
Interlaminar Shear Strength	56 MPa
Tensile Strength (0°)	947 MPa
Ultimate Strain (0°)	0.01081
Tensile Modulus (0°)	102.7 GPa
Shear Strength (±45°)	80 MPa
Shear Modulus (±45°)	24.5 GPa

25.4.3.2. Composite properties.

The Mode I Fracture toughness [23] and interlaminar shear strength (ILSS) [24] were determined for composites formed both with and without the addition of epoxy silane. In both cases the Mode I fracture toughness was approximately 1000 J/m^2 implying that the addition of the epoxy-silane to the AMORLUX resin had no detrimental effects on fracture toughness. The ILSS value was similarly unaffected by the addition of epoxy-silane and was approximately 56 MPa.

The fibre volume fraction and void content [25] was also determined. The fibre volume fraction was found to be variable, it was believed mainly due to the nature of the wet layup process where full consolidation of the composite was not easily achieved. Typical values for fibre volume fraction ranged between 36% to 48%. The typical void content in all laminates was about 2.5%.

The tensile strength, modulus and Poisson's ratio [26] were determined for uni-directional composites formed with AMORLUX 1310 with the addition of epoxy-silane. The shear strength and modulus [27] were also determined. The results are summarised in Table 25.5.

25.5. Application of the DSTO/ABDR system

A number of application techniques were investigated that were designed to simplify and speed ABDR. Easy to use application procedures will ensure consistent application of repairs and improve overall repair quality.

25.5.1. Resin measurement, mixing and dispensing

The AMORLUX resin system comes as a two-part system that must be measured into exact quantities and thoroughly mixed prior to application. This is a critical issue as operator error leading to an improper ratio of resin to hardener may result in poor adhesive and composite properties.

Several solutions to both problems are currently commercially available. Pre-measured quantities of resin and hardener can be packaged in bags or syringes where the resin and hardener are kept separate for storage. For the bags, a stopcock separates the resin and hardener and to mix the two components the stopcock is opened and the contents of one bag is squeezed into the other. This also provides a way of mixing the resin safely without any spillage or accidental contact to the operator. Alternatively, the resin and hardener can be stored in separate syringes. The opening of each syringe is connected to a mixing nozzle and as the two components are plunged through the nozzle they mix and dispense. Both these techniques have been trialed in the laboratory and were shown to be quite simple to implement and offer many advantages for ABDR.

25.5.2. *Pre-bonding surface treatment procedures*

As mentioned previously, to ensure strong and durable bonds it is important to treat the metal surface prior to bonding. The standard technique employed by DSTO and RAAF includes solvent cleaning, mechanical abrasion, treating the surface with a bond enhancing epoxy-silane coupling agent and priming the surface with a corrosion inhibiting primer.

With the AMORLUX 1310 resin, the time taken to apply the surface treatment was reduced by leaving out the priming and consolidating the epoxy-silane treatment into the resin mixing and application step. The epoxy-silane is mixed into the liquid resin and applied to the bonding surface. It is believed that the epoxy-silane molecule migrates to the metal surface and then couples the polymers in the resin with the oxide on the metal surface [28]. This was shown to increase durability and strength over just solvent wiping and grit blasting (see Figure 25.7). Whilst not having the same durability as the full DSTO surface treatment procedure the durability fell within limits set out in the RAAF Engineering Standard C5033 of 5.1 mm of growth in the first 24 h and 6.4 mm of growth within the first 48 h [8]. Also, repair durability is not critical since ABDR is considered to be a temporary repair. Thus, the total surface treatment time was reduced to approximately 1 h.

25.5.3. *Repair consolidation and application*

To simplify the application process for bonded repairs the AMORLUX resin system allows the simultaneous forming and bonding of the composite patch to the damaged structure. The resin has low viscosity and thus wets dry carbon fibres extremely well and consolidation and forming of the composite can be achieved by hand rolling with a roller. If a higher performance repair is required the composite can be laid up, consolidated and pressurised under a vacuum bag. The resin also has high bond strength, fracture toughness and good durability forming excellent adhesive bonds quickly and simply.

25.5.4. *Heating procedures*

The AMORLUX 1310 resin can be cured over a wide range of temperatures, from room temperature to 110°C. This simplifies the cure process, as complex heating systems are not required for AMORLUX 1310 to control the applied cure temperature to tight tolerances. If elevated temperature cure is required heater blankets connected to an analogue or computer-based heater control system can be used. Alternatively, a novel technique used by other researchers [29,30] and employed at DSTO for the cure of very large bonded repairs utilises the electrical conductivity of carbon fibre. A current is applied to the fibres, which creates heat through resistive heating. This technique has proven to be effective with the heat transferred directly to the curing resin. The ship repair mentioned earlier used this technique to cure a vinyl-ester resin associated with a large carbon fibre patch [6].

25.5.5. Vacuum moulding tool

The application of ABDR to highly contoured surfaces can present a challenge. Normally, a vacuum bag would be used in this situation; however, this can be difficult when a strong vacuum cannot be achieved due to leaks through large holes in the structure. In this case, it may be difficult to apply an even pressure to a complex contoured structure in order to form a good quality composite repair. Traditional techniques require a mould to be taken of the area using fibreglass or other materials. This can be very time-consuming and wasteful of materials. One method, which has been successfully employed, utilises a reusable moulding tool consisting of a silicon rubber bladder filled with a porous filler material which packs into a hard mass when a vacuum is applied. This method was previously reported in reference [31] and has been trialed successfully at DSTO.

A high-temperature silicone-rubber bladder is filled with small ceramic microspheres, sealed and a vacuum port attached to one side. The tool is shaken to loosen the filler material and is then applied to the surface. A vacuum can then be applied to the bladder and as the air evacuates the tool becomes rigid and forms to the shape of the structure underneath. The pliable nature of the silicone rubber ensures that even small contours are reproduced faithfully. A repair patch may then be produced from this tool or the tool may be applied on the external side of the patch during the patch application process. This tool was found to be compact, reusable, durable and effective (see Figure 25.8).

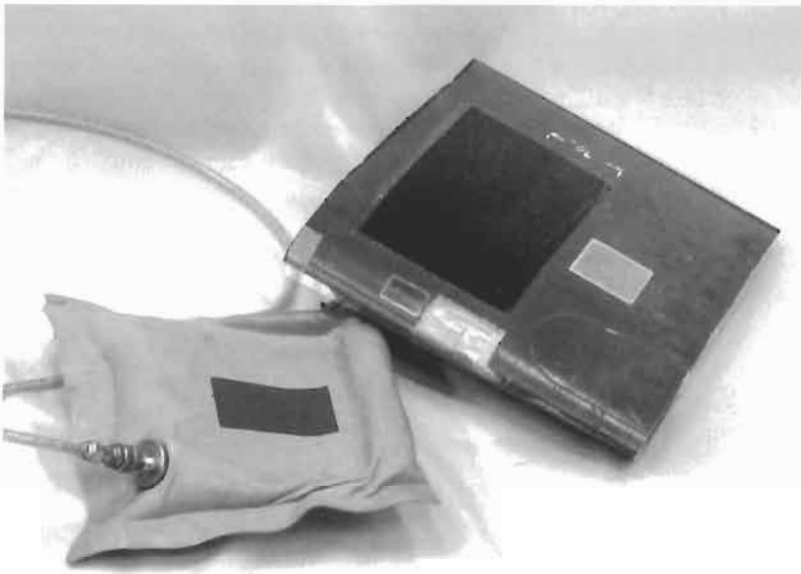


Fig. 25.8. Photograph of vacuum moulding tool demonstrating manufacture of a composite repair for the leading edge of a rotor blade.

Once formed to the shape of the damaged structure the tool will maintain this shape at temperatures up to 200 °C and pressures up to 700 kPa. The tools can be used to cure composite repairs in either an autoclave, by using a mechanical press, or under a vacuum bag for field use.

25.6. Conclusions

Early experimental work showed that bonded composite ABDR performed better than traditional mechanically fastened metallic repairs when loaded in both static and fatigue. This work also indicated that the resin was the limiting factor for the successful implementation of ABDR. Whilst the fibre provides the load bearing capability of the composite repair it is the matrix resin that determines the processing speed, flexibility and sensitivity to pre-bonding surface treatment, which are the paramount elements for ABDR.

At the time no off-the-shelf resin system provided for all these needs. An in house resin system was therefore developed, named AMORLUX 1310. Using this resin system a repair technique was developed for aircraft battle damage based on the use of advanced composites and structural adhesives.

Importantly, the use of this liquid resin simplified the application of the bonded composite technique for ABDR by:

1. The use of the resin simplifies repair manufacture and bonding by forming composites of good quality and creating a void-free bond at low pressures simultaneously. Thus a vacuum bag is sufficient to form the repair rather than an autoclave or press. The system also cures at a range of temperatures giving the operator more flexibility during the cure of the repair.
2. The resin system may be stored at room temperature for at least one year and thus needs no refrigeration.
3. The use of AMORLUX 1310 saves time during the pre-bonding surface treatment of aluminium adherends. This was possible by introducing the epoxy-silane coupling agent to the liquid resin, removing the need for the epoxy-silane to be applied to the adherend as a discrete step. The outcome was that high strength and durable bonds were achieved with the use of only the solvent degrease and mechanical abrasion steps in the AMRL standard surface treatment procedure for bonding to aluminium adherends.

References

1. Baker, A.A. (1984). Repair of cracked or defective metallic aircraft components with advanced fibre composites – and overview of Australian work, composites structures 2, Elsevier Applied Science Publishers Ltd, England.
2. RAAF Technical Manual, Aircraft Battle Damage Repair General, DI (AF) AAP 7002.011.
3. USAF Technical Manual General, Aircraft Battle Damage Repair, TO 1-1H-39, 1 April (1984).

4. Bartholomeusz, R.A., Fry, I.P. and Baker, A.A. (1994). A report on the repair of battle damage to metallic airframe structure, *Aeronautical and Maritime Research Laboratory, Defence Science and Technology Organisation*, DSTO-CIC-0003, Australia, May.
5. Baker, A.A. (1988). Bonded Repair of Aircraft Structures, Chapter 6, Crack Patching: experimental studies, practical applications, (A.A. Baker and R. Jones eds.), Martinus Nijhoff Publishers, Dordrecht, The Netherlands.
6. Grabovac, I., Bartholomeusz, R.A. and Baker, A.A. (1993). Composite reinforcement of a ship structure-project overview. *Composites*, **24**(6), p. 501.
7. Hart-Smith, L.J. (1973). Adhesively-bonded double-lap joints, NASA Langley Research Centre Report, NASA CR-112235, January.
8. RAAF Standard Engineering C5033, *Composite Materials and Adhesive Bonded Repairs*, Issue 1, September (1995).
9. Hart-Smith, L.J. (1988). Bonded Repair of Aircraft Structures, Chapter 3. Design and analysis of bonded repairs for metal aircraft structures, (A.A. Baker and R. Jones eds.). Martinus Nijhoff Publishers, Dordrecht, The Netherlands.
10. Baker, A.A. and Chester, R.J. (1992). Minimum surface treatments for adhesively bonded repairs. *Int. J. of Adhesion and Adhesives*, **12**(2), April, p. 73.
11. Drake, R.S. and Siebert, A.R. (1997). SAMPE Q., July p. 11.
12. Pearce, P.J., Siebert, A.R., Egan, D.R., *et al.* (1995). *J. Adhesion* **49**, p. 245.
13. Bartholomeusz, R.A., Pearce, P. and Vodicka, R. (1999). Repair of Aircraft Battle Damage – Australian Research into the use of Adhesively Bonded Advanced Composites, Defence Science Technology Organisation, DSTO-RR-0144, January.
14. Lee, B.L., Lizac, C.M., Riew, C.K. *et al.* (1980). *J. Natl. SAMPE Tech. Conf.* **12B**, p. 1116.
15. ASTM D 1876–95, Standard Test Method for Peel Resistance of Adhesives (T-Peel Test), Annual Book of ASTM Standards, Section 15, **15.06**, Adhesives, (1996).
16. Kies, J.A. and Clark, A.B.J. (1969). In *Fracture 1969*, (P.L. Pratt, ed.). London: Chapman and Hall, p. 483.
17. ASTM D 648-98c, Standard Test Method for Deflection Temperature of Plastics Under Flexural Load in the Edgewise Position, *American Society for Testing and Materials*, West Conshocken, PA, (2000).
18. ASTM D 1084–88, Standard Test Methods for Viscosity of Adhesives, Method B, Annual Book of ASTM Standards, Section 15, **15.06**, Adhesives, (1996).
19. ASTM D 3762–79, Standard Test Method for Adhesive-Bonded Surface Durability of Aluminium (Wedge Test), Annual Book of ASTM Standards, Section 15, **15.06**, Adhesives, (1996).
20. ASTM D 3433–93, Standard Test Method for Fracture strength in Cleavage of Adhesives in Bonded Metal Joints, Annual Book of ASTM Standards, Section 15, **15.06**, Adhesives, (1996).
21. Kerr, C. and Walker, P. (1987). Some Aspects of Silane Technology for Surface Coatings and Adhesives, *Adhesion 11*, (K.W. Allen ed.), Adhesion Science Group, The City University, London, Elsevier Applied Science, London and New York.
22. Hong, S.G. and Boerio, F.J. (1990). Adhesive Bonding of Oil-Contaminated Steel Substrates, *J. of Adhesion*, **32**, pp. 67–88, Gordon and Breach Science Publishers S.A., United Kingdom.
23. ASTM D 5528–94a, Standard Test Method for Mode I Interlaminar Fracture Toughness of Unidirectional Fiber Reinforced Polymer Matrix Composites, Annual Book of ASTM Standards, **15.03**, High Modulus Fibres and Composites, (1996).
24. ASTM D2344–84, Standard Test for Apparent Interlaminar Shear Strength of Parallel Fibre Composites by Short-Beam Method, Annual Book of ASTM Standards, **15.03**, High Modulus Fibres and Composites, (1996).
25. ASTM D3171–76, Standard Test Method for Fiber Content of Resin-Matrix Composite by Matrix Digestion, Annual Book of ASTM Standards, **15.03**, High Modulus Fibres and Composites, (1996).
26. ASTM D3039/D 3039M – 95a, Standard Test Method for Tensile Properties of Polymer Matrix Composite Materials, Annual Book of ASTM Standards, **15.03**, High Modulus Fibres and Composites, (1996).

27. ASTM D 3518/D 3518M – 94, Standard Test Method for In-Plane Shear Response of Polymer Matrix Composite Materials by Tensile Test of $\pm 45^\circ$ Laminate, Annual Book of ASTM Standards, **15.03**, High Modulus Fibres and Composites, (1996).
28. Digby, R.P. and Shaw, S.J. (1998). *The international collaborative programme on organosilane coupling agents: an introduction*, *Adhesion and Adhesives*, **18**(4).
29. Moriya, K. (1993). On use of joule effects for curing / joining/patching of CFRP composites. In *Proceedings of the Japan.-U.S. Conference on Composite Materials*, 6th, pp. 742–750.
30. Fukuda, H. (1994). Processing of carbon fiber reinforced plastics by means of Joule heating. *Advanced Composite Materials*, **3**(3) pp. 153–161.
31. Frailey, J.A. and Carter, D.W. (1995). Rapid repair of large area damage to contoured aircraft structures. *AGARD Composite Repair of Military Aircraft Structures*, January.

Chapter 26

STANDARDIZED TRAINING AND CERTIFICATION FOR BONDED REPAIR SPECIALISTS

MARTY A. SMITH

Advanced Repair Technology International, Fort Worth, Texas, USA

26.1. Introduction

On April 15, 1997 a corporate helicopter lifted off from New York City's 60th Street Heliport, suddenly rotated to the right, and crashed into the East River killing a Colgate-Palmolive executive. Although the National Transportation Safety Board has yet to rule on the cause of the accident, it is suspected that an unauthorized substitution of blind fasteners for solid rivets caused the loss of the vertical fin and the resulting crash.

US National Transportation Safety Board member John Goglia stated that during the investigation he discovered "it was generally believed by mechanics that blind rivets and solid rivets can be safely interchanged." [1] How can that be? Surely the mechanics involved had received formal training and were either experienced in their trade or working under the supervision of experienced personnel.

The fact that this type of scenario is possible in a trade as well developed as traditional metal working should focus our attention on the importance of training and certification for bonded repairs, which are so much more "process sensitive."

26.1.1. Benefits of improved training and process control – an example

In the past it was common to rely on "factory specifications" for all bonding operations, but they have proved to be ill suited for field applications of structural repairs. Although appropriate for original production of composites and sandwich panels, these specifications are not the best source for guidance on field installations of bonded repairs on metal structure. Max Davis of the Royal Australian Air Force (RAAF) describes a 1992 study of 194 reports of bondline failures. [2] Of these, 79

(41%) were secondary attempts where previous defective repairs had been applied using OEM approved manuals.

In response to this and other incidents, the RAAF instituted its own training and improved procedures aimed specifically at field repairs on metal substrates. Using these stringent training and process control requirements, the RAAF cut the rework rate on bonded repairs from 42% in 1992 to nearly zero. This illustrates the dramatic effect that thorough training in surface preparation and bonded repair installation practices can have. Similar success rates have been achieved by other maintenance and repair organizations which have developed proper training, certification and process controls.

26.2. The task at hand – a uniform approach

26.2.1. Advantages of standardization

Proponents of bonded repairs must occasionally endure the re-telling of anecdotes about “the ones that fell off.” It makes no difference when, where, how or by whom the repairs were installed (or if, in fact, they fell off at all). Any failure or substandard performance of a bonded repair will be around to haunt for years to come. In addition to the legitimate concern for aircraft safety, the effect of such negative perception makes it in the best interest of the entire community to insure that all parties engaging in structural bonding have the necessary information to produce durable repairs.

With the growing acceptance of bonded repairs, engineering and maintenance groups around the world will want to establish their own capabilities. This could lead to a proliferation of differing practices. In some cases, equivalent results can be achieved with different processes. But, whenever deviations are made there is a possibility of producing substandard repairs unless the changes have been approved based on adequate evaluation and testing. Since such justification can be time consuming and expensive it makes sense for the bonded repair community to arrive at consensus around procedures which have been thoroughly tested by the major research labs. Agreement on basic, generic surface preparation methods and installation practices would provide continuity across the industry without compromising proprietary processes.

Standardized design and process methods have two advantages: (1) they provide commonality across the industry avoiding confusion about how any particular repair was accomplished; and (2) when available to all practitioners, standard practices decrease the probability of unreliable repairs with their inherent impact upon the industry as a whole. Since technical innovation is to be encouraged, individual organizations would still be free to improve or tailor procedural details assuming they thoroughly test, justify and document their internal process requirements.

26.2.2. Building a database of reliable repairs – “We’re all in this together”

For people who consider structural bonding to be a new and radical technology nothing is more persuasive than a good track record of successful repairs; and the more repairs cited the better. A fleet manager or airworthiness authority will be much more likely to consider the bonded repair option if it can be shown that, for example, “65 repairs done with these same processes have been flying for an average of 12 years with no failures or maintenance problems encountered.”

Using common design and installation standards allows apples-to-apples comparisons of a large population. Unfortunately, such collected data is currently hard to come by. In order to make service histories retrievable for compilation each organization should keep a database listing minimum essential information including: surface prep method (i.e. Silane/grit blast, PACS, *etc.* – see Chapter 3), adhesive, cure temperatures, and parent/doubler materials. At most repair facilities these descriptions are contained in separate data packages for numerous repairs. Collecting the information in a simple database would be useful within the organization; and sharing common portions would benefit efforts to move the technology forward.

26.3. Current approaches to training and certification

Typically, bonded repairs are implemented by teams of individuals who have gained the necessary knowledge and skills through personal hands-on experience. This system will not provide the infrastructure required to support the technology as it comes into more widespread use. Without a distinct curriculum, the impression will persist that procedures for bonding *primary* structures are just a more tightly controlled version of the ones used for lightly-loaded honeycomb sandwich panels. The specific techniques necessary to produce a repair capable of sustaining primary flight loads over the life of the airframe will not be recognized until formal training and certification programs are implemented in each maintenance organization.

Institutionalized training programs for field installations on metal substrates were found in the RAAF [3], ARTI [4] and the US Navy [5]. All three programs include classroom lectures, hands-on instruction, and fabrication of “Boeing wedge test” specimens (see Paragraph 26.6.1, below). The scope of training can vary according to purpose. For example, the RAAF course is quite broad, producing an individual who emerges as a versatile composites technician skillful in laminate fabrication, temperature measurement and control, honeycomb panel repair, core splicing and other related areas in addition to surface preparation. Training for ARTI personnel (who are dedicated specifically to in-situ structural repairs) is more tightly focused on surface preparation and installation procedures. It is the ARTI model that is presented for consideration in this chapter.

26.4. Formalized trade structure

Outstanding performance is motivated by self-discipline and pride in one's work. Development of a formal trade structure, which recognizes workers as highly-trained specialists, not only provides a framework for organizing and managing the work force but also fosters professionalism on the part of its members. A formal certification plan will provide the industry with a common method for defining and classifying personnel skill sets, a necessary step for quality control.

26.4.1. *The purpose of a trade structure*

Quality assurance in bonded repair activities is dependent predominately on the skill and experience of the specialists who are performing the work. A good analogy is aircraft welding where there is no direct, non-destructive test to determine the strength or durability of any particular weld. For this reason, only specially trained and certified workers are authorized to perform this task. A similar approach, with the opportunity for personnel to advance according to their experience and capabilities is the only way to maintain a pool of qualified technicians to accomplish bonded repairs which are reliable and repeatable. A formal trade structure which confers upon its members the recognition that they are technical specialists will also serve to attract and retain qualified candidates into the field of structural bonding.

26.4.2. *A four-tiered trade structure – the ARTI model*

Most repair installations involve traditional metal work in addition to surface preparation and the typical candidate brings these skills from his/her previous experience. To move into bonded repairs advanced repair technology international (Advanced Repair Technology International) [6] has developed a four-tiered trade structure for certification of individuals who demonstrate the following core proficiencies:

- **Level 1 – Basic proficiencies:** Primary set of applied skills with limited theoretical knowledge. Produces accurate and repeatable results with direct supervision.
- **Level 2 – Intermediate proficiencies:** Refined set of applied skills (improved by experience and practical application). Some knowledge and understanding of applied bonding theory. Limited evaluation skills. Can work without direct supervision within a larger team.
- **Level 3 – Journeyman proficiencies:** Stable applied skill level. Technical knowledge and understanding of applied bonding theory. Basic understanding of composite laminates. Understanding required to fully evaluate existing processes and to propose (but not implement) new processes.
- **Level 4 – Advanced proficiencies:** Advanced applied skill level. Advanced technical knowledge and understanding of applied bonding theory. Fundamental understanding of composite materials and their applications. Thorough understanding of NDI. Able to fully evaluate existing processes and develop new



Fig. 26.1. ARTI technicians in a typical hangar environment performing (a) solvent scrub, (b) water wipe, (c) grit blast and (d) laminate application for repair of an F-16 FS 479 bulkhead.

bonding processes under controlled experimental conditions. Has management and/or supervision capability.

26.5. The ARTI model for training of bonded repair specialists

Training serves multiple functions. In addition to imparting the raw skills and knowledge required to accomplish assigned tasks accurately and reliably, training motivates the work force and assures consistency from one repair to the next.

Rote repetition and memorization of procedural steps may prepare a student to pass the written and practical tests but it will not go far toward insuring a quality product at the end of a long hot day. The course must be designed and administered to instill an appreciation of the need to adhere exactly to approved methods, an understanding of why the details are important, and an awareness of the long term implications of substandard work.

In addition to understanding the tasks required, the bonded repair specialist must appreciate the need for following procedures exactly as written, without deviation. Therefore, even in a very focused course the student is introduced to the precepts of adhesion theory, or more simply put, "What makes things stick?" Other related topics are included, such as characteristics of composites and adhesives, as well as NDI methods and how they relate to bonded repairs. These ancillary topics are covered in increasing depth as the student advances from one level to the next.

It is not the intention to supplant the role of engineers, NDI specialists and the like. Rather, it is to produce bonded repair technicians with a comprehensive understanding of their own field and those with which they will be interacting. Eligibility to participate in the next level of training is contingent upon mastery of the skills of the preceding level. Successful completion of the training will entitle the candidate to certification as a bonded repair specialist. A summary of the curricula for all four levels is presented below.

- **Level 1 – Basic training (18h classroom, 22h workshop):** Introductory level training is planned for five consecutive days. Background material is presented on composite materials, adhesives and NDI methods; but basic training focuses on surface preparation techniques and practices. The first three days are split

Table 26.1

ARTI syllabus for level 1 (basic) training.

<i>I. Introduction to bonding technology</i>	<i>IV. Adhesives</i>
<ul style="list-style-type: none"> ● History ● Terminology ● Current applications 	<ul style="list-style-type: none"> ● Structural vs. non-structural adhesives ● Paste and film adhesives ● Storage and handling
<i>II. Surface preparation and bonding theory</i>	<i>V. Installing bonded repairs on aircraft</i>
<ul style="list-style-type: none"> ● Surface prep procedures and basic bonding theory ● Personal protection and waste disposal ● Control and handling of materials and consumables 	<ul style="list-style-type: none"> ● Facilities requirements and environmental control ● Pre-cured, B-staged and co-cured doublers ● Bagging, pressure and heating options ● Cure cycles
<i>III. Composite materials</i>	<i>VI. Introduction to NDI methods</i>
<ul style="list-style-type: none"> ● Fibers (graphite, boron, Kevlar, fiberglass) ● Resins (thermosets, thermoplastics) ● Prepregs and cloth ● Storage and handling 	<ul style="list-style-type: none"> ● Visual ● Coin tap ● Ultrasound ● Thermography

between classroom instruction and a hands-on workshop. The last two days are used for review and reinforcement, followed by fabrication of two sets of Boeing wedge test specimens. A 90-min period is set aside for a written test.

- **Level 2 – Intermediate training (16h classroom, 16h workshop):** Intermediate level training is planned for four consecutive days. The first two days are spent in the classroom and the last two days are spent in the workshop. In addition to reinforcement of surface prep techniques, this level introduces topics such as the basics of adhesion theory and an overview of non-destructive investigation (NDI). Fundamentals of composite laminate fabrication are also discussed. A 90-min written test is administered at the end.

Table 26.2
ARTI syllabus for level 2 (intermediate) training.

<i>I. Review of bonding technology</i>	<i>V. Surface preparation</i>
<ul style="list-style-type: none"> • Terminology • Examples of past applications • Current developments 	<ul style="list-style-type: none"> • Detailed step-by-step review of procedures • Personal protection and waste disposal • Chemical preparation
<i>II. Characteristics of composite fibers and resins</i>	<i>VI. Fundamentals of laminate fabrication</i>
<ul style="list-style-type: none"> • Graphite, Boron, Kevlar • Various resin systems • Storage and handling of prepreg 	<ul style="list-style-type: none"> • Reading laminate engineering drawings • Cutting plies • Assembling laminate • Vacuum bagging
<i>III. Characteristics of structural adhesives</i>	<i>VII. NDI methods and evaluation</i>
<ul style="list-style-type: none"> • Paste adhesives • Film adhesives • Storage and handling of adhesives 	<ul style="list-style-type: none"> • Visual • Coin tap • Ultrasound • Thermography • X-ray
<i>IV. Introduction to bonding theory</i>	
<ul style="list-style-type: none"> • What makes things stick? • What is a good bonding surface? • What happens during curing? 	

Table 26.3
ARTI syllabus for level 3 (journeyman) training.

<i>I. Surface preparation</i>	<i>VI. Repair implementation</i>
<ul style="list-style-type: none"> • Detailed step-by-step review of procedures • Personal protection and waste disposal • Chemical preparation 	<ul style="list-style-type: none"> • Facilities, tooling and equipment • Fasteners in repair area • Bagging on aircraft • Pressure requirements and options • Controlling cure cycles • Machining procedures
<i>II. Fundamentals of bonding theory</i>	<i>VII. NDI and evaluation (hands on practice)</i>
<ul style="list-style-type: none"> • Mechanical locking • Molecular forces • Electro-chemically active surfaces 	<ul style="list-style-type: none"> • Visual inspection • Tap test • Ultrasound • Thermography • X-ray • Witness strips and test buttons
<i>III. Introduction to laminate theory</i>	<i>VIII. Health, safety and environmental issues</i>
<ul style="list-style-type: none"> • Role of fibers in laminates • Role of matrix in laminates • Ply orientation 	<ul style="list-style-type: none"> • Personal protection • Waste disposal • Government regulations (EPA, OSHA, etc.)
<i>IV. Bondline failure modes</i>	
<ul style="list-style-type: none"> • Adhesive failure • Cohesive failure • Substrate corrosion 	
<i>V. Bonded repair constraints</i>	
<ul style="list-style-type: none"> • Parent materials (metallic and composite) • Structure geometry and near field features • Temperature • Access 	

- **Level 3 – Journeyman training (24 h classroom, 16 h workshop):** Journeyman level training is planned for five consecutive days. Subjects covered at the Journeyman level include fundamentals of adhesion theory, introduction to composite laminate theory, repair constraints, practical considerations in repair implementation, and hands-on practice with NDI equipment. The first four days are split between the classroom and the workshop, with a 90-min written test administered on the fourth day. The fifth day is spent in the shop finishing up previous exercises and practicing NDI and other techniques.
- **Level 4 – Advanced training (25 h classroom, 15 h workshop):** In addition to refining technical knowledge, advanced level training prepares the student to assume supervisory or management roles. It is scheduled for five consecutive

Table 26.4

ARTI syllabus for level 4 (advanced) training.

<i>I. Building quality into bonded repairs</i> <ul style="list-style-type: none"> ● Certification and acceptance of raw materials ● Material control and storage ● Environmental control of work area ● Process control 	<i>V. Prevention of defects in laminates and bondlines</i> <ul style="list-style-type: none"> ● Porosity ● Warping ● Voids ● Poor adhesion
<i>II. Aircraft structures and materials</i> <ul style="list-style-type: none"> ● Common structural configurations as they relate to bonded repairs ● Common aircraft materials as they relate to bonded repairs 	<i>VI. NDI and evaluation (hands on practice)</i> <ul style="list-style-type: none"> ● NDI of pre-cured laminates ● NDI of completed repairs ● Current developments in NDI
<i>III. Review of bonding theory</i> <ul style="list-style-type: none"> ● Mechanical bonds ● Chemical bonds ● Electro-chemically active surface 	<i>VII. Structural failure modes and corrective action</i> <ul style="list-style-type: none"> ● Fatigue repairs ● Stress reduction ● Stress corrosion cracking ● Corrosion repairs
<i>IV. Surface preparation alternatives</i> <ul style="list-style-type: none"> ● Silane ● Phosphoric acid anodizing and PACS ● FPL etch, others ● Abrasion ● Common solvents ● Primers 	<i>VIII. Management issues</i> <ul style="list-style-type: none"> ● Administration and supervision ● Health and safety issues ● Government regulations (EPA, OSHA, etc.)

days. All five days are split between classroom and the workshop, with a 90-min test administered on the fifth day. Topics introduced at the advanced level include material acceptance standards, comparison of various surface preparation techniques, environmental and process control, defect prevention, common structural failure modes and how they relate to bonded repairs.

The courses outlined above are intended for individuals wishing to advance to a higher level in the trade structure. A specialist who is due for semi-annual recertification, but who will be remaining within the same trade level requires only a one-day refresher course, plus successful completion of a written examination and Boeing wedge test.

26.6. Certification of bonded repair specialists

26.6.1. The Boeing wedge test (BWT) – an accepted standard

The Boeing wedge test is so named for the company that brought it into standard practice back in the 1970s. It has become the common practical test for evaluation of surface preparation for adhesive bonding and is codified in ASTM Standard D 3762.7

26.6.1.1. Boeing wedge tests for verification of adequate surface preparation.

BWT specimens are fabricated by performing surface prep on two 6 by 6 inch (150 by 150 mm) aluminum plates and applying a structural adhesive between them. Before putting the plates together a strip of mylar type 0.75 inch wide (20 mm) is applied between them to make one unbonded edge. After the adhesive is cured under heat and pressure, the resulting panel is cut into 1 inch wide (25.4 mm) coupons as illustrated in Figure 26.2. Into the unbonded end of each coupon a

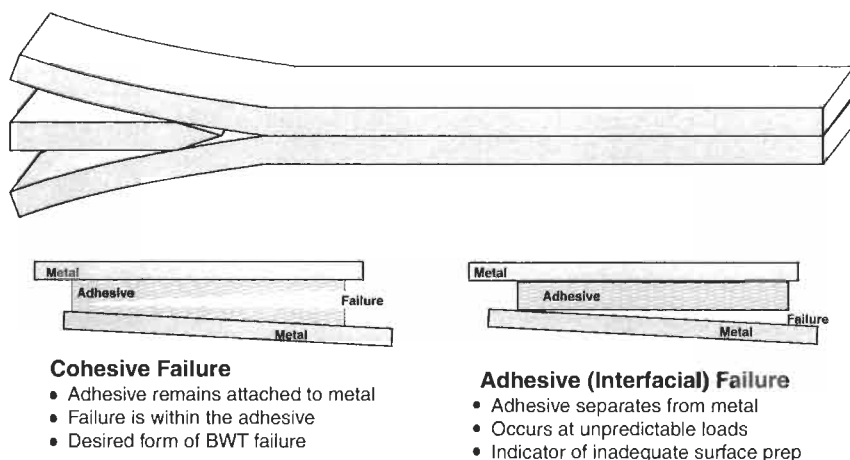


Fig. 26.2. A schematic representation of the Boeing wedge test, showing the desired and undesired modes of induced failure.

metal wedge is inserted and forced between the adherends using a slow press or vice. This starts a crack in the adhesive layer.

For certification purposes the coupons are exposed to a hot-wet environment of 122 °F (50 °C) and condensing moisture (100% relative humidity). The concentrated stress at the crack tip is considerable, and if the surface preparation is not good the adhesive will separate from the metal in a premature failure. The standard generally agreed upon as a “passing mark” is an additional crack growth not exceeding 0.20 inch (5.1 mm) after 24 h. Upon conclusion of the test, the coupon can be completely wedged apart and the resulting failure surfaces evaluated for the percentage “cohesive failure” (separation within the adhesive bondline) and “adhesive failure” (separation between the metal coupon and the adhesive). Cohesive failure is the desired mode.

Fast crack propagation is often associated with the “adhesive failure” mode. Where the adhesive layer pulls away from the metal, it is an indicator of poor surface preparation. The Boeing wedge test is a good qualitative indicator of the adequacy of surface preparation but it cannot be used to quantify the load-carrying capability of the bondline. Also, in the absence of such evidence as fingerprints or obvious contamination it cannot tell us what part of the preparation process was deficient. On the other hand, a good BWT result confirms that the proper techniques were followed to achieve a strong and durable bondline.

26.6.1.2. *An interesting result from a series of Boeing wedge tests.*

Wedge tests are often used to evaluate process details or to compare different materials. An effective solvent used in surface preparation is MEK (methyl ethyl ketone), which is a hazardous material and environmentally unfriendly. Figure 26.3 is a histogram of 74 Boeing wedge tests performed on a proposed MEK substitute, Citra-Safe. The *x*-axis shows the crack growth during 24 h in an environmental chamber. The *y*-axis shows the total number of specimens reaching various crack lengths. Since almost all the specimens fall well within the 0.20 inch limit, the results indicted that Citra-Safe may be an acceptable substitute for MEK. However, the figure is included here for *another reason*.

Note that three of the samples failed the test. These specimens were fabricated by a trained technician who had successfully installed dozens of repairs in the field and was known to be a very conscientious worker. However, due to other assignments, he had not performed surface preparation for over a year when he was asked to assist in laying up these test samples.¹ The disappointing result of this technician's first coupons after an absence from the bonded repair team underscores the “art” of surface preparation and the absolute importance of keeping skills honed through practice.

¹ He would not have been allowed to work on an actual aircraft since his certification was not current.

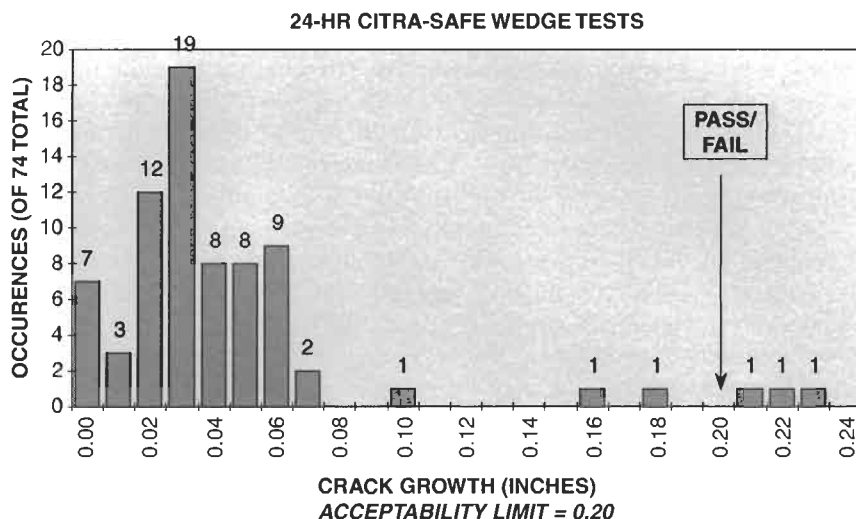


Fig. 26.3. Results of 74 Boeing wedge tests to evaluate a new solvent. The failing specimens were produced by a technician who had not performed surface preparation for over a year.

26.6.2. Administration of certification tests

26.6.2.1. Facilities and instructors.

Resources for bonded repair training are no different than for any other classroom. The instructor must be sufficiently experienced to explain the science behind the processes and to provide authoritative information when responding to students' questions. One instructor can present the material and adequately engage in student interaction with a class size up to 30. (The RAAF consider a class size of less than ten as more appropriate.)

All levels of training include practical hands-on sessions as well, which require laboratory or shop space and the equipment associated with bonding: controlled ovens, grit blasters, autoclaves or platens, primer guns, *etc.* Clean Room conditions need not be provided, and in fact are not recommended, since real repairs are usually implemented under field conditions. All health and safety precautions must also be observed such as hazardous material disposal and personal respirators where required.

Once the class moves to the practice area, one instructor cannot give the individual attention each student will need. In addition to the principal instructor, an aide proficient in surface preparation practices is recommended for every 10 (RAAF 4) students during the practicum.

26.6.2.2. Schedule of re-certification.

At this time ARTI requires re-certification every six months regardless of how intensively the technician is involved with surface preparation and bonded repairs.

Admittedly, this is a cumbersome requirement, but in view of the consequences of a failure it is a burden which has been accepted. The need for absolute reliability is driven as much by outside impressions as by flight safety. Bonded repairs are designed with residual strength sufficient for the parent structure to sustain limit load even if the repair fails completely. Unfortunately, the user community will not be so forgiving where they are unfamiliar with the technology.

One of the most important things about refresher training isn't an update on the latest changes, but rather to insure that no unauthorized changes have crept into the procedures. ARTI recommends semi-annual requalification in those fleets where bonded repairs are not commonly used. The Australians have a twenty year history of installing bonded repairs on metal and use them on a fairly routine basis. The RAAF has determined that their infrastructure supports a transition to annual requalification.

26.6.2.3. Test controls.

What if bonded repair teams are deployed in areas far from the training and testing facilities?

For advancement training (which is a five day course under the ARTI model) courses may be given on-site with the instructor traveling to the students' location. Any facility where bonded repairs are being implemented will have all the equipment necessary for the fabrication of Boeing wedge test specimens. The instructor will return the serialized test panels to the laboratory for processing.

For semi-annual recertification with no advancement in grade level a qualified local supervisor may administer the one-day refresher course and written examination. The student would fabricate the Boeing wedge test panel under local supervision, with the serialized panel being shipped in protective wrapping to the cognizant certification authority for testing.

26.6.2.4. Certification authority.

As in other technologies there are two avenues for obtaining certification and maintenance of the associated records. Larger organizations may elect to support their own internal programs for training, certification and record keeping. For smaller organizations it will be more cost effective to out-source these functions. Currently there is no "higher authority" (such as the CAA or FAA) with a system in place to approve bonded repair training and certification.

National or international airworthiness bodies are the logical parties to eventually assume the task of reviewing and approving certification programs. In the absence of a governing authority, certification standards must be managed by consensus. Specifications such as those cited in Paragraph 26.4, along with existing [8] and up-coming standards [9] form a basis for establishing common criteria. The agreed upon criteria, in turn, will assist civil and military authorities in establishing independent requirements.

In the final analysis it is incumbent upon each organization which installs structural bonded repairs to examine its own practices to insure that adequate control is in place to guarantee reliable and repeatable results.

26.7. Conclusion

From accident reports to rework statistics there is ample proof that effective work force training and certification is directly reflected in the quality of the finished product. This is especially true for adhesively bonded repairs, which are extremely process sensitive. Furthermore, the cost of thorough training is offset by savings in turn-around-time and rejected work. The fact that this is a relatively new technology in many fleets increases the importance of gaining concurrence on the basic methodology and insuring that it is available for organizations attempting to establish their own capabilities.

Proponents of this technology have a vested interest in developing and disseminating commonly accepted core practices for training and certification. Several programs have been cited which offer models upon which to build; with the ARTI model detailed in this chapter. Once the common standards are in place and refined they will be valuable resources as national and international airworthiness authorities assume their roles as independent arbiters for requirements and “best practices.” As bonded repairs become more widely accepted, a proper emphasis on training and certification issues will play a key role in how the technology matures.

References

1. Aviation International News. 1 January, 1999, p. 3.
2. Davis, M.J. (1994). The development of an engineering standard for composite repairs, *AGARD SMP Specialists Meeting*, Seville, Spain, 3–5 October.
3. Royal Australian Air Force, RAAF approved course #627006, “ADHESBONDSTRUC”.
4. Advanced Repair Technology International, ARTI Document Nr. 99A4097, “Training Plan and Trade Structure Policy,” dated 17 January, 1997.
5. Naval Aviation Depot, North Island, California, Process Specification #NI 657, Certification Requirements for Metallic Surface Preparation for Structural Adhesive.
6. Advanced Repair Technology International, 6500 West Freeway, Fort Worth, TX. 76116, USA.
7. American Society for Testing and Materials, Designation D 3762–79 (Re-approved 1993), Standard Test Method for Adhesive-Bonded Surface Durability of Aluminum (Wedge Test).
8. Royal Australian Air Force, RAAF Standard C5033, Composite Materials and Adhesively Bonded Repairs.
9. US Air Force, Wright Laboratories CRMS initiative, Composite Repair of Metallic Structures.

Chapter 27

CASE HISTORY: F-111 LOWER WING SKIN REPAIR SUBSTANTIATION

K.F. WALKER and L.R.F. ROSE

Defence Science and Technology Organisation, Air Vehicles Division, Defence Science & Technology Organisation, Australia

27.1. Introduction

This chapter details the design and substantiation aspects of a safety critical bonded composite repair to the lower wing skin of a Royal Australian Air Force (RAAF) F-111 aircraft. The bonded composite repair was designed according to procedures, which have now been incorporated in an Engineering Standard [1]. These procedures are continually being improved and updated, and they include improvements on the techniques originally presented in the fore-runner to this book [2].

The repair followed the discovery of a crack on the lower wing skin of a RAAF F-111 aircraft during a routine visual inspection. The visual indication was associated with fuel seepage around the crack site. A more detailed inspection revealed a through thickness crack, 48 mm long tip to tip. Fracture mechanics calculations (using a handbook value of $46 \text{ MPa}\sqrt{\text{m}}^{1/2}$ or $42 \text{ ksi}\sqrt{\text{in}}^{1/2}$ as the effective fracture toughness) indicated that the residual strength had been degraded to 168 MPa (24.4 ksi), which is considerably less than the Design Ultimate Stress of 358 MPa (51.9 ksi) specified for this region of the wing. A mechanically fastened metallic doubler was initially considered as a repair option, but this was discarded because of undesirable aerodynamic implications and because the underlying structure would be un-inspectable. Further limitations of traditional repairs are discussed in [2,3]. Thus, the only viable alternative to a bonded repair would have been scrapping the wing.

The repair consisted of a 14 ply boron/epoxy patch adhesively bonded to the wing skin with FM73 adhesive. A co-cure process was used to fabricate the patch in which a layer of FM73 is co-cured with the pre-preg at 120 °C. This layer of adhesive was then grit blasted prior to the cured patch being secondarily bonded

with a second layer of adhesive. The secondary bonding involved a cure for 8 h at 80 °C under a positive applied pressure of 100 kPa. The patch measured approximately 470 mm in the spanwise direction and 320 mm in the chordwise direction, and the lay-up was $[0_2, \pm 45, 0_3]_s$, with the 0° fibers oriented in the spanwise axis. The 45° fibers were added to account for any torsion loads.

Approval and final certification of this repair required a comprehensive validation and substantiation program. There are two main reasons why such a program was required as follows:

The crack had reduced the residual strength below the specified Design Limit Stress of 238 MPa (34.6 ksi), thereby compromising flight safety. Thus, the implementation and approval of any repair option required very stringent scrutiny.

The local geometry of the wing skin at the site of cracking gives rise to a significant stress concentration and to secondary bending in the wing skin. Both of these features constitute a severe test for the adequacy of the design procedure documented in the Engineering Standard [1]. The validation of this procedure for the present repair would therefore provide confidence in its adequacy for other, less critical, applications.

Details of the comprehensive validation and substantiation program are presented in this chapter.

27.2. Crack location and residual strength

Figures 27.1 and 27.2 indicate the location of cracking on the lower wing-skin. The raised portions serve as integral stiffeners and as attachment lands for spars [4]. The cracking occurred in an area lying below the forward auxiliary spar, at the spar station FASS 281.28, where the thickness of the integral stiffener is reduced from

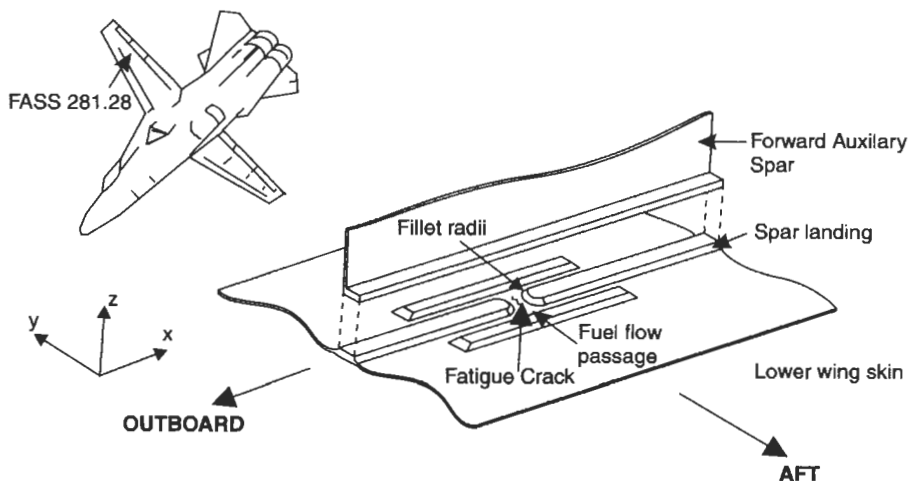


Fig. 27.1. Location of cracking on the F-111 lower wing-skin, at FASS 281.

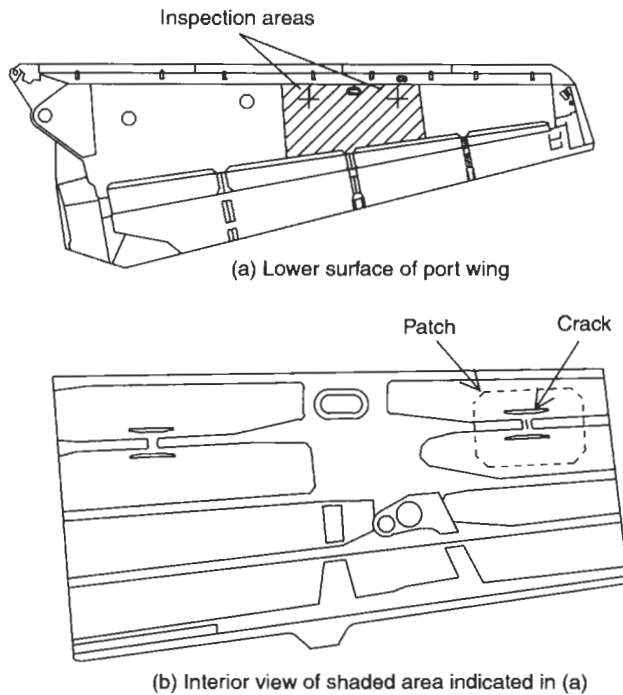


Fig. 27.2. Location of cracking on the F-111 lower wing-skin, at FASS 281, showing also the outline of the repair patch.

approximately 8 mm to the nominal skin thickness (at this location) of approximately 4 mm (with the minimum acceptable thickness being 3.6 mm). The purpose of this depression in the stiffener is to allow full fuel flow and drainage between adjacent bays of the wing-box fuel tank. Two side-stiffeners are used to compensate for the loss of spanwise stiffness due to this fuel-flow passage, as indicated in Figure 27.1. The thickness variation in this region is more clearly illustrated in Figure 27.3. These geometrical features lead to a significant stress concentration factor and to out-of-plane secondary bending at the location of cracking, as discussed in [5,6].

The cracking occurs in the chordwise direction, normal to the direction of the nominal principal stress at that location. The presence of secondary bending results in faster crack growth along the wing-skin's inner surface relative to its outer surface. This discrepancy between the surface traces is further accentuated by the residual compressive stress at the outer surface caused by shot peening. For the purposes of assessing the residual strength, however, it is convenient to assume a straight-fronted through crack, as indicated by the shaded area in Figure 27.3. This leads to the residual strength estimate of 168 MPa cited earlier. This estimate is conservative in two respects. First, the effective toughness for the skin material (2024-T851 aluminium alloy, 3.6–3.8 mm thick, LT orientation) has been found

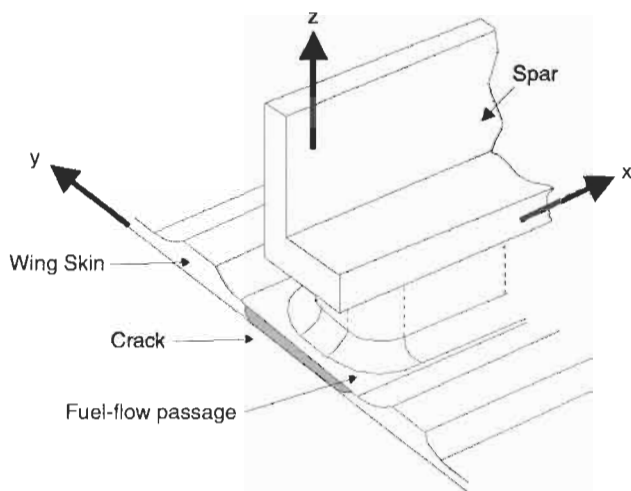


Fig. 27.3. Local geometry of the wing skin in the vicinity of the fuel-flow passage, showing the location of cracking and the coordinate axes used in the text.

experimentally to be in the range $57\text{--}62 \text{ MPa}\sqrt{\text{m}}^{1/2}$, which is significantly higher than the handbook value assumed earlier. Secondly, the beneficial effect of the spar bridging the crack has been ignored in deriving this estimate.

27.3. Repair substantiation requirements

The repair substantiation requirements were as follows:

To validate the repair design by an independent method. In this case, 3D Finite Element Analysis closely coupled with a representative article test program was used.

To verify, through representative article testing, that the structural integrity of the repaired structure has been restored to the level specified (or implicit) for the original certification of the aircraft, with respect to (a) static residual strength, (b) durability and damage tolerance, with proper accounting for environmental effects and for possible detrimental effects of the repair on the structural integrity of the surrounding structure.

27.3.1. Design load cases

The principal load case considered corresponds to a balanced symmetric manoeuvre at Mach 1.4, wing sweep angle = 50° , Gross Weight = 59000 lb, Altitude = 26000 ft, Dynamic pressure = 1030 psf, $N_z = 6.5 \text{ g}$, Temperature = 167°F (75°C). The Design Ultimate Stress for this condition is 51.9 ksi. The design was also evaluated at -40°F (-40°C) being the temperature the aircraft experiences at

cold proof load test (CPLT). The CPLT is conducted at approximately 2000-h intervals. It involves the application of a proof load (the “once in a lifetime” or design limit load, DLL) to the structure at a reduced temperature of -40°F , where the critical D6ac steel material exhibits a reduced fracture toughness.

27.3.2. Fatigue loading

The specified fatigue loading was based on a detailed cycle-by-cycle load spectrum available from multi-channel recorders fitted to RAAF F-111 aircraft. This spectrum is representative of RAAF usage and is currently used for structural management of the F-111 fleet. The loads expressed in terms of the wing-pivot bending moment were converted to nominal stresses at FASS 281 using a stress equation which was verified as part of the development of a detailed 3D FE stress analysis [5–7]. The spectrum from [9] is shown in exceedance diagram form in Figure 27.4 below.

27.4. Validation strategy

The strategy employed to address the repair-substantiation requirements involved a closely integrated program of testing and of detailed stress analysis. The stress analysis was used not only to verify the analytical design formulae, as required above, but also to guide specimen design, and to provide a basis for correlating crack (or damage) growth rates and failure modes between the various levels of testing, thereby providing a high level of confidence in the interpretation of test results and their applicability to the actual in-service repair.

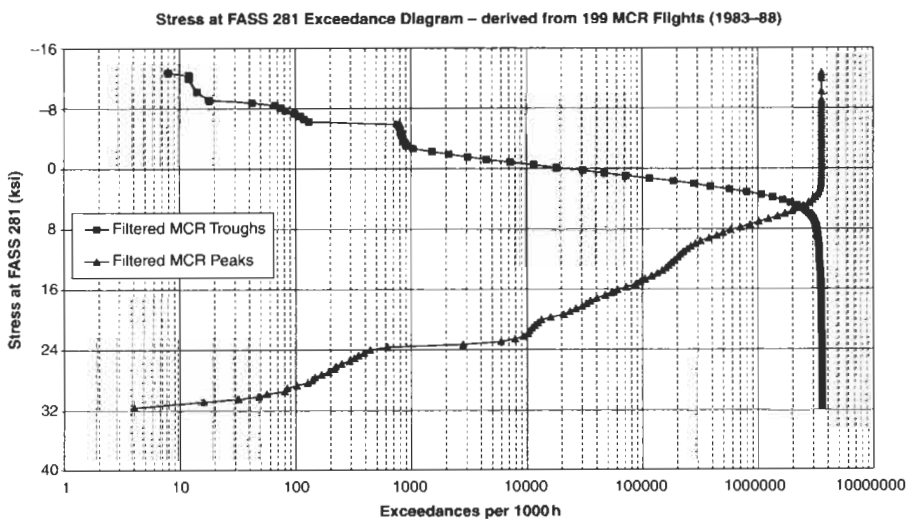


Fig. 27.4. Stress exceedance diagram at FASS 281.

The RAAF requirement with regard to environmental effects and damage tolerance is that the testing conditions should be severe relative to anticipated service conditions, but realistic. The present substantiation package involves three levels of testing, as described below in Section 5. It will also seek to derive the maximum benefit from the extensive previous service and laboratory experience with bonded repairs, as summarised in [3,10–12], particularly in assessing the durability at high temperature [3] and the susceptibility to impact damage [13]. It is also noted that the testing reported below uses axial (spanwise) loading only, but the effect of torsional loads representative of those expected for the present repair has been investigated experimentally in [14].

27.5. Design validation (finite element analysis)

27.5.1. Uncracked, unpatched wing model

A 3D finite element model (see Figure 27.5 below) of the wing skin, supporting spar, adhesive and patch was developed and refined [8].

The model without the crack or patch was calibrated to data available from a strain survey undertaken on a full-scale (uncracked) wing. It was found that the stress distribution prior to cracking is sensitive to the precise thickness variation around the fuel flow passage. Considerable mesh refinement and attention to detail of the local geometry was required to obtain a good correlation. Figure 27.6 below illustrates the excellent correlation obtained, which provides confidence in the

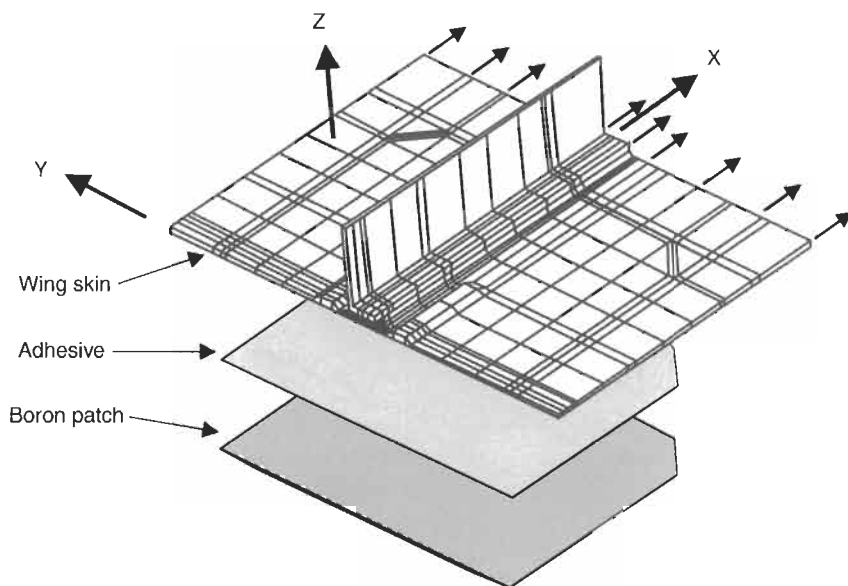


Fig. 27.5. Skin/spar FE model with outline of adhesive and boron patch.

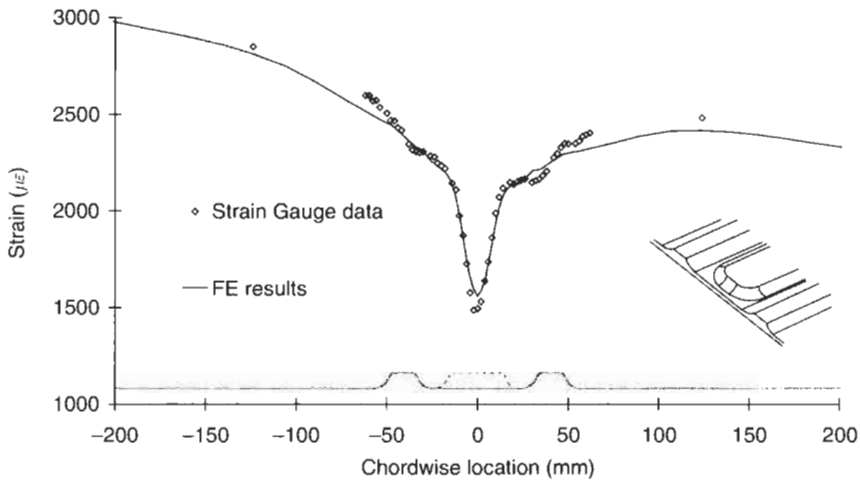


Fig. 27.6. Comparison of strain-gauge data from a static strain survey of a full-scale test wing with predictions from a 3D finite-element model of the region shown in Fig. 27.3. The FE results include a correction for the chordwise variation of the wing-box section. The strains correspond to limit-load (CPLT).

adequacy of the FE model to reproduce the complex stress state around the fuel flow passage at FASS 281.

Calibration of the FE results against the full scale strain survey provided a refined stress equation for that location (i.e. a more accurate relation between the nominal local stress and the wing pivot bending moment than was available from the original, approximate aircraft design calculations). This refined stress equation was used in setting the stress levels for the structural testing.

The FE results indicated the presence of significant stress concentration and secondary bending, both prior to cracking and in the cracked, repaired structure. These effects were not accounted for in the original repair design. However, it was discovered that there was sufficient conservatism in the design procedures [1] that the repair was still acceptable in terms of design.

27.6. Cracked, patched model including thermal effects

The cracked, patched FE model was analysed at the extremes of temperature (-40°C and $+75^{\circ}\text{C}$) including thermal mis-match effects [1]. The significant factors to consider are the stress intensity in the repaired structure, and the shear stress in the adhesive near the crack. The stress intensity factor FE results compared with the C5033 [1] design analysis are shown in Figure 27.7 below.

The adhesive shear stress results are shown in Figure 27.8 and 27.9 below for the -40°C and $+75^{\circ}\text{C}$ cases respectively.

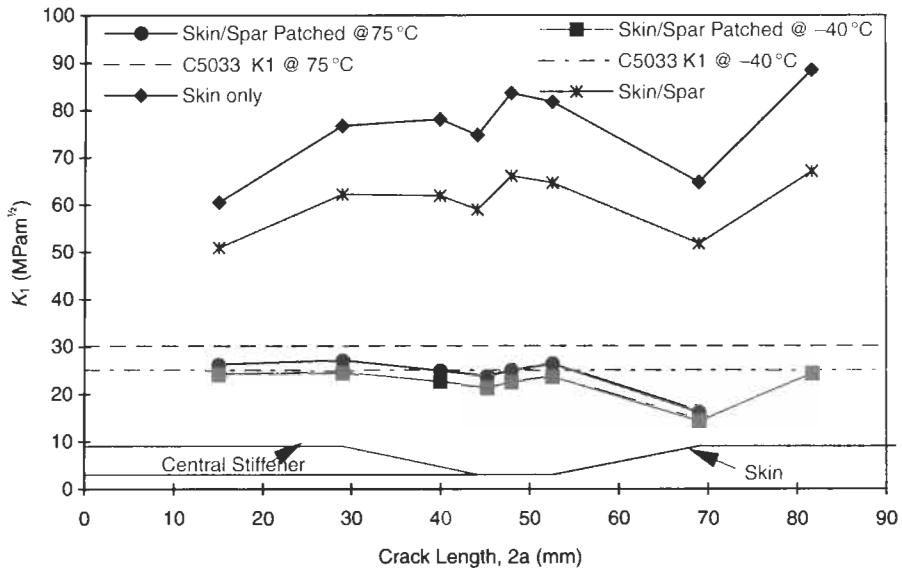


Fig. 27.7. Stress intensity factor versus crack length at design limit load.

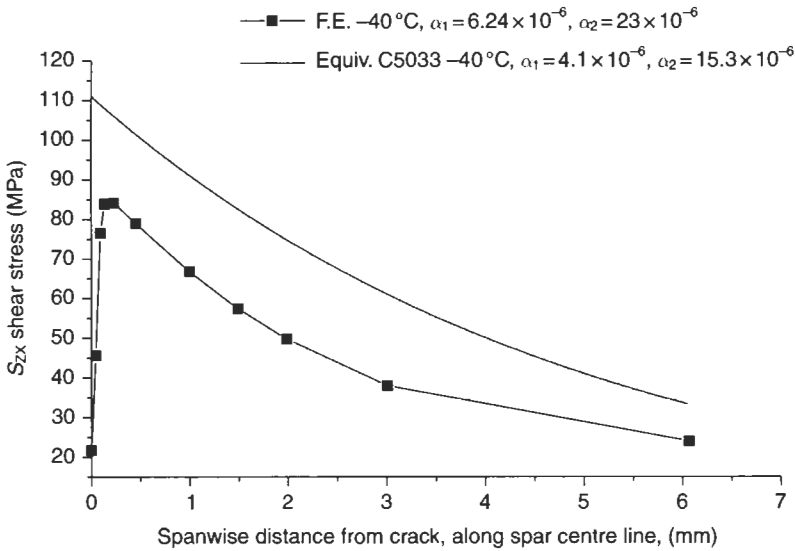


Fig. 27.8. Adhesive shear stress (τ_{zx}) near crack, -40°C, at DLL.

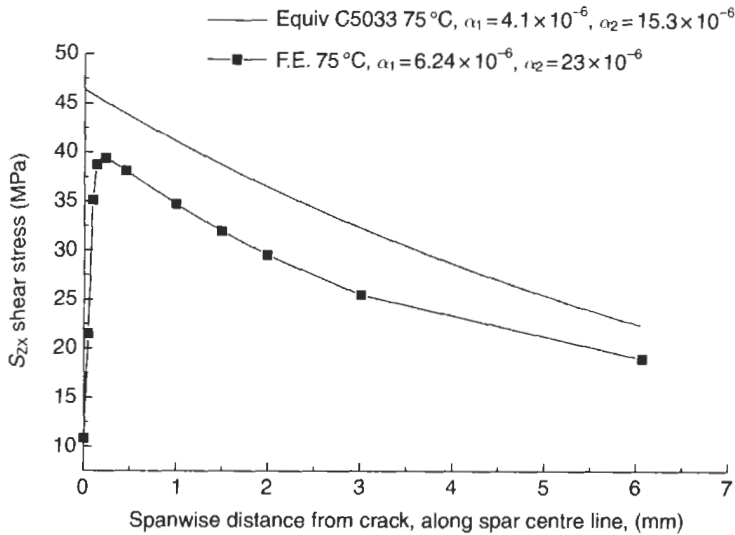


Fig. 27.9. Adhesive shear stress (τ_{zx}) near crack, + 75 °C, at DLL.

These results demonstrate that the original design procedures [1] gave conservative results that compare well with the FE.

27.7. Repair substantiation (representative specimen testing)

Three levels of structural testing were undertaken. Figure 27.10 below details the three levels of testing which are discussed in this section.

The first two levels (the box and panel specimens) are intended to serve as representative test articles. They employ wing skins which contain the structural detail as shown in Figure 27.3. In the case of the box specimens, the restraint due to the spar is also included and the specimens can accommodate the full compressive loads encountered in service. The representative bonded joint (RBJ) specimens were used to quantify the effects of peel stress and extremes of temperature, moisture and simulated damage. The FE analysis provided a theoretical basis for correlation between these various levels of testing and for interpretation of the results.

27.7.1. Representative bonded joints

The RBJ specimens consisted of two 2024-T851 aluminium alloy inner adherends joined and sandwiched between two boron patches to form a double sided bonded joint as shown schematically in Figures 27.10 and 27.11. The specimen was intended to simulate faithfully the combination of adhesive shear and peel stresses that occurs near the crack.

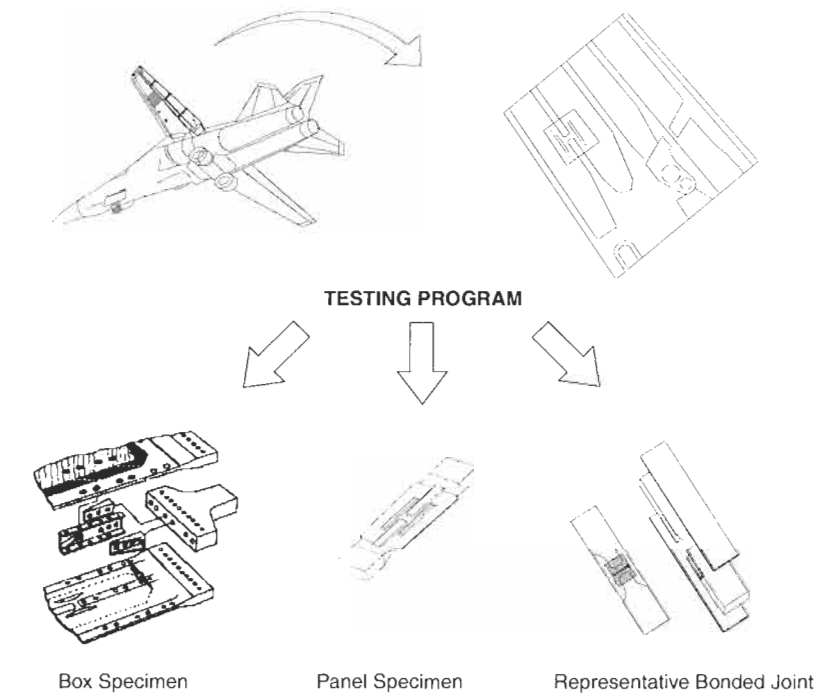


Fig. 27.10. Three levels of representative specimen testing.

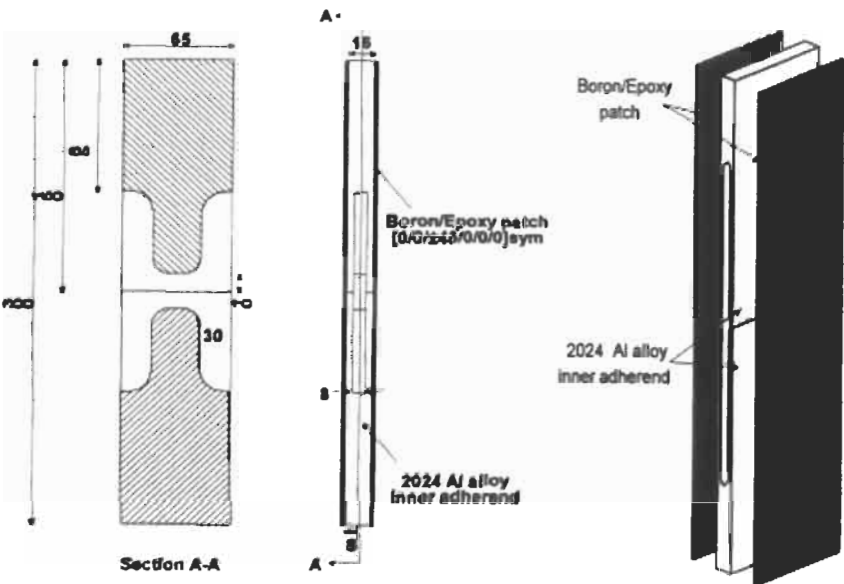


Fig. 27.11. Representative bonded joint specimens.

27.7.2. Panel specimens

The panel specimens (Figure 27.12) contained a test section which was representative of the structural detail at the crack location. They were used to quantify the performance of the repair in terms of the following:

1. Static Strength at room temperature, extreme low temperature of -40°C , and extreme high temperature of $+110^{\circ}\text{C}$.
2. Crack growth rate reduction after patching.
3. The effects of temperature and testing frequency on patched crack growth rate.

The first objective was to verify that the stress and strain distribution in the panel specimen was representative of the full scale wing structure. The results of a strain survey comparison of the uncracked and unpatched panel and box specimens [14] compared with the full scale wing is shown in Figure 27.13 below.

The strain survey comparison coupled with FE analysis demonstrated that the panel and box specimens exhibited far field stress and strain consistent with the full scale wing, but they showed significantly more secondary bending. This is considered to be acceptable because it means that the loading on the panel and box specimens was in fact more severe than the full scale structure, and should therefore provide conservative estimates of the crack growth rate, fatigue life and residual strength.

The results of the static load testing [14] are shown in Figure 27.14 below.

A comparison of the crack growth rates in the panel specimens in the patched versus unpatched condition under spectrum loading [14] is shown in Figure 27.15 below.

In terms of the effects of frequency and temperature on crack growth rate, tests were performed at ambient temperature (23°C) and elevated temperature (80°C), and at frequencies of 0.5 and 5 Hz. The results are reported in [14,15]. No significant effect of temperature or frequency variation on patched crack growth rate was detected. It is particularly interesting that the temperature appeared to have little effect. The adhesive shear stiffness properties change significantly with temperature. At an elevated temperature, the adhesive is significantly less stiff and the crack patching efficiency is reduced, ie the stress intensity reduction is less. However, there is less residual tension stress in the cracked structure due to post

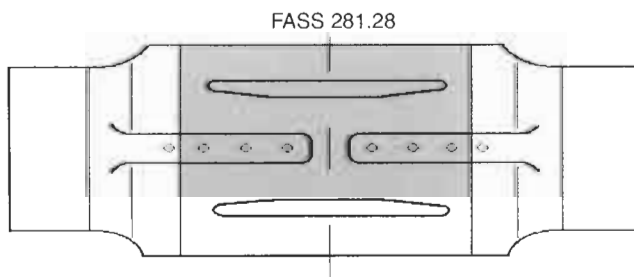


Fig. 27.12. Panel specimen.

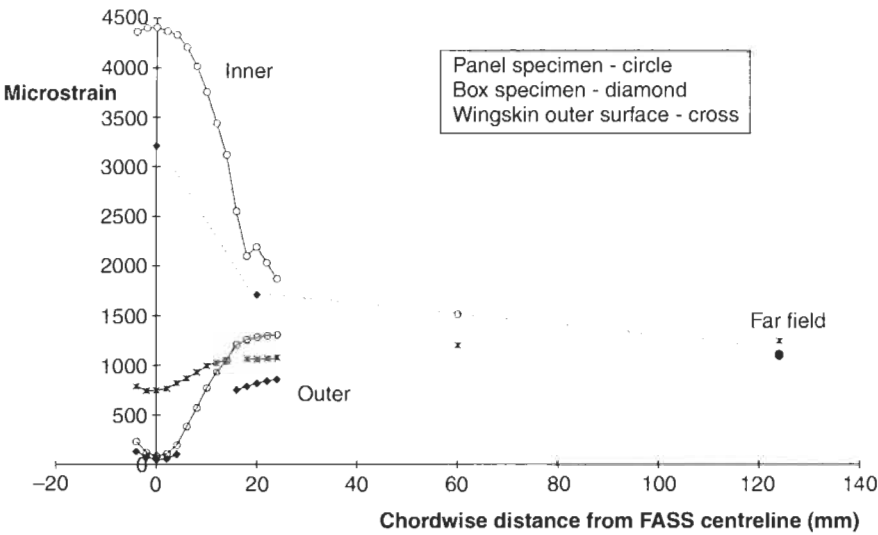


Fig. 27.13. Chordwise strain distribution at 50% DLL.

cure thermal mis-match due to a lower coefficient of thermal expansion for the boron compared with the aluminium. The combination of these two competing effects may cancel each other out such that the patched crack growth rate is relatively unaffected.

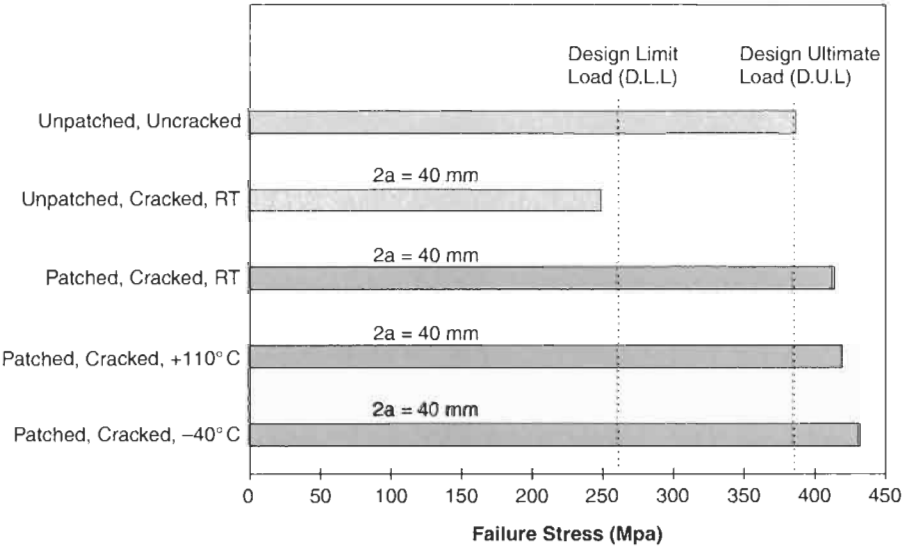


Fig. 27.14. Results of static strength tests on panel specimens.

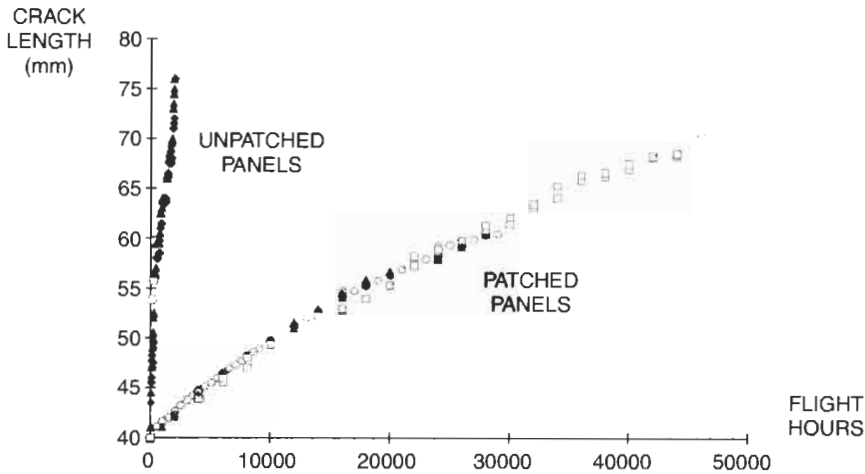


Fig. 27.15. Comparison of patched and unpatched crack growth in the panel specimens.

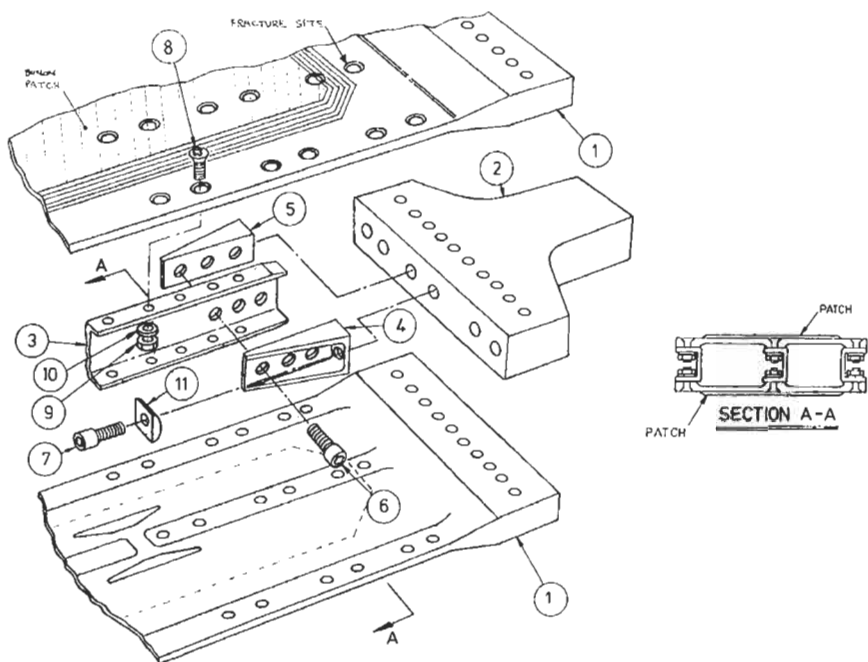
27.8. Box specimens

The box specimen was designed to incorporate the out of plane support and thermal mass provided by the complete built up wing structure, and is large enough to install a full size repair patch. The specimen arrangement is shown in Figure 27.16. The results of the box specimen testing were consistent with the panel specimen as shown in the crack growth comparison in Figure 27.17.

27.9. Repair history

Following the application of the repair, the aircraft flew safely for more than two years and accumulated 665.9 flying hours. The repair was inspected regularly (at least every 100 h) for any evidence of disbonding, degradation or crack growth under the patch. Some small disbond indications were detected at the corners of the repair. These are believed to have been present since the repair was applied and have not developed or progressed in service. They are believed to have been caused by poor consolidation of the adhesive (confined to small regions at the patch corners) and the application methods have now been revised to prevent a recurrence. At the time of writing, a further three wings with similar cracking have also been repaired, and there are plans to apply the repair fleet wide as a fatigue enhancing reinforcement.

The original cracked wing has now been retired from RAAF service. It is being used as a full scale fatigue test article and will be subjected to a full tear down investigation at the conclusion of the test. The wing has now seen a further 8074.4 h of testing under a spectrum representative of RAAF usage with no crack growth or degradation of the repair identified. Further investigation of the minor disbond



indications mentioned earlier revealed that the bond was, in fact, still intact in these small regions. The reason for the indications is still under investigation, but it appears that the adhesive consolidation was to blame and that has now been resolved.

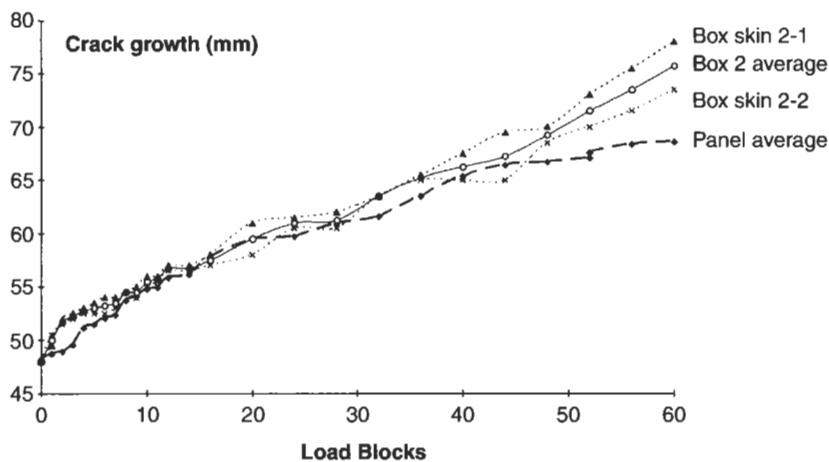


Fig. 27.17. Comparison of box and panel specimen crack growth (1 Block = 500 h).

27.10. Conclusion

A safety critical bonded composite repair to the outer lower wing skin of an F-111 aircraft has been fully validated and substantiated. The first wing to be repaired has now completed 665.9 h of actual operational usage and a further 8074.4 h in a full-scale wing fatigue test. As expected based on the coupon testing and the analyses, there has been no degradation or crack growth detected. A further three wings have now been repaired and returned to fully operational status using this repair technique. The substantiation and validation process demonstrated that the repair design was sound. The combination of an independent analysis (based on 3D Finite Element Analysis) for the validation, closely coupled with representative coupon testing for the substantiation proved to be an extremely efficient and effective method for the validation and substantiation necessary for such a critical repair.

References

1. Composite Materials and Adhesive Bonded Repairs, RAAF Standard Engineering C5033 Issue 1, 4 September, 1995.
2. Baker, A.A. and Jones, R. (eds.) (1988). Bonded Repair of Aircraft Structures, Martinus Nijhoff.
3. Baker, A.A. (1994). Bonded Composite Repair of Metallic Aircraft Components – Overview of Australian Activities, AGARD Specialist Meeting on Composite Repair of Military Aircraft Structures, Seville, 3–5 October.
4. McHenry, H.I. and Key, R.E. (1968). The F-111 Logic: Familiar Materials; Proven Processes, *Metal Progress*, **93**(3), 62–68.
5. Callinan, R.J., Sanderson, S. and Keeley, D. (1997). Finite Element Analysis of an F-111 Lower Wing Skin Fatigue Crack Repair, DSTO-TN-0067, January.
6. Keeley, D., Callinan, R. and Sanderson, S. (1996). A Validated Finite Element Model of an F-111 Lower Wing Skin Structural Detail at Forward Auxiliary Spar Station 281.28, DSTO-TN-0046, June.
7. Keeley, D., Callinan, R. and Sanderson, S. (1996). Sensitivity Study of an AMRL Finite Element Model of the F-111 Lower Wing Skin Structural Detail at Forward Auxiliary Spar Station (FASS) 281.28, DSTO-TN-0060, September.
8. Callinan, R.J., Sanderson, S. and Keeley, D. (1997). Finite Element Analysis of an F-111 Lower Wing Skin Fatigue Crack Repair, DSTO-TN-0067, January.
9. Walker, K. and Swanton, G. (1996). Static and Fatigue Loading Development for an F-111 Bonded Composite Repair Substantiation, DSTO-TN-0063, November.
10. Lincoln, J.W. (1994). Challenges for the aircraft structural integrity program. *Proc. FAA/NASA Symp. on Advanced Structural Integrity Methods for Airframe Durability and Damage Tolerance*, edited by C.E. Harris, NASA CP 3274, September.
11. Raizenne, M.D., Benak, T.J. and Heath, J.B.R. (1994). Bonded Composite Repair of Thin Metallic Materials: Variable Load Amplitude/Temperature Cycling Effects, Report LTR-ST-1979, Institute for Aerospace Research, Canada, August.
12. Belason, E.B. (1994). Status of Bonded Boron/Epoxy Doublers for Military and Commercial Aircraft Structures, AGARD Specialists Meeting on Composite Repair of Military Aircraft Structures, Seville, 3–5 October.
13. Belason, E.B., Rutherford, P. and Miller, M. (1994). Evaluation of Bonded Boron/Epoxy Doublers for Commercial Aircraft Aluminium Structures. FAA/NASA Symposium on Advanced Structural

Integrity Methods for Airframe Durability and Damage Tolerance, (C.E. Harris ed.), NASA CP 3274, September.

14. Boykett, R. and Walker, K. (1996). F-111C Lower Wing Skin Bonded Composite Repair Substantiation Testing, DSTO-TR-0480, November.
15. Walker, K. and Boykett, R. (1996). Repair Substantiation Fatigue Testing Including Temperature and Frequency Effects for a Bonded Composite Repair to an F-111 Lower Wing Skin, Presented at the USAF ASIP Conference, San Antonio, Texas, USA, December.

Chapter 28

CASE HISTORY: COMPOSITE DOUBLER INSTALLATION ON AN L-1011 COMMERCIAL AIRCRAFT

Full-Scale Structural and NDI Validation Tests of Bonded Composite Doublers

D. ROACH

Sandia National Laboratories, FAA Airworthiness Assurance Center

28.1. Introduction

The development and application of new aircraft repair techniques needs to keep pace with the growing understanding of aircraft structural aging phenomena. One of the primary goals of the Federal Aviation Administration's (FAA) National Aging Aircraft Research Program (NAARP) is to foster new technology associated with the repair of civil aircraft. Following a request from the manufacturers and airlines to utilize composite doubler repairs on commercial aircraft, the FAA sponsored a program at its Airworthiness Assurance Center operated by Sandia National Laboratories. A door corner repair, a typical repair for cracks found on many commercial aircraft, was selected as the target application. An industry team consisting of an Original Equipment Manufacturer (Lockheed-Martin) and an airline (Delta Air Lines) was formed. FAA oversight was provided through the Atlanta Aircraft Certification Office (ACO) and the FAA's William J. Hughes Technical Center. The overall goals of this project were to: (1) establish the capabilities of composite doublers, (2) gain FAA approval for composite doubler use on commercial aircraft, and (3) assist the FAA in developing guidance which will assure the continued airworthiness of these aircraft repairs.

Composite doubler use in commercial aircraft repair

In addition to developing general information to support composite doubler use, this program introduced composite doubler technology to the U.S. commercial aircraft fleet. A specific application was chosen – repair of an L-1011 door frame – in order to provide the proof-of-concept driving force behind this test and analysis project. By focusing on a particular commercial aircraft application and encompassing all “cradle-to-grave” issues such as design, analysis, installation,

long term durability, and nondestructive inspection, this program was designed to assess the capabilities of composite doublers. Although a specific application provided the foundation for this project, it should be noted that the data stemming from this study serves as a comprehensive evaluation of bonded composite doublers for general use.

Full-scale structural and NDI test program

Most of the concerns surrounding composite doubler technology pertain to long-term survivability, especially in the presence of non-optimum installations, and the validation of appropriate inspection procedures. Through the use of analysis, laboratory tests, and flight demonstrations on an in-service L-1011 airplane, this project investigated composite doubler design, fabrication, installation, structural integrity, and NDI issues. This chapter summarizes a series of structural tests and NDI inspections that studied the structural response and damage tolerance of Boron-Epoxy doublers installed on representative aircraft structure. The tests were conducted to evaluate the general use of bonded composite doublers to repair metallic aircraft structures. Specific emphasis was placed on select areas of the doubler design which experience the highest strains and must survive large peel stresses. Specimen geometry and load conditions were engineered to exceed design strains corresponding to the worst-case flight conditions. A comprehensive report on this program and the test results is provided in reference [1].

28.2. Fuselage door surround structure tests

28.2.1. Full-scale structural testing philosophy

The goal of structural testing is to determine how structures behave statically and dynamically under realistic loading conditions. It is often necessary to utilize full-scale or large-scale test articles in order to adequately account for all aspect of a structure's configuration – especially the unique aspects of connections and fastened joints – and to properly apply the operating boundary conditions. In this program, use of an actual aircraft fuselage section allowed for the most accurate assessment of stress concentrations, residual stresses, and variations in structural response across fuselage cut-outs and doublers. The understanding and insight gained from these tests include: (1) correlation with analytical models of structural behavior, (2) evidence that the composite-reinforced structure can meet its intended strength and durability requirements, and (3) proof that the doubler and surrounding structure can meet their performance requirements such as fatigue resistance and damage tolerance.

In the case of the aircraft structures addressed here, full-scale tests can be used to determine how much the stress has to be reduced to increase the life a required amount. This is achieved through appropriate comparisons between the test strain data and S-N fatigue curves for the structure's material. The comparison can be based on similar loading as described by the stress ratio, R . Similarly, S-N

characteristics and stress data from aircraft panel tests can be used to assess damage accumulation and make life predictions based on damage tolerance in the presence of different R values. This process is an approximation, however, it serves as a guide for considering the stress levels and the affect of stress reductions on the life of an aircraft structure.

Full-scale tests were conducted on a large fuselage panel cut from retired aircraft. These tests studied load transfer around composite doublers subjected to simulated flight conditions of fuselage pressure and axial stress. The test series utilized a complete L-1011 door surround structure to: (1) assess general composite doubler response in representative flight load scenarios, (2) evaluate the effectiveness of composite doublers in reducing the stresses around a damaged or weakened structure and the associated crack mitigation capabilities, and (3) verify design and analyses methodologies for composite doubler technology. The test bed was instrumented with strain gages and subjected to simulated fuselage pressure differential loads using a customized fuselage test fixture described in this chapter. Nondestructive inspections (NDI) were interjected throughout the test series.

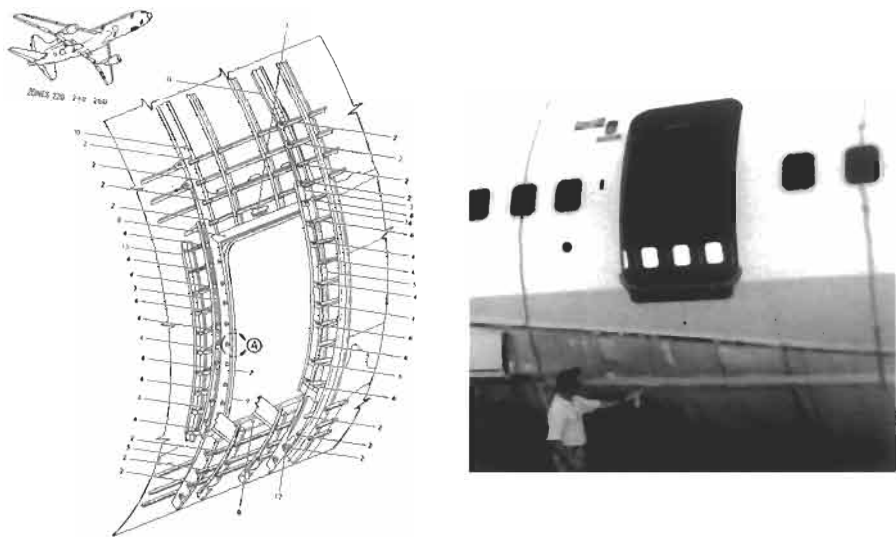
28.2.2. L-1011 fuselage structure

The primary test article was a large fuselage section cut from a retired All Nippon Airways (ANA) L-1011 aircraft. The fuselage test article included a passenger door (P3 passenger door) cut-out and contained all substructure frame, longeron, and stringer elements. The fuselage cross section has a radius of 117.5 in. and the nominal thickness of the 2024-T3 skin in the P-3 door area is 0.68". Figure 28.1 shows the basic L-1011 structure and a photograph of the door surround structure section prior to being cut from the L-1011 fuselage. The door surround structure test article contained eight circumferential frames and six longitudinal stringers, as well as, the upper and lower longeron around the door cut-out. This test bed was instrumented with strain gages and subjected to simulated fuselage pressure differential loads using a customized fuselage test fixture.

28.2.3. Repair of fuselage test article with a composite doubler

Overview of boron-epoxy composite doubler

The important test article modification involved the installation of a Boron-Epoxy doubler to the upper, forward corner of the P3 door surround structure. The door surround structure was tested before and after the doubler was installed to evaluate strain field improvements produced by the composite doubler. The Boron-Epoxy doubler design discussed in this analysis is shown in Figure 28.2. The doubler consists of 72 plies oriented in a quasi-isotropic lay-up of sequence [45, 0, -45, 90]. This type of lay-up is the most effective at reducing inter-laminar peel stresses. In addition, peel stresses in the adhesive bond line are reduced by tapering the edges of the doubler away from the door corner. The rectangular cutout in the doubler is required to facilitate the existing emergency door release handle. Following composite doubler installation, the door surround structure was visually



(a) Structural Configuration of Passenger Door Area

(b) Section Cut from Retired L-1011 Aircraft for Full Scale Tests

Fig. 28.1. L-1011 Door surround structure test article.

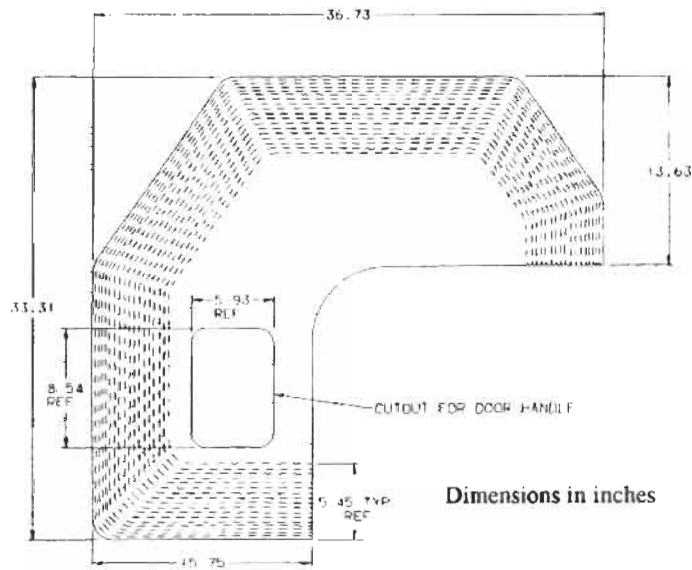


Fig. 28.2. L-1011 Door corner boron-epoxy repair doubler.

inspected and ultrasonically scanned to determine if there were any disbond or delamination flaws.

Doubler stiffness requirements

To provide adequate stress reduction and crack growth mitigation, the doubler was designed to have a minimum stiffness ratio (for extension and shear) of 1.2. In order to avoid an overly stiff doubler that creates stress concentration problems in the skin adjacent to it, this ratio should not be much greater than 1.5. The stiffness ratios are defined as:

Extension:

$$R_x = \frac{(E_x t_{\text{laminate}})_{\text{BE}}}{(E_x t)_{\text{A1}}} \quad (28.1)$$

Shear:

$$R_{xy} = \frac{(G_{xy} t_{\text{laminate}})_{\text{BE}}}{(E_x t)_{\text{A1}}} \quad (28.2)$$

Classical laminated plate theory, along with Boron-Epoxy lamina properties [2], were used to arrive at the cured laminate moduli E_x and G_{xy} . The resulting R_x and R_{xy} values are as follows:

$$\begin{aligned} R_{x(-65^\circ F)} &= 1.55 & R_{xy(-65^\circ F)} &= 1.53 \\ R_{x(\text{RTA})} &= 1.51 & R_{xy(\text{RTA})} &= 1.49 \\ R_{x(180^\circ F)} &= 1.29 & R_{xy(180^\circ F)} &= 1.27 \end{aligned}$$

Thus, the L-1011 doubler provides adequate stiffness without overly restraining the adjacent skin.

28.2.4. Biaxial test facility description

The door surround structure test bed was subjected to a combined load environment of external vacuum (note: external vacuum was used to simulate the internal pressure which generates the primary hoop stresses in the airplane) and axial, or longitudinal, stress. A specialized structural test facility was developed to simulate maximum cabin pressure loads. It used a computerized feedback system to maintain the proper ratio between hoop and axial loads. The differential cabin pressure was generated using a custom vacuum chamber while the axial loads were applied by hydraulic rams. The applied biaxial tension loads approximated the stresses induced by normal flight pressurization (maximum L-1011 cabin pressure differential is $\Delta P = 8.835$ psi). Figure 28.3 is a schematic of the multi-axis load test bed for the curved fuselage panels. It shows the vacuum chamber, the restraints in the hoop direction, and the load trains in the axial direction. Turnbuckles in the hoop direction were used to adjust the boundary conditions in order to assure a

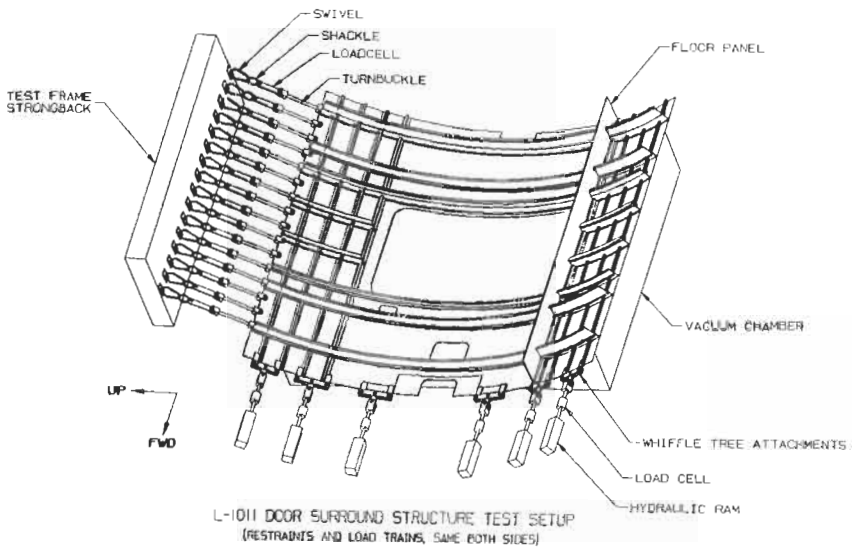


Fig. 28.3. Biaxial test facility design drawing showing the door surround structure mounted in the vacuum chamber and the hoop and axial load application hardware.

uniform load across the width of the door surround structure. As the vacuum load was applied, hoop and axial loads were developed in the test article. Figure 28.4 shows the door surround structure mounted in the biaxial test facility. It shows one

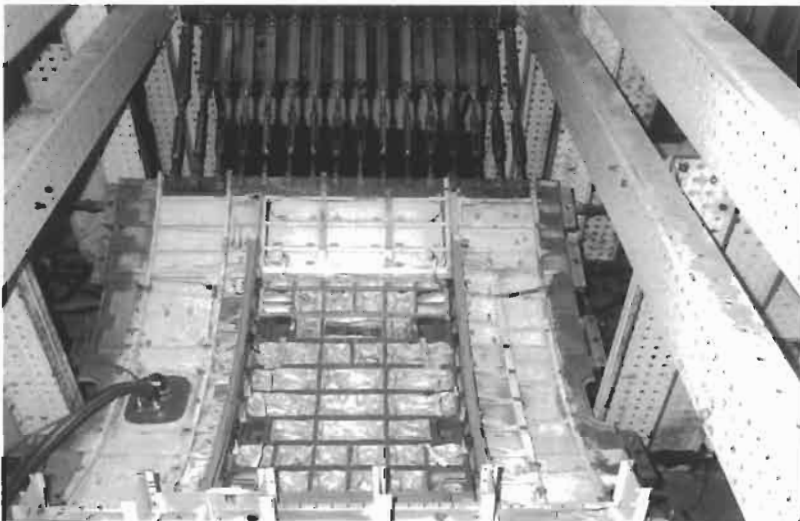


Fig. 28.4. Door surround structure mounted in the biaxial test facility.

side of the hoop restraints and the longitudinal whiffle trees attached to the test article.

The entire stress field on and around the composite doublers was monitored using the strain gages. Load, strain, and pressure data was acquired at 0.5 psi intervals up to the maximum pressure differential test goal of 10.0 psi. The L-1011's maximum operating pressure is 8.835 psi. Vacuum pumps were used to produce the pressure differential across the door surround structure. The pressure differential and longitudinal tension loads were increased in accordance with thin-walled cylinder theory. That is, a ratio of 2:1 was maintained between the hoop and axial stresses.

Instrumentation

The loads applied by the hydraulic tension rams or reacted by the turnbuckle restraints were monitored by load cells. A pressure transducer measured the pressure differential across the fuselage skin. The entire strain field on and around the composite doubler was monitored using a series of biaxial and Rosette strain gages. Data was acquired to study the following issues: (1) load transfer through the doubler, (2) stresses in the doubler and parent structure, and (3) effect of the doubler on the fuselage stresses adjacent to the doubler. Prior to the composite doubler installation, a series of strain gages monitored the strain fields in the "original," unmodified door surround structure. These same gage locations were monitored again after the doubler was installed. A series of Rosette gages were also placed on the aluminium skin within the perimeter of the composite doubler footprint. The locations shown correspond to high strain areas, potential crack initiation sites and important load transition regions along the outer perimeter of the doubler. These gages allowed for "before-and-after" data comparisons to assess the effects of the doubler on the overall strain field. Finally, several external gage locations had matching strain gages mounted on the inside of the door surround structure at the same X, Y location. This allowed for an assessment of the bending strains at those locations.

28.3. Fuselage door surround structure test results

28.3.1. Structural tests before composite doubler installation

Prior to installing the composite doubler, a biaxial test was conducted on the door surround structure test article using the custom test facility and procedures described in Section 28.2. The test loads simulated the maximum cabin pressure loads. Strain data showed that the maximum hoop strains were found at the common cracking location along the vertical portion of the door cut-out and at the door corner radius. The maximum axial strains were found at the the common cracking location along the horizontal portion of the door cut-out, the common cracking location above the door handle cut-out, and at the door corner radius. Finally, large shear strains were monitored at the door corner radius and along the upper (horizontal) leg of the doubler repair area.

28.3.2. Structural tests after composite doubler installation

Upon completion of the structural tests on the fuselage section in its original condition, the 72-ply, door corner repair doubler was installed on the test article. The photos in Figure 28.5 show an overall view of the doubler on the fuselage test article and the strain gages installed on the composite doubler and surrounding aluminium skin. Figure 28.6 shows the 74 channels of strain that were used to monitor: (1) the strain field throughout the composite laminate and aluminium parent material, and (2) the load transfer into the composite doubler.

28.3.2.1. Strain field analysis.

The locations of the peak strain areas after the doubler was installed agree with those found in the “before doubler” test. Their magnitudes, however, are less. Direct before and after comparisons show that the strain field around the door cut-out was not shifted by the doubler. Rather, the strain levels in all areas were uniformly reduced. This data substantiates the doubler design (footprint and stiffness) since it demonstrates that the doubler does not create new stress risers due to excessive doubler stiffness in any one area.

These strain reductions, along with the fact that the doubler did not induce any undesirable stress risers in the door corner area, quantify the realization of the basic doubler design goals: (1) to uniformly reinforce the area (global reduction in door corner strains), and (2) achieve the proper stiffness ratio between the parent skin and composite laminate (excessive stiffness would attract undesirably large loads). Figure 28.7 is a plot of data obtained before and after the doubler was installed and show hoop and axial strain reductions around the door corner radius. The strain reductions were primarily in the 40%–60% range.

28.3.2.2. Stress field analysis

Principal stresses.

The principal stresses were determined from strain data obtained from the Rosette strain gages. From these individual strains, the maximum and minimum principal stresses can be calculated using the following equations:

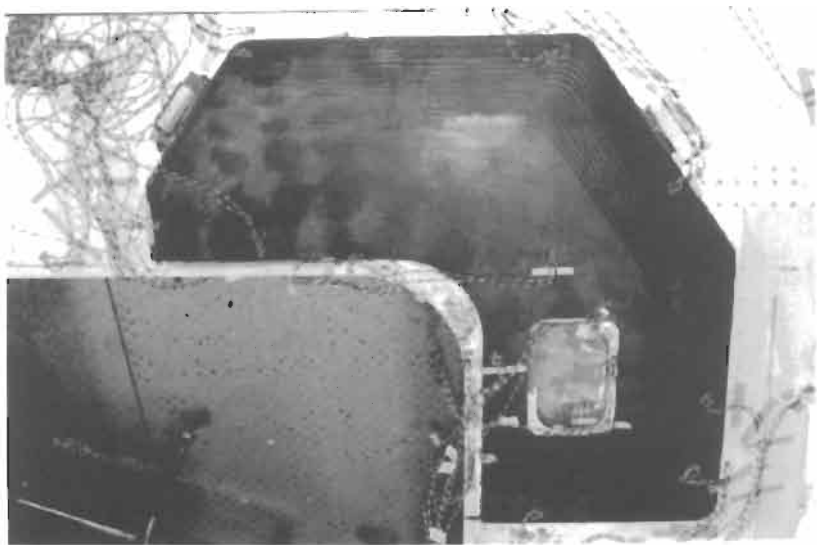
$$\sigma_{\max} = \frac{E(\epsilon_1 + \epsilon_3)}{2(1 - \nu)} + \frac{E}{\sqrt{2}(1 + \nu)} [(\epsilon_1 - \epsilon_2)^2 + (\epsilon_2 - \epsilon_3)^2]^{1/2}, \quad (28.3)$$

$$\sigma_{\min} = \frac{E(\epsilon_1 + \epsilon_3)}{2(1 - \nu)} - \frac{E}{\sqrt{2}(1 + \nu)} [(\epsilon_1 - \epsilon_2)^2 + (\epsilon_2 - \epsilon_3)^2]^{1/2} \quad (28.4)$$

The maximum principal stresses for Rosettes R-8 through R-12 are plotted in Figure 28.8. The largest stress in the aluminium skin was found at R-7 (inside skin) at the door corner radius. The magnitude was 10.6 ksi, down from the 15.3 ksi recorded at that same location before the doubler was installed. The largest Boron-Epoxy stress was 19.3 ksi at the R-8 Rosette gage. This is less than the 22.4 ksi



A. Fuselage Test Article with Composite Doubler Installed; Note Reinforcing Plates Around Perimeter of Fuselage Section for Load Application



B. Close-Up View of Doubler with Strain Gages Installed

Fig. 28.5. Door surround structure test article with strain gages mounted.

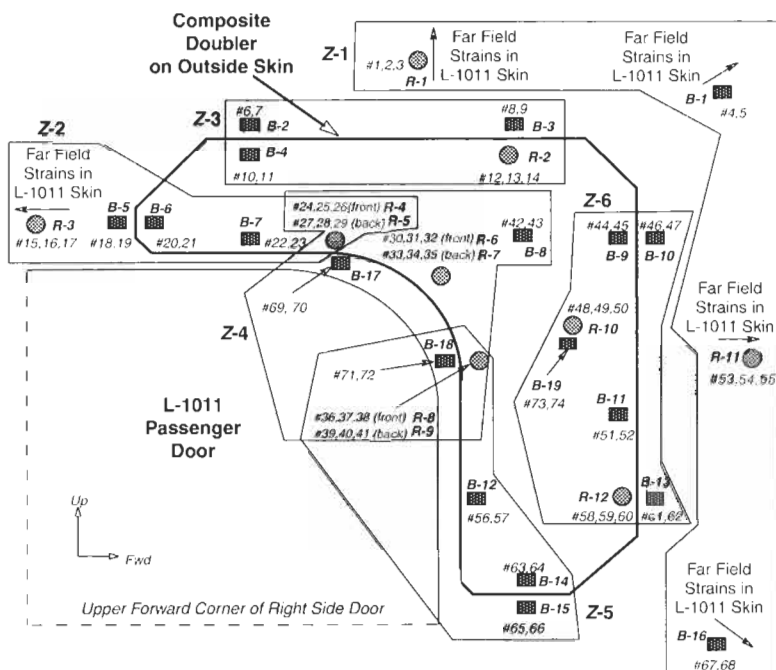


Fig. 28.6. Strain gage layout for fuselage door structure tests after doubler installation.

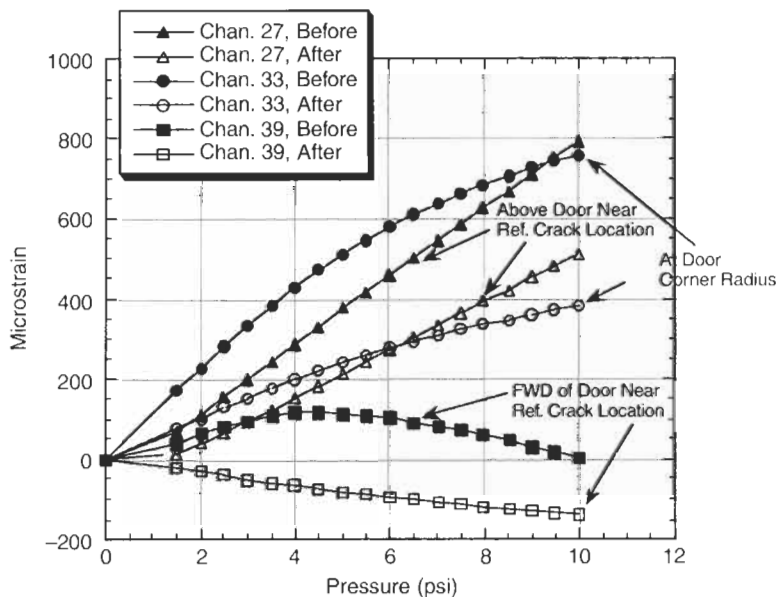


Fig. 28.7. Comparison of strains before versus after doubler installation around door corner radius (Axial Strain Reduction).

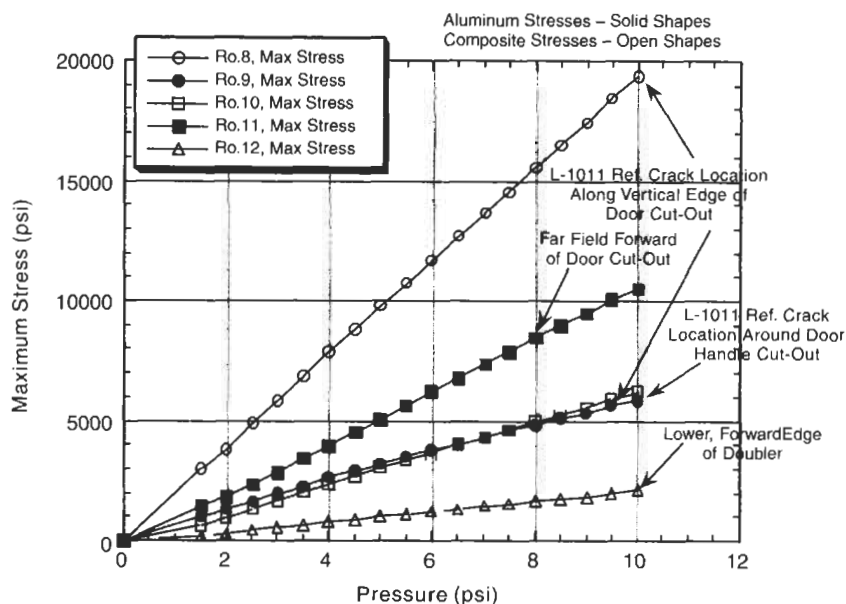


Fig. 28.8. Principal stresses in region of doubler vertical leg.

measured at that same location before the doubler was installed. Similar comparisons of aluminium stresses before the doubler versus aluminium/boron stresses at the same locations after the doubler revealed the stress reductions summarized in Table 28.1. It can be seen that the stresses were reduced by as much as 53% through the application of the reinforcing doubler.

Membrane stresses

The strain data collected from the hoop and axial gages were used to calculate the corresponding membrane stresses using the following equations:

$$\sigma_h = \frac{E}{1 - \nu^2} (\epsilon_h + \nu \epsilon_a) \quad (28.6)$$

$$\sigma_a = \frac{E}{1 - \nu^2} (\epsilon_a + \nu \epsilon_h) \quad (28.7)$$

where E is the modulus of elasticity, ν is Poisson's ratio, σ_h is the hoop stress in the skin, σ_a is the longitudinal stress in the skin, ϵ_h is the hoop strain, and ϵ_a is the axial or longitudinal strain. From Mil-Handbook 5, the modulus of elasticity and Poisson's ratio for 2024-T3 aluminium are $E = 10.5$ msi and $\nu = 0.33$, respectively. For gages mounted on the composite laminate, reference [2] information and the ply lay-up for this doubler generates a Boron-Epoxy laminate modulus $E = 11.87$ msi.

Table 28.1

Principal stress reductions produced by Boron-Epoxy doubler.

Gage identity	Principal stress before doubler (psi)	Principal stress after doubler (psi)	Percent reduction in stress	Location
R.2, Ch. 12, 13 & 14	12701 psi	6879 psi	46%	Outside Skin at Door Corner Radius
R.4, Ch. 24, 25 & 26	9574	6205	35	Above Door Cut-out (Outside Skin)
R.5, Ch. 27, 28 & 29	7448	4911	34	Above Door Cut-out (Inside Skin)
R.6, Ch. 30, 31 & 32	15299	12881	16	Outside Skin at Door Corner Radius
R.7, Ch. 33, 34 & 35	15066	10259	32	Inside Skin at Door Corner Radius
R.8, Ch. 36, 37 & 38	22366	19363	14	Beside Door Cut-out (Outside Skin)
R.10, Ch. 48, 49 & 50	13246	6221	53	Above Door Handle Cut-out

Only one Boron-Epoxy stress exceeded 10 ksi: R-8 hoop stress at the crack reference location along the vertical portion of the door cut-out ($\sigma_h = 19.3$ ksi). Membrane stresses in the aluminium exceeded 10 ksi at the following locations: (1) R-11 axial stress (far field forward of subject area; $\sigma_a = 10.7$ ksi), (2) B-3 hoop stress (far field aft of subject area; $\sigma_h = 12.6$ ksi), (3) B-15 hoop stress (near lower edge of doubler's vertical leg; $\sigma_h = 14.4$ ksi), (4) B-17 axial stress (along upper, horizontal portion of door cut-out; $\sigma_a = 10.2$ ksi), and (5) B-18 hoop stress (crack reference location along the vertical portion of the door cut-out; $\sigma_h = 15.3$ ksi). All of the stresses were well below the 42 ksi nominal yield value for 2024-T3 material.

Bending effects

The primary reason for gaging common locations on the inside and outside of the test article was to obtain information regarding out-of-plane bending in critical regions. The Finite Element Model of the door surround structure and other subelement structural tests highlighted the existence of stress risers at the corner of the door cut-out. Therefore, external Rosettes R-4, R-6, and R-8 were matched by internal Rosettes R-5, R-7, and R-9. Bending strains were calculated using the individual strain gage readings and the following equation:

$$\varepsilon_b(\psi) = \frac{1}{2}(\varepsilon_e + \nu\varepsilon_i)_{(\Psi)} \quad , \quad (28.8)$$

where ε_b is the bending strain, ε_e is the external strain, ε_i is the internal strain, and Ψ denotes the bending direction (hoop, axial, or shear). Comparisons between common strain gage directions revealed the following bending strains in the hoop (h), axial (a), and shear/45° (s) directions:

1. L-1011 reference crack location along the horizontal, upper edge of the door cut-out (R-4 vs. R-5) bending strains: $\varepsilon_b(h) = 62 \mu\epsilon$, $\varepsilon_b(a) = 0 \mu\epsilon$, $\varepsilon_b(s) = 135 \mu\epsilon$.
2. Door corner radius (R-6 vs. R-7) bending strains: $\varepsilon_b(h) = 125 \mu\epsilon$, $\varepsilon_b(a) = -170 \mu\epsilon$, $\varepsilon_b(s) = 552 \mu\epsilon$.
3. L-1011 reference crack location along the vertical, forward edge of the door cut-out (R-8 vs. R-9) bending strains: $\varepsilon_b(h) = 534 \mu\epsilon$, $\varepsilon_b(a) = -163 \mu\epsilon$, $\varepsilon_b(s) = 262 \mu\epsilon$.

These bending strains account for 30% to 50% of the total strain in the structures being monitored. Figure 28.8 also shows the significant amount of bending that occurs across the fuselage skin at R-8/R-9. While the principal stress on the inside skin (R-9) was only 5.9 ksi, the principal stress on the outside skin (R-8) was 19.3 ksi. These results are similar to those obtained during the “before doubler” tests, however, the magnitudes of the bending strains are lower. This shows that the doubler reduced the stress risers in the door corner area.

Load transfer

Percent load transfer values were obtained by calculating the ratio between doubler strains and strains in adjacent portions of the parent aluminium skin $\{\varepsilon_{\text{doubler}}/\varepsilon_{\text{alum(ref)}}\}$. The comparisons focus on strain levels around the outer perimeter of the doubler. References [3–6] determined that this is the critical region of the doubler and that most of the load transfer occurs along the outer, tapered edges of the doubler. As a result, the allowable flaw size – which drives the nondestructive inspection requirements – is smallest around the perimeter of the doubler. The load transfer was consistently in the 40%–60% range. Several outliers were found with minimums of 30% and a high of 80% along the upper portion of the doubler. These load transfer levels agree with the results obtained in references [3,4,7] and, more importantly, match traditional repair design guidelines for reinforcing damaged aircraft structure.

28.3.4. Validation of finite element model analytical results

The performance of the 72 ply composite doubler was analyzed using a finite element model (FEM) of the fuselage structure containing the passenger door [1,3]. The tests described in this document were used to assess the general performance of a composite doubler and to validate the analytical model. Results from the validated FEM were then used to predict the doubler stresses and the reduction in stress in the aluminium skin at the door corner during maximum flight load scenarios.

The FEM of the door region included half of the fuselage circumference between fuselage stations FS769 and FS963. A total of 10150 elements and 167000 degrees-of-freedom were used to model the aluminium skin, the composite doubler, and reinforcing elements such as longerons, frames, and aluminium doublers. The use of proper constitutive properties for the Boron-Epoxy composite laminate and the adhesive layer, as per reference [2], is key to obtaining relevant analytical results. The FEM of the L-1011 fuselage section was able to accurately (within 10%) map out the stress field in the door corner region and correctly locate the Principal Stress

directions. Stress concentrations, stress reductions, and out-of-plane bending components were also correctly identified. The validated FEM was able to assess the damage tolerance and crack mitigation capabilities of the doubler using the complete flight load spectrum. The crack growth analysis revealed that the doubler increases the safety-limit of the fuselage structure by a factor of 2.8. The damage tolerance analysis showed that the doubler exhibits sufficient strength to provide adequate fatigue enhancement over the full spectrum of environmental conditions.

28.3.5. Nondestructive inspection

The inspection requirements for composite doublers involves the identification of disbonds, between the composite laminate and aluminium parent material, and delaminations in the composite laminate. Surveillance of cracks in the parent aluminium material beneath the doubler is also a concern. Eddy current (EC) and X-ray inspections performed on the door surround structure test article did not reveal any cracks in the parent structure. After the doubler was installed and tested in the biaxial load facility, X-ray, eddy current, and ultrasonic inspections did not show any disbond/delamination flaws (composite laminate) or cracks (aluminium) in test article.

28.4. Component level tests: door corner specimen

28.4.1. Door corner test overview

The purpose of this test was to: (1) verify composite doubler analysis techniques, and (2) experimentally assess the potential for delaminations and disbonds in extremely thick composite doubler installations. A Door Corner Specimen, modeled by a C-section test article configuration, was used to study doubler delamination and disbond in extreme bending and peel stress conditions. This test specimen was a subsize mock-up of a skin cut-out with a corner reinforced by a composite doubler. Specimen geometry and load conditions were engineered to exceed design strains corresponding to the worst-case flight conditions of fuselage downbending and pressurization. The important geometric variables, such as door corner radius and load/restraint boundary conditions, match the configuration on the L-1011 aircraft. The aluminium substrate was 0.25" thick (maximum variation in aluminium thickness was 0.01") and the composite doubler was 0.41" thick (maximum variation in composite patch thickness was 0.013").

Figure 28.9 is a photograph of the test specimen mounted in the uniaxial test machine. It is important to note that the composite doubler did not have any edge taper along the horizontal and vertical legs and around the door corner radius. This created a 90° drop off from the full thickness of 72 plies down to the parent aluminium skin. While this does not follow normal doubler design guidelines it does represent the L-1011 door corner repair. Since the doubler needed to have maximum strength in the critical door corner region, it was not possible to utilize a



Fig. 28.9. Photograph of door corner test article mounted in a uniaxial test machine.

tapered edge in this area. This prompted fears about the severity of the shear stresses at the edge of the doubler especially in light of the the loads in the P-3 passenger door area that are well represented by the test described here.

The three structural tests conducted were: (1) Limit Load Test to 10300 lbs., (2) 150% Limit Load Test to 15600 lbs., and (3) Ultimate Failure Test. After reaching 15600 lbs. in the 150% limit Load Test, the load was reduced to 0 lbs. in order to determine if there was any permanent deformation in the test article. In the ultimate failure test, the load was uniformly and continuously increased until structural failure – defined as an inability to sustain an increasing load – occurred. Uniaxial and Rosette (0° , 45° , and 90°) strain gages were installed to monitor the strain field throughout the aluminium skin and the composite doubler. Gage locations were guided by the FEM and were concentrated in the high strain areas around the corner radius. Figure 28.10 shows the strain gage layout.

Pre-test non-destructive inspection

Nondestructive inspection of the test article prior to testing consisted of Thru-Transmission (TTU) and Pulse echo (PE) ultrasonic scans of the doubler. These techniques detect the presence of disbonds, delaminations, and porosity/voids in the material. Figure 28.11 shows the TTU inspection scan of the test article before structural testing. It was found that the specimen contained a flaw in the upper, horizontal leg of the composite doubler (see indication in Figure 28.11). As a result, this test had an element of damage tolerance since the specimen was not in an unflawed, most desirable state. PE ultrasonics was able to determine that the flaw was a disbond at the composite-to-aluminium interface.

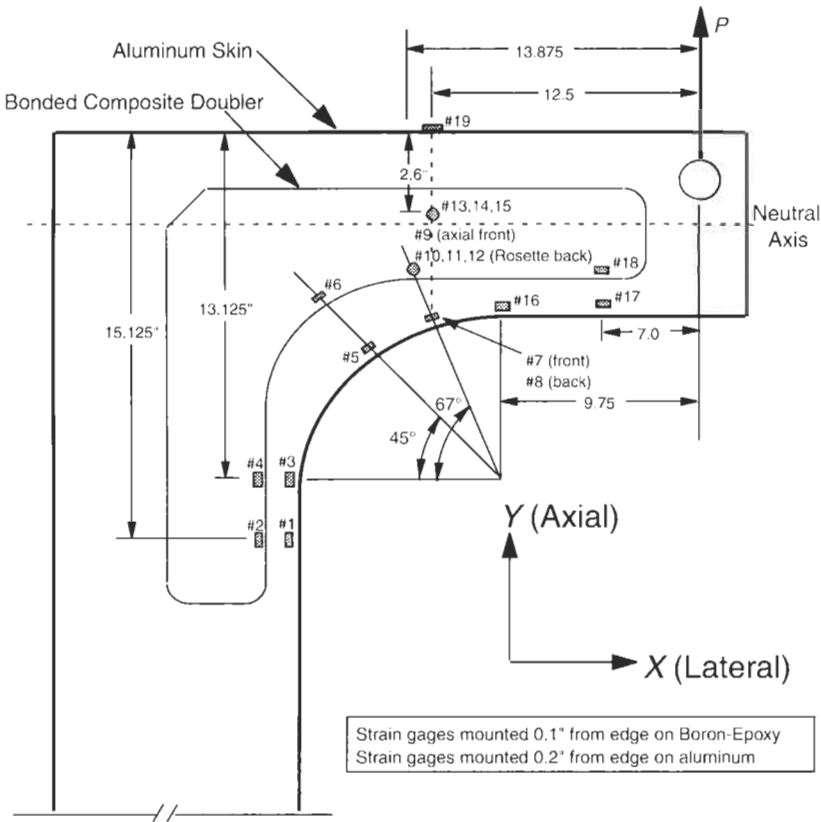


Fig. 28.10. Strain gage locations for door corner test.

28.4.2. Subsize door corner test results

Limit load tests

The test specimen survived the first two load scenarios, up to 15600 lbs. (150% Limit Load) without failure. The aluminium plate, composite doubler, and aluminium angles all survived strain levels which exceeded the design allowable values. In general, the results from the 150% Limit Load Test were linear extrapolations of the data from the Limit Load Test, however, some yielding was observed in the aluminium plate. At the location of maximum strain – 67° around the corner radius (see Figure 28.10) – channels 7 and 8 began to yield slightly. Yielding began at approximately 12500 lbs. when the strain levels reached 5700 $\mu\epsilon$ to 6000 $\mu\epsilon$. Nondestructive inspections revealed that the excursions into the plastic regime did not produce any new disbands nor did it cause the initial installation flaw to grow in size. Table 28.2 summarizes the maximum strains found in the test article during the 150% Limit Load Test.

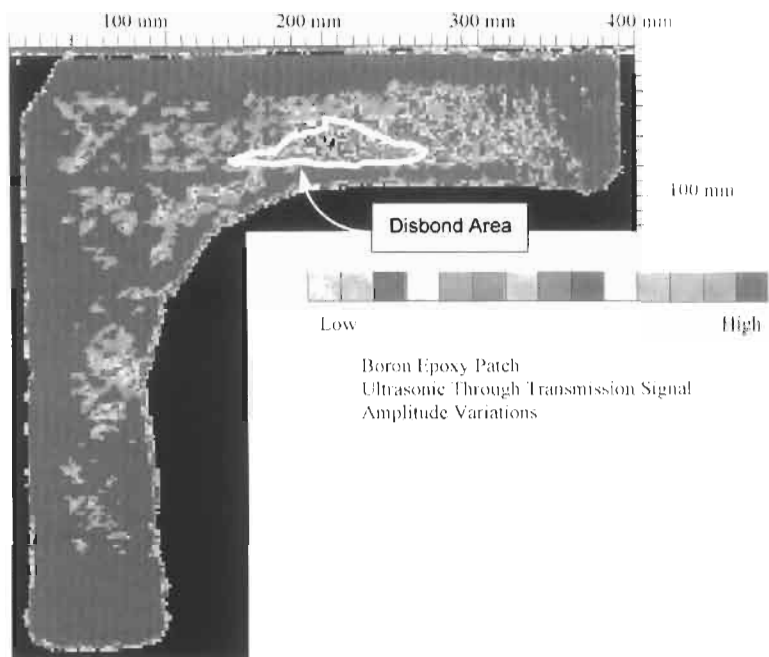


Fig. 28.11. Through transmission ultrasonic C-Scan of composite doubler before structural testing.

Ultimate failure tests

The main concern with bonded doubler installations is that the doubler will disbond due to shear stresses in the adhesive layer. The Ultimate Failure Tests test studied the failure mode of an extremely thick, non-tapered doubler when subjected to severe shear and in-plane bending loads. The Door Corner Test Article

Table 28.2
Summary of maximum strains in the aluminium plate and composite doubler for the 150% limit load test.

Strain gage number	Gage location	Maximum strain at 15600 lbs. ($\mu\epsilon$)	Percent of strain from adjacent aluminium plate
1	Vertical Leg – Alum.	3636 $\mu\epsilon$	1.1. N/A
5	45° on Corner – Alum.	5873 $\mu\epsilon$	N/A
7	67° on Corner – Alum.	7370 $\mu\epsilon$	N/A
16	90° on Corner – Alum.	4859 $\mu\epsilon$	N/A
17	Horizontal Leg – Alum.	3721 $\mu\epsilon$	N/A
2	Vertical Leg – Composite	1304 $\mu\epsilon$	35.8% (vs. Ch. 1)
6	45° on Corner – Composite	1650 $\mu\epsilon$	28.1% (vs. Ch. 5)
9	67° on Corner – Composite	3083 $\mu\epsilon$	41.8% (vs. Ch. 7)
18	Horizontal Leg – Composite	1272 $\mu\epsilon$	34.1% (vs. Ch. 17)

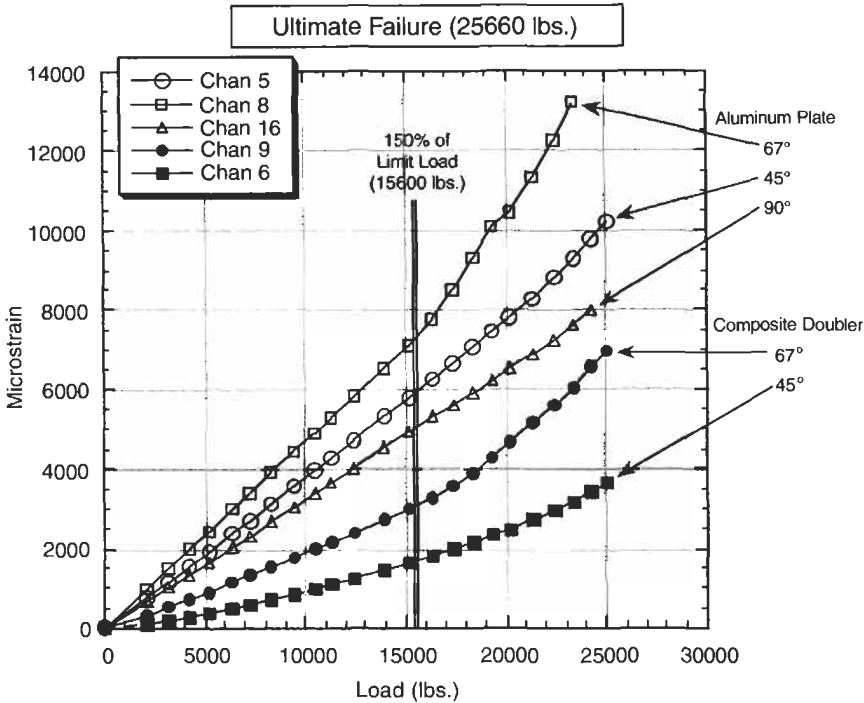


Fig. 28.12. Comparison of critical strains in aluminium and composite material showing load transfer into doubler.

withstood a maximum load, or failure load, of 25660 lbs. The specimen failure load was 2.5 times the limit load for this composite application.

The test specimen's failure stemmed from the initial installation disbond which, unfortunately, was located at the maximum stress region of the test article. As the load was increased beyond the 1.5 Limit Load (15600 lbs.) mark, the aluminium substrate experienced significant yielding. This, in turn, accelerated the load transfer into the composite doubler and produced nonlinear behavior in the doubler's strain field. The installation disbond between the composite laminate and the aluminium substrate, began to grow at the point of maximum strain: 67° around the door corner radius. However, much of the flaw growth corresponded to a cohesive fracture in the adhesive layer. Thus, the full strength of the adhesive was achieved and extreme shear stresses, well beyond normal operating stresses, were needed to produce specimen failure.

Figure 28.12 compares the aluminium and Boron-Epoxy strains for the critical area around the cut-out radius in the Door Corner Test Article. The strain field in the composite doubler was similar to that of the parent aluminium plate with nonlinear behavior noted in the gages located around the radius of the door cut-out (Channels 6 and 9). Note that due to strain hardening applied during the 150%

Table 28.3

Summary of maximum strains measured in the composite doubler for the ultimate failure test (P = 25060 lbs.).

Strain gauge number	Gage location	Maximum strain at 25060 lbs. ($\mu\epsilon$)	Percent of strain from adjacent aluminium plate
6	45° on Corner – Composite	3635 $\mu\epsilon$	35.6% (vs. Ch. 5)
9	67° on Corner – Composite	6979 $\mu\epsilon$	49.3% (vs. Ch. 8)
18	Horizontal Leg – Composite	2169 $\mu\epsilon$	34.2% (vs. Ch. 17)

Limit Load Test, subsequent yielding in the Ultimate Failure Test did not occur until the strain levels corresponding to the previous 15600 lb. test load were exceeded. This yield onset point is indicated in Figure 28.12 by the 150% limit load line. Since Boron-Epoxy material does not normally exhibit the nonlinear stress-strain response or yielding indicated in the figure, the nonlinearities in the curves probably stem from the yielding in the aluminium substrate and the corresponding nonlinear load transfer into the composite doubler. This conclusion is supported by the fact that the onset of the composite's nonlinear response (at the 15600 lbs., 150% Limit Load level) matches the one noted for the aluminium plate.

The maximum strain levels measured in the composite doubler just prior to the failure load of 25660 lbs. (last measurement at 25060 lbs.) are listed in Table 28.3 below. In performing its reinforcing duties, the doubler absorbed approximately 35% to 50% of the load from the aluminium structure beneath it. Strain gage results revealed a large plastic region in the corner of the aluminium plate. This plastic zone caused the strain rate in the doubler to increase. Tests to failure demonstrated that the bondline is able to transfer plastic strains into the doubler and that the parent aluminium skin must experience yield strains before any damage to the doubler will occur. Strain levels along the perimeter of the door corner cut-out (7000 $\mu\epsilon$; Channel nine) were much larger than the strains at the center of the doubler (–2000 $\mu\epsilon$; Channel 13). This supports the design assumption and analyses methods for bonded doublers which indicate that the load transfer takes place in the perimeter (first 1"–2" around edge) of the doubler's footprint. Thus, disbonds have their greatest effect in this area and are less detrimental when present in the "interior" of the doubler's footprint.

In the Ultimate Failure Test, the stress in the composite doubler reached 92.3 ksi before failure occurred. Thus, the stresses required to fail this doubler were found to be 4.8 times greater than the stresses measured during the full-scale fuselage tests (simulated cabin pressure tests described in Section 3). The parent aluminium material beneath the doubler experienced a maximum stress level of 86 ksi. This means that the composite-reinforced aluminium plate was able to withstand stresses in excess of the Mil Handbook ultimate tensile stress value listed for the parent 7075-T6 aluminium material (83 ksi). More importantly, the aluminium stresses measured at doubler failure were 5.6 times greater than the stresses experienced during the full-scale fuselage tests. The C-section test article withstood

a maximum load, or failure load, which was 2.5 times the limit load for this composite application. These results show that the safety factor for this doubler design exceeded the minimum goal of 1.5.

Post-test nondestructive inspection

Nondestructive inspection (NDI) of the test article was conducted after each load test. Using the visual, Pulse-Echo ultrasonic, and Thru-Transmission ultrasonic inspection methods [8], it was determined that there was no disbond growth during either the Limit Load or 150% Limit Load tests. Thus, the composite doubler design began the Ultimate Failure Test having successfully demonstrated a resistance to flaw initiation and growth while enduring shear loads which exceed yield levels.

28.5. L-1011 composite doubler installation

Overview

The best proof that the composite doubler repair technique is viable on commercial aircraft was provided by the installation of a large doubler on a Delta Air Lines L-1011. The aircraft (#755, S/N 193Y-1185) was undergoing a heavy maintenance visit (HMV) during the time of the installation. The Sandia Lab's AANC, Textron Specialty Materials and Delta Air Lines team performed the installation and inspection of the L-1011 door corner composite doubler. It was installed in lieu of the standard repair of four, riveted metallic plates as per the approved process specifications. The aircraft returned to its trans-Atlantic service and subsequent inspections following 45 days, 6 months, and one year of activity did not reveal any flaws in the installation.

28.5.1. Composite doubler repair of L-1011 aircraft passenger door

Figure 28.13 shows the Delta aircraft undergoing maintenance and the doubler installation staging area at the right side, P3 passenger door. Figure 28.14 shows the aircraft skin section which was cleaned and anodized – via a phosphoric acid non-tank anodize (PANTA) process – to support the doubler bonding process [12]. The doubler was placed in an autoclave (150 °F, 80 psi) to debulk/densify the doubler and to bleed out excess resin. The 72 ply Boron-Epoxy composite laminate (post-debulk) is shown in Figure 28.15. The contour around the door corner radius, the cut-out to accommodate the emergency door handle access port, and the tapered edges around the perimeter are evident.

A fiberglass environmental protection ply and a copper mesh lightning protection ply were installed on top of the Boron-Epoxy laminate. Figure 28.16 shows the complete doubler lay-up as it was positioned on the L-1011 door frame. The doubler was placed on the fuselage followed by bleeder cloths, heater blankets, insulation and a vacuum bag assembly. Twenty two thermocouples were installed



Fig. 28.13. Delta L-1011 aircraft during installation of composite doubler (inset – work stand positioned next to the right side passenger door).



Fig. 28.14. Anodized door corner prepared for doubler bonding process.

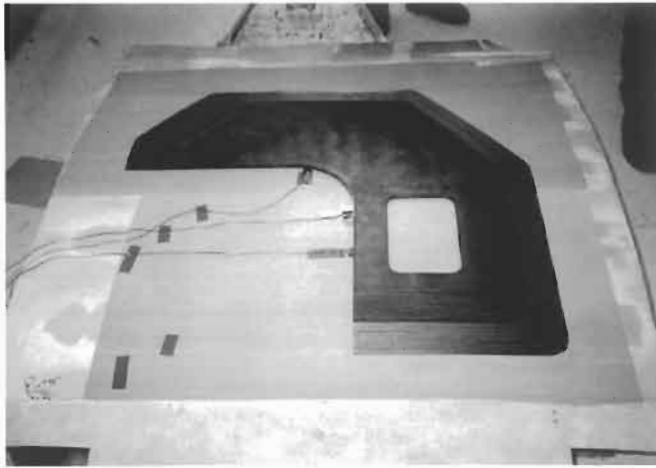


Fig. 28.15. Boron-Epoxy laminate following autoclave debulk process.

to monitor the temperature field around the top and perimeter of the doubler, as well as, the back side of the fuselage skin and substructure elements.

After the heat blankets were turned on, the temperature ramp-up process, which included the placement of heat lamps on the back side of the skin and insulation over heat sink areas, took 2 1/2 h. Figure 28.17 shows the vacuum bag arrangement and the Heat Con blanket controller during the cure process. Figure 28.18 shows the inside structure of the door corner area and the heat lamps that were positioned to minimize the effects of the various heat sinks. In order to optimize the

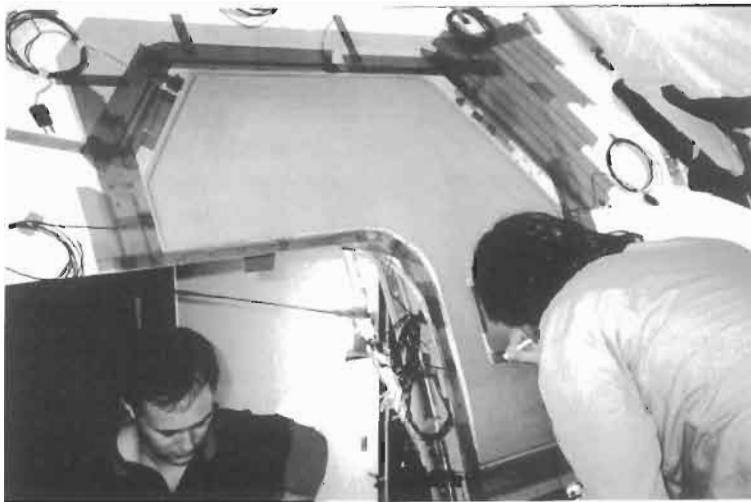


Fig. 28.16. Composite doubler positioned on door for cure process.



Fig. 28.17. Cure process – doubler beneath heat blanket, insulation, and vacuum bag assembly; heat controller is shown in foreground.



Fig. 28.18. Heat lamps positioned inside aircraft to help maintain cure temperature on back skin.



Fig. 28.19. Composite doubler following cure process (prior to application of delta paint scheme).

uniformity and stability of the temperature field, the 190 °F, 6 h cure cycle was used instead of the 210 °F, four-hour cure cycle. Temperature fluctuations were less than 5 °F at any location inside and outside the aircraft. The maximum and minimum temperatures were separated by approximately 25 °F. A close-up view of the completed composite doubler installation is shown in Figure 28.19. To contrast this doubler with the conventional approach, Figure 28.20 shows the series of riveted, metallic plates that are traditionally used to repair the L-1011 door corner. The light colored strip running diagonally across the doubler is a rain gutter.

28.5.2. *Non-destructive inspection of door surround structure and composite doubler*

The NDI techniques deployed in this effort were capable of detecting disbonds, delaminations, and porosity in the composite doubler (ultrasonics), as well as cracks in the parent aluminium material [8–11,13]. The door surround structure was inspected with visual (optical magnification), ultrasonic (UT), X-ray and eddy current (EC) NDI techniques before and after the composite doubler installation. Before the doubler was installed, a drawing was made of the area covered by the doubler footprint. It included the location of all rivets or surface structures which could provide a source of false flaw indications. This drawing was then used as a “template” map to aid the inspections performed after the doubler was installed.

Inspections for cracks in the parent material were carried out using an eddy current procedure applied to both the inside and outside of the structure. Bolt hole eddy current (BHEC) and eddy current surface scan (ECSS) inspections were performed prior to the doubler installation. The aluminium material adjacent to the doubler was also inspected using ECSS after the doubler was installed. Both EC procedures followed existing call-outs in the L-1011 Nondestructive Testing

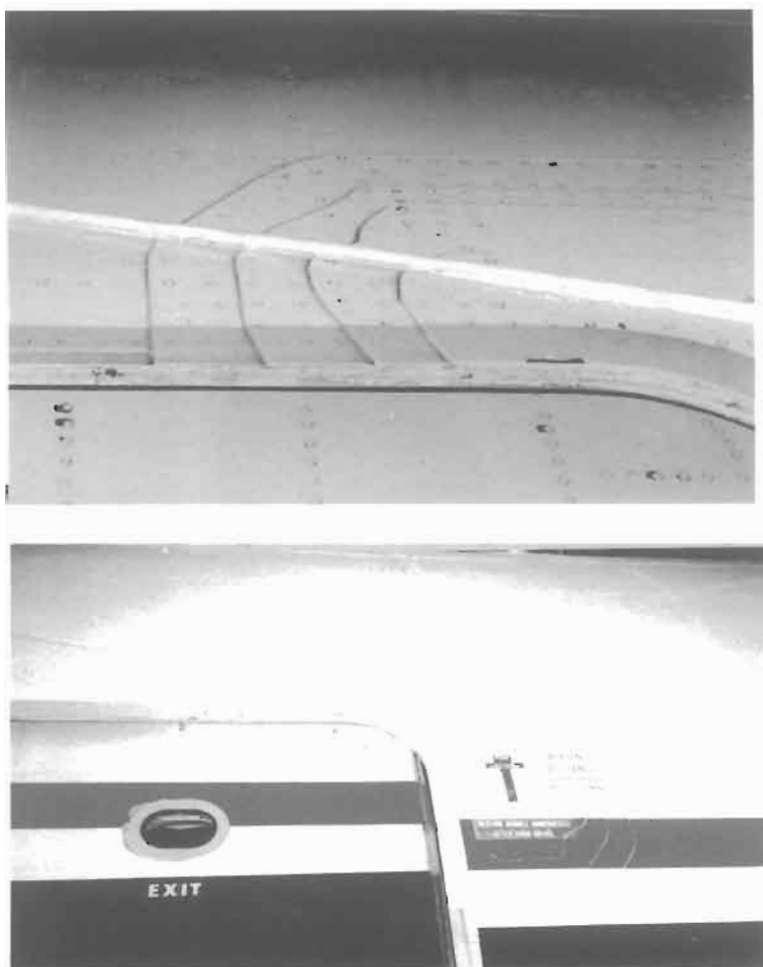


Fig. 28.20. Conventional door corner repair with four, riveted metal plates; close-up view (inset) shows intricate rivet pattern and complex shape of quadrupler plates.

Manual [13]. X-ray inspections, currently in use in the door corner region, were also conducted using the procedure listed in the L-1011 NDT manual. The AANC completed a study to: (1) demonstrate that composite doublers do not interfere with the ability to perform X-ray inspections for cracks in aluminium, and (2) identify proper exposure time and power settings to optimize the sensitivity of X-ray technique when inspecting through extremely thick doublers (72 ply) [8,9]. X-ray inspections were shown to be as effective as before a doubler is installed. The required damage detection threshold for cracks under the doubler is 1.0". X-ray images showed the ability to detect fatigue cracks on the order of 0.38" in length beneath 0.40" thick (72 ply) Boron-Epoxy doublers.

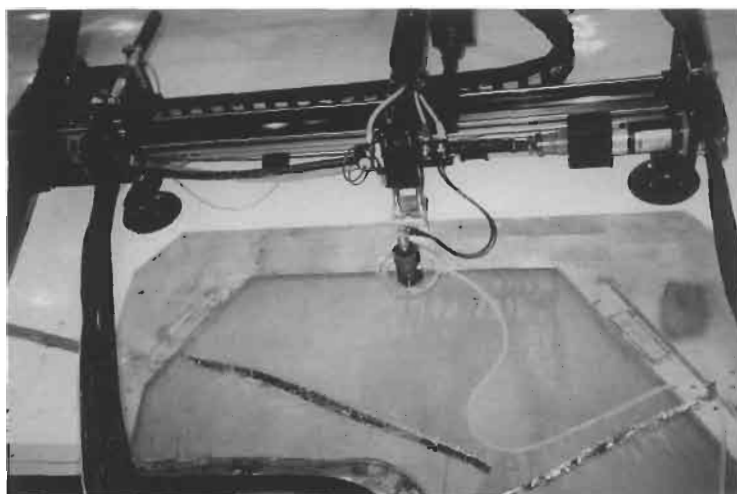


Fig. 28.21. Ultrasonic scanner system inspecting a tapered region of the L-1011 door corner doubler.

Periodic field inspections of the composite doubler for disbonds and delaminations (from fabrication, fatigue, or impact damage) is essential to assuring the successful operation of the doubler over time. After the doubler was installed, disbond and delamination inspections were performed using the Sandia Labs AANC ultrasonics inspection procedure for bonded composite doublers[11]. This procedure is required by reference [14] for the L-1011 application. The doubler was inspected using pulse-echo ultrasonics (UT) and an X-Y scanner system [8]. Most of the flaw detection effort was focused on the critical 1.5" wide strip around the perimeter of the doubler. A 0.5" diameter flaw is the allowable flaw size in this load transfer region. Scans were also produced in the internal region to assure that there were no flaws in excess of the size allowed by the damage tolerance assessment. Away from the doubler edge taper region, the maximum allowable contiguous flaw is equal to 5% of the total, full-thickness area of the doubler. Figure 28.21 shows the ultrasonic scanner system inspecting the upper, tapered region of the door corner doubler. The inspection did not reveal any flaws in the L-1011 doubler. Chapter 23 provides a comprehensive examination of inspection methods for composite doublers.

28.5.3. Inspection intervals for L-1011 aircraft

One of the major outputs from the doubler design effort was the determination of the inspection intervals to accompany the composite doubler installation. The existing crack detection inspections, X-ray, bolt hole EC, and surface scan EC [13], were retained with the following inspection intervals:

Critical Crack NDI Technique		Length (in.)	Inspection Interval
1. X-ray	1.00	after 1st yr. and 4500 flights	
2. ECSS	0.35	after 1st yr. and 5690 flights	
3. BHEC	0.07	after 1st yr. and 10657 flights	

The reference [3] analysis determined the UT inspection intervals for disbond and delamination detection in the composite doubler. The reference [11] inspection procedure was carried out to certify the initial L-1011 doubler installation and to assess the condition of the doubler following 45 days, six months, and one year of service in Delta's fleet. Thereafter, this inspection is scheduled to be carried out every D-check (heavy maintenance visit – approximately every 4500 flights). The sensitivity of the technique to detect 1/4 to 1/2 inch diameter disbonds and delaminations was demonstrated.

The close scrutiny of the doubler indicated by the frequent inspections (short intervals) listed above is due to the newness of this composite doubler technology in commercial aircraft applications. It is believed that with the accumulation of successful flight history, the inspection intervals will be extended and, in some cases, removed altogether. Note that after the initial close surveillance of the doubler (through first year following installation), the inspection interval reverts back to every major overhaul of the aircraft.

28.5.4. *Quality assurance measures*

An overall approach to managing the implementation of composite doubler technology is proposed in reference [15]. Reference [15] suggests the use of an Engineering Standard to guide all design, analysis, and QA issues. A series of quality assurance (QA) measures were included in this project's composite doubler installation process to assure: (1) sufficient strength in the adhesive layer, (2) sufficient strength in the Boron-Epoxy laminate, (3) proper surface preparation to allow the best opportunity for complete adherence of the doubler, and (4) the detection of any flaws in the composite doubler. The first four QA devices involve test specimens which are generated at the same time the doubler is installed. All test specimens are produced using the same temperature and pressure profile as the aircraft doubler cure. The final QA mechanism is nondestructive inspection which is used for the initial acceptance of a composite doubler installation and for continued surveillance over the life of the doubler.

- (a) Wedge test – Two aluminium strips are bonded to the parent structure immediately adjacent to the doubler. A phenolic wedge is used to pry the strips off the aircraft. If adhesive is found on both the aluminium strip and the aircraft skin, this indicates that the adhesive fractured (cohesive failure) rather than disbonded (adhesive failure). Thus, the surface preparation is good and the full adhesive strength has been achieved.

- (b) Lap shear test – These tests utilize one inch wide aluminium coupons with a bonded lap joint. The specimens are pulled to failure to determine the ultimate strength of the adhesive layer. The minimum strength requirement is 3000 psi. Six specimens were tested for the L-1011 door corner doubler. They produced the following strength values: (1) 4720 psi, (2) 4500 psi, (3) 4440 psi, (4) 4880 psi, (5) 4740 psi, and (6) 4390 psi.
- (c) Short beam shear – One inch wide Boron-Epoxy laminate coupons (15 ply unidirectional lay-up) are tested for laminate shear strength as per ASTM specifications. Three specimens were tested for the L-1011 laminate and an average shear value of 10.7 ksi was determined. The cured Boron-Epoxy shear strength should be at least 10.5 ksi.
- (d) Four point bend – One inch wide Boron-Epoxy laminate coupons (15 ply unidirectional lay-up) are tested for ultimate tensile strength as per ASTM specifications. Three specimens were tested for the L-1011 laminate and an average tensile strength of 212 ksi was determined. The established minimum strength requirement is 180 ksi.
- (e) Nondestructive inspection – The tests outlined above determine the strength properties of the installation. However, it is still necessary to detect any flaws in the installation. Initially, the status of flaws in the doubler and bondline must be ascertained to accept the installation. Thereafter, the flaw status of the doubler, bondline, and parent material must be periodically measured. Nondestructive inspection provides the last line of defense in this regard. NDI is the only means for determining if the structural integrity of the repair area changes over time. The NDI methods introduced here and described in detail in reference [8] were used to evaluate the composite doubler installation. Multiple post-installation inspections, spanning three years of aircraft operation, have shown the doubler to be free of flaws. No flaws were detected in the L-1011 composite doubler or the doubler-to-aircraft bond line.

28.6. FAA and industry approvals

The other important products from this program are the series of industry and FAA approvals which: (1) indicate the industry's endorsement of the technology, and (2) allow for expanded use of bonded composite doublers on commercial aircraft. The Lockheed-Martin Service Bulletin 093–53–278 allows the door corner composite doubler to be installed on all L-1011 aircraft. This installation also facilitated the formal introduction of composite doubler technology into the Delta maintenance program. Delta Air Lines, the AANC, and Textron developed the Engineering Repair Authorization (ERA) document which must accompany any new Delta maintenance activity. The ERA generated all of the job cards necessary to support the installation and inspection of the door corner doubler.

In addition to obtaining approval from a Lockheed Designated Engineering Representative (DER), the FAA also approved all data and procedures stemming from this project. An alternate means of compliance (AMOC) was granted by the

FAA and allows for the deviation from the original, metallic repair Service Bulletin (093-53-237) and the L-1011 Aging Aircraft Airworthiness Directive (94-05-1). The FAA letter granting AMOC concludes that the engineering data and installation/inspection specifications listed above provide an "equivalent level of safety" as the metallic doubler called out in Service Bulletin 093-53-237.

Approval form	Document number
1. Lockheed L-1011 Service Bulletin	093-53-278
2. Delta Engineering Repair Authorization	340137-14AD
3. FAA Alternate Means of Compliance	1/19/97 letter ref. L96N1088

With the successful completion of the L-1011 door corner application, the FAA and AANC moved on to a program with Boeing and Federal Express to develop, certify, and install a more generic set of composite doubler applications for a variety of common DC-10 aircraft fuselage skin repairs (See Chapter 35).

28.7. Conclusions

As a result of this program, FAA certification has been received for the use of bonded composite doublers on the U.S. commercial aircraft fleet. Most of the concerns surrounding composite doubler technology pertain to long-term survivability, especially in the presence of non-optimum installations, and the validation of appropriate inspection procedures. The program presented here addressed these uncertainties for general composite doubler installations. In addition, a proof-of-concept aircraft installation was completed in order to demonstrate the successful consideration of all "cradle-to-grave" issues including: design, analysis, installation, damage tolerance, quality assurance, nondestructive inspection, and FAA/industry oversight.

This chapter presents a series of full-scale structural and nondestructive inspection (NDI) tests that were conducted to investigate the performance of Boron-Epoxy composite doublers under realistic flight conditions. Full-scale tests were conducted on fuselage panels cut from retired aircraft. These full-scale tests studied stress reductions, crack mitigation, and load transfer capabilities of composite doublers using simulated flight conditions of cabin pressure and axial stress. Also, structures which modeled key aspects of aircraft structure repairs were subjected to extreme tension, shear and bending loads to examine the composite laminate's resistance to disbond and delamination flaws. Several of the structures were loaded to failure in order to determine doubler design margins. Nondestructive inspections were conducted throughout the test series in order to validate appropriate techniques on actual aircraft structure. The test results showed that a properly designed and installed composite doubler is able to enhance fatigue life, transfer load away from damaged structure, and avoid the introduction of new stress risers (i.e. eliminate global reduction in the fatigue life of the structure).

Comparisons with test data obtained prior to the doubler installation revealed that stresses in the parent material can be reduced 30%–60% through the use of the composite doubler. Tests to failure demonstrated that the bondline is able to transfer plastic strains into the doubler and that the parent aluminium skin must experience significant yield strains before any damage to the doubler will occur. This effort culminated in a successful repair of a commercial aircraft. Subsequent inspections over several years of service provided the ultimate validation of composite doublers in actual operating environments.

Aircraft repair practices must be continuously revisited and expanded to take advantage of new materials, new processes, and new techniques that offer both engineering and economic advantages. Through the steady and comprehensive introduction of test data, analyses, and in-service composite doubler installations on commercial aircraft a critical database is being assembled to accurately guide enhancements to formal maintenance programs. This is an important step in the evolution of composite doubler applications since it will eventually eliminate the need for each bonded composite repair to be preceded by a lengthy research and testing program.

References

1. Roach, D.P. and Walkington, P.W. (1999). Full-scale structural and NDI validation tests of bonded composite doublers for commercial aircraft applications. Dept. of Energy SAND Report SAND98-1015, February.
2. Huang, J., Reeve, S. and Shah, S. (1995). Boron/Epoxy material allowables. Report No. LG95ER0193, Part of Documentation Package for FAA Atlanta Aircraft Certification Office Project No. SP1798AT-Q, November.
3. Jones, K.M. and Shah, S. (1996). Composite repair – upper forward corner of P-3 door-model L-1011 aircraft, strength and damage tolerance analysis. Report No. LG95ER0157, Part of Documentation Package for FAA Atlanta Aircraft Certification Office Project No. SP1798AT-Q, analysis plan December 1995, final report October.
4. Roach, D.P. (1998). Damage tolerance assessment of bonded composite doublers for commercial aircraft applications. Sandia National Laboratories/Dept. of Energy Report No. SAND98-1016, August.
5. Rose, L.R. (1987). Influence of disbonding on the efficiency of crack patching. *Theoretical Applied Fracture Mechanics*, 7.
6. Baker, A.A. and Jones, R. (1988). Bonded repair of aircraft structures. Martinus Nijhoff Pub., The Netherlands.
7. Belason, E.B. (1995). Fatigue and static ultimate tests of Boron-Epoxy doublers bonded to 7075-T6 aluminium with a simulated crack. *Int. Conf. on Aeronautical Fatigue*, Melbourne, Australia, May.
8. Roach, D.P. and Walkington, P. (1998). Development and validation of nondestructive inspection techniques for composite doubler repairs on commercial aircraft. Sandia National Laboratories/Dept. of Energy Report No. SAND98-1014, May.
9. Roach, D.P., Moore, D. and Walkington, P. (1996). Nondestructive inspection of bonded composite doublers for aircraft. *Proc. of SPIE Conf. on Nondestructive Evaluation of Aging Aircraft*, December.
10. Gieske, J.H., Roach, D.P. and Walkington, P.D. (1998). Ultrasonic inspection technique for composite doubler/aluminium skin bond integrity for aircraft. *SPIE Nondestructive Evaluation Techniques for Aging Infrastructure & Manufacturing Conf.*, 3258, April.

11. Walkington, P. and Roach, D. (1997). Ultrasonic inspection procedure for bonded Boron-Epoxy composite doublers. Sandia Labs AANC Specification AANC-PEUT-Comp-5521/4-004, Sandia National Laboratories, Albuquerque, NM; also included in FAA Document SNL96ER0007 under Atlanta ACO Project SP1798AR-Q, FAA approval January.
12. Berg, S.D. (1995). Process specification for the fabrication and application of Boron-Epoxy doublers onto aluminium structures. Textron Specialty Materials Specification No. 200008-001 (may also be referenced as the Boeing Specification D658-10183-1 which was written for Textron), 30 November, Textron Specialty Materials, Lowell, MA, 01851.
13. Nondestructive Testing Manual. Chapter 53, Lockheed California Co., Burbank, CA.
14. Herderich, D., Shah, S. and Izquierdo, I. (1996). Doubler-composite reinforcement, P-3 PAX door, UPR FWD corner, composite reinforcement. Lockheed-Martin Aeronautical Systems Drawing No. LCC-7622-378, April.
15. Davis, M.J. (1995). A call for minimum standards in design and application technology for bonded structural repairs. *Int'l Symposium on Composite Repair of Aircraft Structures in concert with ICCM-10*. August.

Chapter 29

CASE HISTORY: F-111 WING PIVOT FITTING REINFORCEMENT

Dr. R. CHESTER

*Air Vehicles Division Division, Defence Science and Technology Organisation,
Fishermans Bend, Victoria 3207, Australia*

29.1. Introduction

This chapter describes the materials engineering aspects of the development of boron/epoxy doublers to reinforce the wing pivot fittings (WPF) of Royal Australian Air Force F-111 aircraft. The main aim of the doubler is to reduce plastic strain in a critical region of the D6ac steel WPF during the cold proof load test (CPLT). This development was undertaken during 1986 to 1989 [1]. Tests on strain-gauge-instrumented wings confirmed that the required strain reduction of over 30% is achieved in the critical region of the WPF.

The region prone to cracking, depicted in Figure 29.1, is in the upper surface of the wing in the D6ac steel WPF which is close to the bolted splice with the aluminium alloy wing skin. Cracking can develop in the stiffener runout, indicated in Figure 29.1.

An upper wing skin is not expected to experience fatigue cracking problems since in normal flight it experiences predominantly cyclic compressive stress. Generally low levels of cyclic tensile stress are experienced during landing, ground running and some flight manoeuvres. However, as discussed in reference [2], when the aircraft is subjected to very high positive loads, yielding in compression occurs in some of the stiffener runout regions. On unloading, high levels of residual tensile stress develop in the yielded region in these stiffeners, since the length of the yielded material has effectively decreased in comparison with the surrounding unyielded material. The residual tensile stress in combination with stresses resulting from the normal flight loads produces a tensile-dominated fatigue cycle that can result in cracking.

The high loads that cause the local yielding do not arise during normal operation of the aircraft, although in principle they could if the aircraft was flown to its design limits. They actually arise during a proof test on the aircraft, undertaken to screen

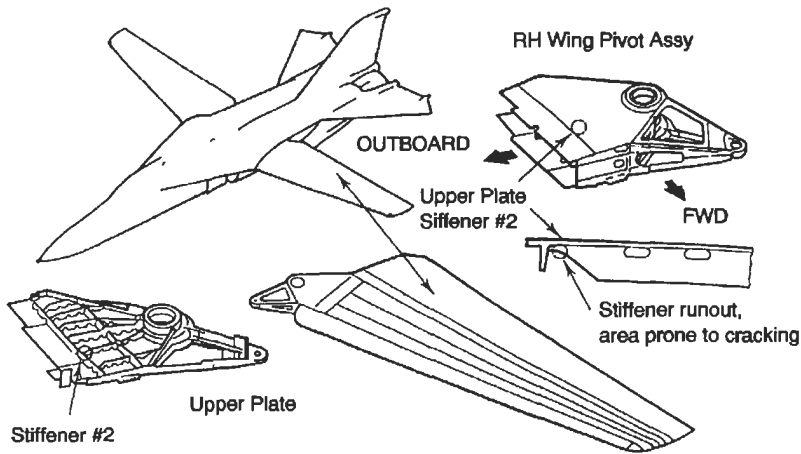


Fig. 29.1. View of F-111 aircraft and wing showing location of critical area.

out undetected flaws [3]. The proof test is performed at -40°C to increase the criticality of flaws in the ultra-high strength D6ac steel components. This ensures that no flaws exist that can cause catastrophic failure at normal flight temperature. The CPLT actually involves loading the aircraft to the nominal flight loads of $+7.33\text{ g}$ and -2.4 g at -40°C (approximate stress of 756 and -248 MPa respectively in the upper plate of the WPF).

In 1984 the RAAF tasked the Defence Science and Technology Organisation to evaluate the feasibility of reinforcing the critical region in the WPF with a doubler. The aim was to reinforce the critical stiffener runout region, (i) to prevent yielding during the CPLT, and (ii) to reduce cyclic stresses during normal aircraft operation in stiffeners where residual stress remained after reworking the region. The reinforcement was to be applied in addition to reworking the critical stiffeners. The aim of the reworking was (i) to remove the existing yielded zone and (ii) to lower the stress concentration factor by increasing the radius of the runout.

29.2. Reinforcement design

As shown in Figure 29.2 and Figure 29.3, the reinforcement consists of two boron/epoxy doublers (over 120 plies, or 15 mm of unidirectional boron), adhesively bonded to the upper surface of the WPF over the stiffeners known to develop high levels of strain during the CPLT. One large doubler covers stiffeners numbers 4 and 5 and a smaller doubler covers stiffener number 2. Structural aspects of the design of the doublers are covered in more detail in [4].

The boron/epoxy composite doublers are bonded to the wing skin with an epoxy-nitrile film adhesive FM73, Table 29.1. Each doubler, Figure 29.3, consists of two segments, the lower segment is bonded to the D6ac steel to provide a bridge level

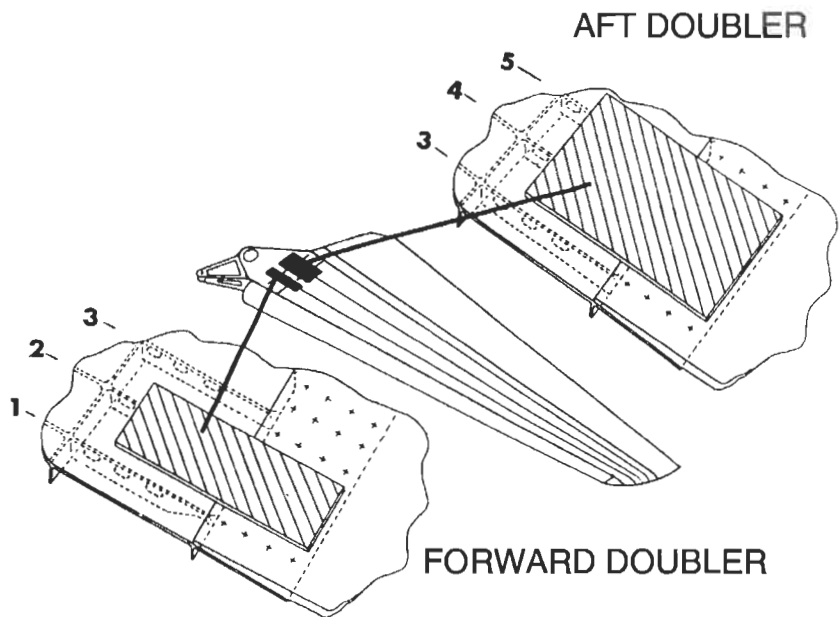


Fig. 29.2. Doubler locations on the F-111 steel WPF and aluminium alloy wing skin.

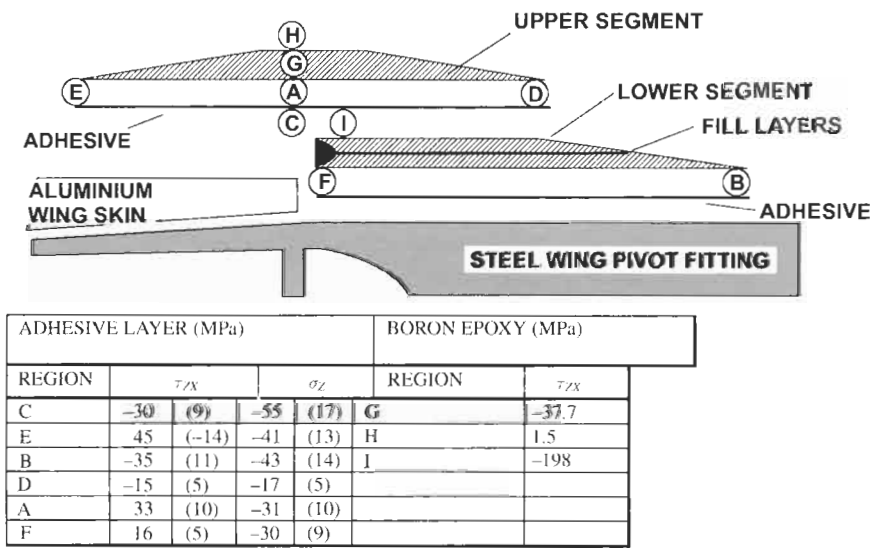


Fig. 29.3. Exploded view of doubler indicating regions where approximate through-thickness stress (σ_z) and shear stress (τ_{xz}) values were estimated. The tabulated values are for the nominal +7.33 g proof load and those inside the brackets are estimated for the -2.4 g proof load.

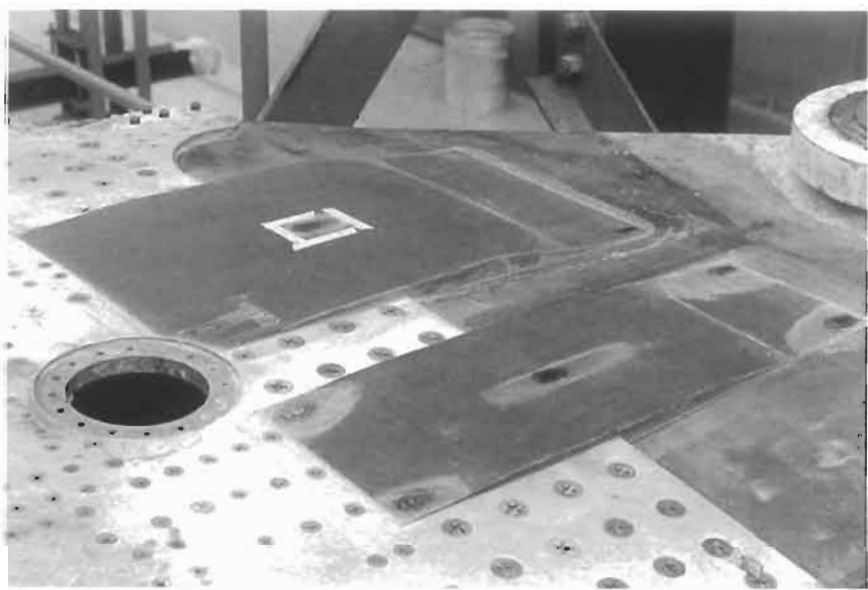


Fig. 29.4. Photograph of the installed doublers; note the step between the aluminium wing skin on the left and the steel WPF on the right.

with the aluminium skin at the step, and the upper segment is bonded to the aluminium skin (over the fasteners) and the lower segment. Each segment consists of about 60 plies tailored (by ply drop-offs) to fit the step and the curved surface of the wing skin and tapered (also by ply drop-offs) to achieve single plies at the extremities of the doublers. The lower segment contains a cut-out region with a

Table 29.1
Typical relevant properties of (a) adhesive FM73 and (b) boron/epoxy 5521/4.

<i>FM-73 Adhesive</i>			
Shear modulus G_A (Gpa)	Shear yield stress τ_y (MPa)	Shear yield strain γ_e	Shear plastic strain γ_u
RT→0.54	31	0.057	0.7
−40 °C→0.77	55	0.071	0.21
(a)			

<i>5521/4 Boron/epoxy</i>		
Elastic modulus E (Gpa)	Strain to failure e_{ult}	Interlaminar shear stress (MPa)
210	0.007	97
(b)		

softening insert (made of the same adhesive) adjacent to the step, designed to reduce the stress concentration at the point of load transfer between the upper and lower doubler.

The doubler design is for unidirectional plies of boron/epoxy as the load in the critical area of the WPF is uniaxial. No off-axis plies are required to prevent splitting and therefore stiffness in the desired direction is maximised. The doublers do require high in-plane shear strength in the fibre direction as mentioned in the next section.

Some results of the finite-element analysis of the doubler are provided in Figure 29.3 (taken from reference [5]) in which only elastic behaviour is considered in the adhesive and reinforcement. Critical shear and through-thickness stresses in the adhesive layer and shear stresses in the boron/epoxy-adhesive interface are indicated. Considering these results and the material's properties provided in Table 29.1 the following comments are made:

- i Comparison of the typical shear yield stress for the adhesive, Table 29.1(a), with the shear stresses predicted by the finite-element analysis Figure 29.3, indicates that the adhesive would not yield during the CPLT. However, modest yielding would have occurred at room temperature around regions A, B and E.
- ii The high shear stress in the boron/epoxy at location I is of concern. However, as it is very localised, failure should not occur since the strain energy density criterion as used in [4] is not exceeded.
- iii Through-thickness stresses under the high +7.33 g load are compressive and are therefore not of concern and only modest tensile stresses arise under the -2.4 g load.

29.3. Selection and evaluation of materials

The aim is to provide a high performance reinforcement, closely conforming to the surface contour of the wing, attached to the wing with an adhesive capable of providing the required level of load transfer at the service temperature. Together with these requirements is the need, (a) to provide high durability in the reinforcement and adhesive systems, (b) to minimise adverse residual stresses, (c) to avoid corrosion, mechanical or metallurgical damage to the wing when applying the reinforcement, and (d) to avoid stiffening other than in the desired directions.

The reinforcement system must be capable of withstanding the service loading and environment experienced by the F-111 wing, especially the severe condition of proof loading at -40°C as well as high temperatures resulting from solar heating or high-speed operation of the aircraft.

The specific requirements for the reinforcement are:

- i a highly directional Young's modulus, to ensure effective reinforcement in desired directions,
- ii high strength, in particular high shear and peel strength, to cope with in-plane shear stresses and out-of-plane tensile stresses,

- iii formability at relatively low pressures and temperatures, to allow shaping and fitting to the complex curvature of the wing,
- iv the ability to incorporate inserts such as a softening strip, and
- v a relatively high thermal expansion coefficient in the reinforcement direction to match that of the metallic structure and thus minimise residual stresses during the adhesive cure cycle. It is not possible to match the coefficients of both steel and aluminium (11×10^{-6} and $23 \times 10^{-6} \text{ } ^\circ\text{C}^{-1}$ respectively) and therefore an intermediate value is desirable.

For the adhesive the requirements are for:

- i moderately high shear modulus, high yield stress and resistance to stress relaxation at the maximum working temperature of $80 \text{ } ^\circ\text{C}$ in order to provide effective load transfer,
- ii high shear strain capacity and peel resistance,
- iii ability to develop high-durability bonds with simple surface treatments, and
- iv ability to cure or gel at a relatively low temperature to ease application requirements and to minimise residual stresses (as described in (v) above).

The requirements for surface-treatments for bonding are:

- i to be effective in promoting high-durability bonds to both the steel and the aluminium alloy structures and the steel fasteners,
- ii to be simple to apply *in situ*, ideally at ambient temperature,
- iii not to encourage corrosion, stress-corrosion or hydrogen-embrittlement, and
- iv to be neither hazardous nor toxic.

As may be expected, no materials or processes would be ideal in all respects. However, for the reinforcement, high performance fibre-reinforced plastics satisfy most of the requirements (Chapter 2), limited mainly by their relatively low peel and shear properties and their low thermal expansion coefficients (compared to metals). Structural film adhesives best satisfy the adhesive requirement, their major drawback being their need for elevated temperature cure. The development of a suitable non-aggressive surface treatment satisfying most of these requirements is described Chapters 2 and 3.

29.4. Selection and evaluation of the reinforcement

The advanced fibre composite boron/epoxy (b/ep) was chosen for the reinforcement because this material offers the highest strength, stiffness and expansion coefficient of available composites although at a high cost premium. The system evaluated was 5521/4 (by Textron Specialty Materials, USA), where the 5521 refers to the resin system (nominally $120 \text{ } ^\circ\text{C}$ curing) and the 4 refers to the diameter of the boron fibre in thousandths of an inch.

Evaluation was aimed firstly at determining the mechanical properties of the material and secondly characterising the cure behaviour and the formability of a semi-cured (B-staged) lay-up to ensure that the doubler can be formed onto the curved surface of the wing before final cure.

29.4.1. Mechanical test evaluation

29.4.1.1. Interlaminar shear evaluation

Standard quality control tests were undertaken to measure the nominal interlaminar shear strength (ILSS) of the b/ep material. The tests were conducted on 16-ply laminates processed under the manufacturer's recommended cure cycle (60 min at 120 °C and 500 kPa) as well as under non-optimum (reduced temperature and pressure) cure cycles required for the F-111 reinforcement. These tests showed that the off-optimum cure cycle resulted in an ILSS reduction of about 10%.

29.4.1.2. Fracture energy assessment

Measurements were made of the mode I fracture energy (G_{IC}) using the double cantilever beam test [6]. The initial work of fracture was 230 J/m² at ambient temperature and 150 J/m² at -40 °C. The significant decrease in G_{IC} with decrease in temperature results from the reduction in strain capacity of the epoxy matrix. This result indicates that the -40 °C condition could be critical for growth of delamination damage in the boron/epoxy doubler under tension which occurs in the wing during the minus g loading. However, other than region I, Figure 29.3, positive σ_z stresses are expected to be modest.

Fracture toughness in Mode II for laminated composites is typically several times higher than that for Mode I. Tests on the 5521-4 boron/epoxy using end-notched flexural (ENF) specimens have confirmed this trend for the material used in the WPF doubler. As the compressive loads applied during the CPLT are three times the tensile loads and the shear stresses in the reinforcement are correspondingly higher in compression (Figure 29.3), it is possible that failure may occur in Mode II. Tests at -40 °C, however, have shown that no significant reduction in Mode II toughness occurs as a result of the temperature decrease, in contrast to the Mode I behaviour.

29.4.2. Cure characterisation and formability studies

An important requirement for the reinforcement resin system is its ability to cure or gel at relatively low temperature. From a series of low-temperature curing experiments [7] and [8], it was concluded that, while the matrix resin 5521 can be satisfactorily gelled at temperatures as low as 80 °C, total cure to acceptable properties is not possible unless a subsequent post cure at 120 °C is carried out. From the co-cure studies, it was concluded that co-curing of FM73 with AVCO 5521 could lead to compatibility problems caused by loss of some of the FM73 curing agent by diffusion into the 5521 resin. It was considered that if this were to occur it might affect the strength of the bond between the FM73 and the metallic substrate. However, if the 5521 is gelled prior to co-cure (as is the situation with the application of the doubler) diffusion of the FM73 curing agent into the 5521 resin should be minimised.

Formability of the doubler material is a very important requirement to match precisely the shape of individual F-111 wings, which show slight variations between

one another in curvature and in the depth of the step created by the joint between the aluminium alloy wing skin and steel WPF, Figure 29.3.

With suitable tooling exactly matching the shape of each F-111 wing, a correctly shaped doubler could readily be formed. However, to avoid the expensive and time-consuming requirement for a custom tool for each aircraft wing, the approach of moulding the doubler directly on each wing was adopted.

Major requirements for *in situ* moulding were that:

- i the b/ep material could be fully compacted and bled (excess resin removed) prior to the cure so that further changes in thickness of the doubler would be minimal and also that there would be only a limited requirement for bleeder layers (resin absorbers) during the cure on the wing, and
- ii the doubler material be sufficiently undercured to allow the initially flat doubler to conform to the curved surface of the wing under moderate temperature and pressure.

Thus the following simple tests were undertaken to establish the required fabrication conditions;

- i lay-up 16 plies of the b/ep prepreg, vacuum debulking every four layers,
- ii compact and bleed for various times from 2 to 4 h at 80 °C over a curved mould (100 mm radius) at a pressure of 580 kPa,
- iii reform onto a flat platen for 8 h at 80 °C, initially under atmospheric pressure (using a vacuum bag) and later under a pressure of 580 kPa, and
- iv cure for 1 h at 120 °C.

The resulting laminate was visually examined for flatness, wrinkles and damage and then sectioned and polished to determine fibre distribution and porosity. Finally, samples were cut for ILS testing. Similar cure tests were also conducted on 60-ply material which is representative of the doubler thickness employed on the F-111. However, only visual and microstructural analysis could be conducted on this material.

Although the 16-ply laminates staged for the various times were all quite acceptable, the 4 h staging at 80 °C appeared to offer the best compromise in controlled movement of the lay-up and minimum further resin flow. No surface damage or wrinkles were apparent and only low levels of porosity were noted on polished sections taken through the test samples. No further loss in ILSS (beyond the 10% for the non-standard cure) resulted from this manufacturing procedure. Finally, examination of the 60-ply material subject to forming after staging for 3 h at 80 °C indicated low levels of porosity and no obvious damage.

29.4.3. Selection and evaluation of candidate adhesives

Epoxy-nitrile film adhesives were considered the most suitable since they provide strong bonds with high plastic strain to failure, have relatively high shear and peel strengths and moduli, cure at 120 °C or below, are reasonably resistant to degradation by absorbed moisture and are capable of providing reasonable load transfer up to temperatures of 80 °C. Adhesive FM73 by Cytec, the main adhesive employed in other Australian repair work, was chosen from several candidate

epoxy-nitrile adhesives for several reasons including low temperature cure capability, large data base and good storage characteristics.

29.4.4. Selection and evaluation of surface treatment procedures

For the F-111 WPF reinforcement, only non-aggressive surface treatments, applicable simultaneously to the steel WPF, aluminium wing skin and steel fasteners could be considered. However, most of the standard surface treatments are specific to the metal being treated and are fairly aggressive in that they involve some form of surface etching. Simplified surface treatments using phosphoric-acid anodising (gel), have been devised for aluminium alloys for use in field repair situations [9]. However, the phosphoric-acid anodising procedure is not applicable to the steel components and, further, there is a serious risk that its use in contact with the ultra-high strength steel components of the WPF could lead to hydrogen embrittlement. Thus, simpler and more effective surface treatments were sought capable of treating simultaneously all of the metallic components. In particular, the use of silane coupling agents was considered, based on previous work at DSTO [10,11], and they were selected as the main approach for this program. Work was also undertaken to investigate the origin of high void contents that were observed in some of the adhesive joint specimens prepared in the test program. This was found to be related to excessive grit blasting and the subsequent adsorption of water vapour on the heavily deformed surfaces [12].

29.4.5. Modifications to doubler system

Following some early failures with the doubler system on aircraft, and experience gained from analysis of the failures, it was decided to modify the doubler system to increase the interlaminar toughness in critical areas. Several new approaches were taken including the use of interleaving adhesive FM300-2 in critical regions. The interleaving adhesive (around 0.025 mm thick) significantly toughens the interfacial regions. This and other modifications reduced the stress concentration in the critical regions and increased the strain capacity and toughness of the doubler system. All aircraft with modified doublers have successfully passed the CPLT.

29.4.6. Residual stress minimisation

This section discusses an approach to reducing the problems of residual stress during application of the F-111 doubler. As mentioned briefly in Chapter 2, the development of residual stresses is perhaps the major disadvantage in the use of high-temperature curing adhesives for composite repairs. Various approaches can be employed to reduce these residual stresses for a given doubler configuration [10], including: (i) minimising the size of the area to be heated, (ii) minimising the cure or gel temperature of the adhesive, or (iii) applying a compressive stress to the metallic component to offset the tensile stresses that arise in this component due to the thermal expansion mismatch. All of these approaches were taken with the F-111

doubler. With regards the second of these, a series of experiments were undertaken in which a boron laminate was bonded on one side of an aluminium plate with FM73 adhesive at a range of different temperatures. By measuring the radius of curvature after the cure was complete, the amount of residual stress was calculated. From this it was calculated that by curing the adhesive for 8 h at 80 °C followed by a 1 h postcure at 120 °C, the level of residual stress was 27% lower than for the standard cure cycle of one hour at 120 °C. It is the ability of adhesive FM73 to cure at a lower than standard temperature which allows this option and was a major reason for its choice for the doubler system.

29.5. Doubler application technology

The selection of the reinforcement and adhesive also dictates certain requirements for the successful application of the reinforcement system to the structure. In the case of the boron epoxy composite and FM73 adhesive, elevated temperature cure and applied pressure are necessary for the production of properly consolidated void-free laminates and bond lines.

29.5.1. Temperature

Since the structure in the repair region is constructed of thick aluminium and steel (approximately 8 to 25 mm and 7.4 mm thick, respectively) which have high thermal mass and are excellent conductors, the amount of heat required for the cure process is significant. Infrared lamps were chosen because they provided a versatile source of high-intensity heat required to raise the temperature of the structure. No direct contact occurred between the heat source and the structure. The system was not therefore affected by problems with thermal contact due to variations in the geometry or curvature of the region. As the power density of radiant heat depends on the distance from the source, the ability to raise or lower the lamps provided another means of control. A number of individually controlled heating banks were required, together with supplementary heating in the form of heater blankets located directly over the doublers. A computer controlled system (now developed commercially as the Novatech HBC-43 system) was established to control these lamps and record up to 16 temperatures around the repair site.

29.5.2. Pressure

The standard vacuum-bag approach can be a very successful method of developing pressure to bond a reinforcement onto a surface that contains no perforations or discontinuities. However, the danger with using a vacuum bag on the F-111 WPF is that contaminants may be drawn into the repair region from either the step at the wing skin or from under the fasteners. Instead, a method to apply direct pressure, based on the use of a rubber bladder, was chosen to overcome these problems. In this approach, the bladder is in direct contact with a

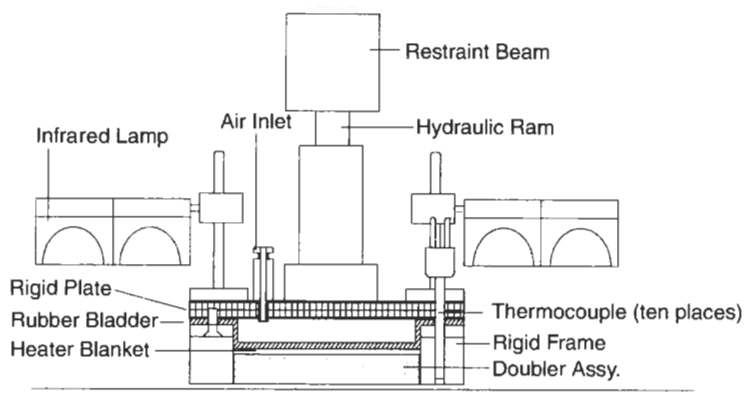


Fig. 29.5. Schematic of the rig employed to form and bond the boron/epoxy doubler to the wing skin (not to scale).

release layer over the repair. The region between the bladder and a stiff plate is pressurised using air to force the bladder down onto the repair. The plate is held firmly against a surrounding frame which also acts as an edge dam, preventing transverse distortion during cure. Loads generated by the pressure were reacted out at hard points on the wing. Figure 29.5 is a schematic of the rig employed in bonding the doubler.

29.6. Doubler fitment

Significant variations in structural geometry are encountered between aircraft due to the original configuration of the region, a wide range of manufacturing tolerances and structural re-work for removal of corrosion. These variations were a major reason that metallic reinforcements could not be used due to the difficulty of forming them to the wing. Fitment problems associated with the B/Ep doublers are mainly solved by matching the thickness of the lower doubler to the step height. A computer program was developed to calculate the location and area of the required fill layers necessary to produce a lower doubler of the correct thickness. The lower doubler is then pre-consolidated to enable close control of thickness, and eliminate problems associated with containment of resin flow on the aircraft. It also reduces the pressure which needs to be applied to the aircraft during *in situ* cure.

The doublers are cured and bonded in a multi-stage operation designed to ensure correct fitment to the wing. This process is necessary to avoid stress concentrations associated with kinked fibres and is carried out at a range of different cure temperatures to minimise residual stresses.

29.7. Fitment to fleet aircraft

Doublers were applied across the RAAF fleet so that the wings had the doublers installed prior to undergoing the CPLT. Once the doublers are fitted to the WPF, they are covered with a range of materials (sealants, honeycomb and fibreglass) that are required to form an aerodynamic surface or fairing over the top of the doublers. As mentioned in Section 29.4.5, two of the first doublers failed during CPLT due to the high strains and low temperatures involved. Modification of the design with FM300-2 interleaf adhesive was an important factor in increasing the strain capability to the required level to pass the CPLT loads. The aircraft are required to undergo CPLT around every eight years at the current rate of fleet flight hours. The doublers were left fitted to the aircraft after the last CPLTs were conducted as a way of reducing the levels of cyclic stress seen in the critical stiffener runouts during routine operation.

Due to the aerodynamic fairing over the doublers, routine inspection of the condition of the doublers was very difficult and in most cases all that was possible was simply a visual inspection of the fairing or sheath itself. The detection of damage on one sheath resulted in its removal and at this time one of the doublers underneath was found to be disbonded. This was the first indication of likely durability problems with the doublers. Inspections have since been undertaken of other sheaths/doublers and to date around a quarter of the doublers have been found to have disbonded. These disbonds appear to have occurred after approximately 800–1000 flight hours of aircraft usage. Previous fatigue durability testing at DSTO [1] did not reveal any likely durability problems and so these disbonds were unexpected. One of the more common reasons for adhesive disbonds is poor surface treatment, however, it is very clear that this was not the cause in this situation. In all cases, adhesive remains bonded to the metallic substructure and the failure location is within the first ply of the composite.

No single factor appears to be cause, however, the following three factors appear to contribute to the problem. Firstly the stepping at the ends of the doublers is not ideal and is more severe than that normally used. This was caused by geometrical limitations at the reinforcement locations together with the desire to keep the doubler size small to reduce the amount of structure that needed to be heated during the cure. The small steps used would increase the level of peel stress at the ends of the doublers. Secondly, the stresses present in the doublers at the location of disbond initiation have been found to be slightly higher than the original analysis predicted, which was for a region over a critical stiffener runout. These two factors are believed to have combined to cause the failures. A detailed fractographic examination of the failed doublers has revealed that in most regions of failure, the adhesive remains bonded to the substrate and the failure is within the ply of the composite adjacent to the bondline. In several cases, small regions of cohesive failure of the adhesive have been found where there were striations on the adhesive fracture surface which indicate that the adhesive has suffered from fatigue crack initiation and propagation. The third factor is the presence of the jet fuel and the various additives it contains. Traces of fuel have been found within the failed

adhesive samples. Laboratory tests at DSTO have shown that the peroxides that develop in fuel as it ages, reduce the properties of the adhesive and it is believed that this further exacerbates the problem. Investigations into the cause of these disbonds are continuing.

From this it can be seen that for repairs that operate at very high stress levels, careful design for fatigue is required. While these doublers were designed with fatigue in mind, there is now much better understanding of the significant influence that peel stresses at the ends of doublers can play in fatigue initiation. Secondly the durability tests that were conducted did not reveal any problems due to the fact that the correct ratio of shear to peel stress was not reproduced at the ends of the doublers. Where representative joint tests are used in repair validation, it is very important that all critical aspects are accurately modelled. This in turn places stringent requirements on the predicted operational stresses that are likely to be generated by a Finite Element Analysis.

This application of bonded repair technology to the F-111 WPF is not typical and indeed the adhesive is operating at very high stress levels under extreme conditions. While the doublers have been successful in reinforcing the WPF during the CPLT which is their most important function, there appears to be a durability problem in this case that is made more difficult by the lack of access to the doublers for NDI inspections. This is a perfect situation for the use of a Smart Patch as described in Chapter 20. The electronics could easily be located between the two doublers underneath the sheath and so a form of remote communication could be used to establish that the doublers were still in good condition. Such a system together with design improvements that may flow from the ongoing disbond investigations, would provide a durable, self-monitoring doubler system that will be effective in extending the life of the F-111.

29.8. Conclusions

A fibre composite doubler system was developed to reinforce a critical region in the wing pivot fitting of the F-111 aircraft. This doubler system has been shown to reduce strain in the region by over 30%. A boron/epoxy composite was chosen as the reinforcement material, together with a structural-film adhesive to provide the required levels of strength, stiffness, formability, ductility and durability. Careful attention to the reduction of residual stress has been an important part of the overall development process. Application procedures have been developed to accommodate the different shape of each wing, together with the stringent requirements for correct application of temperature and pressure. The complex nature of the reinforced region on the aircraft has necessitated the development of a computerised system for control of the infra-red heating lamps.

The doubler system has proved successful in the design objective of reinforcing the WPF during the CPLT. Durability problems have been revealed during subsequent flight operations of the aircraft due in part to the very high stresses that are present in these doublers. Smart patch technology as described in Chapter 20

would be of value in this repair application due to both the significance of the reinforcement and the difficulty of undertaking conventional inspections.

References

1. Baker, A.A., Chester, R.J., Davis, M.J., *et al.* (1993). Reinforcement of the F-111 wing pivot fitting with a boron/epoxy doubler system – materials engineering aspects. *Composites*, **24**, pp. 511–521.
2. Bland, L. (1982). Final engineering report: A8–112 wing pivot fitting failure investigation (Manufacturing Processes). FZM-12–5130, General Dynamics, Fort Worth, USA.
3. Jones, R., Callinan, R.J. and Molent, L. (1987). Preliminary design of a boron/epoxy reinforcement for the F-111C wing pivot fitting. ARL-Struct-Rep-429, Aeronautical Research Laboratory, Melbourne Australia, (August).
4. Molent, L., Callinan, R.J. and Jones, R. (1989). Design of an all boron/epoxy doubler reinforcement for the F-111C wing pivot fitting: structural aspects. *Composite Structures*, **11**, pp. 57–83.
5. Molent, L. (1987). Comparison of theoretical and test results for an F-111C wing pivot fitting boron/epoxy doubler specimen. ARL-Struct-Rep-465, Aeronautical Research Laboratory, Melbourne Australia.
6. Davies, P., Moulin, C. and Kausch, H. (1990). Measurement of G_{Ic} and G_{IIc} in Carbon/Epoxy Composites. *Comp. Sci. and Tech.*, **39**, pp. 193–205.
7. Ennis, B.C., Pearce, P.J. and Morris, C.E.M. (1988). Thermal analysis of epoxide film adhesives, *Thermochimica Acta*, **134**, pp. 187–193.
8. Morris, C.E.M. and Pearce, P.J., Unpublished results.
9. Lock, M.C., Horton, R.E. and McCarty, J.E. (1978). AFML-TR-78–104.
10. Baker, A.A. (1988). Bonded Repair of Aircraft Structures (A.A. Baker and R. Jones, eds.). Martinus Nijhoff, Chapter 6.
11. Baker, A.A. and Chester, R.J. (1992). Minimum surface treatments for adhesively bonded repairs. *Int. J. of Adh. And Adh.*, **12**, pp. 73–78.
12. Chester, R.J. and Roberts, J.D. (1989). Void minimisation in adhesive joints. *Int. J. of Adhesion and Adhesives*, **9**, pp. 129–138.

Chapter 30

CASE HISTORY: BONDED COMPOSITE REINFORCEMENT OF THE F/A-18 Y470.5 CENTRE FUSELAGE BULKHEAD

R.A. BARTHOLOMEUSZ and A. SEARL

Defence Science and Technology Organisation, Air Vehicles Division, Australia

30.1. Introduction

Cracking was predicted to occur in an area of high curvature (the crotch region) of the F/A-18 Y470.5 centre fuselage bulkhead. Boeing recommended that an "engineering change proposal" (ECP) be implemented to the bulkhead to remove any fatigue damaged material and to reduce the stress concentration caused by the present sharp angle. Work at the Defence Science Technology Organisation (DSTO) was aimed at development of a bonded composite reinforcement for this problem. The reinforcement could be applied instead of the ECP or after implementation of the ECP as an added safety factor.

The reinforcement to the F/A-18 Y470.5 bulkhead crotch region was limited by the existence of through-thickness adhesive stresses resulting from the curvature of the region. Through-thickness stresses in bonded joints, or stresses normal to the plane of the adhesive layer, generally arise from out-of-plane loading in the joint. These stresses are called peel, tension, tearing or normal stresses and usually result from the shear stresses developed during load transfer and from the development of secondary bending under non-axial loading. Less commonly they arise in joints with a high degree of curvature. Through-thickness stresses play no part in the desired load transfer in the joint, but can cause failure since adhesives (and composite adherends) have relatively low peel strengths.

The following summarises a work program aimed at development and validation of a bonded composite reinforcement for the Y470.5 bulkhead crotch region [1]. Both a finite element (FE) analysis and an experimental test program were undertaken to determine the suitability of a bonded reinforcement for the bulkhead. A representative structural detail test specimen the "curved beam specimen" (CBS) was designed to identify the stress state in the joint and in conjunction with FE analysis, to determine the through-thickness stresses in the

adhesive. The static and fatigue testing of this specimen were used to validate the reinforcement for the bulkhead.

The Royal Australian Air Force (RAAF) decided to incorporate the Boeing ECP to the bulkhead. Some concerns still exist that this ECP will not produce sufficient stress reduction to give the required fatigue life for the bulkhead. A bonded reinforcement applied to the region post ECP may further reduce the stresses sufficiently to give the required life for the aircraft. As before, FE analysis has shown that the stress in the bulkhead reduces after application of the reinforcement and that high through-thickness and shear stresses were present in the adhesive due to the curvature of the region. The FE analysis and test program however indicated that a reinforcement applied post ECP should extend the life of the bulkhead.

30.1.1. Background

The crotch region of the Y470.5 bulkhead was identified as a potential site for fatigue cracks early in the life of the FA-18 aircraft (see Figure 30.1). The current full-scale fatigue test of the aircraft centre section in Canada showed that cracking will occur in this region under the flight loads likely to be experienced by the RAAF fleet at approximately 6600 test flight hours. Northrop/McDonnell Douglas recommend that an ECP be implemented to the bulkhead to remove any fatigue damaged material and to reduce the stress concentration caused by the present sharp angle (see Figure 30.2). This ECP is planned to be implemented to the RAAF fleet by 2200 flying hours (test life to cracking divided by a safety factor of three) so that the aircraft can safely meet its full design life of 6000 flying hours.

30.2. FE analysis of bulkhead and reinforcement

The existing Northrop/McDonnell Douglas FE model of the Y470.5 bulkhead was refined at AMRL in the crotch region and used to design a bonded composite reinforcement which was applied to the structure. Reinforcements were applied to the model pre ECP and after incorporation of the ECP. The adhesive FM73¹ (an epoxy-nitrile film adhesive) was used for all cases analysed. The model was loaded to the design ultimate load (DUL) condition and the stresses in the bulkhead, epoxy adhesive and boron/epoxy composite were obtained. The analysis showed that a good compromise between stress reduction in the bulkhead versus low adhesive through-thickness and shear stress could be made if a 1.0 mm thick composite reinforcement was used [1].

¹ CYTEC FM73 structural epoxy adhesive.

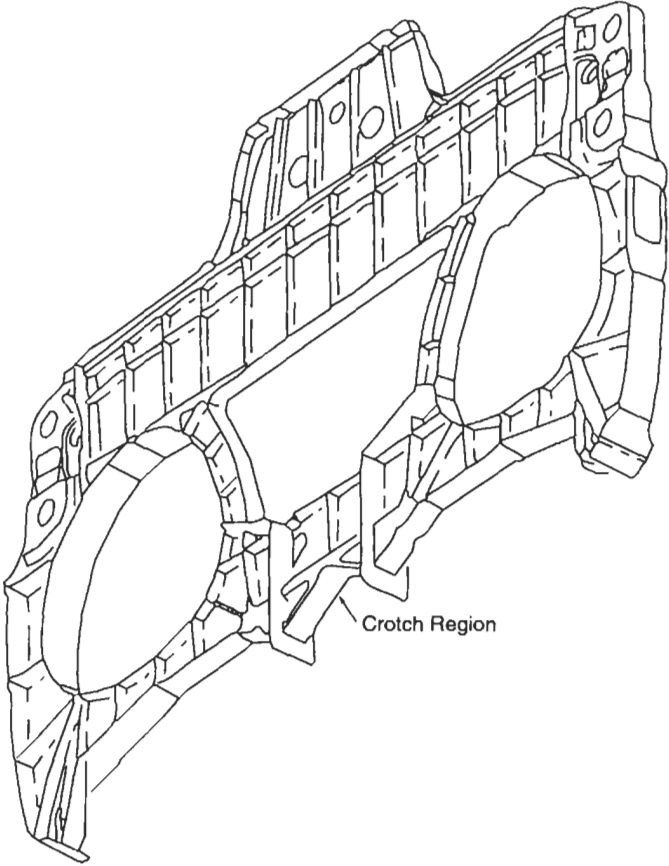


Fig. 30.1. The Y470.5 centre fuselage bulkhead showing location of crotch region.

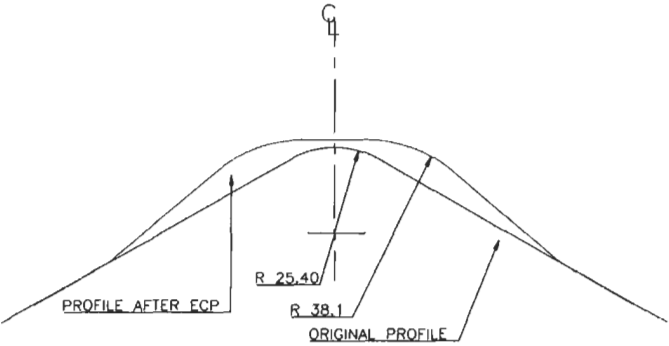


Fig. 30.2. Detail of crotch centreline showing the original and the profile after ECP. All dimensions in millimetres.

30.2.1. Results of the bulkhead FE analysis

The models of the bulkhead were run to determine the stress state in the adhesive at the ultimate load condition for both the pre and post ECP cases. The results for the pre ECP case are summarised in Table 30.1. Figures 30.3 and 30.4 show the adhesive shear and through-thickness stress for the post ECP case.

The 1.0 mm (or eight ply) reinforcement was predicted to achieve 22% reduction in bulkhead peak stress (coincident with the bulkhead centreline) for the pre ECP model and a 15% reduction in the peak stress for the post ECP model. As mentioned above, Table 30.1 summarises the results obtained from the analysis of the bulkhead models for both the pre and post ECP cases.

30.2.2. Measurement of adhesive through-thickness stresses

Through-thickness stresses in adhesives are traditionally measured using butt joints [2]. This test was successfully used by researchers [3,4] to produce fatigue life estimations for adhesives; however, it has a number of disadvantages. The main problems are the difficulties in aligning the specimen halves during manufacture and testing and that the tri-axial stress state at the edge of the joint causes a stress concentration in the adhesive for solid specimens which will fail the joint prematurely. Also, it is difficult to measure the small deflections involved and the large stress concentration at the edge of the joint means that any measurement of failure strength will be approximate. However, some researchers have used FE methods to estimate the stresses in such joints [5].

No design allowable thus exists for adhesives in the through thickness direction and certification of the bonded reinforcement would be difficult, based only on the stresses predicted in the numerical analysis. Experimental testing of a full bulkhead with the reinforcement applied would be prohibitively expensive. To prove the static strength and durability of the reinforcement a structural detail test specimen, the CBS, representative of the crotch region of the Y470.5 bulkhead was developed for both the pre and post ECP case.

Table 30.1

Summary of predicted results from numerical analysis of the bulkhead and the CBS at DUL. All stresses in MPa.

Patch	Bulkhead				CBS			
	Pre ECP		Post ECP		Pre ECP		Post ECP	
	No	Yes	No	Yes	No	Yes	No	Yes
Max ^m XX Stress in Alloy	662	516	524	445	–	–	–	–
Midplane XX Stress in Alloy	662	516	448	368	850	568	450	337
Max ^m Shear Stress in Adhesive	–	–	–	26	–	28	–	26
Max ^m Peel Stress in Adhesive	–	45	–	28	–	50	–	28
Midplane XX Stress in Boron	–	1282	–	1059	–	1261	–	1101

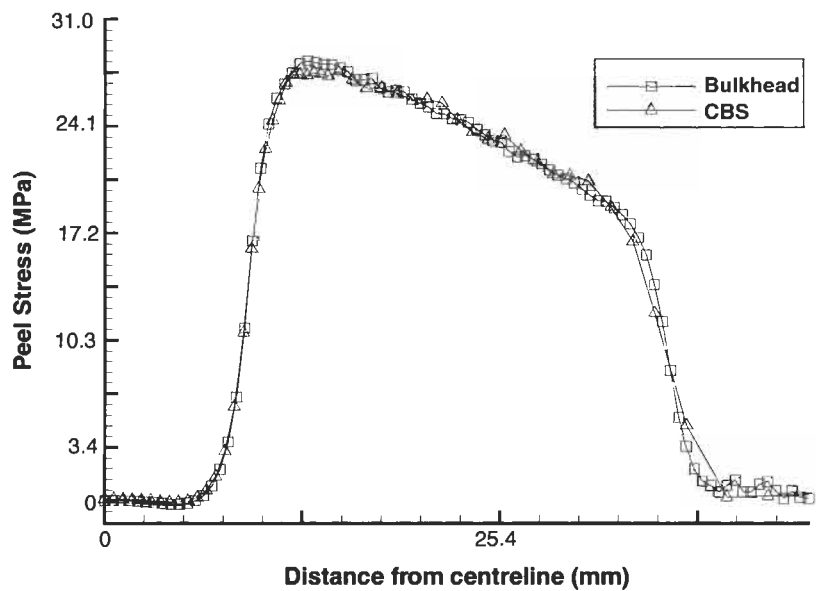


Fig. 30.3. Through-thickness (peel) stress distribution in adhesive post ECP and reinforcement at DUL for both the bulkhead and the CBS.

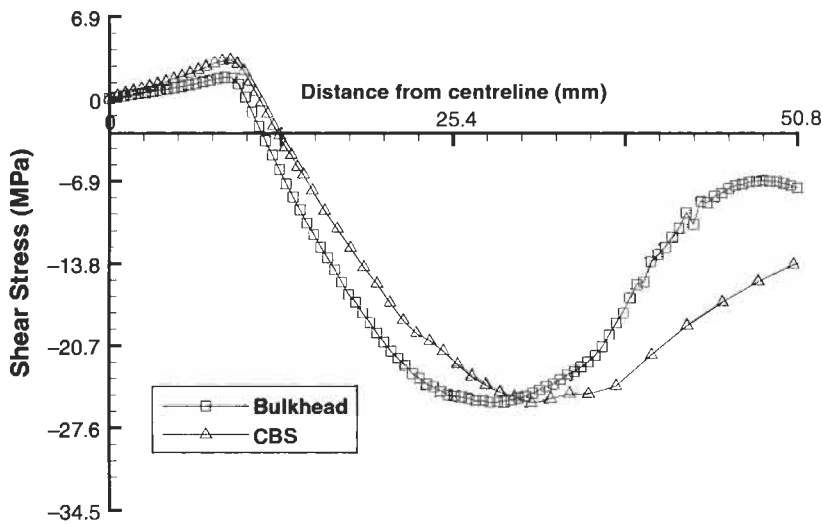


Fig. 30.4. Shear stress distribution in adhesive post ECP and reinforcement at DUL for both the bulkhead and CBS.

30.3. FE design of representative specimen (curved beam specimen)

The CBS was designed to reproduce the stress distribution in the reinforcement and bulkhead material. The two specimens represent the shape of the F/A-18 Y470.5 bulkhead crotch region pre and post ECP, the adhesive and the proposed boron/epoxy reinforcement. Figure 30.5 shows the CBS for the post ECP case. The model of the CBS was analysed at DUL (note that for the pre ECP case DUL is equivalent to a pin load of 72.3 kN and for the post ECP case DUL is equivalent to a pin load of 53.3 kN) and was able to accurately reproduce the midplane bending stresses, the adhesive peel stresses and the adhesive shear stresses when compared with the corresponding bulkhead model. The adhesive shear and through-thickness stress distributions for the CBS post ECP are shown in Figures 30.3 and 30.4 respectively.

30.4. Experimental test program

30.4.1. Static testing of curved beam specimen

For the static test program, repaired CBS's were loaded to 40 kN to validate the FE models and loaded to failure to determine the performance of the reinforcement. Specimens were reinforced with 1.0 mm boron/epoxy composite patches co-cured² and bonded with FM73 epoxy adhesive.

A thermal survey of a FA-18 during ground runs and flight showed that the maximum temperature in the region of the crotch was 49 °C [6]. To be conservative

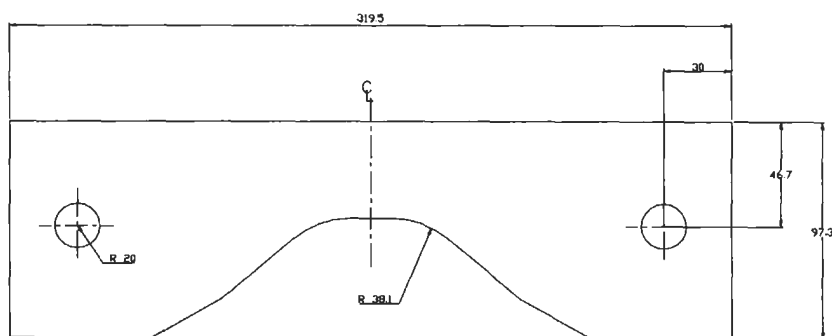


Fig. 30.5. Drawing of CBS for the post ECP case. All dimensions in millimetres.

² To locally toughen the composite matrix, a layer of adhesive can be co-cured to the composite patch. At DSTO this is usually carried out on the bonding surface of a composite to reduce damage to the matrix and fibres during surface treatment.

for the static testing it was decided to test the reinforcement at both room temperature and at 60 °C. For all the tests, the specimens were pin loaded in a servo-hydraulic test machine and load versus strain information was measured using a computer-based data acquisition system. The failure pin load was measured when the strain in the boron/epoxy reinforcement was observed to drop indicating adhesive failure. The results of the static test program are given in Table 30.2 and Figure 30.6 shows a typical failure mode in the radius of the crotch in the CBS.

30.4.2. Durability testing of the curved beam specimen

To determine the long term performance for the reinforcement, CBS's were fatigue tested at both room temperature and 50 °C to be representative of the environmental conditions in the crotch region. For both the pre ECP and post ECP specimens, the FA-18 Y470.5 bulkhead spectrum, truncated to remove all compressive loads, was used for the loading sequence. For the post ECP specimens, to be conservative, the spectrum loads were factored up by 1.5. During the tests strain versus applied loading cycles was monitored. If strain was observed to change over the life of the test this would indicate failure of the reinforcement. Each specimen was loaded to the equivalent of 4.5 aircraft lifetimes or until failure. The adhesives used for bonding were FM73 which can be cured within a temperature range from 80 °C to 120 °C, and FM300-2³ which is cured at 120 °C. FM300-2 is a higher performance adhesive than FM73 with superior elevated-temperature performance, a higher shear yield stress and higher shear modulus. The results of the fatigue tests using the CBS are summarised in Table 30.2.

Table 30.2
Summary of test results for CBS's.

Test conditions	Patch thickness (mm)	Co-cure adhesive	Bonding adhesive	Applied a/c lifetimes	Pin load at failure (kN) (%DUL)
RT, Pre ECP	1.0	FM73	FM73	Static only	94.3 (130)
60 °C, Pre ECP	1.0	FM73	FM73	Static only	68.1 (94)
RT, Pre ECP	1.3	FM73	FM73	Static only	73.4 (102)
RT, Pre ECP	1.5	FM73	FM73	Static only	86.8 (121)
50 °C Pre ECP	1.0	FM73	FM73	0.79	-
RT, Pre ECP	1.0	FM300-2	FM73	4.5	-
50 °C, Pre ECP	1.0	FM300-2	FM300-2	4.5	> 100 (138)*
50 °C, Pre ECP	1.0	FM300-2	FM73	4.6	83.9 (116)*
50 °C, Post ECP	1.0	FM300-2	FM73	4.5	78.2 (147)*
50 °C, Post ECP	1.0	FM300-2	FM73	4.5	65.7 (123)*

*Residual strength after fatigue loading.

The test machine was at maximum load and the specimen did not fail.

³ CYTEC FM300-2 structural epoxy adhesive.

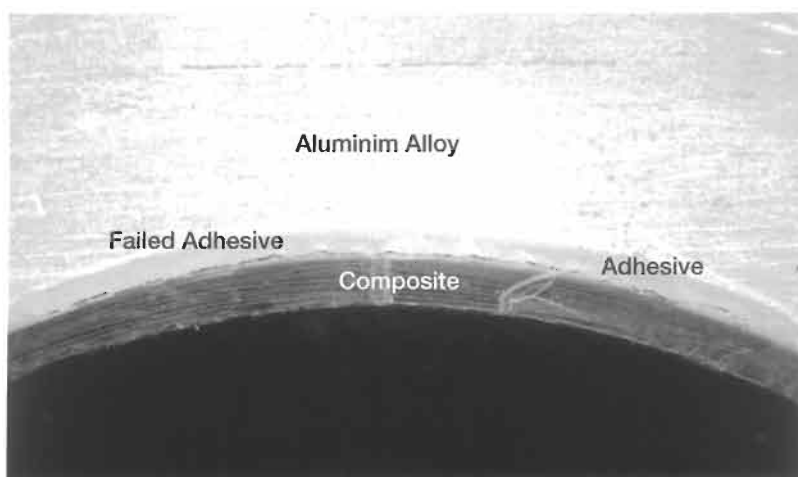


Fig. 30.6. Detail photograph of crotch region in CBS after failure of bondline.

30.4.3. Residual strength after fatigue

Following the fatigue testing, some specimens were statically loaded to failure to determine the residual strength. These tests were carried out as in the static test program and the pin load and strains were measured during loading. When the strain in the boron/epoxy reinforcement was observed to drop, the pin load was recorded as a measure of the residual strength and these results are given in Table 30.2.

30.5. Trial installation of reinforcement to full-scale fatigue test article

To test the installation procedures and confirm the predictions from the bulkhead FE analysis a 1 mm thick reinforcement, co-cured with FM73, was manufactured and forwarded to Canada for application to the Canadian F/A-18 Full-Scale Fatigue Test Article. The reinforcement was bonded with FM73 to the test article pre ECP using positive pressure and a controlled heater system. Comparison of strain measurements before and after installation showed that a 21% [7] reduction in local strain was achieved at the centreline of the crotch which compares favourably with the result predicted by the FE analysis of 22% for the pre ECP case.

30.6. Discussion

30.6.1. Pre ECP reinforcement

The analysis of the bulkhead pre ECP at DUL predicts a high stress of 666.7 MPa (96.6 ksi) at the centreline of the crotch region. This reduces by 22% after application of an eight-ply boron/epoxy composite reinforcement. CBS's, representative of this reinforced case were tested statically, then in fatigue and finally statically to determine residual strength. The results showed that the reinforcement and adhesive were capable of withstanding DUL, surviving 4.5 lifetimes of spectrum fatigue loading and the residual strength was greater than DUL.

FE analysis of the CBS showed that good correlation existed with the stresses calculated by the bulkhead model. This indicated that the CBS was indeed representative of the bulkhead crotch region and thus was a suitable specimen to determine the stress state of the adhesive and reinforcement. The 2D analysis of the CBS was validated against experimental data indicating that the predicted stresses in the model were accurate. For these validation checks, both the model and the test specimen were loaded to 40 kN to avoid any possibility of plasticity. Thus it is important to note that the CBS was modelled and validated using an elastic analysis and some errors will exist for the DUL and failure pin load cases where adhesive plasticity and metal yielding will have occurred. This is also true for the post ECP case.

The analysis showed that through-thickness stress is a maximum and shear stress a minimum at the centreline of the pre ECP crotch region of the Y470.5 bulkhead and the CBS. A bondline thickness of 0.4 mm was chosen to represent the two layers of adhesive that were used first to co-cure to the reinforcement and then later to bond. The model predicted a maximum adhesive through-thickness stress of 45 MPa at the DUL condition.

The static tests showed that the adhesive FM73 fails at a pin load of 93.4 kN at room temperature and at a pin load of 68.1 kN at 60 °C for an eight ply or 1.0 mm thick boron/epoxy reinforcement. Comparing this to the ultimate pin load condition of 72.3 kN it implies that FM73 will not provide the required performance at elevated temperature (noting that the test temperature was slightly greater than the actual temperatures measured on the aircraft).

Visual examination of the failed bondlines in the CBS showed that all the failures occur in the radius of the crotch. This is where the FE analysis predicts the through-thickness stress is a maximum and the shear stress is a minimum implying that the failure is dominated by the through-thickness stress. Close examination of the bondline also revealed that the failures occurred in the co-cured layer of adhesive in the radius of the crotch angle.

Durability testing of the CBS showed that FM73 when used to both co-cure and bond the reinforcement was not suitable at elevated temperature. The failure was again observed in the co-cured layer of adhesive. A higher performance adhesive FM300-2, was trialed and shown to be capable of surviving to 4.5 aircraft lifetimes

when tested at 50 °C with no observed failure. As mentioned above, FM300-2 cures at 120 °C and FM73 can be cured at 80 °C. Reaching a cure temperature of 80 °C during application of a reinforcement to a bulkhead fitted to an aircraft would be much easier than achieving 120 °C. Thus, FM73 would be the preferred adhesive for bonding a reinforcement to an aircraft. As the failures all occurred in the co-cured layer of adhesive, it was decided to trial co-curing the higher performance adhesive FM300-2 to the reinforcement, and then bonding later with FM73. Fatigue testing showed that this combination of co-cured FM300-2 with FM73 for bonding, survived 4.5 lifetimes at 50 °C.

The residual strength after fatigue loading of the specimen co-cured and bonded with FM300-2 after 4.5 lifetimes of spectrum fatigue loading was shown to be higher than the DUL. Also, the specimen that had the combination of the co-cured FM300-2 with FM73 for bonding, had a residual strength of 84.3 kN, which gives a margin of safety of 1.17 over the DUL of 72.3 kN.

30.6.2. Post ECP reinforcement

The rework that will be incorporated during ECP to the crotch was reproduced on the finite element model of the bulkhead. The model was analysed for the DUL condition and the maximum stress was found to be 524.0 (76 ksi). This maximum stress was no longer located at the centreline of the crotch but had moved to the radius of the reworked shape.

An eight-ply boron epoxy doubler co-cured with FM300-2 and bonded with FM73, was applied to the model of the bulkhead post ECP. When analysed at DUL, this reinforcement reduced the maximum stress by 15% to 444.7 MPa (64.5 ksi).

A specimen representative of the bulkhead post ECP was designed. FE analysis of this CBS showed that good correlation existed with the stresses calculated for the bulkhead model. This indicated that this new CBS was indeed representative of the bulkhead crotch region post ECP and thus was a suitable specimen to replicate the stress state of the adhesive and reinforcement during testing. CBS's, representative of the post ECP reinforced case were tested statically, then in fatigue and finally statically to determine residual strength. The results again showed that the reinforcement and adhesive were capable of withstanding DUL, surviving 4.5 lifetimes of spectrum fatigue loading and the residual strength was greater than DUL. For the bulkhead post ECP and reinforcement, the adhesive through-thickness and shear stress distributions for the DUL case show that the maximum through-thickness stress was 28.3 MPa (4.1 ksi) and the maximum shear stress was 26.2 MPa (3.8 ksi). The original model of the CBS, pre ECP, predicted a maximum adhesive through-thickness stress of 45 MPa and a maximum adhesive shear stress of 28 MPa at the DUL condition after reinforcement. Thus, there is a significant reduction in the adhesive through-thickness stress post ECP and reinforcement.

30.7. Conclusions

1. Both FE analysis and an experimental test program using a representative specimen (the CBS) were used to investigate a bonded composite reinforcement for the F/A-18 Y470.5 bulkhead crotch region.
2. FE analysis showed that high shear and peel stresses were present in the adhesive at DUL.
3. A representative specimen (the CBS), for both the pre and post ECP cases, was designed by FE analysis to reproduce the midplane bending stresses, the adhesive peel stresses and the adhesive shear stresses when compared with the corresponding bulkhead model.
4. The experimental test program showed that the reinforcement is capable of withstanding DUL statically and fatigue loading at the operating temperatures of the crotch region.
5. Co-curing FM300-2 adhesive to the lower surface of the boron/epoxy composite increases the static and fatigue performance of the reinforcement.
6. Reinforcement of the crotch region of the bulkhead pre ECP with a 1.0 mm thick patch reduces the peak stresses in the bulkhead by 22% at DUL.
7. Incorporation of the ECP reduces the maximum stress in the bulkhead by 21% at DUL.
8. Reinforcement of the crotch region of the bulkhead after incorporation of the ECP with a 1.0 mm patch reduces the maximum stress by a further 15% at DUL.
9. Installation of a 1.0 mm reinforcement was successfully completed to the pre ECP crotch of the Canadian full-scale fatigue test article. This reinforcement showed a 21% stress reduction in the bulkhead in the critical region.

30.8. Acknowledgments

The authors would like to thank Alan Baker, Richard Chester, Ivan Stoyanovski and Sally Whitehead from DSTO AMRL who have all contributed to the work described in this case study.

References

1. Bartholomeusz, R.A., Baker, A.A., Chester, R.J. *et al.* (1999). Bonded joints with through-thickness adhesive stresses – reinforcing the F/A-18 Y470.5 bulkhead. *Int. J. of Adhesion and Adhesives*, **19**, pp. 173–180, Elsevier Science Ltd.
2. Brinson, H.F. (1990). Technical Chairman, Engineering Materials Handbook, Volume 3, Adhesives and Sealants, Section 5, Testing and Analysis, pp. 321, ASM International, USA, December.
3. Imanaka, M., Kishimoto, W., Okita, K., *et al.* (1989). Fatigue life estimation of adhesive bonded shafts. *Int. J. of Fracture*, **41**, pp. 223–234.
4. Imanaka, M., Fukuchi, Y., Kishimoto, W., *et al.* (1988). Fatigue life estimation of adhesively bonded lap joints. *J. of Engineering Materials and Technology*, **110**, October, pp. 350–354.

5. Adams, R.D., Coppedale, J. and Peppiatt, N.A. (1978). Stress analysis of axisymmetric butt joints loaded in torsion and tension. *Journal of Strain Analysis*, **13**, pp. 1–10.
6. RAAF Minute, AEMS/3050/ET/96/02/TECH Pt 1 (13), 481 WG 8042/96, 8 February 1996.
7. Belanger, P. (1996). Bulkhead 470.5 at Centreline, Presented at the IFOSTP Technical Review Meeting, Canadair, June.

Chapter 31

C-5A FUSELAGE CROWN CRACKING

C. GUIJT and S. VERHOEVEN

Department of Engineering Mechanics, Center for Aircraft Structural Life Extension, US Air Force Academy

31.1. Introduction

One of the problems in the aging C-5A fleet is multiple small-cracks in the upper aft-crown section of the fuselage skin. These cracks are possibly caused due to the usage of stress corrosion sensitive 7079-T6 aluminum. The crown section experiences significant longitudinal tensile bending in addition to biaxial tension due to internal pressurization. Multiple short cracks (25 to 50 mm/1 to 2 inch long) were found (Figure 31.1) in the crown of several aircraft. In the fall of 1995 two bonded-composite repairs were applied at fuselage stations 1700 and 1784 by a team of Wright Laboratory, San Antonio-Air Logistics Center, and United States Air Force Academy personnel [1].

The cracks are believed to have nucleated from the rivet holes of the 7079-T6 aluminum skins due to high fit-up stresses induced in manufacturing and the bending moment caused by the T-tail.

For low temperature applications, analysis and experiments have shown that moderate coefficient of thermal expansion (CTE) composite materials can perform better as fuselage skin repair materials than the more traditional low CTE composite patch materials [2]. The moderate CTE composite material Glare is a viable alternative to traditional composite patch materials such as boron- and carbon-epoxy for pressurized fuselage skin repairs. (Glare is a hybrid laminate of 2024-T3 aluminum sheets and unidirectional S-glass/epoxy composite plies). The moderate CTE patch materials result in a lower K_{repaired} near the crack tip and reduced adhesive shear strains due to the better CTE match with the aluminum skin material. The lower K_{repaired} will result in slower crack-growth, or will stop crack growth. The lower adhesive shear strain is an important advantage in the durability of the bonded repair.

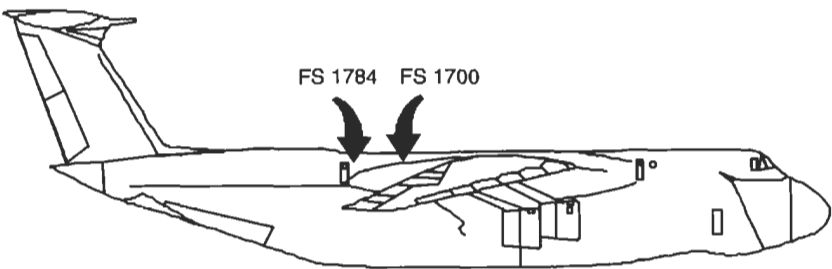


Fig. 31.1. Crack locations in crown section of C-5A.

31.2. Damage tolerance analysis

The cracks are growing in the second rivet row of a 5-rivet row joint. This makes it obvious that the crack is not an ordinary fatigue crack. The direction the crack is growing indicates that the longitudinal stress is the dominant stress to grow the crack. The complicated sub-structure (frame and stiffeners) affects the stress field around the crack.

A typical exceedance table for the C-5A fuselage station (FS) 1700-1784, is given in Table 31.1. The total C-5A life is 30000 flight hours.

Finite element modeling was done to predict more realistic unpatched *K*-values for the crack. A Franc2D-L [3] model was made consisting of the substructure, rivets, and the skin. In order to simplify the model the following modifications were made compared to the actual conditions:

- 1. Shear loads were not applied.
- 2. The crack was modeled as vertical, perpendicular to the longitudinal stress.
- 3. The elliptical patch was modeled as a circular patch.

The result for an applied stress of 120 MPa long/64 MPa hoop is given in Figure 31.2. The lines in the figure indicate the location of the frame, stringer, and the patch. In this figure the patch is not bonded to the skin (simulating the unpatched situation).

Table 31.1
Typical exceedance table for FS 1784-1700.

Stress level	# of exceedances
(MPa/ksi)	per 1000 flight hours
145/19.6	1
130/17.6	10
125/16.9	100
120/16.2	1000
110/14.9	10000
100/13.5	100000
65/8.8	1000000

With the K result from the model and the applied far-field stress, the geometry factor β can be determined.

$$\beta = \frac{K}{\sigma\sqrt{\pi a}} ,$$

where

K = stress intensity factor from the FEM calculation

σ = the applied longitudinal stress

a = the half-crack length in the model (27.66/2 mm) or (1.09/2 inch)

The result for β in the unrepaired case is approximately 0.50. This is not an exact solution due to the simplifications in the model. In general, a biaxial load will reduce the K and K_{repaired} slightly. The substructure lowers the stress in the skin at the crack location by roughly a factor two. The following table gives the stress-intensity factors from the Franc-model at different stress levels (Table 31.2). Limit

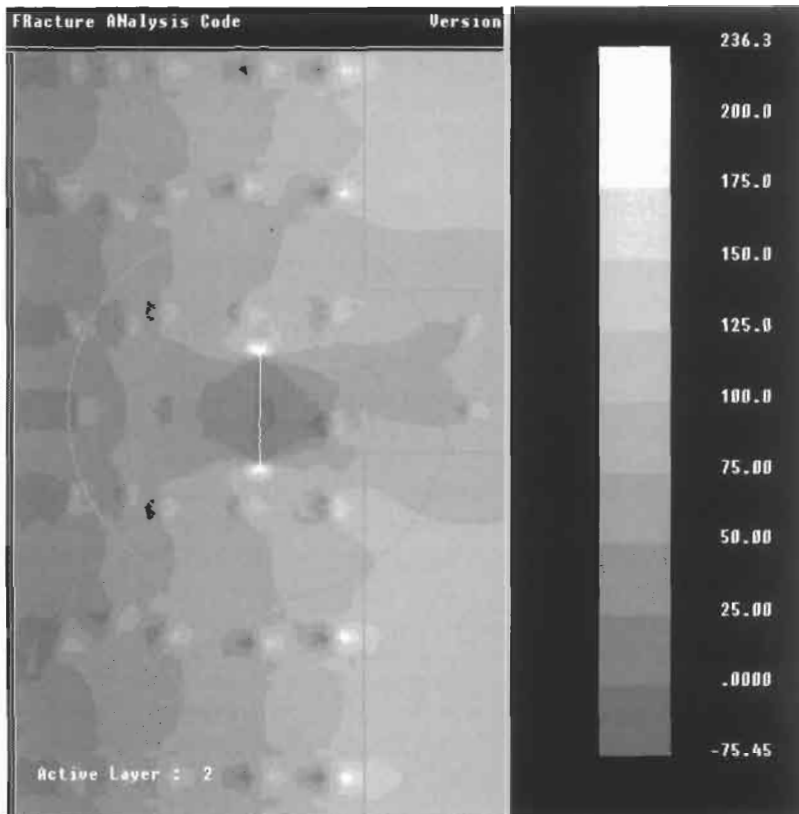


Fig. 31.2. Stresses in the unrepaired skin at FS 1784 (scale in MPa, MPa/7 gives an estimate of ksi, 200 MPa is roughly 28 ksi).

Table 31.2
Stress intensity factors.

Applied stress, long:hoop (MPa.m ^{1/2} /ksi)	80:64/ 10.8:8.7	120:64/ 16.3:8.7	145:100/ 19.6:13.6	160:64/ 21.7:8.7	227:83/ 30.8:11.3
K (Franc2D-L) (MPa.m ^{1/2} /Ksi.inch ^{1/2})	8.5/5.8	12.4/8.5	15.2/10.4	16.4/11.2	23.2/15.9

load is 227 MPa.m^{1/2} (30.8 Ksi) for the longitudinal stress. The unrepaired stress-intensity factor is 23.2 MPa.m^{1/2} (15.9 Ksi.inch^{1/2}) at limit load, this is well below the lowest in the Damage Tolerance Design Handbook [4], 75 MPa.m^{1/2} (51.3 Ksi.inch^{1/2}), the crack is not critical at limit load without a patch. At the time this analysis was performed, the guidelines for bonded repairs were evolving. Limit Load was the load at which the unrepaired defect should not be critical. Since then this load changed to a slightly higher (less likely to occur) load of 1.2*LL. Although the analysis does not address this load, it is obvious that the 20% increased load will not result in a critical crack.

31.3. Repair options

One possible alternative to crack patching the cracked sections on the C-5A's aft upper crown skin is to re-skin the area. Because the rivet pattern in the stringers and frames are hand-drilled, some holes may have edge distance problems. Moreover, re-skinning could be very costly if some frames and stringers have to be replaced due to edge distance problems. Finally, skin replacement must be accomplished in a "fuselage level" condition.

Riveted repairs were attempted. In some cases, new skin cracks grew from the corner rivet holes of the patch. Thus, the most viable repair alternative might be a bonded repair.

Stiffness of the patch material

In order to match patch stiffness to that of the repaired structure, a boron patch will be much thinner than a Glare patch. For very thick sections, or aerodynamic critical areas, the thickness of the patch could play an important role. On a relatively thin fuselage skin in an area where the boundary layer is large, the thickness of the patch will play a minor role; therefore both patch materials are candidates.

Coefficient of thermal expansion

The highest loads in a pressurized fuselage typically occur at low temperatures. The difference in CTE between the patch material and the fuselage plays an important role in patching effectiveness. For all patch materials a stress free state between patch and fuselage skin occurs between the cure temperature and the glass

transition temperature, T_g , of the adhesive. The cure temperature of the adhesive used is typically 100 to 125 °C (212 to 250 °F). After cooling down to room temperature, or to -50 °C (-60 °F) at cruise altitude, in general a moderate- or high-CTE material will cause the crack to be in compression. A low CTE material can actually put the crack in tension. Because of this effect, for this application a moderate- or high-CTE patch material is favorable over a low CTE patch material. Aluminium would be the best alternative from this point of view. However, since the patch is applied over a fatigue crack it is likely that the fatigue crack will propagate through the thickness of the monolithic aluminium patch. Composite patches will not suffer from this problem due to the intrinsic resistance against crack propagation (through the thickness). A Glare patch combines the advantages of composite materials with a higher CTE and is therefore a good candidate for this type of repair.

31.4. Design of the bonded repair

An analytical closed-form computer program was developed, CalcuRep, which allows a quick design of bonded repairs. The 1995 version of the program was used to design the patches and to study the effects of different patch materials, cruise temperature, and cure temperature on the effectiveness of the repair. The results of the predictions were verified using fatigue crack-growth specimens.

However, the program can only handle limited, geometrically simple cases. Therefore, the results are also verified using a 2D finite element model in Franc2D-L [3].

CalcuRep calculations for all load cases

To make a proper patch design the configuration must meet the guidelines for typical loads, limit load and ultimate load. At typical loads, the repair must show durable behavior: the bonded repair should easily outlive the surrounding aircraft structure without causing additional problems. At limit load, no yielding of any component is allowed (except for some limited yielding in the adhesive). At ultimate load (1.5 times limit load) the structure shall not fail; the stresses should be under ultimate strength of the components.

CalcuRep calculates the five most important design parameters for a bonded repair.

1. K repaired
2. Patch stress
3. Skin stress at patch tips
4. Shear strain of the adhesive
5. Minimum patch length vs. load transfer length

Table 31.3 shows the design limits used for these variables at the different load cases.

For the typical repair configuration on an aluminum 7079-T6 crown panel this results in the guidelines given in Table 31.4. The CalcuRep input file, used to design the patches is given in Table 31.5.

Table 31.3
Design limits used for bonded repairs.

	Typical loads	Limit load	Ultimate load
K		$<K_c/1.5$	$<K_c$
σ_{patch}	<0.5 yield	$<\text{yield}$	$<\text{ultimate}$
σ_{tip}	<0.5 yield	$<\text{yield}$	$<\text{ultimate}$
γ_{adhesive}	$<0.5 \gamma_e$	$<1.2 \gamma_e$	$<1.5 \gamma_e$
P_l	$40 \times \text{LTL}$	$40 \times \text{LTL}$	$40 \times \text{LTL}$

Table 31.4
Design limits for bonded GLARE[®] 2 patches on 7079-T6 skins.

	Typical loads	Limit load	Ultimate load
K (MPa.m ^{1/2} /Ksi.inch ^{1/2})		<50	<75
σ_{patch} (Mpa/ksi)	$<236/32$	$<472/64$	$<1100/149$
σ_{tip} (Mpa/ksi)	$<236/32$	$<472/64$	$<1100/149$
γ_{adhesive}	<0.0446	<0.10704	<0.1338
P_l	$40 \times \text{LTL}$	$40 \times \text{LTL}$	$40 \times \text{LTL}$

Table 31.5
CalcuRep input file for patches @ FS 1700 & FS 1784, both 7079-T6.

	FS 1700	FS 1784
Skin thickness (mm/inch)	1.3/0.05	1.3/0.05
Crack length (mm/inch)	12/0.47	22/0.89
Frame spacing (mm/inch)	628/24.7	508/20
Stringer spacing (mm/inch)	155/6.1	155/6.1
Long stress typical* (Mpa/ksi)	121/16.4	121/16.4
Hoop stress typical (Mpa/ksi)	100/13.6	100/13.6
Long stress @ limit (Mpa/ksi)	223/30.2	227/30.8
Hoop stress @ limit (Mpa/ksi)	81/11.0	83/11.3
Patch thickness (mm/inch)	GLARE [®] 2-3/2 1.4/0.055	GLARE [®] 2-4/3 1.55/0.061

* Load which occurs 500 times per 1000 flight hours (15000 per life).

Additional inputs were:

1. Heat blanket 275 × 275 mm/10.8 × 10.8 (inch)
2. Cure temperature 125 °C/250 °F
3. Cruising altitude: 10000 m (33000 ft) typical, 1000 m (3300 ft) limit/ultimate
4. Taper thickness 0.3 mm/0.012 (inch)
5. Patch length: 100 mm/3.94 (inch)
6. Patch width: 90 mm/3.54 (inch)
7. Ultimate load: 1.5 × Limit

The results of the calculations for FS 1700 are given in Table 31.6.

Comparing the calculated results with the table for the design limits shows that all guidelines are met except for patch length (100 instead of 153 mm) and adhesive

Table 31.6
CalcuRep results for FS 1700.

FS 1700	Typical	Limit	Ultimate
K (Mpam ^{1/2} /ksi(inch) ^{1/2})	3.03/2.07	7.13/4.88	19.6/13.43
σ_{patch} (Mpa/ksi)	148/20.1	268/36.3	394/53.4
σ_{tip} (Mpa/ksi)	195/26.4	352/47.7	517/70.1
γ_{adhesive}	0.0343	0.0805	0.1523
P_1 (mm/inch)	153/6.02	153/6.02	153/6.02

Table 31.7
CalcuRep results for FS 1784.

FS 1784	Typical	Limit	Ultimate
K (Mpam ^{1/2} /ksi(inch) ^{1/2})	2.67/1.83	6.98/4.78	20.7/14.18
σ_{patch} (Mpa/ksi)	133/18.0	246/33.3	363/49.2
σ_{tip} (Mpa/ksi)	199/27.0	364/49.3	533/72.2
γ_{adhesive}	0.0276	0.0723	0.1361
P_1 (mm/inch)	157/6.18	157/6.18	157/6.18

shear strain, γ , at ultimate (0.1523 instead of 0.1338). The patch length is 26 times the load transfer length, which should still provide sufficient resistance to creep of the adhesive. Also, the loads carried at the frame location are significantly lower than the skin loads in the middle of the bay, see the DTA section with the determination of $\beta = 0.5$. At ultimate load, the adhesive is allowed to go to the maximum plastic-strain, γ_p ; for the adhesive used (3M's AF163) this is typically a lot higher than 1.5 times γ_e .

For FS 1784 the results are given in Table 31.7. All guidelines except patch length are met. Adhesive shear strain at ultimate is only slightly over the recommended value. The patch length used is, again, about 26 times the LTL, which should be sufficient to prevent creep due to the β of 0.5.

Fit patch to structure

CalcuRep can be helpful to determine an optimized patch configuration, but the program cannot design the actual patch shape to fit the existing structure. CalcuRep will give the proper patch dimensions but the final outline largely depends on location of splices, doublers, stringers and frame configurations, and the existing rivet pattern.

Figure 31.3 shows the rivet pattern, substructure, and the patch location on the aircraft for FS 1784. In the critical areas at the patch tips, the patch covers all the rivets. By covering the rivet a double stress concentration due to the patch tip and the rivet is prevented. At the time when these patches were installed, there was only experience with elliptically shaped patches. A better fit to the structure can be achieved using a square patch with rounded corners. Recently-gained experience and current research would have resulted in using such a patch for this repair.

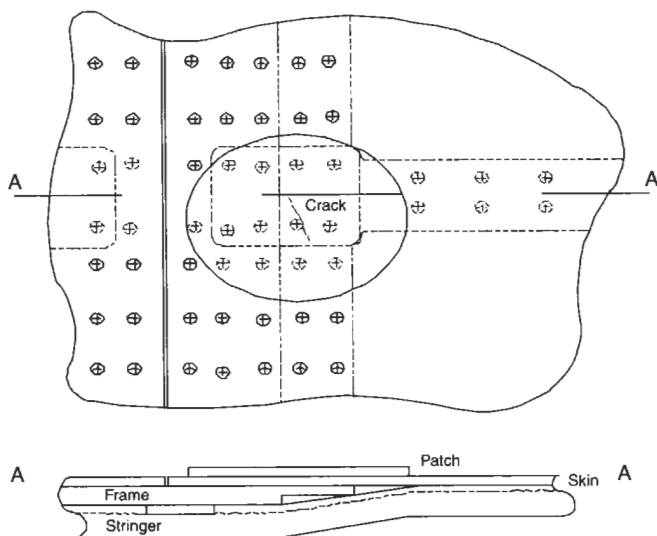


Fig. 31.3. Patch at FS 1784.

Patch manufacturing

Once CalcuRep gives the rough dimensions of the patch, a paper tracing of the actual crack and the rivets can be used to fine-tune the final patch dimensions. A sheet of Glare bigger than the patch is cold rolled to match the curvature of the fuselage. The outline of the ellipse is drawn on the Glare sheet and a shear cutter is used to cut it to the rough dimensions. A belt sander is used to trim the patch to the final outside dimensions.

In order to decrease secondary bending at the patch tips, the patch is tapered. For the taper a minimum of 0.2–0.3 mm (0.008–0.012 inch) is used, which is the thickness of the last aluminum layer, to prevent a knife-edge effect. The taper angle is normally 1/10 up to 1/20. Drawing a smaller ellipse on the patch, and filing the material from that line up to the last aluminum layer of the patch defines the taper angle. Due to the nature of applying the taper this way, Glare patches have a “wedding cake” taper. In order to handle the patch while making the taper, the patch is fastened to a wooden template with double-sided tape.

Big scratches in the taper are removed with a fine file and waterproof sandpaper. After degreasing the pre-treated patch surface (PAA & BR-127 primer) with a solvent, like MEK or Acetone, the patch is ready to be bonded to the fuselage skin. The patch can be prepared anytime during or before the process.

Very few bonding procedures can give the desired durability needed for structural repairs. Achieving this under field conditions is even more difficult. The procedure used for this repair is the grit blast silane procedure (GBS) developed by the US Air Force at the AFRL/ML division [5], AFRL also installed the patches

on the aircraft. The adhesive used was AF163-2M with a cure cycle of 125 °C/250 °F.

31.5. FEM model of the patched crack

The patched configuration was modeled in Franc2D-L. The resulting stresses with the patch bonded to the structure are shown in Figure 31.4.

The effect of the repair on the crack is drastic, compared to the unpatched situation. A summary of the results obtained with Franc2D-L is given in Table 31.8.

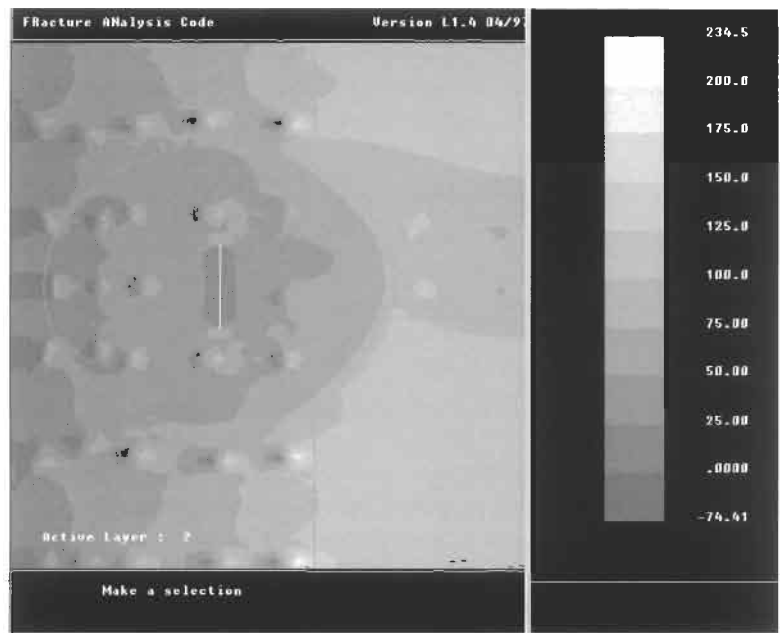


Fig. 31.4. Patched crack at FS 1784 (scale in MPa, MPa/7 gives an estimate of ksi, 200 MPa is roughly 28 ksi).

Table 31.8
Results from Franc2D-L calculations.

Applied long stress (Mpa/ksi)	K_{repaired}	σ_{patch} (Mpa/ksi)	σ_{tip} (Mpa/ksi)	γ_{adhesive}
80/10.8	2.49/1.71	46/6.2	75/10.2	0.018
120/12.4	3.67/2.51	67/9.1	110/14.9	0.024
145/19.6	4.47/3.06	82/11.1	137/18.6	0.030
160/21.7	4.84/3.32	89/12.1	145/19.6	0.033
227/30.8	6.86/4.70	126/17.1	202/27.4	0.045

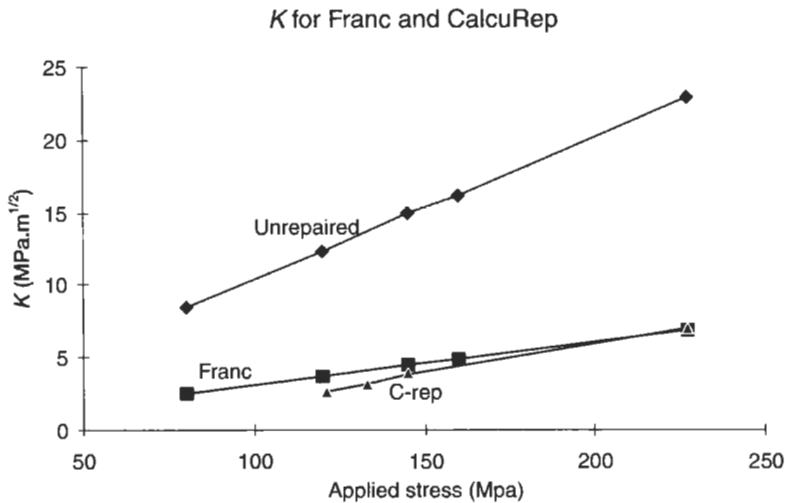


Fig. 31.5. K_{repaired} for Franc and CalcuRep models.

Both analysis methods have weaknesses. CalcuRep does not model the substructure properly and therefore overestimates the applied stress in the repaired area. Franc does not model the thermal issues. A comparison of the results for K_{repaired} between the two methods is given in Figure 31.5.

Testing

In order to verify the predictions of the CalcuRep code, several fatigue specimens were built and tested. Coupon tests were performed on boron and Glare patched panels. The configuration of the panels used was:

1. Panel width, length 152, 400 mm/6, 15.7 inch
2. Initial fatigue crack length 25 mm/1 inch
3. Uni-axial loading, $R=0.05$ (Glare) and $R=0.1$ (Boron), maximum stress 120 Mpa/16.3 ksi
4. Adhesive AF163-2, 0.13 mm/0.005 inch thick

Patch size optimized per material

Figure 31.6 shows the results for an unpatched panel and both Glare and Boron patched panels. Both patch materials extend the fatigue life of the panels considerably. The Glare repair results in a lower K_{repaired} . The now lower $\Delta K_{\text{repaired}}$ in more load cycles for the crack to reinitiate.

The boron repair results in a relatively higher K_{repaired} than the Glare repair, and it takes fewer cycles for the crack to reinitiate. These tests were all run at room temperature. At lower temperatures these differences might even be more

Patch performance of low and moderate CTE patches on 2024 T3

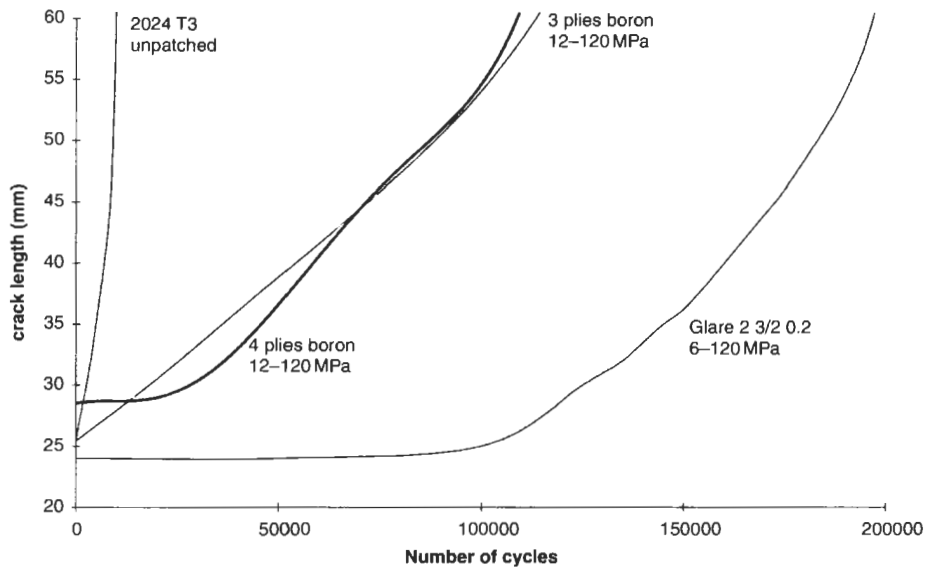


Fig. 31.6. Performance of bonded repairs using GLARE[®] and boron patches.

pronounced due to the increasing thermal stresses. On the other hand, the repairs were applied to unstiffened panels. An actual structure (with substructure and only partly heated) will have a lower CTE than an unrestrained panel, and therefore the lower CTE of the boron will better match the effective CTE of the actual structure [2].

The next test was to evaluate the performance of the repairs on the actual fuselage skin, 7079-T6. Since this material is not available, some scrapped panels from a C-5A were used to prepare the specimens. The panels had multiple rivet holes from installation on the aircraft. All the holes outside the patched area were filled with rivets. The configuration of the specimens was similar to the earlier tested specimens. A pre-crack was cut and fatigued up to the initial starter length after which the patches were bonded to the panels. The results of these fatigue tests are given in Figure 31.7.

The first noticeable (and expected) difference between 2024-T3 and 7079-T6, is the higher unrepaired crack-growth rate in 7079 at the same fatigue level. This indicates that an effective bonded repair is necessary. The first patched panel gave no fatigue crack growth after the bonded repair was applied. The second panel gave an initial retardation period, after which the crack slowly grew until it terminated in one of the existing rivet holes under the patch.

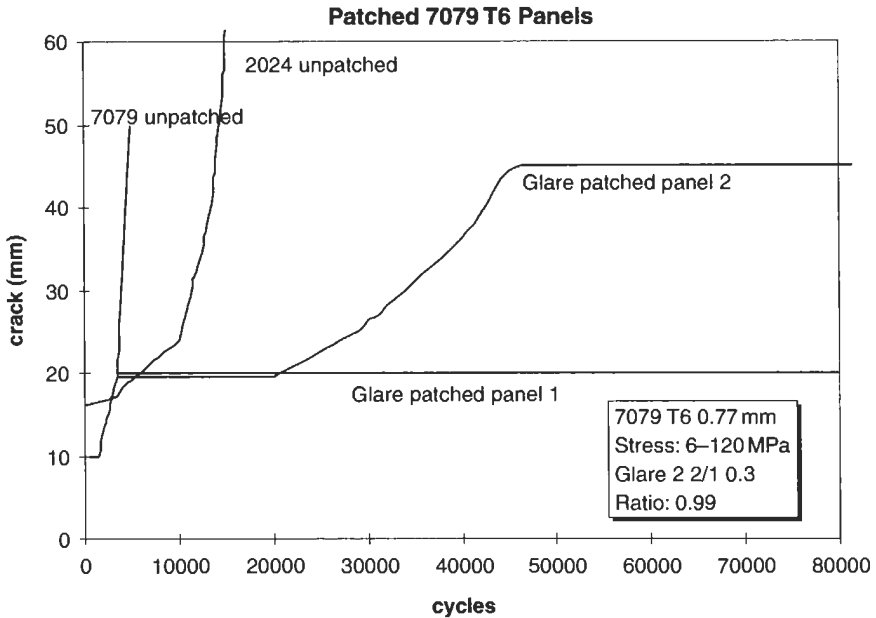


Fig. 31.7. GLARE[®] patched 7079-T6.

Spectrum testing

Obtaining the loads for this section of the aircraft was done using the input for the Lockheed crack growth prediction code. However, the problem is that these loads are used in a statistical prediction code and therefore consist of non-integer load cycles. In order to perform a fatigue test, these non-integer loads were transformed into integer values. A computer program partially based on the procedure used in the Lockheed program regarding plastic zone size/retardation (bucket filling) was used for this task [6]. Partial cycles were stored in a so-called “bucket”, until the bucket would fill up to a pre-set integer value (normally 1 or 2). At that point, the load pair was placed in the spectrum.

In order to reduce the retardation effect, the specimens were pre-cracked to a crack length of 25 mm/1 inch, at a lower cyclic stress level (maximum stress-to minimum stress: 60–6 Mpa (8.1–0.81 ksi)). If a higher pre-crack stress level is used, the relatively large plastic zone from the unpatched crack causes retardation (and scatter in the results) after the patch is applied. Aluminum 7075-T6 alclad sheets (1 mm/0.04 inch) were used for the specimens. The patch was GLARE[®] 3/2–0.2 with a total thickness of 1.1 mm/0.043 inch.

The results from patched specimens under spectrum loading are given in Figure 31.8. The data shows that the bonded repair can easily provide the life extension needed for the C-5A.

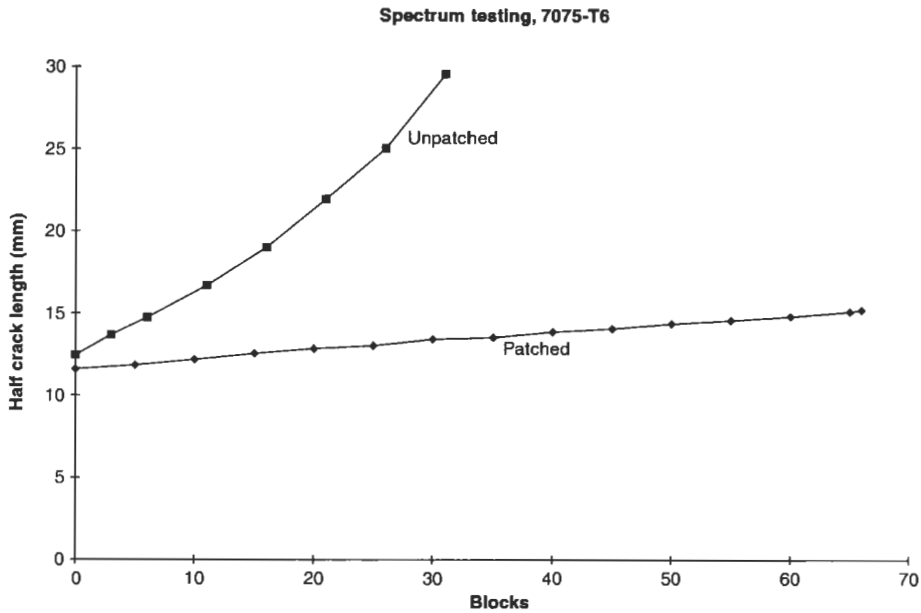


Fig. 31.8. Crack growth under spectrum loading.

31.6. Conclusions

Two bonded repairs were applied as a prototype repair on a C-5A. Since October 1995 the patches have been in service and are stopping further crack growth in the skin of the aircraft. The repairs are technically a viable solution for the crown-cracking problem of the C-5A. With respect to the remaining service-life of the C-5A, the high initial cost of bonded repairs vs. the lower cost of mechanically fastened repairs, might prohibit a more durable (bonded) repair option.

This example described two different analysis methods: (1) CalcuRep addresses the thermal issues and helps to optimize and size the repair, while (2) the finite element program Franc2D-L can model the substructure as well as the skin and the repair as a verification of the CalcuRep results. The finite element model was used to predict K in the unrepaired case and verify the load carrying capabilities of the cracked structure before a repair was applied. The analysis methods were verified using fatigue experiments. The performance of the bonded repairs was tested under C-5A spectrum loading, and easily extended the life of the cracked structure one full lifetime.

References

1. Fredell, R., Guijt, C., Conley, D., *et al.* (1996). Design development of a bonded fuselage repair for the C-5A. *Proc. of the 1995 USAF Structural Integrity Program Conf.*, WL-TR-96-4094, August.
2. See Chapter 14 on: Glare Patching Efficiency Studies.
3. 2D Finite Element Program available from Kansas State University.
4. Gallagher, J. Damage Tolerant Design Handbook, MCIC-HB-01R.
5. Kuhbänder, R.J. and Mazza, J.J. (1993). Understanding the Australian Silane Surface Treatment. *Proc. 38th Int. SAMPE Symp. and Exhibition*, Anaheim, California, May.
6. Verhoeven, S., Guijt, C., Collas, E., *et al.* (1997). Qualification of a Bonded Repair to C-5A Fuselage Cracking under Spectrum Fatigue Loading. *Proc. of the USAF Aircraft Structural Integrity Program Conf.*, San Antonio TX.

Chapter 32

CASE HISTORY: F-16 FUEL VENT-HOLE REPAIRS

C. GUIJT¹ and J. MAZZA²

¹*Department of Engineering Mechanics, Center for Aircraft Structural Life Extension, US Air Force Academy*

²*Materials and Manufacturing Directorate, U.S. Air Force Research Laboratory (AFRL/MLSA)*

32.1. Introduction

An adhesively bonded boron/epoxy repair has been designed and installed to repair fatigue cracks in the vicinity of the F-16 fuel vent hole [1,2]. This repair is compared to a mechanically fastened alternative. While both repairs succeed in slowing crack growth and extending the aircraft life, the bonded repair has significant advantages as outlined below.

Several F-16 aircraft developed cracks, between 2500 and 3500 flight hours, forward and aft of the fuel vent hole in the lower left wing skin, which is about 5 mm (0.2 in) thick. These cracks (Figure 32.1) occurred in the first 144 aircraft prior to a modification requiring the use of interference fit fasteners in the fuel vent hole area.

32.2. Damage tolerance analysis

The first repair option considered was a traditional metal repair. A nonlinear finite element (NASTRAN) static analysis, modeling an aluminum doubler repair, was used to determine the stress-intensity factor at the crack tip. This information was needed for the damage tolerance analysis of the repair. For bonded repairs, this damage tolerance analysis has more restrictive guidelines as directed by the US Air Force's Aeronautical Systems Center, Engineering Directorate. According to the finite element analysis, the maximum stress reduction with the aluminum doubler installed was approximately 10%.

To perform a proper crack growth analysis, the correct β -factor representing the effect of the local geometry must be determined to calculate the stress intensity

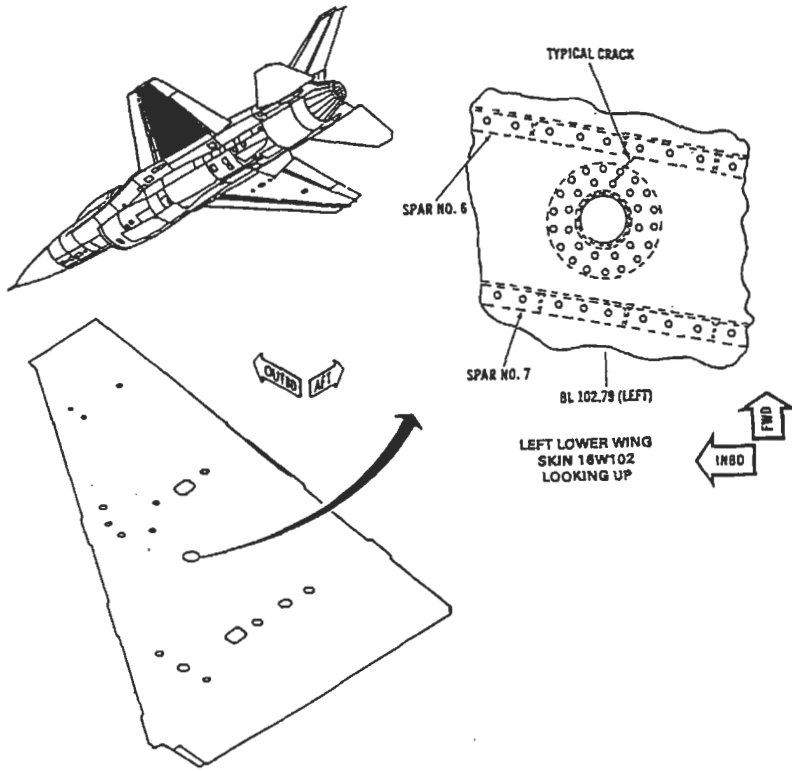


Fig. 32.1. Typical crack location.

factor at the crack tip.

$$K = \beta \cdot \sigma \sqrt{\pi \cdot a} ,$$

K Stress intensity at the crack tip

β Geometry factor depending on type of loading and the geometry of the part and shape of the crack

σ Applied gross or far field stress level

a Half crack length

Cracks 90 software was used to perform the crack growth analysis. In this program, several (standard) β -solutions were given, but none of them matched the situation around the fuel vent hole. NASTRAN was used to model the geometry and determine the proper β -factor. The stress intensity at a crack tip element was then calculated. With the applied stress and the crack length known, the β -factor could be calculated for several crack lengths (see figures 32.2 and 32.3). This was done for three situations:

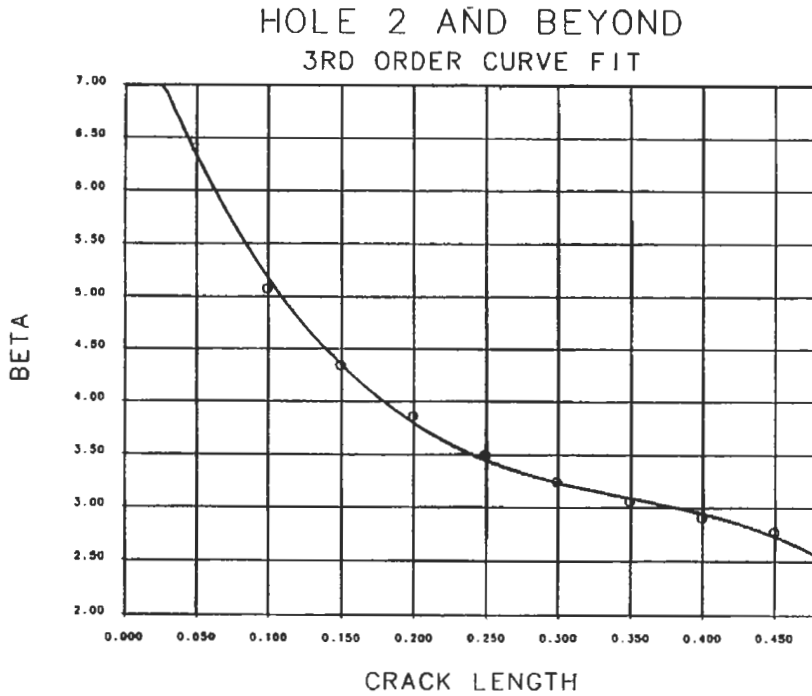


Fig. 32.2. β -factor for different crack lengths (inch) beyond the second row [2].

1. Crack growing from the first fastener row towards the cutout.
2. Crack between the first and second row of fasteners.
3. Crack beyond the second row of fasteners.

If the crack grew longer than approximately 13 mm (0.5 in) beyond the second row of fasteners, it became critical: the stress intensity became higher than the fracture toughness of the wing material, $K > K_C$. If cracks reach this length, the lower wing skin must be replaced. With the β -factors known, the crack growth analysis could be performed using this input in Cracks 90.

Without a repair installed, the cracks in this area require reinspection every 150 flight hours.

32.3. Repair options

In order to extend the life of these aircraft, a mechanically fastened aluminum repair was designed by Lockheed Martin (then General Dynamics). The intent was to design a repair that could be installed at the field level, if at all possible. It was also recommended that interference fit fasteners be installed since no cracks had

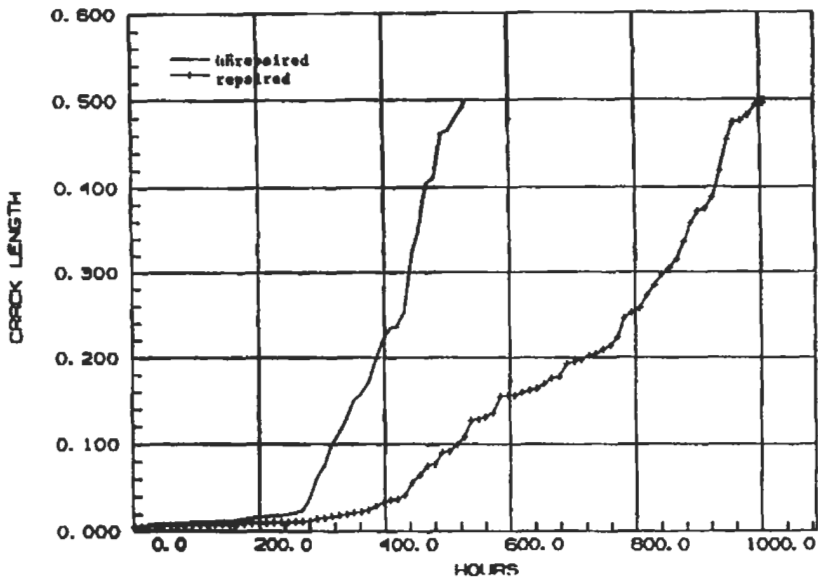


Fig. 32.3. Crack growth prediction in inches (Cracks 90) beyond second row, using calculated β -factors [2].

occurred in aircraft where interference fit fasteners were used. According to analysis, the external aluminum patch, in combination with an internal steel 17-4 PH 1100 ring doubler, would indeed extend the life, but not to the desired two lifetimes of the aircraft. It was also time consuming to install since the upper wing skin had to be removed, and an additional 24 fasteners installed around the fuel vent hole. All the fatigue-susceptible holes would be cold worked at this time. If cracks extended beyond the second row of fasteners, they had to be stop-drilled and cold worked.

32.3.1. Mechanically fastened aluminum patch

The preferred aluminum patch material was 7475-T7351, with 7075-T7351 as an alternative in case of availability problems. The thickness was 5 mm (0.20 in), tapered down to 2.5 mm (0.10 in) with a 45° final taper angle.

The analysis of the life extension of the repair could be improved if the following effects were considered:

1. Stop drilling and cold working the hole,
2. Cold working the fasteners around the vent hole before cracking occurred and installing interference fit fasteners, and
3. Stress reduction due to use of the internal steel doubler (the steel doubler was not used in the analysis since it cannot be installed during a field level repair).

These effects given above were not taken into account in the analysis due to practical reasons and modeling difficulties.

Some disadvantages associated with the mechanically fastened aluminum repair include:

1. Removal of the blind fasteners can result in debris in the wing, which can cause foreign object damage (FOD),
2. Removal of the fasteners can cause damage to the existing holes, which may require case-by-case engineering solutions,
3. The vent tube and other plumbing can be damaged in the process,
4. Improper sealing of the repair and the (additional) fasteners may cause fuel leaks,
5. A depot-level modification is preferred, since the upper wing skin can be removed,
6. Excessive cost, and
7. Excessive aircraft down time.

32.4. Design of the bonded repair

Because of the limited life extension obtained using the aluminum patch, a bonded boron/epoxy repair was evaluated and designed. The advantages for the bonded fuel vent hole repair are:

1. Lighter patch with lower external moldline profile,
2. More efficient load transfer capability,
3. No additional fastener holes, thus preventing new fatigue cracks or fuel leaks,
4. Easier to apply in less time (no need to remove upper wing skin),
5. Crack growth under the patch can easily be detected using eddy-current or ultrasonic NDI,
6. Field-level application,
7. Minimum impact on aircraft readiness, and
8. Much lower cost than mechanically fastened alternative.

Since the aluminum patch design was already tested, the boron/epoxy patch was designed to have the same stiffness (and minimally the same strength) as the original aluminum design. The final boron patch design was a square 18-ply (0.13 mm or 0.0052 in/ply) patch, [$\pm 45/0^\circ$]_s, with a symmetrical stepped-down taper (see Figure 32.4.1).

IDEAS [2] software was used to create a finite element model of both the wing and the patch. In order to allow the fuel vent hole to be operative after installation of the patch, a hole was cut in the patch. The hole was cut after precuring the patch, but before installation on the wing. After installation, the patch covers some fasteners around the fuel vent hole. The adhesive was modeled using linear spring elements. The loads in the spring elements were analyzed to try to assess the durability (in terms of shear strain and creep) of the adhesive.

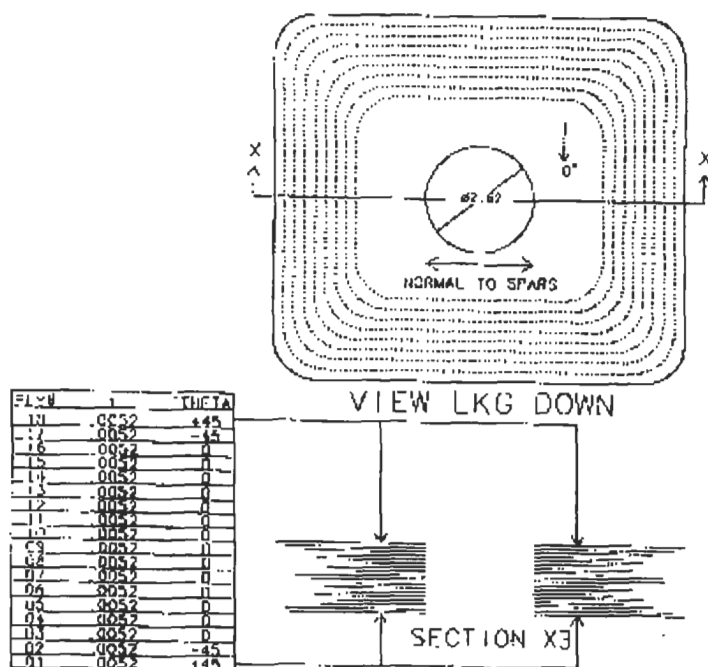


Fig. 32.4. Boron patch design [2].

32.4.1. Operating temperatures

Both the maximum and the cumulative temperature exposure of the patch and the adhesive were investigated. The major components affecting the heat transfer in the region are:

1. Lower wing skin: 5 mm (0.2 in) thick,
2. Spars: 20 cm (7.8 in) spacing, and
3. Support doubler for the fuel vent tube: attached to the lower wing skin.

The patch, with dimensions approximately $216 \times 241 \times 2.4$ mm ($8.5 \times 9.5 \times 0.094$ in), drops off close to the wing spars and covers the doubler with the fuel vent tube welded to it. A SINDA [2] thermal transient finite element model was used to predict the heat transfer in this region.

32.4.2. Maximum operating temperature

Two maximum-endurance missions were used to predict the maximum operating temperatures:

1. A mach 0.96 (30 min) and a mach 1.12 (5 min) sea-level hot day mission (MIL-STD 210-A hot day), resulted in maximum temperatures of $T_{\max} = 90.5^{\circ}\text{C}$ (195°F) and $T_{\max} = 100.5^{\circ}\text{C}$ (213°F) and

2. A supersonic mission with a maximum mach 2.05 at 36000 ft resulted in $T_{\max} = 102^{\circ}\text{C}$ (216°F).

These missions result in the maximum temperature expected. The output of this analysis is a time vs. bondline temperature profile. In this analysis, the fuel tanks were assumed to be empty.

32.4.3. Cumulative temperatures

The cumulative temperature of the bondline (total time above a temperature) was predicted over the 8000 h service life by using a computer procedure named "life time temperature spectrum (LTTS)." This program predicts the adiabatic wall/skin temperatures depending on the mission mix and conditions during the flight. Two types of conditions were analyzed: one with a normal mix of hot, standard and cold conditions, and one with only hot conditions. The output of the program is a table of specified skin temperature exceedances over the life of the aircraft (see Figure 32.5). The bondline temperature was assumed to be equal to the skin temperature.

The result of the analysis was that the bondline temperature was over 82°C (180°F) for 17.5 h per 8000 h during the lifetime of the aircraft in a normal mix of conditions. With only hot conditions (warm weather), the result was 54.7 h above 82°C . These results led to the selection adhesives that had slightly higher service temperatures than traditional 121°C (250°F)-curing adhesives. Two adhesives from Cytec, FM 87-1 and FM 300-2, were considered acceptable for the repair.

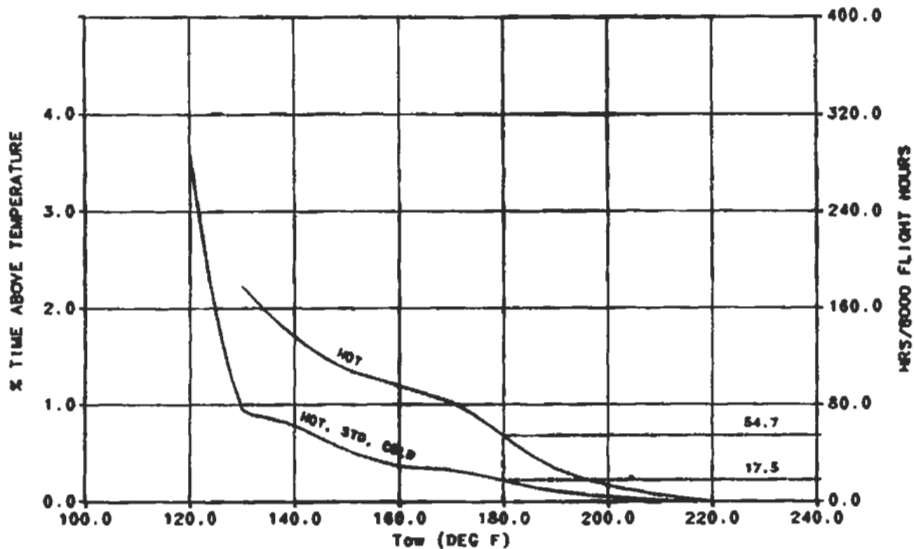


Fig. 32.5. Total flight hours above indicated temperature [2].

32.5. Testing

32.5.1. Fatigue analysis of the aluminum doubler

The spectrum used in the analysis was the standard Block 15 General Dynamics Fort Worth spectrum. The spectrum had a maximum stress of 211 MPa (30.67 ksi) and represented 500 flight hours. In order to predict the effect of the patch, two cases of the spectrum were run: one with the given stresses, and one at 90% of the spectrum stresses (to simulate the 10% far field stress reduction due to the repair). A diagram of the specimen used is given in Figure 32.6. Note that the stress reduction simulating the applied patch will yield conservative results. When the crack starts to grow, the patch will transfer more load due to the higher compliance of the cracked structure. An actually installed patch would probably result in a more constant K_{repaired} , but the assumed 10% stress reduction results in an increasing K with an increasing crack length, and therefore results in conservative (shorter) life predictions.

Since some aircraft had cracks extending beyond the second row of fasteners, this situation was modeled as well. In the unrepaired case, Cracks 90 [1] predicted a life of 3384 flight hours for crack initiation, which was close to the observed amount of hours (2500–3500). The same calculations were repeated at the 10% lower stress level. Even the most conservative result, in which the patch was applied before cracks were present in the area, predicted an increase in service life of only 2316 h. The total life was now 3384 (the current amount of hours) + 2316 (the maximum life extension for preemptive patching) = 5700 h. Although the repair resulted in an increase in service life, the design life goal of 8000 h was not met. Note that if the actual patched configuration would have been tested vs. the 10% stress reduction, this repair might have been sufficient.

32.6. Bonded repairs

Two component-size test articles were produced, and boron/epoxy patches were applied to the precracked fuel vent hole. The specimen size was limited to roughly the width of the patch, even though it is preferred to use specimens wider than the patch to allow for load attraction into the patched area. The spectrum used for both the precracking and the testing of the patched fuel vent hole was a normal severity usage spectrum for the Block 30 fleet. The spectrum represented 500 flight hours and 38257 load points ranging from 100% tension, down to –32.4% compression. The precracking was stopped when a crack had grown from the first row of fasteners to the fuel vent hole, and then from the first row of fasteners half way towards the second row of fasteners around the fuel vent hole. At this point the boron/epoxy patches were applied.

The first specimen was precracked for 959 flight hours before the patch was applied. After patch installation, the crack started to grow after approximately 1000 h of additional testing. After removal of the patch, it was found that the orientation of the patch was 90° off from the intended orientation. This highlighted the fact that, especially when using a symmetric patch, it is very important to

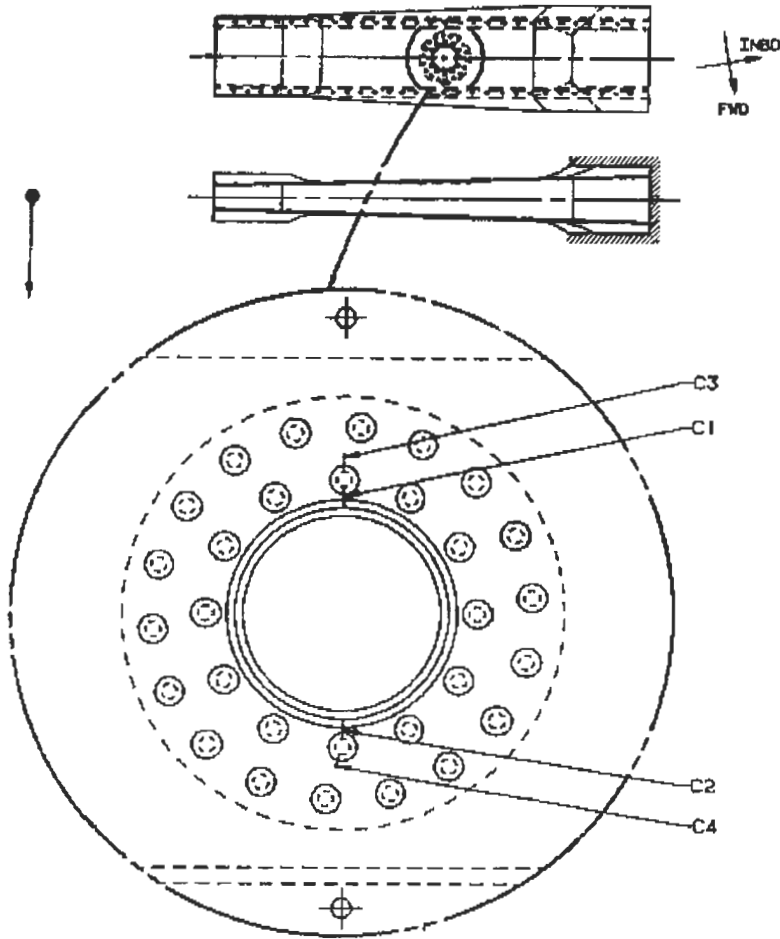


Fig. 32.6. Crack locations and specimen configurations [2].

indicate the fiber orientation or the patch orientation (fwd-aft, inbrd-outbrd, *etc.*) on the patch, to prevent confusion during installation.

A new patch was properly applied, and no further crack growth occurred up to 7230 flight hours when the specimen failed in the load introduction area. This specimen was later tested statically (after regripping) where it failed at a uniaxial tensile load of 458 kN (102960 lbs). The crack path was exactly in line with the fatigue crack, perpendicular to the spars. The patch failed at the interface between the $\pm 45^\circ$ plies closest to the skin and the first 90° layer. The two $\pm 45^\circ$ plies remained bonded to the skin.

The second specimen was precracked for 2150 h before the patch was applied. No indication of debonding or crack growth occurred up to 11800 flight hours when the panel failed in the load introduction area.

Both test articles, with the patches applied, failed in the grip area away from the test area, at 7230 and 11800 flight hours without additional crack growth after patch installation. Neither test reached the two lifetimes of the aircraft needed to prove the damage-tolerant character of the repair. However, since no crack growth occurred in any of the specimens, it was decided that these patches would extend the fatigue life of the fuel vent hole area sufficiently. However, it must be noted that both panels were tested dry at room temperature (about 24 °C).

During the tests, the crack was monitored using nondestructive inspection (NDI) techniques. Eddy-current and shear wave ultrasonic inspections were used to monitor crack growth. Due to the fasteners around the fuel vent hole, eddy-current was insensitive in a range of about 6 mm (0.25 in) around the fasteners, therefore the shear wave technique was selected to monitor crack growth. No crack growth was detected. Ultrasonic inspections (pulse-echo and contact) revealed some minor disbond growth around the crack, but the debonding did not affect crack growth.

32.6.1. Repair installation procedures

Patch installation procedures were developed by the Air Force Research Laboratory (AFRL/MLSE). The all-important surface preparation step was conducted using a grit-blast/silane (GBS) process recently developed by MLSE and based on a similar procedure originally developed by the Australian Aeronautical and Maritime Research Laboratory [3,4]. The process included application of Cytec BR 127 adhesive primer, which was precured prior to patch installation. The silane drying and primer cure steps were conducted using infrared heat lamps, having several bulbs that were independently controlled. Temperatures in the repair area were monitored using a minimum of eight thermocouples, with feedback used to adjust heat lamp power settings. The F-16 vent hole repair represented the first on-aircraft use of the MLSE GBS process.

Thermal surveys were conducted on F-16 wings in order to determine the best approach for heating the repair area to the required temperatures. It was determined that a large (760 × 760 mm or 30 × 30 in), electrical resistance heat blanket positioned above the repair area on the top wing skin could greatly minimize the heat sink effect of the wing. This was useful for silane drying and primer cure as well as adhesive cure. In fact, the upper blanket could be used to directly heat the repair area (lower wing skin) to roughly 70 °C (160 °F) while maintaining a temperature of about 121 °C on the upper skin immediately under the heat blanket. With the upper blanket in place and fiberglass insulation covering a second heat blanket installed directly over the repair on the lower surface, temperatures in the repair area could be maintained in an acceptable 110–127 °C (230–260 °F) range. Heat blankets were held in place under vacuum bags, and vacuum pressure was applied to hold the precured patch to the aircraft during adhesive cure. Temperatures in the repair were monitored with a minimum of eight thermocouples. Hot bonder units were used to power the heat blankets control to the highest-temperature thermocouple. Adhesive cure time was based on the lowest temperature in the repair area, using a range of time-temperature cure conditions

available for the adhesives. The boron/epoxy patch must also be surface treated to obtain acceptable bond strength. Fortunately, for composites based on thermosetting matrices, mechanical activation is all that is required. This was achieved by abrading or tearing off a resin-rich nylon peel ply cured onto the bond surface of the patch and then lightly grit-blasting the surface with 50 micron alumina. During patch application, the fuel vent hole itself was filled with a silicon rubber plug sandwiched between two metal plates connected through the rubber with a fastener. Tightening the fastener expands the plug to fill the vent hole and creates a vacuum-tight seal. Fasteners in the repair area, to be covered by the patch, were checked for leaks. Leaking fasteners were replaced prior to patch bonding. In some cases when "leaks" only represent fuel trapped around the fastener without a direct path into fuel puddles in the wing, infrared lamps were used to remove the fuel prior to surface preparation for bonding. There was no attempt made to allow for access to the fasteners under the patch. One side benefit of permanently covering the fasteners in the fuel vent area was the elimination of these fasteners as sources of potential fuel leaks.

Since the first installation in 1993, 20 bonded vent hole repair patches have been applied to F-16s in the United States, the Netherlands and Denmark. The first repair utilized FM 87-1 adhesive, while all remaining repairs have been installed with FM 300-2M (0.06 weight) adhesive. A new grit-blast/sol-gel surface preparation (refer to Chapter 3) was used in lieu of GBS for the last five repairs. This procedure is similar to GBS but uses a more reactive chemical that does not require the GBS elevated-temperature drying step. This process also includes the use of cocured Cytec BR 6747-1 waterborne adhesive primer rather than BR 127. Significant time savings are achieved, and heat lamps are no longer necessary, with the elimination of the silane and primer heating steps.

32.7. Conclusions

The F-16 fuel vent hole bonded repairs are considered highly successful since no crack growth or disbonds have been detected since the patches were applied in 1993. In addition to their effectiveness in preventing crack growth, the patches are much easier and therefore less costly to install and inspect and much less damaging to the parent structure than mechanically fastened alternates.

References

1. Phelps, N. (1997). Composite Patch for Fuel Vent Hole, Status, MEMO TO USAFA, Hill AFB.
2. Palmer, B. (1991). Fuel Vent Hole Cracking, GD OOALC, BMP0007:OG-AS:91-03:705, F42600-90-C-0007-F-16.
3. Mazza, J.J., Avram, J.B., Kuhbander, R.J., Grit Blast Silane (GBS) Aluminum Surface Preparation for Structural Adhesive Bonding, WL-TR-94-4111 (Interim report under US Air Force contracts F33615-89-C-5643 and F33615-95-D-5617).
4. Kuhbander, R.J. and Mazza J.J. (1993). Proc 38th Int. SAMPLE Symp., May 10-13, p. 1225.

Chapter 33

REINFORCEMENT OF THE F/A-18 INBOARD AILERON HINGE

R. CHESTER

Defence Science and Technology Organisation, Air Vehicles Division, Fishermans Bend, Victoria 3207, Australia

33.1. Introduction

F/A-18 inboard aileron hinges are susceptible to fatigue cracking in the aft strut fillet due to higher than originally expected flight loads. The hinge and the location of cracking are shown in Figure 33.1. The cracks are normally detected at less than half the anticipated life of the hinge and there is currently no repair possible for cracked hinges. The only currently accepted solution is to replace the cracked hinge. This procedure is difficult for some operators of this aircraft as the entire aileron has to be sent to the US for the hinge replacement to be undertaken. Because of the lengthy delays and costs involved for these replacements, the present investigation was undertaken to see if it would be possible to repair some of the cracked hinges without removing them from the aileron.

There are several possible ways to address the problem of fatigue cracking in these hinges. The first approach is to reduce the level of fatigue strain in uncracked hinges so as to delay the onset of crack initiation. In this case, depending on the level of strain reduction, it may be possible to extend the life of the current hinges out to the life of type of the aircraft and therefore avoid any further need to replace or repair hinges. For hinges that are already cracked a second approach is necessary. The fatigue cracks would firstly need to be removed and this could be done either without particular concern for the resulting shape of the strut or alternatively by calculating a precise new geometry for the strut which minimises the tensile stresses which cause cracking. This latter approach is known as Structural Optimisation. After the crack is removed, it may then be necessary to reinforce the strut to replace the stiffness that is lost by the removal of material. Reduction of fatigue strain and reinforcement to replace stiffness lost due to

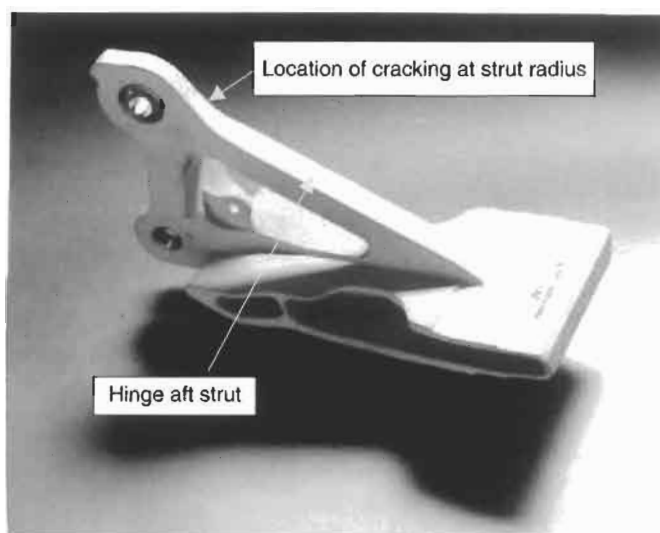


Fig. 33.1. Photograph of the aileron, showing the hinge aft strut and location of fatigue cracking.

reworking, are both possible through the use of advanced composite materials and adhesive bonding.

33.2. Load cases

A significant amount of work has been undertaken by the aircraft manufacturer (Boeing) to determine the reason for the fatigue cracking. Part of this work was to establish the magnitude and nature of the critical loads for the aileron hinge [1]. Under certain flight conditions, the aerodynamic pressure on the aileron acts vertically upwards and this type of pressure distribution causes the aft strut of the hinge to be subjected to a tensile force. This force combined with the stress concentration caused by the radius in the aft strut fillet region, generates high stresses at the radius which is the location of the cracking. The critical load case for this tensile stress condition is known as WO 39. When the aileron is extended upwards during flight, the aerodynamic force acts to push the aileron back to the level condition and in this case, a compressive force develops in the aft strut. The critical load case for this compressive stress condition is known as WO 42. The absolute magnitude of this compressive stress is slightly higher than the tensile WO 39 stress, however, in service this is not a problem as it is only the tensile stress that causes fatigue cracking. However, when considering a bonded composite reinforcement, it is necessary to address both load cases as the shear stress that will be developed in the adhesive layer will be equally damaging for both tensile and compressive stresses in the strut. The shear stress in the adhesive layer will simply be reversed in sign. Two stress magnitudes are referred to in this section for these

load cases. Design limit load (DLL) is considered to be the maximum stress the aircraft is likely to see during its life, while design ultimate load (DUL) is 1.5 times DLL.

These two load cases were used in both the finite element (FE) design work as well as the static test program. The work described in reference [1] confirms that these two load cases are greater than the most severe loads that the aileron is exposed to in flight and therefore it is conservative to use them for this work.

33.3. Design and stress analysis

A numerical stress analysis was undertaken to design an appropriate reinforcement for the aft strut of the aileron hinge. The approach followed is to first remove existing cracks with a suitable precise rework shape before reinforcement. This precise rework shape is determined using structural optimisation procedures, to minimise the peak stresses for an un-reinforced hinge. Since in practice various crack lengths will exist before possible enhancement, it is proposed here to consider the limiting case where the rework depth is 2 mm at the crack location. Secondly, this optimal shape for the no reinforcement case is further slightly adjusted to minimise peak adhesive stresses when a reinforcement is bonded on. Full details of the procedures used in this work are given in [2].

For all analyses isotropic material behaviour under ambient conditions was assumed for the aluminium hinge, the steel bush, and the FM73 adhesive layer. Conversely for the elements comprising the boron/epoxy reinforcement the material was taken as orthotropic. The material properties were as follows; (i) for the aluminium hinge the Young's modulus, E , was taken as 70.38 GPa, Poisson's ratio, ν , was taken as 0.33; (ii) for the steel bush in the lower lug, Young's modulus was taken as $E = 213.90$ GPa, and Poisson's ratio was $\nu = 0.30$; (iii) for FM73 adhesive, $E = 1.43$ GPa, $\nu = 0.35$; (iv) for the boron, $E_{11} = 208.95$ GPa, $E_{22} = E_{33} = 19.18$ GPa, $\nu_{12} = 0.21$, $\nu_{23} = 0.3$ and $\nu_{31} = 0.02$ where 1 refers to the direction of the fibres and 2 and 3 are the transverse fibre directions. The basic mesh used is shown in Figure 33.2(a).

Rework optimisation was achieved using a design sensitivity optimisation technique available in the MSC/NASTRAN code. This technique involves changing the position of nodes defining a boundary shape based on the computation of the rates of change of nodal stresses with respect to changes in nodal positions. This approach has been successfully developed and implemented in prior DSTO work, for the purpose of minimising peak stress at reworks for 2D idealisations [3,4]. The method is also discussed in Chapter 10 of this book.

Firstly the shape of the hinge was optimised for the case where no subsequent reinforcement would be required (referred to as the "O" profile). The resultant finite element mesh shape obtained after seven iterations of the rework optimisation is shown in Figure 33.2(b). The shape obtained is compared to the initial boundary in Figure 33.3(a), while the corresponding stresses are given in Figure 33.3(b). It can be seen that the stresses for the rework have been rendered

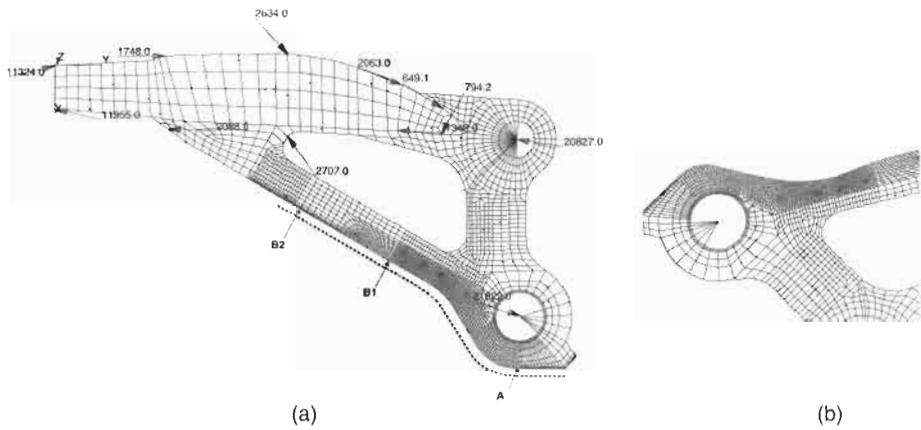


Fig. 33.2. Finite element mesh discretisation for (a) the nominal unworked hinge analysis, and (b) 2 mm depth rework shape after completion of optimisation procedure. In (a) the load vectors shown are for the WO 39 load case and the dotted line represents the patch location. In (b) the diagram has been rotated with respect to Fig. 33.2(a) so as to be consistent with the orientation of Fig. 33.3(a).

constant in the critical region, and are essentially the same magnitude as those for the nominal geometry, even though 2 mm of material depth has been removed. If a typical non-optimal rework shape had been used instead, the peak strut stresses could be expected to be about 20% higher.

Secondly the rework profile for a hinge that will be subsequently reinforced, was further developed to meet the needs of minimal peel and shear stress in the adhesive, in addition to minimising the peak stress in the strut (referred to as the “OSR” profile). If a reinforcement is applied directly to the rework as described previously, there is a local peak stress in the adhesive, at the location near $x = 40$ mm (the peak is due to the local change in curvature of the optimal profile shape at $x = 40$ mm) which would be greater than the adhesive yield stress, at DLL.

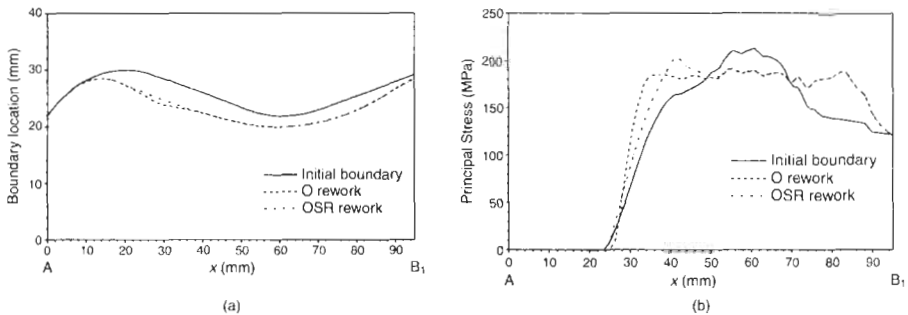


Fig. 33.3. (a) The profiles of the 2 mm (O) and (OSR) reworks are compared with the unworked hinge; (b) the corresponding stresses along the strut edge are shown for the unworked and 0.2 mm (O), (OSR) and (OSR) reworks and the unworked hinge. A and B₁, are shown on Fig. 33.2(a), indicating the range of these plots.

Thus, in order to decrease the adhesive stresses, this slight curvature discontinuity in the O rework profile (near $x=40$ mm) is manually smoothed/removed, which then resolves this problem regarding this adhesive stress peak. Of course as expected, the trade off due to this profile change is a 9% increase in the strut stresses if the patch were to be removed. This effect is clearly shown in Figure 33.3(b) by comparing strut stresses for the “O” and “OSR” profiles.

In the design of a typical bonded reinforcement to a component, there are two particular regions of concern for the adhesive layer. These are respectively; (i) near the end of the doubler where shear stresses can be very high, and (ii) locations under the doubler where it is desired to reduce the stress concentration in the repaired component; typically shear and/or peel stresses are high here. Since the bonded reinforcement functions by transferring load from the strut to the doubler, the doubler effectiveness increases with increasing numbers of plies, while simultaneously the adhesive stresses at the two key locations also increase. Hence a suitable final reinforcement design will be a compromise between these two requirements, ie adequate reinforcement effectiveness for reasonable adhesive stress magnitudes. Details of the design process for this reinforcement are given in reference [7]. The beneficial effect of the reinforcement is demonstrated in Figure 33.4 which shows the principal stress along the aluminium edge for both the un-reinforced and reinforced cases. It can be seen that there is a predicted 20% reduction in stress at the crack location.

An important aspect of this reinforcement is the presence of through-thickness or peel stresses in the adhesive as well as the usual shear stresses. Peel stresses can arise in a bonded joint for a number of reasons and good design practice is to minimise them as adhesives do not perform well in through-thickness tension. In this case, they arise from the curvature in the joint and it is not possible to design them out altogether. It should be noted that the magnitude of the peel stresses is influenced

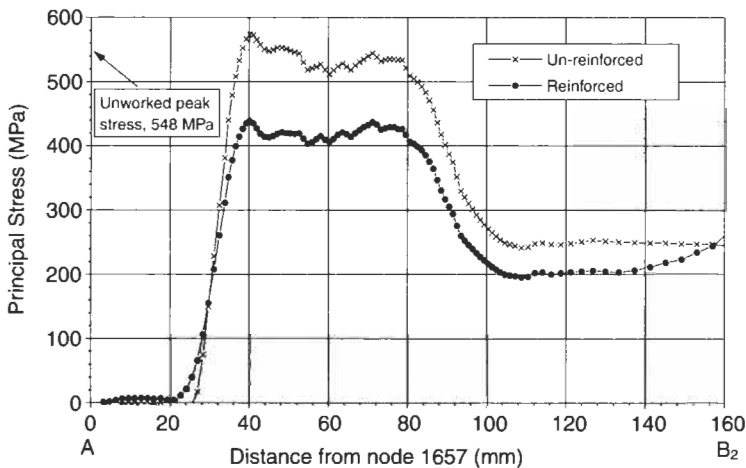


Fig. 33.4. FE prediction of principal stress along the strut edge for the OSR 2 mm rework geometry for the WO 39 load case. A and B₂ are the points shown in Fig. 33.2(a).

by various aspects of the design, such as the thickness of the composite reinforcement and the exact profile of the surface, and where possible the level of peel stress has been minimised. Other work at DSTO has recognised the presence of peel stresses and sought to establish an indication of the allowable level of peel stress for a structural film adhesive [5]. From this work a preliminary figure of 35 MPa has been proposed for FM 73 adhesive under constrained tension [6]. Figure 33.5 shows the distribution of both shear and peel stresses for the adhesive along the strut radius at the DUL WO 39 condition. The shear stress is seen to peak at $x = 30$ mm and the magnitude of the stress is high. It is important to note that the peaks in the shear and peel stress distributions do not coincide. The issue of fatigue durability is more significant in situations where these stresses are both high at the same location (Chapter 5).

The adhesive will yield at these loads, however, this is acceptable providing failure does not occur at the DUL condition. While the adhesive has been shown to be capable of tolerating these static loads, consideration must also be given to the fatigue loading that the hinge will see. This is considered further in a later section. The peel stresses while high compared with a conventional flat joint, are comfortably below the proposed peel allowable. Note that the peel stresses become positive for the tensile WO 39 design load case.

The composite reinforcement was manufactured from Textron 5521/4 boron/epoxy pre-preg, because of the superior compressive properties, absence of galvanic corrosion problems and higher coefficient of thermal expansion of boron compared with carbon (Chapter 2). This helps to minimise residual thermal stresses which result from the elevated temperature cure. The adhesive used in the test program was Cytec FM 73, although a combination of FM 300-2 co-cured with the boron and then secondarily bonded with FM 73 is also possible. This co-cured

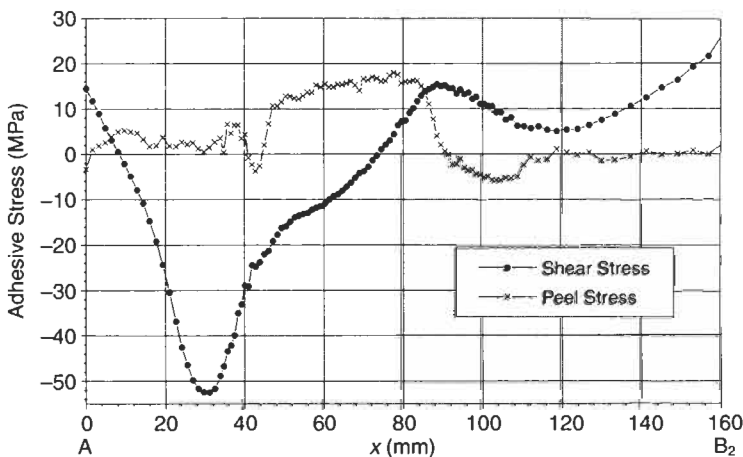


Fig. 33.5. Adhesive stresses occurring along the adhesive bondline for the OSR 2 mm rework hinge for the WO 39 load case. A and B₂ are the points shown in Fig. 33.2(a).

combination may be used for the future reinforcing of the hinges as it has previously shown excellent elevated temperature fatigue performance [5].

33.4. Static testing and repair validation

To validate the FEA, a static test program was undertaken on a series of hinges using both the WO 39 and WO 42 load cases. A test rig was constructed in which the hinges could be loaded at the correct angles as shown in Figure 33.6. The required series of fittings were fabricated and attached to the end of the hinges through which the applied loads were reacted. Strain gauges were applied to the hinges to measure the strains in the radius region during the test. One new hinge was tested in the original condition to validate the base FE model and very good correlation of strain in the critical region was achieved. Further tests were conducted on hinges which had been reworked to a variety of different rework depths as reported in [7] and then again after the composite reinforcement had been applied.

The tests were carried out at a range of different loads with checks made to ensure linear behaviour at low loads and consistency between different tests. The final tests were conducted to both DLL to check for no permanent deformation of the hinge and then to DUL to confirm that no failure occurred. These successful tests proved the structural integrity of the reworked and reinforced hinge.

The strain behaviour of the hinge under the different test configurations can be seen in Figure 33.7, where the strains along the radius can be seen. The original

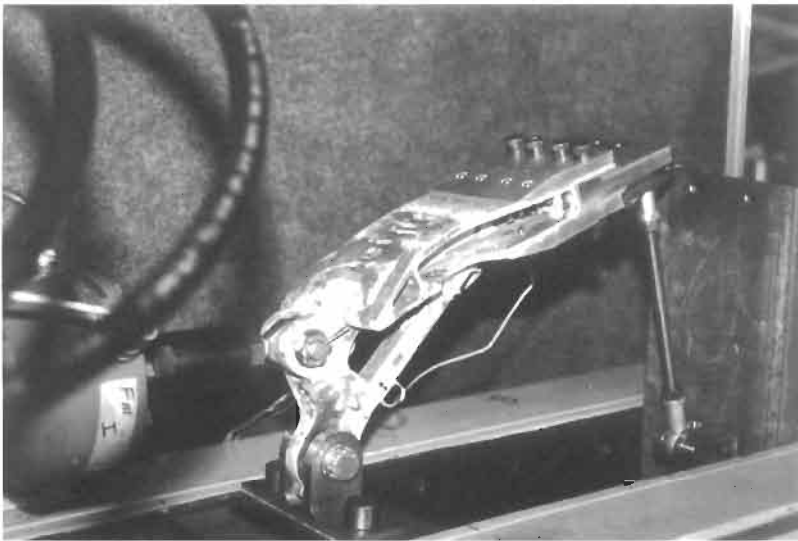


Fig. 33.6. Close up photograph of test article in WO42 configuration. Test fixtures can be seen at the end of the hinge.

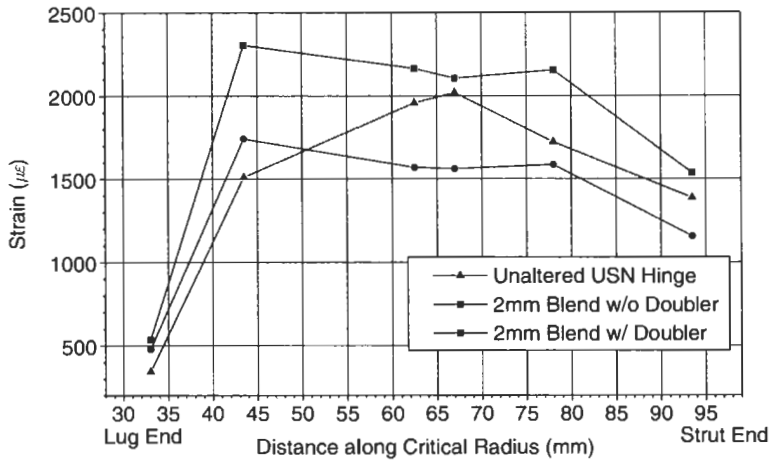


Fig. 33.7. Measured strains for the unaltered, 2 mm blended without reinforcement and 2 mm blended with reinforcement ex-USN hinge at 50% DLL in the WO39 load configuration. These strains were measured along the side of the strut.

geometry shows the peak in tensile stress at 67 mm as described previously in the stress analysis section. The effect of the 2 mm deep rework can be seen as the region of high stress is broadened and the location of peak stress shifts closer to the lug end (compare Figure 33.7 with Figure 33.4). The subsequent effect of reinforcement is seen to significantly reduce the strain at all locations in the critical radius region with the peak stress having been reduced by 16% compared with the original uncracked hinge geometry.

This observed strain behaviour confirms and validates the predicted strains from the FE models of the hinge. Importantly the models are seen to correctly predict the location and magnitude of the maximum stress in the hinge for the various conditions (original, reworked and reinforced). This provides confidence in the accuracy of the observed stress behaviour of the hinge.

The measured strains in the boron/epoxy composite reinforcement are shown in Figure 33.8, where the results from strain gauges mounted on the surface of the composite are compared with strains measured on the side of the aluminium hinge strut for both the DLL and DUL WO 39 load cases. The strains shown in this figure are higher than the strains that would normally be expected for a composite-reinforced aircraft component, however, this is often the case for repairs where less design freedom is available and geometrical constraints are more severe. On the other hand during the design of composite repairs there is often less uncertainty about the stress state than there is during the initial design of a much larger component, and therefore it is sometimes possible to use higher design allowables for a repair than for component design. The strains in the boron at DUL are around 75% of the ultimate material strain and no failure was observed during the DUL testing. Both WO 39 and WO 42 load cases were applied during these tests.

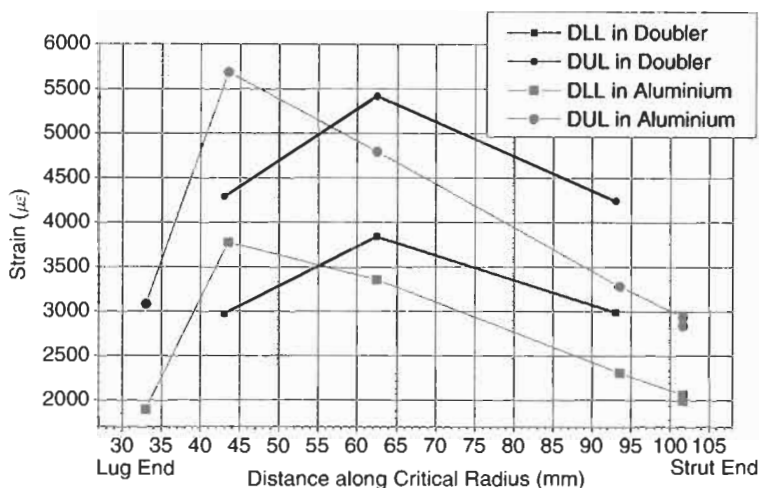


Fig. 33.8. Measured strains from DUL test (WO 39) showing strains on both the aluminium (side of strut) and boron at $1.06 \times \text{DLL}$ (14800lbs) and DUL (21000lbs).

33.5. Certification and implementation to aircraft

Before the proposed reworking and/or reinforcement design can be applied to an aircraft, it will require certification by an airworthiness authority. Further issues such as fatigue durability of the reworked hinge and the composite reinforcement would need to be completed for certification as well as consideration of environmental durability and degradation possibly by hot/wet mechanical testing. An important aspect of the certification relates to the confidence in the long term structural integrity of the composite reinforcement. Consider the OSR profile for the 2mm blend which by itself slightly increases the stress at the critical radius as compared to an uncracked hinge of standard geometry. If it can be shown that there is an acceptably low probability of failure for the reinforcement, then full credit can be given for the stress reduction it provides and the original inspection intervals for the component could be maintained. If it could not be shown that the reinforcement was unlikely to fail, it would not be possible to rely on the reinforcing effect of the doubler. In this case it would be necessary to quantify the exact stress increase and calculate a reduced inspection interval. Less extensive reworks have been shown in this project [7] to reduce the stress concentration at the radius. For these cases there is no increased risk of fatigue cracking and the original inspections could be maintained. If a composite reinforcement was applied the additional stress reduction it permits could permit a reduction in the inspection intervals.

To fully satisfy the requirements for certification, it is necessary to consider inspection and application issues as well. To confirm a new fatigue crack could be detected under the proposed reinforcement, a hinge has been blended to the 2mm

rework geometry and a series of very fine slots has been machined into the high stress region using electro-discharge machining. These slots (representative in size of fatigue cracks) have been located using ultrasonic NDI methods both when the reinforcement is bonded in place and when it is absent. The technique involved sending and receiving the pulses from the back face of the strut.

To apply the reinforcement to an aileron hinge a set of simple tools have been designed and manufactured. The first is a set of hardened steel guides which contain the profiles that were determined from the structural optimisation design process (Section 33.3). These tools are attached either side of the hinge and are used as guides in both the removal of fatigue cracks and in the subsequent re-profiling of the hinge to the required profile. The second is a tool which allows a rubber bladder to be held firmly against the outer surface of the reinforcement. When the bladder is inflated with air, the tool reacts out the loads and provides a positive pressure to the adhesive during cure.

33.6. Conclusions

A design approach is described which combines structural optimisation methods with bonded composite repair technology. This approach was used to design a proposed reinforcement for fatigue cracked F/A-18 aileron hinges. This design includes high through-thickness stresses in the adhesive layer which have been minimised where possible. The design was validated using a full-scale static test program, and the test hinges and composite reinforcements have been satisfactorily tested to design ultimate load. This reinforcement provides a cost effective option to the replacement of the hinge which is the only other alternative.

References

1. Anon. (1997). F/A-18 A/B/C/D Trailing Edge Flap and Aileron Hot Spot Analysis – Final Report, McDonnell Douglas Aerospace Report MDA 96A0138, Revision A 27, March.
2. Chester, R.J., Heller, M., Whitehead, S., *et al.* (1999). Life extension of an F/A-18 Aileron Hinge using structural optimisation and bonded composite reinforcement. *Proc. of the Int. Conference on Aeronautical Fatigue*, Seattle, August.
3. Kaye, R. and Heller, M. Life extension options for FA 18 470 bulkhead using sensitivity based shape optimisation, for publication in the *Int. J. for Numerical Methods in Engineering*, DSTO File M1/8/1156.
4. Searl, A. and Heller, M. Constrained shape Optimisation for Minimising Stress concentrations, DSTO Research Report, Australian Department of Defence, File M1/9/409.
5. Bartholomeusz, R., Searl, A., Baker, A., *et al.* (1997). Bonded composite repair of the F/A-18 Y470.5 bulkhead – applications with through-thickness stresses. *Proc. of the Int. Aerospace Congress (IAC 97)*, 1, Sydney, 24–27 February.
6. Ignjatovic, M., Chalkley, P.D. and Wang, C. The Yield Behaviour of a Structural Adhesive under Complex Loading, *DSTO Technical Report DSTO-TR-0728*, Australian Department of Defence.
7. Chester, R.J. (ed.). Life Extension of F/A-18 Inboard Aileron Hinges by Shape Optimisation and Composite Reinforcement, DSTO Technical Report DSTO-TR-0699, Australia, Department of Defence.

Chapter 34

UK APPLICATIONS

P. POOLE

*Structural Materials Centre, Defence Evaluation and Research Agency,
Farnborough, Hants, UK*

34.1. Introduction

Adhesively bonded gr/ep patches have been used in the UK to repair a range of aircraft structures. Early work at British Airways [1] involved the use of paste adhesives for wet laminated gr/ep patch repair of various structures, including wing leading edge panels, elevons and body fairing panels on Concorde, and engine cowling and pylon fairing panels on Boeing 747 aircraft. The repairs to Concorde wing leading edge panels were particularly successful, with good in-service performance and large cost savings. Although surface pretreatment was limited to grit blasting or Deoxidine 202 treatment, long term performance was good, i.e. no crack growth was detected under patches which were in service for 5–7 years. British Airways has also used wet laminated patches to repair composite structures, such as the aileron and rudder on Boeing 757 aircraft [2]. These repairs were extremely cost effective and have been in service for over 12 years.

British Aerospace has investigated the use of bonded gr/ep patches for the repair of metallic components and carried out design studies for the repair of primary structures on military aircraft, as described in Section 34.2 below. However, to date only two primary structure repairs have been applied to RAF aircraft. These repairs, together with repairs to various secondary structures and reinforcements of fuselages to improve birdstrike resistance, are described in Section 34.3 below. GKN Westland Helicopters have used bonded gr/ep patches to repair fatigue damage on the EH101 development standard full scale fatigue test specimen, as described in Section 34.4 below.

34.2. Design studies

A programme of work to identify, design and apply a series of in-service gr/ep patch repairs to primary metallic aircraft structures was undertaken by British Aerospace [3], under a Ministry of Defence contract. Known service defects, with existing metallic repair schemes, were assessed for their suitability to be repaired using adhesively bonded gr/ep patches. Applications considered included:

- (a) Harrier fuselage skin cracking [various locations]
- (b) Harrier airbrake beam cracking
- (c) Hawk leading edge upper wing skin cracking
- (d) VC10 spar centre member cracks
- (e) VC10 wing tip skin cracks
- (f) VC10 undercarriage bay sidewall cracks
- (g) Tornado leading edge slat skin impact damage
- (h) Tornado wing pen nib fairing cracks
- (i) Victor alternator cold air intake skin cracks
- (j) Hercules rear fuselage sloping longeron cracks

The following assessment criteria were used to identify suitable candidates for bonded composite patch repair trials:

- The repair would act as a fatigue life enhancement only
- There was suitable access for repair application and inspection
- The number of mechanical fasteners would be reduced significantly
- The aircraft had a significant anticipated service life ahead of it
- Selected candidates would cover different aspects of bonded patch repair

Using these criteria, candidates b, d, e, f and j were eliminated. For the other candidates, bonded patch repairs were designed and repair drawings were issued. The repair designs were based on stiffness matching and simple closed form analytical methods. The effectiveness of these methods were substantiated with empirical data and finite element analysis. Individual trial repair designs were not verified directly by test.

The repair designs for Hawk upper wing skin and Harrier rear fuselage side skin at frames 37/38 involved co-cure of prepreg and adhesive at 125 °C. This method is best suited to relatively thin [<1 mm] patches, where satisfactory patch consolidation may be achieved using vacuum bags and heater mats. It was calculated that these repairs offered manhour savings of 65–75%, when compared to conventional metallic repairs, although manhours associated with any additional inspections were not included. The repairs to Harrier fuselage skins at frames 30/31 and 51, and to Tornado leading edge slat and Tornado wing pen nib fairing, involved adhesively bonded precured patches. For these repairs, it was estimated that cost savings would be 40–60%, compared to corresponding conventional metallic repairs. The repair scheme for the Victor alternator cold air intake skin involved wet lay-up of woven graphite cloth. In general, this method is considered to be suited to secondary structures only, due to the variation in patch properties that can occur. However, it was selected for the intake duct repair, owing to severe double curvature of the region to be repaired. Of the seven repairs outlined above,

only the Hawk wing skin and Harrier rear fuselage [frames 37/38] repairs have been applied to RAF aircraft [see Section 34.3.2 below].

British Aerospace, Military Aircraft carried out additional work to design and assess bonded composite patches for the repair of skin splice joint and wing spar specimens. The skin splice specimen was based on Harrier guidelines, using typical fastener pitches and assembly methods. The specimen was 300 mm wide with a butt strap attached by six rows of rivets [two rows with 13, 14 or 15 rivets]. 20 mm length fatigue cracks were grown in the skin from the two centre rivet holes in the outer rows; this was achieved using oversize rivets and notching. Patch design was again based on stiffness matching and simple analytical formulae. Skin surfaces were subjected to a grit blast/silane surface treatment before two precured gr/ep patches [T300/914] were bonded to each specimen using a 125°C epoxy film adhesive [Redux 312/5]. Although constant amplitude fatigue tests demonstrated that fatigue life was increased by up to eight times by patching, it was concluded that further work was required to account for the observed fatigue performance and to develop an optimum patch design. Similar materials and procedures were used to repair wing spar specimens, which were cut from scrap Hawk wings and comprised rear spar/skin sections between ribs 13 and 16. Simulated cracks were introduced at various locations, including the spar web where a 19 mm length slot was spark eroded from the edge of a transfer hole. Constant amplitude $R = 0.1$ loading was applied by three point bending, and patching was carried out after a 1 mm fatigue crack had grown at the end of the slot. Patching was very effective and resulted in crack arrest, i.e. no crack growth was detected after fatigue loading for 16.5 times the number of cycles required to grow the crack by 1 mm. For one specimen, the patch was removed and crack growth recommenced almost immediately. It was estimated that bonded composite patch repair of the spar web would result in manhour savings of 69%, compared to a conventional metallic repair.

At present, British Aerospace is investigating the feasibility of using bonded gr/ep patches to repair internal damage in narrow structures where access is difficult. It is planned that artificial damage will be introduced at various locations in a Hawk tailplane, and that fatigue testing will be carried out to assess the effectiveness of the bonded patches in retarding crack growth.

34.3. Repairs to RAF aircraft

34.3.1. Secondary structure repairs

The RAF has used gr/ep patches to repair a variety of secondary structures [4]. In general, patches were applied by wet lay-up and cured under pressure at 60–80 °C using vacuum bags and heater mats. One of the earliest repairs concerned the CSDU air intake fairing on Victor aircraft [4]. Wet laminated woven gr/ep patches were used to repair cracked, double curvature aluminium alloy skins, as illustrated in Figure 34.1. The first trial repair was very successful and most Victor aircraft were subsequently repaired in this way. These repairs were extremely cost effective,

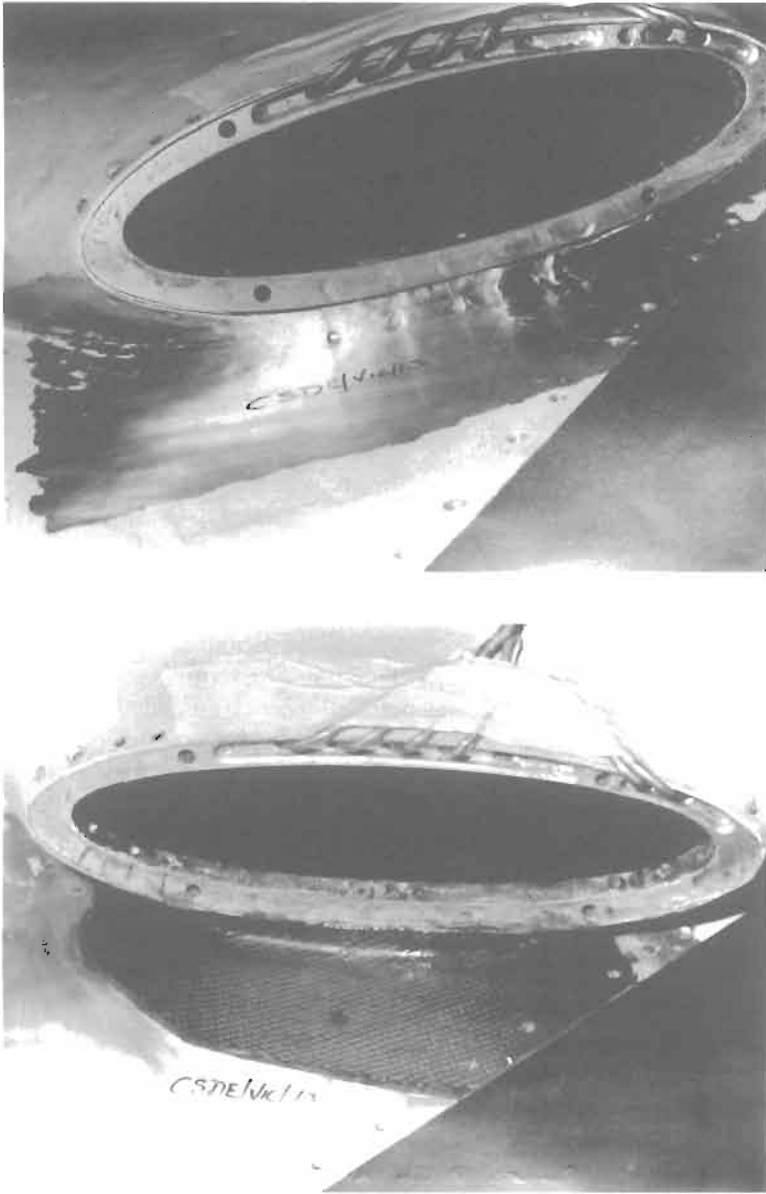


Fig. 34.1. Victor CSDU air intake before and after patching.

since conventional mechanically fastened metal patch repair was not feasible. Furthermore, in-service performance was very good with no problems reported after several years.

Other secondary structures repaired by the RAF include:

- (a) Harrier T4 engine door. Cracking from panel fastener holes was repaired effectively using a four ply woven gr/ep patch. The composite patch repair was preferable to a conventional metal repair because it avoided the need to gain access to the rear face to apply rivets. No problems were reported after 824 flying hours.
- (b) Harrier GR3 inter-nozzle fairing. Panel cracking, which occurred along a partial frame due to longitudinal flexing, was overcome using unidirectional and woven graphite to produce patches which improved the stiffness over local selected areas. This repair was accepted as a reinforcement prior to damage occurring. Six repaired fairings have been flown for up to 779 h, with no problems reported.
- (c) Tornado GR1 pylon rib fairing. Cracking occurred along a line joining machined webs, after only 19 flying hours in some cases. Wet laminated gr/ep patches, comprising three plies of unidirectional graphite between two plies of woven graphite, were used to repair sixteen cracked fairings. These cost-effective repairs performed very well in-service; some were flown for 900 h with no problems reported.
- (d) Harrier gun pod fairing. Impact damage occurred due to expelled links not delinking and then flailing the aluminium alloy skin. This problem was overcome by reinforcing the panel with a four ply kevlar/epoxy wet laminated patch. This solution was more cost effective than a proposed metal repair involving a stainless steel doubler.
- (e) Harrier air pipe. Wet lay-up patches were used successfully to recover pipes which had suffered surface abrasion damage.
- (f) VC10 tailplane bullet fairing. Fatigue damage was repaired using a wet laminated gr/ep patch, with an outer layer of woven glass to provide erosion resistance.

Other bonded patch repairs have been applied successfully to Hunter drop tanks, a Chinook aft pylon servicing platform and a VC10 stub wing. The RAF is currently investigating the use of bonded composite patches for a range of additional repairs, and it is anticipated that this repair technology will be used more extensively in the future.

34.3.2. Primary structure repairs

To date, composite bonded patches have been used for only two primary structure repairs on RAF aircraft. The first concerned the Hawk upper wing skin where fatigue cracks grew from fastener holes positioned behind the leading edge. Buffet loading was believed to be responsible for this cracking. The traditional repair involved a large number of fasteners and eight main components, and affected a large area around the defect [3]. The composite version was designed on a stiffness basis, utilising finite element analysis and fatigue crack growth prediction data to clear the repair as a fatigue life enhancement on a Special Trial Fit basis. It was predicted that patching would result in very low stress intensity factors and

that crack arrest would occur, even though there was some uncertainty concerning in-service loading. The surface of the aluminium alloy wing skin was subjected to a grit blast/silane treatment and patching was carried out using a vacuum bag and heater mat to co-cure four plies of woven gr/ep prepreg and epoxy film adhesive at 125 °C. No debonding was detected by simple tap tests or ultrasonic inspection. Two aircraft were repaired and in both cases crack length was monitored by eddy current inspections carried out at intervals consistent with those specified for unrepaired structure. No crack growth was detected before the wings were removed from service after 398 and 990 flying hours.

The second primary structure repair concerned fatigue cracks in Harrier fuselage side skins. The traditional metal repair involved many fasteners and a number of components. The bonded composite patch repair was designed, applied, inspected and cleared for flight using the same techniques/procedures as described above for the Hawk wing. Two aircraft were repaired and eddy current inspections were again carried out at intervals consistent with those specified for unrepaired structure. No crack growth was detected after 70 and 209 flying hours when the aircraft ceased flying.

34.3.3. Birdstrike protection

Bonded Kevlar composite patches have shown considerable promise for improving the birdstrike resistance of front fuselages of Hawk aircraft. It has been reported [4] that birdstrike damage to thin skinned areas forward of the cockpit cost the RAF thousands of manhours to maintain and months of aircraft downtime. Thus, wet laminated Kevlar composite patches were applied to four Hawk aircraft, as a Special Trial Fit, where the main objective was to prevent penetration which would cause damage to the pressure bulkhead. However, no in-service birdstrikes were reported for the reinforced areas on these aircraft and, thus, it was not possible to assess their effectiveness. Nevertheless, in-service experience with the reinforcements was good, with no debonding detected up to six years after application.

Bird-gun trials were carried out on life expired Harrier GR3 fuselages, where Kevlar/epoxy patches were applied to frame 1–3 areas directly in front of the windscreen and to areas on the port and starboard sides of the cockpit. The effects of patch thickness and resin type were studied, and it was shown that 9-ply Kevlar 29/MY750-HY956 patches can substantially reduce structural damage by deflecting 1 kg birds at impact velocities up to 420 knots. Best performance was observed when patches were precured and bonded with a 120 °C curing epoxy film adhesive.

Further development work and trials were planned, but these did not proceed due to a substantial reduction in birdstrike occurrences. This reduction was caused by improved bird control methods at airfields and amendments to operational procedures, as a result of an increased awareness of bird migratory patterns.

34.4. Repairs to EH101 development airframe full scale fatigue test specimen

As part of the structural substantiation of the EH101 helicopter main load path, a full scale fatigue test of a development airframe has been carried out by GKN Westland Helicopters [5]. The main load path test specimen was a complete cabin structure, with a dummy main rotor head fixed to a locked main rotor gearbox. 25 servo hydraulic actuators were used to apply three load programmes:

Programme A – Low level manoeuvre loads, following an assumed flight profile.

Programme B – Medium level manoeuvre loads, which were 1.3 times higher than A.

Programme C – High frequency loads, which simulated blade passing vibratory loads.

The loads were applied in blocks and at the end of the test the airframe had achieved the following cycles: programme A – 95985 cycles, programme B – 4545 cycles, programme C – 2.708×10^6 cycles. This test life was considered sufficient to substantiate the Navy requirement for a safe life of 10000 h.

During the test a number of primary structure fatigue failures occurred, mainly at lightening holes and curved and tapered flanges on side and roof frames. These fatigue cracks were repaired with gr/ep patches applied by wet lay-up or by bonding precured patches with a paste adhesive [6,7]. Three-dimensional finite element analysis and strain gauge measurements were used to determine the stresses that resulted in cracking and to develop bonded patch repair designs. In general, shear webs were repaired using $\pm 45^\circ$ Brochier 833 graphite fabric applied by wet lay-up with a room temperature curing epoxy paste adhesive. Patches of similar thickness to the web were applied to both sides of the web. In cases where the crack had reached the edge of the web or propagated into or along the flange, 0/90° woven graphite plies were used to form a nested angle between the web and flange before the $\pm 45^\circ$ plies were applied. Flanges were repaired by bonding precured unidirectional gr/ep [XAS/913] patches with a paste adhesive, using a vacuum bag to apply pressure. Patch thickness was approximately 70% of flange thickness. All patches were applied within 3 h of reactivating the surface anodic film. The main features of repairs to a shear web lightening hole failure and to a curved flange failure are shown in Figures 34.2 and 34.3, respectively.

Table 34.1 summarises the various gr/ep patch repairs carried out on the fatigue test specimen, and indicates the number of cycles of each load programme at which failure occurred and the number of cycles the repair withstood. All repairs were very effective and were unfailed at the end of the test. It can be seen from Table 34.1 that the repairs successfully withstood extensive fatigue loading, and that the oldest repair [Item 1] withstood 80625 test flight cycles. When four of the oldest repairs were examined by X-radiography after the test, no further cracking was detected for Items 3, 7 and 8 but an additional crack was detected in the case of Item 1. Although no detailed explanation for the development of the additional crack was provided, it was noted that 0/90° plies were not used for this oldest repair and therefore patching may not have been as effective as for subsequent repairs [6].

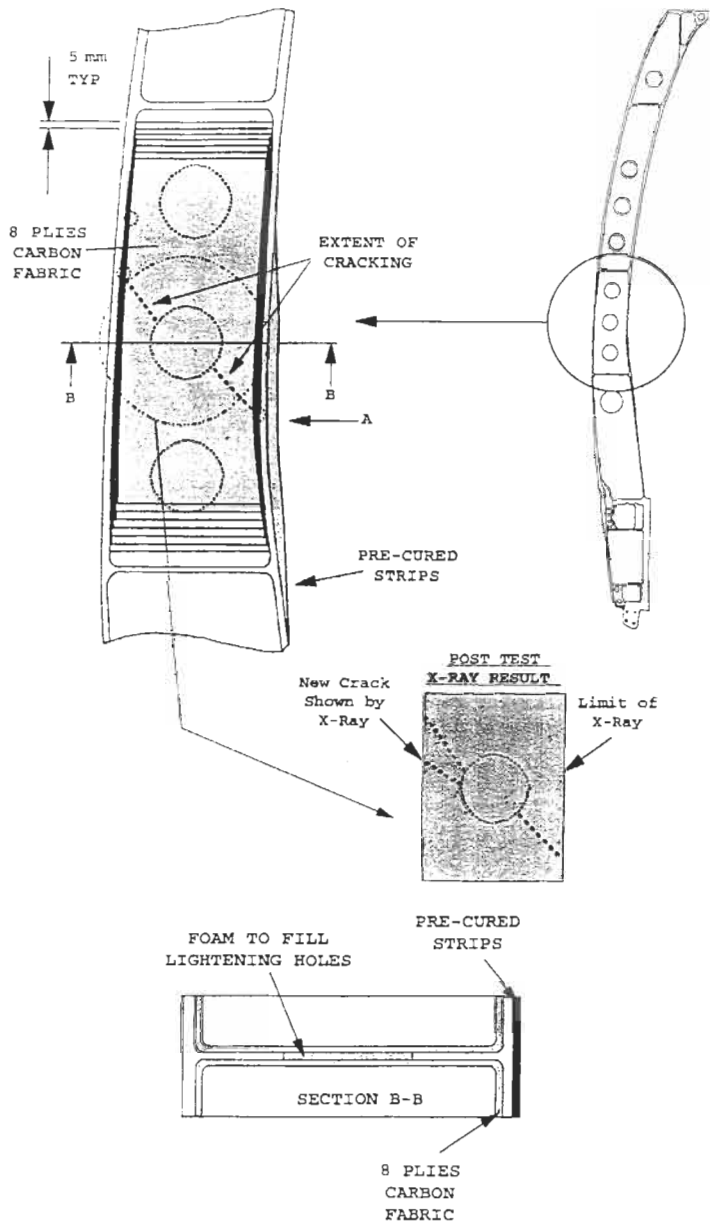


Fig. 34.2. Repair details of X8875 port side frame WL2121 unflanged lightening hole failure.

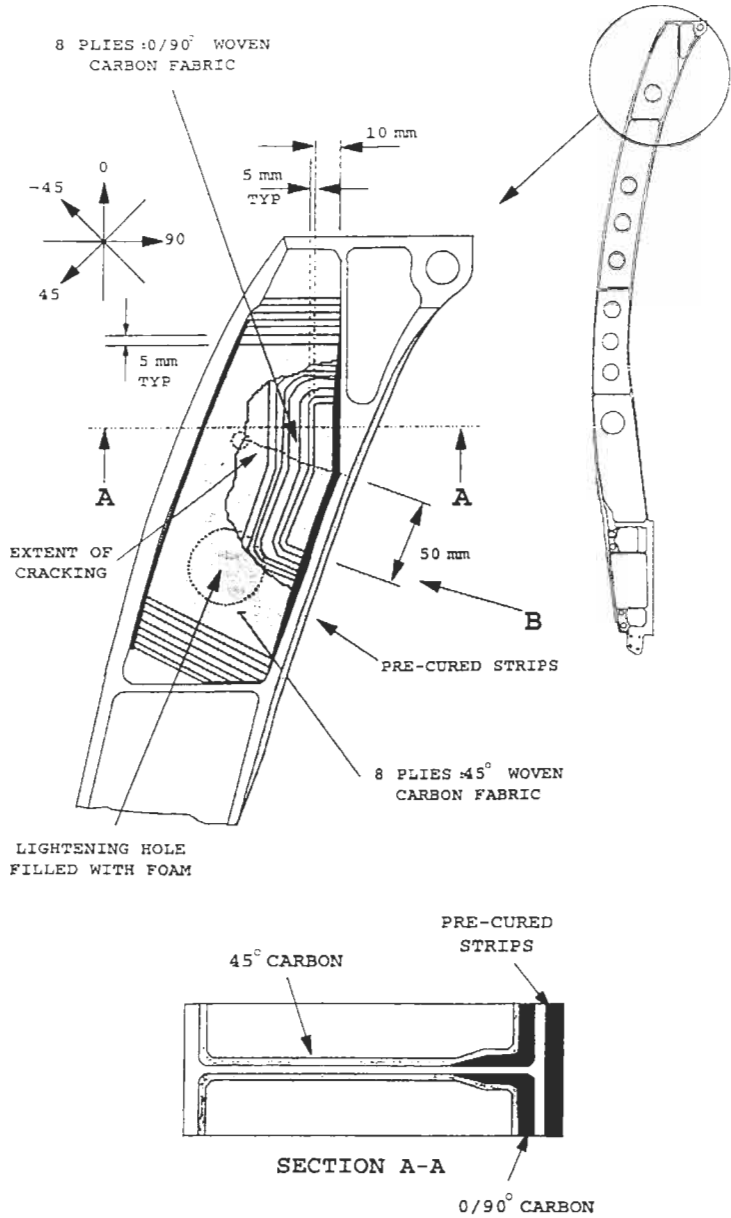


Fig. 34.3. Repair details of X7875 port side frame WL3038 flange failure.

Table 34.1

Summary of repairs to EH101 development airframe fatigue test specimen [6].

Item No.	Failure location and remarks	No. of cycles at failure	Repair details	Repair performance, cycles
1	X8875 Side Frame Port. Unflanged lightening hole failure W12121. Crack propagated at 45° to both inner and outer flanges then along web/flange angle. "U" shaped section of inner flange pulled away. Web $t = 2.5$ mm. Flange $t = 5.5$ mm	A. 18792 B. 1113 C. 1.14×10^6	Cracks stop drilled. Eight plies $\pm 45^\circ$ woven each side of web. 32 plies (16 pairs) pre-cured u/d on inner flange damage.	A. 77193 B. 3432 C. 1.568×10^6
2	X7875 Side Frame Port. Frce flange below WL3250 failed at junction with stiffener due to 3D warping behaviour. Crack then propagated through web. Web $t = 2$ mm. Flange $t = 2$ mm	A. 22962 B. 1113 C. 1.14×10^6	Crack stop drilled. Eight plies 0/90° woven per side applied at web/flange angle then eight $\pm 45^\circ$ woven plies overlaid in web. 16 plies pre-cured u/d on flange.	A. 39573 B. 2207 C. 0.86×10^6 Note: This repair was unfailed when repair No. 10 was installed.
3	X8875 Side Frame Stbd. Unflanged lightening hole failures WL1500–2310. One crack from each hole propagating at 45°. Cracks did not reach the flanges. Flange $t = 5.5$ mm. Web $t = 2.5$ mm	A. 23362 B. 1113 C. 1.14×10^6	Cracks stop drilled. Eight plies per side of $\pm 45^\circ$ woven over each web.	A. 72623 B. 3432 C. 1.568×10^6
4	N/A	A. 23362 B. 1113 C. 1.14×10^6	Preventative repairs of L165 rings; carbon patches applied to holes at-risk of failure.	A. 72623 B. 3432 C. 1.568×10^6
5	X8875 Roof Frame BL277 Port. "Axial" failure of unflanged lightening hole. Crack at 90° did not reach flange. Flange $t = 10$ mm. Web $t = 2.5$ mm	A. 27000 B. 1113 C. 1.14×10^6	Crack dressed out. 4 plies 0/90° woven per side of web.	A. 68985 B. 3432 C. 1.568×10^6
6	N/A	A. 27000 B. 1113 C. 1.14×10^6	Further preventative repairs applied.	A. 68985 B. 3432 C. 1.568×10^6
7	X6875 Roof Frame. Outer flange at BL1046 stbd. broken on aft side. Crack propagated into web. Flange $t = 3.5$ mm. Web $t = 3.0$ mm	A. 35550 B. 1113 C. 1.36×10^6	Crack stop drilled. Eight plies 0/90° woven applied at web/flange join. Four plies $\pm 45^\circ$ woven overlaid in web. 24 plies of pre-cured u/d applied to outer surface of flange.	A. 60435 B. 3432 C. 1.348×10^6 Repair still intact when further repair in this area installed. See item no. 12
8	X8875 Side Frame Port. Unflanged lightening hole failure at WL2421. Crack propagated at $\sim 30^\circ$ and completely failed inner flange. Adjacent repair (Item 1) may have overloaded section since not identified as at risk. Flange $t = 7.5$ mm. Web $t = 2.5$ mm	A. 35550 B. 1113 C. 1.48×10^6	Eight plies 0/90° woven applied at web/flange join. Eight plies $\pm 45^\circ$ then overlaid in web. 40 plies of pre-cured u/d applied to failed inner flange.	A. 60435 B. 3432 C. 1.228×10^6

Table 34.1
(Continued).

Item No.	Failure location and remarks	No. of cycles at failure	Repair details	Repair performance, cycles
9	X8875 Roof Frame. Failure of outer flange at BL900 stbd. Cracks propagated through the outer flange, into the adjoining web and along the web/centre flange join. Flange $t = 12$ mm. Upper web $t = 5$ mm. Lower web $t = 3.5$ mm (Note: lower web had been reinforced ref. Item 4).	A. 53320 B. 3320 C. 2.00×10^6	Steel strap repair to flange since insufficient bond area for carbon strap. Top end with six bolts into tapped bar, bottom end with 4 through bolts. Carbon repairs to webs of eight plies $\pm 45^\circ$ woven.	A. 42665 B. 1225 C. 0.708×10^6
10	X7875 Side Frame Port. Failure of inner flange just below barrel nut housing at WL3210 similar to Item 2. Flange $t = 2.00$ mm	A. 62535 B. 3320 C. 2.00×10^6	Steel copy milled part frame WL2900-3250 installed. Carbon angles of eight plies woven $\pm 45^\circ$ carbon used to reinforce remaining horizontal stiffeners at WL2900. 16 ply u/d pre-cured strap on inner flange across joint.	A. 33450 B. 1225 C. 0.708×10^6
11	X7875 Roof Frame Port. Failure of WL3250 bolt pad at inner bolt positions. Pad $t = 3$ mm.	A. 64085 B. 3320 C. 2.00×10^6	Angled stiffener machined away. Nested repair of 20 plies $0/90^\circ$ woven carbon installed. Steel throat plate to prevent peel.	A. 31900 B. 1225 C. 0.708×10^6
12	X6875 Roof Frame. Failure of outer flange propagating from BL910 stbd. walk-way fillet thorough flange and web and down web/vertical stiffener join. Flange $t = 10$ mm. Web $t = 3.00$ mm	A. 87403 B. 4428 C. 2.708×10^6	Cracks stop drilled. Vertical stiffener machined away. Web repaired with eight plies $\pm 45^\circ$ woven per side. Slot cut in walkway support member and 48 plies pre-cured u/d applied to outer flange.	A. 8582 B. 117 C. 0

The ease, speed, cost effectiveness and fatigue performance of the above bonded patch repairs indicated that they were attractive for in-service applications, although further qualification work was required to quantify the effects of impact damage and environmental degradation and to determine failure modes of the repairs. However, it should be noted that design and material changes were subsequently incorporated in the production design, and that a stand-alone fatigue test of a production standard roof and side frame demonstrated that the changes eliminated the fatigue failures observed for the development airframe [5].

34.5. Acknowledgements

The author is grateful to K.B. Armstrong [Consultant], M.L. Overd [GKN Westland Helicopters], Wg. Cdr. S. Welburn and Sqn. Ldr. S. Reed [RAF] for providing information used in this review.

© British Crown Copyright 2001. Published with the permission of the Defence Evaluation and Research Agency on behalf of the Controller of HMSO.

References

1. Armstrong, K.B. (1983). In: *Proc. of SAMPE Conf. on Engineering with Composites*, pp. 8.1–8.12.
2. Armstrong, K.B. (1989). In: *Proc. of Conf. on Bonding and Repair of Composites*, Birmingham, pp. 93–99.
3. Poole, P., Young, A. and Ball, A.S. (1994). In: *Composite Repair of Military Aircraft*, AGARD-CP-550, pp. 3.1–3.12.
4. Ford, T. (1989). *Aerospace Composites and Materials*, **1**(2), pp. 4–7.
5. Overd, M.L. (1997). In: *Proc. of 19th ICAF Symp. Proc.*, Fatigue in New and Ageing Aircraft, EMAS, pp. 347–364.
6. Overd, M.L. (1994). A Survey of the Design and Performance of Carbon Composite Repairs on the Main Load Fatigue Test, Westland Helicopters Report EA53B001W.
7. Overd, M.L. (1993). *Composite Structures*, **25**, pp. 557–565.

Chapter 35

CASE HISTORY: REPAIR APPLICATIONS ON DC-10/MD-11 AIRCRAFT

D. ROACH

Sandia National Laboratories, USA

35.1. Introduction

Boeing-Long Beach and Federal Express have teamed with the Sandia Labs AANC to optimize and properly focus composite doubler applications. The team also includes participants from the FAA Long Beach Aircraft Certification Office (ACO), and the FAA's William J. Hughes Technical Center so that FAA oversight remained constant throughout the project. Using the data accumulated to date, the team has designed, analyzed, and developed inspection techniques for an array of composite doubler repairs with high-use fuselage skin applications. The general DC-10 repair areas which provide a high payoff to FedEx and which minimize design and installation complexities have been identified as follows:

1. gouges, dents, lightning strike, and impact skin damage
2. corrosion grind outs in surface skin (exceeding 20% allowable and requiring repair)
3. scab repairs for skin fatigue cracks (unpressurized surfaces).

Following a successful pilot program, the plan is to accommodate the routine use of composite doublers by adding their designs alongside the riveted metallic repair tables commonly found in OEM Structural Repair Manuals (SRM). Using these look-up tables, maintenance facilities can have the option of choosing the traditional metallic repair or the "equivalent" composite doubler repair. Examples of existing SRM riveted metallic repairs that can be replaced by the family of composite doublers developed in this DC-10 program are shown in Figures 35.1 and 35.2.

An infrastructure for supporting routine use of composite doublers was demonstrated at the Federal Express maintenance facility. For example, the family of composite doublers was laid up in advance and was quickly available for repairs.

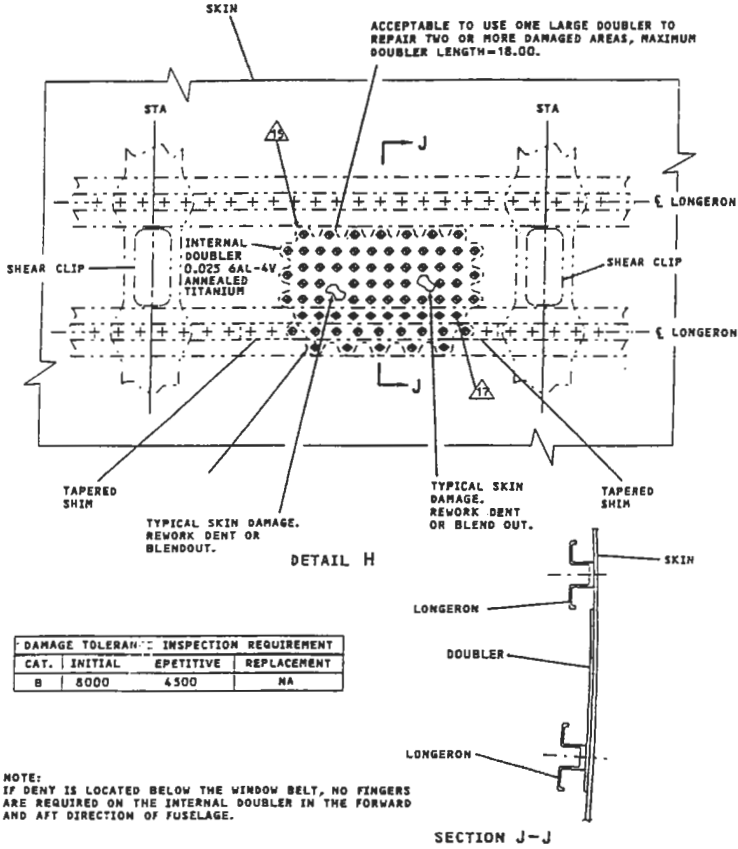


Fig. 35.1. Typical fuselage skin corrosion damage to be repaired by composite doublers.

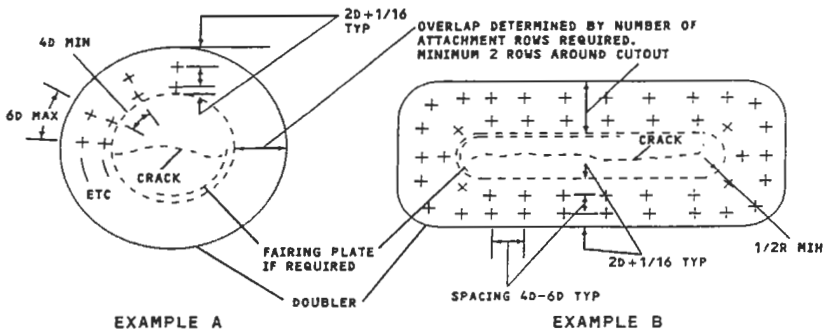


Fig. 35.2. Typical fuselage skin crack damage to be repaired by composite doublers.

Other unique issues pertain to the production of composite doubler installation job cards, specialized training for composite shop and NDI shop personnel, and the ability to shift the emphasis from sheet metal workers to composite shop technicians to facilitate repairs. Each doubler was closely monitored by frequent inspections to accumulate flight performance history and to validate the entire repair process as implemented by a commercial carrier. This approach was demonstrated to the FAA that composite doubler repair technology can be safely transferred to industry.

35.2. Repair development and validation tasks to support on-aircraft installation

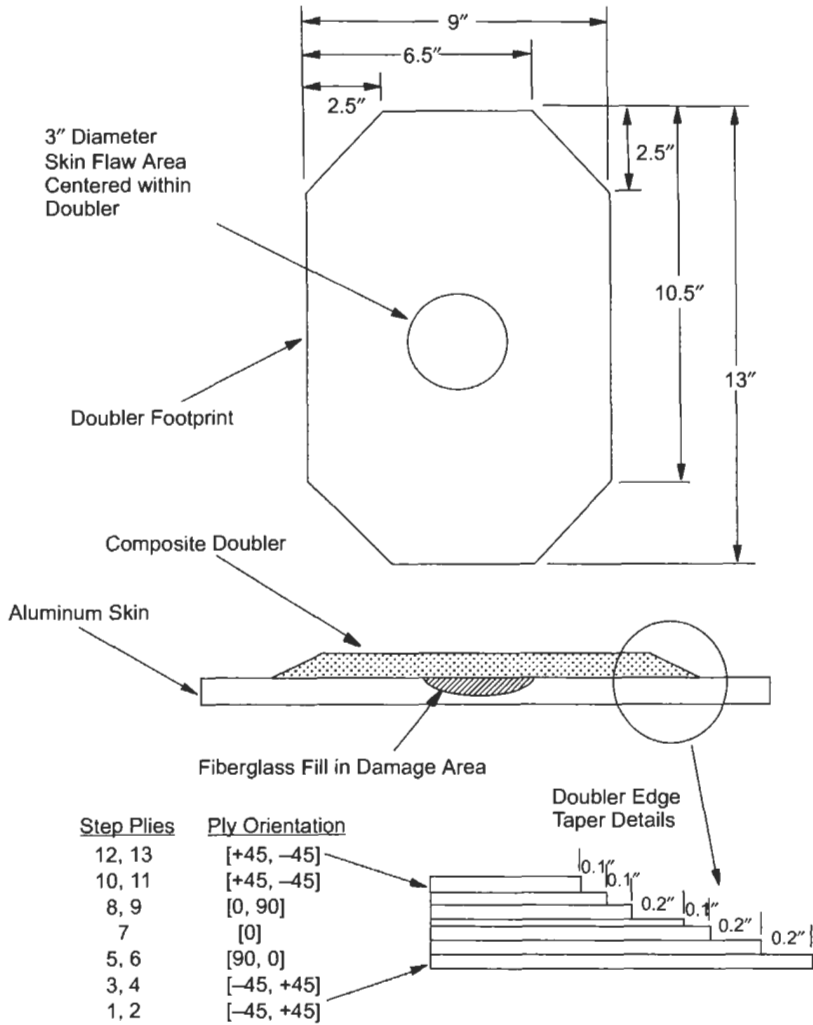
35.2.1. Repair design

The family of composite doublers developed in this program will allow for the repair of corrosion (internal and external), impact damage, gouges, and lightning strike damage to the DC-10 and MD-11 fuselage skins. The doubler designs restore the original static, fatigue, and durability capability of the structure. A representative skin repair from the DC-10 Structural Repair Manual is shown in Figure 35.1. This repair schematic shows the conventional riveted, metallic doubler. The design and analysis process was conducted to produce a composite repair set that could be applied over the majority of the DC-10/MD-11 fuselage structure. Fuselage skins up to 0.080" thick can be repaired with the composite doublers. The doubler footprint can include frames, longerons, and other substructure elements but not production joints or finger doubler joints. Repairs for 1", 3", and 5" diameter damage have been designed and analyzed. All of the repairs are 13 ply, quasi-isotropic doublers with symmetrical lay-ups. The footprint of each doubler was adjusted to accommodate the size of the damage. Figure 35.3 provides the details of the composite doubler design for 3" diameter flaws.

Formal design drawings were prepared to guide the fabrication and installation of all composite doublers. It includes the footprints for all three repair designs, as well as, a comprehensive set of notes to guide all fabrication, installation, QA, and inspection activities for the DC-10/MD-11 repairs.

35.3. Repair analysis

Stress and damage tolerance analysis was performed in accordance with applicable Federal Aviation Regulation (FAR) requirements. The analysis also compared the undamaged original structure with the same damaged structure containing a composite doubler. The stress analysis was performed using NASTRAN and NASA FRANC2D/L FEM codes. A worst-case load scenario, including extreme shear loads, was applied to the design. In addition, the analysis conservatively assumed zero load transfer in the damaged area. The applied



Skin: Aluminum 2024-T3

Patch: Boron/Epoxy, nominal lamina thickness = 0.0057

Install Per: Boeing Specification No. D658-10183-1
(also listed as Textron Specialty Materials
Specification No. 200008-001)

Fig. 35.3. Composite doubler design for 3" diameter skin flaws on DC-10 aircraft.

loading was a worst case DC-10/MD-11 stress spectrum of: $\sigma_{x(\text{axial})} = 10.4$ ksi, $\sigma_{y(\text{hoop})} = 20.7$ ksi, and $\tau_{xy(\text{shear})} = 20$ ksi.

Analysis Stress Output – The maximum stresses produced in the composite doubler, adhesive layer, and surrounding skin during the worst case DC-10/MD-11 stress spectrum were as follows:

Design for 3" Diameter Repair

- Maximum Stress in Aluminum Skin

$$\sigma_1 = 44.2 \text{ ksi } (\sigma_{\text{yield}} = 47\text{--}50 \text{ ksi})$$

$$\sigma_2 = -1.6 \text{ ksi}$$

$$\tau_{\text{max}} = 22.4 \text{ ksi } (\tau_{\text{allowable}} = 39 \text{ ksi})$$

- Maximum Stress in Adhesive

τ_{zy} = component has lower magnitude and is less critical than τ_{zy}

$$\tau_{zy} = 4.1 \text{ ksi } (\tau_{\text{allowable}} = 5.6 \text{ ksi})$$

- Maximum Stress in Composite Doubler – Based on maximum strain failure criteria, the laminate critical load is determined from the transverse ply strain (ϵ_z) in the -45° ply at the second tapered step up from the patch edge (base). The Margin of Safety is calculated based on the largest strain value found in the FEM.

$$\frac{\epsilon_z(\text{Critical location in } -45^\circ \text{ ply})}{\epsilon_z(\text{Allowable})} = +0.77$$

$$M.S. = +0.23$$

- A sample contour plot for a Maximum Principal Stress tensor is shown in Figure 35.4. The significant effects of the shear loading are evident. Note that the peak doubler stresses are confined to a small region where the doubler has its full thickness. Furthermore, the stresses in the critical tapered region of the doubler (primary load transfer zone) are 30% to 50% of those found in the surrounding skin. This type of load transfer matches general design goals for stress distribution around aircraft skin repairs.

Damage Tolerance – The analysis studied skin, patch, and adhesive stresses, as well as potential failure modes. All of the designs produced acceptable margins of safety when subjected to the worst case flight load spectrum. The stress intensity (K_I) for the repaired and unrepaired configurations was determined using the CalcuRep program for aircraft repair analysis. Table 35.1 provides a comparison for the three composite patch sizes. The crack is assumed to be initially the same size as the grind out (damaged area). The stress level is 20.68 ksi.

Using Walker's equation, below, with $C = 6.76125\text{E-}10$, $p = 3.71980$, $q = 0.64647$ and $R = 0.0$, da are determined for the above K_I (see Table 35.2).

$$\frac{da}{dn} = C \times [(1 - R)^q \times K_I]^p$$

Damage Tolerance and Inspection Intervals for DC-10/MD11 Doubler Analysis – Results from analyses and tests validated the three DC-10/MD-11 skin repair

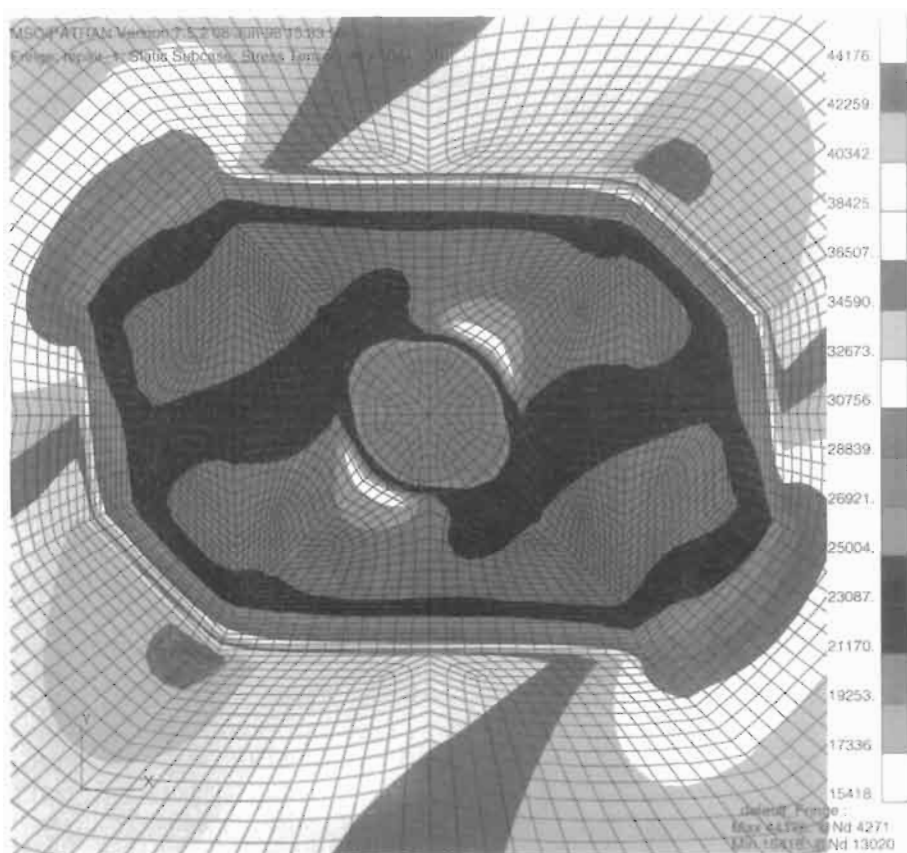


Fig. 35.4. Maximum principal stress tensor σ_1 in composite doubler and aluminum skin for 3" diameter repair design and worst case load spectrum.

designs. The results show that the doubler and adhesive exhibit sufficient strength to provide adequate fatigue enhancement through a wide range of environmental conditions. The crack growth analysis with and without the doubler present allows us to conservatively bound the inspection requirements. The rate of growth for the repaired configuration is significantly smaller than the unrepaired configuration. Note that the crack growth mitigation remains the same with the doubler in place regardless of the length of the crack beneath the doubler. The design approach uses a typical maintenance rule that since the doubler is less than two bays in size, normal maintenance activities are already in place to find any cracks that may originate in this area.

Even in the presence of extensive damage in the original structure (cracks, material loss) and in spite of non-optimum installations (adhesive disbonds), the composite doubler allowed the structure to survive multiple design lifetimes of

Table 35.1
Stress intensity factors for unrepaired skin and skin
repaired with composite doubler.

Patch size 4.5" × 3.75"		
Crack length	K_I Repaired	K_I Unrepaired
1.0"	9.32	25.94
1.5"	9.32	31.77
2.0"	9.32	36.69
2.5"	9.32	41.02
3.0"	9.32	44.94

Patch size 13" × 9"		
Crack length	K_I Repaired	K_I Unrepaired
3.0"	9.06	44.94
3.5"	9.06	48.54
4.0"	9.06	51.89
4.5"	9.06	55.03
5.0"	9.06	58.01
6.0"	9.06	63.55
7.0"	9.06	68.64

Patch size 21" × 13"		
Crack length	K_I Repaired	K_I Unrepaired
5.0"	8.85	58.01
5.5"	8.85	60.84
6.0"	8.85	63.55
6.5"	8.85	66.14
7.0"	8.85	68.64
8.0"	8.85	73.38
9.0"	8.85	77.83
10.0"	8.85	82.04

Skin: AL 2024-T3 ($t = 0.080$ ").

fatigue loading. The crack growth analysis shows that the doubler increases the safety limit of the structure by a factor of 45. Associated test results showed that it would take two to three aircraft fatigue lifetimes (72000–108000 cycles) for a crack to propagate 1" beneath a reinforcing composite doubler. The doublers provide acceptable safety factors and the strain levels throughout the doublers and in the surrounding skin area are below the allowable levels. Finally, the damage tolerance analyses and comprehensive testing indicate that disbond and delamination flaws experience almost zero growth under normal operating environments. Thus, the

Table 35.2
Crack growth parameters for unrepaired skin and skin repaired with composite doubler.

Patch size 4.5'' × 3.75''		
Crack length	da for n = 1 Repaired	da for n = 1 Unrepaired
1.0''	2.729e-6	123.122e-6
1.5''	2.729e-6	261.355e-6
2.0''	2.729e-6	446.510e-6
2.5''	2.729e-6	676.158e-6
3.0''	2.729e-6	949.492e-6
Patch size 13'' × 9''		
Crack length	da for n = 1 Repaired	da for n = 1 Unrepaired
3.0''	2.457e-6	949.492e-6
3.5''	2.457e-6	1265.00e-6
4.0''	2.457e-6	1621.00e-6
4.5''	2.457e-6	2017.00e-6
5.0''	2.457e-6	2454.00e-6
6.0''	2.457e-6	3446.00e-6
7.0''	2.457e-6	4589.00e-6
Patch size 21'' × 13''		
Crack length	da for n = 1 Repaired	da for n = 1 Unrepaired
5.0''	2.251e-6	2454.00e-6
5.5''	2.251e-6	2930.00e-6
6.0''	2.251e-6	3446.00e-6
6.5''	2.251e-6	3998.00e-6
7.0''	2.251e-6	4589.00e-6
8.0''	2.251e-6	5883.00e-6
9.0''	2.251e-6	7323.00e-6
10.0''	2.251e-6	8909.00e-6

Skin: AL 2024-T3 (*t* = 0.080'').

inspection interval of 4500 flights (every ‘‘C’’, ‘‘D’’, or heavy maintenance check) is sufficient to provide more than one opportunity to find any doubler installation flaws.

35.4. Repair design validation

Strength and fatigue tests were completed to validate the composite doubler designs. The reliability and sensitivity of NDI was determined as it pertained to the

damage tolerance of the repairs. The goal of this effort was to validate the following aspects of the DC-10/MD-11 composite doubler repair initiative: (1) repair design, (2) repair analysis approach – stress analysis and damage tolerance, (3) finite element analysis models, (4) assessment of post-repair fatigue life, and (5) nondestructive inspection procedures. Two specimens were tested. One specimen contained a corrosion flaw with the maximum allowable material removal (50% thinning) and another specimen contained a skin impact flaw with the extreme out-of-plane deformation of $3/8''$.

Test Approach – (1) start with the DC-10/MD-11 fuselage pressurization stress spectrum in tension-tension testing (0–10 ksi) and magnify to a 70% overtest by applying a 0–17 ksi tension load spectrum, (2) conservatively test each specimen for up to four lifetimes of DC-10 aircraft (160000 cycles), (3) measure static strain fields at different stages of fatigue testing – assess changes in stress field and associated

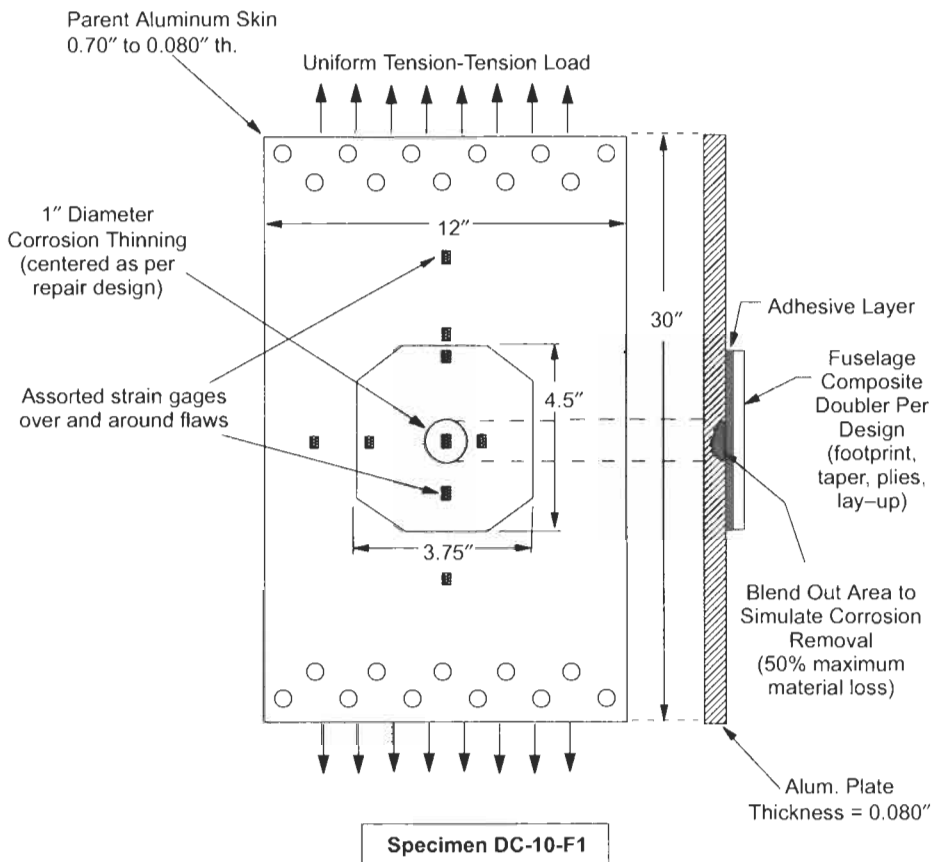


Fig. 35.5. Design and NDI validation test specimen for family of DC-10 composite doubler skin repairs (corrosion skin flaw).

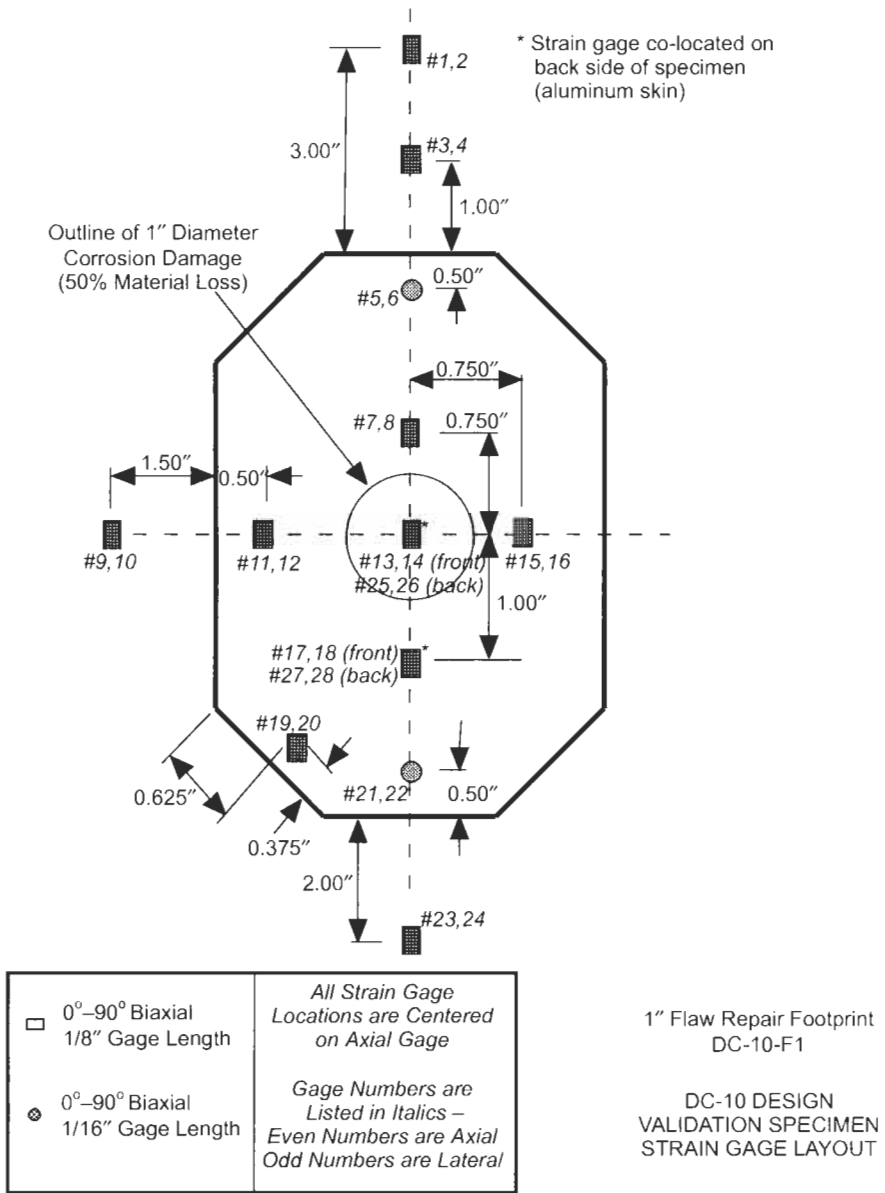


Fig. 35.6. Strain gauge layout for one inch flaw repair design validation test.



Fig. 35.7. Set-up for DC-10 composite doubler validation test.

performance of composite doubler, (4) frequently apply ultrasonic resonance (Bondmaster) NDI to each test specimen, and (5) follow fatigue tests with a static ultimate test (residual strength) to determine design margins and performance of composite doublers when the parent material yields (plastic strain regime). Figure 35.5 shows one of the design validation test articles for the extreme skin corrosion flaw and Figure 35.6 shows the associated strain gage layout. Results highlighted in this section will focus on the corrosion flaw repair. The validation specimens contained representative, yet upper extreme, flaws and the corresponding Boeing-designed doubler. Figure 35.7 shows a DC-10 doubler design validation test article undergoing fatigue and strength testing.

Strain Field Assessment – In general, it was observed that all strain responses from the simulated fuselage pressurization loads were linear. No residual strains were noted when the specimens were unloaded. Subsequent failure tests showed that the strains induced by the fatigue load spectrum, despite representing a 170% fuselage overpressure, were well inside the linear elastic regime for the 2024-T3 aluminum and Boron-Epoxy composite materials. The strains monitored in the

load transfer (tapered) region around the perimeter of the doubler were approximately 40%–50% of the total strain in the aluminum plate. The strain in the aluminum plate beneath the doubler was reduced in accordance with the strain picked up by the composite doubler. The load transfer values remained constant over four fatigue lifetimes indicating that there was no deterioration in the bond strength. To supplement the nondestructive inspection results, strain field assessments were used to show that there was no effect of multiple fatigue lifetimes on the patch performance. The strain field remained unchanged over 160000 fatigue cycles.

Ultimate Strength Results – Attempts were made at subjecting the design validation test specimen to ultimate tensile strength tests following the 160000 cycles of fatigue loading. The uniaxial load was uniformly increased until the specimen failed. Failure was defined as the point at which the structure could no longer sustain an increasing load. Figure 35.10 shows the strain field in specimen DC-10-F1 up through failure. The aluminum plate away from the doubler

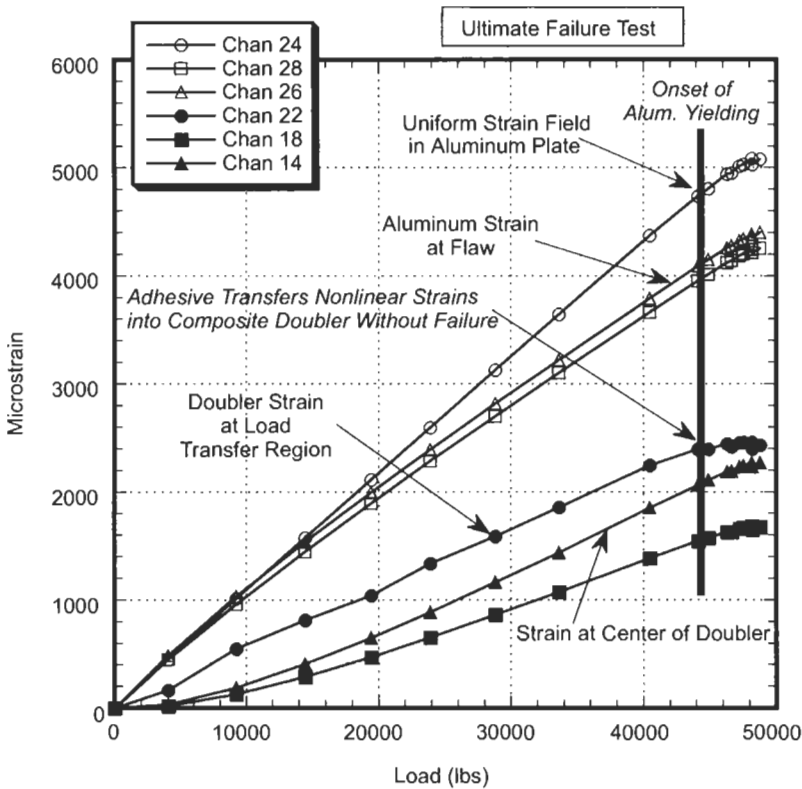


Fig. 35.8. Axial strain field during ultimate failure test of DC-10-F1 design (repair of 1" diameter flaws – 50% material thinning flaw).

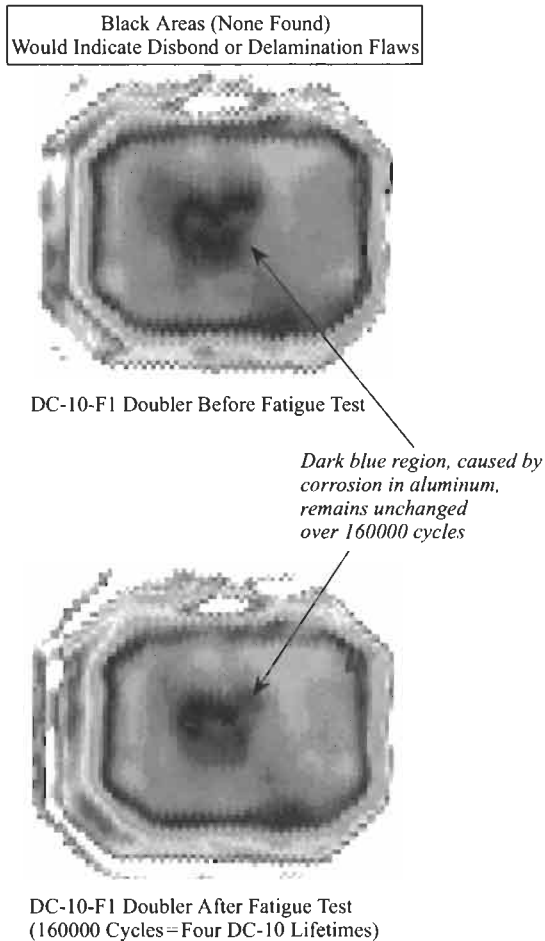


Fig. 35.9. Ultrasonic C-Scan of DC-10-F1 composite doubler before and after 160000 fatigue cycles (four lifetimes of DC-10 aircraft).

(channels 24) began to yield at approximately 44000 lbs (45.8 ksi), while the doubler continued to increase its load in a linear fashion. Unfortunately, failure occurred at the holes used to grip the specimen (55.7 ksi) and ultimate strength values for the repaired area could not be achieved. However, the ultimate strength tests were successful in loading the DC-10-F1 specimen into the plastic regime (past yielding).

The aluminum began its nonlinear response at the yield point indicated in Figure 35.8. Similarly, the composite doubler showed a slightly nonlinear behavior at this same load level. But the Boron-Epoxy laminate did not yield. The material properties for Boron-Epoxy indicate a yield stress of 185 ksi. Further, after specimen failure, the strain gages on the doubler returned to zero

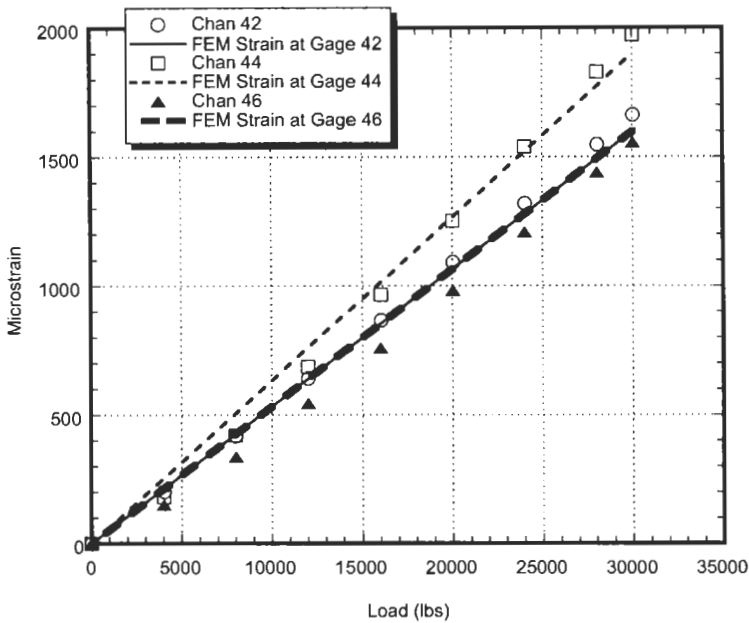


Fig. 35.10. Comparison of experimental and analytical (FEM) strains in the composite doubler.

indicating that the doubler did not undergo any plastic deformation. Thus, the nonlinear response in the doubler strain gages shows that the doubler is absorbing more strain and mirroring the response of the parent aluminum skin. Figure 35.8 illustrates an important performance feature of bonded composite repairs in that the adhesive is able to transmit stresses in the plastic regime and that yielding/loading beyond the initial aluminum yield level is required to fail the repair installation.

Inspection of Specimens Before and After Fatigue Tests – The repair design validation tests assessed the potential for loss-of-adhesion flaws (disbonds and delaminations) to initiate and grow in the composite doubler installation. Through transmission ultrasonic (TTU) inspections were conducted in an immersion tank and represent the most accurate and sensitive form of nondestructive inspection for this type of structure. It is not fieldable for most aircraft applications but it served as the optimum reference for the hand-held ultrasonic resonance and pulse-echo techniques. Both resonance and pulse-echo ultrasonic techniques were applied to the test specimens while in the fatigue test machine and are the techniques that are used for aircraft installations. Comparisons between the TTU and resonance/pulse-echo inspection methods showed excellent agreement and further validated their use for inspecting composite doublers in the field. The two C-scan images in Figure 35.9 compare

the specimen flaw profile before and after the fatigue and ultimate strength testing. Side-by-side comparisons show that the original corrosion flaw, which was detected prior to testing, remained unchanged even after multiple fatigue lifetimes and loads that exceeded yield strength of the aluminum skin. More importantly, the scans show that no disbond or delamination flaws were produced by the fatigue overtest of four aircraft lifetimes.

Validation of Analysis – The performance of the composite doubler repairs was analyzed using a finite element model (FEM) of the fuselage structure and Boron-Epoxy laminate. Results from the validated FEM were then used to predict the doubler stresses and the reduction in stress in the aluminum skin during maximum/extreme flight load scenarios. In general, comparisons with experimental data indicated that the FEM had sufficient accuracy (and conservatism) to support the Boron-Epoxy doubler design and analysis. Figure 35.10 compares experimental and analytical strain levels in the composite doubler and aluminum skin. In both cases the FEM is able to accurately predict the stress/strain field. The FEM predictions were particularly good in the area of greatest concern around the flawed region of the skin. The computer analysis and test data both verified the primary goal of the reinforcing doubler: reduce stress risers. Furthermore, the FEM was able to assess the damage tolerance and crack mitigation capabilities of the doubler using the full flight load spectrum. The associated damage tolerance analysis showed that the doubler exhibits sufficient strength to provide adequate fatigue enhancement over the full spectrum of environmental conditions.

35.5. Non-destructive inspection

Initial qualification of a repair prior to releasing an aircraft for service is an important consideration as is in-service inspections of repaired flaws. Validation efforts for the DC-10 inspections revealed that ultrasonic resonance and pulse-echo (dual-element pitch/catch mode) test methods work well in detecting flaws and mapping out flaw shapes in composite doublers. These two inspection methods were pursued because they are hand-held techniques involving relatively low-cost instruments and can be easily applied in the field. Inspection procedures have been written, validated, reviewed by Boeing, and are currently being incorporated into FedEx-approved process specs.

All of the DC-10 inspection work was built on the foundation of the extensive NDI validation activities conducted for the L-1011 composite doubler repair [see L-1011 application discussion in this chapter and nondestructive inspection section in Chapter 23]. Approval for the application of specific NDI techniques was granted by the FAA via an Alternate Means of Compliance for ultrasonic inspections, as well as, through the Service Bulletin that covered the entire L-1011 door corner repair and inspection process.

35.6. Current status of DC-10/MD-11 commercial aircraft repairs

The Pilot Program installations on FedEx aircraft were recently completed. Formal documentation, which will allow the FAA to properly direct the use of this technology, is also being completed. Six composite repairs were installed on DC-10/MD-11 aircraft. The repairs are being closely monitored for one year and inspections will occur every D-check thereafter. During the first year of operation, the doublers are being inspected at 60 day, six month, and one year intervals. A quality assurance inspection was also conducted immediately after each doubler was installed. In preparation for these aircraft repairs, appropriate installation and NDI training was conducted with FedEx's composite and NDT shops. All aspects of the composite doubler fabrication, installation, and quality assurance measures were incorporated into a Federal Express engineering order (EO). The EO generates all of the job cards needed to build, install, and inspect the repairs at the FedEx maintenance depot.

With the successful completion of the Pilot Program, the DC-10 Structural Repair Manual is being formally modified to include the family of fuselage skin composite doubler repairs. The SRM revision will take the form of a look-up table that will allow users to match flaw type and size with either a metallic repair or the equivalent composite doubler repair. The engineering drawings for the composite repairs will also be integrated into the SRM.

The Pilot Program and associated manual revisions represent a major milestone in the evolution and application of composite doublers. This effort is validating composite doublers for a number of high use applications. It is also streamlining the design-to-installation process in order to make the technology more amenable to wide scale use. In order to govern the appropriate use of composite repairs, an FAA Advisory Circular is being prepared. The AC will list the training, procedures, design guidelines, quality assurance, and inspections required for a maintenance depot to utilize this technology. It will be used by the FAA to assure the uniform and safe application of composite doublers by qualified maintenance depots using qualified personnel. Recent inquiries from transport, commuter, and general aviation manufacturers indicates an increase in support for composite doubler repairs on commercial aircraft. As more and more maintenance depots adopt composite doubler repairs, the Advisory Circular will help assure that this technology is applied properly and safely.

The project activities discussed here have helped eliminated obstacles to the use of composite doublers and have allowed airlines to take advantage of potential time and cost savings. A myriad of strength, fatigue, and failure tests have demonstrated that composite doublers are able to withstand extensive damage and non-optimum installations while significantly improving fatigue life and ultimate strength of the parent structure. The DC-10/MD-11 composite repair Pilot Program is now accumulating critical flight performance history to establish a track record for composite doubler repairs in the U.S. commercial aircraft industry. Overall, this program is demonstrating how composite

doubler repairs can aid aircraft Service Life Extension Programs and the technology transfer tasks are helping to foster widespread use of composite doubler repairs.

Chapter 36

CASE HISTORY: CF-116 UPPER WING SKIN FATIGUE ENHANCEMENT BORON DOUBLER

D. RAIZENNE

*Institute for Aerospace Research, National Research Council, Ottawa, Ontario,
Canada*

36.1. Introduction

The CF-116 A/D Freedom Fighter (CF-5) was last used in Canada as the lead-in trainer for the CF-18. It was first introduced into military service in Canada in the mid 1960s. Due to policy decisions by the Canadian Forces, it was prematurely retired from service in 1995. At the time of its retirement there were 44 aircraft in the fleet with an average fuselage life of 3500 flying hours.

In 1991, during a depot level inspection, fatigue cracks were found in the upper wing skin fastener holes directly above the wing critical radius where the wing skin was fastened to the root rib and the 44% rear spar.

The focus of this chapter is on the development of a composite bonded doubler as an enhancement for the CF-116 upper wing skin.

An earlier paper [1] described the progress of the work up to 1993. As a case history contribution to this book the following topics are described: the problem, the repair approach, the doubler design analysis processes, the installation process, the structural qualification program and in-service experience.

36.2. Background

The CF-116 uses a single wing box structure – six ribs and six spars per side sandwiched between an upper and lower wing skin. The two wing skins are chem milled from Al 7075-T651 plate. The upper wing skin is fastened to the underlying structure with Hi-Lok fasteners and the lower wing skin with interference fit fasteners. The upper wing skin is 0.335 in. (8.5 mm) thick at the fastener hole

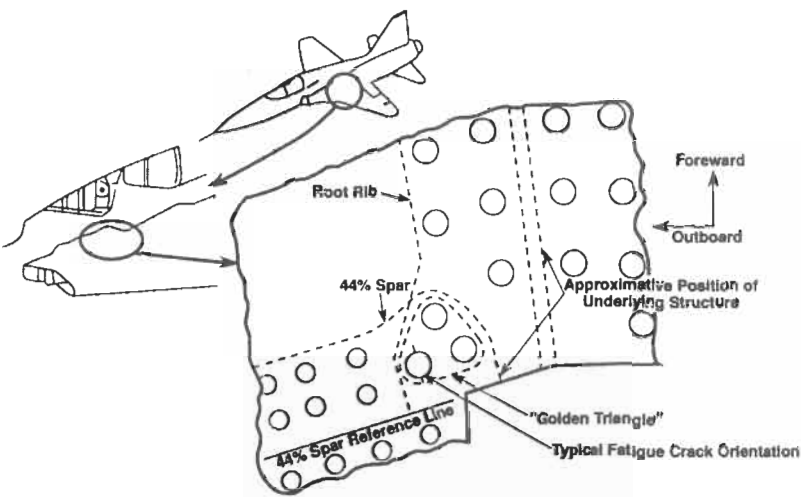


Fig. 36.1. CF116 and location of upper wing skin fastener hole cracks.

locations. Figures 36.1 and 36.2 show the location and details of the “golden triangle” fastener holes.

Using eddy current and liquid penetrant inspection techniques, fatigue cracks were found in 8 of 18 aircraft inspected. The cracks in the bore and countersink of the fastener holes ranged in length from 0.030 to 0.105 in. (0.76 to 2.67 mm). In Figure 36.3 the orientation and size of a typical fatigue crack in this area are shown. Fractographic analysis [2] confirmed that the crack propagation mechanism was fatigue. The crack initiation mechanism was assumed to be a tensile residual stress zone caused by a compressive overload – high positive “g” maneuver.

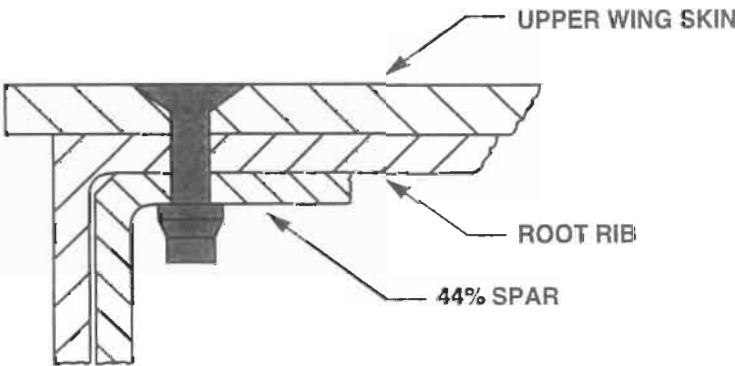


Fig. 36.2. Fastener hole configuration.

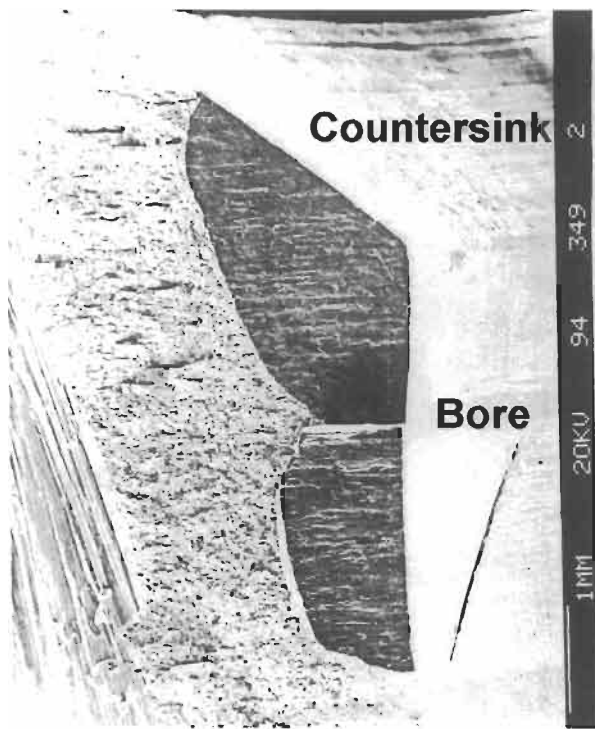


Fig. 36.3. SEM photograph showing orientation and size of fastener hole fatigue cracks.

36.2.1. Compression induced fatigue cracking

Fatigue cracking in a compression load dominated structure such as an upper wing skin is not a common occurrence. However if the wing experiences a high positive “g” loading, the resultant compressive stress in the wing skin when coupled with the stress concentrations in the fastener holes can result in localized compressive yielding in the form of hole elongation. This compressive yielding is balanced by a tensile residual stress zone that can raise the local mean applied stress level such that a fatigue crack can initiate and grow in a compression dominated environment.

Literature on compression induced fatigue cracking is limited. In a review of this subject, Conor [3] sites 15 cases of fighter aircraft and helicopter components where compression induced fatigue cracks were identified. In only one instance was the fatigue crack growth found to decrease as the crack grew longer. Fractographic analysis of the CF-116 fastener holes indicated there was no evidence that the striation spacing was reducing as the cracks grew outward from the hole (see Figure 36.4) [2]. This implied that there were sufficient negative “g” maneuvers in the aircraft load spectrum to propagate the crack under tension loading after it had initiated and propagated through the residual tensile stress zone.

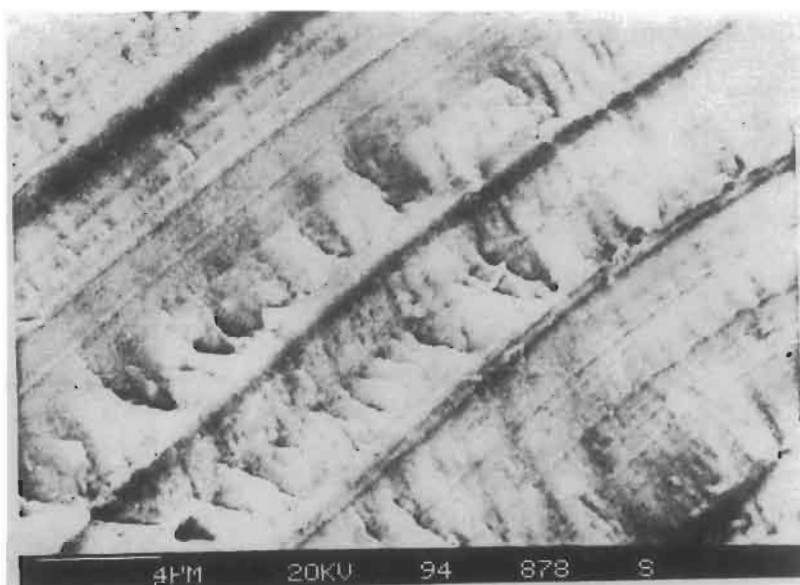


Fig. 36.4. (SEM) striation spacing at crack front, 0.025 in. (0.64 mm) from countersink face.

36.3. Repair considerations

The repair process carried out consisted of a metallic repair that met the residual strength, static and fatigue design requirements for the wing skin. A composite fatigue enhancement doubler was to be bonded onto the wing skin to reduce the strain levels in the affected area.

The details of the metallic repair included:

- oversize each hole to remove any eccentricity, evidence of fatigue cracking and potential plastic zone;
- take an additional “confidence cut” to produce a “zero time” hole;
- install a press fit steel bushing and blind interference fit fastener (to replace the original Hi-Lok fastener).

The use of a press fit bushing with an interference fit fastener was the basis for the metallic repair scheme. The approach was similar to that developed for compression induced fatigue cracks on the F-15 wing upper spar cap [4]. The press fit bushing will reduce the tensile stress range in the skin. The blind interference fit fasteners will assist the press fit bushing, transfer compressive stress across the fastener hole and reduce the hole stress concentration effect.

The problem with a press fit bushing combined with a blind hole interference fit fastener is the clamp up process is difficult to control. This was highlighted when measurements were taken of the original Hi-Lok fastener hole diameters that were inspected for cracking. The interference fit varied from 0.0 to +0.0025 in. (+0.0064 mm).

Continuing inspection of the area was also a concern, for no reliable inspection technique had been developed that would detect similar cracks with the bushing and fastener installed. Reliable inspection could only be achieved by wing disassembly, removal of the fastener and bushing and inspecting with an eddy current bolt hole probe and liquid penetrant. This inspection requirement imposed a severe penalty to the fleet operations. In addition, the collateral damage caused by bushing and fastener removal limited the number of inspections.

36.4. Bonded composite doublers

In parallel to the development of the above repair scheme, the NRC and Canadair were requested to carry out the design, analysis and development of a bonded composite doubler that would be applied over the golden triangle fasteners. This doubler would be a fatigue “enhancement” and no benefits from it were considered in the design and approval processes for the metallic repair scheme.

Bonded composite doublers have several advantages over conventional riveted or bolted metallic doublers: the elimination of additional fastener hole stress concentrations, a smaller doubler size, ease of application and lower cost. The main disadvantage is that the application of a bonded doubler is very process dependent with particular attention to the surface treatment of the metallic substrate.

A bonded composite doubler was selected over a bolted titanium doubler for two reasons:

- the limited clearance between the upper wing skin and the fuselage placed a limit on the doubler thickness, and
- a bolted titanium doubler would have required a large area for load transfer with many additional fastener holes.

36.5. Doubler design and analysis

The design for the CF-116 doubler faced several challenges:

- The CF-116 upper wing skin with a thickness of 0.335 in. (8.5 mm) was a thick section bonded repair application. With a 50% wing skin stress reduction target, this meant very high peel stresses at the edge of the doubler.
- The doubler was to be bonded to one side of the wing skin that would cause out-of-plane bending effects.
- The wing skin was highly loaded in compression, $-4500 \mu\text{in/in.}$ limit load.
- The doubler was to be bonded over 26 steel fasteners.

A three phase design process was used for the doubler. In the first phase the doubler was sized using extensional stiffness and strength to match the stress reduction criterion for the “golden triangle” area. In the second phase the adhesive bondline was analyzed under limit load conditions to determine the magnitude of the adhesive shear stress distributions. In the third phase detailed finite element

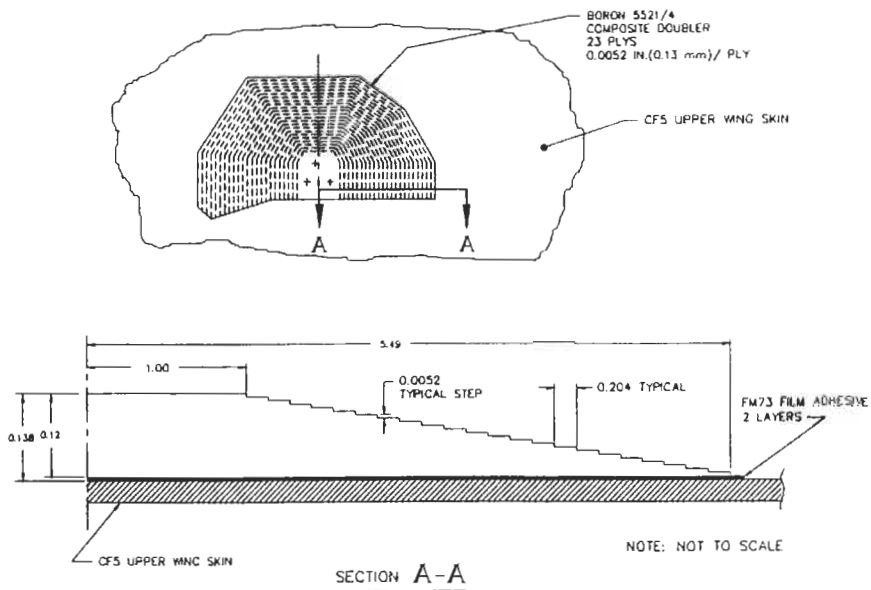


Fig. 36.5. Details of boron doubler.

analysis was carried out to predict the effect of the doubler on the stress level in the wing skin. The details of the final doubler design are provided in Figure 36.5.

Step 1: Limit load conditions

The limit load condition P_{limit} for the golden triangle area of the upper wing skin was a +7g maneuver. This corresponded to a running load of $-15,800 \text{ lbf/in}$ (-2.77 kN/mm) and a strain level of $-4500 \mu\text{in/in}$.

Step 2: Critical load direction

The primary loads (P_x) in the golden triangle area run parallel to the 44% spar. This agrees with the fractographic analysis [2] that determined that the cracks grew perpendicular to the spanwise direction. Chordwise bending (P_y) and shear (P_{xy}) were neglected in the doubler design.

Step 3: Repair section stiffness design goal

An average upper wing skin strain reduction of 40% was set as a doubler design goal.

Step 4: Doubler and adhesive materials

Textron Specialty Materials boron 5521/4 prepreg was selected for this application because of its superior strength and stiffness under compressive loading conditions (see Appendix A) and for its low (250°F) cure temperature. Boron has a coefficient of thermal expansion closer to that of aluminum than graphite. This reduces the thermal residual strains induced in the wing skin during the bonding process. Boron's low electrical conductivity reduces galvanic corrosion with aluminum and allows eddy current inspection of the substructure.

The choice of a structural film adhesive for bonded repair is driven by the adhesive's shear strength, fatigue resistance and environmental resistance to moisture and temperature variations. An adhesive used in many bonded repair applications that satisfies these criteria was Cytec's FM73, an epoxy nitrile system with a recommended cure temperature of 250 °F.

To minimize the thermal residual stresses for an elevated temperature cure, the cure temperature was set at 185 °F. Both boron 5521/4 prepreg and FM73 adhesive can be cured at 185 °F over a longer cure cycle. Similar mechanical performance to the recommended 250 °F cure cycle can be achieved. It was also decided to cocure the boron prepreg and adhesive in order to eliminate a secondary bond between a precured doubler and the adhesive layer. The boron doubler was B-staged [5] prior to bonding in order to eliminate excessive porosity. One of the disadvantages of cocuring bonded repairs was that the design allowables for the adhesive and the composite prepreg were reduced to reflect out-of-autoclave cure conditions.

Step 5: Doubler stacking sequence and overlap thickness

The section stiffness ratio, S , is the ratio of the doubler extensional stiffness to that of the wing skin. It was used to determine the doubler thickness t_R . The equivalent compression modulus for a composite doubler is a function of the doubler's stacking sequence. As explained in Step 2, the doubler was used to reduce the load in the spanwise direction only. Consequently the optimal stacking sequence was unidirectional, parallel to the 44% wing spar. The doubler's equivalent compression modulus was the 0° compression modulus for the unidirectional boron prepreg. This optimized the doubler for stiffness and thickness. A stiffness ratio of 1.1 required 23 plies of unidirectional boron 5521/4 at 0.0052 in./ply (0.0132 mm). See Appendix A for boron 5521/4 properties.

Step 6: Doubler overlap length, taper angle and shape

The full thickness length of the doubler L_R is a function of the load transfer length, β^{-1} , from the edge of the overlap for a 95% reduction in the adhesive shear stress. Rose [6] defines the load transfer length by the adhesive shear stress decay from the edge of the overlap in the y direction:

$$\tau_A(y) = \left(\frac{N_X}{E_p t_p} \right) \left(\frac{G_A}{t_A} \right) \left(\frac{\sinh \beta y}{\beta \cosh(\beta L_R/2)} \right),$$

where the load transfer occurs over a length β^{-1} at the edges of the doubler where β^{-1} is a function of doubler stiffness, plate stiffness and adhesive properties G_A and t_A .

$$\beta^{-1} = \left\{ \left(\frac{G_A}{t_A} \right) \left(\left(\frac{1}{E_{AI} t_{AI}} \right) + \left(\frac{1}{E_p t_p} \right) \right) \right\}^{-0.5}$$

Using the RT/DRY properties from Appendix A, $\beta^{-1} = 0.8$ in. (20.3 mm) β^{-1} can be used to size the overlap length L_R of the doubler. Baker [7] recommends a conservative overlap length of $6\beta^{-1}$. Hart-Smith [8] describes L_R as a multiple of

the substructure thickness (≈ 30 to 80 times) depending on how the joint is modeled (double-lap to single-lap unsupported).

Using the Baker criterion, $L_R = 6 \times 0.8 = 4.8$ in. (121 mm)

Using the Hart-Smith criterion, $L_R = 30 \times 0.33 = 10$ in. (254 mm)

An L_R of 2.0 inches (50.8 mm) was selected for the CF-116 doubler that was unconservative based on the above criteria. The “undersizing” of L_R was balanced by the selection of the doubler taper angle. A doubler must be tapered from the full section thickness t_p in order to minimize adhesive peel stresses and to gradually transfer the load into the doubler. A taper angle of 1.25° was selected that corresponds to a 5.5 inch (140 mm) taper length. For the CF-116 doubler there were 23 single ply drop-offs spaced 0.2 in. (5.08 mm) apart (see Figure 36.5).

The design process must ensure that the initial plies at the edge of the taper are capable of withstanding the strain levels that are transferred into the doubler from the substructure. This issue was addressed in the bondline analysis.

The doubler aspect ratio (length to width) will affect the stress reduction in the structure. The optimum aspect ratio is 1. A rectangular shape is less efficient than an elliptical shape [9]. For an edge application like the CF-116 a semi-circular doubler shape was the optimum shape.

Step 7: Bondline analysis

A bondline analysis was required to determine the elastic and elastic-plastic stress distributions in the adhesive and the stress distribution in the doubler. A design goal for the bondline was to maintain an elastic state of stress up to limit load conditions. A closed form 2D analysis computer program A4EI [10] was used to verify the initial design assumptions. A4EI accounts for adherent properties: stiffness, stiffness imbalance, thermal expansion mismatch, step thickness and step length, adhesive properties (deformations, thickness, disbands and porosity), and loading conditions (tension, compression and in-plane shear). The program does not predict the adhesive peel stresses that are highest at the edges of an externally bonded doubler. A4EI also assumes a cohesive failure mode in the bondline and does not consider an interfacial (adhesion) failure mode.

For the A4EI analysis a 23 ply unidirectional boron 5521/4 cured doubler was bonded to a Al 7075-T651 plate that was representative of the CF-116 upper wing skin. This is an idealized model, for the effects of the 26 fastener holes and the load transfer of the underlying substructure were not considered in the analysis. The material properties for the boron, aluminum and adhesive are provided in Appendix A. The A4EI analyses were used to determine the static margin-of-safety for the doubler in compression under RT/DRY and HOT/WET conditions. The following assumptions were applied to the analyses:

- As the doubler was considered a fatigue enhancement, there was no requirement to use the ultimate load case. Only limit load conditions were used;
- The doubler taper angle was sufficiently small to preclude concerns over peel stresses;
- A cohesive bondline failure mode would prevail;
- A 0.75 knockdown factor, K_1 , for RT/DRY to HOT/WET for the boron 5521/4;

- A 0.80 knockdown factor, K2, for boron 5521/4 cured at 185 °F for 8 h under vacuum bag pressure;
- A 0.70 knockdown factor, K3, to account for variations within the FM73 adhesive cured at 185 °F for 8 h under vacuum bag pressure;
- Out-of-plane bending caused by doubler and by thermal mismatch between the boron doubler and the aluminum wing skin was neglected;
- Thermal residual strains (positive) were neglected. A high level of mechanical restraint on the wing skin was assumed to limit thermal expansion during cure;
- The stress concentrations caused by the 26 fastener holes covered by the doubler were neglected.

The results are summarized in Table 36.1 for two bondline thicknesses, 0.009 and 0.018 in. (0.29 and 0.58 mm). These results were then compared to the limit load/elastic bondline design criteria of $-4450 \mu\text{in/in.}$ strain or -15800 lbf/in. (-2.78 kN/mm) running load. As seen in Table 36.1 a two ply bondline will satisfy the design criteria for the RT/DRY condition.

The limiting factor for the elastic-plastic strength of the bondline was the compression allowable (-23000 lbf/in (-4.03 kN/mm)) for the aluminum wing skin. The boron compression allowables (-1530 lbf/in (-0.267 kN/mm) per ply RT/DRY and -1150 lbf/in (-0.201 kN/mm) per ply HOT/WET) were never exceeded in the analyses. The bondline strengths are limits against which operating running load values can be compared to determine the loading of the adhesive.

Step 8: *Adhesive margin-of-safety calculation*

The adhesive margin-of-safety was based on the elastic joint strength for two layers of FM73 calculated by A4EI. The formula used for the calculation is the following:

$$\text{Margin-of-Safety} = \left[\left(\frac{1}{(P_{\text{limit}}/\text{Elastic Joint Strength})} \right) - 1 \right]$$

Using an P_{limit} running load of -15800 lbf/in (-2.77 kN/mm) and using the adhesive values in Table 36.1, the margin-of-safety calculations for an elastic joint are $+0.07$ for RT/DRY and -0.44 for HOT/WET. A suggested value for RT/DRY was $+0.25$.

Table 36.1
A4EI bondline strength values for one and two layers of FM73.

	Elastic Joint Strength lbf/in (kN/mm)	Elastic-Plastic Joint Strength lbf/in (kN/mm)	Potential Joint Strength lbf/in (kN/mm)
RT/DRY (one layer)	-13900 (-2.43)	-23000 (-4.03)	-31300 (-5.48)
HOT/WET (one layer)	-7200 (-1.26)	-16000 (-2.80)	-16000 (-2.80)
RT/DRY (two layer)	-16900 (-2.96)	-23400 (-4.10)	-37500 (-6.57)
HOT/WET (two layer)	-8930 (-1.56)	-22900 (-4.01)	-22900 (-4.01)

Although the margins-of-safety are low, the allowables and the knockdown factors used in the A4EI analyses were conservative and the elastic performance of the bondline was only a design goal and not mandatory.

Step 9. *Finite element analysis*

A finite element analysis of the doubler and wing skin was carried by Canadair to predict the effect of the doubler on the stress level in the wing skin [11]. The adhesive between the doubler and the skin was not modeled because the adhesive shear strains in the golden triangle area are low. The FEM analysis predicted a 47% stress reduction on the exterior surface of the wing skin under the doubler and a 37% stress reduction on the interior surface of the wing skin.

The FEM analysis also predicted a significant (28%) out-of-plane bending effect at the edge of the doubler. This was attributed to the shift in the neutral axis of the wing skin caused by the one-sided doubler.

36.6. Doubler manufacturing and installation procedures

A detailed doubler manufacturing and application procedure [12] was written and is summarized as follows.

For boron doubler manufacturing:

- Lay up reverse stacking sequence 23 ply boron doubler.
- B-stage doubler in autoclave at 195 °F and 100 psi (689 kPa) pressure for 30 min.

For boron doubler application:

- Remove paint from wing skin using chemical strip.
- Remove sulfuric acid anodizing using 75 μ m diameter aluminum oxide grit blast.
- Blow off loose grit with nitrogen gas.
- Apply 1% γ -glycidoxypropyltrimethoxy silane solution.
- Apply Cytec BR127 corrosion inhibiting primer.
- Place two layers of Cytec FM73 film adhesive over bondline.
- Place B-staged boron doubler over FM73 adhesive.
- Vacuum bag as shown in Figure 36.6 and cocure adhesive and doubler for 10 h at 12 to 14 psi (83 to 96 kPa) vacuum pressure at 185 °F.
- Inspect doubler using ultrasonic pulse echo technique.

The complex aluminum substructure at the doubler location required a heat survey to measure the heat distribution during the cure cycle. Large thermal gradients in the bondline area (185 °F \pm 40 °F) were measured when a single zone heater blanket was used. A customized etched foil silicone three zone heat blanket was designed and manufactured that provided a uniform bondline temperature of 185 \pm 4 °F.

For process control, each boron doubler application included ASTM wedge crack growth [13] and single lap shear [14] tests on “traveler” coupons.

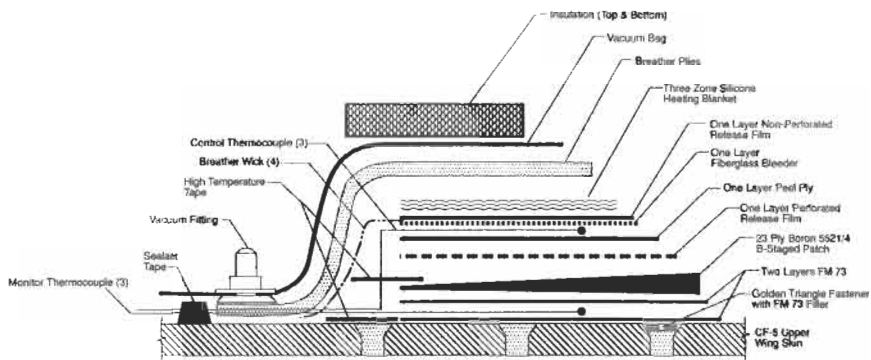


Fig. 36.6. Boron doubler bagging sequence. (Note location of embedded thermocouples in bondline.)

36.6.1. Doubler qualification testing

The CF-116 upper wing skin doubler was structurally qualified in two stages. The first stage was a coupon test program. An instrumented test coupon, shown in Figure 36.7, was used to verify the A4EI analysis and to measure the fatigue resistance of the bondline. The test coupon was strain gauged in the bondline and on the boron doubler to verify the strain reduction in the aluminum plate. For the bonding procedure the aluminum plate was constrained to limit the amount of thermal expansion and out-of-plane bending that simulated the constraint on the wing skin. The test coupon was loaded to $N_{ultimate}$ ($-6600 \mu\text{in/in}$) in a -35°F enclosure. Fatigue testing included 3000 cycles from 0 to P_{limit} and 50000 cycles from 0 to $0.5P_{limit}$. The test coupon passed both the static and fatigue testing and the measured strain levels approximated those predicted by the A4EI analysis. Given the conservative allowables/knockdown factors used in the A4EI analyses failure of the test coupon was not expected.

The second qualification stage involved applying a doubler to the CF-116 full scale durability and damage tolerance test (FSDADTT) that was carried out at Canadair from 1990 to 1994. The objective of the CF-116 FSDADTT was to extend the fuselage life from 4000 to 6000 h and investigate the possibility of a further extension to 8000 h. The CF-116 FSDADTT afforded an excellent opportunity to validate the metallic repair and the effectiveness of the doubler using a realistic loading spectrum. In the CF-116 load spectrum the $+7 \text{ g } P_{limit}$ was applied on average once every 14 simulated flight hours.

A boron doubler was bonded onto the wing skin on the right side while on the left side there was no reinforcement. Strain gauges were installed on both sides of the wing in order to compare the strain distributions on the upper wing skin with and without the doubler. Figures 36.8 and 36.9 detail the strain gauge locations and their respective limit load strain levels. In Table 36.2 a comparison is made of the strain levels between the patched and unpatched sides of the wing. In the golden triangle area the strain level reduction was 50% (comparing PA-5 and ZA-13) on

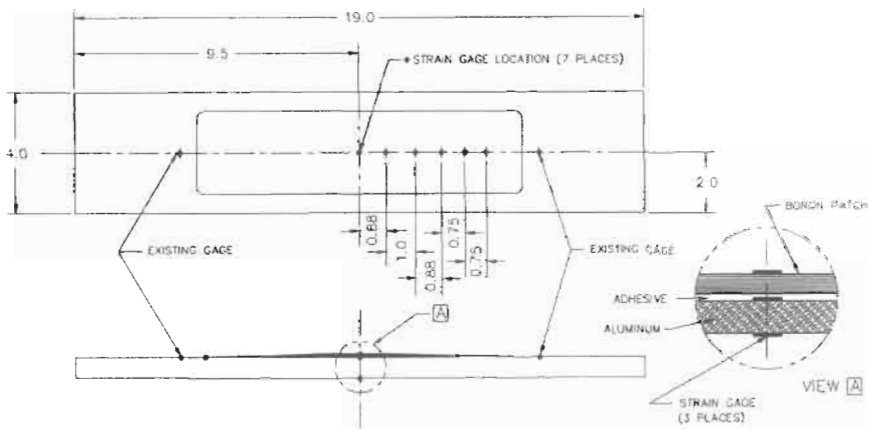


Fig. 36.7. Static and fatigue test coupon.

the surface of the wing skin. This strain reduction would decrease towards the underside of the wing skin that would result in an average through-the thickness strain reduction approximating the design goal of 40%.

The stiffening effect of the doubler increased the local strain level in the wing skin at the edge of the doubler. Comparing PA-9 and ZA-37, there was a 20% increase. This localized increase in strain could cause wing skin cracking or initiate doubler disbonding.

These measured strain values described above were in good agreement with the FEM results.

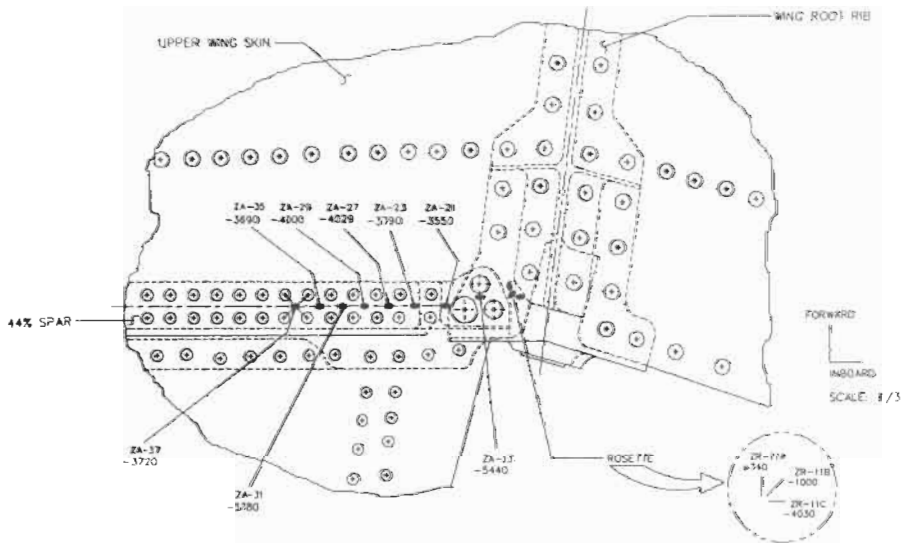


Fig. 36.8. Limit load strain data on unpatched left side of CF116 FSDADTT.

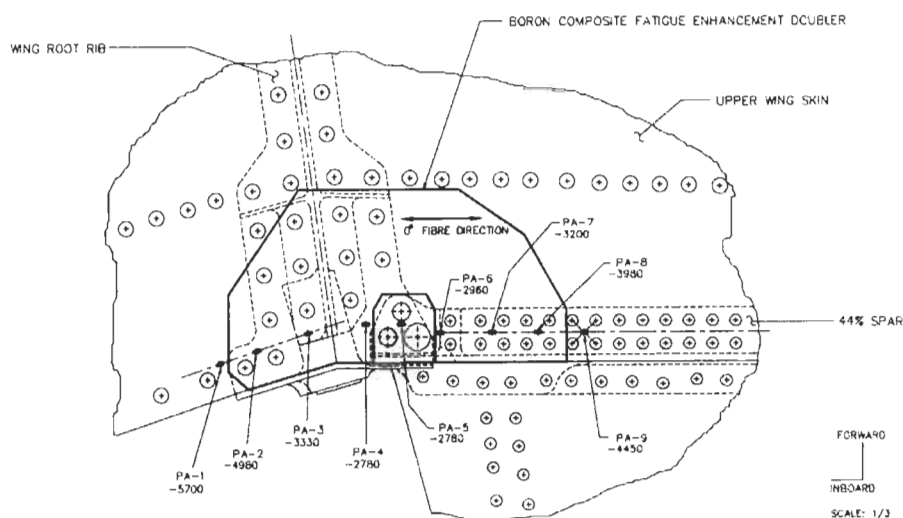


Fig. 36.9. Limit load strain data on patched right side of CF116 FSDADTT.

Table 36.2

Comparison of patched and unpatched wing skin strain levels ($\mu\text{in./in.}$).

No Doubler	-3720	-3780	-4029	-3550	-5440	-4030
Fig. 36.8	(ZA-37)	(ZA-31)	(ZA-27)	(ZA-21)	(ZA-13)	(ZR-11C)
With Doubler	-4450	-3980	-3200	-2960	-2780	-2780
Fig. 36.9	(PA-9)	(PA-8)	(PA-7)	(PA-6)	(PA-5)	(PA-4)

Using ultrasonic NDE, disbonds were detected at the outboard and inboard edges of the doubler after 1500 h of spectrum loading. The disbonds then grew inward toward the golden triangle area. At 2000 h, with the doubler effectiveness over the golden triangle area reduced by 50%, the doubler was removed. Figure 36.10 shows the location and size of the disbonds. A series of matrix cracks were also observed that ran parallel to the fiber direction. These cracks were not unexpected as the doubler was designed with chordwise strength provided by the matrix material only.

A second doubler was installed that remained completely effective for 3800 h after which the test was stopped. Matrix cracking was detected after 1500 h.

36.7. Doubler fractographic analysis

An examination of the fracture face of the first doubler indicated that the disbond initiated at the first ply between the boron fiber/matrix interface (Figure 36.11). The disbond followed the same path for the complete disbond.

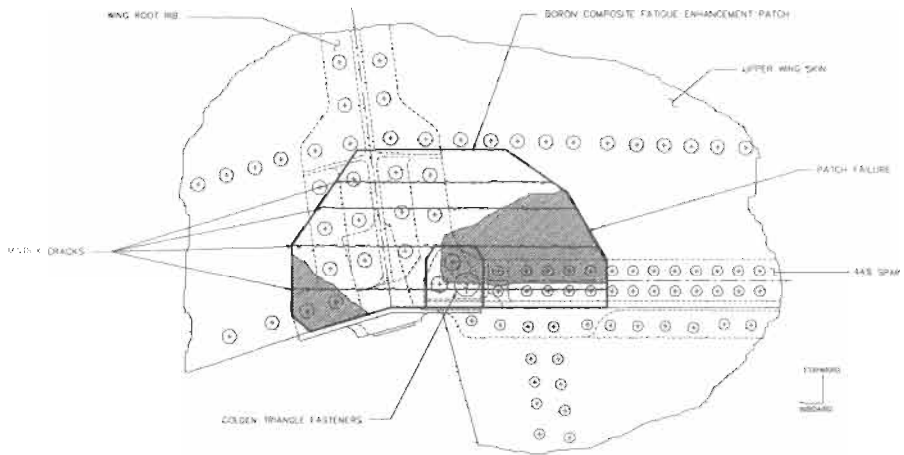


Fig. 36.10. Doubler disbond after 2000 h of spectrum testing.

There was no evidence of cohesive failure of the FM73 adhesive or interfacial failure between the aluminum wing skin and the FM73 adhesive.

A scanning electron microscope (SEM) examination was then carried out on selected locations. The dominant fracture mechanism is illustrated in Figure 36.12 –



Scale: 20x's

0° Fibre Direction

Fig. 36.11. Photomicrograph of fracture face showing primary failure mode interfacial failure between the boron fibers and the epoxy matrix.

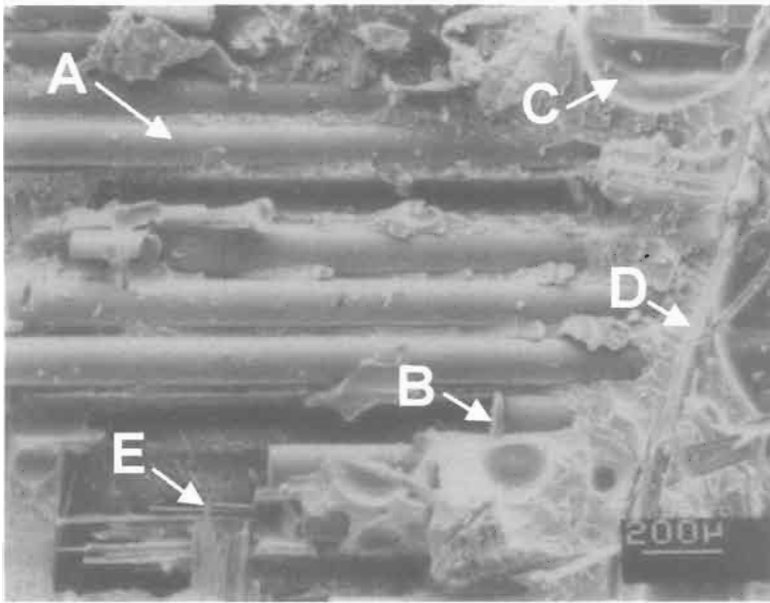


Fig. 36.12. (SEM) Key fracture features (a) fiber/matrix interfacial failure (b) fiber fracture (c) adhesive porosity (d) adhesive carrier (e) prepreg carrier.

interfacial failure between the boron prepreg matrix and the boron fiber. There are no significant hackles in the matrix, which indicates that the interfacial failures occurred before a general fracture in the matrix could develop. The majority of the fracture plane was on or in the doubler ply adjacent to the FM73 adhesive. The fracture surface of the locally exposed matrix in the second and third doubler plies (Figure 36.13) looks different from the dominant fracture surface on the first ply discussed earlier. Here the fiber/matrix bond remained generally intact and the matrix fracture shows shallow hackle and cusp formations. This indicates that the boron fiber/matrix interfacial failure observed in the first ply had not progressed into the adjacent plies.

There is a limited amount of fractured boron fibers, as shown in Figure 36.14. The exposed cross sections of these fibers show conical fractures with radially oriented lamella-like surface ridges. The flush light spot in the fiber centers is the remnant of the tungsten wire on which the boron was deposited during the production of the fiber. The radial ridges or river markings on the fracture face indicate the locations of the initiation sites on the circumference of the fiber.

36.8. Fleet experience

It should be noted that the CF-116 fleet was undergoing an upgrade program during this period of time that included new wings. The new wing skins were

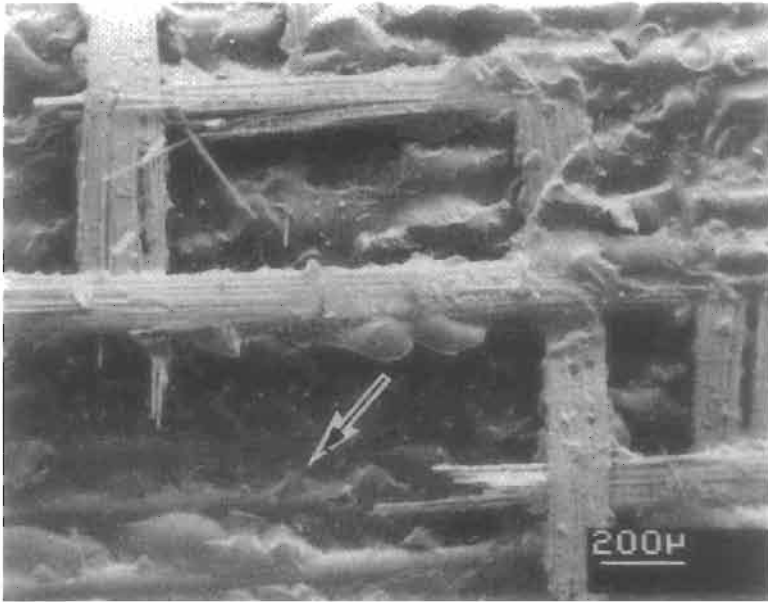


Fig. 36.13. (SEM) Matrix hackles and cusps on top of second boron ply.

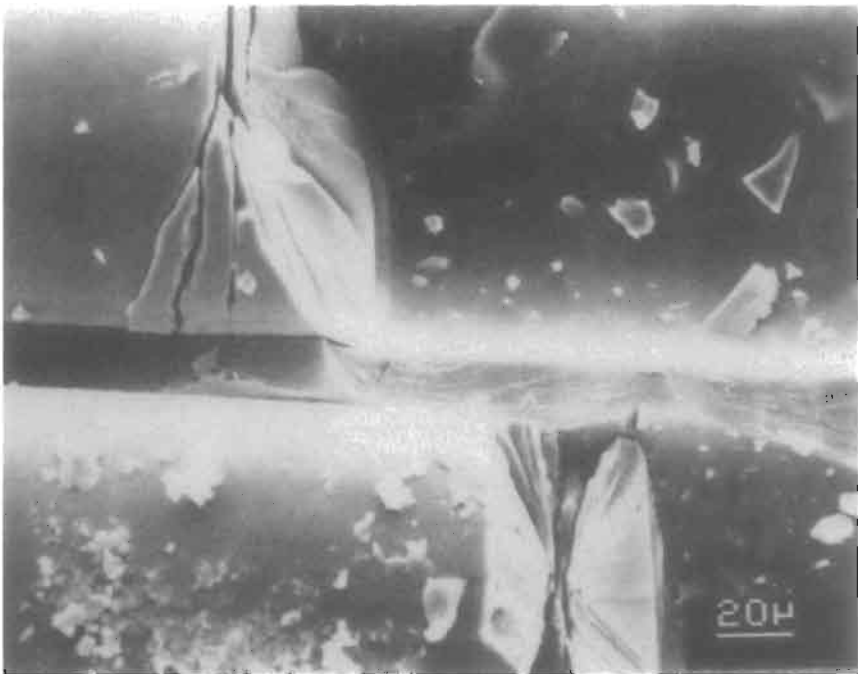


Fig. 36.14. (SEM) fracture faces from two boron fibers.

Table 36.3
CF116 fleet data.

Wing# (Tail #)	Wing hrs at retirement	Doubler hrs	Comments
1065 (704)	2673	323	
1005 (705)	1690	283	
1059 (826)	4146	383	Disbond, edge of doubler, detected at 180 h
1002 (702)	1765	75	Disbond, golden triangle area, detected at 18 h
2015 (721)	4375	442	Disbond, outside golden triangle area, detected at 430 h
2029 (829)	2560	195	
2030 (830)	2439	80	
1068 (759)	2840	216	Disbond, outside golden triangle area, detected at 20 h
2001 (801)	2559	60	
2002 (802)	2142	179	
1040	3201	111	
1009 (1004)	3302	205	
BAW101*	228	228	
BAW102*	157	157	
BAW104*	138	138	
BAW105*	16	16	

* New wings, no repair scheme with boron doublers

manufactured from machined Al 7075-T651 plate. Hi-Lok fasteners were used in the golden triangle fastener holes. Boron doublers were also used on the new wings.

Before the CF-116 fleet was retired from service there were data collected on the performance of the doublers. The performance data were in the form of ultrasonic inspections that were carried out at intervals of 20 flying hours. The portion of doubler inboard of the golden triangle fasteners was not inspected because it was under the fuselage skin. The data are provided in Table 36.3 and are summarized below:

Repaired wings flown:	12
New wings flown:	4
Boron doublers installed:	32
Doubler partial disbonds:	4
Doubler complete disbonds:	0
Total boron doublers flying hours:	3100
High time wing hours (with disbond):	442
High time wing hours (without disbond):	323
High time wing calendar time (months):	24

Observations with respect to the data are the following:

- Three of the disbonds initiated in the golden triangle area. These disbonds did not show evidence of growth after detection.
- The fleet inspection data did not show evidence of matrix cracking that was found in the full scale test.

- The single edge disbond was approximately 2.75 in. (70 mm) along the edge of the doubler and 0.75 in. (19 mm) into the doubler.
- The disbanded doublers remained in place. The failure morphologies could not be confirmed.
- The doublers with disbands were installed by one of the three organizations that installed doublers indicating possible processing problems.

36.9. Discussion

Fastener hole cracking in the CF-116 upper wing skin was an example of compression induced fatigue cracking, a rare form of fatigue cracking given the predominance of compressive loading in the upper wing skin. With fatigue cracks detected in 8 of 18 aircraft inspected, this problem was not isolated to a single overload incident on one aircraft. The usage role for the CF-116 aircraft fleet would have included significant numbers of high positive “g” maneuvers for crack initiation as well as large numbers of high negative “g” maneuvers for continued crack propagation.

The metallic repair scheme was developed through analysis to meet the residual strength, static and fatigue requirements without the composite doubler. Inspectability of the fastener holes through disassembly of the repair scheme posed a problem.

The use of a bonded composite doubler as a fatigue enhancement was viewed as insurance for the metallic repair scheme. As long as the doubler was in place the strain level surrounding the fastener holes was reduced by approximately 40%. The qualification of the composite doubler as a fatigue enhancement was carried out quickly through analysis, a limited test program and the development of a detailed doubler application specification. This allowed for a timely resolution of a major operational problem for the Canadian CF-116 fleet.

No doublers were applied to cracked or unrepaired fastener holes. Had it become necessary to raise the status of the doubler from an “enhancement” to a full repair scheme for primary structure, it was recognized that an extensive test program would have been required to ensure that the probability of failure of the patched structure was equal to or less than the probability of failure demanded by the original wing design requirements.

36.10. Conclusions

- Fatigue cracks were found in the CF-116 upper wing skin fastener holes. Crack initiation was believed to be the result of high compressive loading. There was no fractographic evidence to indicate that the crack growth rates decreased as the crack extended past the tensile residual stress zone at the edge of the fastener hole.

- The mechanical repair scheme for the wing skin fastener holes consisted of damage removal and hole oversizing followed by a press fit steel bushing and a blind hole interference fit fastener. Through analysis, the repair met the required residual strength, static, and fatigue requirements for the upper wing.
- A boron doubler was designed as a fatigue enhancement to reduce the strain level in the wing skin area by 40%.
- Qualification of the doubler was carried out analytically and through testing. Analyses of the boron doubler, the adhesive and the upper wing skin were carried out using both closed form solutions and finite element analysis. Coupon tests and the CF-116 full scale test were used for static and fatigue qualification of the doubler.
- After 1500 h of fatigue testing on the CF-116 full scale test, two disbonds at the edge of the doubler were detected using ultrasonics. At 2000 h the doubler was removed. Subsequent failure analysis indicated that the doubler disbond mode was a boron fiber/matrix interfacial failure.
- A manufacturing and processing specification was developed for the boron doubler.
- The fleet experience with the 32 installed doublers indicated good performance.

36.11. Composite repair lessons learned

In Canada, as a first application of composite bonded repair technology to thick highly loaded primary structure, the following points were noted where future applications would benefit:

- No adhesive peel stress analysis was carried out for the subject application. This is an important component that should be included in future analyses. One of the difficulties with a peel stress analysis is finding the required adhesive (elastic modulus and flatwise tension strength) allowables.
- Writing a detailed specification for the manufacturing and installation of the composite doublers was essential for the success of the program. Three organizations used the specification for the installation of the boron doublers. Great care was taken during the development of the specification to ensure that the adhesive bonding process, in particular the aluminum surface preparation, produced durable bonds.
- Determining the failure mode for the composite doubler was essential to improving the design and analysis process. For the CF-116 doubler, an interfacial failure between the boron fibers and the surrounding matrix material was not accounted for in the design process. This interface was in fact weaker than the adhesive.
- Although a doubler stacking sequence 0° is very efficient, matrix cracking can cause collateral damage to the doubler. This can be addressed by including $\pm 45^\circ$ plies in the lay up.

36.12. Acknowledgements

The author would like to acknowledge the partial funding support provided by the Canadian Department of National Defence and the technical contributions provided by Canadair and Bristol Aerospace.

References

1. Raizenne, D., Simpson, D.L., Zgela, M., *et al.* (1993). CF-116 upper wing skin compression induced fatigue cracking: a case study. *17th ICAF Symp.*, Stockholm, June.
2. Lafrance, A. (1991). Investigation of fastener hole cracks in the golden triangle area of the CF-116 upper wing skin, Quality Engineering Test Establishment Report A026490, July.
3. Conor, P.C. (1998). Fatigue Induced by Compressive Loading. NRC LTR-ST-1673, July.
4. Rich, D.L., Pinckert, R.E. and Christian, T.F. (1986). Fatigue and Fracture Mechanics Analysis of Compression Loaded Aircraft Structure, ASTM STP 918, (C.M. Hudson and T.P. Rich, eds.), pp. 243–258.
5. Heath, J.B.R. and Raizenne, M.D. (1990). A Preliminary Investigation of An Out-of-Autoclave Cure Procedure for Thermoset Composite Systems, NRC LTR-ST-1775, November.
6. Rose, L.R.F. (1988). Bonded Repair of Aircraft Structures, Chapter five, Theoretical Analysis of Crack Patching, (A.A. Baker and R. Jones, eds.), Martinus Nijhoff Publishers, Dordrecht, pp. 81–82.
7. Baker, A.A. (1988). Bonded Repair of Aircraft Structures, Chapter six, Crack Patching: Experimental Studies, Practical Applications, (A.A. Baker and R. Jones, eds.), Martinus Nijhoff Publishers, Dordrecht, pp. 150–151.
8. Hart Smith, L.J. (1988). Bonded Repair of Aircraft Structures, Chapter three, Design and Analysis of Bonded Repairs for Metal Aircraft Structures, (A.A. Baker and R. Jones, eds.), Martinus Nijhoff Publishers, Dordrecht, p. 32.
9. Bateman, G.R. (1990). Composite Patch Repairs to Cracked Metal Sheets, Cranfield College of Aeronautics M.Sc. Thesis, September.
10. Hart Smith, L.J. (1983). A4EI Bonded Joint Program, McDonnell Aircraft Company Report A8372.
11. Smith, J. (1994). Design and structural validation of CF-116 upper wing skin boron doubler. *Composite Repair of Military Aircraft Structures, AGARD Conf. Proc. 550*, October.
12. Raizenne, M.D., Heath, J.B.R. and Benak, T.J. (1992). Processing Specification for CF-5 Upper Wing Skin Boron 5521/4 Fatigue Enhancement Doubler, NRC LTR-ST-1884, November.
13. ASTM D 3762. Standard Test Method for Adhesive-Bonded Surface Durability of Aluminum (Wedge Test). ASTM Standards **15.06**, Sec. 15, 1990.
14. ASTM D 1002. Standard Test Method for Strength Properties of Adhesives in Shear by Tension Loading (Metal to Metal). ASTM Standards **15.06**, Sec. 15, 1990.
15. AFML, Advanced Composites Design Guide. 3rd edn., **IV**, Materials, 1973.
16. MIL-HDBK-5F, **1**, November 1990.

Appendix A

Material properties

Textron Specialty Materials boron 5521/4 [0°] A-basis properties [15]

Compression:	RT/DRY	RT/DRY* Cocure	HOT/WET** Cocure
E_x^c Msi (GPa)	33.4 (230)	33.4 (230)	33.4 (230)
E_y^c Msi (GPa)	3.5 (24)	3.5 (24)	3.5 (24)
σ_x^{cu} ksi (MPa)	-353 (-2433)	-282 (-1944)	-211 (-1454)
σ_y^{cu} ksi (MPa)	-40 (-275)	-32 (-220)	-24(-165)
ϵ_x^{cu} e-06	-11000	-8800	-6600
ϵ_y^{cu} e-06	-15400	-12320	-9240
Tension:			
E_x^t Msi (GPa)	3.1 (21.3)	3.1 (21.3)	3.1 (21.3)
σ_y^{tu} ksi (MPa)	10.4 (71.7)	8.3 (57.2)	6.3 (43.4)
ϵ_y^{tu} e-06	3850	3100	2325
t_B in/ply (mm/ply)	0.0052 (0.132)	α_B 2.5 PPM/°F	
ω lbm/in ³ (kg/m ³)	0.0725 (2006)	fiber volume fraction 0.50	

* Apply K2 to RT/DRY properties for cocure at 185 °F, vacuum pressure for 10 h.

** Apply K1 to RT/DRY Cocure properties for 185 °F/WET conditions.

Al 7075-T651 RT compression
A-basis properties [16]

E_x^c Msi (GPa)	10.6 (73.1)
σ_x^{cy} ksi (MPa)	-67 (-461)
ϵ_x^{cy} e-06	-6500
α_{Al} PPM/°F	13
ν	0.33
ω lbm/in ³ (kg/m ³)	0.101 (2795)

FM73 adhesive properties [10]

RT/DRY with 2 h cure at 250 °F, 80–100 psi (550–690 kPa) autoclave pressure.			
τ_{max} ksi (MPa)	5.15 (35.5)	G_A ksi (MPa)	51.5 (355)
γ_{max}	0.600	$\gamma_{elastic}$	0.100
t_A in.(mm)	0.018 (0.46)		
185 °F/WET with 2 h cure at 250 °F, 80–100 psi (550–690 kPa) autoclave pressure.			
τ_{max} ksi (MPa)	1.61 (11.1)	G_A ksi (MPa)	8.24 (56.8)
γ_{max}	1.000	$\gamma_{elastic}$	0.195
t_A in.(mm)	0.018 (0.46)		

Chapter 37

IN-SERVICE DURABILITY OF BONDED COMPOSITE REPAIRS – COMMERCIAL DEMONSTRATOR PROGRAMS

R.A. BARTHOLOMEUSZ and R. C. GEDDES

Defence Science and Technology Organisation, Air Vehicles Division, Australia

37.1. Introduction

Bonded-composite repair technology has been mainly used for the repair of in-service damage to military aircraft. The Defence Science Technology Organisation (DSTO) has undertaken a number of collaborative demonstrator programs with commercial aircraft manufacturers and operators to assess the durability of bonded-composite repairs exposed to in-service environmental conditions. These collaborations, with the Boeing Commercial Airplane Company (Boeing), Ansett Airlines and QANTAS Airways Limited were initiated in the late 1980s and continued for approximately 10 years before the demonstrator repairs were removed.

The first demonstration program was in March 1989, when the application of two boron/epoxy reinforcements to an aircraft in service with Ansett Airlines, B767-200 VH-RMF, restored stiffness in a keel beam damaged by corrosion [1]. This repair was inspected and some problems were discovered which will be discussed later in the chapter. The second was in November 1989, when a boron/epoxy doubler was applied to a lap-joint of an aircraft in service with Australian Airlines,¹ B727-200 VH-TBM [2]. In the second program there was no prior damage, the application was simply to demonstrate the feasibility of doubler application and its durability. DSTO has also applied bonded-composite repairs to fatigue cracks in the Boeing full-scale fatigue-test fixture at Everett, in the USA [3]. The bonded boron/epoxy patches were applied to five fatigue cracks typical of in-service damage.

In October 1990, a repair team from DSTO and DSTO's Australian licensee company Helitech Industries Pty Ltd (Helitech) applied nine demonstration doublers to a QANTAS Boeing 747-300 aircraft VH-EBW. These doublers were

¹ Now part of QANTAS.

applied under field conditions to typical problem areas (no prior damage present), which are exposed to severe in-service environmental conditions.

The application areas were known to be prone to corrosion damage, bird strikes, stone and foreign object damage (FOD), oil and grease. In August 1999, when DSTO personnel inspected the repairs, aircraft VH-EBW had accumulated 57045 airframe hours (afhrs) and 10905 landings during service and at doubler removal in September 2000 the aircraft had flown 61248 afhrs and 11628 landings. The repairs were fitted in October 1990, when the aircraft had flown 20010 afhrs and undergone 3885 landings. Therefore the repairs had seen 37035 afhrs of service and 7020 landings in a nine-year period when they were inspected and a total of 41238 afhrs of service and 7743 landings when the doublers were removed. During this period the aircraft's movements were typically international, departing from Sydney, with the main destinations being Rome, Denpasar, Christchurch and Los Angeles. Thus the doublers have experienced a variety of environmental conditions, from the heat and humidity of the tropics to the cold of Europe in mid-winter. Also, they regularly experienced temperatures as low as -50°C whilst the aircraft was cruising at high altitude.

This chapter summarises the application processes used for the demonstrator repairs to the QANTAS aircraft and details the results of the above-mentioned inspection. In addition, some of the lessons learnt from the demonstrator programs undertaken by DSTO will be discussed.

37.2. Demonstrator doublers

37.2.1. QANTAS demonstrator program

As mentioned earlier, the demonstrator doublers were applied to areas exposed to severe service environmental conditions. Referring to Figure 37.1 [1], the locations were:

- (a) The external fuselage-skin longitudinal lap-joint located at BS 2050 at stringer 46L.
- (b) Left hand side, inboard trailing edge midflap. Located on the upper, aft midspar panel 300 mm from the outboard edge and 150 mm aft of the teflon rubbing strip.
- (c) Left hand side inboard trailing edge midflap. Located on the lower forward midspar-panel, 460 mm from the outboard edge and 150 mm aft of the forward edge.
- (d) Number two engine-pylon aft fairing on the hydraulic bay access door 150 mm forward of the aft edge.
- (e) The left-hand side wing, fixed leading-edge nose, located at inboard leading edge station 395.
- (f) The lower leading-edge skin panel of the left hand horizontal stabiliser, station 397, 300 mm forward of the front spar.

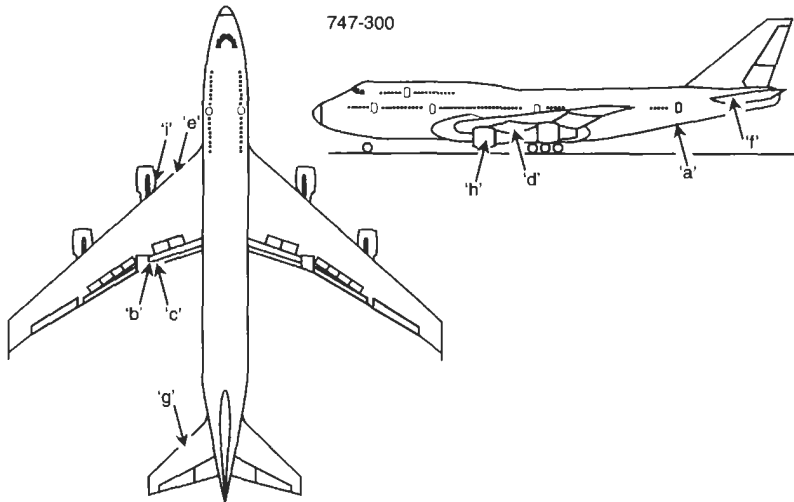


Fig. 37.1. Location of doublers on QANTAS B 747-300 aircraft.

- (g) The leading-edge nose skin panel of the left-hand horizontal stabiliser, station 390.
- (h) The thrust reverser cowl, translating-sleeve number two engine, serial number 12758, located outboard at the eight o'clock position (looking forward), on the external skin, at the aft edge of the sleeve.
- (i) The thrust reverser cowl, translating-sleeve number two engine, serial number 12758, located inboard at the four o'clock position (looking forward) on the external skin at the aft edge of the sleeve.

Table 37.1 details the repair geometry and adhesive systems used for each repair. Each repair was square, with dimension "A" indicating the side length. Two adhesive systems were trailed in this program, the epoxy film adhesive CYTEC FM73 and a room temperature curing vinyl-ester Lord Versilok 201. This allowed some flexibility in the application of repairs to areas that were unsuitable for elevated temperature adhesive cure.

37.2.1.1. Adhesive load transfer

It should be noted that the doublers whilst not repairing cracks or defects in the structure would act as reinforcements and load would be shared, based on stiffness, between the doubler and the skin. It follows that the adhesive was thus transferring load in shear between the skin and the doubler. The composite doubler and adhesive were thus subjected to both severe environmental conditions and the normal flight loads for the structure.

Table 37.1
Details of doublers applied to QANTAS aircraft.

Repair location	Adhesive type	Cure time (hours)	Cure temperature (°C)	Size "A" (mm)	Plies
"a"	FM73	8	80	200	12/4
"b"	FM73	8	80	100	4
"c"	V201	1	RT	150	4
"d"	V201	1	RT	150	4
"e"	FM73	1	120	200	4
"f"	V201	1	RT	146	4
"g"	FM73	1	120	100	4
"h"	FM73	1	120	110	3
"i"	V201	1	RT	110	3

RT = Room Temperature; V201 = Lord Versilok 201 acrylic adhesive; FM73 = Cytec FM73 epoxy adhesive.

37.2.2. Ansett keel beam reinforcement

Corrosion damage found in a keel beam of an Ansett Airline, B767-200, was found to be out of limits and two demonstrator reinforcements were applied to reduce the stress in the region. The corrosion damage was located in an extremely severe service environment due to the presence of hydraulic fluids and the overflow from the toilets. It was believed that this would provide a very demanding environment for a bonded repair and as such the demonstrators were applied. Subsequently, the location was re-analysed by Boeing and the limits for corrosion damaged increased. Although no longer required as reinforcement the repairs were left on the aircraft and monitored to determine durability over time. The reinforcements were made up of 12 layers of boron epoxy, one of the doublers was bonded with FM73 epoxy adhesive and the second doubler was bonded with Versilok 201 acrylic paste adhesive (see Figure 37.2).

37.3. In-service environment and repair location

Careful consideration must be given to the possible service environmental exposure a bonded repair may see, in the design phase, to ensure the long-term durability of the repair. Other important factors include the loads and the sub-structure. The most critical environmental issues included temperature, foreign object damage, exposure to aircraft fuels and lubricants and high velocity airflow.

37.3.1. Temperature

The temperature on an aircraft structure varies considerably due to the speed, altitude, local conditions and proximity to heat sources such as the engine or jet efflux. When designing a bonded composite repair it must be understood that

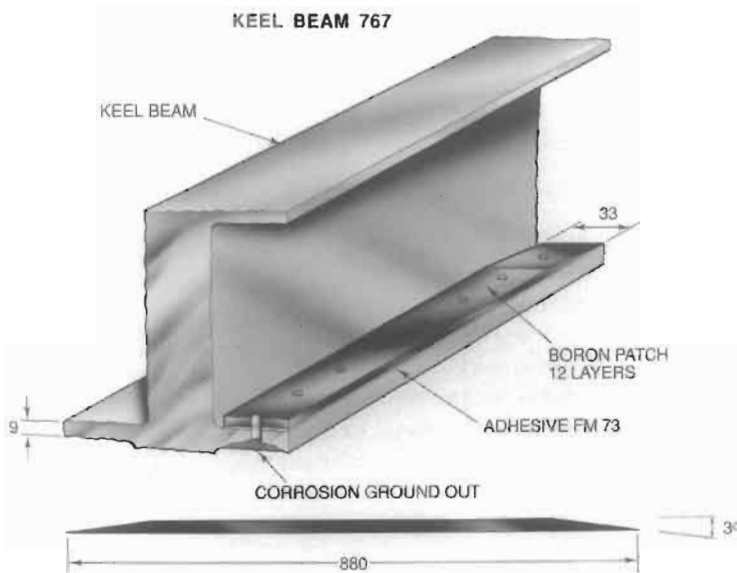


Fig. 37.2. Reinforcement applied to Ansett airlines B767-300 keel beam.

adhesives and composite materials, like all materials, have an operating temperature envelope. Outside the limits of this envelope the repair may not perform adequately. Careful selection of the repair materials is required to ensure that the repair will survive the temperature extremes the structure will experience.

Besides temperature limits set by altitude and generated by high-speed flight, allowances for radiated heat near the engines and jet efflux from engine and missile exhausts must be made. Also, the effects of icing and de-icing equipment should be carefully considered, especially in aircraft whose systems use internal heating via compressor bleed air to de ice the leading edges of the wings and other surfaces.

To ensure that the correct design parameters are used AMRL advocates the direct measurement of the temperature at the repair location. If such data is unavailable, operating temperature envelope data is usually available from the aircraft manufacturer. If the temperature of the environment falls outside the repair limits, then a different repair system must be used.

37.3.2. Foreign object damage

Composite materials have relatively low impact damage tolerance especially in the through thickness direction. Impacts can cause delaminations or pitting damage to the outer layers of a composite patch. Care must be taken when locating such repairs to ensure that they are not in direct the path of foreign objects, for example runway debris thrown up by the wheels or carried by the jet efflux. If a bonded composite repair is to be placed in such a location some thought must be given to application of a covering protective layer.

37.3.3. *Airflow and erosion*

High velocity airflow on its own does not seem to present a problem to bonded composite repairs. The combination of airflow and fine particulates such as dust, ice or rain can cause erosion damage to both the adhesive flash and outer layers of composite in the repair.

37.3.4. *Aircraft fuels, hydraulics and lubricants*

Some aircraft fuels and lubricants can chemically attack adhesive and matrix systems of bonded composite repairs, particularly some of the additives present in aircraft fuels and hydraulic liquids. Care must be taken when locating repairs that adequate protection be given to the repair to shield it from such materials and to use approved repair systems that have been tested and cleared for use in the presence of aircraft fuels, hydraulics and lubricants for long periods.

37.3.5. *Miscellaneous*

It is also important to note the following issues when designing and locating bonded composite repairs:

1. In regions subject to ground handling that may lead to impact damage of the repair. Appropriate signs indicating the presence of a bonded repair and the special maintenance considerations required for such a repair should be placed near the repair to assist ground crews.
2. Any issues with clearance when a repair is placed near adjacent parts that may rub and wear the outer layers of the composite repair.
3. Thin skins that may buckle during repair cure. In these cases it might appropriate to select a low temperature curing adhesive system to prevent buckling of the skin.

37.4. **Bond durability and surface treatment**

Bond durability and surface treatment has been discussed elsewhere and it is well understood that surface treatment is the major factor when determining bond durability. Arnott, *et al.* [4], have compared different surface treatment methods by using the Boeing wedge test, and Figure 37.3 clearly shows the advantages of the DSTO standard preparation that includes solvent cleaning, mechanical abrasion (in the form of grit blasting) followed by application of the silane-coupling agent. Other work has shown that the addition of a corrosion inhibiting primer further improves the bond durability [5] and for the QANTAS demonstrator program the standard DSTO preparation followed by the application of a primer was used to treat the metallic aircraft structure prior to bonding. In the ANSETT keel beam demonstrator program, a less durable treatment was used, that included only solvent cleaning, abrasion with pads and application of the silane-coupling agent.

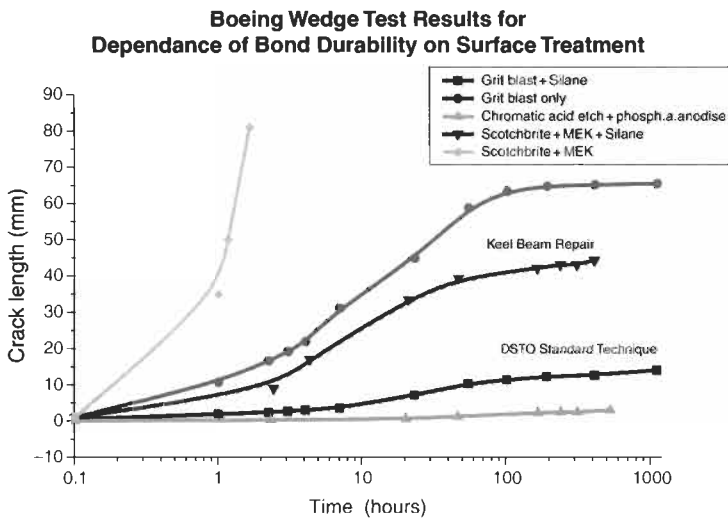


Fig. 37.3. Boeing wedge test results showing durability of bond versus different surface preparation techniques [4].

37.5. Case study results

Only two of the demonstrator programs will be discussed in this chapter. The majority of the results are from the QANTAS program, however, the results of a recent inspection of the ANSETT keel beam reinforcement demonstrator are also presented.

37.5.1. QANTAS program

37.5.1.1. Inspection of the doublers

Of the nine doublers applied to VH-EBW, seven of them could be inspected. The two doublers that were applied to the engine thrust reverser cowls could not be inspected as the cowls were moved to another aircraft. All remaining repairs were inspected visually and using a tap hammer to look for delaminations or disbonds. Some of the inspected doublers showed signs of erosion damage, most of which was minor. The doublers sheltered from foreign object impingement showed no signs of damage. One doubler, at location “b”, showed signs of a disbond or delamination.

Locations “h” and “i” were not inspected as engine 12758 had been moved to another aircraft.

The following types of erosion damage were found on the doublers:

1. Eroded adhesive flash.
2. Multiple impact sites leaving pits across the surface of the repair.
3. Fibres that were stripped from the outer layers of the composite doubler.

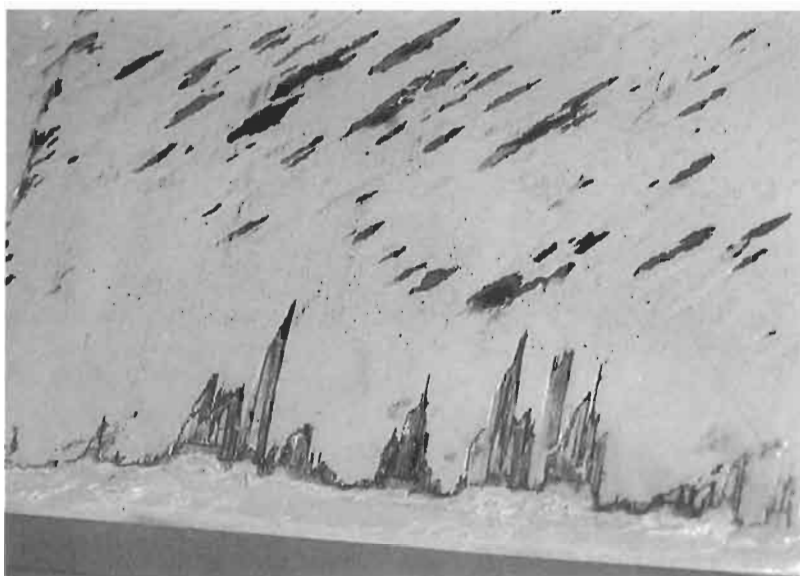


Fig. 37.4. Erosion damage at leading edge of doubler.

Figures 37.4 and 37.5 show the sort of damage that was found on the doublers. Figure 37.4 shows the extent of erosion damage that was seen on some of the doublers. The damage was seen particularly on the leading edge of the doublers where in this case the adhesive flash and the first 10 mm of the doubler had eroded completely away. Figure 37.5 shows a doubler with some of the fibres in the outer layer of the composite patch completely removed.

37.5.1.2. Application of erosion shields

The erosion seen on some of the doublers was of concern and an erosion shield was applied to the leading edge wing and the two horizontal stabiliser doublers as a trial after the inspection. The material chosen was 3M 8681 outdoor-grade, polyurethane, protective tape. This tape is aerospace qualified and is used to protect leading edges of aircraft wings from erosion damage [6]. The tape is 0.36 mm thick and has excellent resistance to ultraviolet light.

Any loose fibres, resin or adhesive were carefully removed and the patch and surrounding area were wiped clean with solvent. The tape was cut to size and positioned to cover the doubler and extend 10 mm around the doubler edge. The edges of the tape for the doubler on the lower horizontal stabiliser were covered with QANTAS decal seal and the edges of the tape for two of the doublers were covered with a thin layer of Proseal PS870 B2, a rubber based sealing material.

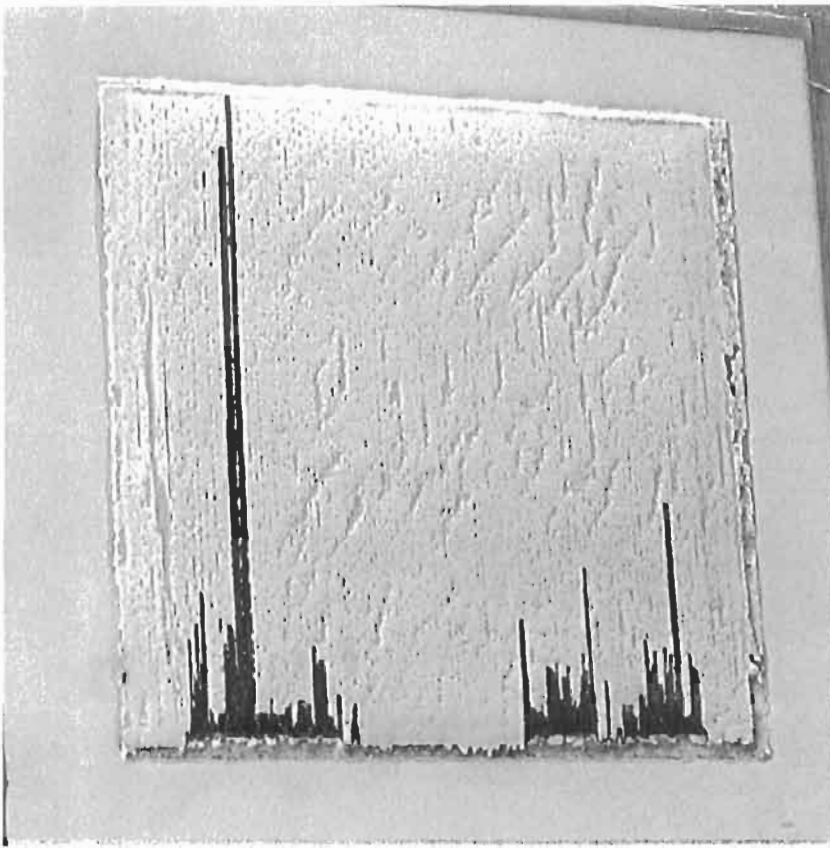


Fig. 37.5. Lower stabiliser repair showing missing fibres along the length of the repair.

37.5.1.3. Removal of QANTAS doublers

In September 2000, all the doublers were removed from the aircraft. Doubler “b” on the upper mid flap, that had shown signs of disbonding, was removed by QANTAS staff. Both the skin under the doubler and the doubler were removed. Some corrosion damage was evident in the disbonded region.

The remaining doublers were removed by DSTO staff. The composite plies of each doubler were carefully removed using a grinder. On exposure of the adhesive layer it was inspected for damage in the form of disbonds or corrosion. Some disbonding and surface corrosion was evident under the lap-joint doubler (see Figure 37.6). During installation of the Lap Joint doubler, a teflon insert was also placed in the adhesive layer in the centre of the doubler to simulate a disbond. The adhesive around this region was carefully removed so that any disbond growth could be identified. Figure 37.6 shows the location of the insert and the close-up view of the disbond. No disbond growth was evident after adhesive removal and inspection of the area.

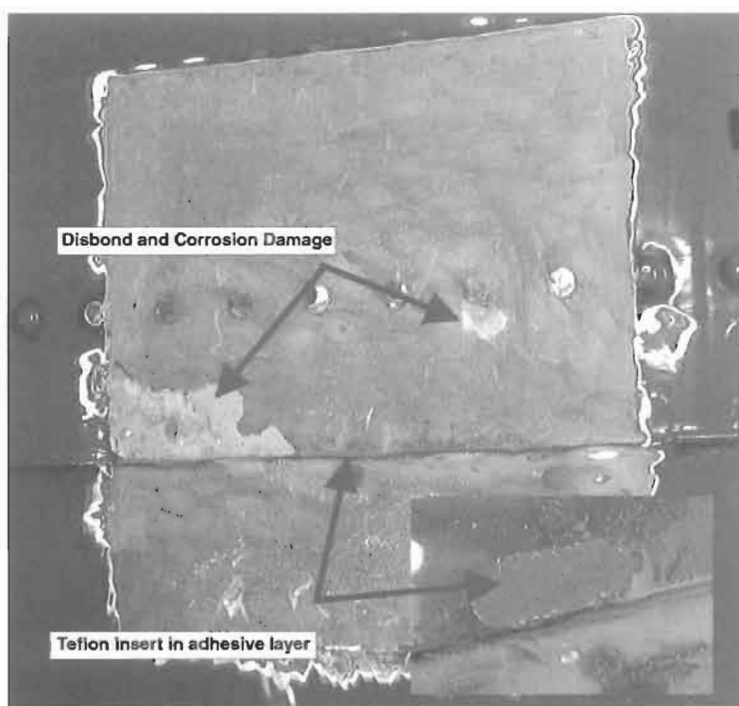


Fig. 37.6. Lapjoint doubler showing disbond and corrosion damage with a close up of the teflon insert in the centre of the doubler in the adhesive layer.

Figures 37.7 and 37.8 show the exposed adhesive layers for two doublers bonded with V201 and FM73 respectively. The adhesive layer was then removed using Rollock sanding disks. The bare metal was inspected for signs of damage. For the Lap-joint doubler, whilst removing the adhesive layer the disbonded region was also lightly sanded removing all signs of the surface corrosion.

The doublers with the trial erosion shields were closely examined for any further signs of impact damage prior to removal. No signs of damage were found.

37.5.2. Ansett keel beam demonstrator reinforcement

The results of a recent inspection, in December 1999, showed that the demonstrator reinforcements had disbanded over almost the entire length indicating that the surface preparation used for the program was inadequate. The reinforcements and the surrounding area were found to be covered in hydraulic fluid.²

² Sykdrol fire resistant hydraulic fluid.

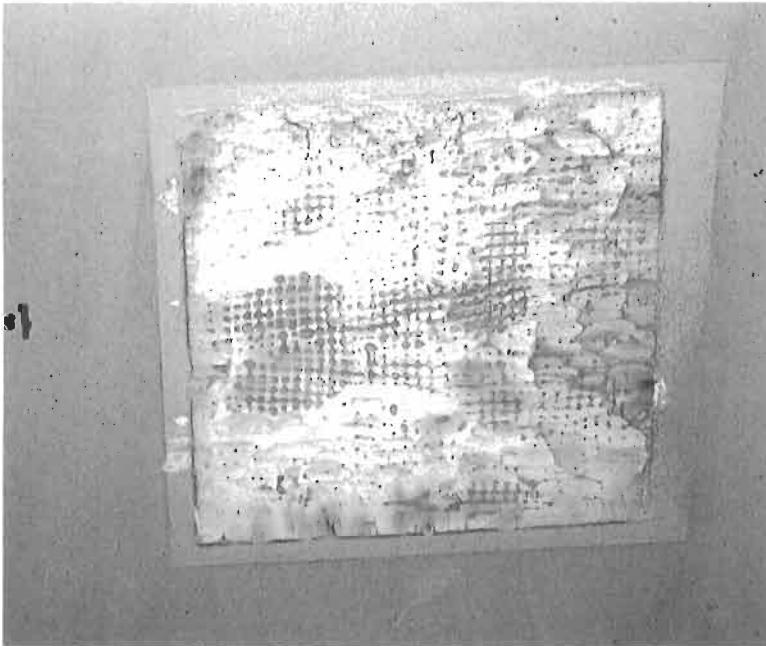


Fig. 37.7. V201 adhesive layer under doubler "c" on the lower mid flap.

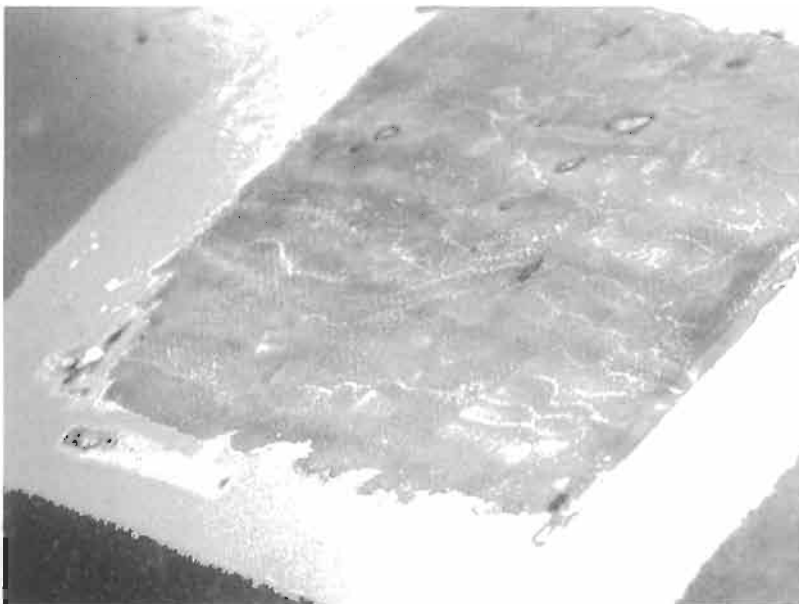


Fig. 37.8. FM73 adhesive layer under doubler "g" on the upper horizontal stabiliser.

37.6. Discussion and lessons learnt

The inspection of the demonstrator repairs on the QANTAS aircraft showed that despite exposure to severe environmental conditions, the bond integrity of the doublers was maintained if the standard DSTO surface preparation was used. Erosion due to FOD was seen mainly on the leading edges of the repairs and to a lesser extent on the sides. This would be expected as the airflow and any object carried by the airflow would impact the leading edge and front of the repair first. Airflow alone does not seem to erode the repair. This is demonstrated by the integrity of the repairs on the Lap Joint (a) and No. two Pylon (d), which were sheltered from FOD, yet were exposed to high velocity airflow.

The most eroded doubler was the top surface of the horizontal stabiliser (location "g"), followed by the wing leading edge, (location "e") and the lower surface of the horizontal stabiliser (location "f"). Doubler "g" was in line with the exhaust gas path of the number two engine. During takeoff and landing, with the aircraft in a nose high position, the exhaust gases ricochet off the runway and will carry any loose material up at high velocity towards the horizontal stabiliser. The top surface of the stabiliser is more exposed than the lower surface while the aircraft is in this flight condition. This is due to the negative trim setting angle of the stabiliser which leaves the leading edge of the stabiliser rotated downwards with respect to the trailing edge, exposing more of the top surface than the lower surface to direct airflow. Doubler "f", on the lower surface of the stabiliser, would have experienced the same type of airflow environment as doubler "g".

The source of the impact damage to the doubler at location "e", the leading edge of the wing, was most probably due to material being thrown up from the nose wheels during landing and takeoff. This was characterised by the angle of the FOD markings or pits on the doubler that traced a direct line between doubler and nose wheel bogey. The disbonded region on the doubler at location "b" was examined optically and it is believed that the disbond was caused by hydration of the oxide layer in the aluminium skin. The surface was also analysed using energy dispersive spectroscopy (EDS) and no chromium was detected in the region where the bond appeared to have degraded. This implies that inadvertently the primer was left out of the surface treatment process. This may explain why the disbond grew under the doubler.

The disbond under the lap-joint doubler initiated from a region where the adhesive flash had eroded at the leading edge of the doubler near the lap-joint step. The eroded adhesive layer exposed the bond to moisture and a disbond slowly grew under the doubler. The small disbond at the rivet head can be similarly explained. Holes were made in the doubler to allow the dome head rivets used to install the lap-joint to protrude through. It is believed that moisture worked its way in through one of the holes and caused a small disbond to grow.

There were no signs of cracking in any of the aluminium skin surrounding any of the repairs, implying that their presence did not lead to other structural problems such as fatigue cracking of the skin.

The Versilok 201 adhesive demonstrated excellent durability over the life of the program implying that it would be a suitable adhesive for room temperature bonding applications. In the QANTAS program it proved to be as durable as the elevated temperature curing film adhesive FM73.

The reinforcement on the Ansett keel beam was applied following a very basic surface treatment procedure, this being solvent cleaning, abrasion with pads and then application of the silane coupling agent. Figure 37.3 shows that this pre-bonding treatment is not as durable as that used on the QANTAS demonstrator program. Additionally the reinforcement was located in an extremely severe environment for adhesive bonds, where it was soaked in hydraulic fluid and overflow from the toilets with no protection. This explains the bond failure of the reinforcement and implies that bonding in such environments should be undertaken only if the most durable surface treatments are applied and some form of protection is provided for the repair.

37.6.1. Erosion protection by the use of shields

To minimise erosion of bonded composite repairs exposed to FOD, effort must be made to protect the repair. The evidence from the QANTAS trial implies that only the leading edge and sides of the repair need protection, however, to be conservative the entire repair could be covered for regions that have a high exposure to FOD. Trials at DSTO are examining the use of polyurethane tape and PR compounds to cover the repairs. The trial of such a system on some of the more exposed doublers on the QANTAS aircraft for eleven months showed that this may be a suitable technique to protect the doublers.

37.6.2. Repair location and design

The recognition and understanding of the operating environment and flight profiles of civil and military aircraft is important when considering the application of bonded repairs to the aircraft, especially on an external skin. Location issues, such as surface temperature, exposure to aircraft fuels, hydraulics and lubricants, interference with control surfaces, areas exposed to direct airflow and or susceptible to FOD must all be considered at the repair design stage, as they may play a major part in the long-term performance of the repair.

37.6.3. Applicability of demonstrator programs

The service environment that the bonded composite repairs experienced in both the QANTAS and Ansett demonstrator programs was typical of the operations that a large passenger commercial aircraft will see. The doublers on the QANTAS B747-300 have experienced a variety of environmental conditions, from the heat and humidity of the tropics to the cold of Europe in mid-winter. Also, they regularly experience temperatures as low as -50°C whilst the aircraft is cruising at high altitude. The reinforcement applied to Ansett B767-200 was soaked

throughout its life in hydraulic fluid and also exposed to the overflow from the toilets, a very corrosive environment that would not be conducive to bond durability. A number of lessons were learnt from these demonstrator applications including:

1. The need to protect bonded composite repairs from FOD.
2. The implications of using less rigorous pre-bonding surface treatments on bond durability.

It can be implied that although these demonstrator repairs were applied to a civilian aircraft, the lessons learnt from this program are directly applicable to military transport aircraft and at least the environmental durability aspects of fighter aircraft.

37.7. Conclusions

The doublers applied to the QANTAS B747-300 were exposed to a severe environment over a period of nine years, in excess of 37000 h of service and 7020 landings. The inspection of the demonstrator bonded repairs showed that correctly applied bonded boron epoxy repairs are extremely durable.

The demonstrator program has shown that repairs placed in areas of high susceptibility to FOD like leading edge surfaces need to have some form of protection to prevent erosion damage.

Repairs that are parallel to the airflow, like the sides of pylons, or slightly sheltered like the rear fuselage lap repair, have been demonstrated as needing little or no additional protection.

Using less durable surface treatments for adhesively bonded repairs is not recommended, as it is likely that the repair will fail by disbonding.

This demonstrator trial was considered successful, with valuable information relating to the long-term effects of in service environmental damage to bonded composite repairs being obtained and reported on for future work in this area.

References

1. Civil Aviation Authority-Australia, Supplemental Type Certificate – No. 157-1, Holder: Helitech Industries Pty. Ltd., dated 12 July, 1991.
2. Taylor, J.L. (1991). The practicalities of ensuring the continued structural integrity of aging aircraft in an airline environment. *Proc. Int. Conference on Aircraft Damage Assessment and Repair*, IEAust, ISBN (BOOK) 85825 537 5, Melbourne, Australia, 26–28 August.
3. Molent, L. and Roberts, J.D. (1990). Bonded Repair Application to the Boeing 747-400 Pressure Test Article-August 1990. ARL-STRUCT-TM-573, Aeronautical Research Laboratory, DSTO Melbourne, Australia.
4. Arnott, D.R., Wilson, A.R., Rider, A.N., *et al.* (1993). *Applied Surface Science*, 70/71, pp. 109–113.
5. Baker, A.A., Chester, R.J., Davis, M.J., *et al.* (1993). Reinforcement of the F-111 wing pivot fitting with a boron/epoxy doubler system – materials engineering aspects. *Composites*, 24(6).
6. Palmer S.J. (1999). 3M Aerospace repair system. *Int. J. of Adhesion and Adhesives*, 19, pp. 209–216.

Chapter 38

CASE HISTORY: BONDED COMPOSITE REPAIR OF A CH-47 CARGO HOOK BEAM

B.J. HARKLESS, A.P. KERR and M.A. SHUPICK

Advanced Repair Technology International, Fort Worth, Texas, USA

38.1. Introduction

A corroded region was identified on the forward cargo hook beam of a CH-47 aircraft. The beam is shown in Figures 38.1 and 38.2. Standard maintenance practice required that this beam be removed and replaced at considerable labor and material cost. An alternative to replacing the component was to repair it *in situ* with a hot-bonded composite doubler. The doubler was sized to carry loads derived from the material ultimate strength of the beam. This chapter provides the analytical justification for the sizing the doubler and presents margins of safety on the repair components. It should be noted that a bonded repair on primary structure requires careful surface preparation in accordance with controlled process specifications. The analysis in this paper assumes that the repair is installed in accordance with ARTI process specifications by certified personnel.

38.2. Defect description

The damage consisted of a single corrosion pit as shown in Figure 38.2. After the corrosion was blended in accordance with standard practices to remove all visual signs, the defect was as shown in Figure 38.3. The defect is an ellipsoid with a maximum depth of 5.59 mm length of 38.1 mm and width of 25.4 mm. It is located nearly on the centerline of the beam with the long axis aligned with the longitudinal axis of the part. A 3D drawing was generated to verify that the blend did not leave excessively thin substructure. As shown in Figure 38.5, the minimum edge distance between the defect and the edge of the part is 6.35 mm.

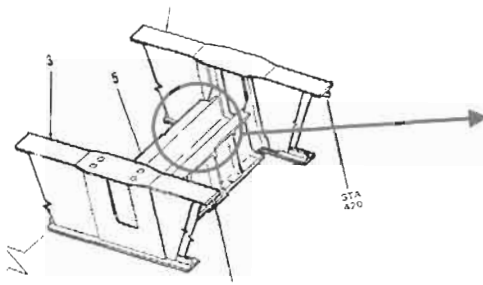


Fig. 38.1. Crane support beam and adjacent floor frames.

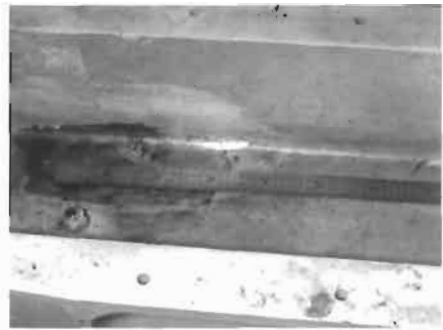


Fig. 38.2. Corrosion on support beam.

38.3. Justification of approach

A simple loads analysis showed that the horizontal web of the support beam is not a load critical region. However, a design load case was conservatively derived from the material ultimate strength. The specific alloy and temper of the beam was unknown, however, it was conservative to assume that it is 7075T6 due to its prevalence on the aircraft and its high tensile strength. The repair was sized to carry loads equivalent to the yield strength of 3.81 mm thick material (maximum web thickness) with an allotment for bypass loads carried under the repair by the undamaged substructure.



Fig. 38.3. Defect after blending to remove visual corrosion.

38.3.1. Loads analysis

Cross sections of the support beam at the defect location are shown in Figure 38.5. The corrosion is located on a 3" wide support that forms the attach point for the crane hook. As such, there is ample material at the defect site. The beam is in bending due to the crane loads, but the caps, not the horizontal web, carry this force because the horizontal web is nearly on the neutral axis of the beam. The horizontal web is present mainly to support the vertical webs and provide a barrier to the external environment. Any loads present at the defect location would therefore be minimal. The main purpose of the repair is to eliminate the stress concentration caused by blending the defect, prevent future growth of damage, and seal the area from future environmental ingress.

38.3.2. Design loads

Although the actual stresses in the web are minimal, a design load case was derived for use in sizing the repair. The design load for the bonded repair was based on material yield strength with knockdown factors to account for the presence of undamaged carry through structure. The undamaged material under the corrosion site will still carry significant load, as shown in Figure 38.5. Since the repair was designed before the actual grind-out was performed, it was necessary to make some conservative assumptions regarding the depth of the damage. It was assumed that no more than half of the thickness would be removed during corrosion removal. It was also assumed that the design ultimate load for this region would be no more than the material yield strength. The design limit stress is therefore derived as follows with the 50% knockdown factor being equivalent to the repair nominal load if half of the beam section was removed:

$$\sigma_{DLL} \leq \frac{\sigma_{mat\ yield}^*}{1.5} 50\%$$

The yield stress for 7075T6 extrusion (A Basis) is 476 MPa. Therefore, the DLL for the repair design will be 159 MPa. The DUL is DLL times the standard 1.5 reserve factor, or 238 MPa.

38.3.3. Static strength analysis

An elastic-plastic bondline analysis was performed to determine adhesive stresses, parent stresses, and doubler stresses. As shown in Figure 38.5, the local thickness at the defect is substantial. To facilitate repair sizing, the defect was analyzed as a through hole in the web. The repair is sized to restore adequate load capability in the presence of this defect. The analysis tools have been well substantiated by Royal Australian Air Force (RAAF) experience [1]. Features of the analysis are:

- The analysis is 2D and therefore conservatively assumes all loads across the defect width are transmitted through the adhesive and carried by the repair. In actuality, some load would be diverted around the defect where the repair serves as a doubler on undamaged substructure.
 - The peak stress and strain in the adhesive are calculated based on an elastic-plastic adhesive analysis.
 - Thermally induced stresses caused by the difference in thermal coefficient of expansion between the doubler and parent material are included in the analysis.
- The material properties used in the analysis are provided in Table 38.1. Metal properties are derived from Mil-HDBK-5. Manufacturer furnished properties at room temperature were used for the adhesive. Plain weave 250 °F curing graphite cloth was selected as the repair material due to its conformability, availability, and high strength.

Margins of safety at DUL are shown in Table 38.2 based on the design loads above. The margins of safety on the parent stress near the defect have been reduced by a factor of 1.15 to account for any stress concentration due to the blend-out [3].

Table 38.1
Material properties used in bond analysis.

<i>Beam properties</i>	
Material	7076T651 Plate, A Basis
E	72400 MPa
σ_{yield}	476 MPa
σ_{ult}	538 MPa
α	0.000023 mm/mm/°C
T	3.81 mm
<i>Doubler properties</i>	
Material	250 °F Cure Graphite/Epoxy Prepreg
E	68900 MPa
T	2.95 mm (16 plies)
σ_{ult}	690 MPa
α	0.00000156 mm/mm/°C
Lay-up	16 plies 0/90/Symmetric 0/90 3 k Plain Weave
<i>MB1146 adhesive properties</i>	
G	393 MPa
T	0.127 mm
τ_{plastic}	39.3 MPa
γ_{c}	0.10 mm/mm
γ_{max}	1.16 mm/mm

Table 38.2
Static analysis margins of safety.

Property	MS at DUL
Doubler Stress	2.6
Parent Stress	2.2
Near Defect	
Adhesive Shear	7.1
Strain	
Overlap Length	56.1 mm

The analysis shows that the repair and bondline have a maximum load capacity of 1087.8 N/mm.

38.3.4. Fatigue analysis

A conservative fatigue analysis of the bondline was performed by assuming that a once-per-flight load equivalent to 60% DLL is applied to the structure. The maximum adhesive strain in this condition is 0.15 mm/mm, 1.5 times the elastic limit of the adhesive. Previous experience indicates that the adhesive is capable of excellent fatigue performance up to two times the elastic limit assuming a once per flight load at that level.

A fatigue analysis of the metal under the repair was not required because the stress levels are lower than that associated with the filled hole in a nearby region. The fatigue-limiting factor on the part is the stress concentration at the bolthole, not the blended region. The repair restores the load path lost by the corrosion, prevents the growth of any damage from the blended region, and seals the region against further environmental damage.

38.3.5. Proof testing

Because the repair is not structurally critical, no static strength coupons were tested. Coupons were constructed to demonstrate that the doubler manufacturing and cure process would produce an acceptable part. To demonstrate the process, trial repairs were applied to a representative piece of angle. The angle included the same radius as the actual part, and contained a representative blend-out. The repairs were applied using the same lay-up and cure methods as the actual installation. A release agent was applied under the repair to facilitate removal of the part after the cure for examination. The examination focused on the following areas:

- Whether vacuum pressure used in the field was sufficient to consolidate the patch and insure a void free part
- Whether the fiberglass/film adhesive defect filling technique would produce acceptable results
- Whether the graphite would conform to the sharp fillet radius in the part

- Whether the patch would “sag” over the defect

A total of six trial bonds were performed to perfect the lay-up and cure technique. Destructive visual examination of a part produced using the finished procedure showed excellent results.

38.4. Patch system and environmental protection

Graphite was chosen as the repair material because of its ability to conform to the necessary repair geometry. Some potential concerns arose because of the potential of galvanic action between the repair and the aluminum substrate. The film adhesive has been shown to be an effective electro-chemical barrier between the graphite and aluminum [2], however, and it was deemed that no additional protection was necessary under the bonded repair. A layer of fiberglass pre-preg was added on top of the graphite repair to protect the surface of the repair. That sacrificial layer along with the edge sealant provides sufficient environmental protection for the bonded repair.

38.5. Repair procedure

The repair procedure is provided on the doubler drawing contained in Figure 38.6. An overview of the repair procedure is as follows:

- The corroded region was blended to approximately a 5:1 taper ratio to remove the corrosion and minimize any stress concentration.
 - The bonding surface was prepared in accordance with the standard ARTI process specifications. The governing specifications are: PS101, “Solvent Cleaning of Metallic Surfaces”, PS127, “Alumina Grit Blasting”, PS128, “Preparation, Application, and Cure of Silane Coupling Agent” and PS130, “Application, Drying and Curing of Cytac BR127 Primer”.
 - The defect was filled with film adhesive and dry fiberglass cloth in a 2:1 adhesive to cloth ratio.
 - The doubler was laid-up from uncured prepreg directly onto the repair surface over one layer of MB1146 film adhesive.
 - The doubler was debulked under vacuum for 20 min.
 - The doubler was cocured and bonded in place under full vacuum pressure using a 250 °F for 90 min cure with a 30-min dwell at 190 °F to insure adequate flow.
 - The repair was inspected visually and by tap test.
 - A hole was counter-bored through the repair to allow access for the crane safety retaining bolt and nut.
 - The repaired area was sealed, primed and painted in accordance with standard aircraft maintenance procedures.
 - Installation and recurring inspection entries were made in the aircraft log.
- The finished repair installation is shown in Figure 38.4.



Fig. 38.4. Bonded repair before sealing.

38.6. Continuing airworthiness/inspection

Due to the low levels of stress associated with the region, and the fact that the repair is not the limiting factor for the fatigue life of the part, no inspection of the repair is technically required. However, good aerospace practice dictates that the repair be inspected visually and by tap test during phased inspections. In addition, a one-time inspection after 50–60 h is suggested to assure the application was correct and to provide user confidence. These entries will be recorded in the aircraft inspection log under form 2408-18.

References

1. Baker, A.A. and Jones, R. (eds.). (1988). *Bonded Repair of Aircraft Structures*, Martinus Nijhoff Publishers.
2. Harkless, B. and Kerr, A. (1999). *Laboratory Examination of Bonded Repairs for Corrosion Damage*, ASIP Conference, San Antonio, TX.
3. Young, W.C. (1989). *Roark's Formulas for Stress and Strain*, Table 37.3. McGraw Hill.

ARTI Process Specifications

PS101, "Solvent Cleaning of Metallic Surfaces"

PS127, "Alumina Grit Blasting"

PS128, "Preparation, Application, and Cure of Silane Coupling Agent"

PS130, "Application, Drying and Curing of Cytac BR127 Primer".

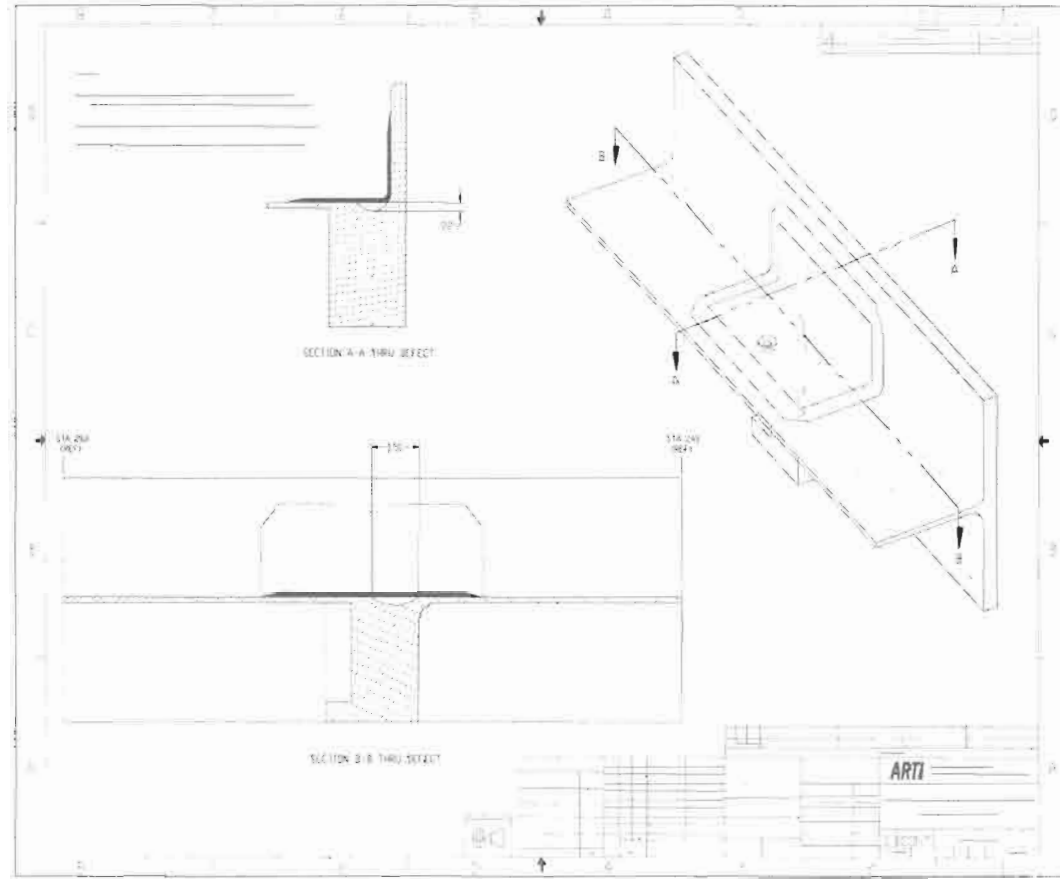


Fig. 38.5. Defect layout drawing.

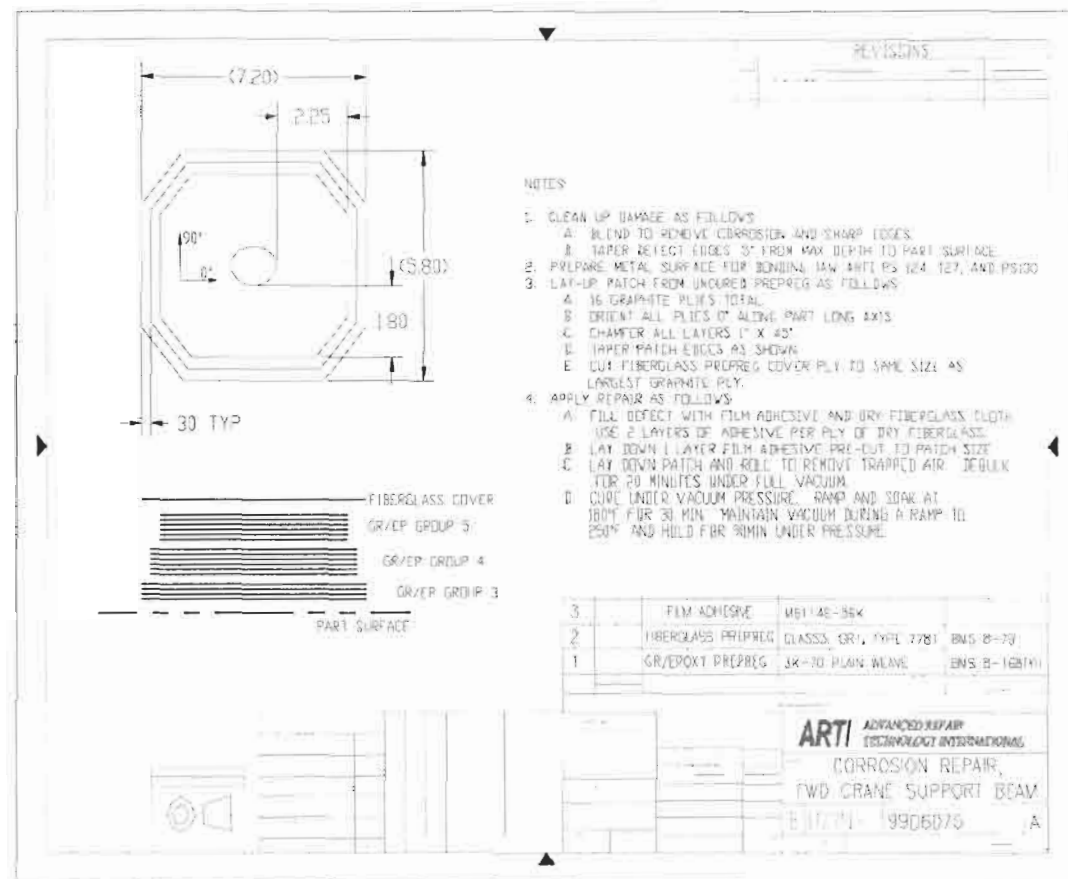


Fig. 38.6. Repair doubler drawing.

Chapter 39

CASE HISTORY: APPLICATION OF BONDED REPAIR TECHNOLOGY TO LARGE AREAS

B. HARKLESS and A. KERR

Advanced Repair Technology International (ARTI)/Dyncorp, Fort Worth, TX

39.1. Background

Application of bonded repair technology has traditionally been limited to small repairs of cracks and corrosion damage. Past efforts in Australia one and more recently in the United States have proven that field installation of permanent bonded repairs to metallic aircraft structure can be reliably performed. Over 25 years of service history exists to demonstrate the long-term durability of repairs applied with the grit blast/silane process even in challenging environments such as fuel tank interiors. Not only are the repairs technically more efficient and more effective than riveted repairs at preventing crack growth, but they are also frequently more cost effective to install. Although numerous applications have proven successful on aircraft such as the F-111, C-141, F-16, and AH-64 the majority of these repairs have been confined to small damage areas.

In today's aging aircraft structures, problems are often not confined to small areas, but instead are widespread across significant portions of structure. Widespread fatigue damage, multi-site damage, and corrosion are all examples of common issues that affect large areas of aging fleets. In order for bonded repairs to have a more significant impact in reducing the cost, increasing the safety, and extending the life of aging airframes, their application must be extended to large areas. Current industry reluctance to apply repairs to large areas has stemmed from a misconception that current application techniques cannot be scaled up without sacrificing bond integrity. The purpose of this paper is to review the state of the art on bonded repair application processes and show that with relatively minor changes, large areas can be addressed conveniently and economically with bonded repairs. Applications of large area bonded doublers to aging airframe repair, structural life extension, and restoration of fail-safety will be discussed.

39.2. Examples of applicability to large areas

39.2.1. Full length rotor blade doublers

Large disbands are occurring between elements in the main rotor blades on the AH-64 Apache helicopter. Allowable limits were established for these defects, and blades with defects beyond these limits were being scrapped. Inventory cost for these scrapped blades was in the order of nine million dollars per year. A bonded repair has been developed with the capability of restoring the integrity of blades that would have been scrapped because of these defects. The repairs for these blades are significant because of their size, 6 m long. The techniques used to apply the repairs are the same as those used to apply the more familiar and much smaller "crack-patching" repairs. The large area is prepared in a piecewise manner where segments of the repair are applied in sequence and spliced together by employing carefully designed ply terminations.

39.2.2. Large scale wing reinforcement

The C-141 "Weepole" repairs are well known for their success and numerous applications. Not as well known are some of the repairs for incidental damage that were also incorporated by both the government and contractor groups during this project. Repairs to scratches on the lower wing surface up to 1.2 m long were incorporated.

Heat damage and corrosion repairs on the lower wing surfaces of C-130 aircraft have been applied in field locations. These patches have been as large as 1.8 square meters, and have been applied using the same "crack patching" application processes. Repairs like this are being applied by the USAF Warner Robins personnel quite routinely.

39.2.3. Large scale fuselage reinforcement

One fuselage repair example currently being considered uses bonded repair techniques to stabilize the sides of a fuselage against compressive buckling. Cracks resulting in this structure because of the buckling impact on the structural integrity of the aircraft.

Another example of a large-scale fuselage repair is the 1.5 square meter reinforcement of an L-1011 passenger doorframe, done jointly by the FAA Airworthiness Assurance Center at Sandia Labs, the FAA, Delta and Lockheed. This repair has completed an estimated 9000 flight hours of trouble-free service since February 1997.

Surface preparation for the L-1011 repair was accomplished using the PACS process (Chapter 28), whereas the grit-blast/silane process was used in the other examples mentioned. Both processes work effectively on smaller areas typical of most repairs; and although they were used successfully on the larger areas, they were working at the practical extreme for the current technology level.

39.3. Current state of the technology

39.3.1. Critical features of the bonding process

The criticality of the bonding process cannot be overstated if a durable bonded repair is to be achieved. The term durability as applied to bonded repairs usually refers to environmental durability, as opposed to structural durability or fatigue. It is not possible today to inspect non-destructively for bond strength. Numerous NDI techniques exist to find disbonds, voids, and other such defects, but a typical bonded repair is very tolerant to such defects. Similarly, the adhesives used to bond the composite or metallic repairs to the parent structure have excellent fatigue properties. Under typical aircraft loads and fatigue spectra, the fatigue strength of the repair is usually not the limiting factor. Once adequate static strength is verified in the presence of “knock-down factors” used to account for the effects of temperature and moisture on composite materials, fatigue capability can be assessed by test. This is usually adequate. In general, epoxy film adhesives used in bonded repair applications are not sensitive to high frequency, low load cycles, but are more sensitive to continuous low frequency, high load cycles. Because normal aircraft fatigue spectra include relatively few high load cycles, the bonded repair tends not to be the limiting fatigue factor for the repaired structure, except possibly in the case of highly loaded primary structure. Most aircraft structures include more critical local stress concentrations for example at fastener holes. A possible exception where general stresses are high is in fuselage repairs, where internal pressure dominates the fatigue loading. However, the high stresses are still at the local stress concentrators. Fortunately, fuselage skins are relatively thin structure, and the adhesives in use today have high enough strength that even fatigue loads due to pressure are not a limiting factor. Standard repair adhesives have enough strength that in a properly designed joint, the adhesive capability far exceeds the yield strength of transport fuselage skins.

Unfortunately, the aspect not understood by some is that bonded repair strength and fatigue resistance is compromised without correct surface preparation on the substrate (Chapter 3). In addition, surface prep requirements for structural bonding are different from those currently associated with honeycomb assemblies. Numerous horror stories exist of bonded joints simply peeling apart after a few months or years of service even though the loads on the bondline are inconsequential. Even fatigue testing conducted after 30-day exposure to hot/wet conditions, a common justification procedure, may not show up surface preparation difficulties. The only industry accepted means to justify surface preparation procedures is the Boeing Wedge Test 2.

An issue that arises with the Boeing Wedge Test and other accelerated tests is that they cannot, as yet, be directly correlated to service life. ARTI/Dyncorp uses a passing mark of 5.08 mm of crack growth after 24 h of specimen exposure to a 50 °C, 100% relative humidity environment. This number is chosen based on service experience. Over 25 years of history with the grit blast/silane process have shown that if surface preparation is tested to the 5.08 mm standard, excellent service

history will result. Even so, no data exists to make quantitative statements such as "7.62 mm of crack growth would be good for at least five years." This forces surface preparation methods to err on the side of conservatism, because inevitably bad surface preparation will lead to total and unpredictable failure of the repair bond.

39.3.2. Grit blast/silane process steps

The grit blast/silane surface preparation process three was developed in the 1980s. The Aeronautical and Maritime Research Laboratory (AMRL) in Australia is recognized in the industry as a leader in bonded repair research, and they have over 25 years of service history on early C-130 repairs for outer wing cracks. References [1,4] contain numerous other examples including the well known wing pivot fitting repair on the F-111. All these repairs were done with the grit blast/silane process. silane is non-toxic and unlike acid etches, is inert. It has demonstrated excellent results over a broad span of materials including all the common aluminum alloys and stainless steels used in aircraft. The grit blast/silane process contains the following steps:

1. Thorough solvent scrub. The solvent scrub is used to remove all traces of surface contamination from the bonding surface. Past work at ARTI/Dyncorp has shown some sensitivity to the type of solvent used, and the degree of scrubbing employed. Currently, the process is performed manually using Scotch-Brite abrasion. After a carefully controlled procedure is used for the scrub, the surface is checked with a water break test.
2. Grit blast. The grit blast step is used to expose a fresh chemically active layer on the metallic surface. 50 micron aluminum oxide grit is used with high purity nitrogen as a propellant. The use of high purity nitrogen guarantees that hydrocarbon contaminants will not work their way onto the surface. Removal of the surface oxide layer is critical to obtaining a good coupling between the silane and the metal. For this reason, the time span between the end of the grit blast and the silane application is carefully controlled and limited in duration.
3. Silane application and cure. The silane molecule chemically couples the epoxy adhesive used in the repair to the metal substrate. It is sprayed or brushed onto the surface in an aqueous solution. After the surface is wetted for a prescribed amount of time, the area is dried, and heat is applied to cure the silane.
4. Primer application and cure. A corrosion inhibiting bonding primer, usually BR127, is used to improve the integrity of the bond and the resistance of the surface to corrosion, which is tied to the durability of the bond. A very thin layer of primer is applied, and the structure must be heated again to cure the primer.
5. Application of the repair. Repair application involves the actual lay-up of the film adhesive with the composite or metallic doubler and curing of the adhesive under temperature and pressure. Temperature can be achieved using heat lamps, hot air circulation, heat blankets, or by projection heating. Pressure is applied with vacuum or using positive pressure. Positive pressure is advantageous

because it tends to produce a less porous bondline than vacuum pressure, especially when bonding over fasteners or other unsealed surfaces. This process takes about 12 h to complete, and must be executed without interruption. Minimizing the chance of contamination during every step is critical; however, the process is easily accomplished in the field with the proper precautions.

39.4. Process areas requiring adaptation

Although straightforward to implement in a limited area, the current manual scrubbing process is difficult to scale upward economically. The main limitations are:

- Difficulty in performing the solvent scrub step on the large area without contamination from adjacent areas also being cleaned.
- Difficulty in grit blasting a large area quickly enough to prevent reoxidation of the surface.
- Heating the structure during the silane, primer, and adhesive cures.

39.4.1. Solvent scrubbing step

It is possible, without adaptation, mechanization or automation of existing surface preparation techniques, to break the area into small, manageable pieces, cure on the individual repairs, and splice each segment to the previous one. A splice section requires special care in the design phase to ensure that the splice effectively transfers both static and dynamic loading and that the substrate area is not adversely affected by additional cure cycles. In general a 3 to 4 mm per ply stepping of the splice would be required. This issue may require R&D to evaluate fatigue strength issues. As an extreme example, assume that a repair doubler 3 m by 9 m is to be applied on top of an aircraft wing. Based upon ARTI/Dyncorp's experience, one applicator can reasonably scrub a 0.3 m by 1 m section in a given cleaning cycle. Using this as the baseline, it would take 100 bond cycles to complete the doubler installation. It would be possible to decrease the overall project time by utilizing multiple teams of applicators preparing surfaces adjacent to each other. This would also allow the use of larger repair segments and reduce the number of splices, since one repair could be applied over several "zones." Using this type of team approach, it may be feasible to complete the project in 20 shifts. However, although the total elapsed installation time would be decreased using this method, the labor cost would be the same. Assuming one applicator per zone, the doubler would require 1200 man-hours to install.

In the case of the wing doubler, a traditional solution may involve replacing planks or skin panels. Replacing the skins would require drilling out fasteners, aligning the new skins, back-drilling the hole locations to match, and reinstalling new fasteners. Assuming 25.4 mm fastener pitch and 457.2 mm plank spacing, over 5000 fasteners would be involved. Figuring the labor at 30 min per hole leads to a project cost of 2500 h, twice the bonded repair solution. In addition, the skin

replacement method would require alignment jigs and fixtures that the field-installable bonded repair would not. This example shows that even with today's methods, large area bonded repairs can be more cost efficient than alternative solutions.

The example chosen is extreme in the sense that re-skinning wings is not a common occurrence. In order to increase the appeal of large area bonded repairs additional cost incentive is required. To accomplish this, better methods for completing the solvent scrub process are required.

39.4.2. Grit blast step

The main issue with scaling the grit blast operation is completing the operation quickly. Commercial blasting systems exist that can blast large areas and still maintain the cleanliness and quality required for bonding preparation. The essential parameter is the time to complete the step. Currently a 15 min window is specified between the completion of the grit blast and the application of the silane. Although the methods are not implemented in repair installations today, multiple large capacity grit blasters may be required to meet this goal. Close coordination between the applicators performing the grit blast, the quality inspectors, and the silane application team will be required. However, the solution is straightforward – apply the silane as the rest of the area is blasted. Although the blast equipment must be carefully examined from a contamination viewpoint, the grit blast step is not considered a disqualifying factor. Another possibility is using a non-hazardous abrasion/cleaning mix instead of the grit. Plastic micro-beads and a water based solvent like Citra-Safe could be used to quickly clean the surface while not presenting the collection and disposal problem associated with the aluminum grit. However, this requires investigation as plastic beads may contaminate the surface.

39.4.3. Heating methods

A significant challenge in any repair application is how to heat the substructure during cure of the silane and primer (where direct contact with the surface is not permitted) and cure of the repair (where surface contact is possible). This challenge is significantly magnified in large area applications because:

1. The required heating power is significant.
2. The applications for large areas will tend to be specialized, making it difficult to implement a generic tool. This necessitates additional non-recurring engineering and tooling costs.
3. Other aircraft systems and components will naturally be exposed to the heat and must be protected if necessary. This may require insulating any surrounding parts not rated for temperature, or possibly additional disassembly.

Again, this is a solvable problem which can be handled with engineering, and will not require relaxation of quality standards or the use of alternative heating systems. The experience base to date with epoxy film adhesives makes their use preferable in any repair application. They are readily available, have well understood properties,

and excellent performance. New technologies such as e-beam and UV curing resins are emerging that may someday eliminate the need for heat cure of epoxy systems. However epoxy-based adhesives are now preferred.

The technology exists today for large scale heating. Numerous OEM's utilize large bonding fixtures (although many times heat and pressure are applied in an autoclave, which is not suited to on-aircraft work). In the wing doubler example, heat could be applied via heat lamps from above the wing, blankets from inside the wing, projection heating from the backside of the wing or numerous other methods. There will be a cost penalty to scaling up heating systems that will increase the non-recurring cost for large area repair applications. Power management will also be an issue. If more efficient methods are found to complete the solvent scrubbing and other labor intensive portions of the repair application, these non-recurring costs can be tolerated.

39.5. Large area repairs in a production environment

The AH-64 main rotor blade repair described previously has been implemented on a large scale production-like environment by Composite Technology Incorporated and Dyncorp. To date over 120 blades have been repaired using more than 1200 bonding operations averaging 20 completed blades per month. The repair rejection rate due to insufficient bonding has been miniscule, while the rejection rate due directly to human error has also been minimal.

No true process modifications were made for this repair. Solvent scrub of the blade was done by hand in approximately $2\text{ m} \times 0.5\text{ m}$ sections. Special non-contact infrared heater ovens were manufactured to cure silane and primer, while another tool cured the repair adhesive using positive pressure bladders and heater blankets.

Figures 39.1–39.10 detail the steps involved in this repair process. When blades arrive at the facility, they are inspected for disbonds. Once the disbonds are located, the old adhesive is removed and the area cleaned. The disbonds are then shot with an anaerobic adhesive and clamped in place to cure. Since the bonded repair will completely replace the old load path along the blade, the disbond fills serve only to provide a good bonding surface and reinforce the blade. If very low areas exist along the spar seams, they are filled with room temperature cure adhesive before patches are applied. This minimizes the risk of disbonds later on.

Each blade is hand scrubbed using MEK and Scotchbrite to remove gross contamination, shed oxide layers and provide a water break free surface. The metal blade surface is then grit blasted to reveal fresh chemically active metal and provide a rougher surface to encourage mechanical interlocking of the adhesive. Silane is applied by hand to the blade and then cured using non-contact infrared ovens. The blade temperature is monitored by infrared thermocouples mounted on the top of the heating ovens. A very fine layer of corrosion inhibiting primer is applied and cured using the same ovens that cured the silane. Film adhesive is applied to the patches which are then placed on the rotor blades. Thermocouples are arranged on



Fig. 39.1. Disbond repairs.



Fig. 39.2. Solvent scrub process.



Fig. 39.3. Rotor blade in grit blast chamber.



Fig. 39.4. Silane application.

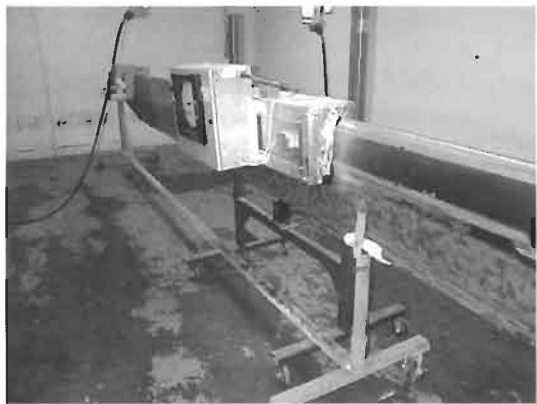


Fig. 39.5. Non-contact heating oven.



Fig. 39.6. Primer application.



Fig. 39.7. Patch application.



Fig. 39.8. Heater blanket positioning.



Fig. 39.9. Pressure bladder tool.



Fig. 39.10. Finished patch.

the patches and the surrounding blade surface to ensure proper heating control and monitor cure conditions. A large heating blanket is draped over the blade surface and the pressure tool, complete with heating controllers is lowered onto the blade. The repair cure is done in two steps to protect the delicate fiberglass and honeycomb portions of the blade. First, a low temperature, high pressure step allows the adhesive to flow and fill any uneven areas. Second, the pressure is reduced and the blades are heated to ensure adequate performance at elevated temperature.

Although the basic process was unchanged and the repairs were relatively straightforward, several obstacles had to be overcome before the specific repair procedures were fine tuned. Since the repair was designed to replace the existing load path along the entire length of the blade, the patches had to be effectively continuous. This was done by scarfing the ends of each repair section and bonding them together. This resulted in the overlap section seeing two cure cycles. In addition, if a repair section had to be removed there was a possibility of damaging the previously installed good patch during the removal of the defective one. A thorough thermal imaging and tap test regimen was done to each side of the rotor blades as each repair section was installed. These tests showed no damage associated with a redundant cure cycle. Also, as long as extreme care was taken in removing rejected repair patches, no more than cosmetic damage was done to the accepted patches.

Overall, as of 6 February, 2001, Dyncorp has repaired 124 blades for a total of 1240 individual patches installed. Only 16 patches or 1.3% were rejected for disbonding between the patches and the blade surface. These disbonds were caused almost exclusively by not filling low areas of the blades adequately and not allowing adequate "settling time" for the repair. All of these disbonds occurred during the beginning stages of production while the team was fine tuning the processes. Three minor changes that were made to the production process eliminated all of these

disbond problems. First, whenever a low point on the bonding surface was discovered, primarily due to improperly done field repairs and/or mismatched C-spar joints, extra adhesive was added to the area as to ensure good contact by the repair. Second, after the patch was taped into place for cure, the positive pressure bladders on the curing tool were inflated for half an hour without heating to allow the repair to settle before the adhesive would begin to flow. Third, the blades were allowed to cool to 23 °C before the pressure was removed.

39.6. Conclusions

Large area bonded repairs offer new possibilities in aircraft maintenance. Bonded repairs could be used for problems never before considered as candidates. Thickening a skin panel or repairing a large disbond becomes easier than ever before with the use of bonded repairs. Rivet intensive repairs that require large scale rigging and disassembly could be simplified by an order of magnitude by using large area bonded repairs, with a savings in down time and cost as well.

While this promise has not yet been reached, the technology threshold is here. The state of the art in bonded repairs is poised to cross into the large area regime. One of the last remaining hurdles to viable commercial application of these large area bonded repairs is to efficiently scale up the labor intensive solvent scrub step so that a few technicians can complete the task quickly. Money is needed to fund such scale-up studies to ensure that economically preparing a large area will provide an acceptable bonding surface. Additionally, issues governing workforce training requirements, regulatory acceptance and generic large area tooling design need to be considered and funded. ARTI/Dyncorp and its partners are leading the way in this regard with preliminary tooling designs, use of a prescribed training program, and adaptation of existing processes to large areas.

ARTI/Dyncorp has examined the issues related to large area bonded repairs, most visibly with a disbond repair for the AH-64 main rotor blade. Other situations with large transport aircraft have arisen and are under consideration. This market could be potentially tapped for major structural upgrades to meet increased load, mission and lifetime requirements.

Large area bonding is already employed in many original production aircraft assemblies. Entire wings are bonded together and bonded joints have been used for decades. *In situ* bonded repairs are also becoming more commonplace. With a technological pedigree over 25 years old, bonded repairs are recognized for their efficiency at crack stopping and corrosion control. The next step is to move large area bonding from the factory floor to the maintenance hangar, and the technology base is present to make this transition. ARTI/Dyncorp supports the transition by examining new applications for bonded repairs and continuing to develop techniques to make such applications commercially viable.

Now more than ever, large area bonded repairs could be an extremely valuable tool for both commercial and military aircraft operators. With the potential savings

in both time and money, large area repairs can be an effective part of an overall life extension or maintenance program.

References

1. Baker, A. and Jones, R. (eds.). (1998). *Bonded Repair of Aircraft Structures*, Martinus Nijhoff Publishers.
2. ASTM Designation D 3762, Standard Test Method for Adhesive-Bonded Surface Durability of Aluminum (Wedge Test).
3. Baker, A.A. and Chester, R.J. (1992). Minimum surface treatments for adhesively bonded repairs. *Int. J. of Adhesives and Adhesion*, **12**, pp. 73–78.
4. Baker, A.A. (1994). Bonded Composite Repair of Metallic Aircraft Components, Paper one in AGARD-CP-550 Composite Repair of Military Aircraft Structures.

Chapter 40

CASE HISTORY: COMPOSITE PATCH REINFORCEMENT OF T-38 LOWER WING SKIN

M.M. RATWANI, J. HELBLING, B. HEIMERDINGER and N.M. RATWANI
*R-Tec, 28441 Highridge Road, Suite 530, Rolling Hills Estates, CA. 90274-4874,
USA*

40.1. Introduction

Repair of cracked metallic structures with bonded composites is finding increased use in service [1–7] due to the several advantages offered by the repair concept. The cracked structures, which would not meet fail safety requirements with conventional mechanical fastening repair concept, can meet these requirements with bonded repairs. Hence, the structural components, which would normally be scrapped due to safety problems, can be put in service with bonded repairs and result in significant cost savings. The in-service applications of this repair concept in USA are found in T-38 lower wing skin near “D” panel [1], C-141 weep holes [5], F-16 lower wing skin at fuel access hole [7], *etc.*

Machined lands in T-38 lower wing skin between 39% and 44% spars at W.S. 78 have developed cracks during service. In order to extend the service life of the wing, there is a need to develop a reinforcement concept that will reduce stresses in the pocket area and thereby reduce the tendency towards crack initiation and also retard crack growth. Preliminary studies indicated that a conventional mechanically fastened repair would degrade the structural integrity of the lower wing skin and jeopardize the safety. Three different bonded concepts namely – (1) aluminum, (2) graphite, and (3) boron were considered. The reinforcement can be bonded on the outer moldline of the wing only due to one side access availability. High stresses at the location of machined pockets precluded the use of aluminum due to very thick reinforcement design. A graphite/epoxy reinforcement design was thicker compared to boron/epoxy design. A thick reinforcement, bonded on one side, causes excessive out-of-plane bending and thereby reduces the effectiveness of the reinforcement. Thus, relatively thin boron/epoxy reinforcement and better thermal compatibility with aluminum compared to graphite reinforcement provided the

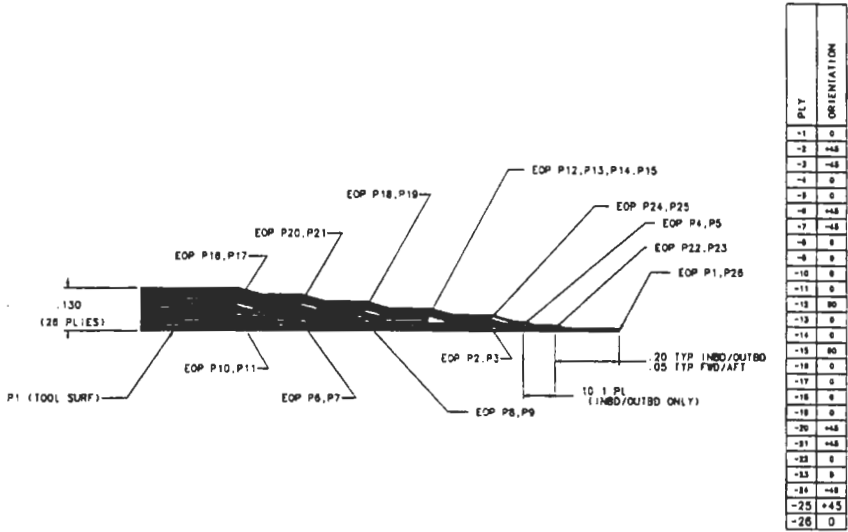


Fig. 40.1. Composite patch repair definition.

best load transfer and life extension prospect. A detailed design and analysis of the bonded boron concept was carried out. A 26-ply boron/epoxy patch, shown in Figure 40.1, was selected. The potential location of the boron reinforcement on the wing skin is shown in Figure 40.2. Due to the complexity of the structural configuration (pocket area with variable skin thickness) it was considered necessary

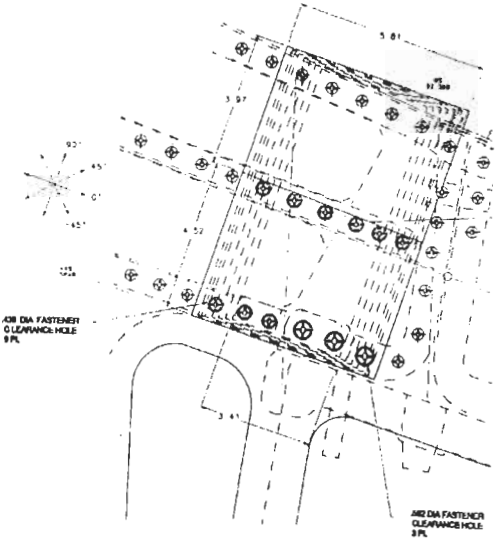


Fig. 40.2. Composite patch repair on the T-38 wing structure.

to carry out a test program to verify the design and analysis so that confidence can be assured in the repair concept.

40.2. Validation testing

A test validation program was carried out to verify composite patch reinforcement design and verify by test the predicted life extension obtained with the composite reinforcement.

40.2.1. Test specimen description

The test specimen configuration is shown in Figure 40.3. The pocket area in the test specimen was designed to represent the cracking location in T-38 lower wing skin pocket between 39% and 44% spars at WS 78. The thickness and pocket dimensions were representative of the actual dimensions in the wing skin. Each specimen had two pockets so that two sets of data can be obtained from each specimen. The cracks in the two pockets were sufficiently apart so that there was no interaction between the cracks in each specimen. Two specimen were fabricated, one to be used as a baseline specimen without composite reinforcement and other to be repaired with composite reinforcement.

Initial flaws were introduced in the test specimens in the pocket area on the side representing the inner moldline of the wing. The flaws were semicircular with 0.125-inch radius. The length of the flaw on the specimen surface being 0.25 inch and

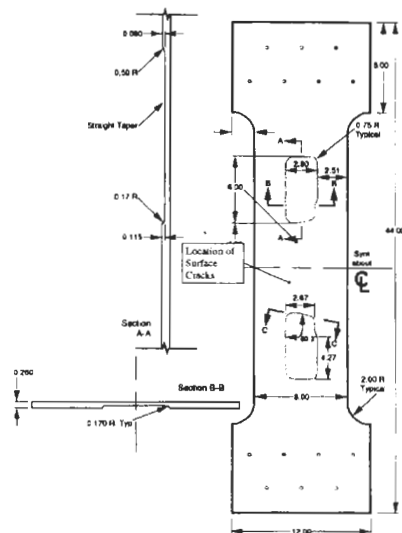


Fig. 40.3. Wing skin test specimen configuration.

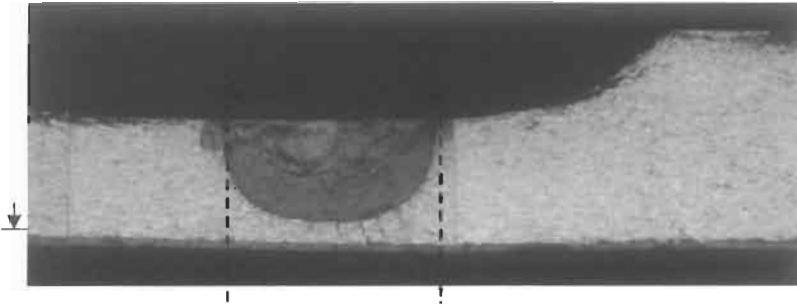


Fig. 40.4. Photomicrograph of EDM area in failed test specimen.

depth of flaw through the specimen thickness being 0.125 inch. The flaws were introduced by electric discharge machining (EDM) process to produce a flaw 0.005-inch thick. Figure 40.4 shows a photomicrograph ($7.5\times$) of the EDM machined area from the tested specimen.

40.2.2. Composite reinforcement fabrication and bonding

A requirement for the lower wing skin reinforced with boron/epoxy composite patch is having access to the fasteners connecting lower wing skin to 44% spar at the location of the reinforcement. This required that the holes be drilled through the reinforcement at the exact location of the holes in the wing skin. The ply orientations and configuration are shown in Figure 40.1. During the cure Teflon plugs were installed in the holes in the laminate to control resin bleed and maintain the hole dimensions. The plugs were installed to the thickness of the laminate in order to maintain uniform pressure over the laminate surface during the cure process. The laminate was cured in an autoclave at a pressure of 90 psi and a temperature of 240 °F for 60 min. Non-destructive inspection (NDI) using through transmission was performed on each laminate. NDI showed the laminate to be of good quality free of defects.

The patch area of the validation test specimen was anodized using the phosphoric acid non-tank anodize (PANTA) process. The bond surface was primed with Cytec BR127 primer and cured at 200 °F for 1 h. The bond surface of the boron patch was prepared for bonding by abrading the surface with 240 grit silicon carbide abrasive sheet. The surface was then solvent wiped with MEK and wiped dry with a clean dry cloth. On ply of Cytec FM73 film adhesive was applied to the boron patch and the patch was installed on the bond surface of the test specimen. The assembly was vacuum bagged, placed in an oven and cured at 210 °F for 120 min under a vacuum pressure of 12 to 15 inches of mercury. The bonded assembly was ultrasonically inspected for disbonds and the “C” scans showed no defects.

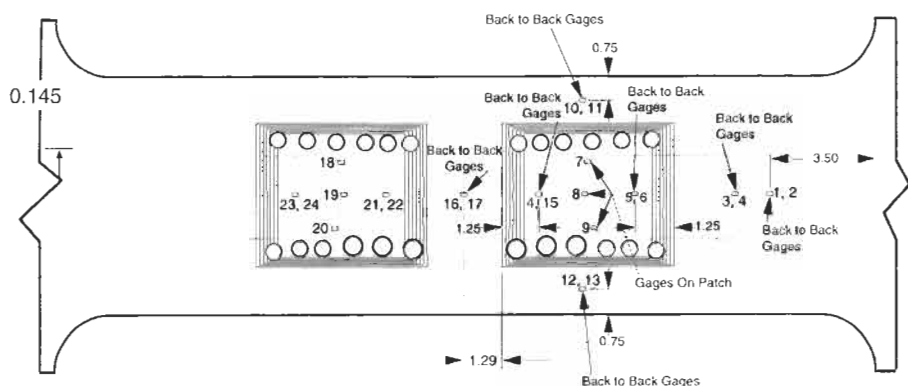


Fig. 40.5. Strain gage locations on test specimen.

40.2.3. Strain gage installation

Nine strain gauges were installed on the baseline specimen without the composite patch and twenty four gauges were installed on the test specimen with the boron patch at the locations shown in Figure 40.5.

40.2.4. Test spectrum and equipment

All the specimens were tested to a stress spectrum representing the T-38 Lead-in-Fighter usage. One pass through the test spectrum represented 1000 flight hours. Maximum spectrum stress was 34.675 ksi.

The tests were conducted on two-post MTS servohydraulic test frames using 442 console controllers. All crack measurements were made visually on the surfaces of the specimens using Bausch and Lomb stereo microscope.

40.3. Test results

40.3.1. Strain gage results

The observed strains at 29% of the maximum spectrum load in test specimen without composite reinforcement are shown in Figure 40.6. The figure shows that the strains in the center of test specimen are almost the same on both surfaces i.e. the surfaces representing inner and outer moldline of the wing skin, indicating no bending in the center of the specimen. Also, the back to back gauges in the center of the pocket area show identical strains, indicating no local bending in the center of the pocket. The gauge near the grip area on the surface of the specimen representing inner moldline of the wing skin shows lower strains compared to the

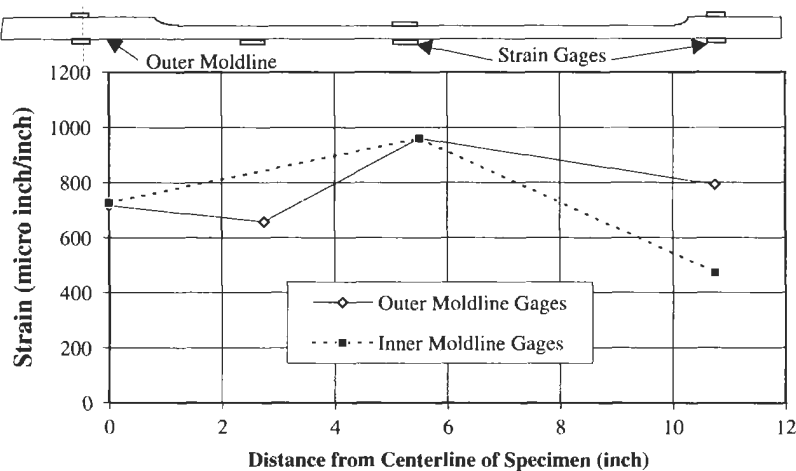


Fig. 40.6. Strains in baseline specimen without composite reinforcement.

one on the back side due to the gauge being close to the machined pocket. The skin strain has to gradually reduce to zero at the end of the pocket.

The strains in the test specimen with composite reinforcement are shown in Figure 40.7. These strains are shown at 29% of maximum spectrum load. The strain gauge data shows that the strain in the center of specimen is not the same on both surfaces of the specimen. The strain gauge on the composite reinforcement side shows strains that are 60% higher than those on the side without reinforcement. This indicates significant amount of bending caused by the composite reinforcement.

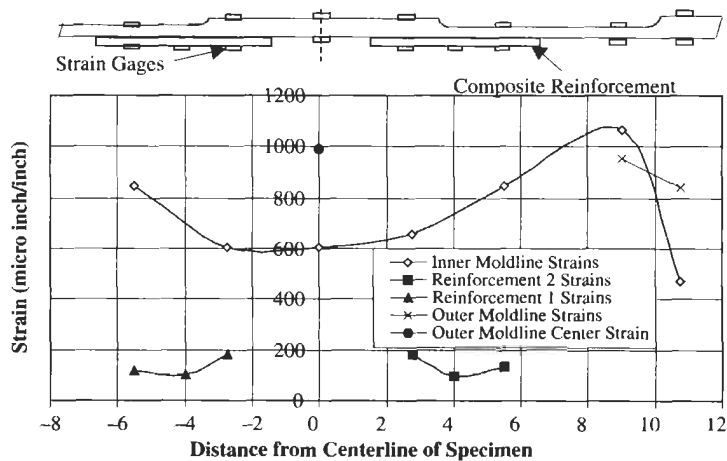


Fig. 40.7. Strains in specimen with composite reinforcement.

A comparison of metal strains in the pocket at locations where there is no composite reinforcement (9 inches from specimen centerline) and location where there is reinforcement (5.5 inches from specimen centerline) indicates that the strain in metal is reduced from 1065 micro inch/inch to 848 micro inch/inch. This represents a reduction of about 20% in strain. Thus, the effect of composite reinforcement is to reduce pocket strain by 20%. Figure 40.7 shows relatively small strains in composite reinforcement compared to skin strains. It may be noted that the modulus of composite reinforcement in loading direction is 20.5×10^6 psi compared to 10×10^6 psi for aluminum.

40.3.2. Crack growth results

During the testing it was observed that the crack tips in both the test specimens were growing at almost the same rate initially for about 1500 flight hours of spectrum testing. However, when the crack tip adjacent to the end of the machined pocket was closer to the pocket edge it grew much slower compared to the other tip which was away from the edge of the pocket. The crack growth rate was found to be significantly different at the crack tips in both the pockets of the test specimen. This behavior was observed for the specimen with and without composite reinforcement.

Crack growth in baseline specimen without composite reinforcement

The half crack length as a function of flight hours for the left and right crack tips is shown in Figure 40.8 for upper pocket. The half crack length is measured from the centerline of the EDM flaw. The figure also shows average crack length. It is seen that after about 1200 flight hours the right crack tip is growing considerably slower as compared to left crack tip. At 7000 flight hours the half-crack length at the left crack tip is 50% longer than that at right crack tip. The slower crack growth of the crack tip adjacent to the edge of machined pocket is attributed to the stiffening provided by the thicker skin out side the pocket and there by reducing the

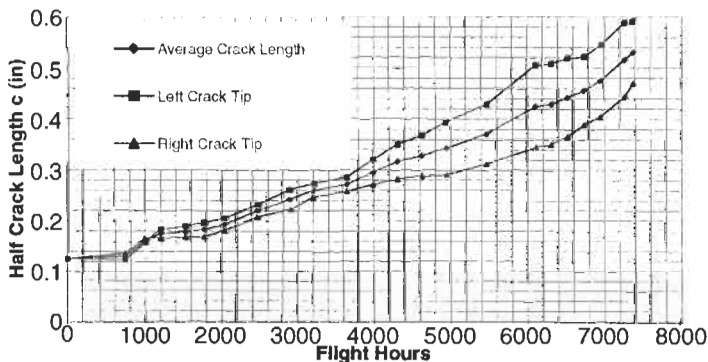


Fig. 40.8. Crack growth in baseline test specimen without composite reinforcement (upper pocket).

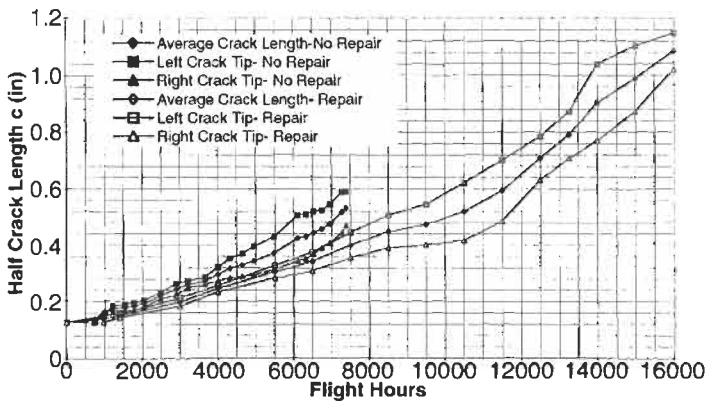


Fig. 40.9. Comparison of crack growth in test specimens with and without composite reinforcement (upper pocket).

stress intensity factors ahead of the crack tip. A similar crack growth behavior was observed for the lower pocket.

Crack growth in specimen with composite reinforcement

The crack growth in the upper pocket of the specimen with composite reinforcement is shown in Figure 40.9. The figure also shows crack growth in the specimen without composite reinforcement for comparison. It is seen that once again the right crack tip closer to the machined pocket edge grows considerably slower as compared to the crack tip away from the pocket edge. Each of the crack tips in the specimen with reinforcement grows slower as compared to the crack in specimen with no reinforcement. The presence of reinforcement significantly increases crack growth life.

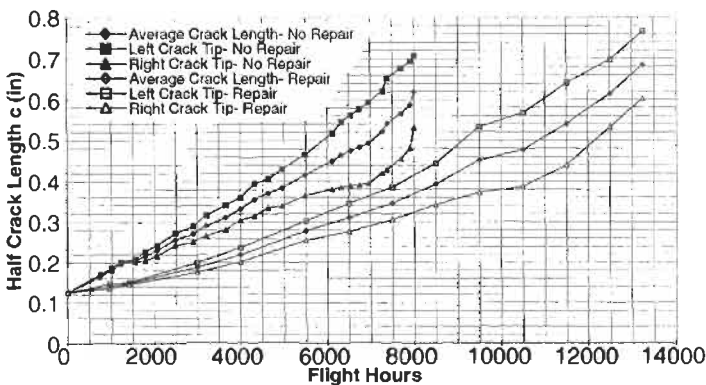


Fig. 40.10. Comparison of crack growth in test specimens with and without composite reinforcement (lower pocket).

The crack growth in the lower pocket for the specimens with and without reinforcement is shown in Figure 40.10. The figure shows significant increase in crack growth life. It is seen that at 8000 flight hours the average crack length in the specimen with reinforcement is about half of that in the specimen without reinforcement even though the starting crack lengths in both the specimens were the same.

40.4. Comparison between test results and analytical predictions

The analytical predictions of crack growth in specimens with and without composite reinforcement were not straight forward due to the fact that the initial flaw was introduced at radius in the pocket area. The crack tips experience stiffening due to thicker section on one side of the crack surface. In addition, the crack growth predictions become complex due to one crack tip experiencing the stiffening effect of machined pocket edge and the other crack tip being away from the edge. The crack growth predictions were further complicated due to the fact that one crack tip was growing at half the rate as compared to the other tip. All the crack growth models assume same crack growth rate at both the crack tips. Considering the complexity of the crack growth, no attempt was made to predict crack growth at individual crack tips of the specimens but techniques were developed to predict average crack length.

Crack growth predictions in specimen with no composite reinforcement

The thicker wing section in the pocket area along the crack plane in the chordwise direction affects the crack growth in the machined pockets. In addition, the crack tip near the thicker section of the pocket experiences stiffening due to thicker section in the spanwise direction. To account for these stiffening effects the stress intensity factors for a through crack geometry need to be modified. In reference [8], analytical stress intensity factors have been developed for cracks at root radii in skins with lands. These stress intensity factors were used to account for the effect of stiffening in the chordwise direction. The influence of one crack tip experiencing the stiffening effect due to thicker section in the spanwise direction was accounted for by using stress intensity factors for through cracks in sheets with different thickness from reference [9]. The modified stress intensity factors were used in Forman equation to make crack growth predictions under spectrum loading. The unequal crack growth at the crack tips was accounted for by modifying crack growth constant c in the Forman equation. As the test data indicated crack growth rate at one crack tip to be one half of that at other crack tip, average value of c equal to 0.75 times the normal value was taken in Forman equation for crack growth predictions.

A comparison of predicted crack growth and observed crack growth is shown in Figure 40.11 for upper pocket. The figure shows a good correlation between predicted and observed average crack length.

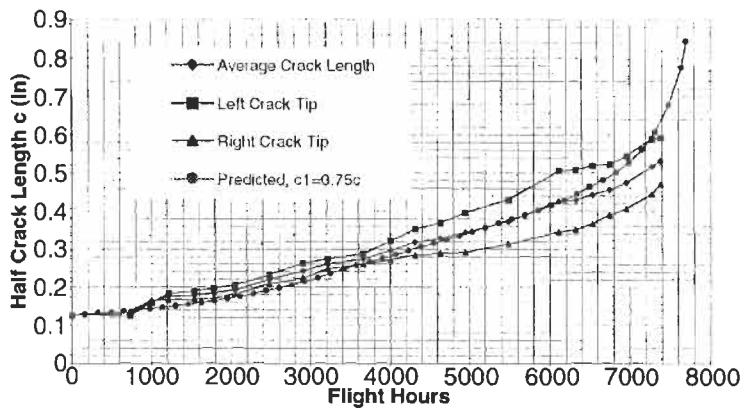


Fig. 40.11. Comparison of test and predicted crack growth in specimens without composite reinforcement (upper pocket).

Crack growth predictions in specimen with composite reinforcement

To make crack growth predictions in test specimen with composite reinforcement the stress intensity factors for the test specimen without reinforcement were modified to account for the influence of the reinforcement. The modification was done using the analytical techniques developed in reference [10] and incorporated in the Air Force computer code AFGROW [11]. The AFGROW code was used to obtain stress intensity factors for a cracked sheet with bonded repair. These stress intensity factors were multiplied by the stress intensity factors for pocket area with no reinforcement. The stress intensity factors thus obtained were used in Forman equation to predict crack growth life. The constant c in Forman equation was taken as 0.75 times the normal value for 7075-T73 aluminum to compensate for unequal crack growth at two crack tips. The predicted and observed average crack growth in the upper pocket of the specimen with composite reinforcement is shown in Figure 40.12. The figure also shows predicted and observed crack growth in

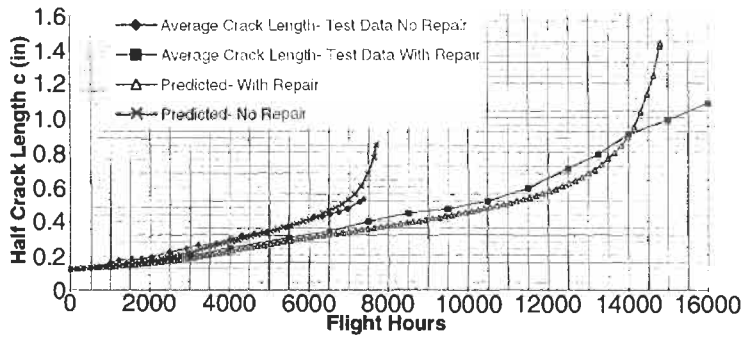


Fig. 40.12. Comparison of test and predicted crack growth in specimens with and without repair (upper pocket).

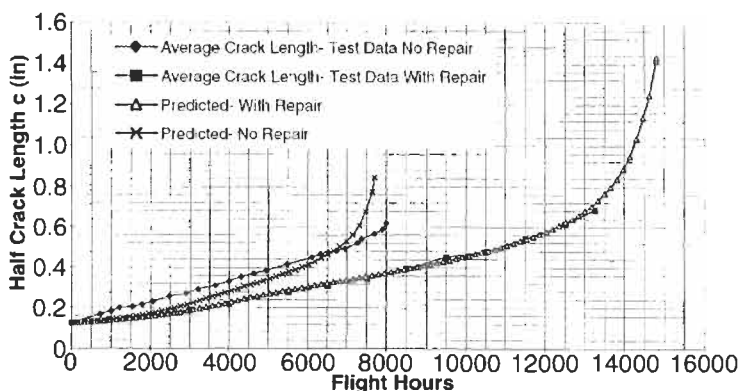


Fig. 40.13. Comparison of test and predicted crack growth in specimens with and without composite reinforcement (lower pocket).

specimen without composite reinforcement for comparison. The comparison between predicted and observed crack growth is excellent. The composite reinforcement doubles the crack growth life.

The comparison of predicted and observed crack growth behavior in lower pocket is shown in Figure 40.13 for specimens with and without composite reinforcement. Once again comparison between predicted and observed crack growth for specimen with composite reinforcement is excellent. These results indicate that the analysis of references [10,11] can be used with confidence for damage tolerance analysis of metallic structures bonded with composite reinforcement.

40.5. Application of composite reinforcement to a full scale wing test

A T-38 wing is undergoing full scale durability test under Lead-in-Fighter spectrum loading at Wright Patterson Air Force Base, Ohio, as a part of Air force Contract F33615-9-C-3201, entitled "Advanced Technology Redesign of Highly Loaded Structures (ATROHS)". Prior to the commencement of fatigue testing, composite reinforcements were bonded to both left and right wings in the pocket areas between 44% and 39% spars and 39% and 33% spars. The wing has undergone 3500 h of spectrum load testing. No problems have been encountered with the composite reinforcement so far. Nondestructive inspection has not shown any disbonding of the reinforcement.

40.6. Conclusions

The following conclusions are drawn from the present studies:

1. Composite patch reinforcement concept can be effectively used to retard crack growth at complex structural details such as skins with variable thickness (pockets).
2. Modified stress intensity factors accounting for the presence of pocket areas can be used to predict crack growth life with good accuracy.
3. The crack growth in the pocket areas of skins is influenced by variation in skin thickness, resulting in significantly different crack growth rates at the crack tips. This behavior can be accounted for in crack growth life predictions by modifying stress intensity factors and crack growth rate constants.
4. The composite patch repair analysis in AFGROW can predict crack growth behavior in repaired structure with good accuracy.

References

1. Ratwani, M.M., Koul, A.K., Immarigeon, J.P., *et al.* (1997). Aging airframes and engines. *Proc. of Future Aerospace Technology in the Service of Alliance, Volume 1 – Affordable Combat Aircraft, AGARD-CP-600*.
2. Baker, A.N. (1995). Bonded composite repair of metallic aircraft components. *AGARD Proc. Composite Repair of Military Aircraft Structures*, January.
3. Belason, E.B. (1995). Status of bonded boron/epoxy doublers for military and commercial aircraft. *AGARD Proc. Composite Repair of Military Aircraft Structures*.
4. Poole, P., Young, A. and Ball, A.S. (1995). Adhesively bonded composite patch repair of cracked aluminum alloy structures. *AGARD Proc. – Composite Repair of Military Aircraft Structures*, January.
5. Cockran, J.B., Christian, T. and Hammond, D.O. (1988). C-141 Repair of Metal Structures by Use of Composites, *Proc. of ASIP meeting*.
6. Fredell, R.S. (1994). Damage Tolerance Repair Techniques for Pressurized Fuselage, WL-TR-94-3134, June.
7. Mazza, J.J., Forte, M.S. and Cramer, B.D. (1996). F-16 Fuel Vent Hole Bonded Repair Update. *Proc. of Air Force 4th Aging Aircraft Conference*, United States Air Force Academy, Colorado, July.
8. Ratwani, M.M. (1981). Stress Intensity Factors for Cracks at Root Radii in Skins With Lands, NOR 81-58, July.
9. Tada, Paris and Irwin, *Stress Intensity Factors Handbook*.
10. Ratwani, M.M. (1978). Analysis of Cracked Metallic Layer Bonded to an Orthotropic (Composite) Layer, NOR 78-32, March.
11. "AFGROW" Computer Code Developed by Wright Patterson Air Force Base, Ohio.

Chapter 41

CASE HISTORIES: ADVANCED COMPOSITE REPAIRS OF USAF C-141 AND C-130 AIRCRAFT

W.H. SCHWEINBERG and J.W. FIEBIG

Structures Branch, Technical and Engineering Sciences Division, Technology and Industrial Support Directorate, Warner Robins Air Logistics Center, Robins Air Force Base, Georgia 31098

41.1. Background

The C-141 aircraft is experiencing primary structure fatigue cracking due to age, and increased and expanded mission requirements. This can degrade the fail-safe capability of the aircraft and adversely impacted aircraft availability. Many of the cracks are in areas that are not readily repairable using conventional methods. Earlier studies by Lockheed Martin Aeronautical Company (LMAC) demonstrated that bonded advanced composite repairs presented real possibilities as a viable repair method for many of the cracks. In 1993 a widespread fatigue cracking problem was identified in the Inner Wing lower surface weep holes. This condition required some aircraft grounding and/or placed severe flight restrictions on many of the aircraft. The intent of this chapter is to address the actions taken to transition advanced composite repairs from a LMAC study to a major and intense repair effort crucial to correcting the weep hole problem and to the point that advanced composite repairs are now the repair option of choice for many primary structure repair applications on the C-141 and C-130.

The C-141 aircraft was designed by LMAC primarily for strategic airlift and 284 were manufactured for the United States Air Force between 1964 and 1967. The aircraft was designed for a service life of 30000 h and a full-scale fatigue test to 90000 cyclic test hours was accomplished. Analysis of the full-scale wing/fuselage fatigue test article was completed in 1981 through a residual strength test and partial tear down. The aircraft was modified in the late 1970s and early 1980s to lengthen the fuselage by approximately 6 m and provide an air-refueling capability. As part of the modification, a durability and damage tolerance analysis (DADTA) was accomplished on the complete structure. The analysis used information from the full-scale fatigue test and tear down, the design stress analysis, and the service

history. As a result, 121 areas were identified (69 of which were in the wing) for further analysis and closer monitoring. With expanded missions made possible by the modifications, changing military needs and with much of the fleet in excess of 30000 h, the need for new and flexible repair methods became evident.

In 1986, Warner Robins Air Logistics Center (WR-ALC) contracted with LMAC to evaluate and demonstrate the viability of using bonded advanced composite repairs for a priority group of areas selected from the original 121. Five candidate repair locations were identified (Figure 41.1). Composite repair designs were developed and finite element analysis (FEA) was accomplished on all five areas. Application procedures were developed and necessary equipment identified. Both boron and graphite were identified as candidate repair materials, and two demonstration repairs were applied using both materials. The LMAC effort [1] was quite extensive and proved that advanced composite repairs were definitely a viable repair option from a structural standpoint.

WR-ALC has, for many years, been accomplishing metal bond and composite overhaul, remanufacture and redesign. During WR-ALC review of the LMAC effort for possible depot use, concerns were identified with the LMAC approach as to the method of composite doubler application, particularly as to the surface preparation flexibility and consistency. In 1991 WR-ALC identified these concerns to Air Force Research Laboratory (AFRL) as to the need for a nonacid surface preparation method for on aircraft use which would still provide phosphoric acid

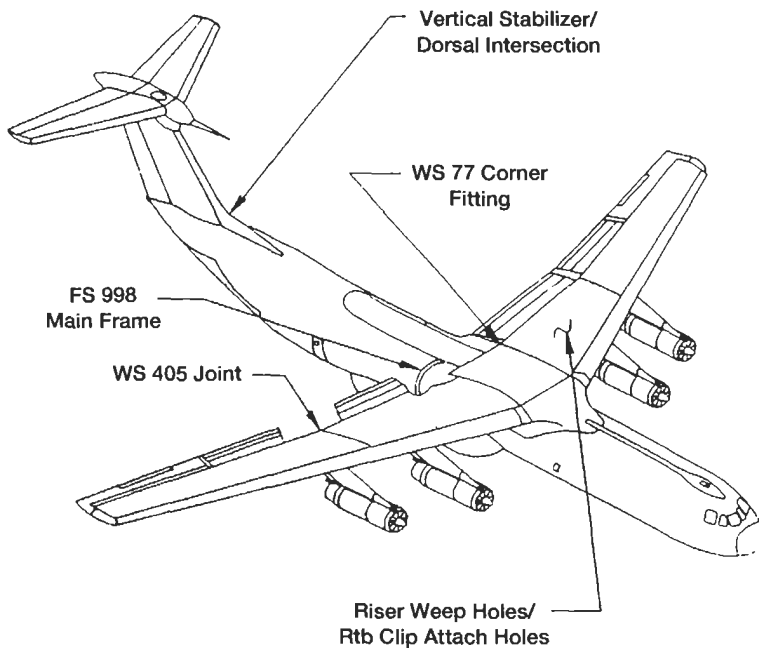


Fig. 41.1. Lockheed selected potential composite repair sites for the C-141.

anodize (PAA) tank or near tank quality for long term durability. AFRL worked with the University of Dayton Research Institute (UDRI) to identify possible methods and alternatives. The standard wedge test (ASTM D 3762) was used as the primary method of comparison. Several methods were explored including a Grit-Blast/Silane and Prime (GBS) method similar to that of the Australian Research Laboratory (ARL) which had been synopsized in several technical papers relating to composite repair. Significant testing was accomplished under the "Nonmetallics, Test and Evaluation" contract (F33615-89-C-5643) to quantify all of the parameters and all results were openly published without restriction.

When the LMAC DADTA was accomplished, the longitudinal spanwise lap splices between the lower surface inner wing panels were identified as an area of definite concern and one that warranted additional inspection and evaluation. During a LMAC teardown of a retired C-141 aircraft wing to evaluate this and other structural areas, a significant cracking problem was identified with the Inner Wing weep holes. The weep holes are 6.35 mm diameter holes drilled near the base of the wing risers (Figure 41.2) which allow all fuel to be accessed by the fuel pumps and to allow ready drainage of tank condensation. There are approximately 750 weep holes in each Inner Wing. The advanced composite repair of this area was one of the five candidate locations analyzed by LMAC and it was recognized that an advanced composite repair was the only viable repair option if the magnitude of the

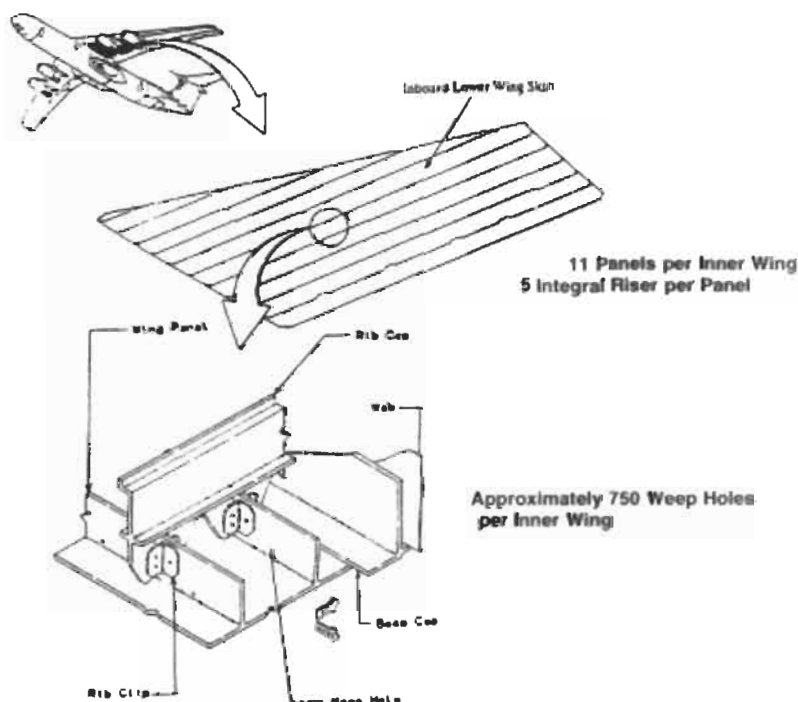


Fig. 41.2. View of C-141 inner wing structure showing integral risers and weep holes.

problem was as serious as the teardown indicated. Restrictions were placed on individual C-141 aircraft based on total wing lower surface damage hours. This included gross weight limits and in some cases grounding. WR-ALC developed a comprehensive four step plan to address the problem. The four basic steps were:

1. Accomplish a fleet wide inspection of all weep holes on all aircraft (over 375000 holes) using a bolt hole eddy current inspection technique.
2. Attempt to remove the smaller cracks by reaming the hole, in incremental steps, to a larger size and then cold working the hole to increase the fatigue resistance (this step corrected approximately 82% of the cracked holes).
3. Apply a bonded boron repair to those holes which did not clean up through reaming.
4. If there was a significant quantity or cluster of cracked holes that would not cleanup, then the whole wing plank was replaced – all 10 m of it.

An effort of this magnitude, complexity and criticality was a total team effort which required considerable effort and innovative approaches by many Air Force organizations and contractors.

41.2. Repair design

A very conservative engineering approach was taken for the composite repairs by assuming the member was totally severed and the stress increase immediately adjacent to the repair was to be kept to a minimum. The composite repairs were required to last 15000 flight hours.

Substantial FEA was accomplished for both the repair and the parent structure. The stress field for the lower wing surface is well known and is a near uniaxial condition spanwise with nearly equal loads in tension and compression. LMAC's original analysis had clearly shown that a composite repair would significantly reduce the stress at the crack location. The initial WR-ALC effort was to look quickly at the issue of proximity in that it would not be a single repair but the possibility of several repairs in close proximity to one another. A coarse two panel wide shell element analysis was accomplished to evaluate the proximity issue. Using this coarse model, initial evaluations were also made on the overall repair concept to simplify the repair by eliminating the two internal wing surface doublers of the original five planned in the LMAC study (Figure 41.3) and using only three doublers and increasing the number of plies in the external wing surface doubler.

Particulars of the composite doubler design as to length and capability were based on criteria presented in the LMAC report [1] and other articles [2–5]. Ply stacking, ply step-off and doubler shape was based on WR-ALC experience with composite repairs of composite structures and numerous department of defense (DoD) programs on repair of composite structures. Using these basic inputs, a detailed 2D shell element analysis of an assumed standard repair was accomplished to look at ply by ply stresses and further optimize the repair as to doubler shape, size, location and quantity. This FEA showed that a three doubler configuration was acceptable with the exterior doubler in a semi-elliptical shape and extending

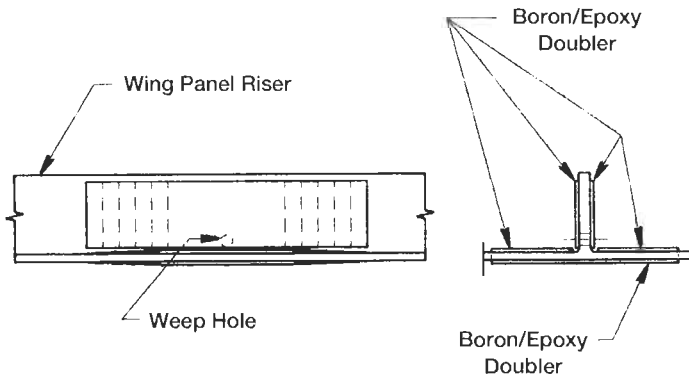


Fig. 41.3. View of C-141 wing panel section showing original planned five doubler repair scheme and eliminated inner doublers.

beyond the interior doublers. Various materials for the doublers were also studied. For this application it was found that graphite would work as well as boron. However, boron was selected due to material availability and the need to eliminate the problems of galvanic corrosion when fastening through the doublers was required.

With favorable initial results, a considerable amount of additional very detailed 3D FEA was accomplished (Figure 41.4) to further evaluate repair size, shape, stress reduction, and impact on surrounding structure. Results of the 3D analysis were very similar in many respects to the 2D shell FEA, but it was found to be more accurate, realistic and less conservative than the shell FEA. To validate the 3D FEA model, a segment of an actual wing plank was repaired to identically match the model (Figure 41.5), instrumented, and statically tested. Correlation between

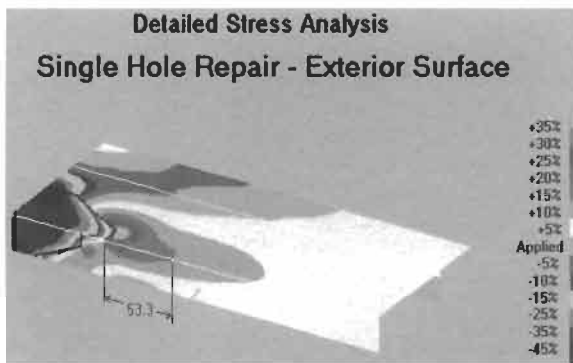


Fig. 41.4. 3D finite element analysis of C-141 wing plank showing estimated wing plank stress levels with boron doubler repairs.

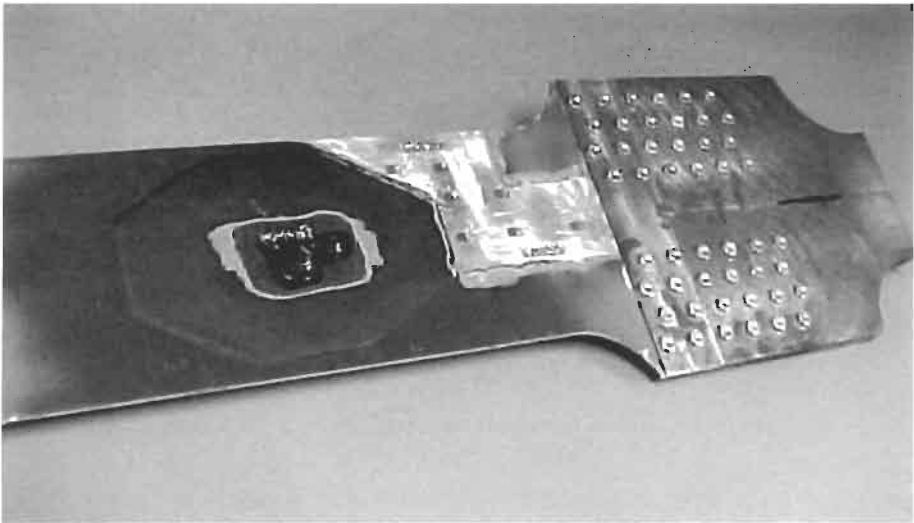


Fig. 41.5. Static and fatigue test specimen made from a C-141 wing plank with three doubler bonded composite repair.

FEA predicted results and the actual was quite good. The shape and appearance of the stress contours for the 3D analysis were basically identical to those for the shell analysis but the stress levels were lower in the surrounding structure with less impact on adjacent repairs which allowed for closer spacing of repairs. The analysis also showed that several smaller doublers in close proximity actually resulted in lower surrounding stress than one larger doubler to span the area between the doublers. From this it was found that the best approach was to use a thick-thin-thick doubler. This used the two smaller doublers to repair the crack with a thinner overlay doubler between to reduce the stress impact on the surrounding area. The analysis also identified the need to closely control the location of the ends of the doubler repairs due to a stress increase (Figure 41.6) but identified that the stress increase dropped quite quickly to the maximum desired 15% increase. The 3D analysis did show some out of plain bending effects due to the switch to three doublers in lieu of five, but the impact was small (Figure 41.6). All FEA was linear with SDRC Supertab for the model development and analysis and CSA-NASTRAN as the solver.

Due to the magnitude of the repair effort and the need for expeditious resolution of the problem, contractual support was used to supplement both the inspection and composite repair of the weep holes. Composite Technology Incorporated (CTI) was contracted to install doublers at Robins AFB. There were some differences in the doubler designs between WR-ALC and CTI, but both designs followed the same basic principles and were very conservative in nature.

Time was a premium and considerable additional engineering actions and FEA were accomplished concurrently with the actual repair effort. Based on the detailed

Deleted Stress Analysis

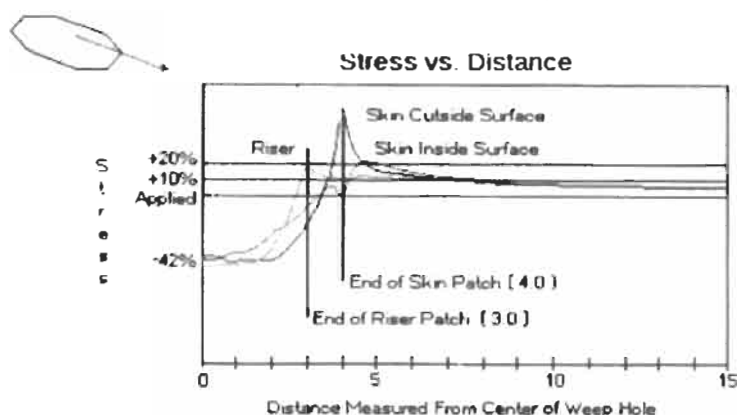


Fig. 41.6. Analysis of stresses in the wing plank at the ends of the bonded composite doublers.

FEA, a damage tolerance analysis (DTA) [6] was performed. The DTA showed that for a crack running down the riser, the doublers increased the safety limit by 33 times over the nonrepaired configuration and a 60 times increase for a crack running up the riser. The DTA was later validated by actual fatigue testing to a critical flight spectrum for the area. The specimens were precracked to a rather large crack of approximately 6.35 mm. Unrepaired the cracked specimens reached critical crack length of greater than 57 mm in 13000 to 15000 equivalent flight hours (EFH). Other precracked specimens were repaired in the same manner under the same conditions and by the same personnel as used for the actual repairs. When fatigue tested at room temperature there was no measurable crack growth in the repaired specimens following 30000 EFH and no appreciable crack growth following 15000 EFH when tested at -54°C . Long term thermal shock (> 1000 h) and salt fog (> 1000 h) testing were also accomplished on a freestanding repaired specimen with no negative results.

41.3. Installation development

As part of the joint AFRL/UDRI effort to develop an on aircraft nonacid surface preparation method, an external composite repair was demonstrated on an F-16 wing. The timing of this demonstration was quite fortuitous. With the success of this demonstration, WR-ALC tasked AFRL with the tremendous effort of developing the baseline procedures for bonding the boron weep hole doublers to the C-141 wing. A very large segment of an Inner Wing was supplied to AFRL for this development effort. Thermal surveys were accomplished, equipment modified, surface preparation procedures were definitized for the application and practice

repairs accomplished. Demonstration installations of composite repairs were then accomplished at Robins AFB on actual cracked weep holes by AFRL using their developed procedures, and then by CTI with their own independently developed proprietary procedures. Both approaches proved acceptable. The repairs were evaluated for bond integrity using ultrasonics, but it was quite apparent that some other method of non-destructive inspection (NDI) would be required for the overall repair effort.

41.4. Industrialization and repair

Though the repair demonstrations went well, considerable work remained to basically industrialize the effort to allow repair on a production scale while maintaining the highest quality possible. Considerable equipment was procured and modified to meet the specific needs of the repair procedure. Several key certified senior bonding mechanics and engineers were identified and trained by AFRL on the surface preparation and installation procedures developed by AFRL. Subsequent training was accomplished by WR-ALC using the AFRL trained personnel. CTI accomplished their own personnel training for their proprietary process. All mechanics however were required to qualify in the appropriate surface preparation technique through standard wedge testing (ASTM D 3762). The WR-ALC wedge test specimens were prepared totally by each mechanic in the aircraft hangar using the equipment, materials, and procedures to be used for the actual repairs. All specimens for all mechanics were tested by AFRL to ASTM D 3762, tested at 49 °C and 95 to 100% relative humidity, with a 5.1 mm maximum crack growth with 100% cohesive failure in 24 h as the acceptance criteria. For the WR-ALC repair effort, the AFRL baseline procedures were used to develop a much more detailed process specification to address additional safety and environmental concerns and also to include numerous quality and NDI steps. All repairs were accomplished in heated hangars. The AFRL developed surface preparation method requires a continuous non-stop effort from the time the aluminum surface is initially scuff sanded to remove the corrosion protection until the bonding primer is cured. This normally required about 12 to 14 clock hours and did require flexible personnel management and work hours to assure there were no breaks in the effort.

Since the repair sites were basically flat, the large majority of the doublers were pre-cured in an autoclave to maximize the material properties. Bonding the doubler to the wing was accomplished by vacuum bag and heat blanket. In most cases, the doublers for the risers inside the fuel tank and the external doubler were applied simultaneously. Due to the amount of surrounding structure in several repair locations, thermal uniformity was a problem and did require multi-zone heating capability or supplemental heating with external infrared lamps. The number and orientation of boron plies in the repair doublers were basically standardized. It was also hoped that the size of the doublers could be standardized for efficiency and consistency. However there was enough variation in location, adjacent fasteners, quantity of holes and surrounding structure, that each doubler was specifically

made for each repair site with variations in size and to some extent shape. The external doubler sizes varied from a routine 120 mm by 200 mm to 250 mm by 940 mm. The internal doubler repairs varied a little in height; length varied with respect to the external doubler. Several times on larger doublers, co-curing and/or a mix of pre-cure and co-cure was accomplished using a double bag method to reduce the porosity in the adhesive bond line. In locations where there were several cracked holes in close proximity, the required doubler was applied to the crack and a thinner overlay doubler was used over the surrounding area to reduce the stress concentrations and impact on the surrounding structure. Some of the shapes for the external doublers became quite unusual when there were several cracks in close proximity.

WR-ALC developed a conservative accept/reject criteria for the composite doublers and for the installed adhesive bond integrity. No delaminations were allowed in the composite doublers, and when installed no adhesive disbonds/voids were allowed in the ply transition area or within one inch of any edge or within one inch of the crack. In all other areas, a total of 5% of the remaining area could be disbonded with no single disbond greater than 12.5 mm in the longest direction. Several non destructive inspection (NDI) methods and equipment types were evaluated, none proved truly satisfactory. Luckily, WR-ALC had a portable thermal imaging capability available that was used for a different application. NDI calibration standards were developed using actual C-141 wing plank sections with intentional doubler interply delaminations and doubler to metal disbonds based on the above accept/reject criteria. The portable thermography unit was capable of clearly and consistently identifying both the delaminations and disbonds. The thermography NDI method has proven to be quite accurate, consistent, flexible and quick, and allows for easy recording of the installed doubler condition for future reference and follow-up inspections. Additional thermal imaging equipment was procured and used quite effectively by both WR-ALC and CTI. Considerable additional application development with advanced equipment has been accomplished by WR-ALC for the use of thermal imaging of bonded repairs.

41.5. Success and failures

The whole weep hole repair effort was a tremendous task including not only the repair efforts of inspection, ream/cold work, composite repair and panel replacement, but required considerable manpower and effort in management, engineering, scheduling, planning and procurement. The overall repair effort began in September 1993 and was completed in December 1994 with all 243 aircraft being returned to unrestricted flight. Follow up inspections of all weep holes continues to be accomplished on the aircraft at every depot overhaul with a few additional weep holes requiring repair every year. Approximately 770 boron weep hole repairs were made on 170 aircraft by five different sources/contractors at four different sites, though the majority were accomplished by WR-ALC and CTI at Robins AFB. The specific breakout is as follows (some aircraft were repaired by multiple sources):

	# of repairs	# of aircraft
WR-ALC	350	90
CTI	255	52
LMAC	85	18
Chrysler Tech. Airborne Systems	62	9
Air Force Research Laboratory	18	4

The overall removal rate for doublers installed by WR-ALC that did not meet the accept/reject criteria was less than 15%, and less than 5% once the learning curve was overcome.

Follow-up thermography inspections are accomplished on the repairs at every depot overhaul with the results compared to recordings of the original inspections. The field is accomplishing routine eddy current surface scan around all external doublers and there have been no reports of cracks emanating from under the composite doublers.

To date, only one riser doubler set installed by WR-ALC has been known to have disbonded and that one was traced to human error and one external doubler installed by CTI required replacement due to some minor delamination. However, several doublers installed by LMAC have suffered near total delamination. The failures were near total adhesive failure at the adhesive to wing surface interface and are attributed to poor surface preparation of the metal surface (See

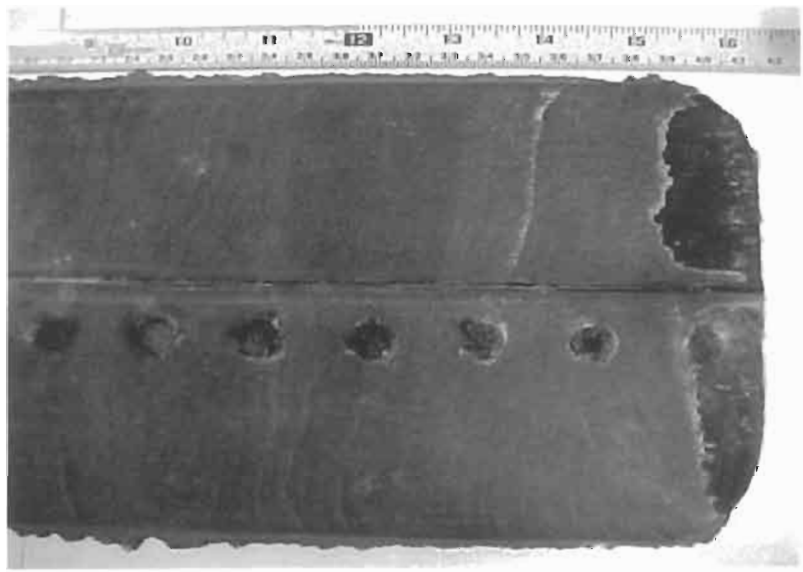


Fig. 41.7. Failed doubler near total adhesive failure.

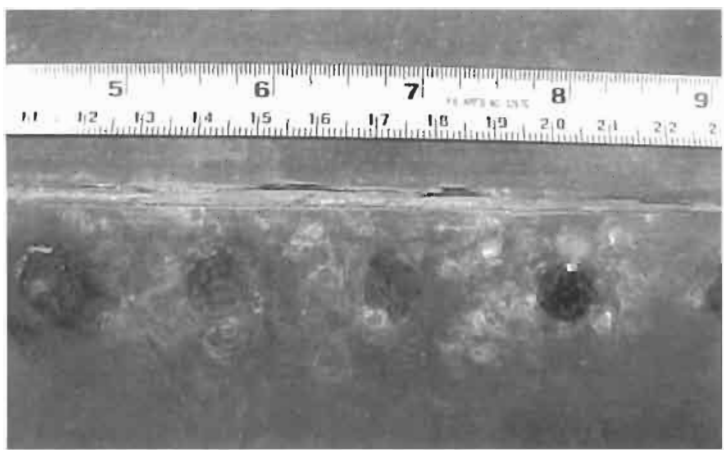


Fig. 41.8. Failed doubler showing adhesive failure and corrosion products residue.

Figures 41.7–41.9). LMAC used a sulfuric acid/sodium dichromate paste etch in lieu of GBS. The failed wing and patch surface had noticeable corrosion products with severe corrosion pitting of the steel fasteners. Other LMAC installed doublers on the same aircraft or even in the same area of the wing were found still be firmly bonded.

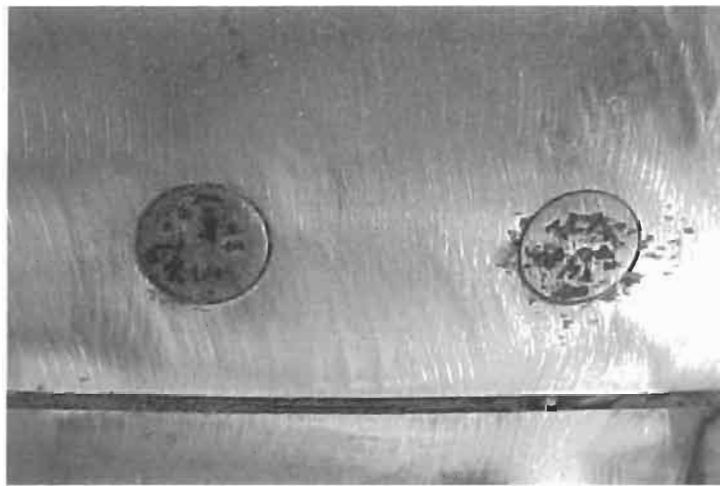


Fig. 41.9. Wing surface after removal of most of the corrosion, note panel joint and taper lock fasteners.

41.6. Other applications

C-141

The basic weep hole repair effort was completed in December 1994. The success of the repair effort clearly showed the viability, flexibility and durability of bonded composite doublers for repair of aircraft primary structure. Do to the success of the repair methodology numerous other primary structure repair applications have been undertaken since 1994 and the size, thickness and complexity of the applications has increased. Other bonded boron repair applications include the Wing Station 77 Corner Fittings and the Vertical Stabilizer/Dorsal Intersection identified in the original 1986 LMAC [1] development effort and are shown in Figure 41.1. The Wing Station 77 repair is 680 mm long and 180 mm wide and 33 plies thick. The Vertical repair is 790 mm long and 115 mm wide and 22 plies thick. The same standard installation procedures developed for the weep hole effort were used for these applications, though some additional steps were added to help in achieving a vacuum and both applications required detailed thermal surveys. Both repairs have been used to repair visible cracks in the structure, and the Vertical Stabilizer repair in particular has been accomplished numerous times.

Boron composite repairs have also been used for repair of other cracks in the C-141 wings that normally would have required replacement of a whole wing panel or a very complicated metal repair. One particular repair that has been accomplished numerous times is for cracks in the lower wing planks at a riser run-out where the wing panels join with the lower fwd spar cap. The repair requires two doublers that are up to 810 mm long with a combined width of up to 310 mm and 22 plies thick. One of the repairs is shown in Figure 41.10.

One special effort accomplished was the repair of a C-141 which sustained ballistics damage. The aircraft sustained two ballistics hits in the wing panels resulting in three significant damages, two entrance sites and one exit. The holes were approximately 19 mm to 25 mm in diameter and two of the hits struck on the riser and panel interface causing damage to the riser and spanwise cracking, one

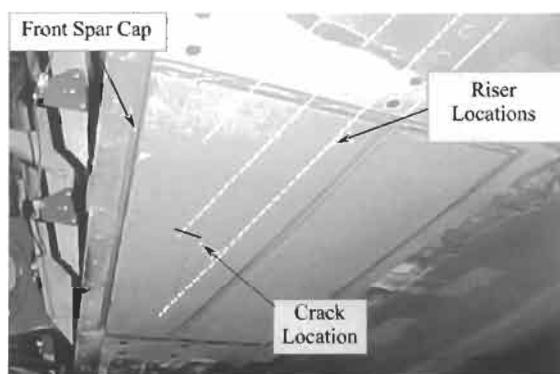


Fig. 41.10. Bonded composite repair over cracks in the lower wing skin of the C-141.

was over 50 mm between the riser and the plank surface. For the most severe damage, precured "L" angle graphite (IM7/977-3) doublers were made for the internal riser repair along with graphite external doublers. Boron was used for two damages, including one that required an "L" angle doubler. All repairs were completed in 10 days allowing quick return of the aircraft to service.

Doubler sizes on the C-141 have grown to as large as 610 mm by 1.12 m and up to 36 plies thick and all were to primary structure. The overwhelming majority of the repairs have been for fatigue cracks with a small amount for corrosion problems. The number of additional bonded composite repairs accomplished on the C-141 since 1994 is in excess of 150 with over 500 total repairs accomplished.

C-130 [7]

As the viability and flexibility of composite repairs became known, applications on the C-130 have developed. In most of the C-130 applications boron repairs have been used to restore the strength to areas that have been ground deeply to remove corrosion. The primary application is to correct severe and wide spread corrosion pitting of the lower center wing surface immediately aft of the inboard engines and under the aft nacelle fairing. The wing panels in the area of concern are approximately 3.05 mm thick 7075-T7351. The wing panels run the whole length of the center wing and are mechanically fastened to large hat sections which also run the whole length of the wing. Each wing panel is over 11 m long and 0.66 m wide and is secured to the hat sections with over 3800 interference fit fasteners. Analysis has shown that isolated corrosion damage up to 0.5 mm deep could be simply removed and no repair is required. However, the corrosion has been found to be much deeper and wide spread and long-term durability, and in the worst cases structural integrity, dictate a repair. Corrosion pitting has been found that extends up to 450 mm by 610 mm with depths normally up to 1.65 mm and in a few rare cases up to all the way through the panel. A typical panel condition is shown in Figures 41.11 and 41.12. The standard Technical Order (T.O.) repair for general structural damage to the lower wing panels is to install a fastened metal doubler. However the size and severity of the standard T.O. repaired damage is severely restricted in length and width (one hat section) due to the loading, type of construction and the need to install a large number of additional interference fit fasteners. This causes additional structural, damage tolerance and durability problems so bonded composite repairs were selected as the repair methodology of choice. The only choices are replacement of the whole panel, which is very expensive and time consuming due to the size of the panels, or a bonded composite repair. The bonded composite repair option was selected except for the most extreme cases.

The same basic repair development was accomplished as was done for the C-141 repairs to include detailed FEA and in-service thermal evaluation of the repair site. As for the C-141, the particulars of the composite doubler design as to length and capability were based on criteria presented in the LASC report [1] evaluation of different designs and changes in the variables and material properties. The doubler



Fig. 41.11. Corrosion pitting damage in the lower wing skin of a C-130 aircraft, numbers refer to measured pit depths.

sizes, shapes and thicknesses are tailored for the depth and area of corrosion on each application.

Installation includes replacement of all button head fasteners with flush head, removal of all corrosion pits through grinding, GBS surface preparation and

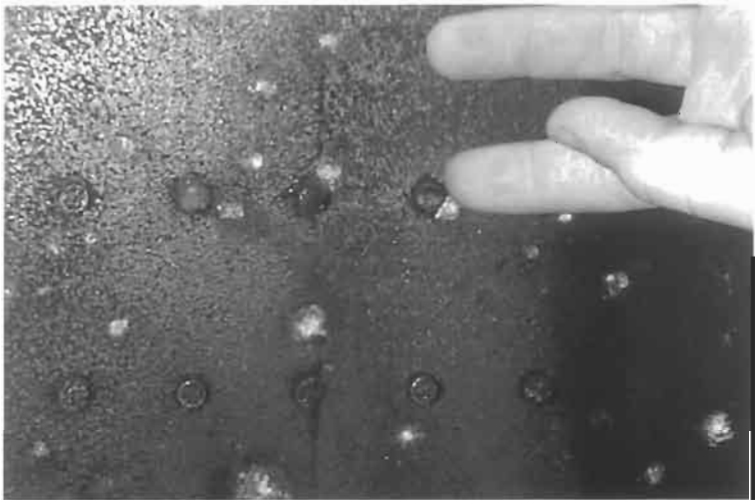


Fig. 41.12. Corrosion pitting damage in the lower wing skin of a C-130 aircraft after initial cleanup note pitting extending under the fastener head.

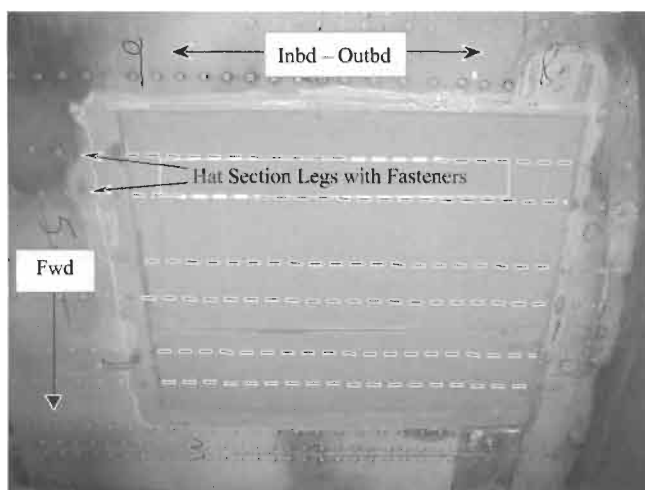


Fig. 41.13. An installed bonded repair doubler used to repair corrosion in the C-130 wing.

secondary bonding of pre-cured boron composite doublers over the corroded area. The ground-out areas are filled with additional adhesive prior to installation of the repair doubler. An installed doubler is shown in Figure 41.13. The doubler sizes vary up to 710 mm by 460 mm and up to eight plies thick. Over 130 repairs on over 80

C-130 aircraft have been accomplished.

On site repairs

To better support the operational squadrons, WR-ALC has developed a mobile repair trailer that can accomplish all forms of bonded repairs in the field (Figure 41.14) with a depot field team. The trailer allows the depot to go to the aircraft wherever it may be and greatly reduces the schedule difficulties and cost incurred with having to return the aircraft to the depot for a bonded composite repair. The trailer is totally self-contained and requires only service stands from the field organizations. The depot field team is responsible for the whole repair, but relies on the operational squadrons for aircraft jacking, fuel and de-fuel operations and final painting. The trailer contains a diesel generator, filtered air compressor, freezer, bond controllers, thermography inspection equipment and all of the associated equipment and material to accomplish two repairs at a time. The trailer and tractor combination is 11 m long, 2.5 m wide, 2.5 m high and weighs 11111 kg and is air transportable by C-130/C-141/C5/C17 as well as over the road. The repair trailer approach has proven quite successful and saves the users approximately \$100000 per aircraft over having to fly the aircraft back to Robins AFB for one specific repair. WR-ALC currently has two units in operation. To date, the repair trailers have been used to accomplish over 115 repairs on over 73 C-



Fig. 41.14. WR-ALC mobile bonded repair trailer.

141's and C-130's at over 15 stateside locations and three overseas locations including eight aircraft for allied nations.

41.7. Cost savings

The bonded composite repair methodology was developed primarily to provide a repair option for primary structure where conventional methods were not viable from a technical or logistics perspective. Significant cost and schedule benefits have also been realized from bonded composite repairs compared to alternative methods.

For the WR-ALC weep hole effort alone, bonded composite repairs eliminated the need to replace 263 wing panels. The cost to replace a wing panel including the removal of the old panel, the cost of a new panel, over 600 new fasteners and all of the man-hours for drilling and installation was over \$165000 per panel. For 263 panels this cost would have been over \$43 million dollars. The total cost for the bonded composite repairs to the 263 panels (many panels required more than one weep hole repair) including the engineering, personnel training, equipment, materials and the actual repairs was \$4.7 million or a savings of over \$38 million. No attempt has been made to calculate a savings for the savings in schedule or aircraft downtime, which would be considerable since the panels and fasteners in the necessary quantities were not on hand nor was there available hanger space for such a protracted replacement effort.

In the case of the C-130 corrosion repairs, a panel replacement costs approximately \$180000 and requires normally 45 days to accomplish with the aircraft at the depot. A bonded composite repair costs approximately \$14000 per repair and normally requires four to five days to complete and can be accomplished in the field with the repair trailers and a depot field team.

41.8. Additional research

Since 1996 WR-ALC has sponsored over \$3 million dollars of applied research at Southwest Research Institute for testing to quantify the interaction of numerous variables in the design process and to further define the limits and capabilities to the application of bonded composite repairs. The following is a short synopsis of some of the programs.

Doubler design optimization [8]

The optimization effort was to develop a method to optimize the design of basic doublers. The testing was to determine the interaction of seven doubler design variables (Stiffness Ratio, Transfer Length, Ply Step-off Rate, Adhesive Thickness, Stacking Sequence, Doubler Shape and Doubler Width) on the performance of the doublers. Over 45 single sided doubler configurations were used and tested on a cracked 3.1 mm thick 7075-T6 plate in uniaxial tension up to 95% of tensile yield. All specimens were strain gauged in the same manner and many of the doublers were also coated with a photoelastic sheet to obtain a visual representation of the doubler response. The testing showed a wide difference in the impact of the design variables. Using the strain gauge readings, a statistical design of experiment approach was used to develop a mathematical prediction capability for key strain gauge ratios given user selected inputs of the seven design variables. The predictions were then compared to FEA predictions that were developed in the blind and to actual test data. A regression analysis was performed to determine fit based on the coefficient of determination (R^2), in all cases the R^2 value was in excess of 96%. The prediction capability is limited to a uniaxial load case with the parameter values limited to the ranges tested. While the prediction capability was never intended to replace FEA or the current design criteria it is a very useful tool by allowing the user to change the design variables to optimize the doubler design. A subsequent test program followed that fatigue tested (plus/minus loading) several designs developed with under the optimization program and the results correlated quite well.

High compression loads [9]

Static and fatigue tests were run on boron and graphite doublers bonded to one side of a cracked 31 mm thick 7075-T6 plate. The specimens were loaded uniaxially. The static loads were up to 95% of compressive yield. The fatigue loads were at 40% and 60% of compressive yield. Some of the key design parameters identified in the optimization program were varied. The testing did show a serious limitation in the

fatigue performance of the doublers at the 60% fatigue load level. The testing also showed that graphite doublers with a tougher resin system performed better. The problem with the poor performance was traced to the residual thermal stresses from bonding. The aluminum test panel was not constrained during the cure cycle which produced the most severe ΔCTE (thermal expansion) condition.

Corrosion repairs [10]

Static and fatigue tests were run on boron doublers bonded to one side of simulated corrosion grind outs in a 31 mm thick 7075-T6 plate. Two simulated grind-out shapes, two grind-out depths (20% and 80% of the panel thickness) and two basic doubler designs were tested. The boron doublers were both co-cured to the panels with the plies made to follow the contour of the grind-outs and pre-cured with the grind-outs filled. The fatigue testing was to a C-141 flight spectrum with a target life 45000 simulated flight hours. The doublers performed quite well, with 15 of 16 doublers tested reaching the 45000 h target.

High aspect ratio repairs [11]

Static and fatigue tests were run on boron doublers bonded to one side of a cracked 31 mm thick 7075-T6 plate. The testing was to test for any performance degradation as the aspect ration (Doubler Length/Doubler Width) increased. The basic doubler designs were developed from the optimization effort. One basic doubler design was used and only the lengths were varied. Aspect ratios evaluated were 4/1, 8/1 and 24/1. The fatigue testing was to a C-141 flight spectrum with a target life of 45000 simulated flight hours. An un-repaired aluminum panel was tested and failed at 19000 simulated flight hours. The 4/1 and 8/1 aspect ratio doublers all exceeded 42000 flight hours before failure and the 24/1 ratio doublers reached 33000 h. There was a degradation in performance, but not as pronounced as predicted by FEA.

Heavy frame repair [12]

Two large thick frame members from a C-141 were tested with graphite doublers over a fatigue crack to determine the feasibility of repairing such large thick members with complex stress fields and confining geometry. The test was not intended to mimic precisely the actual loads on the C-141 frame nor develop an actual repair, but to use the available frames for a feasibility investigation. The frame members are 7075-T6 forging and are an "I" in cross section. The height of the "I" is 280 mm with a web thickness of 8.9 mm and a flange thickness of approximately 13 mm. A very detailed FEA was accomplished to best determine the site to induce the failure and for development of the composite doubler. The first member was saw cut at a high stress location in the web of the "I" at a systems pass through hole and the crack was grown to failure with the intent of establishing a base line. The speed and direction of crack growth on the first member was unexpected and while the failure was not totally useable as a base line, it did identify the loads and crack growth direction for the subsequent test. The second member was saw cut in the same manner and the crack was grown to just short of



Fig. 41.15. Large C-141 fuselage main gear frame showing graphite/epoxy bonded doublers over a crack.

the point of fast fracture. Two “L” graphite doublers were then co-cure bonded on either of the web and up under the outer flange (Figure 41.15). Due to geometry constraints and the complex stress fields, the largest doubler that could be installed had a stiffness factor of only 0.54 in the direction of the crack growth. Fatigue testing was continued at the original load levels with a considerably slowed crack growth. In the interest of time and money the load level was doubled and additional fatigue testing was accomplished. Due to time constraints and concern for possible fatigue failure at the attachment end of the test fixture, it was decided to cease fatigue testing and accomplish a residual strength test. The load was tripled from the original with no failure. The flanges were then cut to a point to induce failure (Figure 41.16) with interlaminar failure of the doublers. At the point the fatigue testing was stopped, the bonded graphite/epoxy doublers had increased the fatigue life by 400%. The success of the test program was quite impressive and has lead to a follow-on effort to further explore the possibilities of bonded composite repairs as a repair option for actual problems on heavy substructure.

Fuselage skin repair [13]

A test fixture was developed and initial testing accomplished to demonstrate that realistic and cost effective testing could be accomplished on less than a whole fuselage sections using sections from retired aircraft and that bonded composite repairs were a viable repair option. The test fixture was developed to cyclically apply all appropriate hoop, shear and bending loads under simulated cruise altitude temperatures appropriate for a large transport type aircraft (Figure 41.17). Six 3.1 m by 3.1 m fuselage sections were cut from retired C-141 and C-130 aircraft. Two constant section C-141 sections were selected for initial viability testing. Two

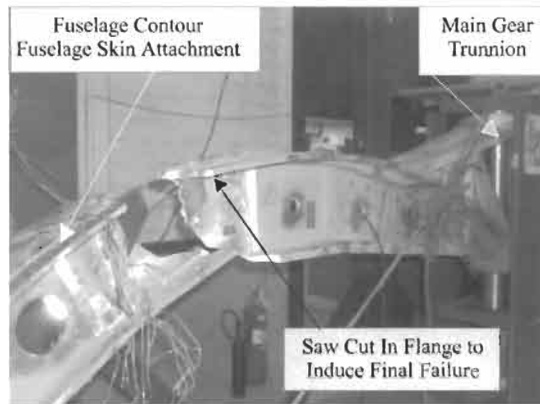


Fig. 41.16. C-141 fuselage main gear frame, as shown in the test fixture, after failure in the patch region after cutting of the top flange.

additional complex C-141 sections and two aft upper crown C-130 sections were obtained for possible future testing. One constant section C-141 section was instrumented and tested to a typical C-141 Ground-Air-Ground (GAG) flight spectrum cycle. Recoded stresses were compared to the predictions from a detailed FEA. It was found that the test fixture properly simulated inflight loading and the stresses in the center 1 m by 1 m section very closely approximated the predicted stresses.

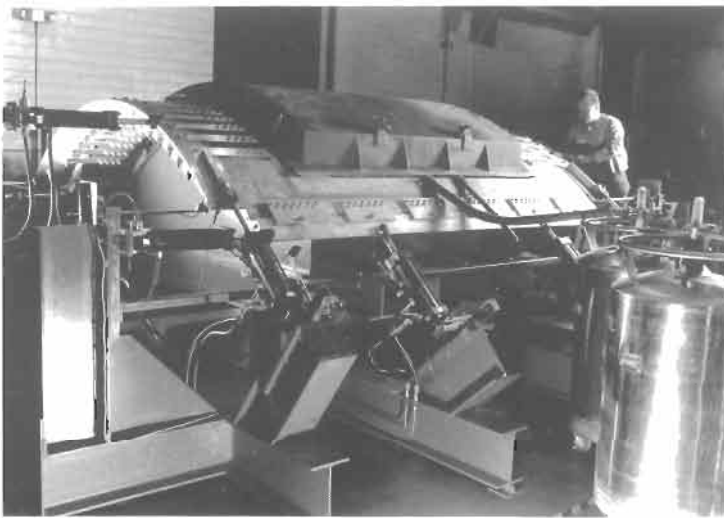


Fig. 41.17. Fuselage test fixture with 3.1 m by 3.1 m C-141 section installed for testing.

Two 35 mm saw cut flaws were made between fasteners at two identical, but separated structural joints. The saw cuts were grown to sharp 38 mm cracks through application of 6600 GAG cycles. An eight ply 127 mm by 127 mm cocured octagonal external boron doubler was then bonded to repair one of the cracks. Testing was continued to the planned 40000 GAG cycles. The test areas were cut from the test article and subjected to metallurgical examination. The repaired crack grew from 38 mm to 46 mm whereas the unrepaired crack grew from 38 mm to 102 mm. There was no degradation of the boron doubler or the adhesive bond line. The repaired crack growth rate was stable and linear. The unrepaired crack growth rate was increasing and testing vacuum pressurization was becoming difficult to maintain.

The program demonstrated both the testing methodology and the viability of bonded composite doublers to fuselage applications. Additional testing on the more complex C-141 (access door) and C-130 (aft upper crown) sections will be accomplished as need and funds dictate. The test fixture is totally operational and available for testing.

41.9. Lessons learned

In any effort of this magnitude there are always a multitude of problems to go with the success. Some of the problems were anticipated, but for many we only proved that "Murphy" is alive and well. Some of the key lessons learned that may be beneficial to others are as follows:

1. Composite repairs are not a panacea and several areas on the C-141 and C-130 have been evaluated and found inappropriate for composite repair due to accessibility, structural loading or offered no improvement over conventional sheet metal repairs.
2. The personnel making and bonding the doublers must be highly experienced in composites and metal bond. Due to the magnitude of the effort, not all of the personnel were certified in metal bond and composites, but at least one person on a team assigned to a repair was certified and had a minimum of 12 months current experience in metal bond and composites. In addition all were trained on the AFRL process and all successfully prepared and bonded a wedge test specimen. Space inside the wings was tight and contorted in many locations and required some personnel of small stature, young and limber.
3. Attention to detail is paramount. Start to finish, the surface preparation and bonding of the doublers required, on average, 18 to 20 clock hours. This meant that the repairs stretched over three shifts and three repair crews. Personnel overlaps at shift change were required along with a written shift log to assure nothing was missed. At key steps in the process, triple checks were required by two certified mechanics and the shift supervisor. Engineering personnel were either assigned to all shifts or were on 24 hour call to address any technical problems and monitor the process.

4. Past experience with composites on the aircraft has shown a problem with field personnel using paint stripper on composite replacement parts. Previous testing had shown that a layer of fiberglass and film adhesive, on top of the structural composite, works quite well as a sacrificial protection. In addition decals were painted on the external doublers warning field personnel not to paint strip the boron doublers.
5. To provide a better bond surface on the doubler and improve protection of the doubler against contamination, all doublers were bonded in the autoclave with resin rich "Natural" non treated peel ply on both surfaces.
6. Due to layered structure and joints, vacuum leaks were common and quite frustrating. When in doubt a practice bag was found to be quite helpful before working with the doubler, adhesive, heat blanket, thermal couples, *etc.* and then having leaking problems.
7. Due to the amount of metal mass involved, it was found that at hangar temperatures below 15°C, obtaining adequate adhesive cure temperatures was quite difficult.
8. Due to hanger availability purposes, many times we have been asked to perform the repairs out doors. Obviously it can be done, but never promise a schedule or manhours required. Changes dew point, high winds, storms and rain will always ruin the best plans.
9. On larger repairs or the repairs requiring multi-zone heating, it was not uncommon to use 30 thermocouples to track adhesive cure temperature which lead to a bewildering array of wires along with the usual jumble of vacuum hoses, power leads *etc.* Preplanning, a detailed "map" of what thermocouple went where, color coding and labeling of each thermocouple, neatness and anticipation of what temperature lead or lag to expect was necessary to prevent total confusion and a nervous breakdown.
10. Controlling the materials required for the repair over three shifts with multiple aircraft in a hanger in various stages of repair and making sure they were fresh and not contaminated was difficult. Kitting of the key materials in sizes applicable for a single repair helped significantly.
11. Several methods of determining the quality of the surface preparation and adhesive cure were tried; none were totally satisfactory. Tension adhesion testing per ASTM D 4541 worked the best but it also had problems. In developing accept/reject criteria in a shop environment on a flat surface it worked quite well, but at the repair site it was not always definitive and could be misleading.
12. No easy way of removing a doubler was found. Chemical, thermal and brut force were tried with no success. Careful grinding with a diamond impregnated disc to the adhesive layer proved to be the only effective method. Having to remove a doubler in this fashion over your head or in a cramped fuel tank convinced many a mechanic that attention to detail during doubler installation was paramount.
13. Thermal shock and residual thermal stresses due to the thermal differential of the materials was addressed and changes were made in the process to minimize

the thermal effect. With no real chordwise structural load, no composite plies were required in the external doublers in the chordwise direction. In bonding the external composite doubler at the bolted spanwise lap joint between the wing panels, the external doubler simply spanned the joint which simplified installation. Embarrassingly, the unrestrained chordwise thermal growth of the lap joint aft of the bolts was not considered. This thermal growth, while quite small, provided enough residual stress to produce a visible hairline crack in the doubler matrix parallel to the fibers with some fiber breakage. While this cracking did not impact the efficiency of the doubler in stopping the crack, there were concerns as to long term environmental degradation due to an exposed edge and bond line and the overall philosophical concern of a visual crack in the doubler. A special cutting tool was developed and all doublers that spanned the joint were cut lengthwise, effectively creating two parallel doublers, inspected and thoroughly sealed.

14. The surface preparation techniques used require aggressive blasting of the surface with 50 μ aluminum oxide. From the outset of the program this was identified as an area of special concern when working inside the fuel tanks. Special containment devices and procedures were developed to contain and clean up the aluminum oxide. This, along with the normal tank cleaning and fuel sampling accomplished whenever the tanks are opened, and multiple engine fuel filters was considered adequate for assuring no fuel contamination. The contamination potential was severely underestimated. Several aircraft experienced inflight engine rollback problems when the fuel controls were contaminated by minute quantities of aluminum oxide. This resulted in grounding of all aircraft that had been composite repaired to that time (Jan. 1994) and required that all fuel tanks were drained, all internal surfaces cleaned by hand and then refueled and retested. This was a large and costly task. The composite repair effort was stopped for a period of time until better procedures and containment methods were developed and tested. These improved procedures require a double containment system at the blast site, additional vacuum inside the first containment device, and meticulous cleaning of all inside surfaces after repair. Since the improved methods and procedures were developed and implemented in March 1994, no further fuel contamination problems have been encountered.
15. The fuel tanks on the aircraft at the depot are thoroughly fluid purged and the explosive levels (LEL) in the fuel tanks are quite low so the safety concerns of using electrical equipment and heaters on the aircraft are not a serious concern from an explosive position. However the field units can only, at best, air purge. With aircraft with foam in the fuel tanks, you cannot get to a safe explosive level by only air purging. One solution is to totally fill the tanks and reduce the potential for fuel fumes. When working on fueled aircraft in the field, special steps must be taken as to the wiring, connectors, grounding, heat blankets, *etc.*, and all equipment and procedures must be thoroughly reviewed by safety. All equipment must be thoroughly checked prior to use and all personnel must be especially alert to safety issues.

41.10. Summary

From a limited research and demonstration effort, bonded composite repairs have, due to need, fortuitous timing, and with considerable effort, become a very efficient and useful repair method at WR-ALC. In nine years, over 1100 bonded composite repairs, representing over 2700 bonded doublers, have been applied to primary structure on over 390 C-141 and C-130 aircraft. Technically the composite repairs have proven to be very robust, structurally efficient and flexible. From a logistics standpoint, the repair method has proven to be cost and time efficient with over 45 million dollars in cost savings. Additional research and testing being accomplished by several organizations is continuing to expand the technical understanding of the design methodology and the areas of application on other aircraft.

However, bonded composite repairs are not a panacea. They do require a thorough understanding of aircraft structures, knowledge of advanced composites and adhesive bonding, definite attention to detail and procedures, special equipment and facilities and a firm commitment to quality. If these requirements are clearly understood, we believe bonded composite repairs have a great future potential for military and civilian applications, especially in the area of aging aircraft – misunderstood, improperly applied or without the commitment to quality and failures will occur and the methodology will not receive wide spread acceptance.

References

1. Lockheed Martin Aeronautical Company, C-141 Repair of Metal Structures Using Composite Material, Report LG87ER0039, August 1988, Air Force Contract Number F09603-86-G-0455-0011.
2. Baker, A.A. Fibre composite repair of cracked metallic aircraft components – practical and basic aspects. *AGARD, Conf. Proc. No. 402*.
3. Poole, P. Effect of Adhesive Bonding Variables on the Performance of Bonded CFRP Patch Repairs of Metallic Structures.
4. Hart-Smith, L.J. (1985). Designing to minimize peel stresses in adhesive-bonded joints. *Delamination and Debonding of Mat. ASTM STP 876*, (W.S. Johnson, ed.), American Society for Testing and Materials, Philadelphia, pp. 238–266.
5. Raizenne, M.D., Heath, J.B.R. and Benak, T.J. (1992). Process Specification for CF-5 Upper Wing Skin Boron 5521/4 Fatigue Enhancement Doubler. LTR-ST-1884, November Revision.
6. Lee, Capt. D.L. and Register, D.C. Damage tolerance analysis of C-141 weep hole cracks with boron composite repairs. *Proc. of 1994 USAF Aircraft Structural Integrity Program Conf.*, pp. 289–304.
7. Schweinberg, W., Fiebig, J., Adams, S., *et al.* Bonded composite doubler repair of severely corroded C-130 primary wing structure. *The 4th Joint DoD/FAA/NASA Conf. on Aging Aircraft*.
8. Spigel, B., Buckingham, J. and Wieland, D. Composite Doubler Design Optimization and Thermally Compatible Repair Material, Southwest Research Institute Project No. 06-8311, Deliverable Report on Air Force Contract F09603-95-D-0176, Subcontract No. 10600EVF5S, Delivery Order No. 14881E-03.
9. McMaster, F., Feiger, J. and Griffin, K. Bonded Composite Repair Efficiency for Highly Compression Loaded Thick Primary Structure, Southwest Research Institute Project No. 18-1072-

- 600, Deliverable Report on Air Force Contract F09603-95-D-0176, Subcontract No. 18763EVF7S-08.
10. Spigel, B., Buckingham, J. and McMaster, F. Application of Composite Doublers to Corrosion Grind-Out, Southwest Research Institute Project No. 18-01072-200, Deliverable Report on Air Force Contract F09603-95-D-0176, Subcontract No. 18763EVF7S-08.
 11. Spigel, B., Buckingham, J. and McMaster, F. Performance of High-Aspect-Ratio Composite Doublers, Southwest Research Institute Project No. 18-01072-400, Deliverable Report on Air Force Contract F09603-95-D-0176, Subcontract No. 18763EVF7S-08.
 12. Wieland, D., Cutshall, J. and Griffin, K. Composite Repair of Large Fuselage Frame Structure, Southwest Research Institute Project No. 18-1072-900, Deliverable Report on Air Force Contract F09603-95-D-0176, Subcontract No. 18763EVF7S-08.
 13. Griffin, K., Cutshall, J., Kimball, E., *et al.* Composite Repair of Fuselage Skin Structure, Southwest Research Institute Project No. 18-1072-800, Deliverable Report on Air Force Contract F09603-95-D-0176, Subcontract No. 18763EVF7S-08.

Chapter 42

CASE HISTORY: BONDED COMPOSITE REINFORCEMENT OF SHIP STRUCTURES

I. GRABOVAC

*Defence Science and Technology Organisation, Maritime Platforms Division,
Fishermans Bend, Victoria 3207, Australia*

42.1. Introduction

There are six US designed FFG-7 class of guided missile frigates in service with Royal Australian Navy (RAN), Figure 42.1. The frigates have a steel hull with continuously welded aluminium alloy (5456) superstructure extending over about 55% of the ship's length. As a result, these aluminium structures receive a very significant proportion of the cyclic loading imposed on the hull as it flexes in a seaway, Figure 42.2. The superstructure breadth varies from 10.1 m forward to 7.3 m in the midship region and 14.3 m aft.

The finite element analysis (FEA) contours represent the axial stress in the aluminium plating in the direction along the length of the ship. Figure 42.2(a) shows the stress contours as a result of ship passing over a wave peak, which results in a tensile force (hogging). In contrast Figure 42.2(b) shows mid-ship area passing over a trough of a sea wave. This induces a compressive load in the plating (sagging). Both figures show that a critical stress area occurs where the deck becomes somewhat reduced in width. This occurs because a smaller area supports the same amount of load. FEA also shows that the stress contours are non-symmetrical. This is due to the difference in the internal structure on either side of the ship centreline.

All ships in the FFG-7 Class have experienced some form of superstructure cracking. The first incidents were reported in 1981. Since that time the majority of vessels experienced varying degrees of deckhouse cracking occurring in critical midship areas on 02-deck. By 1984 it was clear that the deckhouse cracking issue was no longer identified as ship unique, but an overall Class problem.

Of particular concern is a transverse, welded butt joint in the necked, midship region. The combination of relatively poor weld quality, weld alignment of



Fig. 42.1. RAN FFG-7 Adelaide class guided missile frigate.

longitudinal and deck butt joint, high overall nominal stress at the knuckle (2.6 times higher than at the 02-deck centreline) and stress concentration has lead to the initiation of fatigue cracks in aluminium [1–3]. Additionally, the “necking” of the superstructure aggravates the situation. In extreme sea-state conditions these cracks have the potential to cause a major superstructure failure, Figure 42.3.

Investigations by the USN and subsequently by the RAN using modelling and sea trials lead to the introduction of various fixes. All the proposals put forward basically involved adding varied amounts of new structure with aim to increase the section modulus of the superstructure especially in areas of high stress concentration. Design changes accepted by both navies involved the introduction

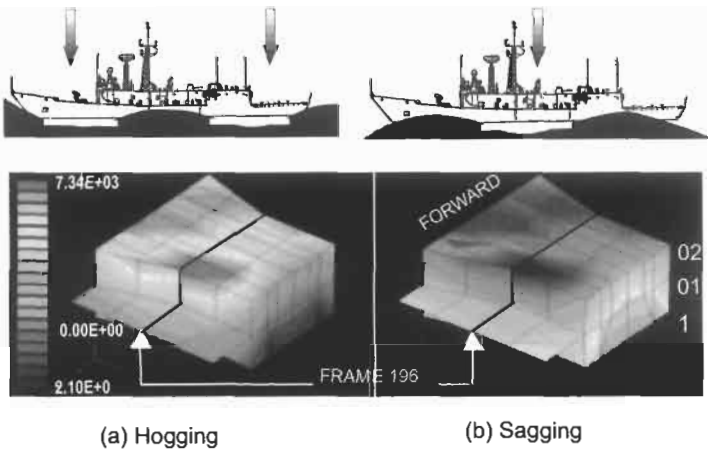


Fig. 42.2. FE analysis of superstructure response to wave action (mid-ship region 02-deck).

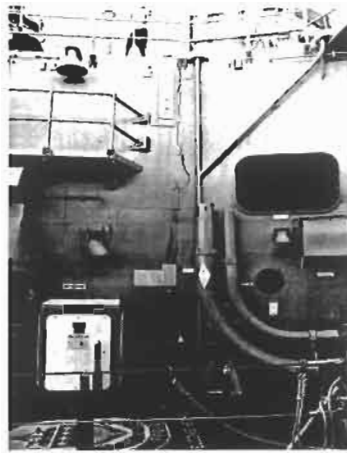


Fig. 42.3. Major crack at the knuckle (Frame 196).

of a larger radius at the superstructure knuckle (frame 196) in conjunction with thick plate inserts in areas of high stresses, Figure 42.4. In spite of these alterations the RAN vessels experienced further cracking thus it became obvious that the USN design will not provide long-term solution to the problem. This “setback” prompted the RAN to investigate alternative strengthening methods involving adhesively bonded advanced fibre composite reinforcements that have been successfully developed at the Defence Science and Technology Organisation (DSTO) Australia for the reinforcement or crack repair (“crack patching”) of aircraft structures [4–6]. The Royal Navy (RN) also reported successes in using adhesively bonded fibre composite for superstructure reinforcements of Type 21 frigate [7].

In close cooperation with DSTO, the Directorate of Naval Ship Design (DNSD), Department of the Navy has carried all preliminary feasibility studies focusing on stress analysis and methods of reducing stresses in high stress concentration areas to an acceptable level. The principal stresses at the knuckle (frame 196) was found to be around 76 MPa (11 ksi) which coincided with the USN findings. By

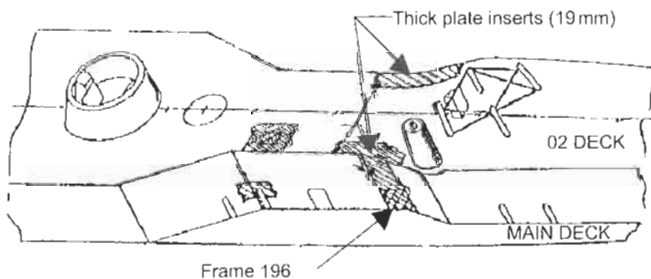


Fig. 42.4. Phase 1 fix for superstructure cracking.

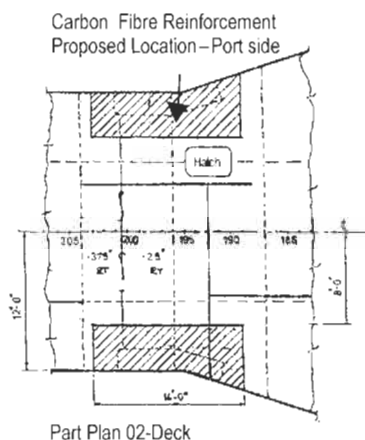


Fig. 42.5. Upper mid-ship region of aluminium superstructure, FFG-7 class frigate.

application of Carbon Fibre (CF) reinforcement the analytical models indicated a stress reduction of between 18 and 40% in aluminium plates of varied thickness used on 02-deck. The target value for the average longitudinal stresses were set at around 55 MPa (8 ksi) which is roughly a 20–25% reduction [8].

In practice to achieve the stress reduction of this magnitude a number of factors were considered. The research work conducted at DSTO involved extensive development of materials and processes since no appropriate codes or standards were available. The only guidelines were DSTO staff experiences with “crack patching” and adhesive bonding for aerospace applications, manufacturers data sheets and the RN experiences with composite reinforcement of Type 21 ships. Thus it was proposed to reinforce both the port and starboard sides with a composite demonstrator measuring 5 m × 1 m and comprising 25 plies (7 mm thick) unidirectional carbon fibre. The design also included a glass/resin polymer (GRP) protection layer to provide in-service protection to underlying CF reinforcement. The proposed locations of composite demonstrators relative to high stress concentration area are shown in the engineering drawing, Figure 42.5 (shaded area).

42.2. Materials development and characterisation

A naval ship is continually exposed to varied operational and environmental conditions which subject the ship structure to cyclic loads, high sea-states, IR and UV radiation, water and salt corrosion, mechanical abrasion, impact and structural fatigue deterioration. These factors can have direct influence on performance and durability of composite reinforcement and therefore must be taken into the account at the design stage. The project development carried out between the late 1980s through to early 1990s is briefly outlined here and given in greater detail elsewhere [9,10].

Resin development – In laboratory studies several candidate thermoset resin systems were considered for the adhesive role [11]. The most suitable resin was found to be the vinyl-ester resin system. The resin provided high strength adhesion, it cured at ambient temperature and possessed good elevated temperature performance to more than 80 °C (solar heating of 02-deck could reach over 60 °C while the ship is in port). The vinyl-ester resin was modified to enhance toughness needed to maximise resistance to peel and cleavage forces.

For example, resin modification increased fracture toughness from the nominal value $G_{IC}=172\text{ J/m}^2$ for standard resin to $G_{IC}=1074\text{ J/m}^2$ for DSTO modified version. Similarly, the peel resistance (T-peel) has increased from 0.89 N/mm for a standard product to 2.64 N/mm for modified resin. However, the glass transition temperature, T_g (tan δ , determined by DMTA) was reduced from 129 °C to 120 °C due to presence of a modifier [11]. Resin modification also increased viscosity from about 350 MPa.s to 580 MPa.s at 25 °C. This small reduction in properties is regarded as a good “trade-off” for considerable improvement in resin toughness that enhances uniform stress distribution for optimised adhesive bonding to both metal and composite.

Resin toughness can also minimise the effect of mismatch in thermal expansion between CF and aluminium plating at the composite/deck interface. The resin provided good wetting of the substrate and it was also found suitable for use as the composite matrix. To aid processing especially on board the ship the resin formulation could be tailored to adjust cure conditions such that the relatively long induction time (pot-life) required for the *in-situ*, wet lay-up of large composite reinforcements can be achieved over a wide ambient temperature range. The selection of the same resin system for both an adhesive and the composite matrix also eliminated all potential compatibility problems.

Adhesive bond – The principal role of an adhesive bond is to transmit shear forces between adherends. Properly designed bond will not deteriorate in service either mechanically or chemically for the life of the bonded structure. Adhesive bond line should be uniform and preferably $<500\text{ }\mu\text{m}$. Suitable scrim materials are used to control the uniformity of a bond line thickness. Adhesive also acts as a physical barrier which controls potential corrosion between adherends. It is well known that two dissimilar materials (i.e. Carbon fibre, aluminium) due to electro-potential difference will in presence of an electrolyte form a galvanic cell and initiate localised corrosion [12]. In this project adhesive bond is also used as electrical insulator. A method was developed to post-cure both, resin matrix and adhesive by application of a Joule heating principle (see later).

Surface pre-treatment – The methods of surface pre-treatment for aluminium bonding often refer to the use of inflammable solvents and corrosive chemicals not really recommended for ship applications. For that reason a simplified surface pre-treatment method was developed that consisted of grit blasting and silane application. In contrast to other methods this process could easily be reproduced and performed on site and independent of the scale of operation or dockyard conditions. Grit blasting resulting in surface profile $>50\text{ }\mu\text{m}$ has been found suitable for physical bonding in all laboratory tests. Considerable improvement in

the strength of a bond is achieved if resin compatible silane coupling agent is used as adhesion promoter. Silanes are organofunctional molecules capable of forming a strong chemical bond between polymer and inorganic substrate thus increasing adhesion and bond strength [13]. Among various products tested the methacrylate silane proved to be the most effective in wedge test experiments conducted under hot/wet (50 °C, 96% RH) and simulated marine conditions (35 °C, 5% salt fog) [11]. See Chapter 3, Section 3.3 and 3.4 for additional details.

Composite development – The development of a suitable technique leading to the production of a large-scale composite reinforcement on board the ship posed some challenge. The wet lay-up resin application technique was the “choice of the day” however; this “traditional” method required modification primarily to reduce the time needed for resin wetting of 25 layers (5 m long \times 1 m wide) carbon fibre preform.

Laboratory study indicated that good wetting and vacuum bag consolidation of fibre preform is achievable if measured quantity of resin is applied only to the selected carbon fibre layers. Therefore, instead of resin application to all 25 individual layers, the resin was dispensed to only four layers i.e. 0, 2, 12 and 22nd. This method significantly reduced the composite production time and was well inside the pot-life of resin. The composite manufactured by this method was found to contain minimal fabrication defects i.e. voids, density variation and the volume fraction of fibres (V_f) was close to 60%. The composite ends (aligned along the axis of the ship) were designed so that both terminate in approximately 2–3 degrees tapered joint at the composite/deck interface. The purpose of this is to minimise peel and shear stress concentration at the beginning of adhesive bond.

Scale-up work – Conditions of work on board the ship are vastly different from those in the laboratory. Being a new demonstrator technology the required skills within the dockyard was not available. For that purpose it was decided that the DSTO staff, involved in the project from the beginning, would carry out a simulated “dry-run” to perfect various segments of work prior to ship applications. It should be pointed out that beside the technical development there is often other, more critical aspect involved and that is the performance, durability and eventual acceptance of new technology that will be judged by the industry. Therefore, it was vital for DSTO personnel to adjust to the working conditions on board the ship and ensure those composite demonstrators are properly installed.

Reinforcing fibre – Carbon fibres were selected as the most suitable reinforcement for the composite. The fibres are lightweight, easily wetted by vinyl ester resin and possess excellent mechanical properties primarily, very high strength in both tension and compression and a high resistance to corrosion and creep. For this application only unidirectional fibre reinforcement was employed since the cyclic load causing the stress concentration at the weld is directed along the axis of the ship. The commercially available carbon fibres employed in this project had an intermediate tensile modulus of 230 GPa, a tensile strength of 3.53 MPa and a density of 300 g/m². The scanning electron microscope (SEM) showed presence of fibre sizing which was separately identified by fourier transfer infrared (FTIR) analysis to be an epoxy based surface finish. Fibre sizing is applied at the point of

fibre manufacture basically to protect fibres from damage, improve handling and to promote fibre/matrix interfacial bond strength.

Postcure – A parallel study has been carried out on resin postcure. Initial resin reaction at low ambient temperature ($<20^{\circ}\text{C}$) normally produce less than optimal crosslinking reaction, however, by application of heat the resin reaction is advanced resulting in improvement of its physical and mechanical properties. Postcuring of bonded ship reinforcement can be achieved by several methods such as solar heating of 02-deck or application of heater blankets. Both methods have certain shortcomings. Solar heating is the most economical way, which will in time achieve partial postcure, but the process is uncontrolled. Alternatively, a large heater blanket (i.e. at least $5 \times 1 \text{ m}$) is expensive, requires a large power input (240 VAC) and is an inefficient method to heat-up the adhesive bond layer due to a huge heat-sink effect of aluminium superstructure. However, a better and more effective method was developed in-house, which generated heat within the composite itself thus enabling resin postcure in both the composite and adhesive bond.

This method uses low voltage ($<120 \text{ VAC}$) resistance heating (Joule heating) utilising the electrical conductivity of carbon fibre. The electrical conductivity of carbon fibres is highly anisotropic. For instance, conductivity along the fibres is of the order of 10^4 S/m , while in the direction perpendicular to the fibres this value is several orders of magnitude lower i.e. between 10^{-3} and 10^{-1} S/m [14]. As a result, far less amount of current is required to heat the CF composite in the latter case. In early laboratory tests a 25-ply CF composite ($1350 \times 1000 \text{ mm}$) bonded to 6 mm aluminium plate reached a temperature in excess of 105°C when the electrical current (4 A and 108 V) was applied perpendicular to the direction of fibres. The initial resistance at ambient was 28.6Ω for a 1 m width, however, after 4 h of postcure this value dropped to 23.9Ω . It is most probable that the matrix resin volume reduction due to additional crosslinking reaction causes fibres closer contact and hence a decrease of electrical resistance.

Composite fatigue performance – Various tests were conducted in the course of materials development which are described in greater detail elsewhere [9,10]. Still, the fatigue performance of composite reinforced aluminium specimens simulating ship deck reinforcement was considered to be the ultimate test. Two test specimens were produced each 1.2 m long and instrumented with 18 strain gauges, Figure 42.6.

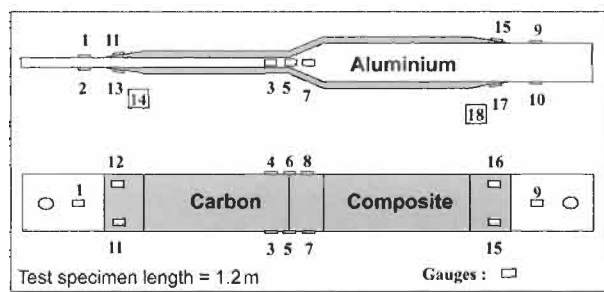


Fig. 42.6. Fatigue test specimen.

Both sides of the specimen were reinforced to avoid bending in tension and in compression the anti-buckling plates were used to minimise aluminium buckling on load application. The FEA, static and the fatigue tests indicated about 50% reinforcement efficiency in the underlying aluminium metal [10]. Each specimen was tested at increasing load levels including the peak load of 91 kN (equivalent to ± 76 MPa peak service stress range [8]) for up to 90000 cycles. Although, the last 5000 cycles were tested at the level twice the peak load before the fracture of aluminium, there was no evidence of composite reinforcement failure. Non-destructive evaluation tests confirmed no debonding and there were no signs of degradation in the adhesive bondline. The other fatigue test specimen was assessed at 35 °C and the maximum load of 91 kN for 10^5 cycles without failure.

Impact protection – Consideration was also given to in-service protection of CF reinforcement from impact damage, exposure to elements and surface erosion. The location of both composite reinforcements on 02-deck (port and starboard side) is on a walkway used by both the ship's crew and maintenance personnel. In addition, this area is often used as an offloading point from an overhead crane and for the erection of scaffolding required for maintenance of the ship's main mast.

For these reasons and including constant exposure to solar effects, water, salt *etc.*, the GRP protective layer for the reinforcement was designed and tested in the laboratory. Out of several candidate systems considered the modified vinyl ester resin used for adhesive and composite matrix was chosen again. The GRP composite containing this resin performed well in impact tests spanning the kinetic impact energy level from 11–56 Joule. No resulting damage to underlying CF composite bonded to aluminium plate was evident. Moreover, the choice of selected resin assured total compatibility with the rest of composite lay-up.

Environmental exposure and durability – The durability of structural bonded joint is often considered more important than its initial strength. The rate of bond degradation is subject to many factors, all of which can be grouped in three main categories: (a) environment, (b) material and (c) stress. Temperature, moisture, solar radiation and aggressive chloride ions in the marine environment dominate the climate. The GRP protective layer designed for impact protection was also made to provide environmental shielding to CF reinforcement. In the design, a provision was made for an extra sacrificial edge protection to the composite reinforcement extending the GRP cover an additional 100 mm in width and length to coincide with the size of adhesive bond layer. The other two categories, material and stress, were addressed through research and development of selected materials and the design of bonded reinforcement (size, strength and position) as discussed above.

42.3. Installation of composite reinforcement

Sydney March/April 1993

The work on board the ship (*HMAS Sydney*) was uneventful. Apart from preparation of work area (temporary removal of obstructing equipment and

erection of weatherproof canopy) all segments of composite installation (port and starboard) proceeded as planned. The work schedule was well planned and completed in about 12 days, although unexpected daily temperature fluctuations had to be accommodated on several occasions. A detailed description is given elsewhere [15,16]. In this article only basic steps taken in the process of composite strengthening of 02-deck superstructure will be presented.

Surface preparation – The preparation of 02-deck surface for adhesive bonding was the most time consuming and difficult work. It included removal of surface paint coating and preparations for grit blasting. Due to varied size of thick plate inserts especially on the port side the step-up angles between the original plate and the insert plates were reduced to about 10–15 degrees with epoxy filler paste. A crack uncovered after paint stripping is shown in Figure 42.7. The crack was re-welded prior to reinforcement application and the grit blasting followed by application of a silane solution developed for aluminium surface in the earlier laboratory trial.

Fabrication of adhesive bondline – The construction of adhesive bondline, manufacture of CF composite and the GRP protective layer were all separate processes requiring overnight resin cure in each case. A wet lay-up technique (as described above) and the vacuum bag fibre consolidation was simply a repetition of work developed in the laboratory for the large-scale ship application. Resin diffusion through the dry fibre preform worked well and produced composites of good quality.

Resin postcure – The postcure was carried out on full size bonded reinforcement (5 m × 1 m) in a single step. The resistance heating of CF composite, adhesive bond and inevitably the deck to about 75 °C was achieved by using a single-phase AC power supply. Four transformers were utilised each attached to the carbon composite supplying a low voltage current (31 V, 21 A). The total power consumption by the composite was only 2.5 KW. The heating process required a 2-h heat-up stage followed by a 4-h resin postcure period. Surface heat losses were minimised by the use of a blanket consisting of 50 mm fibreglass insulation and a

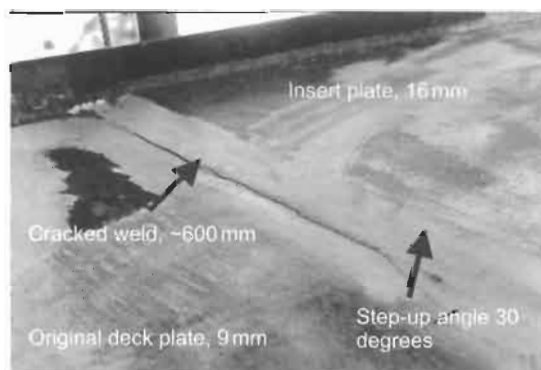


Fig. 42.7. Welded connection between 9 and 16 mm plate insert (Note the length of crack).

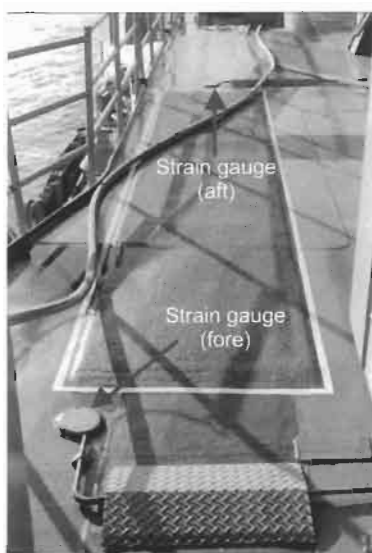


Fig. 42.8. CF reinforcement in service – starboard side.

15 mm thick felt material. To monitor selected heat-up rate and temperatures at the various locations on composite surface a total of 14 surface bonded thermocouples were employed. After the postcure period the power supply was discontinued and that section of 02-deck allowed to cool down overnight.

Composite protection and surface finish – The fabrication procedure for GRP protective layer was identical to that used for adhesive bond layer and CF composite as given earlier. Original design allowed for an additional sacrificial edge protection thus extending an additional 100 mm in width and length to coincide with the size of adhesive bond layer (i.e. $5.2\text{ m} \times 1.2\text{ m}$). A standard navy surface protection applied by DSTO staff was a two-coat coverage of an epoxy-based primer. This was followed by a standard navy paint scheme that included the final non-skid layer applied to the walkway. At the time this coverage consisting of a multiple-coat of paint was considered appropriate and adequate. The final in-service appearance of a starboard reinforcement is shown in Figure 42.8.

42.4. Reinforcement efficiency assessment

According to the original engineering estimates, only a 7 mm (25-ply) CF composite bonded to critical areas on port and starboard side was needed to reduce the stress concentration by approximately 20%. RAN numerical analysis indicated a stress reduction of this magnitude was expected to stop or significantly relieve cracking episodes re-occurring most commonly due to inherent weld flaws on the 02-deck plating.

For assessing the effectiveness of bonded composite reinforcements strain measurement trials were conducted before and after composite application to determine their effect on stress levels in the superstructure. Sea trials were conducted over time for given sea-states and ship speeds during alternating conditions of longitudinal hull bending (sagging and hogging). Strain output data were collected using a combination of uni- and multi-directional strain gauges installed at predetermined 02-deck locations including the sides to reach the main deck, Figure 42.9. Data analysis indicated up to 18% reduction in strain levels along the sides (Frames 188–212) and other areas between the composite reinforcements, however, there is a corresponding 20% increase in strain next to either end of reinforcements [17].

Installation of CF composite reinforcements also affected strain distribution in the vertical plating welds at frame 196. The three strain gauges (rosettes) positioned at each superstructure level (i.e. 1, 01 and 02) also showed a beneficial effect of reinforcement in the longitudinal strain. The anomaly in the output of strain gauges G4 and G5 (02-deck starboard side, fore) indicated the influence of a crack (see Figure 42.7) present during the initial collection of experimental data which was rewelded between the two sets of sea trials.

Strain data results produced clear evidence, which indicated that adhesively bonded composite reinforcements are an effective means of reducing the strains and hence stress in the critical regions of 02-deck. Strengthening of weaker regions was found to transfer some of the stresses to the ends of reinforcement into the area of a stronger part of the superstructure.

Non-Destructive Evaluation (NDE) – Two non-destructive evaluations (NDE) were conducted by DSTO since bonding the reinforcements. The first was carried out in February 1994, approximately a year after superstructure strengthening, and

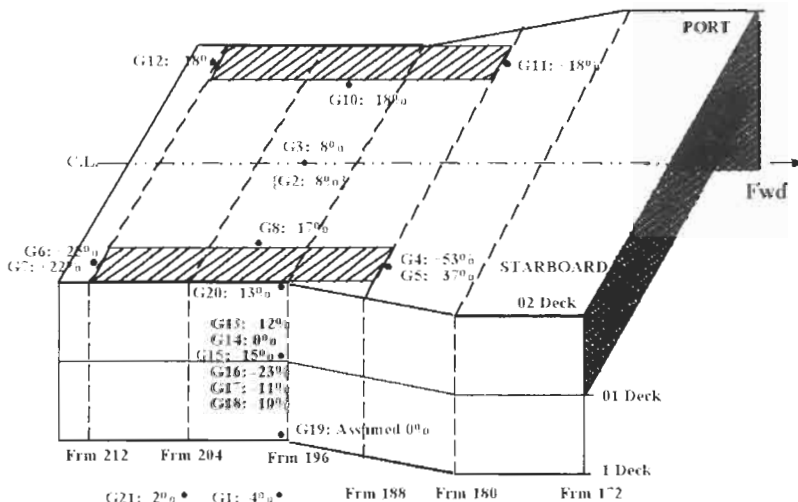


Fig. 42.9. Changes in strain intensity level after composite reinforcement (neck-down region).

the second in October 1995. Although the tests were conducted only approximately 18 months apart, the findings indicated that no detectable deterioration (i.e. debonding) of the adhesive interfaces had occurred. See Chapter 23, Section 23.2.1 for related details.

42.5. Service performance

The attitude adopted from the outset by DSTO researches was that there is a “one-off” chance to demonstrate the new technology. The target for service endurance was (arbitrarily) set to seven years. This goal has now been exceeded. In that period *HMAS Sydney* has been posted twice to the Gulf on the UN missions, have encountered high sea states around Australia and was among the first ships to enter East Timor’s territorial waters. The composite reinforcements remain adhesively bonded in spite of exposure to extreme marine conditions; very high temperatures in the Gulf, high operating loads at high seas and abrasion from crew traffic and service personnel. At the same time composite is continuously exposed to most harmful elements that affect adhesive bonds i.e. temperature fluctuation, water, solar radiation and saline atmosphere.

Through-life maintenance – It is not surprising, given the exposure that the 02-deck experienced a local debonding of GRP protective layer at the GRP/aluminium interface. After about two years at sea the sacrificial edge area on both the port and starboard GRP composite developed untidy appearance basically due to failure of surface paint coating combined with the effect of water locks caused by undulated deck surface, Figure 42.10. The underlying CF composite was unaffected but if this condition were left unchecked the progressive debonding of adhesive layer would have compromised the integrity of both reinforcements. Water is known to be the most harmful environment for bonded joints. Bond deterioration is caused due to



Fig. 42.10. Weathering of composite reinforcement (Starboard side) and typical damage inset (a) and (b).



Fig. 42.11. Physical damage to CF composite.

water absorption by adhesive, adsorption at the interface and corrosion of the substrate surface. Therefore, the most important factor in the long-term durability of bonded joints is the stability of interfacial adhesion against moisture [18].

The repair consisted of all-round GRP edge removal followed by reconstruction of affected areas using the same techniques and materials as described above. In addition, a new enhanced edge sealing method was developed in the laboratory and applied to both composite reinforcements thus ensuring that a standard navy coating is not the only protection against water ingress. The new edge sealing method included a glass reinforced polysulphide elastomer among other materials to account for differences in thermal expansion prevalent at the critical GRP/aluminium interface. The new seal comprising this material was also expected to provide additional protection against water attack [15,16]. A second call for assistance by the Navy was of an entirely different nature. In January 1998 the port side CF reinforcement suffered mechanical damage during a maintenance schedule. High-pressure (40000 psi) rotary water jet equipment, used for surface paint removal, had accidentally digressed onto the composite reinforcement. The type and the extent of damage are shown in Figure 42.11. The repair comprised removal of all damaged material until sound structure was encountered. The size of the repair was around 900 mm in length and 400 mm in width and included edge reconstruction. Because of total composite penetration by water jets the reconstruction sequence followed normal composite fabrication procedure. On the occasion a 1 m length of edge sealing strip was also repaired. No further incidents have occurred since January 1998.

42.6. Technology improvement

In view of changes in safety regulations in Australia taking place at the workbench level, especially in the second part of 1990s, together with ever-

increasing financial constraints on research, subsequent work in the development of marine composite reinforcement required modification. Retrospectively, the work carried out in 1993 was demanding both in terms of time and labour. Furthermore, the semi-automated technique required workers to be exposed to chemicals to a small extent. For these reasons the requirements and conditions of the work conducted in 1993 can no longer apply. At least two new approaches for improvement of composite reinforcement technology have been explored by DSTO.

One is to employ the limited shelf-life, carbon fibre/epoxy prepreg systems in conjunction with epoxy-based, aerospace structural film adhesives. These materials cure at elevated temperatures (i.e. 120 °C, 180 °C) and the DSTO developed heat-generating method (Joule heating), has been successfully used to produce composite reinforcements bonded to marine aluminium.

The other approach is based on a vacuum bag resin infusion technique (VBRI) [19]. This method is a "closed-mould" technique in which a (preformed) reinforcement of glass or carbon fabrics is positioned onto a substrate (or mould) and pre-consolidated under a vacuum bag. A liquid resin is then injected into the fibre preform by creating a vacuum inside the bag. After curing of the resin the bag is removed leaving composite reinforcement bonded to the substrate. The VBRI method is neat, quick and produces very good quality product while practically eliminates hazards associated with workers exposure to chemicals. In addition, this technique can also use the current heating method for resin cure and postcure. Overall, this new technology that is now made available offers a significant reduction in both human and financial resources. This aspect alone could make the composite reinforcement technology potentially attractive not only to naval fleet operators but also to a large commercial sector in the marine industry.

42.7. The current status – year 2000

For the last eight years no cracking has been reported in the vicinity of composite reinforcements on 02-deck. The last visual inspection (May 2000) confirmed the integrity of both reinforcements with no evidence of any deterioration at the critical composite/aluminium interface. It is believed that the composite reinforcement technology "screening" process is now complete after eight years of real life shipboard evaluation.

In the meantime the interest in technology is slowly on the increase, the last significant step being DSTO licensing the technology to an Australian company.

42.8. Conclusion

A combined effort involving RAN and the DSTO research into carbon fibre reinforcement technology suitable for marine structures has been successfully demonstrated on *HMAS Sydney*. After strengthening the superstructure, no

further cracking has occurred in the region of interest and after eight years the reinforcements remain in good condition despite exposure to severe marine conditions.

In addition, DSTO's capability to develop materials and relevant new technology, carry out repair and maintenance as deemed necessary has also been demonstrated. Furthermore, the durability of bonded structural composites indicates good interfacial stability and therefore low through-life maintenance.

DSTO made refinement to the original technique thus improving the technology through quality, simplicity and speed. The cost of reinforcement manufacture has been reduced which represent good incentive to fleet operators. Improved technology observes new regulations applicable to safe working practices and it complies with the new stringent occupational health and safety (OHS) requirements now in force in Australia.

42.9. Acknowledgement

The author gratefully acknowledges the contributions made by Dr. Alan Baker, R. Bartholomeusz, and J. Retchford in the initial stages and P.J. Pearce, A.W. Camilleri, K. Challis, and J. Lingard towards project development and completion. Supply of FEA data by Dr. Stuart Cannon and Matthew Gudze of DSTO is appreciated. In addition, the assistance of Navy staff in Canberra, Navy officers on *HMAS Sydney* and Garden Island dockyard personnel are recognized.

References

1. Toman, R. (1986). An engineering review of steel and alloy superstructures on surface warships. *Australian Naval Engineers Symp.*, Sydney, August.
2. Toman, R. (1984). CCB Proposal for Recommended Solutions to the FFG-7 Class Superstructure Cracking Issue, PMS 399.11, April.
3. FFG Aluminium Superstructure Cracking. Directorate of Naval Ship Design, Technical Memo A012695, TSC 061, Department of Defence (Navy Office), Commonwealth of Australia.
4. Baker, A. (1979). Evaluation of adhesives for fibre composite reinforcement of fatigue cracked aluminium alloys. *SAMPE J.*, No. 15, pp. 10–17.
5. Baker, A. (1984). Repair of cracked or defective metallic aircraft components with advanced fibre composites – an overview of Australian work. *Composite Structures*, No. 2, pp. 153–181.
6. Baker, A. (1988). In *Bonded Repair of Aircraft Structures*, (A.A. Baker and R. Jones, eds.), Martinus Nijhoff, Dordrecht, pp. 107–173.
7. Allan, R.C., Bird, J. and Clarke, J.D. (1988). Use of adhesives in repair of cracks in ship structures. *Materials Science and Technology*, (October) 4, pp. 853–859.
8. Design Investigation of Fibre Composite Repair of FFG Aluminium Superstructure, Directorate of Naval Ship Design, Technical Memo A012840, Department of Defence (Navy Office), Commonwealth of Australia, Feb. 1987.
9. Grabovac, I., Pearce, P.J., Baker, A.A., *et al.* (1993). Carbon-fibre-composite reinforcement of aluminium superstructure. Paper presented at the 9th Int. Conf. on Composite Materials (ICCM-9), Madrid, SPAIN, July 12–16.

10. Grabovac, I., Bartholomeusz, R.A. and Baker, A.A. (1993). Carbon fibre composite reinforcement of a ship superstructure – project overview, *Composites*, **24**(6) pp. 501–509.
11. Grabovac, I. and Pearce, P.J. (1997). Composite Reinforcement of a Ship Superstructure, Part 1: Adhesive/Matrix Resin Development, *DSTO-IPIC-0017*, AMRL, Department of Defence Australia.
12. Alias, M.N. and Brown, R. (1993). Corrosion behaviour of carbon fibre composites in the marine environment. *Corrosion Science*, **35**(1–4), p. 395.
13. Walker, P. (1994). Silane and other adhesion promoters in adhesive technology. In *Handbook of Adhesive Technology*, (A. Pizzi and K. L. Mittal, eds.), Pub. Marcel Dekker Inc. Ch. 4, pp. 47–63.
14. Moriya, K. (1993). On use of Joule effects for curing/joining/patching of CFRP composites. *Proc. Japn – U.S. Conf. on Composite Materials*, 6th Publisher; Technomic, Lancaster, PA, p. 742.
15. Grabovac, I., Pearce, P.J., Camilleri, A., *et al.* (1999). Are composites suitable for reinforcement of ship structures. *Paper presented at the ICCM-12*, Paris, France, July 5–9.
16. Grabovac, I., Pearce, P.J., Camilleri, A., *et al.* (2000). Composites for reinforcement of ship structures. Published in *Composites in Manufacturing by Composites Manufacturing Association of the Society of Manufacturing Engineers*, USA, Third Quarter **16**(3).
17. Phelps, B.P. (1995). Bonded repairs to RAN FFG superstructure strain gauge data analysis, *DSTO RR-0046*, AMRL, Department of Defence, Australia.
18. Mays G.C. and Hutchinson, A.R. (eds.) (1992). Adhesive joints. In *Adhesives in Civil Engineering*, Published by Cambridge University Press, Ch. 4, p. 116.
19. Summerscales, J. (2000). Clean efficient manufacture of composite vessels using resin infusion under flexible tooling (RIFT). Paper presented at the International Conference *Lightweight Construction – Latest Developments*, London, 24–25 February.

INDEX

- A*-scan *see* ultrasonics
- abrasion of surface, 51–53, 60
- acid etch *see* etch
- acoustic emission, 689–692
- acoustic fatigue cracking, 531–568
 - aft fuselage, 559–560
- acousto-ultrasonics, 595–597
- acrylic adhesives, 29–30
- adherends, 20–28
 - aluminium, 69–74
 - steel, 77–78
 - taper profile, 286–288
 - thermoset composites, 78–80
 - titanium, 74–77*see also* surface preparation; wetting
- adhesion, 20–21, 41–45, 727–730, 791
- adhesive bonding, 7–9, 42–44
 - composite adherends, 79
 - environmental effects, 44–45
 - hot solution treatment, 81–82
 - SMART patches, 597–599
 - sol-gel technology, 80–81
- adhesive cure, 20
 - bondline pressurisation, 42–43
 - residual stress, 167–174
- adhesive disbonds, 71, 200–202
 - damage tolerance, 468–469
 - inspection, 664–694
 - leaky interface waves, 681–683
- adhesive fillet, 38, 281–285
- adhesive primer *see* primer
- adhesive stresses, 141–144
 - finite element analysis, 281–285
 - load transfer, 269–313
 - patch tapering, 186–189, 272–296
- adhesives, 28–32, 41, 87–100
 - bondline thickness, 65
 - data for fuselage, 561–562
 - degradation, 54–57
 - fillet, 38, 281–285
 - shelf life, 20, 34–35
 - test procedures, 34–35
 - thickness, 251–258
 - voids minimised, 65–66
- aft fuselage cracking, 536–537
 - finite element model, 557–562
- aileron hinge, 300–308, 897–906
 - aileron hinge, 902
 - non-destructive inspection, 710–714
 - SMART patch, 603–611
- Airbus
 - fatigue tests, 474–477
 - fuselage lap joint, 464
 - lap joints, 449–450
- alkanes, 51–53
- aluminium adherends, 22, 43, 49–53
 - double overlap joint, 104–114
 - moisture absorption, 65
 - surface preparation, 69–74
- aluminium patches, 23–24
- AMORLUX for battle damage, 772–779
- anaerobic adhesives, 28
- analyses, 207–265, 621–637
 - bonded crack-patching, 177–205
 - CF-116 doubler repairs, 941–946
 - damage tolerance, 487–488
 - fatigue crack growth, 353–373
 - random response, 537–538
 - repaired cracked plate, 551–553
 - thermal stress, 317–350
 - wing repair, 341–349*see also* stress intensity
- analytical methods, 137–174
 - aileron hinge, 300–308
 - lower wing skin, 1005–1007
 - stepping in patch taper, 272–280
 - stresses in circular plate, 318–335
- anodisation, factory processes
 - aluminium, 69–71
 - titanium, 74–76
- anodisation, repairs, 32–33, 60–61
 - aluminium, 72
- ARALL patches, 10, 21, 23
- aspect ratios of patches, 141, 310–313
- ASTM tests, 88–94
- atomic force micrographs, 50
- B-stage adhesive, 34, 38, 476
- battle-damage repairs, 6, 761–779
 - composite patches, 438–440
- beam-spring theories
 - adhesive joint, 107
 - skin doubler, 115–117
- bend test, 715
- bending effects, 139–141, 157–167
 - fuselage door surround, 824–825

- one-sided patches, 200–204
- bi-axial loading
 - cracked holes, 258–262
 - door surround, 817–819
- birdstrike protection RAF, 912
- bismaleimide adhesives, 29
- block end skin doubler, 115–117
- Boeing
 - B-737, 443
 - B-747 demonstrator, 477–480
 - fuselage, 459–464
 - lap joints, 444–449
 - multi-site damage, 443–482
 - see also* wedge test
- bolting versus bonding, 11–14, 765–770
- bond durability, 20–21, 30, 47–56, 985
- model, 53–56
- surface treatment, 964–965
- surfaces, 49–53
- see also* adherends; adhesives
- bonded repairs, 7–9, 14, 44
- acoustic fatigue cracking, 531–568
- applications, 727–757
- battle damage, 765–770
- commercial demonstrators, 959–972
- cracked plate, 103–104
- damage tolerance, 103–104
- environmental effects, 127–135
- fracture mechanics, 127–135
- large areas, 983–995
- load transfer, 141–144
- material selection, 731–732
- non-destructive inspection, 659–723
- quality control, 659–723
- residual stresses, 197–200
- safety requirements, 615–639
- shape optimisation, 269–313
- UK applications, 907–918
- bonding versus bolting, 11–14, 765–770
- bondline
 - defects, 427–433
 - pressurisation, 42–43
 - thickness, 65
- boron doubler CF-116, 937–957
- boron fibres, 24–25
- boron-epoxy/aluminium, fracture mechanics, 127–135
- boron/epoxy patches, 9, 685–689
- analysis, 294–296
- double overlap joint, 104–114
- efficiency studies, 375–398
- versus graphite/cpoxy, 424–427
- Bragg grating sensors, 580–587
- bulkhead, 24, 707–709
 - finite element analysis, 860–864
 - reinforcement, 297–300, 859–870
- C-130/C-141, 1009–1032
- C-5A fuselage crown, 871–883
- C-scan *see* ultrasonics
- CalcuRep C-5A fuselage, 875–878
- calibration standards, 715–723
- calorimetry, 34
- cantilevers stressed, 48
- case histories
 - Ansett keel beam, 968–972
 - C-130/C-141, 1009–1032
 - C-5A fuselage crown, 871–883
 - CF-116 upper wing skin, 937–957
 - CH-47 cargo hook beam, 973–981
 - composites on ship structures, 1035–1049
 - DC-10/MD-11, 919–935
 - F-111 lower wing skin, 797–811
 - F-111 wing pivot, 845–858
 - F-16 fuel vent-hole, 885–895
 - F/A-18 aileron hinge, 897–906
 - F/A-18 fuselage bulkhead, 859–870
 - L-1011 doubler, 813–842
 - large areas, 983–995
 - QANTAS doublers, 965–968
 - T-38 lower wing skin, 997–1008
- certification
 - aileron hinge, 905–906
 - airframe structure, 2–3
 - bonded repairs, 14–16, 615–639, 783–795
 - critical repairs, 643–656
 - F/A-18 aileron hinge, 905–906
- CF-116 upper wing skin, 937–957
- CH-47 cargo hook beam, 973–981
- chemically active surface, 734–739
- chromate conversion coatings, 73
- chromate inhibitors, 63
- chromic acid anodise, 70, 75
- chromic acid etch *see* etch
- circular plate stresses, 318–335
- cleavage tests, 46–48
- clip gauge, 11–12
- closed-form analyses, 177–205
- coefficient of thermal expansion, 9–10, 22, 24, 27
 - boron fibres, 25
 - C-5A fuselage, 874–875
 - graphite fibres, 26
 - laminates, 333–335
 - repairs, 35–36
- cohesive failure, 45, 47, 71, 727–730, 791
- commercial aircraft

- demonstrators, 959–972
- doubler repairs, 485–515
- L-1011 repairs, 813–842
- composite reinforcement, 1042–1046
- composite repairs, 9–11, 14, 21
 - design, 137–174
 - test procedures, 34–35
- composite surfaces, 79
 - surface preparation, 21, 78–80
- contact angle of adhesive, 42, 52
- contaminants of adhesive, 20
- contamination of surface, 21, 42, 44
 - bond durability, 51–54
 - hydrophobic, 66–67
- conversion coatings for steel, 78
- corrosion, 3–6, 23, 968, 974, 1019–1024
 - inhibitors, 33, 63, 78
 - metal patches, 23
 - patch design, 191–192
 - universal charts, 189–190
- cost fibres, 24–26
- coupling agents, 33
 - aluminium, 70
 - surface preparation, 51–53, 61–63, 73–74, 986–987
- crack growth, 3–5, 48–49
 - acoustic fatigue, 455–557
 - damped repair, 563–565
 - fuselage lap joint, 459–464
 - fuselage skin, 921–926
 - graphite/epoxy patches, 420–440
 - monitoring, 703–707
 - nacelle inlet, 533–546
 - nacelle inlet panel, 540–546
 - patch materials, 399–413
 - stress intensity model, 376–379, 526–530
 - T-38 lower wing skin, 1003–1008
- crack growth rate, 11–14, 96–97
 - curves, 51–53
 - doubler, 504–505
 - fatigue tests, 134–135
- crack patching
 - asymmetric analysis, 294–296
 - closed-form analysis, 177–205, 354–361
 - stress intensity analysis, 376–379
- crack tips, 150–154
 - stress-intensity factor, 200–202
 - Rose analysis, 180–183
- crack-closure analysis, 354–361
- cracks, 3–4
 - acoustic fatigue, 531–568
 - avoid by design, 194–196
 - beneath composite doubler, 694–701
 - F-111 wing skin, 798–811
 - holes, 233–236
 - bi-axial loading, 258–262
 - lugs, 236–242
 - one-sided repairs, 162–163
 - panels, damped repairs, 546–557
 - plates, 103–104, 551–553
 - size, 150–154
 - stationary, 357–361
 - stiffened panels, 192–194
- critical repairs certified, 643–656
- critical strain, 27
- crosslinks
 - adhesives, 20, 42
 - sol-gel, 80–81
- curing, 20, 31–32, 742–748
 - F-111 reinforcement, 851–852
 - residual stress, 167–174
 - temperature, 20, 42, 78, 341–349
 - voids, 36–38
 - see also* heating
- curved beam analysis, 864–870
- curved surfaces, 10, 39
 - boron fibres, 25
 - graphite fibres, 26
- cyanoacrylate adhesives, 28
- cyclic loading patches, 392–394
- damage detection *see* SMART patches
- damage on impact, 433–435
- damage tolerance, 3, 103–105, 632–635
 - C-5A fuselage crown, 872–874
 - doubler repairs, 485–515
 - F-16 fuel vent-hole, 885–887
 - multi-site damage, 468–474
 - non-destructive inspection, 660–664
 - SMART patches, 572–573
- damped repairs panels, 546–557
- damping data aft fuselage, 561
- database of adhesives, 87–100
- DC-10/MD-11, 919–935
- DC-9 test bed, 687–689
- defects in bondline, 427–433
- degreasing surface, 57–58
- delamination inspection, 664–694, 716–718
- demonstrators
 - Ansett keel beam, 962
 - B-747, 477–480
 - commercial aircraft, 959–972
 - multi-site damage, 474–480
 - QANTAS doublers, 960–962
 - SMART patches, 599–611
- density, 9, 26–27

- depot repairs, 6, 45
 - see also* on-aircraft
- design, 15–17, 27–28
 - airframe structure, 2–3
 - allowables, 621–626
 - analytical methods, 137–174
 - crack avoidance, 194–196
 - F-16 fuel vent-hole, 889–895
 - inspections, 27–28
 - loads, 2, 626–630
 - CH-47 cargo hook beam, 975
 - F-111 wing skin, 800–801
 - numerical analysis, 207–265
 - operating temperature, 26–27
 - patches, corrosion, 191–192
 - reinforcements, 297–308
 - stress limit, 395–396
 - UK bonded repairs, 908–909
- differential equations, 245–251
- differential scanning calorimetry, 34
- diffusion coefficients, 99–100
- disbond-tolerant zone, 104, 634
- disbonds, 716–718
 - crack growth, 381–391
 - crack-tip stress-intensity, 200–202
 - detection, lamb waves, 680–681
 - double overlap joint, 108–114
 - inspection, 664–694
 - skin doubler, 120–123
- displacement and frequency, 552–553
- door corner testing, 826–832
- double cantilever beam, 128–129
- double overlap joints, 11–13, 124–125
 - fatigue specimen, 104–114
- doubler repairs
 - CF-116, 941–946
 - cracks beneath, 694–701
 - damage tolerance, 485–515
 - inspections, 479–480
 - L-1011, 813–842
- Drucker-Prager/cap plasticity model, 92–94
- drying surface, 63–64
 - composites, 79–80
- durability, 3, 32
 - curved beam, 866
 - see also* bond
- eddy-current inspection, 694–701
 - aileron hinges, 712–714
- education of practitioners, 68, 755, 783–795
- efficiency charts
 - isotropic patches, 183–186
 - orthotropic patches, 196–197
- efficiency studies
 - boron/epoxy patches, 375–398
 - fatigue, 644–648
 - GLARE patches, 399–413
 - graphite/epoxy patches, 425–440
- EH101 helicopter, 913–917
- elastic energy release, 49
- elastic-plastic analysis, 49
 - multi-site damage, 456–459
 - stress analysis, 456–459
- electrical conductivity, 10, 23, 26
- electro-mechanical impedance
 - SMART patches, 593–595
- electroformed nickel, 24
- element stiffness matrix, 210–212
- elliptical patches, 184–186
- environmental effects
 - bonding repairs, 464–468
 - fracture mechanics, 127–135
 - humid atmosphere, 43–44, 47, 49
 - patching efficiency, 648–654
 - temperature, 962–963
- epoxy adhesives, 29
 - hydrogen bonding, 42, 50–51
- erosion shields, 966
- etching surface, 60, 78
 - acid etch, 69–71, 73, 78
 - chromic acid, 32, 60
- exfoliation *see* corrosion
- F-111
 - lower wing skin, 704–707, 797–811
 - wing pivot, 689–691, 845–858
- F-16 fuel vent-hole, 885–895
- F/A-18
 - aileron hinges, 300–308, 710–714, 897–906
 - bulkhead, 297–300, 707–709, 859–870
 - nacelle inlet, 539–546
 - thermal environment, 562–568
- factory processes, 44, 69–71, 74–76
- fail-safe approach, 2–3, 631
- failure modes, 45–46, 401, 513
- fatigue, 23, 134–135, 381–391
 - CH-47 cargo hook beam, 977
 - damage criteria, 124–125
 - F-16 fuel vent-hole, 892
 - lifetimes, 508
 - patching efficiency, 644–648
 - repair design, 630–635
 - ship structures, 1041–1042
 - strain, 27
- fatigue cracks, 4
 - analysis of repairs, 353–373

- propagation tests, 379–381
- upper wing skin, 939–940
- see also* acoustic fatigue
- fatigue loading, 96–97, 506
- F-111 wing skin, 801
- fatigue testing
 - battle damage, 769–770
 - doubler, 500–507
 - EH101 helicopter, 913–917
 - generic bonded joints, 103–125
 - multi-site damage, 459–468
 - service environment, 134–135
 - skin doubler, 121–123
- FE analysis *see* finite element
- fibre diameter boron, 24–25
- fibres, safety, 752
- Fickian diffusion coefficients, 99–100
- field repairs, 6, 45
 - see also* on-aircraft
- fillet, adhesive, 38, 281–285
- finite element analysis, 208–215
 - adhesive stresses, 281–288
 - aft fuselage, 557–562
 - bulkhead, 860–864
 - C-5A fuselage, 879–883
 - curved beam, 864–870
 - damage sensing, 603–611
 - double overlap joint, 106–107
 - F-111 wing skin, 802–803
 - fracture mechanics, 131–132
 - fuselage door surround, 825–828
 - heat stress, 324–341
 - nacelle inlet, 539–546
 - one-sided repairs, 157–167
 - overload effect, 361–365
 - plate stress, 281–285
 - shape optimisation, 270–296
 - skin doubler, 115–120
 - stress analysis, 456–459
 - stress concentration, 309–313
 - symmetric repairs, 144–155
 - wing, 343–348
- flaws in adhesive, 505–506
- flow of adhesive, 20, 34
- FM300, 88–89, 96–97
- FM73, 89–96
 - database, 98–100
 - doubler overlap joint, 104–114
- Fokker surface contamination tester, 67
- foreign object damage, 963
- forest products laboratory etch, 70–71
- formulation *see* analytical
- Fourier transform IR spectroscopy, 67
- fractographic analysis, 949–951
- fracture control plan, 486–490
- fracture energy, 46
- fracture mechanics, 48
 - allowables, 94–97
 - environmental effects, 127–135
 - skin doubler, 123–124
 - testing procedures, 129–132
 - toughness data, 100
- fracture toughness, 129–134
- frequencies, 551–552, 566–568
- fuselage, 558
- full scale testing repairs, 637
- fuselage, 24, 536–537
 - bulkhead, 859–870
 - crown, 871–883
 - door surround, 814–826
 - finite element model, 557–562
 - lap joints, 459–464
 - reinforcement, 984
 - skin repair, 1027–1029
- galvanic corrosion, 23–26
 - see also* corrosion
- gases giving voids, 37
- generic bonded joints
 - fatigue testing, 103–125
- geometrically linear analysis, 157–162
- geometrically non-linear analysis, 163–167
- geometries of patches *see* patches
- GLARE patches, 23–24
 - efficiency studies, 399–413
- glass transition temperature, 99
- graphite/epoxy patches, 9, 25–26
 - efficiency studies, 415–440
 - versus boron/epoxy, 424–427
- grit-blasting surfaces, 49–50, 60, 77, 986–994
- safety, 752
- guided waves, 680–684
- hardness fibres, 25–26
- Hart-Smith design data, 89–91, 98
- health of patch *see* SMART patch
- health of workers
 - chemical hazards, 45
 - graphite fibres, 26
 - see also* safety
- heating
 - AMORLUX, 777
 - on-aircraft repairs, 742–748, 988–994
 - residual stress, 170–171
 - see also* curing
- helicopter, 913–917

- high energy surface oxide, 60–61
- HMAS Sydney, 675, 1042–1046
- hole-in-a-plate problem, 311
- holographic interferometry, 691–692
- honeycomb structure, 30, 46
- hot solution treatment, 81–82
- hot/wet environments, 43–49, 53–57
 - composite patches, 436–438
 - fatigue tests, 465–466
 - fracture mechanics, 127–135
 - void formation, 65
- humid atmosphere, 43–44, 47, 49, 53–57
 - void formation, 65
- hydration of surface, 21
- hydrocarbon contamination, 44, 51–53
- hydrofluoric acid etch, 73
- hydrogen bonds, adhesives, 42
- hydrolysis coupling agent, 62
- hydrophobic contaminant, 51–53, 66–67
- hydroxyl content, 50–51
- impact damage
 - composite patches, 433–435
 - damage tolerance, 469–472
- in-flight demonstrators, SMART patches, 599–611
- in-plane shaping effects, 308–313
- in-service environment *see* environmental
- in-service management
 - commercial demonstrators, 959–972
 - inspection, 637–638
 - quality control, 714–719
- inclusion model, 144–147
 - stress fields, 178–180
- infrared spectroscopy, 67
- inlet nacelle, 533–546
- inspection of aircraft, 3–5, 27–28, 490
 - adhesion failure, 664–694
 - CH-47 cargo hook beam, 979
 - cracks beneath doubler, 694–701
 - delaminations, 664–694
 - disbonds, 664–694
 - doubler, 479–480, 492–500
 - in-service management, 637–638
- interactions in bonding, 42
- interfacial failure, 47, 727–730
- interfacial loading, 49–50
- interfacial peel, 49–50
- interfacial shear component, 50
- interferometry, 691–692
- interlaminar shear test, 35
- interlayer cracks, 699–701
- Iosipescu testing, 98
- isotropic patches, efficiency charts, 183–186
- joints, 104–105, 646–648
 - two dimensional strip, 337–339
 - see also* strip joints
- K-gauge, 518–530
- keel beam, 968–972
- Kevlar, 23
- KI measurement, 519–530
- Knoop value, boron fibres, 25
- L-1011 door surround, 673, 813–842
- lamb waves, disbond, 680–681
- laminates, 9, 21–24, 399–400
 - lap joints, 444–450
 - thermal analysis, 333–335
- lap shear strength, 34, 715
- leaky interface waves, 681–683
- linear analysis repairs, 157–163
- load transfer in repairs, 8
 - adhesive stresses, 269–313
 - bonded reinforcement, 141–144
 - doubler, 510
 - SMART patches, 578–587
 - surface roughness, 50
- loading, 4, 30–31, 45–46, 626–630
 - aileron hinge, 300–308, 898–899
 - CH-47 cargo hook beam, 975
 - in-plane shaping, 308–313
 - multi-site damage, 444–450
 - static, 89–94
- maintenance of ageing aircraft, 3–4
- material non-linearities, 243–251
- materials engineering, 35–39
 - see also* voids
- MD-11/DC-10, 919–935
- mechanical abrasion *see* grit-blasting
- mechanical joints, 7–8
- mechanical tests, 45–46
 - F-111 wing pivot, 851
- mechanically fastened patch, 7–9
 - battle damage, 765–770
 - F-16 fuel vent-hole, 888–889
- membrane stress, fuselage, 823–824
- metal laminates *see* laminates
- metal oxides, 42–51
- metallic adherends *see* adherends
- metallic airframes, ageing, 3–5
- metallic patches, 21–24
 - versus composite patches, 9–10
- micrographs, 50, 53–59, 950–952, 1000

- MIL tests, 88–94
- Mirage III aircraft, 212
- modal shapes, 551–552
 - aft fuselage, 558
- mode I fracture, 45–46, 95, 155–156
 - environmental effects, 127–135
 - toughness data, 100
- mode II and mixed mode fractures, 95–96
- mode of fracture, 53–57, 155
- modelling
 - aft fuselage, 557–562
 - bond durability, 53–56
 - bonded crack-patching, 177–205
 - crack bridging, 162–163, 521–530
 - Drucker-Prager/cap plasticity, 92–94
 - F-111 wing skin, 803–805
 - fracture mechanics, 131–132
 - in-plane shaping, 308–313
 - patch shape, 270–272
 - stress intensity, 376–379, 521–530
- modulus, shear, 27
- moisture absorption, 99–100
 - adhesive film, 64–65
- monotonic fracture toughness, 129–131
- multi-load-path design, 2–3
- multi-site damage, 443–482
- multi-step taper, 274–275
- nacelle inlet, 533–546
- nickel as repair material, 24
- non-destructive inspection, 8, 10, 17, 28, 715
 - boron fibres, 25
 - damage tolerance, 505–506, 660–664
 - fuselage door surround, 826–840
 - fuselage skin, 932–934
 - graphite fibres, 26
 - guided waves, 680–684
 - quality control, 659–723
 - resonance test, 683–685
 - ships, 1045–1046
 - thermography, 685–689
- non-linear analysis, 163–167
- non-linearities in materials, 243–251
- non-metallic repair materials, 24–26
- notation, space design analysis, 139–141
- numerical analyses
 - aileron hinge, 300–308
 - design, 207–265
 - see also* analytical
- occupational health and safety, 750–752
 - see also* health; safety
- octagonal patches, 184–186
- on-aircraft repairs, 45
 - aluminium, 72–74
 - anodisation, 60–61, 72
 - composites, 78–80
 - etching, 73
 - heating procedures, 742–748
 - steel, 78
 - titanium, 76–77
 - see also* case histories
- optical reflectivity, 68
- optically stimulated electron emission, 67
- optimisation
 - shape of repairs, 269–313
 - F/A-18 bulkhead, 297–308
 - through-thickness shaping, 288–296
- organosilane coupling *see* coupling agents
- orthotropic patches, 328–330
- overload effect, 361–365
- oxidation of surface, 21, 50–51
 - oxide removal, 60–61, 77
- P2 etch, 71, 73
- panel thickness, 387–388
- panels F-111, 807–809
- parametric studies, patches, 400–413
- Pasa-Jell pastes, 73–77
- patch length, shear strain, 276–277
- patch tapering
 - adhesive stresses, 186–189, 272–296
 - stepping formulation, 272–280
- patches, 6–10
 - aspect ratios, 310–313
 - corrosion damage, 191–192
 - crack growth, 381–383
 - cracks in stiffened panels, 192–194
 - end step geometries, 114–115
 - epoxy materials, 9
 - isotropic, 183–186
 - materials, 21–28
 - metal and composite, 7–10
 - one-sided bending, 202–204
 - panels, stress intensity, 517–530
 - parametric studies, 400–413
 - shapes, 184–186
 - finite element analysis, 285–296
 - taper angle, 114–115
 - thickness, 23, 384
 - universal efficiency charts, 183–186, 196–197
 - see also* panels; SMART patches
- patching efficiency, 7–8, 26
 - environmental durability, 648–654
 - fatigue, 644–648
 - SMART patches, 654–656

- peel ply method, 79
- peel stress, 31, 332
 - double overlap joint, 106–107
 - skin doubler, 115–123
- peel tests, 46
- phenolic adhesives, 28–29
- phosphate fluoride, 75
- phosphoric acid anodise, 69–70
 - on aluminium, 72
- phosphoric acid etch *see* etch
- piezotransducer, 593–611
- pitting *see* corrosion
- plasma oxidation experiments, 50
- plastic adhesive
 - design analysis, 149–150
- plastic strain, adhesives, 31
- plate stress, analysis, 281–285
- Poissons ratio, 139, 145
- polarity epoxy resins, 50–51
- polyimide adhesives, 29
- polymeric surfaces, preparation, 21
- polyurethane adhesives, 28
- power spectral density, 537
 - displacement, 552–553
- practitioner education, 68, 755, 783–795
- prebonding surface treatment, 9
- preured patches, 80
- pressure during repairs, 32, 748–750
 - voids, 38
- primary structure, 2
 - RAF aircraft repairs, 911–912
- primers, 33, 739
 - aluminium, 69–71
 - surface preparation, 63
- probability of detection, 660–663
 - cracks, 697–701
- process control coupons, 68
- profile angle of surface, 49
- pulse-echo ultrasonics *see* ultrasonics

- QANTAS demonstrators, 960–962
- quality assurance tests, 34, 714–715
 - L-1011 repairs, 839–840
- quality control, 752–754
 - in-service, 714–719
 - non-destructive inspection, 659–723
 - surface treatment, 66–68

- R* ratio, fatigue, 384–386
- RAF bonded repairs, 909–912
- random response analysis, 537–538
- reflectance colourimeters, 68
- reflectivity, optical, 68

- reinforcements, 141–144
 - designs, 297–308
 - F-111 wing pivot, 846–849
 - materials, 21–28
- repairs, 2–9, 21–26
 - aircraft wing skin, 212–215
 - applications, 730–750
 - cracked holes, 233–236
 - bi-axial loading, 258–262
 - cracked lugs, 236–242
 - damped, 546–557
 - demonstrators, 474–480
 - design, 619–637, 1012–1015
 - differential equations, 245–251
 - large areas, 983–995
 - multi-site damage, 443–482
 - one-sided (asymmetric), 139, 157–167
 - pressure, 748–750
 - shape optimisation, 269–313
 - skin components, 416–418
 - surface flaws, 242–243
 - surface treatment, 41–82
 - symmetric design, 144–155
 - thick sections, 229–233, 262–265
 - efficiency studies, 418–424
 - wing analysis, 341–349
 - see also* case histories; depot; efficiency studies; factory; field; on-aircraft; workshop
- residual strain technique, SMART patches, 588–593
- residual strength, 661
 - b/ep patch design, 396
 - curved beam, 866–867
 - F-111 wing skin, 798–800
 - patched panels, 389–391
- residual stress *see* thermal residual
- resin development, 772, 776–779, 1039
- resonance test, 683–685
- reviews bonded composites, 15
- Rose closed-form analysis, 177–205
- Rose inclusion model, 521–530
- rotor blade doublers, 984
- rust removal, steel surfaces, 77

- safe-life approach, 2, 572–573, 631
- safe-life zone, 104, 634
- safety by inspection, 3–5, 572, 632–633
- safety of chemicals, 33, 45
 - chromate inhibitors, 63, 70
 - hydrofluoric acid etch, 73
 - repair process, 76–77
 - solvents, 58, 751
- safety requirements, repairs, 615–639

- salt environment, 466–468
- sawtooth surface, 49–50
- scanning electron microscopy, 53–56, 950–952
- scanning technology, 585
 - adhesive failure, 666–669
- secondary structure, 2
 - RAF aircraft repairs, 909–911
- sensors, 39
 - SMART patches, 571–612
- service environment *see* environmental effects
- shape optimisation, 269–313
 - aileron hinge, 303–308
 - finite element analysis, 285–296
- shear components, 49–50
- shear mode, design analysis, 155–156
- shear modulus, 27, 538
- shear strain, 109–114
 - patch length, 276–277
- shear strength, adhesives, 31
- shear stress
 - double overlap joint, 106–107
 - skin doubler, 115–123
- shear stress-strain data, 89–94, 98
- shear tests, 35, 46, 715
- shear-tension/compression, 91–94
- shelf life of materials, 34–35
- ship structures, 1035–1049
- short beam shear test, 35, 715
- silane *see* coupling agents
- skin components, 416–418
- skin doubler, 114–125, 578–587
- slow-crack-growth *see* safety by inspection
- SMART patches, 15, 39, 571–612
 - damage detection, 578–599
 - demonstrators, 599–611
 - patching efficiency, 654–656
- smut on steel surface, 78
- sol-gel technology, adhesives, 80–81
- solution-gelation, 80–81
- solvents, 987–994
 - contaminant, 58–60
 - degreasing, 57–58, 733–734
 - giving voids, 37
 - safety, 58, 751
- sound causing cracks, 531–568
- spectroscopy
 - infrared, 67
 - X-ray photoelectron, 51
- spectrum loading, 367–372
 - b/ep patch design, 394–396
 - C-5A fuselage, 882–883
- spew fillet, 38
- standard tests, 47–48
 - see also* cleavage; fracture; wedge
- static analysis, repair design, 626–630
- static loading, 95
- static strength, 2
 - CH-47 cargo hook beam, 975–977
- static testing
 - battle damage, 769–770
 - F/A-18 aileron hinge, 903–905
 - F/A-18 fuselage, 865–866
- steel adherends, 22
 - surface preparations, 77–78
- stepping patch taper, 272–296
- stiffness, 7–9, 24–25
- strain
 - residual, 588–593
 - T-38 wing, 1001–1003
- strain field measurements, 507–514
 - fuselage door surround, 820–823
- strain gauges, 519–530, 1000–1003
 - fuselage skin, 926–929
- strain-energy release rate, 95–97
 - double overlap joint, 109–114
 - fracture mechanics, 127–135
 - skin doubler, 124–125
- strength, 10
 - non-metallic materials, 24–25
- strength of bonds, 21
 - see also* bond
- stress analysis
 - aileron hinge, 899–903
 - multi-site damage, 453–459
 - wing, 1012–1015
- stress based diffusion model, 53–55
- stress concentrations, 7–9
 - load transfer, 269–313
 - voids, 37
- stress displacement plots, 11–13
- stress distribution, 53–57
- stress fields, 820–825
 - inclusion model, 178–180
- stress intensity factor, 10
 - acoustic fatigue cracking, 538–546
 - crack growth, 365–372
 - crack tips, 180–183
 - model, 376–378, 521–530
 - one-sided repairs, 157–167
 - patch materials, 402–405, 416–418
 - patched cracks, 376–379
 - patched panels, 389–391, 517–530
 - Rose inclusion model, 521–530
 - skin, 553–555
 - symmetric repairs, 144–155
- stress ratio, 10, 141

- stress reduction, 145, 312
 - see also* universal efficiency charts
- stress states, 88–94
 - double overlap joint, 106–107
 - skin doubler, 115–120
- stress wave technique, 595–597
- stress-corrosion cracks, 4
- stress-strain data, 89–94
- stresses
 - cantilevers, 48
 - circular plate, 318–335
 - design limit, 395–396
 - fatigue studies, 383–384
 - plate, 281–285
 - residual, 10
 - wing, 346–349
 - see also* adhesive; thermal
- strip joints, 330–332, 337–341
- structural adhesives *see* adhesives
- structural degradation, 2–6
- structural repair manual, 2
- structure tests, door surround, 814–826
- surface oxide *see* oxidation
- surface preparation, 21, 32
 - abrasion, 58–60
 - aluminium, 69–74
 - bond strength, 732–742
 - composite adherends, 78–80
 - degreasing, 57–58
 - drying, 63–64, 79–80
 - research, 80–82
 - steel, 77–78
 - titanium, 74–77
 - see also* coupling agent; oxidation; primers
- surface tension, bonding, 42
- surface treatment, 9, 21, 32, 1039
 - battle damage, 767–768
 - bond durability, 964–965
 - quality control, 66–68
 - Fourier transform IR, 67
 - optical reflectivity, 68
 - process control coupons, 68
 - waterbreak test, 66–67, 78
 - work function, 67
 - repair bonding, 41–82
 - see also* wedge test, 74, 76
- surfaces
 - bond durability, 48–56
 - contamination, 51–53
 - cracks, 679–699
 - curved, 10
 - energy, 41–42
 - flaws, 242–243
 - symmetric repairs *see* repairs
 - symmetric stepped patches, 272–273
 - T-38 lower wing skin, 997–1008
 - taper angle of patch, 114–115
 - taper profile, 114–115
 - adherend, 272–296
 - skin doubler, 117–120
 - tapered end skin doubler, 117–120
 - temperature
 - adhesion, 20
 - adhesive selection, 30
 - aircraft use, 26–27, 435–436, 962–963
 - F/A-18, 562–568
 - changes for repairs, 35–36
 - curing, 36, 42, 341–349
 - F-111 wing, 854–855
 - F-16 fuel vent-hole, 890–891
 - fatigue studies, 384–391
 - fracture toughness, 127–135
 - glass transition for FM73, 99
 - ramp rate, 64
 - repairs, 44, 76–77
 - residual stress, 168–170
 - see also* thermal
 - tensile strength, 511–514
 - tensile tests, 46
 - adhesive, 91–92
 - damage tolerance, 472–474
 - tertiary structure, 2
 - test procedures, 740–742
 - bonding, 46
 - Fourier transform IR, 67
 - fracture mechanics, 129–132
 - physical tests, 46
 - ASTM and MIL, 88–94
 - shear tests, 46
 - waterbreak test, 66–67
 - see also* quality assurance
 - thermal cycling of patches, 10, 129–135
 - thermal effect F-111, 803–805
 - thermal expansion coefficient *see* coefficient
 - thermal loading
 - tapered skin doubler, 119
 - wing, 341–349
 - thermal residual stress, 35–36, 197–200
 - acoustic fatigue cracking, 563–565
 - adhesive curing, 167–174
 - aft fuselage, 560–561
 - analysis, 317–350
 - crack growth, 365–372, 384–391
 - skin doubler, 115–120
 - thermocouples, 747–748

- thermodynamics, 42
- thermography, 685–689
 - stress analysis, 692–694
- thermoplastic composites, 23
- thermoset composites, 23
 - surface preparation, 78–80
- thick sections, 229–233, 262–265
 - efficiency studies, 418–424
- thickness of adhesive, 251–258
 - bondline, 42, 65
 - non-linearity, 256–258
- thickness of patches, 23, 384
- through-thickness shaping
 - aileron hinge, 300–308
 - bulkhead, 297–300
- through-thickness stresses, 31
- titanium adherends, 22
 - surface preparations, 74–77
- titanium patches, 23
- trade structure, 786
- training technicians, 68, 755, 783–795
- transfer function method, SMART patches, 595
- TURCO 5578, 75
- UK bonded repairs, 907–918
- ultraflat surface, 49–50
- ultramilling preparation, 49
- ultrasonics, 585, 721–723
 - aileron hinges, 710–714
 - fuselage skin, 932–934
 - non-destructive inspection, 665–679
- unbalanced repair, skin doubler, 115
- uniaxial loading, 310–313
- unidirectional patches, 9
- universal charts, corrosion, 189–190
- universal efficiency charts
 - isotropic patches, 183–186
 - orthotropic patches, 196–197
- vacuum moulding tool, 778
- validation, 740–742
 - DC-10/MD-11 repairs, 926–932
- viscoelastic behaviour of joins, 11
- viscosity of adhesive, 20, 42
- voids, 65–66
 - cure pressure, 36–38, 42
 - solvents, 63
- Wang crack bridging model, 521–530
- water
 - degrades bond, 21
 - giving voids, 37
- waterbreak test, 66–67
 - composite surfaces, 78
- wedge durability test, 47–57, 715, 791–794
 - aluminium, 74
 - battle damage, 773–776
 - titanium, 76
 - validation, 740–742
- weight, 28
- Westergaard equations, 519–521
- wetting of adherend, 20, 60–61
 - hydrophilic, 58
 - surface energy, 41–42
- wings
 - analysis of repairs, 341–349
 - C-141 repairs, 1013–1015
 - reinforcement, 984
 - skin crack repairs, 212–215
 - see also* F-111
- work function, 67
- workshop environment, 45
 - see also* on-aircraft
- X-radiographic inspection, 701–703
- X-ray photoelectron spectroscopy (XPS), 51, 54
- yield criterion for FM73, 98–99
- yielding, crack-closure, 354–361
- Young equation, 42
- Youngs modulus, 139, 157, 538

Advances in the Bonded Composite Repair of Metallic Aircraft Structure

The availability of efficient cost-effective technologies to repair or extend the life of aging military airframes is becoming a critical requirement in most countries around the world, as new aircraft become prohibitively expensive and defence budgets shrink. To a lesser extent a similar situation is arising with civil aircraft, with falling revenues and the high cost of replacement aircraft.

Fortunately a repair/reinforcement technology based on the use of adhesively bonded fibre composite patches or doublers can provide cost-effective life extension in many situations.

From the scientific/engineering viewpoint, this technology, although simple in concept, can be quite challenging, particularly when used to repair primary structure. This is because it is based on interrelated inputs from the fields of aircraft design, solid mechanics, fibre composites, structural adhesive bonding, fracture mechanics and metal fatigue. The technologies of non-destructive inspection (NDI) and, more recently smart materials, are also included. Operational issues are equally critical, including airworthiness certification, application technology (including health and safety issues) and training.

Most of these issues and the latest developments are discussed in this book, which contains contributions from leading experts in this technology from Canada, UK, USA and Australia. Most importantly, the book contains real case histories of application of the technology to both military and civil aircraft.

The cover picture is an Australian F-111 Aircraft, showing, schematically, a boron/epoxy repair patch applied to lower wing skin. Details of the region inside the wing where fatigue cracks develop are shown in the sketch. This repair is described in Chapter 27.

ISBN 0 08 042699 9



9 780080 426990